

Volume I  
SYSTEMS AND PROGRAM


Final Report  
MISSION DEFINITION STUDY  
FOR  
STANFORD RELATIVITY SATELLITE

Prepared for  
MARSHALL SPACE FLIGHT CENTER  
of  
NATIONAL AERONAUTICS AND SPACE ADMINISTRATION

Contract No. NASW-2284

Report F71-07  
22 December 1971

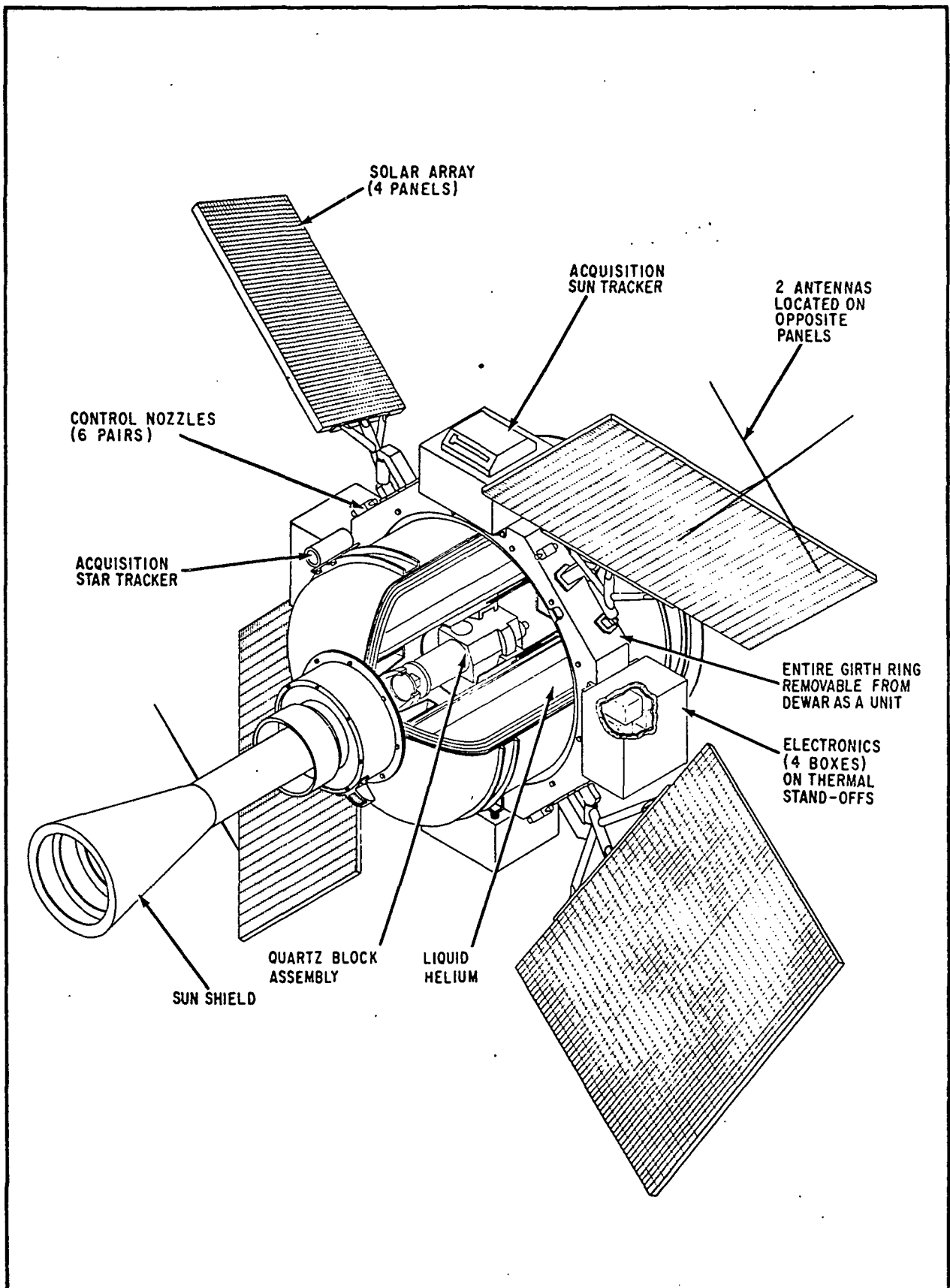
APPROVED:

  
F. P. Dolder  
Vice President

  
R. M. Ringo  
Vice President  
Aerospace Division



**BALL BROTHERS RESEARCH CORPORATION**  
SUBSIDIARY OF BALL CORPORATION  
BOULDER, COLORADO



STANFORD RELATIVITY SATELLITE



## FOREWORD

This is the final report of a funded study under Contract NASW-2284 issued by the National Aeronautics and Space Administration. It defines a mission for measuring the drift of a gyroscope due to the effects predicted by Einstein's General Theory of Relativity. The development of the gyroscopes and telescope used to detect the relativity effect has not been completed. The study assumes an interface for these components based on the present state of the development. Major changes in the assumed mechanical and electrical interface would have an important impact on the orbiting hardware but would probably not affect the rest of the mission.

The work reported here was performed in close cooperation with personnel of the Stanford University Departments of Physics, and Aeronautics and Astronautics. It is based on the extensive theoretical and practical work that has been done there since 1962.



## SUMMARY AND CONCLUSIONS

The objective of the Stanford Relativity Satellite mission is to perform the experiment originally suggested by L. I. Schiff in which a gyroscope in motion about the earth undergoes a relativistic precession with respect to the fixed stars. Two main effects are predicted. The geodetic effect is due to the motion of the gyroscope about the earth and yields a drift rate,  $\Omega_G$ , of approximately 6.3 arc-seconds per year for a 500 nautical mile orbit. The motional effect, due to the rotation of the earth, is much smaller and yields a drift rate,  $\Omega_M$ , of approximately 0.05 arc-second per year.

Performance of this experiment would give a clear test between the General Theory of Relativity of Einstein, and the various modifications of the theory that have been proposed by others. In addition, this is the only experiment proposed to date, which would confirm the existence of the motional drift.

The performance of the experiment to its design accuracy of 0.001 arc-second per year would measure the geodetic drift to an accuracy of 0.015 percent and would allow determination of the coefficient  $\gamma$  of the relativity equation to two parts in  $10^4$ . It would also allow measurement of the motional term to 2 percent. Performance of the experiment to 0.2 arc-second per year would allow a clear test between the Einstein theory and the Brans-Dicke theory which is the leading contender.

As a result of this study, a mission is defined, along the lines originally suggested by Stanford, in which the measurement of the geodetic term to 0.2 arc-second per year is clearly achievable and the measurement of both terms to an accuracy of 0.001 arc-second per year, though extremely difficult, may be possible.





The difficult mechanical stability goals are made feasible by making the entire telescope-gyroscope assembly from fused quartz parts which have been optically contacted together. These are all at the temperature of liquid helium where thermal expansion and creep are greatly reduced. The cryogenic environment also provides the means for superconducting magnetic shields to be used around the gyroscope to reduce drifts caused by magnetic fields. Nearly torque free gyro attitude readout is possible by the use of the London Moment caused by the superconducting coating on the spinning rotor.

The Frontispiece shows the "flying dewar" satellite needed to maintain the experiment at cryogenic temperatures. Inside a central cavity in the dewar, in thermal contact with the liquid helium, is the experimental apparatus consisting of a startracking telescope and four gyroscopes mounted together and supported in a two-axis gimbal. The telescope looks out a window at one end of the cavity, through the sun shield, at the star Rigel near the celestial equator. Two of the gyroscopes are mounted with their spin axes aligned with the optical axis of the telescope. These two make redundant measurements of both the geodetic effect and the motional effect. The other two gyroscopes are aligned mutually perpendicular to each other and to the telescope axis. One of these makes an independent measure of the geodetic effect and the other an independent measure of the motional effect.

The satellite needed to support the experiment is straightforward. The total weight is about 600 kg, easily launched by the Delta launch vehicle into the polar orbit. The data rate of 84 bps, and the few commands necessary for operation, require very limited support from the chosen ground stations of Fairbanks, Ororal and Santiago.



The design described in this report will perform the experiment to the required accuracy. There are, however, some assumptions inherent in the design which must be proven to be correct before the program can succeed.

At present, there is very little knowledge of the performance of a helium dewar in a space environment. The fundamental problems of preventing liquid venting and slosh must be investigated. Stanford has proposed and ground tested a "superfluid plug" which shows great promise of preventing liquid venting and BBRC has proposed, in this report, a scheme for preventing slosh. These methods can only be adequately tested in orbit.

The gyroscopes required for this experiment have not yet been demonstrated. Hardware with tolerances approaching that required has been fabricated for test, but small problems have delayed a demonstration of the spin up. Such a test is, of course, a fundamental first step. Once this is done, the gyroscope performance must be extensively evaluated in the laboratory. The laboratory drift performance of the gyroscope will be possibly a million times worse than in orbit, because of the required 1 g support force. In addition, spin-up characteristics of the gyroscope in orbit may be different from those on the ground and the system used to keep the balls suspended is different. Adequate evaluation of gyroscope performance can only be made in an orbital environment.

The magnetometer required for the London Moment readout system has not been perfected to a state where it could be used reliably with adequate sensitivity and noise characteristics. Work is being performed on this problem but significant improvement must be made over what can be demonstrated now.



The optical contacting method suggested for providing the dimensional stability of the entire assembly is at present an optician's art. We have found no engineering data regarding strength of joints in tension or shear. This kind of information must be developed so that the quartz block can be designed to survive launch.

Almost perfect magnetic shielding of the gyroscopes is required to allow the performance of the experiment to the design goal. There are practical conflicts between the magnetic shielding techniques contemplated and the technique of optical contacting to meet the stringent stability criteria. This problem must be resolved by an engineering test program to evaluate the solutions which have been proposed.

From our study, it seems that in most areas Stanford has made careful and adequate paper studies of the requirements and the phenomena of importance to the program. Also, Stanford and MSFC have developed some experimental hardware which has been given preliminary testing. We feel that in the near term, this work on development hardware and technology advancement should be greatly expanded to solve the engineering problems outlined above. An engineering flight test program is needed to test some of the vital components which cannot be adequately evaluated on the ground. Further laboratory work is required to be ready to proceed with the main program in an orderly manner. It seems possible for the flight test program and the laboratory work to be performed in a time frame which would allow a main program start in late 1973, with a target launch date of mid-1976.

The successful performance of the liquid helium dewar and the gyroscopes in space will make possible whole new areas of investigation in the fields of cosmic ray physics, infrared astronomy and space navigation.



## INTRODUCTION

This report is in three volumes:

- Systems and Program
- Test Flights
- Appendices

Volume I provides general information on the mission to the sub-system level and a description of the program necessary to perform the mission. The first section, Mission Objectives, describes the science involved in this mission. The second section is a summary or overview of the total mission covering the orbiting hardware, the orbit and launch vehicle and operations from fabrication through data reduction. Section 3 describes the system considerations for the orbiting hardware. Included are a description of the system functional diagram, the satellite configuration, and a tabulation of satellite requirements and subsystem budgets. Section 4 is the program plan. This section includes discussions of technology advancements that must be made before the mission can be performed, the program schedule and a cost estimate.

Sections 5 and 6 contain the details of the experiment and spacecraft subsystems and mission support items. Each subsystem section starts with the requirements for the subsystem, then describes the subsystem. The final part tabulates the predicted performance for the subsystem and describes any tradeoffs or analysis performed.



Section 7 provides the details of support for the orbiting hardware. These include the orbit, booster and operations including all activity from fabrication to data reduction to extract the relativity drift.

Volume II describes an engineering flight test program which results in orbital tests of a dewar and later a dewar with a gyroscope assembly.

The final volume contains the appendices, that provide further detail which may be of interest to specialists.



## GLOSSARY

CRYOGENIC ACTUATOR - A solenoid used to develop the force to move the quartz block. The coil of the solenoid will be superconducting and the slug will be of paramagnetic material.

EXPERIMENT - The quartz block assembly and associated electronics that are mounted in the experiment dewar.

EXPERIMENT DEWAR - The "dewar within a dewar". This dewar contains its own liquid helium supply and will keep the experiment cold for several days. The experiment is "spared" at this assembly level.

GEODETIC DRIFT - The relativity drift caused by the motion of the satellite around the earth. The drift is about the orbit normal, and is in the direction of satellite motion.

GIRTH RING - The main structure of the spacecraft which bolts to the main dewar outer shell and supports all the spacecraft hardware.

GUIDE STAR - The star to which the telescope points and the celestial reference for measuring relativity drift.

INSTRUMENTATION ELECTRONICS - The processing electronics for the scientific data. It consists of the telescope electronics, AGC amplifiers, the ten second data integrators, the magnetometer, the roll encoder and the resolvers.

LONDON MOMENT - The dipole moment created when a superconductor spins. The moment is aligned with the instantaneous spin axis, and is proportional to spin rate.



MAGNETOMETER - The gyro loops and associated electronics used to determine the flux crossing the plane of the gyro position readout loop.

MAIN DEWAR - The large dewar consisting of the outer shell to which the girth ring and attach fitting are attached, inner shell inside which the experiment dewar slides, helium vessel which contains the one year's supply of liquid helium, and super insulation, the approximately 10 cm section inside the outer shell which insulates the liquid helium.

MOTIONAL DRIFT - The relativity drift caused by Earth rotation. The drift is about Earth's spin axis and in the direction of Earth's motion.

PROOF MASS - The ball inside the quartz block used to establish a geodetic orbit. The translation control system causes the satellite to follow the proof mass.

QUARTZ BLOCK ASSEMBLY - The assembly of the substrate block, the four gyroscopes, and, telescope and electronics which are attached to the substrate block.

REFERENCE TELESCOPE - The telescope which is part of the quartz block assembly and is maintained in the cryogenic environment.

ROLL REFERENCE STAR - The star that is near  $90^\circ$  to the guide star and used as a celestial roll reference.

SATELLITE - The total piece of orbiting hardware that is separated from the launch booster.



SPACECRAFT - The portion of the satellite that does not include the experiment dewar and instrumentation electronics.

STARTRACKER - The external startracking device used for coarse acquisition of the guide star.





## CONTENTS

Section		Page
	FOREWORD	iii
	SUMMARY AND CONCLUSIONS	v
	INTRODUCTION	ix
	GLOSSARY	xi
1	MISSION OBJECTIVES	1-1
2	MISSION DESCRIPTION	2-1
	2.1 Orbiting Hardware	2-4
	2.2 Orbit and Booster	2-10
	2.3 Operations	2-11
	2.4 Program	2-13
3	SATELLITE SYSTEM	3-1
	3.1 Configuration	3-1
	3.2 System Functional Description	3-3
	3.3 Reliability	3-18
	3.4 Requirements and Budgets	3-20
4	PROGRAM PLAN	4-1
	4.1 Feasibility and Problems	4-1
	4.2 Overall Schedule	4-1
	4.3 Plan for Technology Advancement	4-3
	4.4 Satellite Development Plan	4-14
5	EXPERIMENT AND DEWAR	5-1
	5.1 Telescope	5-2
	5.2 Gyroscopes	5-39
	5.3 Experiment Electronics	5-67
	5.4 Helium Dewar	5-91
6	SUBSYSTEMS	6-1
	6.1 Structure	6-1
	6.2 Thermal Design	6-31
	6.3 Power	6-48
	6.4 Control System	6-65
	6.5 Communications	6-148



## CONTENTS (Cont.)

Section		Page
7	MISSION SUPPORT	7-1
	7.1 Orbit and Booster	7-1
	7.2 Tracking and Data Support	7-20
	7.3 Operations	7-26

## ILLUSTRATIONS

Figure		Page
1-1	Relativity Drift Program	1-4
2-1	Simplified Systems Functional Diagram	2-6
2-2	Orbit Characteristics	2-11
2-3	Overall Program Schedule	2-15
3-1	Helium Used Versus Temperature	3-2
3-2	Particle Radiation	3-35
3-3	Probability of Micrometeor Hit on Satellite	3-36
4-1	Overall Program Schedule	4-2
4-2	Dewar Technology Program	4-7
4-3	Gyro Technology Program	4-11
4-4	Preliminary Design and Definition Schedule	4-15
4-5	Satellite Development Schedule	4-17
5-1	Sun Shield, 30-Degree	5-6
5-2	Sun Shield, 22-Degree	5-8
5-3	Telescope Optical System	5-9
5-4	Transmission and Reflectance of Dereflected Gold	5-10
5-5	Reflectance of Front-Surface Silver-Coated Mirror	5-13
5-6	Reflectance of Front-Surface Enhanced Aluminum Mirror	5-13
5-7	Fiber Optics Relay	5-15
5-8	Chopper Servo Schematic	5-17
5-9	Linearity Error Versus Pointing Error	5-22



## ILLUSTRATIONS (Cont.)

Figure		Page
5-10	Effects of Image Nonuniformity	5-27
5-11	Image Offset	5-33
5-12	Positive Detector Angle Versus Error Angle	5-34
5-13	Rigel Location and Neighbors	5-40
5-14	Procyon Location and Neighbors	5-41
5-15	Gyroscope Basic Parts	5-43
5-16	Gyroscope Shielding Detail	5-46
5-17	Gyroscope Optical Contact	5-47
5-18	End View of Quartz Block Assembly	5-50
5-19	Side View of Quartz Block Assembly	5-50
5-20	Quartz Block and Window Portion of Dewar	5-51
5-21	Quartz Block Gimbal	5-55
5-22	Typical Instrumentation Channel and Signal Processing Loop	5-69
5-23	Cryogenic Vibrating Plane Magnetometer	5-72
5-24	Gyroscope Readout Loop	5-74
5-25	Gyro Readout Loop Transfer Function and Noise Characteristics	5-75
5-26	Single Axis Telescope Electronics	5-80
5-27	Telescope Electronics Waveform	5-82
5-28	Servo-Type Integrating Analog-Digital Converter	5-84
5-29	Simplified Diagram of Electromechanical Resolver	5-89
5-30	Graphical Representation of Resolver Function	5-89
5-31	Functional Diagram of Roll Encoder	5-90
5-32	Dewar Cross Section	5-94
5-33	Superfluid Plug	5-95
5-34	Quartz Block Gimbal	5-97
5-35	Thermal Conductivity of Unidirectional Epoxy-Fiberglass Composite	5-108
5-36	Support Thermal Paths	5-109
5-37	Vapor Shield Support Heat Transfer Attachment	5-110



## ILLUSTRATIONS (Cont.)

Figure		Page
5-38	Fixed Dewar Support	5-112
5-39	Retractable Dewar Support	5-119
5-40	Shell Stress Comparison	5-123
5-41	Concept For Gyro Spinup	5-127
5-42	Schematic For Inside Valving	5-127
5-43	Schematic For Outside Valving	5-128
5-44	Vacuum Support Unit	5-129
5-45	Operation of Helium Management Scheme	5-131
5-46	Cell Assembly for Helium Management Scheme	5-133
6-1	Structure Layout (Dimensions in Inches)	6-4
6-2	Inner Dewar Layout, Bottom View	6-5
6-3	Delta Fairing Outline	6-6
6-4	Launch Configuration	6-7
6-5	Deployed Configuration	6-8
6-6	Attachment Fitting	6-12
6-7	Satellite Sine Vibration Input	6-19
6-8	Solar Panel and Sun Shield Sine Vibration Input	6-19
6-9	Electronics Box Line Vibration Input	6-20
6-10	Quartz Block Sine Vibration Input	6-20
6-11	Spacecraft Exterior Finishes	6-33
6-12	Electronic Boxes Thermal Design	6-34
6-13	Temperatures of Sun-Facing Surfaces at One Astronomical Unit	6-37
6-14	Second-Surface Mirror Assembly	6-37
6-15	Thermal Network for Electronic Boxes	6-38
6-16	Thermal Nodes	6-42
6-17	Solar Array Transient Temperatures	6-46
6-18	Typical Electronics Transient Temperatures	6-46
6-19	Dewar Top and Bottom Transient Temperatures	6-47
6-20	Dewar Fore and Aft Transient Temperatures	6-47
6-21	Power System Block Diagram	6-49



## ILLUSTRATIONS (Cont.)

Figure		Page
6-22	Solar Array Cell Configuration	6-51
6-23	Solar Array Power Gain Due to Angular Sunlight Incidence and Shadowing	6-53
6-24	Orbit Shadowing	6-53
6-25	Total Solar Array Power Gain	6-54
6-26	Master Regulator Simplified Block Diagram	6-56
6-27	Reliability Diagram	6-64
6-28	Cryogenic Actuator, Section View	6-71
6-29	Thruster, Cross-Section View	6-73
6-30	Pitch-Yaw Pointing Controls	6-74
6-31	Day-Night Operation	6-79
6-32	Roll Control System	6-84
6-33	Translation Control System	6-86
6-34	Sun Sensor Position and Field of View	6-89
6-35	Two-Stage Modern Pitch-Yaw Controller/Estimator	6-132
6-36	Antenna Pattern	6-152
6-37	Communications Concept	6-153
6-38	Telemetry Format	6-156
6-39	Command Message Format	6-161
6-40	Critical Command List	6-164
7-1	Day and Night Density Profiles in the Upper Atmosphere	7-10
7-2	Relativity Drift Versus Circular Orbit Altitude	7-10
7-3	Thor-Delta Payload Capability	7-11
7-4	Particle Radiation for Circular Polar Orbits	7-12
7-5	Ground Station Visibility Plot	7-21
7-6	Communications Time Chart	7-22
7-7	Typical Black Box Fabrication, Assembly and Test Sequence	7-29
7-8	Experiment and Main Dewar Assembly and Test	7-32
7-9	Ground Station Tape (One Pass)	7-35



## ILLUSTRATIONS (Cont.)

Figure		Page
7-10	Verification of Optical Alignment Using Autocollimating Telescope	7-37
7-11	Satellite Integration and Test Sequence	7-40
7-12	Centering Errors Affecting Center of Mass Location	7-43
7-13	Vacuum Support Unit	7-49
7-14	Polar Mount for Experiment and Control System Tests	7-51
7-15	Self-Aligning Artificial Star Source	7-53
7-16	Polar Axis Mounted Inertial Test Stand	7-56
7-17	Cross-Section Schematic, Ultra-Low Magnetic Field Facility	7-57
7-18	On-Line (Near Real-Time) Data Processing and Operation	7-59
7-19	Off-Line Data Reduction Sequence	7-60
7-20	Launch Site Operations	7-62
7-21	Launch and Initial Acquisition Sequence	7-63
7-22	Backup Acquisition Sequence	7-65
7-23	Aberrated Guide Star Motion	7-67
7-24	Aberrated Guide Star Motion and Motional and Geodetic Drift	7-68

## TABLES

Table		Page
1-1	Relativity Theories	1-6
1-2	Mission Objectives	1-7
2-1	Mission Requirements	2-2
3-1	Satellite Requirements	3-21
3-2	Gyro Readout - Full Scale	3-26
3-3	Gyro Acceleration Budget	3-27
3-4	Perpendicular Gyro Alignment Budget	3-28
3-5	Sensor Noise	3-28



## TABLES (Cont.)

Table		Page
3-6	Roll - Error Budget	3-28
3-7	Dewar Heat Leaks	3-29
3-8	Mass and Moment of Inertia	3-29
3-9	Electronic Box Allocations	3-30
3-10	Satellite Margins of Safety	3-30
3-11	Satellite Resonant Frequency (Hertz)	3-31
3-12	Power Budget	3-32
3-13	Outer Satellite Disturbance (Gas Budget)	3-33
3-14	Control System Closed Loop Break Frequency (Hertz)	3-34
3-15	Telemetry Budget	3-34
3-16	Command Budget	3-34
3-17	Reliability Budget	3-35
5-1	Telescope System Requirements	5-3
5-2	Telescope Parameters	5-12
5-3	Linear Expansion Coefficient for Fused Silica	5-29
5-4	Wiring per Gyroscope	5-48
5-5	Coordinates of Leads from Gyroscopes	5-49
5-6	Gyroscope Acceleration Sources	5-59
5-7	Gyroscope Acceleration Estimates	5-61
5-8	Gyro Readout Performance	5-77
5-9	Instrumentation Loop Performance	5-86
5-10	Dewar Performance Characteristics	5-99
5-11	Dewar Heat Leak Summary	5-102
6-1	Electronics Allocations	6-9
6-2	Resonant Frequencies (Hertz)	6-10
6-3	General Information	6-13
6-4	Weights and Moments of Inertia	6-14
6-5	Satellite Load Factors and Interface Moments	6-15
6-6	Margins of Safety	6-16



## TABLES (Cont.)

Table		Page
6-7	Spacecraft Thermal Design Requirements	6-31
6-8	Some Stable Thermal Control Finishes	6-34
6-9	Thermal Model of Exterior Finishes	6-43
6-10	Steady State Temperatures of Selected Nodes	6-45
6-11	Power Budget	6-58
6-12	Orbit Performance Data	6-59
6-13	Initial Acquisition Steps	6-90
6-14	Backup Acquisition Steps	6-97
6-15	Outer Satellite Peak Disturbance (Gas) Budget (Normal Operation)	6-101
6-16	Single-Stage Linear Second Order Pitch-Yaw Controller	6-130
6-17	Two-Stage Modern Pitch-Yaw Controller	6-136
6-18	Roll Control System Characteristics	6-140
6-19	Translation Control System Characteristics	6-144
6-20	Gyroscope Suspension System Characteristics	6-149
6-21	Submultiplexer Channel List	6-157
6-22	Command List	6-162
6-23	Communications Performance	6-165
6-24	560 K Bit Memory Comparison	6-168
7-1	General Orbit Requirements	7-2
7-2	Orbit Description	7-6
7-3	Orbit Trade-off Considerations	7-9
7-4	Booster Requirements	7-14
7-5	Performance of the Thor-Delta Launch Vehicle	7-16
7-6	Payload Capability and Cost Comparison for Alternate Launch Vehicle Configuration	7-19
7-7	Orbit Determination Requirements	7-24
7-8	Static Balance - Center of Mass Location Errors	7-44
7-9	Dynamic Balance Errors	7-45
7-10	Systems Test Equipment	7-47
7-11	Standard Facilities Requirements, Integration and Test	7-55
7-12	Computer Requirements	7-61





Section 1  
MISSION OBJECTIVES

The General Theory of Relativity has been of deep interest to scientists of several specialties since it was proposed by Einstein in 1916.

The theory has three important aspects:

1. The special theory of relativity which gives the relationship between space, mass, time and energy.
2. The equivalence of gravitational and inertial mass, and
3. The equations of motion for matter moving through a gravitational gradient.

In his original paper on general relativity, Einstein proposed three experimental verifications of the theory, now often called the "classical tests": (1) the gravitational shift of light to longer wavelengths (the red shift) when going from a stronger to a weaker gravitation field; (2) the deflection of starlight as it passes through the strong gravitational field close to the surface of the sun; (3) the slow rotation of the perihelion of the planets, in particular, the planet Mercury.

The gravitational red shift was first observed in the spectra of the sun and two white dwarf stars, Sirius  $\beta$  and 40 Eridani  $\beta$ . However, the most precise measurements were performed in terrestrial laboratories, where nuclear Mossbauer radiation was used over vertical distances up to 22.5 meters (74 feet).



The theoretically predicted red shift  $\Delta\nu/\nu = gh/c^2$  has now been verified with an accuracy of about one percent.

The second test predicts that light rays from stars should be refracted towards the sun through an angle of  $4GM/c^2r$  radians, where  $r$  is the distance of closest approach of the ray to the center of the sun. This produces 1.75 seconds of arc when the ray grazes the limb of the sun. The evidence to date has been obtained during total eclipses, when stars are visible close to the limb of the sun. The observations are not in disagreement with the theory, but are uncertain by roughly 20 to 30 percent and so cannot be regarded as strong support for Einstein's theory.

The third of the "classical tests" of general relativity is the precession of the perihelia of the inner planets. For an isolated planet, Newtonian theory predicts that the orbit is a closed ellipse with the sun at one focus. However, perturbations caused by other planets, which can be calculated from Newtonian theory, cause these ellipses to rotate slowly. The orbit of Mercury, which is closest to the sun and hence provides the best test of general relativity theory, is affected most by Venus (since it is closest) and Jupiter (since it is most massive). These perturbations can be calculated very accurately. When this is done, it is found that about 8 percent of the observed precession (43 arc-seconds per century) cannot be accounted for by planetary perturbations. Einstein's theory predicts an additional precession of  $6 \pi GM/c^2r$  radians per orbital revolutions, where  $r$  is the mean orbit radius. The value for Mercury is about 43 arc-seconds per century.



The close agreement between the predicted and observed precession was considered for many years to be very strong evidence in support of Einstein's theory. Recently, however, Dicke and Goldenberg have reported observations indicating an oblateness in the visual shape of the sun, the equatorial diameter exceeding the polar diameter by the fractional amount  $(5 \pm 0.7) \times 10^{-5}$ . If the sun has a quadrupole mass moment corresponding in magnitude to this visual oblateness, it will cause an additional purely Newtonian precession of the perihelion of Mercury of 3.4 arc-seconds per century. The remainder of the 43 arc-seconds is presumably still relativistic in origin, but the amount is less than the Einstein prediction. With this interpretation, the Einstein theory is incorrect, or at least incomplete. The Brans-Dicke scalar-tensor theory of gravitation is a way of explaining the smaller relativity component of the precession. There has been intensive debate about the significance of the visual oblateness measurements and thus which theory is correct. While no universally agreed answer yet exists, it is clear that the results of the Dicke-Goldenberg experiment must be taken very seriously.

It is of extreme importance in physics to perform additional experiments which can give information on the theory of general relativity especially with respect to a scalar component. The purpose of this mission is to perform a new test of the third aspect of relativity theory. This test was proposed by L. I. Schiff. It involves observing the drift of a free gyroscope in a satellite.

Schiff has shown that a gyroscope in orbit about a massive body such as the earth undergoes a relativistic precession in the framework of the fixed stars. Two effects are predicted. The first (geodetic effect) is done solely to the orbital motion of the gyroscope about the earth, and yields a predicted precession of 6.3 arc-seconds per year in a 500 nautical mile orbit. The

second (motional effect) is due to the rotation of the earth itself and is about 0.05 arc-second per year. For a satellite moving in a polar orbit, the two effects are at right angles as shown in Fig. 1-1.

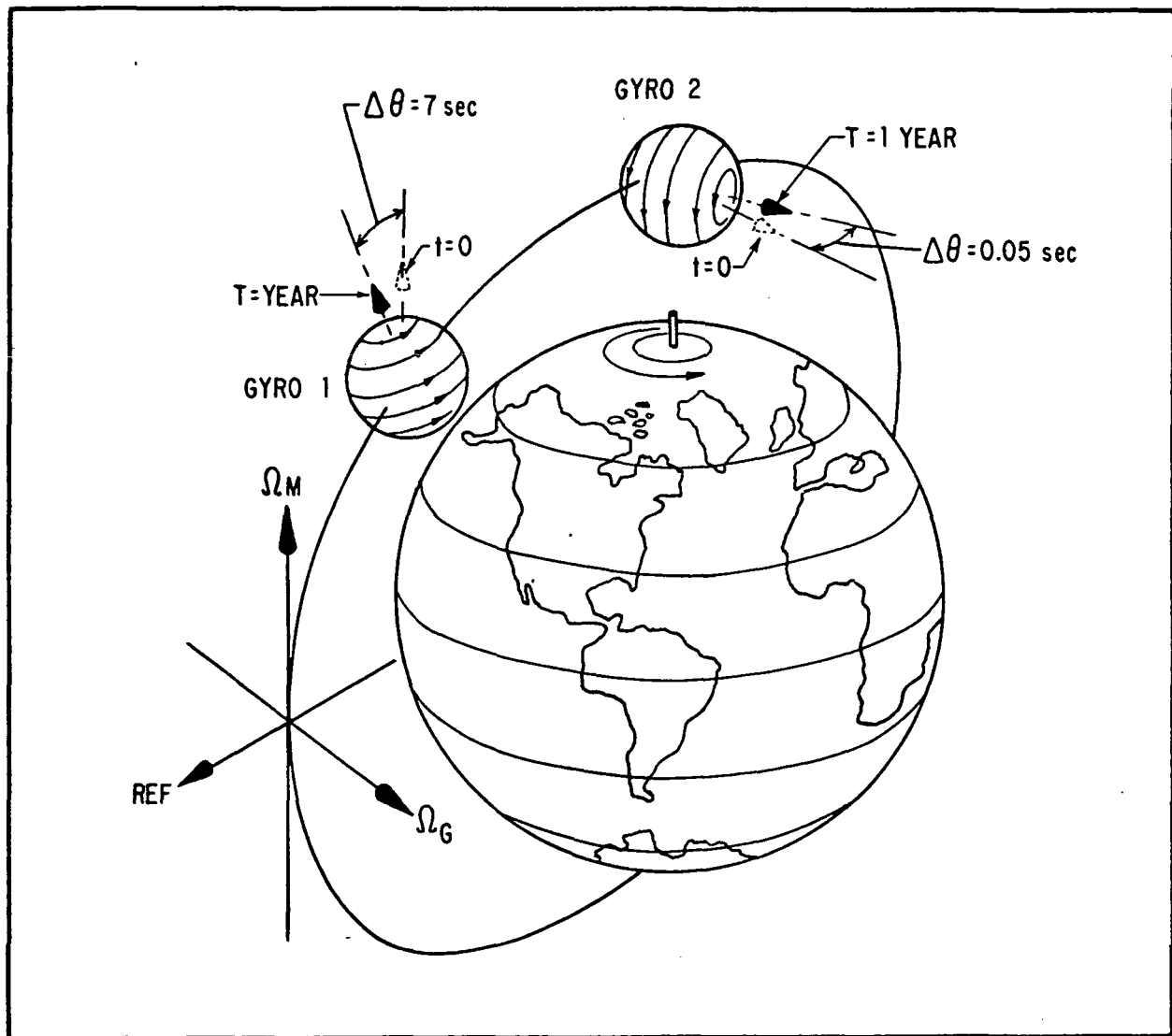


Fig. 1-1 Relativity Drift Diagram



The precessions expected by certain alternative theories of gravitation, including the Brans-Dicke scalar-tensor theory, are appreciably different from the predictions of Einstein's theory. Thus, the experiment is designed to provide a decisive test of the theories. The experiment will measure the drift of two pairs of gyroscopes with reference to a fixed star (the guide star). The design goal is to make measurements accurate to 0.001 arc-second per year. However, the flight would provide useful results at considerably reduced accuracy.

Table 1-1 lists the predicted geodetic drifts for a 500 nautical mile orbit according to the Einstein theory and a number of alternative theories of gravitation for which calculations are available. Note that an accuracy in the geodetic term of  $\pm 0.2$  arc-second per year is needed to distinguish between the Einstein and Brans-Dicke theories. The value of the various theories listed is a matter for debate. Many workers feel that some of them can be disposed of on other grounds. Another approach to defining the significance of the geodetic measurement is a representation originated by Eddington and is subsequently applied and extended by Schiff, K. Wordvedt and K. Thorne and C. Will. This representation, which is known as the parameterized post-Newtonian (PPN) formulation keeps the same broad conceptual framework as Einstein's theory, but introduces certain free parameters in the metric whose values may differ in different theories. The formulation is restricted to metric theories. For theories within this class, the starlite bending and radar ranging effects are proportional to  $(1 + \gamma)$ , and the geodetic precession of a gyroscope to  $(1 + 2\gamma)$ , where  $\gamma$  is one of the free parameters already mentioned which in Einstein's theory is equal to unity. A 0.001 arc-second per year measurement of the geodetic effect would determine  $\gamma$  to  $\pm 0.02$  percent compared with present observations which are good to about 5 to 10 percent.



Table 1-1  
RELATIVITY THEORIES

<u>Theory</u>	<u>Annual Geodetic Drift (Arc-Seconds)</u>
Einstein	+6.3
Brans-Dicke	+5.7
Birkhoff	+3.9
Whitrow-Morduch	+1.5
Belinfante-Swihart	-2.6

This will be sufficiently accurate to allow a good understanding of astronomical observations near massive bodies such as black holes. On the other hand, making hardware to measure drifts less than 0.001 arc-second per year appears very expensive.

A summary of the mission objectives is given in Table 1-2. The mission will demonstrate an advance in technology in several important areas; thus there are several secondary objectives. The gyroscope drifts will be millions of times less than the best terrestrial units. The readout loops have a very large dynamic range (106 db), and can be used over 360° for control purposes. This system could be used to point a satellite anywhere in the celestial sphere to 1 arc-second.

The environment near absolute zero will be very useful for detectors that need to be cold to reduce noise to low levels or that require superconductivity. Many kinds of infrared astronomy become feasible only in this environment. Precision pointing of an instrument to a small part of an arc-second using the telescope would be useful in pointing large telescopes at stars to study such things as minute details of nearby nebula.



Table 1-2  
MISSION OBJECTIVES

PRIMARY

Measure Relativistic Motional Precession	Accuracy Goal: 0.001 arc-sec/year Design Minimum: 0.01 arc- sec/year
---	---

Measure Relativistic Geodetic Precession	Accuracy Goal: 0.001 arc-sec/year Design Minimum: 0.01 arc- sec/year
---	---

SECONDARY

Low Drift Gyroscopes	0.001 arc-sec/year
Cryogenic Environment	<2°K for 1 year
Precision Pointing	±1/20 arc-sec about 2 axes
Telescope	0.001 arc-sec stability

Definitions:

Goal: Design will meet this limit if total mission costs are not greatly impacted.

Design Minimum: The mission plan will require review if this design limit cannot be met.



## Section 2

### MISSION DESCRIPTION

To provide an overall view of the mission, its various parts are described here in the following sequence:

- Orbiting hardware
- Orbit and booster
- Operations
- Program

These elements are described in greater detail in later sections. Table 2-1 lists the important mission requirements that have been derived in the study. The basic experiment requirements for linearity and stability ( $\sim 0.0005$  arc-sec/yr), accurate orientation in inertial space (0.05 arc-sec over a year), a liquid helium environment of  $< 2^\circ\text{K}$ , a low acceleration environment ( $< 10^{-9}$  g's) and a particular spatial geometry dictate the other requirements either directly or indirectly. These requirements are derived in the detailed discussion of the subsystem and the operation sections that follow.

Operations, as defined in this report, include all the activities starting with assembly of the various black boxes and concluding with data reduction to determine the relativity drift of the gyroscopes.





Table 2-1  
MISSION REQUIREMENTS

ITEM	REQUIREMENT	REASON
<u>ORBITING HARDWARE:</u>		
Gyro & Readout Electronics	Drift + Nonlinearity <0.0006 arc-sec per yr	Allow total system to approach 0.001 arc-sec per year drift measurement.
Telescope & Readout Electronics	Stability and Nonlinearity <0.0005 per year Telescope Linear Range 0.05 arc-sec	
Helium Storage	Keep Experiment <2°K for one year	Keep parts at a very low thermal coefficient of expansion.
Control System	Point Telescope to 0.05 arc-sec  Roll about the guide star at rate having 5 hour period Keep translation acceleration to <10 <sup>-9</sup> g's	Allow accurate subtraction of body motion from gyro signal.  Reduce net drift on gyroscopes and reduce long term electronic drift requirement. Control gyro drift due to steady state accelerations.
Power	Provide >100 watts continuous power for sat. Very high reliability on suspension electronics	Power budget plus 20 watt pad. Suspension failure on all gyros aborts mission.
Telemetry	84 bps R.T. and 2.3K bps P.B.	Provide experiment data at 20 words/min and a suitable housekeeping data rate -- provide memory dump (P.B.) in <4.5 minutes.
Command	140 Discrete; 30-12 bit instruction Missed Commands <1 in 100 Misinterpreted <1 in 1000 Spurious <5 in year	Provide necessary mode changes and satellite control. Limit operations problems.
Memory	>100 minutes storage	Assures negligible data lost with chosen ground stations.
Life	1 year	Time to assure annual aberrations are subtracted out accurately.
<u>MISCELLANEOUS</u>		
Guide Star	<ul style="list-style-type: none"> <li>&gt;1 magnitude</li> <li>&lt;10° to equatorial plane.</li> <li>&gt;20° to ecliptic plane.</li> <li>Proper motion known</li> </ul>	Set telescope aperture for noise <0.1 arc-sec & 10 Hz bandwidth. Keep motional effect drift near maximum Set design limit for sun shade. Achieve mission accuracy
<u>LAUNCH</u>		
Orbit	Inclination 90±0.04°  Height of perigee >875 km Height of apogee <1000 km	Keep orbit within ±2° of guide star for a year. Limit air drag. Keep prediction of relativity drift simple (near circular orbit), and keep particle radiation manageable.



Table 2-1 (Cont.)

ITEM	REQUIREMENT	REASON
Booster	Put 700 kg satellite in-orbit • Fairing envelope 2.2 M (86 in.) dia. by 4.1 M (161 in.) high • Attitude error before separation (2 hr. after lift off) $<0.5^\circ$ • Separation rates $<1^\circ/\text{sec}$	Allowable for a Thor-Delta with 3 strap-ons. Set maximum satellite size. Attitude reference for spin-up of parallel gyros. Limit control torque impulse needed by satellite.
<u>OPERATIONS</u>		
Orbit Determination Accuracy	Orbit Inclination Uncertainty $<10$ arc-sec Ascending node uncertainty $<20$ arc-sec Radial position uncertainty 300 meters. Velocity uncertainty $<0.5$ m/sec. (The velocity uncertainty must be as small as 0.05 to 0.2 m/sec at some point in each orbit to allow for error propagation from initial conditions.)	Limit $\Omega_M$ corruption by $\Omega_G$ $<0.0003$ arc-sec, and $\Omega_G$ corruption by "worst case" annual aberration to 0.02 arc-sec over two months. Limit $\Omega_G$ corruption by "worst case" annual aberration to 0.02 arc-sec over two months.
Tracking Stations	Fairbanks, Ororal, Santiago; and Tananarive Record Memory Dumps. Make Real-Time Data checks. Send 2 Commands/Orbit Average. Use Standard STADAN Equipment.	Provides $>5$ minute pass for life of mission. Necessary functions to control spacecraft and recover data.
Operations Control Center	Monitor housekeeping data schedule memory dumps control acquisition sequence. Coordinate emergency operations.	Necessary functions to assure spacecraft operation properly and recover data.
Data Processing	Strip housekeeping TWX selected channel. One complete orbit/day sent weekly. Strip relativity - send weekly. Provide frame count to GMT correlation to 0.1 sec.	Monitor S/C and experiment performance. Ability to subtract orbital star aberration -- correlation of data sample to satellite ephemeris.



## 2.1 ORBITING HARDWARE

The frontispiece shows an overall view of the 600 kg (1400 pound) satellite required for the mission. Because the satellite is designed exclusively for the Stanford gyro experiment, the usual separation of the spacecraft from the experiment is not desirable or even possible. Therefore, the system has been defined as an integrated satellite with considerable overlap between experiment and spacecraft in structure, thermal design and controls.

The main structural element is a large dewar containing about 135 kg (300 pounds) of liquid helium, enough for over 1.5 years of operation. Fastened to the dewar is a ring carrying all the electronics packages and the solar array. The ring is easily separable from the dewar so this portion of the satellite can be assembled and tested separately. The outer skin of the dewar is covered with a second-surface mirror material made of aluminized teflon. This coating produces a dewar outer skin temperature of  $-50^{\circ}\text{C}$ , an important factor in conserving the helium.

The inner container of the dewar, carrying the liquid helium, is supported by rigid, hollow titanium rods extending through the insulation to take the launch loads. When in orbit, these rods are retracted and the container is held by fiberglass bands of very low heat conductivity. Multiple layers of aluminized mylar (super insulation) lie in the evacuated space between the liquid helium container and the outer shell, to reduce the heat radiated into the helium. In addition, three concentric heat shields, in the form of thin metal shells, are suspended in this space. The cold helium boil-off vapor is passed through tubing on these shields to intercept heat leaking into the dewar from external sources. The vapor also cools the telescope windows to intercept heat flowing through them. As a result of these measures, the heat entering the liquid helium is only about 80 mw.

A superfluid plug is placed in the dewar exhaust line to limit the flow of liquid helium out of the dewar to only that required to absorb the heat entering the dewar. Honeycomb-like cells are



located within the liquid helium space to hold the helium in place by surface tension forces. These forces are calculated to be small ( $10^{-4}$  g) compared to the 1 g on earth, but are large compared to the forces encountered in orbit.

Helium is carried in an annular tank surrounding a hollow cylindrical cavity. A fused quartz block is suspended by a two-axis gimbal within this cavity. The four fused quartz gyroscopes used to measure the relativity drift are optically contacted to the block. A star tracking telescope is also made of fused quartz and is also optically contacted to the quartz block. It provides the absolute reference for measuring gyroscope drift.

The telescope is a diffraction-limited Schmidt-Cassegrain system of 140 mm (5 1/2-in) aperture and 2.54 m (100-inch) focal length. It looks out through windows at one end of the cavity at the star Rigel. Rigel is chosen because it is a very bright, distant star with a small proper motion, because it lies near the celestial equator, and because the closest approach between the sun and the star is more than  $30^\circ$ . A two-stage sun shield on the outside of the window greatly reduces the scattered sunlight falling on the telescope.

The entire quartz block assembly is maintained at about  $1.6^\circ\text{K}$ . This temperature is necessary to keep the thermal coefficient of expansion and creep of the quartz near zero and provide super-conduction for gyro attitude readout and magnetic shielding.

Figure 2-1 is a systems diagram for this satellite.

A two-stage pitch-yaw attitude control system operating from error signals generated by the telescope keeps the optical axis pointed at the guide star, Rigel. Proportional gas jets, using the helium vapor from the Dewar, provide attitude control of the satellite body with respect to the guide star to an accuracy of about  $\pm 1$  arc-second while an inner actuator controls the gimballed quartz

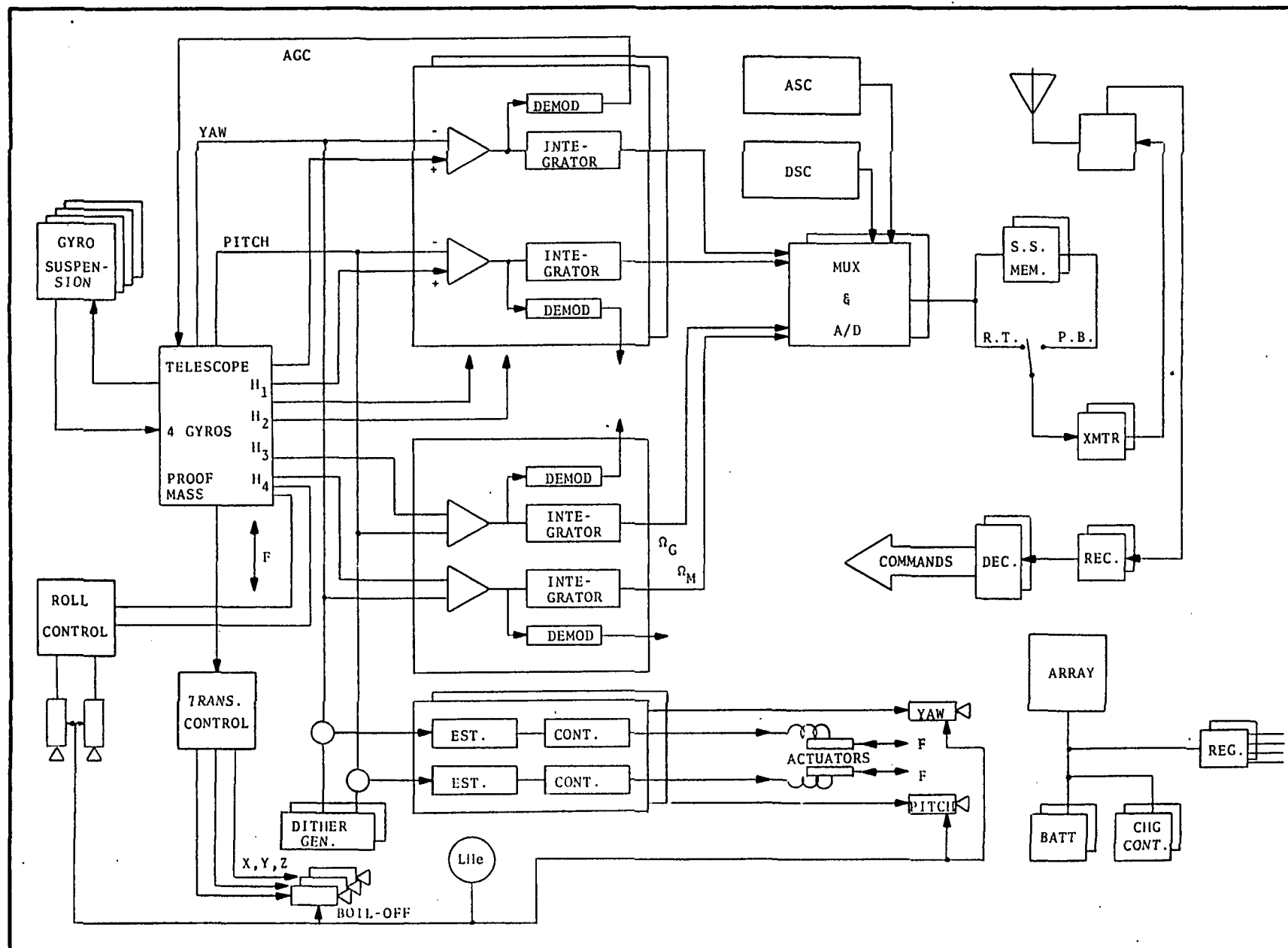


Fig. 2-1 Simplified Systems Functional Diagram



block with respect to the star to keep the pointing error within the 0.05 arc-second linear range of the telescope. The guide star will appear to move around by as much as 20 arc-seconds due to stellar aberration. This is an effect predicted by Einstein's special theory of relativity and is due to the velocity of the satellite in orbit and the velocity of the earth in its orbit.

The gyroscope rotors are nearly perfect fused quartz spheres coated with niobium and electrically suspended within spherical cavities. The superconducting niobium generates a magnetic dipole moment (London Moment) aligned with the instantaneous spin axis of the rotor. This dipole moment causes a current to flow in a superconducting pickoff loop. The current is proportional to the sine of the angle between the spin axis of the rotor and the plane of the loop. The magnitude of the current is measured with a precision modulator and AC amplifier.

Two of the gyroscopes have their spin axes aligned along the telescope axis. With this orientation, the gyroscopes are sensitive to both of the relativity drifts. These gyroscopes provide a check on one another.

The other two gyroscopes have their spin axes oriented mutually perpendicular to each other and to the telescope axis. One is aligned essentially to the earth's spin axis and the other essentially normal to the orbit. In these orientations, the first gyroscope is sensitive only to geodetic drift and the second only to the motional drift. These gyroscopes independently measure the relativity drifts as a further check.

The satellite rolls slowly about the telescope axis to reduce some causes of gyroscope drift and to allow the detection and compensation of possible null shifts in the gyroscope and telescope readout systems.



The relativity data is obtained by subtracting the telescope error signal, which is linear to better than 0.001 arc-second, from the gyroscope readout signal which is also linear to this accuracy. The resulting signal is integrated in the satellite for ten seconds and on the ground for five hours in order to extract the mean value of the data to 0.001 arc-second.

The acceleration due to solar radiation pressure and aerodynamic drag can cause gyroscope drift. To eliminate this cause of drift, the satellite is made drag-free. The error detector for the drag-free control system is the proof ball mounted in the quartz block. Electrodes in the cavity for the proof ball measure the distance between the proof ball and the cavity. The control system then moves the satellite using helium boil-off, so that it follows the proof ball around the orbit. Since the proof ball sees only gravitational forces, it and the total spacecraft fly in a nearly perfect gravitational orbit.

The communications system is straightforward with a multiplexer and digital and analog subcommutators. The real time bit rate is 84 bits per second with a playback rate of 2.3 kilobits per second. This allows memory dump to occur in about 4 1/2 minutes. The telemetry transmitter has 1/2 watt output, which provides ample link margin at this bit rate and also provides for beacon tracking using the minitrack system.

The command system provides both discrete and instruction word commands. Discrete commands are used to change the states of relays while instruction words are a bit stream used to load small memories, such as the offset point generator. The system is a highly secure digital one compatible with existing STADAN equipment. Security is obtained by inhibiting command execution until a complement



of the command word is sent and checked in the spacecraft. The command message is 38 bits long and consists of a 7 bit decoder address, a 12 bit command word and the complement of these. Thus a total of 38 bits must be sent correctly or no command is executed.

Turnstile antennas are mounted on two of the solar array panels. These omni-directional antennas are shared by the command and telemetry system.

Power is provided by a combination of solar cells and batteries. The solar array panels (with cells on both sides) are set at  $45^\circ$  to the axis of the satellite so that power will be generated at any sun angle. The pitch of two of the panels is reversed with respect to the other two to prevent windmilling when the sun or airstream is along the axis. The hinge line for the array is set askew so that the panels will lie down flat against the cylinder for launch.

The solar array generates about 220 watts during the time of year when the sun is occulted for about 30 minutes per orbit. This amounts to an average regulated power to the loads of about 110 watts. Power during the occulted period is provided by three strings of nickel-cadmium cells. This battery provides 12 ampere-hours of capacity. The output voltage of the power system is regulated +28 volts for general purposes, regulated  $\pm 15$  volts for operational amplifiers, and regulated +5 volts for logic circuits.

All surfaces of the satellite, except for the solar array, are coated with a second-surface mirror. This material works like a mirror for the solar spectrum, and as a plastic with high emissivity in the IR. Thus only a small amount of solar energy is absorbed but heat is radiated from the dewar very well. The effective temperature of the outer skin of the dewar is about  $220^\circ\text{K}$ . Since solar cells are a good absorber in the





solar spectrum, the solar panels run at a little over 80°C when normal to the sun. The electronics boxes are insulated so that the inside runs a little below room temperature.

## 2.2 ORBIT AND BOOSTER

The satellite will be flown in a 500 nmi circular, true polar orbit. The orbit plane will contain the guide star. In a true polar orbit, the very small motional effect can be clearly distinguished from the very much larger geodetic effect since they occur at right angles to each other. Figure 2-2 is a view looking from slightly above the ecliptic plane. The orbital plane is the plane of the paper. The guide star is 30° below the ecliptic plane which makes it relatively easy to build the sun shade. A star with a much higher declination would start to appreciably reduce the motional relativity drift. When the sun is on either side of the spacecraft, and normal to it, the earth does not provide any shadowing, and continuous sunlight orbits are achieved. When the sun is 90° to this position (that is at the left or right hand part of the picture) the occult periods are about 30 minutes. The occult period becomes shorter and shorter as the sun moves away from this position.

The 600 kilograms (1320 lbs) satellite can easily be launched on a Delta vehicle equipped with the new 96 inch fairing. A near Hohmann transfer is required. The launch would be out of the Western Test Range. The satellite would use the Delta guidance package for attitude control when the perpendicular gyros are spun up. This requires that the satellite remain attached to the vehicle for about one hour after injection. Very low separation rates and accelerations are required from the vehicle. We propose that the vehicle back away from the satellite rather than use separation springs.

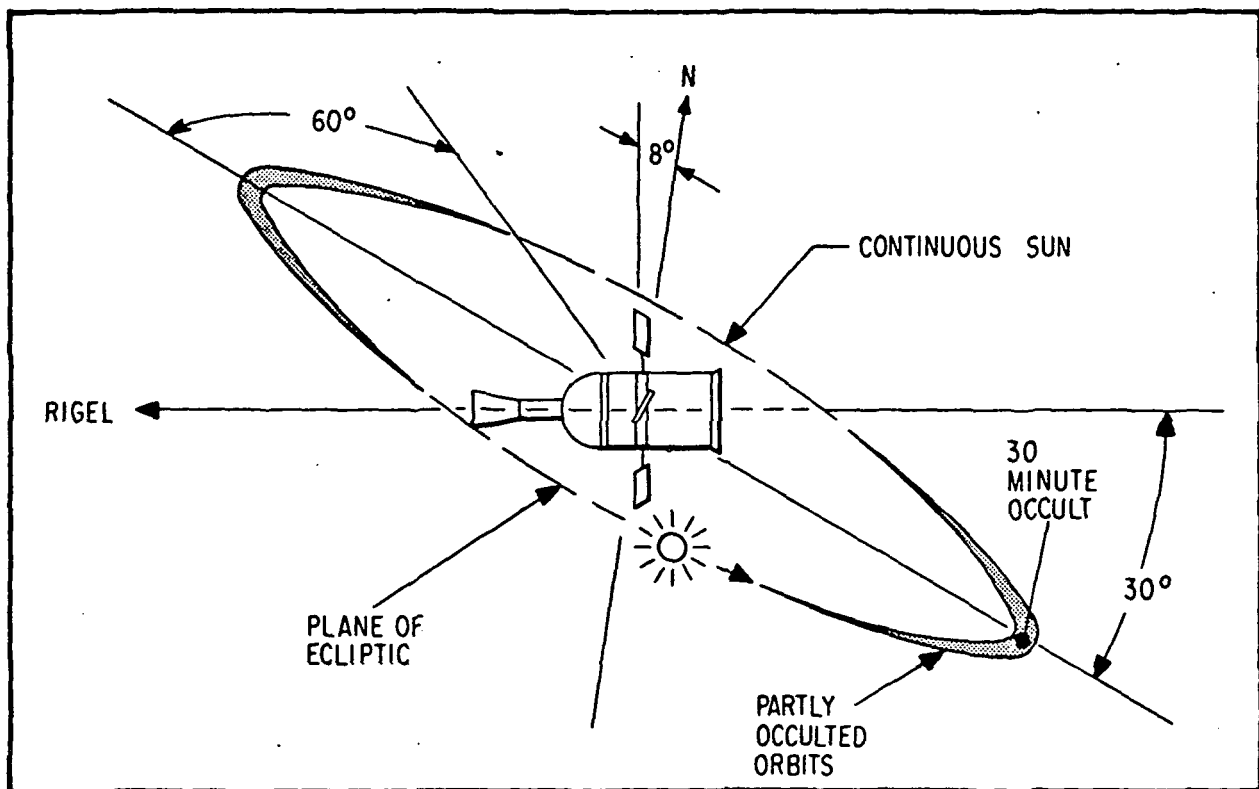


Fig. 2-2 Orbit Characteristics

### 2.3 OPERATIONS

Assembly and test of this spacecraft will be conventional except for three items:

- Helium servicing
- Experiment maintainability
- Stability checks

A superconducting shield is used to prevent the earth's field from torquing the gyroscopes. In order to maintain a low internal field, this shield must be made superconducting, while in a field environment less than  $10^{-6}$  gauss. The instrument package may then be removed from the low field environment but must be kept at cryogenic temperatures from this point through the end of the mission. For the approximate year of testing, the dewar must be supplied with



liquid helium and vacuum pumps will be required to keep the insulation and experiment cavity evacuated, and keep the helium vent line at about 20 millimeters pressure. This will require a 10 hp mechanical pump, 7 1/2 hp roots blower, and 2-100 L/S ion pump. Since it is essential that a reasonably good vacuum be maintained for the one year period, this equipment must have suitable backup to prevent any appreciable pressure rise.

If a failure occurs within the quartz block assembly requiring disassembly, there is a further complication beyond having to warm up the experiment package. At this point in the development of optical contacting, there is a high probability that the parts will be destroyed or badly damaged upon disassembly. To avoid the long delays, a complete spare quartz block assembly, already demagnetized and at cryogenic temperatures, is kept ready for immediate installation in the satellite during the integration and test period.

It would be desirable to show that the flight telescope and gyroscopes have stabilities consistent with the 0.001 arc-second mission goal. In a 1 g environment this will not be possible. Heavy reliance will have to be made on indirect tests and the results of the engineering flight tests.

The launch will be conventional except that the helium support package will be needed until about three hours before liftoff, and that the satellite will be attached to the launch vehicle for a long period. A post-burn maneuver will be required to align the telescope axes to the guide star within the tolerance of the guidance package. A roll maneuver is also required to align the spacecraft Z-axis with the North Pole (roll axis reference). If the launch vehicle performs normally, setup for normal orbit operations will be relatively straightforward. If the launch vehicle guidance package does not align the satellite properly, a backup system will be used which will require considerable support from the Operations Control Center.



In-orbit operations will be very simple, consisting primarily of dumping the memory once per orbit. The data reduction program will be quite sophisticated. There are two basic tasks. The first task is to integrate approximately 5 hours of real time data, gathered while pointing at the guide star, until the average gyro orientation is obtained accurate to better than a milliarc second. The second task is to take the actual orbit parameters for the same interval of time and predict what the relativity drift would have been, based on Einstein's equation, or on a competing theory.

#### 2.4 PROGRAM

At this time the program appears feasible but there are several areas where advancement of technology is required. These areas are:

- Dewar Design
- Gyroscopes and Readout
- Magnetic Shielding
- Instrumentation Loops
- Telescope Design Evaluation
- Optical Contacting
- Control System

In order to allow the development of the Stanford Relativity Satellite to proceed in an orderly manner once it has started, we have described an accelerated effort aimed at obtaining solutions to problems in the areas listed above. Evaluation of both dewar design and gyroscope design require orbital engineering test flights while the other areas require further laboratory work.



For the relativity mission itself, two flights will be budgeted. Engineering models of all black boxes requiring extensive development will be made. A qualification spacecraft will be made and tested. Common spares for the qualification unit, Flight 1, and Flight 2 if needed, will be made. Refurbishment of the qualification spacecraft will be used for Flight 2. The two flights will provide about a 90% chance that the primary mission objectives can be accomplished. This requires that the satellite have a reliability of about 69%. This reliability can be realized and is comparable to the 70 to 80% reliability computed for OSO series spacecraft.

Figure 2-3 is a simplified schedule of the program. The necessary technological advancements will be completed by mid 1973. In-orbit verification of the advanced technology will be completed by mid 1974. Start of detailed design of the actual flight spacecraft will begin in mid 1973. Completion of the testing and launch will occur in mid 1976. If the mission goes as planned, sufficient relativity data will be gathered by late 1976 to verify which if any of the contending relativity theories are correct.

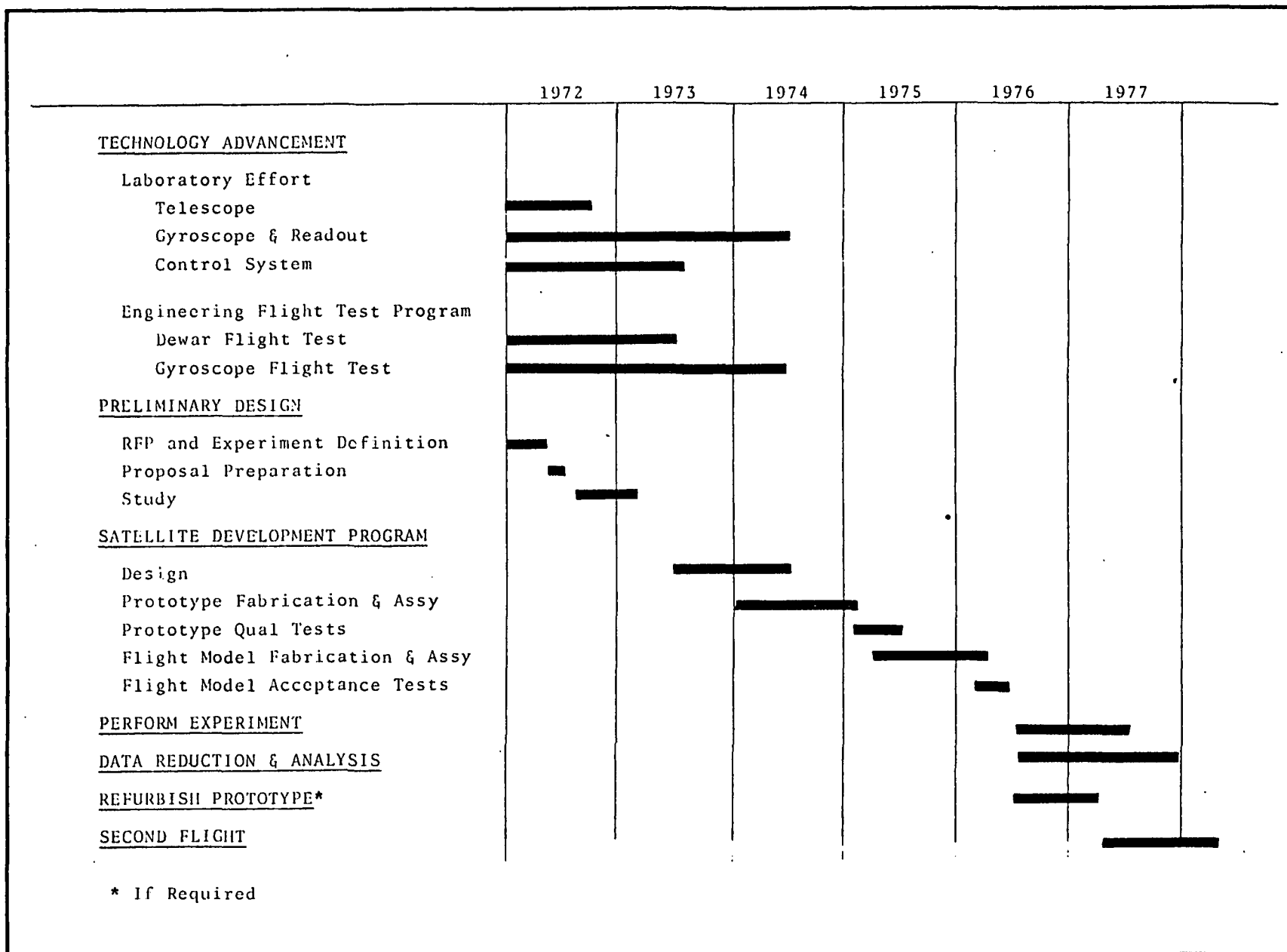


Fig. 2-3 Overall Program Schedule



### Section 3 SATELLITE SYSTEM

This section describes the system aspects of the orbiting hardware. The following items are covered:

- Configuration
- The system functional diagram
- Satellite requirements and budgets

Sections 5 and 6 discuss details of the individual subsystems.

#### 3.1 CONFIGURATION

In order to provide the experiment with a  $<2^{\circ}\text{K}$  temperature environment for the one year mission, approximately 900 liters of liquid helium are required. This makes the spacecraft configuration essentially a flying dewar. The size of the dewar is dictated by the required helium volume and the requirement for a 48 cm (19-inch) diameter cylinder through the center of the helium tank to mount the experiment dewar.

The volume of helium needed is a function of the dewar heat leak. To keep the dewar small, its outer skin temperature is kept as low as practical. The skin is made cold by minimizing blockage of thermal radiation and by making the dewar surface a good infrared radiator but a poor absorber of sunlight. Figure 3-1 shows the importance of the outer skin temperature for the particular design chosen.

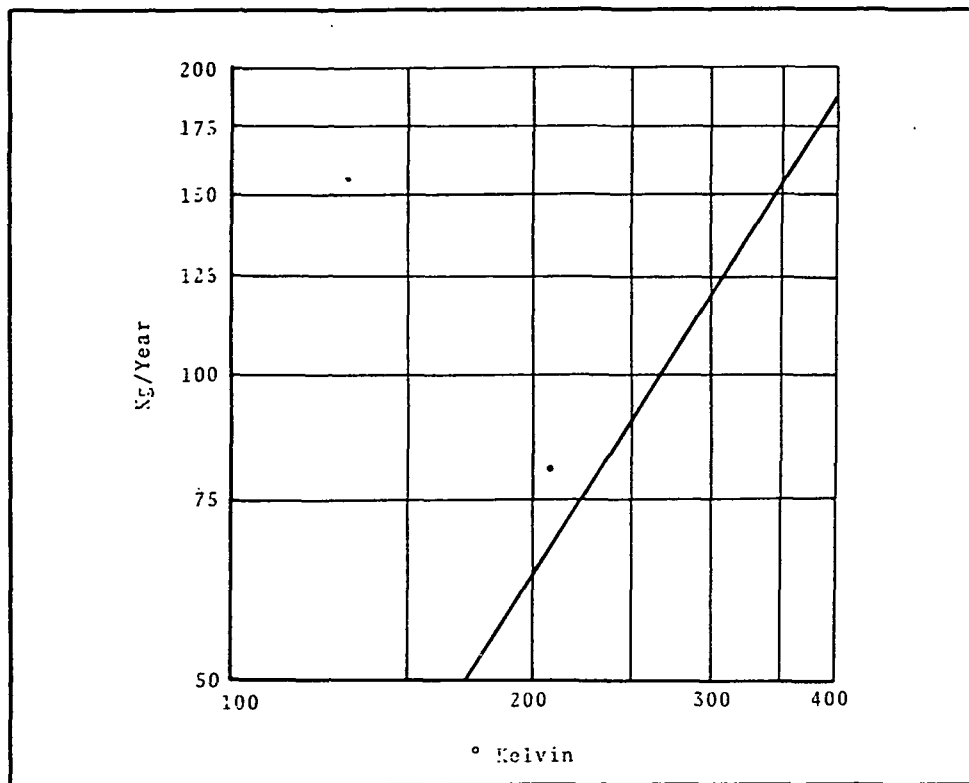


Fig. 3-1 Helium Used Versus Temperature

Rolling the spacecraft is important to get the desired relativity accuracy and confidence in the measurements. Since the mission is to last one year, the solar array must either be omni-directional or track the sun. If a pointed array is used, disturbance torques are generated by transferring momentum in and out of the array, due to the "slip-stick" action of friction at very low speeds. Also there is added complexity with a driven array. Four paddles would still be needed with either array so the only saving is that cells are needed on only one side and the paddles could be a little smaller because they would run cooler. Therefore, the fixed omni-directional array was chosen.

The angle that the plane of the array panels makes with the vehicle center line was chosen so that the variation in power (when averaged over an orbit) was least dependent on the length of day caused by the seasonal variations in the sun position.





The configuration was constrained to have a difference in moment of inertia less than 15 kilogram-meters<sup>2</sup>, to make the geogravity gradient disturbance comparable to that expected from peak aerodynamic drag torques and the expected magnetic torque. Solar pressure and aerodynamic drag can cause torques because of an offset between center of pressure and center of mass. Torques produced by this effect can be minimized only by keeping the distance between the center of pressure and center of mass small, since the area of the spacecraft is dictated by other subsystems. This offset is kept small by making a satellite geometrically symmetrical about the center of gravity. The array paddles are set at  $\pm 45^\circ$ , so that windmill torques from air and solar pressure will tend to cancel.

The configuration of the sun shade is dictated by the closest angular approach of the sun to the vehicle centerline. This angle is  $30^\circ$  for the planned mission, i.e., using Rigel for the guide star. The sun shade shown in the frontispiece is for a  $20^\circ$  star to sun angle. The shade can be shortened if Rigel is confirmed as the guide star and additional attenuation from the shade is not required. A rotating sun shield was considered but was not used because of added complexity and "slip-stick" torques.

### 3.2 SYSTEM FUNCTIONAL DESCRIPTION

In Section 2.1 the orbiting hardware was generally described with reference to a simplified block diagram. In this section, a more detailed description of this hardware will be covered with attention to the overall systems aspects of the satellite, showing the very close interrelations between the experiment and the spacecraft. This discussion will refer to the systems function diagram bound to the back of this volume. More detailed discussions of the experiment and spacecraft subsystems making up the satellite are found later in this volume.



The heart of the system is the quartz block assembly (zone 9 of the diagram) carrying the four relativity gyroscopes, the reference telescope and the proof mass. This assembly is located in the cold central cavity of the Dewar. The relative orientation geometry of these critical parts is shown schematically. The telescope is aimed at the guide star toward the left with north being toward the top of the page. Roll of the satellite takes place about the telescope axis. Each gyroscope is identified by an H with the arrow giving the direction of the spin axis and the London Moment. Gyroscope H-4 is shown pointing away from you into the page. Each gyroscope has three loops for reading out the London Moment, identified by L 1 through L3 for each gyro. The arrow out of the loop is normal to the plane of the loop, and shows the direction for positive output. When the angular momentum vector is in the plane of the loop, there is no output. When the angular momentum vector points out of the loop, the loop reads out the vector component of the London Moment that is normal to the loop. Functional details of these loops are given in Section 4.

### 3.2.1 Gyroscopes

The four gyroscopes on the quartz block each consists of nearly perfect niobium coated fused quartz spheres, electrically suspended, and spinning freely within spherical housings. The spinning superconducting niobium coating generates the London Moment magnetic dipole along the instantaneous spin axis which is measured by the three readout loops to determine the orientation of the spin axis. The outputs of these loops provide the relativity data and also signals for the satellite control system.



Parallel Gyroscopes. Gyroscopes H1 and H2 are called the parallel gyroscopes; they are oriented with their spin axes parallel to the telescope. They are affected identically by both the motional relativity drift ( $\Omega_M$ ) and the geodetic relativity drift ( $\Omega_G$ ) and provide redundant measurements. Loops L1 and L3 are the loops that read out gyro drift. Loop L1 reads out the geodetic term when the roll angle ( $\phi$ ) is zero, and motional term  $90^\circ$  later. Loop L3 is  $90^\circ$  out-of-phase with this\*. Thus, for each gyro these loops are redundant. Loop L2 reads out the gyroscope spin rate. The outputs from loops L1 and L3 go to a summing amplifier which subtracts the telescope signal. This removes the motion of the quartz block from the data. Thus, the quartz block does not have to be pointed to 0.001 arc-second. The summing amplifier, voltage-to-frequency converter, up-down counter, and D/A converter serve as a very accurate integrator. The loops work by incrementing the counter until the D/A converter output equals the gyro signal minus the telescope signal. The time constant of this operation is 10 seconds, which provides 10-second averaging on the data that is telemetered to the ground.

Night Pointing Signal. The rest of the parallel gyroscope read-out block is concerned with the way the control system error signal is derived for satellite control during stellar night and how the telescope AGC signal is derived. During night (when the guide star is occulted by Earth) the satellite is controlled by the gyroscopes. This is accomplished by holding the count in the bi-directional counter, which provides a constant output from the D/A converter. Thus, any pointing error caused by motion of the satellite is seen by the gyroscope and fed directly through the

---

\*Loop outputs are:  $L1 = \Omega_M \sin \phi + \Omega_G \cos \phi$

$$L3 = \Omega_M \cos \phi + \Omega_G \sin \phi$$



summing amplifier to the control system, shown as outputs E and F. This points the spacecraft at the dusk position of the guide star.

Because the satellite rolls, the angle to the star in body fixed coordinates will change. For instance, if the error at dusk is 0.01 arc second in pitch, and if the satellite rolled 90° at night, this error would be 0.01 arc second in yaw. To account for this, the inertial coordinates of the star position, which is the information on the right side of the resolver, is resolved into a body fixed angle that tracks as the spacecraft rolls during the night. This is done by driving the "shaft" input of the resolver at the known roll rate.

AGC Signal. In order to subtract the quartz block motion as detected by the telescope, the gain of the telescope must be equal to the gain of the gyro. Since the maximum pointing error expected is 0.05 arc second, and the desired accuracy is 0.001 arc second, a gain match to 1 percent (an error of 0.0005 arc second) is sufficient. To match these gains in spite of telescope photomultiplier degradation, the quartz block is mechanically dithered in pitch and yaw at a frequency of 0.1 radian per second. This dither is detected by both the gyroscope and the telescope. If the gains are matched, this motion will be zero at the summing amplifier output. Gain mismatches will produce an output. The data integrator described above causes this signal to be lowpass filtered with a break point of 0.1 radian per second. This signal is then amplified through a high pass filter with a break point of 0.1 radian per second. These two filters primarily pass the dither signal which is demodulated with a synchronous demodulator. The output is the gain mismatch with the proper polarity to determine whether the



mismatch requires higher or lower telescope gain. This error signal causes the voltage-to-frequency converter to drive the counter in the proper direction to match the gains. The output of the counter is fed to a D/A converter and which in turn drives the telescope AGC amplifiers.

The dither signal is 0.03 arc second. In order to get a 1 percent gain match this signal must be driven down to 0.0003 arc second. Because of the 1.4 arc second (rms) gyroscope noise on the dither signal it requires about 30 hours to average this signal to the desired level. For an initial fast gain match, several stages of the counter are bypassed to get a gain match of 3 percent which will take about 3 hours.

Perpendicular Gyroscopes. Gyroscopes H3 and H4 have their spin axes oriented perpendicular to the telescope axis. Gyroscope H3 measures the geodetic effect since its momentum vector is in the plane of the orbit. Loop L1 measures the spin rate of this gyroscope. Loop L2 is the relativity readout, since the gyro will drift about the pitch axis (drift in the plane of the paper). Loops L1 and L3 are used to read out satellite roll angle. Loop L1 reads out the cosine of the roll angle, and loop L3 reads out the sine of the roll angle. These two signals are processed by the roll encoder. The output of the encoder is a 19 bit word indicating the roll angle.

Loops L1 and L2 are used similarly to read out pitch angle during the pitch maneuver to the roll reference star. Loop L1 reads out the cosine of the pitch angle, and loop L2 reads out the sine of the pitch angle. When the telescope is pointed at the guide star, loop L2 provides a pitch angle error signal in inertial coordinates.



During spin-up of the parallel gyros this signal and the yaw signal from gyroscope H4 are fed to resolver 2 in order to resolve these inertial coordinates into body fixed coordinates for control purposes.

Gyroscope H4 is the motional gyro. The rotating earth causes it to drift about a vertical axis (drift out of the plane of the paper). Loop L2 is used to readout the motional drift. Loop L3 reads out the spin rate of the gyroscope. Loops L1 and L3 are used for a back-up to gyroscope H3 for roll information. Loop L1 is used for roll control during the acquisition sequence.

The relativity data from H3 loop L2, and H4 loop L2 are processed as discussed above for the parallel gyros. However, these gyroscopes read out inertial coordinates instead of body fixed coordinates; i.e., the output is independent of roll angle. However, the motion that the telescope reads is in body fixed coordinates, thus the body fixed telescope coordinates must be resolved into inertial coordinates in order to subtract them from the gyroscope signals. Resolver 4 is used for this purpose. During one roll cycle, one telescope axis will be subtracted from both gyroscopes. To subtract to a 1% accuracy, gyroscopes must be matched in gain to 1 percent. This will be accomplished by spin rate adjustment of one of the perpendicular gyros.

Gyroscope Readout System. When a superconductor spins, it produces a dipole moment called the London Moment, which is aligned with the instantaneous spin axis. If a superconducting readout loop surrounds a spinning superconductor and this gyroscope moves with respect to the readout loop, the number of magnetic flux lines through the loop will change. The current in the readout loop changes by the amount required to buck out this change in flux. Thus, the current in the readout loop measures the position of the spin axis of the gyro.



The circuit for reading out this current is shown in the upper left hand corner of the functional diagram. The readout loop (detector) is connected in series with a second superconducting loop (modulator). The inductance of the second loop is modulated at 100 kHz, which in turn modulates the current in the loop. Thus, an alternating current is generated proportional to the original dc current. The system is made resonant with a capacitor and the ac current is coupled out by the transformer shown on the upper portion of the diagram. This signal is amplified and synchronously demodulated to produce a dc signal proportional to the current in the loop. A narrow-band filter is used at the modulation frequency in order to reduce the noise level so that the output amplifiers are not saturated. In order to obtain the extreme accuracy and stability required, feedback is used around the total loop. This feedback consists simply of a resistor to convert the output voltage to current. The current is coupled back into the loop by a transformer.

### 3.2.2 Telescope

The telescope is a 140 mm aperture, 2540 mm focal length Schmidt-Cassegrain stellar telescope optically contacted to the quartz block. This telescope provides the absolute reference to the fixed stars from which relativity drift measurements will be made. It also provides the satellite control signals when the star is in view. The telescope has a field of view of three arc minutes. The diffraction limited image of the reference star is approximately 1 arc second in diameter but only the central 0.1 arc second portion of the image is linear enough to be used in processing the relativity data to an accuracy of 0.001 arc second. Thus the control system must always keep the telescope centered on the star to within its  $\pm 0.05$  arc second linear range.



The image of the star formed by the telescope is split to produce images for pitch and yaw. Each image falls on a roof prism where it is again subdivided and fed to an external detection system. In the null position the energies on each side of the roof prism are equal. At null, the telescope is aligned with the apparent star except for errors arising from image aberration and starlight from neighboring stars within the field-of-view of the telescope. The signals from the two halves of the prism are modulated by a light chopper and fed to a single photomultiplier. The output is thus a chopped square wave with amplitude proportional to the pointing error. The pitch and yaw signals are separately processed through an intensity monitor and AGC loops, which match the telescope gains to those of the gyroscopes. Separate AGC systems are required to allow for the differences in spin rate and loop gains in each gyro. The output of the AGC amplifier is demodulated and runs through a low-pass filter and dc amplifier.

The intensity monitor provides a signal for telemetry proportional to the intensity seen by the two photomultipliers. Thus, there is an intensity for yaw axis and intensity for pitch axis. The photomultiplier outputs are also summed and run through a threshold detector to produce a stellar day/night signal on lead Y. Additional circuitry, such as a timer, may be necessary to distinguish between light from the star and that from cities and the band of atmospheric glow.

The gain of the gyroscopes can be predicted before flight to better than 5 percent. The AGC circuits match the telescope output signals to the gyro gains. Therefore, after the AGC circuits settle, the telescope gains are known to 5 percent even though the photomultiplier gains might vary by a factor of 2. Thus the error signals derived by the telescope and used for the pointing control can be taken off the output of these AGC circuits.





### 3.2.3 Control System

The satellite control system must keep the telescope pointed at the reference star to within its linear range of  $\pm 0.05$  arc second by moving the quartz block in its gimbals, and keep the satellite oriented at the star within a few seconds of arc to keep the gimbals away from their stops. It must also slowly roll the satellite about the telescope axis to reduce some of the effects of drift on the gyroscopes. Finally, it must keep the satellite in a "drag free" orbit based on control signals from the proof mass.

The gimbals are controlled by cryogenic actuators, essentially superconducting solenoids, and the satellite body is controlled in rotation and translation (drag free) by directing the flow of the boil off helium through appropriate nozzles.

Day Control. During stellar day the satellite is controlled using the telescope. The telescope signals are summed with the dither signals used for the AGC control. These error signals are processed by an estimator to derive the motions (state variables) of the quartz block and the satellite. An optimal controller is used to determine the required drive by the proportional thrusters and the gimbal actuator. Integral control is used to increase the gain at the disturbance frequencies (twice orbital rate) without having excessive closed-loop bandwidth.

The thrusters are driven in quads such that attitude about an axis and translation along an axis uses the same four valves. For instance, the pitch and Z-axis thrusters are the same. Section 6 gives more details on the attitude control system.



During stellar night, the gyros are used to obtain error signals as discussed above. The error signals are processed by the day control system but the bandwidth will have to be reduced. This is necessary to limit the acceleration in the quartz block since the gyro signal is much noisier than the telescope signal.

Roll Control. The roll signal for acquisition backup search and the normal roll maneuver is derived as shown in the lower center of the diagram. The spacecraft clock is integrated to produce time. The gain of this clock is set to produce the two roll rates by the command system. Time is summed with the roll angle (output of the roll encoder) and fed to a D/A converter and filtered. The output of this is an error signal proportional to the difference between the programmed position, i.e., time, and the actual position. The filter is used to filter out the 2.5 arc seconds steps produced because roll angle is in digital form. The roll controller is a simple lead-lag system.

Description of the operation of the roll control circuitry is given in Section 6.

Drag-Free Control. The proof mass is a metal ball 1.5 cm in diameter. The cavity for it has a pair of electrodes at either end of three mutually perpendicular axes. A capacity readout device is used to detect the error in centering the ball.

The satellite is translated by the helium thrusters to keep it centered about the proof mass. A capacitance bridge is used to measure the error in centering the proof mass within its cavity. The bridge is powered by a three phase generator, so that the proof mass is always at ground potential. The output of the bridge is amplified and synchronously demodulated to produce the position error signal. This signal is fed to a control system which controls the translation jets.



#### 3.2.4 Gyro Suspensions

The gyros are quartz balls coated with superconducting Niobium. There are electrodes in the housing similar to the proof mass. The position is sensed as with the proof mass but using a 1 megacycle frequency. The correcting drive is applied to the same plates, but at 20 kHz frequency. The error signal is modulated at a 20 kHz rate. The output of the modulator goes to a phase splitter to produce push-pull drive. This combined signal of preload and restoring force is fed to the power amplifier which in turn is fed to the plates to drive the gyro to the center position.

#### 3.2.5 Telemetry System

Digital Multiplexer. The digital multiplexer is a straightforward time multiplexer that serially gates out data stored in the various buffers. A gate causes the output buffer to read serially the data stored in it. Each word contains nine bits. Two words are used for relativity data and three words are used for roll angle data. The frame rate for these digital words is 20 times per minute. Thus the relativity data and roll angle are read out every 3 seconds. The multiplexer also drives five sub-multiplexers. Four of these multiplexers accept analog data and convert it to 9-bit digital words. This is used for housekeeping data that appears in analog form, such as voltages, gyro spin rates, control system error signals, etc. One commutator accepts bilevel signals, and is used to monitor the status of the spacecraft. It monitors such things as the position of relays, what bits are loaded into status registers (such as the offset generator), etc. The digital multiplexer is redundant but the submultiplexers are not. The output of the multiplexer is fed to both the memory and the transmitter. The transmitter normally transmits this data real-time continuously, while the memory stores this data. When commanded



over a ground station to dump the memory, the transmitter is switched to the memory, and the memory is played back through the transmitter. The antenna is shared with the command system. The command system is completely redundant and provides both discrete and instructional commands (data commands) for controlling the spacecraft.

### 3.2.6 Power System

Power is generated by eight solar array panels, whose output is connected directly to the continuous bus. This bus provides power to the suspension electronics and other items that are never to be shut down. Battery charging also is provided by the array. Third electrodes are used to determine when the batteries are fully charged. The third electrode circuitry senses full charge and opens the direct connection to the continuous bus. Diodes are provided around this relay to provide power at dusk or for high surges. A shunt regulator is used to control voltage when the batteries are disconnected from the line and to control charge rate when the battery voltage is high. An undervoltage switch protects the spacecraft from shorts downstream from the undervoltage switch. The threshold of the undervoltage switch is set so that the loads will be removed if the battery voltage nears the command system operating threshold. This prevents the spacecraft from being lost because it cannot be commanded. The output of the power system is regulated 28 volts for use in driving the pneumatic valve, suspension electronics, etc;  $\pm 15$  volts regulated, used for driving operational amplifiers; and +5 volts for logic circuitry.



Launch Sequence. The perpendicular gyros are spun up while the satellite is on the booster so that an attitude reference is established.

If the booster performs normally, the perpendicular gyros will be spun up within  $0.5^\circ$  of the desired orientations. In order to establish a roll angle reference, the spacecraft is pitched up to the roll reference star (probably Polaris). The pitch error signal for this maneuver is derived from gyroscope H3 loops L1 and L2. These represent the sine and the cosine of the pitch angle to the guide star. These signals are fed to resolver 1. The resolver produces an output equal to the difference between the pitch angle (the input), and the "shaft" angle. The pitch programmer provides an input to the "shaft" terminals. An error signal is developed which is the difference between the programmed angle and the actual angle. This is used by the control system to make the satellite follow the pitch programmer. Gyroscope H4 loop L1 is used by the roll control system to hold the roll angle at zero. In other words, the satellite is pitched about the axis of gyroscope H4.

After pitching back to the guide star, the satellite is pointed at the true (not aberrated) position of the guide star, and rolled rapidly (0.2 rpm) while the parallel gyros are spun up. The acquisition star tracker, resolver 2 and offset generator are used for this purpose. The acquisition star tracker locks onto the star and points the outer spacecraft at the aberrated star. The alignment between the acquisition telescope and the fine telescope cannot be made better than  $\pm 5$  arc-minutes. Therefore, the satellite is caused to scan about the guide star in a 10 by 10 arc-minute raster. The raster generator has an interrupt line that can be programmed from the ground such that the raster does not occur during stellar night. This assures that this star will be found by the fine telescope in the shortest amount of time with no retracing over the same area. When the fine telescope sees the star, the output on line Y transfers control to the inner telescope.



After telemetry data verifies that the star has been acquired, the necessary offset coordinates to move from the aberrated star to the true star position are loaded in the offset generator. The offset coordinates are valid for one particular point in the orbit. When the satellite is in this position, which will be chosen to be over a ground station, the perpendicular loops are zeroed by heating. When the satellite is put on gyro control, it will point to this point in inertial space.

During spin-up of the parallel gyros the satellite is rolled around the true guide star position with a roll period of about 5 minutes. Since the perpendicular gyros provide inertial information on the true guide star position, they are resolved into body coordinates by resolver 2. The output of resolver 2 provides the error signal to control the spacecraft in pitch and yaw during the spin-up maneuver.

Launch Sequence Backup. To provide a backup in case the vehicle puts the satellite in a useful orbit, but not in a proper attitude, a backup system is provided. This system is shown in the block to the left of the main control system. This system is designed to work for arbitrary attitude and arbitrary rates.

When launch sequence backup is commanded, the auxiliary pitch and yaw rate gyros drive the pitch and yaw high pressure (nitrogen) control system. The auxiliary roll rate gyro is biased to produce a roll period of 5 minutes. The coarse sun sensor is a fan beam that extends over 180 degrees. At some point during a roll cycle, this sensor will see the sun. When this occurs, a sun-present signal (e) will change the bias on the roll rate gyro from that required for a 5 minute roll period to a roll position signal. This signal plus the rate gyro will result in locking on the sun in roll.



The output of the sun sensor in pitch is digital. Its output is run through a D/A converter and is summed with an offset generator. The offset generator is loaded with the angle between the sun and the guide star for the time six hours after launch. This signal is fed to the coarse pitch control system. When the sun has been acquired in both roll and pitch (as indicated by the null indicator and the sun-present signal) yaw control is switched off and the yaw rate gyro is biased for a 30-minute scan period. This causes the satellite to cone about the sun line at the given offset angle. The guide star will be seen by the coarse star tracker within one revolution if the earth did not occult the sun and guide star. If solar night should occur before the star is seen, the sun-present signal will go to zero. This will switch all gyros to the integrator mode. This attitude hold mode holds the satellite attitude within about a degree (the drift rate of the rate gyros) and the scan can be started the next dawn. Since the guide star will be occulted at different times than the sun, it may take several revolutions before the star is seen by the coarse star tracker.

When the star is seen by the coarse star tracker, a star-present signal transfers control in pitch and yaw to the coarse star tracker. When the coarse star tracker has settled onto the guide star, the null detector switches the control mode to star telescope acquisition. Fine acquisition now occurs by scanning as discussed previously. When the star is occulted, the star-present signal drops to zero and the system reverts to the attitude-hold mode. With the star telescope locked on the guide star and the sun in the fan shaped field-of-view of the sun sensor, the pitch and yaw attitude are proper for spinning up the perpendicular gyros.



However, the roll attitude is a function of season. The roll attitude is corrected by calculating the required roll offset angle and ground-commanding the roll offset timer to torque the roll gyro through the proper angle. After offsetting in roll, the control system is switched to the attitude-hold mode and the perpendicular gyros are spun up. The system then reverts to the normal post-separation acquisition sequence.

### 3.3 RELIABILITY

On any program, some rather arbitrary decisions about the reliability of each flight must be made. The Program Office can adjust three parameters that affect reliability:

- Amount of redundancy in the spacecraft.
- Amount of care taken in building the spacecraft (functional and environmental tests, screening of components, quality control, etc.).
- The number of flights to accomplish the mission.

The Program Office usually does not have the authority to make changes in the launch vehicle.

For this program, we picked as a target a 90 percent chance of success using two flights as noted in the proposal. Appendix A presents a crude analysis based on the factors mentioned above, indicating that this is a reasonable number if the total cost of the mission is to be minimized.





A 90 percent chance of mission success in two flights corresponds to a reliability of 0.685 for one flight\*. Dividing this by the vehicle reliability of 0.9, gives the satellite a reliability number of 0.76. This reliability was allocated to the various subsystems as shown in Table 3-17.

This reliability is achievable as demonstrated by the predicted numbers for the various OSO flights. The spacecraft part of the OSOs (not including experiments) had reliability numbers that range between 0.7 and 0.8, depending on the complexity of the particular flight. The total SRS satellite should not be much more complex than the OSO spacecraft. Also the numbers computed for the OSO spacecraft were probably not low, since there have been 7 successes for 7 tries.

To achieve 0.76, some redundancy will be provided. In general, we will not have any single point failures that would cause complete loss of the mission. The following redundant hardware is proposed:

- Telemetry hardware involved in readout of the prime loops.
- Command hardware.
- Hardware for initial acquisition.
- Pointing control hardware, except for valves.

---

\*From probability theory it can be shown that:

$$P = 2p - p^2$$

P = probability of success in two tries.

p = probability of success for each try.



- Roll encoder.
- Telescope chopper and readout electronics.

Gyroscope readouts are redundant by having four gyroscopes, any two of which can fail without complete loss of the mission.

Redundant suspension electronics are not used, because it has been assumed that a bottoming ball would not cause a chain reaction which would bottom the rest of the balls. If this turns out not to be the case, redundant suspension electronics must be provided. This will be very difficult since transfer to the backup system must be done in several hundredths of a second, without start up transients.

Translation control is not redundant since its loss would increase gyro drift, but would not cause complete mission loss. This assumes that the valves will produce only a small translation force due to valve unbalance (offset and gain) compared to external forces. It appears that the valve can easily meet this requirement.

Housekeeping telemetry channels are not redundant since that loss alone would not cause complete loss of the mission.

### 3.4 REQUIREMENTS AND BUDGETS

This section lists the requirements for the orbiting hardware and the budgets for the various subsystems. These were derived from the mission requirements and the subsystem interfaces established during the study.

The information available from Stanford at the beginning of the program was used to generate preliminary mission requirements. The orbiting hardware portion was used to initially scope the subsystems. As the subsystem design developed, systems level trade-offs were made which resulted in more detailed requirements for the subsystems and definition of interfaces between subsystems



(interface agreements). This iterative process, of course, continues for the rest of the program. The tables and figures that follow document the requirements and budgets as they stand at the end of the study.

Table 3-1  
SATELLITE REQUIREMENTS

<u>Item</u>	<u>Requirement</u>	<u>Reason</u>
<u>EXPERIMENT</u>		
Gyro and Readout Electronics	• Drift + nonlinearity <0.0006 arc-sec/year	Mission Requirement.
	• Linear range >32 arc-sec	See Table 3-2.
	• Extended range readout to >5° with accuracy <10 arc-sec	To readout initial position of gyros accurate enough to reduce corruption of motional drift by geodetic drift to <0.0005 arc-sec.
	• Perpendicular Gyro spin axis perpendicular to star line within 1°	Limit geodetic coupling into motional drift, limit effect of pitch/yaw pointing errors, limit gravity gradient drift.
Telescope and Readout Electronics	• Misalignment <3 arc-sec optical axis to prime loops	Ability to determine absolute alignment of gyros in inertial space to 10 arc-sec (see budget table 3-6).
	• Instability & nonlinearity <0.0005 arc-sec/year	Mission requirement.
	• Linear range >±0.05 arc-sec	Allow subtraction of block motion.
	• Field of view >±1.5 arc-min	Limit number of scan lines.
<u>DEWAR</u>	• Storage = 135 kg LHe	Set outer size of dewar.



Table 3-1 (Cont.)

<u>Item</u>	<u>Requirement</u>	<u>Reason</u>
	<ul style="list-style-type: none"> <li>Boil-off &lt;135 kg/year</li> <li>Provide boil-off rates of 135, 700 and 1350 kg/year by command</li> </ul>	<p>Mission life of 1 year.</p> <p>Control peak torques (see Table 3-13), and provide for emergencies.</p>
<u>STRUCTURE</u>		
Mass Properties	<ul style="list-style-type: none"> <li><math>\Delta I &lt; 15 \text{ kg-m}^2</math></li> <li>Dynamic imbalance &lt;0.4 kg-m<sup>2</sup></li> <li>(CP-CG) x area &lt;1.5 M<sup>3</sup></li> <li>CG &lt;1 cm from experiment ref.</li> <li>Total weight &lt;700 kg</li> </ul>	<p>Keep gravity gradient torque <math>2 \times 10^{-5} \text{ n-m}</math> (see Table 3-13).</p> <p>Keep unbalance torques <math>&lt; 5 \times 10^{-9} \text{ n-m cm}</math> at 5 hour roll period (see Table 3-13).</p> <p>Keep solar pressure and aero torques <math>&lt; 10^{-5} \text{ n-m}</math> (see Table 3-13).</p> <p>Gyro acceleration budget (see Table 3-13).</p> <p>Allowable for Delta with 3 strap-ons.</p>
Residual Magnetic Dipole Moment	<ul style="list-style-type: none"> <li>500 pole cm<sup>3</sup></li> </ul>	<p>Keep magnetic torques <math>&lt; 2 \times 10^{-5}</math> (see Table 3-13).</p>
Resonant Frequency	<ul style="list-style-type: none"> <li>Translation, with launch locks, higher than in Table 6-2</li> <li>Translation and rotation-orbit condition &gt; in Table 6-2</li> <li>Middle to outer body &lt;27 Hz</li> </ul>	<p>Keep transmissibility at vehicle frequencies &lt;1.5.</p> <p>Keep interaction with control system small.</p> <p>Attenuate separation shock to &lt;0.2 g's or <math>&lt; 5 \times 10^{-6} \text{ m}</math>.</p>



Table 3-1 (Cont.)

<u>Item</u>	<u>Requirement</u>	<u>Reason</u>
<u>THERMAL</u>		
Temperatures	• Dewar $<240^{\circ}\text{K } T^2 \times$ area average over one year	Set limits for flight tem- peratures. Numbers in- clude:
	• Batteries 0 to $25^{\circ}\text{C}$	Modeling errors
	• Elect boxes $-10^{\circ}$ to $+30^{\circ}\text{C}$	D/N variations
	• Array cells $+90^{\circ}$ to $-100^{\circ}\text{C}$	Orbit plane to sun variation
	• Outer window $<240^{\circ}\text{K}$	Solar intensity variation
Flux	• Peak albedo $<30\text{ mW}$	These numbers should be increased by a minimum of $10^{\circ}\text{C}$ on each end for de- sign limits (qualification temperatures).
	• Yearly av. albedo $<4\text{ mW}$	Limit telescope warpage.
		From boil-off budget (see Table 3-7).
<u>POWER</u>		
	• Output $>100\text{ W}$ aver- aged over worst case orbit	See power budget, Table 3-12.
	• Voltages	
	28 $\pm$ 4 V contin- uous	For suspension
	+28 V $\pm$ 5%	For "off the shelf equip- ment", motors, valves etc.
	+15 V $\pm$ 2%	For operational amplifiers
	-15 V $\pm$ 2%	and general electronics.
	+5 V $\pm$ 5%	For logic circuits.
<u>CONTROLS</u>		
Quartz Block Accelerations	• Jitter at gyros $<3 \times 10^{-8}\text{ g's}$	Limit gyro drift to $<0.0005$ arc-sec/year from suspension dependent torques (see Sect. 5)-Gyro arrangement and acceleration.
	• Steady $<10^{-9}\text{ g's}$	
	• Maximum short dura- tion $<10^{-5}\text{ g's}$	Prevent gyro bottoming by saturating ball suspension.



Table 3-1 (Cont.)

<u>Item</u>	<u>Requirement</u>	<u>Reason</u>
	NOTE: High, short-duration accelerations must only occur several times per mission or integrate to less than 10 m/sec velocity	If 10 m/sec exceeded, drift will be excessive and high drift portion of data will have to be thrown out.
Pointing Accuracy	<ul style="list-style-type: none"> <li>Quartz block - &lt;0.05 arc-sec continuously for 50% of most orbits</li> <li>Satellite - &lt;1 arc-sec</li> </ul>	<p>Pointing excursions due to biases, noise and dither within telescope linear range.</p> <p>Limit gimbal travel to <math>\approx 1</math> arc-sec.</p>
Roll	<ul style="list-style-type: none"> <li>Period - orbit period <math>\times \pi = 314</math> minutes</li> <li>Tolerance <math>\pm 1\%</math></li> <li>5 min roll period</li> <li>Readout Error &lt;5 arc-sec</li> </ul>	<p>Short enough to integrate gyro and electronic drift and long enough to keep centrifugal forces on gyros to <math>&lt;10^{-9}</math> g's and keep phase shift in data integrator to cause &lt;0.0003 arc-sec error.</p> <p>Assures roll period will not produce a low "beat frequency" with the orbital period. Effectively, average gyro torques and readout errors; assure knowledge of roll angle is &lt;3 arc-sec between samples (see Table 3-6).</p> <p>To average cross torques on parallels during spin up.</p> <p>Keep total roll error &lt;10 arc-sec (see Budget Table 3-6).</p>
<u>COMMUNICATIONS</u>		
Telemetry	<ul style="list-style-type: none"> <li>84 bps real-time</li> <li>2.3 k bps playback</li> </ul>	<p>See TM budget, Table 3-15.</p> <p>To limit playback time to 4.5 minutes.</p>



Table 3-1 (Cont.)

<u>Item</u>	<u>Requirement</u>	<u>Reason</u>
Command	• 140 discrete commands	Mode changes, power control etc. (see Budget Table 6-22).
	• 30-12 bit instruction	Stored functions (see Budget Table 6-22)
	• Missed commands <1 in 100	Limit operations problems
	• Misinterpreted commands <1 in 1000	
	• Spurious commands <5 in year	
Memory	• >100 minutes	Assures negligible data lost with chosen ground stations.
Environments	• Particle radiation per Fig. 3-2.	Environment at 500 nm
	• U.V. <15 mW/cm <sup>2</sup> over 2000 to 4000 Å	
	• μ meteorites per Fig. 3-3	



Table 3-2  
GYRO READOUT - FULL SCALE

	<u>Plane of Loop</u>	
	Vertical	Horizontal
Aberrations	$\pm 20$	$\pm 12.5$
Relativity Drift	0.1	$\pm 3.5$
Initial Offset	$\pm 3$	$\pm 3$
Loop Misalignment	$\pm 3$	$\pm 3$
One Quantum Flux	$\pm 3$	$\pm 3$
	<hr/>	<hr/>
TOTAL	$\pm 27$	$\pm 23$





Table 3-3  
GYRO ACCELERATION BUDGET

	<u>Pitch</u>	<u>Yaw</u>	<u>Roll</u>
<u>Bias (g's)</u>			
Geogravity gradient (for the guide star 2° out of the orbit plane)	$5 \cdot 10^{-10}$ (or $6 \cdot 10^{-9}$ )*	0	0
Self Gravity Gradient	0 (or $5 \cdot 10^{-10}$ )*	0 (or $5 \cdot 10^{-10}$ )*	$5 \cdot 10^{-10}$ **
Satellite CG Acceleration	$5 \cdot 10^{-10}$	$5 \cdot 10^{-10}$	$5 \cdot 10^{-10}$
Total (RSS) for a Rolling Satellite	$7 \cdot 10^{-10}$	$3 \cdot 10^{-10}$	$7 \cdot 10^{-10}$
<u>Sinusoidal (g's)</u>			
Geogravity Gradient	$1.3 \cdot 10^{-8}$	$2.6 \cdot 10^{-8}$	$2.6 \cdot 10^{-8}$
Self-Gravity Gradient	$5 \cdot 10^{-10}$	$5 \cdot 10^{-10}$	----
Roll Centrifugal Acceleration	$1.5 \cdot 10^{-9}$	$1.5 \cdot 10^{-9}$	----
Quartz-Block Rotations	$10^{-8}$	$10^{-8}$	$10^{-8}$
Satellite CG Acceleration	$2 \cdot 10^{-9}$	$2 \cdot 10^{-9}$	$2 \cdot 10^{-9}$
Telescope Gimbal Offset Acceleration	$5 \cdot 10^{-9}$	$5 \cdot 10^{-9}$	----
Gyro Suspension Noise	$10^{-8}$	$10^{-8}$	$10^{-8}$
TOTAL (RSS)	$2.2 \cdot 10^{-8}$	$3.1 \cdot 10^{-8}$	$3.1 \cdot 10^{-8}$

\* For a non-rolling satellite stabilized at "zero" roll angle (can be reduced to about  $10^{-9}$  g for all 4 gyros for a 30° roll offset angle).

\*\* Requires careful mass compensation especially near the perpendicular gyros.



Table 3-4  
PERPENDICULAR GYRO ALIGNMENT BUDGET

Gyro Spin-up Alignment Error	±10	arc-min
Alignment of Satellite with Vehicle	±10	" "
Vehicle Error	±30	" "
Launch Window	± 2.5	" "
TOTAL (RSS)	<u>34</u>	arc-min

Table 3-5  
SENSOR NOISE

Telescope	<.03 arc-sec @ 100 rad/sec BW (assuming Rigel)
Gyro	<1.4 arc-sec rms @ 100 rad/ sec BW

Table 3-6  
ROLL ERROR BUDGET

<u>Instrumentation</u>	<u>Error</u>
• Encoder	5 arc-sec
• Loop Alignment	6 arc-sec
• Roll Reference	3 arc-sec
• D/A & Filter	3 arc-sec
<u>Control</u>	
• Jitter Error	4 arc-sec
• Bias Error	<u>3</u> arc-sec
	10 arc-sec (RSS)



Table 3-7  
DEWAR HEAT LEAKS

	<u>Launch</u>		<u>Orbit</u>
Multilayer Insulation	Negligible	W	0.3 mW
Fiberglass Supports	Negligible	W	8.6 mW
Power Dissipation & Wires	Negligible	W	29.0 mW
Albedo	Negligible	W	2.0 mW
Plumbing	Negligible	W	16.4 mW
Titanium Sleeve Conduction	Negligible	W	24.4 mW
Window Radiation	Negligible	W	0.2 mW
Sleeve Radiation	Negligible	W	0.1 mW
Launch Support		6.4 W	---
		<hr/>	<hr/>
TOTALS		6.4 W	81.0 mW

Table 3-8  
MASS AND MOMENT OF INERTIA

	<u>MASS</u> <u>kg</u>	<u>ROLL MOI</u> <u>kg-m<sup>2</sup></u>	<u>TRANS MOI</u> <u>kg-m<sup>2</sup></u>
Instrument	54.4	0.6	3.9
Dewar	202.6	46.3	100.0
Helium	136.0	21.9	34.2
Solar Array	50.8	146.1	76.8
Electronics	81.6	69.9	36.5
Sun Shield	9.0	0.3	24.7
Girth Ring	36.4	19.9	15.7
Attach Fitting	26.0	11.6	6.1
	<hr/>	<hr/>	<hr/>
TOTAL (with He)	596.8	316.6	297.9
TOTAL (without He)	460.8	294.7	263.7



Table 3-9  
ELECTRONIC BOX ALLOCATIONS

	<u>Total</u>	<u>Exp.</u>	<u>Power</u>	<u>Control</u>	<u>Comm.</u>	<u>Dist.</u>
Volume, m <sup>3</sup>	0.15	.046	.025	.028	.037	.014
Mass, kg	81.5	18.1	24.9	13.6	18.1	6.8

Volume Margin 20%

Table 3-10  
SATELLITE MARGINS OF SAFETY

$$M.S. = \frac{\text{Allowable}}{\text{Actual}} - 1$$

<u>Item &amp; Mode of Failures</u>	<u>Condition</u>	<u>M.S.</u>
Pressure Vessel, Tension	Internal Press (22.5 Psig.)	4.8
Outer Shell	External Press, (22.5 Psig.)	.53
Press Vessel to Outer Shell Launch Locks, Tension	Launch (thrust)	3.70
Electronics Box Standoffs, Compression	Longitudinal Vibration	36.6
Outer Shell at Interface, Stability	Launch (thrust)	13.9
Sun Shield, Bending	Lateral Vibration	8.8
Solar Panel Tie Down, Bolt Tension	Lateral Vibration	19.9



Table 3-11  
SATELLITE RESONANT FREQUENCY (Hertz)

	<u>Translation</u>						<u>Rotation</u>		
	<u>Locked</u>			<u>Unlocked</u>			<u>Unlocked</u>		
	X	Y	Z	X	Y	Z	$\phi$	$\psi$	$\theta$
Array to Dewar	High	16	16	10	10	10	10	10	10
Middle to Outer Dewar	104	81	81	25	40	40	6	20	20
Total Satellite to Attach Fitting	High	81	--	--	--	--	--	--	--
Sun Shade	277	43	43	277	43	43	High	43	43



Table 3-12  
POWER BUDGET

<u>Item</u>	<u>Average Power/ Orbit (watts)</u>
Proof Ball (drag free) Electronics	2.0
Optimal Estimate, Control, System Electronics	5.0
Gyro Suspension Electronics	10.0
Gyro Readout Electronics	7.2
Telescope Electronics	3.0
Gyro Instrumentation Loop Electronics (includes 3 electronic resolvers)	41.2
AGC Electronics	1.2
Roll Encoder	4.0
Roll Control Electronics	1.5
Control Signal Processing Electronics	0.8
Cryo Actuator	0.2
VHF Transmitter	2.0
VHF Receiver	0.5
Decoders	0.3
Memory	6.0
PCM System	2.0
Housekeeping Electronics	2.0
Valve Electronics	3.0
	<hr/> 91.9
Array Output (average over worst orbit)	110.3
Average Load	<hr/> 91.9
Minimum Power Margin	18.4 Watts



Table 3-13  
OUTER SATELLITE DISTURBANCE (GAS) BUDGET  
(Normal Operation)

Item	Critical Parameter Values	Force (Newtons)	Torque (N-M)
Solar Pressure	$A = 5\text{m}^2$ , $\ell = 0.3\text{m}$	$3 \cdot 10^{-5}$	$10^{-5}$
Atmospheric Drag	$A = 5\text{m}^2$ , $\ell = 0.3\text{m}$	$3 \cdot 10^{-5*}$	$10^{-5*}$
Magnetic Interaction	$D = 500 \text{ pole} - \text{cm}^3$	---	$2 \cdot 10^{-5}$
Gravity Gradient	$\Delta I = 15 \text{ kg-m}^2$	---	$2 \cdot 10^{-5}$
Static Roll Imbalance	$\omega_R = 3 \cdot 10^{-4} \text{ rad/sec}$ $\delta = 6 \text{ kg-m}$	$7 \cdot 10^{-7}$	---
Dynamic Roll Imbalance	$\omega_R = 3 \cdot 10^{-4} \text{ rad/sec}$ $\delta_D = 0.4 \text{ kg-m}^2$	---	$5 \cdot 10^{-8}$
Slewing While Rolling	$\dot{\theta} = 0.1 \text{ arc-sec/sec}$ $\omega_R = 3 \cdot 10^{-4}$	---	$5 \cdot 10^{-8}$
Probable Worst Case Sum	Per axis during normal operation	$5 \cdot 10^{-5}$	$5 \cdot 10^{-5}$
Control Gas Available (per axis)	$M = 135 \text{ kg/year}^{**}$ $I_{sp} = 100 \text{ sec}$	$5 \cdot 10^{-4}$	$5 \cdot 10^{-4}$

\* Air drag averages about 1/30 this large so its total impulse is small.

\*\* About 1/2 kg of helium is required for spinning up 4 gyros and about 2 kg will be lost during the 3 hour final built-in hold and the launch sequence. Also, system noise and cross coupling between axes cause about a 10 percent reduction in linear range.



Table 3-14  
CONTROL SYSTEM CLOSED LOOP BREAK FREQUENCY (Hertz)

Outer Pitch/Yaw Control	0.5
Inner Pitch/Yaw Control	2.2
Roll Control	0.3
Translation	0.05
Gyro Suspension	6.0

Table 3-15  
TELEMETRY BUDGET

	<u>Total</u>	<u>Spares</u>	<u>Exp.</u>	<u>Thermal &amp; Structure</u>	<u>Power</u>	<u>Control</u>	<u>Comm.</u>
Digital	56 bps	8 bps	46 bps	--	--	2 bps	--
Telltails	2 bps	1.37 bps	.17 bps	.09 bps	.08 bps	.19 bps	.1 bps
Analog	18 bps	6 bps	5 bps	1.5 bps	2 bps	2 bps	1.5 bps
Formatting	8 bps	--	--	--	--	--	8 bps
R.T. Total	84 bps						
P.B. Total	2.3 k bps						

Table 3-16  
COMMAND BUDGET

	<u>Total</u>	<u>Spares</u>	<u>Experiment</u>	<u>Power</u>	<u>Control</u>	<u>Comm.</u>	<u>Structure</u>
Discrete	140	67	26	17	15	14	1
Instruction Word	30	7	15	--	8	--	--



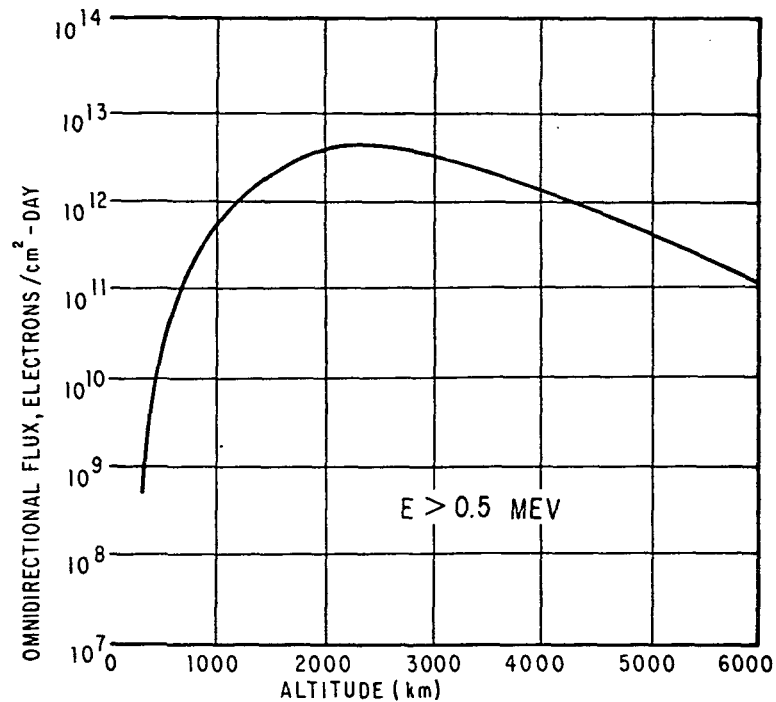


Fig. 3-2 Particle Radiation

Table 3-17  
RELIABILITY BUDGET

	<u>Rel.</u>	<u>Failures/Yr</u>
Experiment	0.923	0.077
Power	0.96	0.040
Control	0.93	0.070
Telemetry	0.97	0.030
Command	0.98	0.020
μ Meteorite Hit	<u>0.997</u>	<u>0.003</u>
R =	0.76	0.24

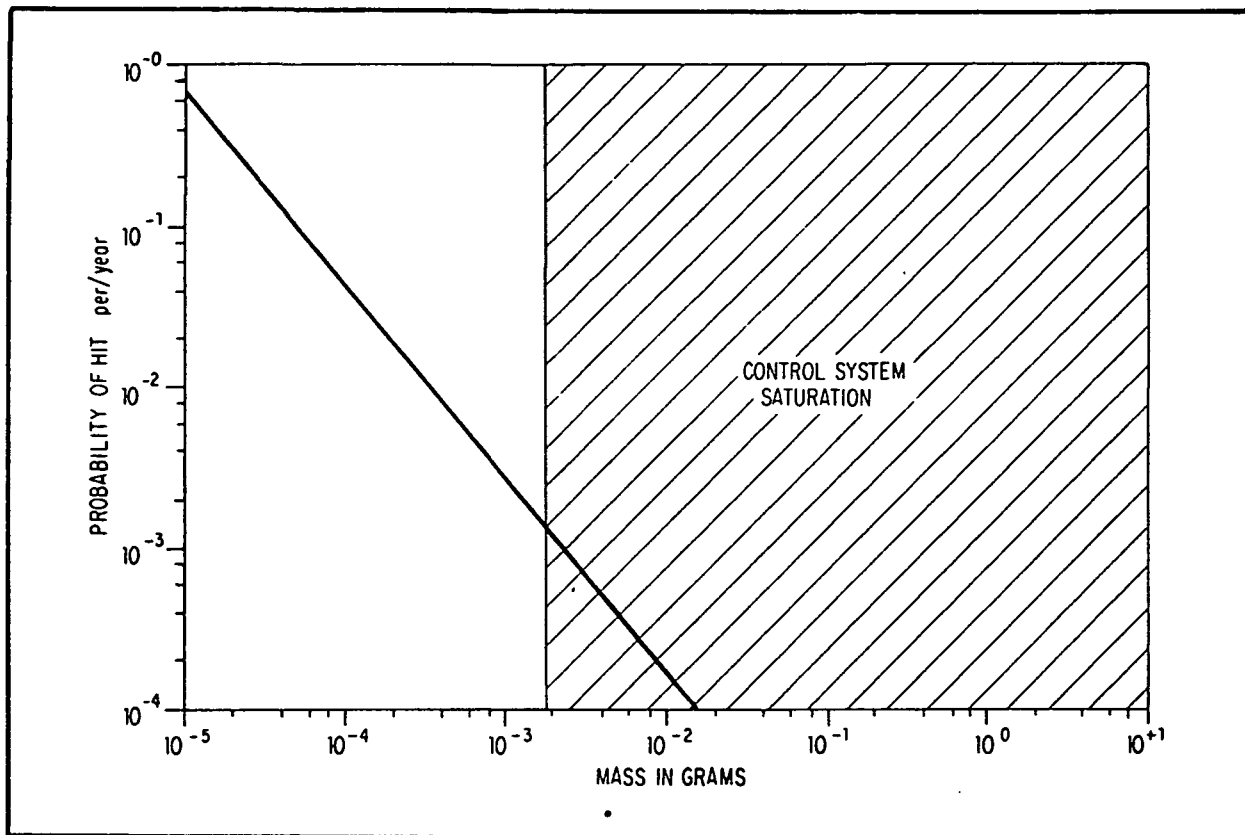


Fig. 3-3 Probability of Micrometeor Hit on Satellite



## Section 4 PROGRAM PLAN

### 4.1 FEASIBILITY AND PROBLEMS

This study was undertaken with the assumption that the gyroscopes needed for the experiment could be built to perform to the required accuracy. Based on this assumption, the mission appears to be quite feasible. The conventional spacecraft subsystems, with the exception of the control system, are of straightforward design. The control system is difficult but is certainly feasible. The Delta launch vehicle of 1976 will have the performance necessary to place the satellite in the desired orbit. The post launch operations are within present capabilities.

The difficulties of the program lie with the gyroscope-telescope assembly, the cryogenic environment needed to support them, and the attitude control system. For the mission to be successful, a considerable advancement of technology must be made in these areas. In order to minimize the risk of the main flight, the program described in this section calls for an intensive effort toward the solution of these problems by a preliminary phase of technology advancement and orbital flight evaluation of dewars and gyroscopes. Commitment to the main flight should be based on the results of this preliminary effort.

### 4.2 OVERALL SCHEDULE

Figure 4-1 shows the overall program schedule.

The technology advancement program is an accelerated continuation of the present work going on at Stanford University with the addition of the engineering flight test program which would evaluate the dewar and gyroscopes in an orbital environment. This work

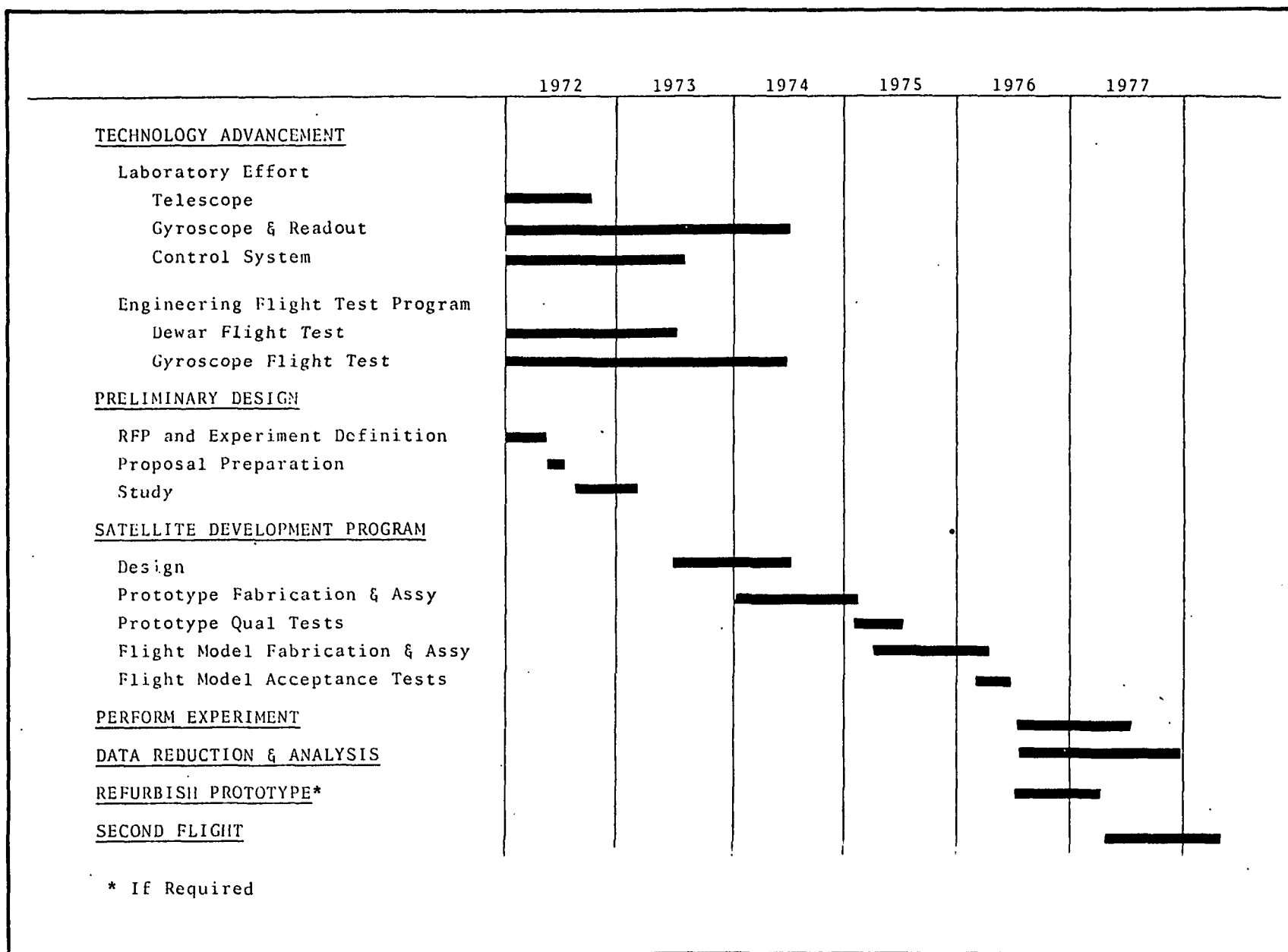


Fig. 4-1 Overall Program Schedule



would last until mid-1974, overlapping the preliminary design phase in which the experiment is further defined and the spacecraft preliminary design studies are performed. It also overlaps the beginning of the satellite development program.

The satellite development program begins in mid-1973. A conventional development program of a prototype and flight model is shown. The prototype satellite has completed qualification tests by mid-1975. The flight model starts in early 1975 and is ready for its first year flight in mid-1976.

Data reduction would take place throughout the flight and be completed six months after the conclusion of the mission.

#### 4.3 PLAN FOR TECHNOLOGY ADVANCEMENT

Advances in technology are required in the following areas:

- Dewar Design
- Gyroscope and Readout
- Instrumentation Loop
- Magnetic Shielding
- Optical Contacting and Stability
- Telescope Evaluation
- Control System

The problems in the various areas have been discussed in the sections of the study concerned with those areas and will only be



briefly described here. In addition, Volume II is devoted to describing a flight test program which supports this plan for technology advancement.

Because solutions to problems in these areas must either be in hand or readily obtainable before it would be reasonable to commit major effort to the flight of the final experiment, it is necessary to make an intensive effort on these problems in the next two and one-half years.

#### 4.3.1 Dewar

The problems in dewar design are in the areas of venting and helium management.

Venting. A superfluid plug design has been proposed by Stanford to solve the venting problem. The design analysis needs some additional work, further laboratory work is necessary and a dewar with this type of vent must be tested in orbit to verify the performance of the vent.

- Design Analysis - An analysis of the performance of a superfluid plug was made by P. M. Selzer, W. M. Fairbank, and C. W. F. Everitt in their paper "A Superfluid Plug for Space". Further paper analysis must be done. The exact design parameters for a plug to match the heat leak and plumbing characteristics of the orbital test dewar must be determined. This includes such parameters as diameter of the plug, spacing between layers, length of re-entrant tubing, orifice size (if required) etc. This effort most logically should be spent by Fairbank and Everitt et al at Stanford.



- Laboratory Testing - The superfluid plug should be tested in Stanford's laboratory to verify its performance as well as possible on the ground. The dewar used in previous tests should be modified to accept the new plug design. Tests would be made with the plug both in and out of the liquid, in both superfluid and normal helium. The ability of the plug to keep the helium superfluid in the presence of internally generated heat would also be tested. This plug or one of similar design would then be used for the engineering flight test.
- Flight Testing - A dewar of sufficient capacity to last at least a month in orbit is necessary to perform the test of the superfluid plug as well as to verify other aspects of the design. The dewar flight would also be designed to test the basic design of the final experiment dewar by incorporating the same type of insulation, inner container supports and central cavity. It would also be designed to be compatible with the engineering flight test of the gyroscopes. Careful measurements of temperature, superfluid film thickness, liquid and superfluid film location, and boil-off rate are required. Sensors must be developed to measure the location and thickness of the superfluid film and the bulk liquid.

A specially designed, relatively simple spacecraft is recommended for this test.



It would be launched as a secondary piggyback payload on a Thor Delta and would be separated after the primary payload. This same spacecraft design with some modifications could be used for the gyroscope test which must follow (see Section 8 for details).

Helium Management. A scheme using honeycomb-like cells has been suggested to prevent the helium from sloshing and also to control the C.G. of the helium mass as helium is used up over the year. This scheme can hold the helium against forces of up to  $10^{-4}$  g. The concept is still an idea and considerably more analysis and flight testing needs to be done. Some modeling may also be done along with the analysis.

- Design Analysis - A further study into the cells scheme is required in order to be able to specify an arrangement that will not be damaged during launch and will hold the helium in orbit. Further study is also required to determine what hole size to use in the various cells to assure draining of the cells in the proper order to keep the C.G. at the desired location. Testing of this system using models of the cells with some other fluid may be possible, but will not give conclusive data on the operation of the system.
- Flight Testing - The helium management scheme can be tested on the same flight as the superfluid plug. The cells can be incorporated within the helium space of





the dewar without affecting the superfluid plug test. Instrumentation similar to that required for measuring the location of the bulk helium would be used to determine the order in which the cells empty. The spacecraft must maneuver with low acceleration to simulate the final Relativity Satellite and must also perform programmed accelerations to test the holding power of the cells.

Schedule. The schedule for this portion of the technology advancement program is shown in Fig. 4-2. Work must start early in the first quarter of 1972 to allow a test flight in mid-1973 before beginning the main satellite development program.

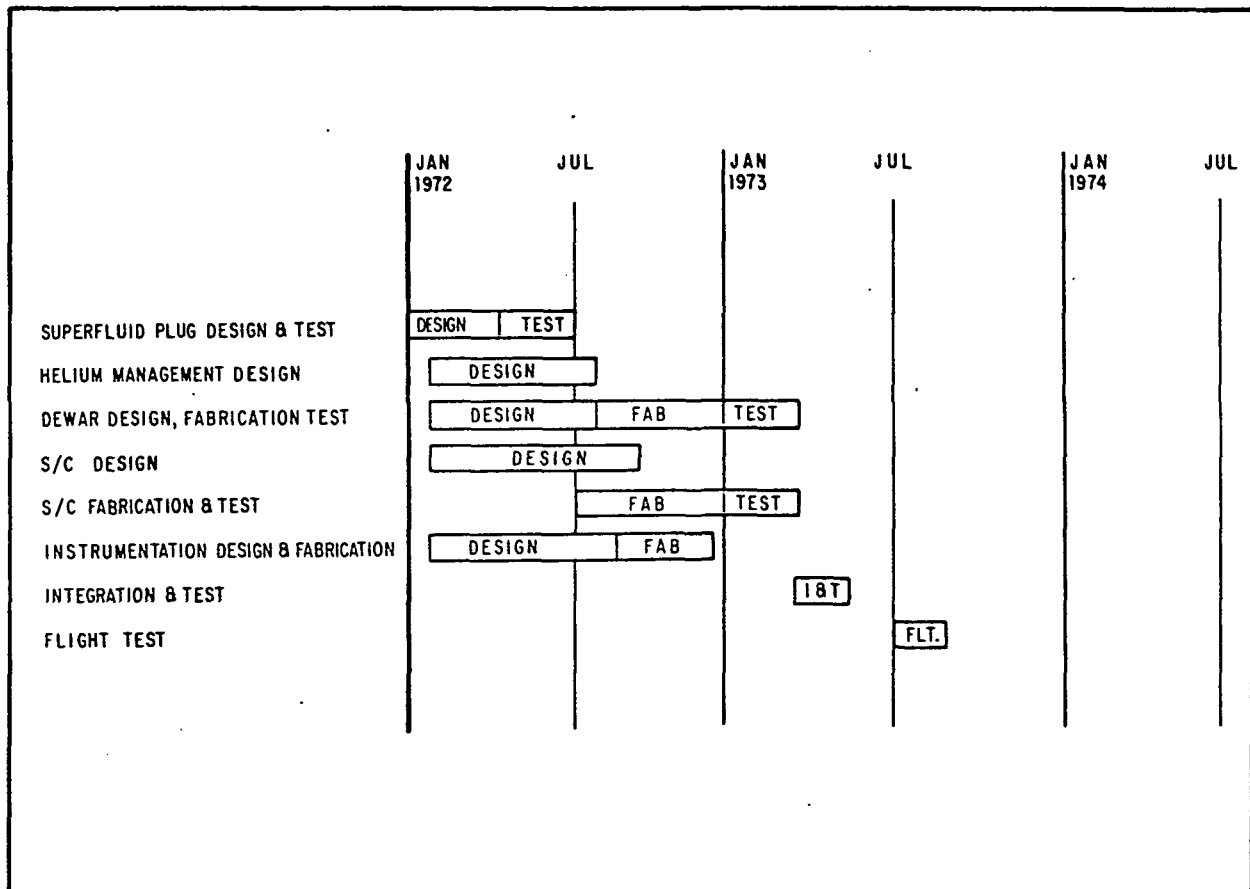


Fig. 4-2 Dewar Technology Program



#### 4.3.2 Gyroscope and London Moment Readout

At this time, the gyroscope has not yet been spun up. Two different housing designs are being developed, one by Stanford and the other by MSFC. Both programs are aimed at a spin-up test in early 1972. In both programs, the parts are nearing completion, the suspension electronics exist and the test facilities are ready. A successful spin-up test will bring the gyroscope a long way toward its ultimate development in that it will demonstrate that the 1 g electrical suspension and the gas spin-up systems are compatible. Spin-up in orbit should be easier to accomplish because of the lower suspension voltage required.

Assuming a successful spin-up takes place in early 1972, work must be directed toward the design, fabrication and flight testing of an orbiting gyroscope system. This includes the low voltage suspension system, a gyroscope with three readout loops and a suitable magnetometer for the London Moment readout. A flight test gyroscope assembly must be built and incorporated into the spacecraft and dewar design used for the dewar test flight. A test flight must then be performed.

Gyroscope. Extensive evaluation of the spin-up characteristics must be made in order that the orbital suspension system can be designed. The disturbance forces and frequency imparted to the rotor during spin-up must be determined to establish the dynamic range and frequency response required of the orbital suspension system. This system must then be designed and built and a means devised to test the system on the ground before committing it to an orbital test.

The spin axes of the two parallel gyroscopes in the Relativity experiment must be aligned to the telescope to within 10 arc-seconds. The method presently contemplated to achieve this is



to roll the satellite about the desired orientation axis during spin-up. Ground testing of this technique must be done to determine whether the desired accuracy can be obtained. If it cannot, an alternate means of controlling the spin axis orientation must be developed.

Neither housing design presently being made can accommodate the three readout loops needed. The exterior of the housing must be redesigned to accept three mutually perpendicular loops. Gyroscopes of this configuration must then be fabricated and ground tested and then made ready for an orbital test flight.

London Moment Readout. The London Moment developed by the spinning superconducting rotor is of the order of  $10^{-4}$  gauss. To read this to an accuracy of 0.001 arc-second requires a magnetometer with sensitivity and stability of the order of  $6 \cdot 10^{-13}$  gauss.

Two approaches to such a magnetometer are now under investigation at Stanford. A Josephson junction magnetometer is presently being used for the initial testing while a vibrating plane magnetometer is being developed. Either system is a candidate for the final design. In either case, further work must be done to demonstrate that the required accuracy and stability can be achieved in the laboratory.

For the engineering test flight, a flight quality magnetometer of somewhat less accuracy ( $\sim 6 \cdot 10^{-12}$  gauss) would be acceptable.

Development of the magnetometer is difficult and is a vital step in the technology advancement program. The plan is to carry the development of both the Josephson junction and the vibrating plane magnetometers along in parallel until a clear choice can be made.



Flight Test Program. The orbital performance of the gyroscopes cannot be determined on earth because of the effects of gravity. The ground drift rate is predicted to be millions of times worse than that in orbit. A flight test program is required to establish even the order of magnitude of drift to be expected. The flight test would also verify the performance of the suspension system, spin-up and alignment of the spin axes.

An assembly of three gyroscopes on a quartz block must be fabricated and ground tested. This assembly with its magnetometers would be mounted within the central cavity of a dewar of the same design as used for the dewar flight test. The spacecraft would also be of the same design with the addition of a roll reference star tracker. Boil-off helium would be used for attitude control. One gyroscope would be spun up and then would become the attitude reference for the spacecraft. The other two gyroscopes would be spun up and compared to the reference gyroscope over a period of one to two months. Details of this flight test are described in Vol. II.

Schedule. The schedule for the gyroscope technology advancement program is shown in Fig. 4-3. This schedule is arranged so that at the time of the proposed start of the relativity experiment's main program in mid-1973, the gyroscope package is about ready for assembly and test. It is assumed that there would be sufficient laboratory data on the gyroscopes and magnetometers to allow the program to proceed. The engineering flight test data would not be available for one more year.

It is important to note that the level of effort required for this program is considerably greater than that presently being expended. An increased level of effort is required early in 1972 to meet this schedule.

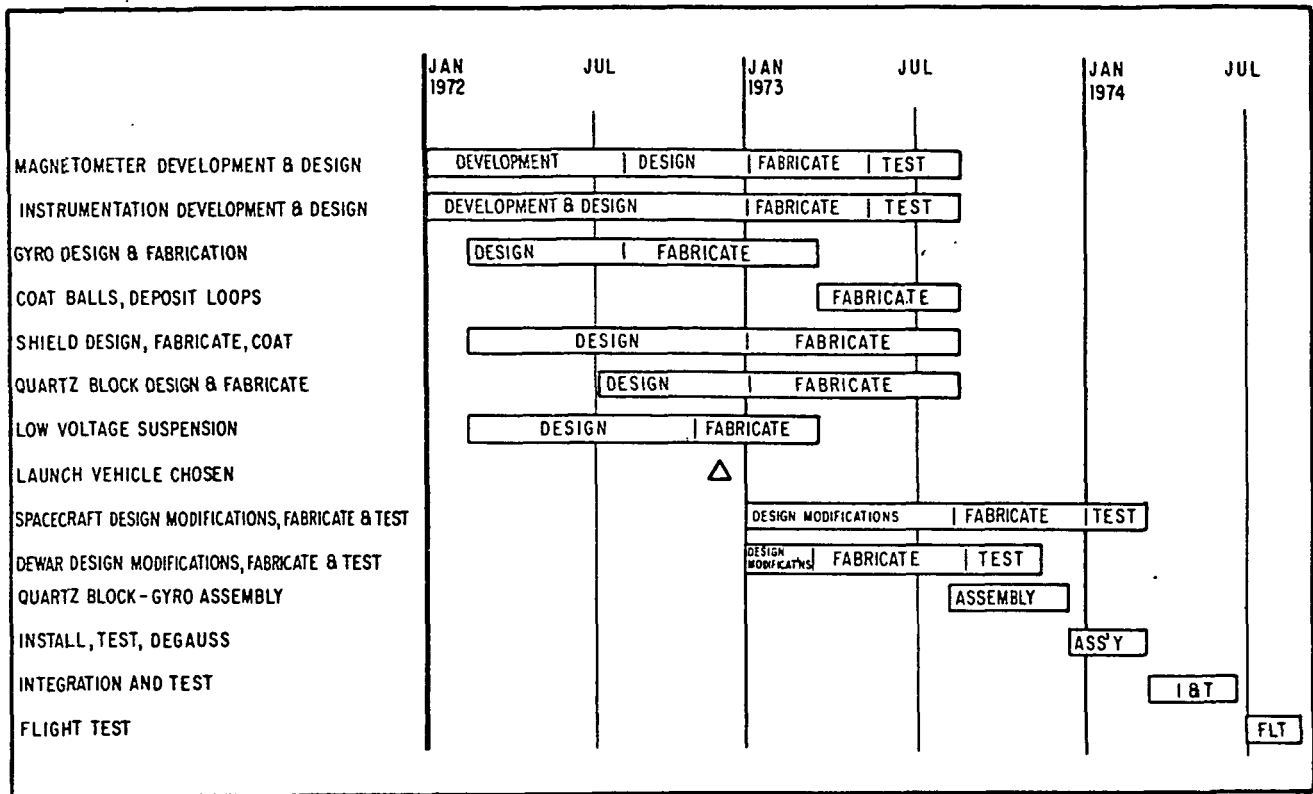


Fig. 4-3 Gyro Technology Program

#### 4.3.3 Instrumentation Loop

Two elements of the instrumentation loop that generates the relativity information are presently state-of-the-art devices for laboratory use. These devices are the voltage-to-frequency converter and the digital-to-analog converter. Both must be accurate to better than one part in 100,000. In order to have confidence that these designs can be converted to flight hardware, breadboard models of these two items must be made using flight type components. This will involve evaluating packaging concepts that assure adequate thermal control and elimination of stray emf's due to thermocouple effects, capacitive coupling of transients, etc.



#### 4.3.4 Magnetic Shielding

Laboratory methods of making nearly perfect superconducting magnetic shields have been developed at Stanford over the past years. Application of these techniques to the specific problem of shielding the gyroscope and its readout loop, while still allowing optical contacting, must be done. This is required for the gyroscope engineering flight test programs and therefore must be done in the time frame of that program. It is one of the most knotty problems and affects the detailed gyroscope design.

In order to make a superconducting shield exclude all flux, the shield must be made superconducting in a field of the order of  $10^{-6}$  to  $10^{-7}$  gauss. Such a facility is under construction at Stanford as part of another program. This program requires successful completion of that facility or an alternate method of obtaining a low field.

#### 4.3.5 Optical Contacting and Stability

At present there are no engineering data on the strength and stability of optically contacted parts. A program must be undertaken to develop these engineering data. Davidson Optronics, which is fabricating an engineering model telescope for this program, has used this technique for a number of years but has had no need to generate the data required for the design of flight hardware.

The program should consist of fabrication of a number of typical optically contacted joints which would be subjected to tensile and shear strength tests at room temperature and at liquid helium temperatures. If at all possible, a nondestructive method should be developed to determine the strength of joints so flight hard-



ware can be inspected. Data must also be gathered on the long term dimensional stability of these joints at liquid helium temperatures. A possible method would be to differentially autocollimate from two parallel optically contacted pieces which are stored within a liquid helium dewar.

These data are required for design of the gyroscopes of the engineering flight test program and must therefore be done in that time frame.

#### 4.3.6 Telescope Evaluation

The engineering model telescope being fabricated by Davidson Optronics for this program is very close to the final design needed. Careful evaluation of the image quality, stability at cryogenic temperatures and performance of the readout system will provide excellent data for the design of the final telescope. An elaborate artificial star must be designed and built to test the telescope stability and linearity.

#### 4.3.7 Control System

Work is presently going on at Stanford on the development and evaluation of an engineering model proportional valve and thruster using the boil-off helium gas as the propellant. This work should be completed and the system applied to the attitude control of the engineering test flight satellites for the dewar and gyroscope tests.

During this study a considerable amount of work was done by Stanford and BBRC in evaluating the proposed control system. At the conclusion of the study there was still a question on the characteristics of the flex pivots for the pitch-yaw controller.



The possibility of eliminating the inner control loop entirely was also unresolved. There is still concern that the system noise is incompatible with the gyro acceleration limits, but a dead zone in the suspension electronics may solve the problem. A continued effort of analyzing and simulating the control system should be undertaken to determine the proper mechanization so the main program can proceed smoothly once it is started.

#### 4.4 SATELLITE DEVELOPMENT PLAN

##### 4.4.1 Introduction

The satellite development plan described in this section is aimed at having a launch in 1976 as recommended by the National Academy of Science. It is constrained at the front by the assumption that funds would first be available for the main program in fiscal 1974. It is assumed that the funds necessary for the technology advancement program would be available in fiscal 1973 or possibly earlier.

We feel that such a schedule, although difficult, is possible. It will require some technical risk in that a number of activities that can affect each other are going on in parallel. Exceptionally close coordination between NASA, the experimenter and the spacecraft contractor must be maintained, especially during the formative portion of the program. It is NASA's stated desire that two competitive preliminary design studies be let for the spacecraft design effort and that the winner be the spacecraft integration contractor. It should be noted that the technology advancement program must overlap these competitive studies as well as the beginning of the main program. This could result in a significant change in experiment definition between the beginning of the studies and the beginning of the main program. By the time of the beginning of the main program, the experiment definition





would be sufficiently frozen to allow a spacecraft contractor to proceed without risking excessive changes.

There is a problem in defining the relative responsibilities of the experimenter and of the spacecraft contractor in the area of the dewar and the control system. The establishment of responsibilities in these areas must be done prior to the issuance of the RFP for the two Preliminary Design Studies.

Because of the very close interaction between these subsystems and the experiment, and because of the experimenter's capabilities in these areas, it is assumed that the experimenter will have design input and design approval authority for these subsystems.

#### 4.4.2 Preliminary Design and Definition Phase

The schedule shown in Fig. 4-4 is for the preliminary work leading up to the award of a contract for the Stanford Relativity Satellite.

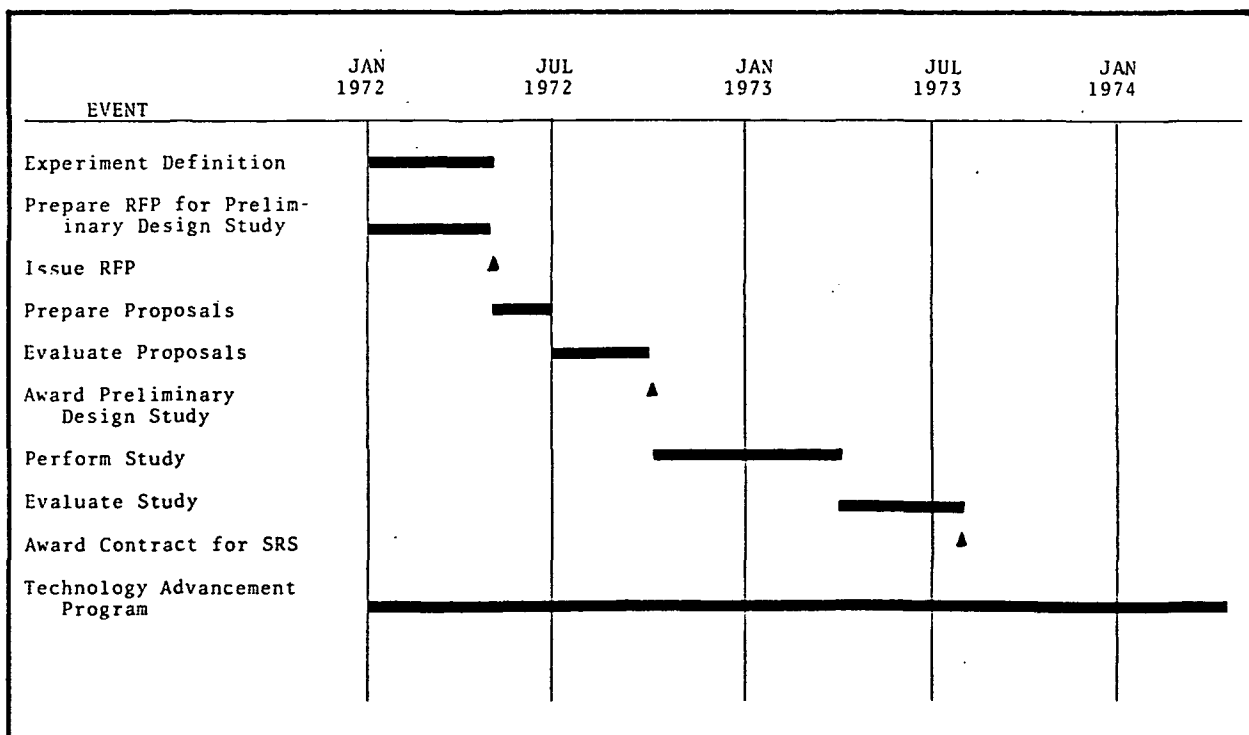


Fig. 4-4 Preliminary Design and Definition Schedule



During the first four months of 1972, an RFP would be prepared for the preliminary design study for the SRS spacecraft. At the same time Stanford would be preparing the base line experiment definition for the study. Two months are scheduled for preparation of proposals followed by a three-month evaluation period. The study contracts would be let in September of 1972.

The six-month study would establish the preliminary design of the spacecraft and operations needed to support the experiment. It should be noted that the technology advancement program is going on throughout this period. The resulting changes in experiment definition will have to be accommodated in some way.

Four months are allocated for evaluating the studies and choosing a contractor for the spacecraft. Contract award would be in August of 1973.

#### 4.4.3 Stanford Relativity Satellite Development Phase

Figure 4-5 shows the schedule for the satellite development phase including both the spacecraft and the experiment. A go-ahead is assumed in August 1973. At that point in time the technology program would have advanced to the point that the dewar test flight was completed and the gyroscopes for the gyroscope test flight were fabricated and ready for test. The experiment definition would be well established.

For both the spacecraft and experiment the major design effort takes approximately one year. Design modifications continue as test data and production problems require changes.

The prototype spacecraft fabrication starts about five months after the beginning of the design phase. Testing of components and subsystems follows shortly behind. As soon as the dewar is

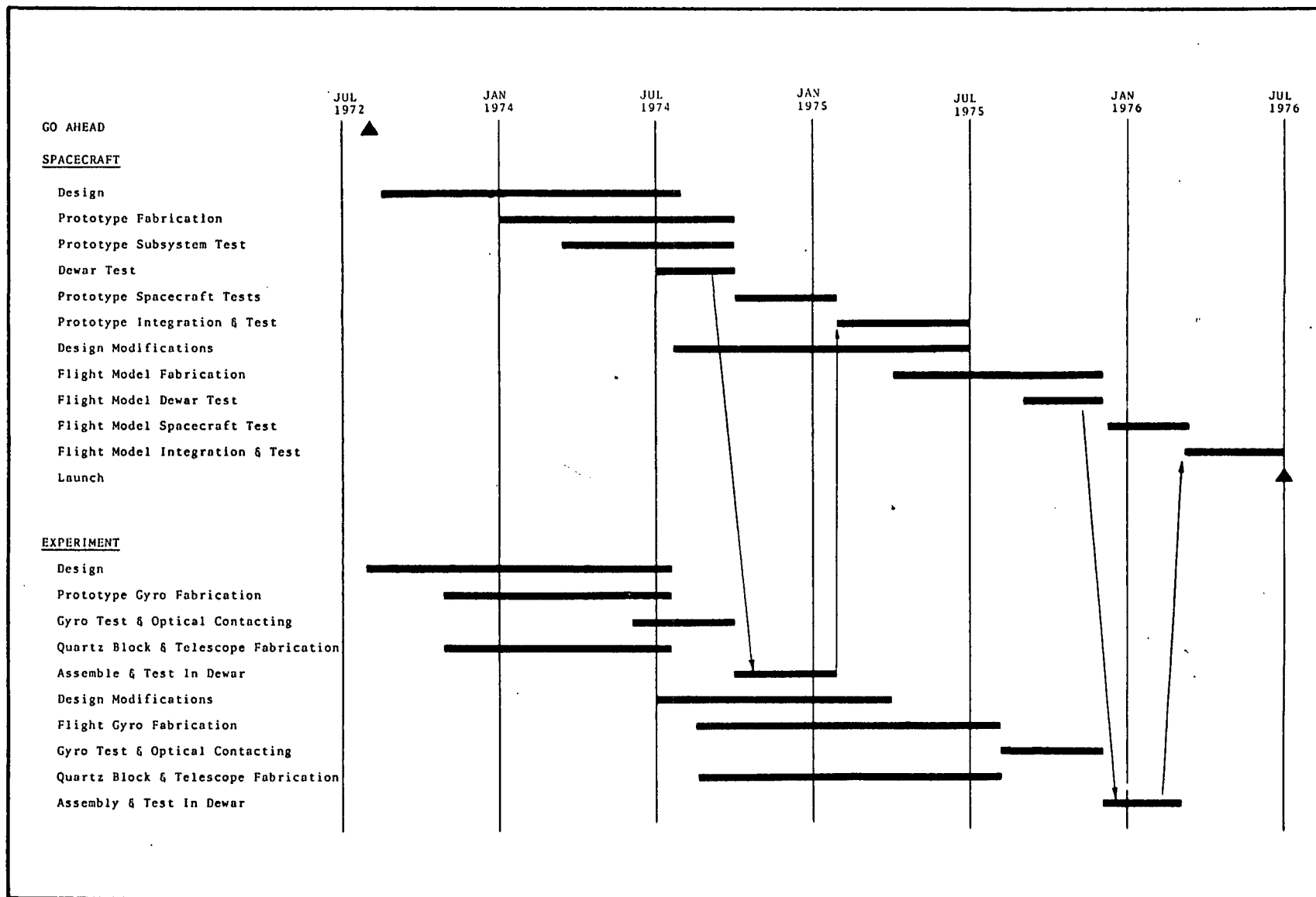


Fig. 4-5 Satellite Development Schedule



completed and tested it is delivered to the experimenter to allow him to incorporate the experiment package in the dewar and check out any problems in his own facility. The portable cryogenic ground support equipment vacuum pumps, helium transfer equipment, etc.) would be delivered along with the dewar.

The start of experiment hardware fabrication is leading the spacecraft hardware by two months due to the long lead time required to fabricate the optical parts for the gyroscopes, quartz block and telescope. It would be desirable to start earlier but this start is timed with the completion of laboratory tests with the gyroscopes being fabricated as part of the technology advancement program. It might be required to start the search for the fused quartz raw material during the technology advancement program in order to have proper quality materials on hand. The nine months allocated to the optical part fabrication is extremely tight. During the preliminary design study, special attention should be paid to establishing a program to ease this particular schedule bind.

The gyroscopes are then assembled with the telescope to form the quartz block assembly. This is tested, assembled in its "dewar within a dewar" and degaussed in the special low magnetic field environment and kept cold from this point on. It is then installed in the prototype satellite dewar for final experiment checkout. The required electronic subassemblies have been following along to be ready for the test phases. Following checkout, the experiment system would undergo the vibration and thermal/vacuum qualification tests.

The satellite dewar with this instrument installed is delivered back to the spacecraft contractor along with the cryogenic ground support equipment to keep the dewar cold.



While this experiment package is being installed and tested in the dewar, the spacecraft system is being assembled and qualification tested, using a dummy dewar. Upon completion of these tests and the delivery of the "live" dewar these two major parts are assembled together.

Once assembled, the satellite is ready for testing. The satellite qualification tests would consist of vibration testing, thermal vacuum testing and thermal balance testing. A centrifuge test would be performed if it was felt to be necessary. Between test sequences, performance tests would be done. Performance tests are done by inserting signals in appropriate portions of the system to determine their proper operation. "All-up" system tests are done on the special, highly stable, polar axis mount using an artificial star. Extreme care must be taken at this time to avoid jarring of the system or inadvertent loss of suspension voltage while the gyroscopes are spinning.

The flight model spacecraft and experiment follow essentially the same kind of sequence except that more time is allotted to the fabrication of the gyroscope-telescope assembly. The integration and test period is reduced from five months to four months, and the thermal balance test is not performed. The flight model would be ready for launch in July 1976.

#### 4.4.4 Spares Plan

Because of the importance of the scientific aspects of the program and the long lead time required for building an entire new satellite in case of a launch vehicle failure, we have not recommended a proto-flight type of program. Instead, we recommend a program in which the prototype is refurbished to a flight condition in case of a launch vehicle failure. This can also be done if it is desired to reflly the experiment in an improved or modified



configuration. Flight spares would be available on a major sub-assembly level, so that an immediate replacement would be available during testing in case of a failure. These same spares would be used to refurbish the prototype. In this case a selected set of spares would be built to support the second mission.

We recommend that there be a complete, tested, spare gyroscope-telescope assembly already degaussed, kept cold in its "dewar within a dewar" and ready to be substituted for the one under test. The recycle time in case of the most insignificant problem requiring work inside this package is at best a month and more likely two months. Any major work on the assembly could take much longer. Once the integration and test program starts, this directly delays the schedule, with the attendant increased cost.



## Section 5

### EXPERIMENT AND DEWAR

A large part of the satellite is the helium dewar which contains the experiment. This section describes the experiment and the helium dewar. The experiment is contained in a smaller dewar which fits into the larger one-year life dewar. The description is separated into the telescope, the gyroscopes, the electronics and both of the dewars.

The telescope is a three-element Cassegrain. All of its pieces are optically contacted together and to the gyroscope (quartz block) assembly. This section also presents analysis for possible errors and establishes the performance requirements of the various parts of the assembly.

The gyroscopes were defined by Stanford University. They are the basis of deriving the relativity data and are made of highly uniform fused quartz machined to an extremely close tolerance. Coating the gyroscope balls with a superconductor allows superconducting loops to sense a shift in the gyroscope spin axis. Each gyroscope has three orthogonal loops. Because of the requirement of low magnetic fields, each gyroscope is magnetically shielded using a superconductor.

The electronics for the gyroscope and telescope are discussed. Also, included are the orbiting signal processing electronics including matching of the telescope and gyroscope gains and extracting the scientific data. The system is extremely sensitive to noise and thus the gyroscope signal preamplifiers are located within the dewar but are insulated to operate at 200°K. A total system block diagram is presented in Section 3, but those circuits critical to the gyroscope signals, control and telescope signals are presented here along with the appropriate analysis



and discussion. The gyroscope suspension system is discussed in Section 6.4.

The last section deals with the configuration and construction of the helium dewar. This includes both the main dewar and the experiment dewar (the dewar within a dewar). Discussion and analytical techniques are presented for the thermal performance and structural design. The main dewar has two sets of supports, one for launch and the other for orbital operations. A discussion is also presented for the window-neck assembly as well as for suggested methods of bringing the electrical wires out and routing the plumbing. The plumbing for initial gyroscope spin-up is presented and the paths for evacuation of the cavity are shown.

## 5.1 TELESCOPE

### 5.1.1 Requirements

The reference telescope provides a fix in inertial space from which the gyroscope drifts are measured. The telescope must generate the error signals which are used by the control system to keep it and the gyroscopes oriented to the star to an accuracy of  $\pm 0.05$  arc-second. These same error signals are subtracted from the gyroscope readout signals to determine the orientation of the gyroscopes with respect to the guide star to 0.001 arc-second. Stability and linearity must, of course, be better than 0.001 arc-second.

The star telescope provides a fix in inertial space from which the positions of the gyroscope are measured. The star telescope error signals are subtracted from the gyroscope readout signals to compensate for the small misalignment of the quartz block and guide star. The telescope system requirements are summarized in Table 5-1.





Table 5-1  
TELESCOPE SYSTEM REQUIREMENTS

Target Star	Rigel ( $m = 0.3$ )
Noise	$<0.030$ arc-sec in 100 rad/sec
Inherent Linearity	$0.0005$ arc-sec
Linear Range	$>0.05$ arc-sec
Light Shield Rejection Ratio	$2 \times 10^7$
Alignment Stability	$0.0003$ arc-sec

#### 5.1.2 Telescope Description

The basic structural material of the telescope is fused quartz which is optically contacted during assembly and alignment. The material is selected for its inherent stability. The choice of material and method of attachment minimizes changes in alignment which could occur as the assembly is cooled to cryogenic temperatures.

Light from the target star passes through the sunshield which rejects light from the sun, earth, spacecraft body and other sources of background, and then through three plane-parallel windows, each of which has one surface coated with a material which transmits visible light and reflects infrared light. The light is then imaged by a telescope consisting of a corrector plate and three spherical mirrors and after being split by a beam splitter falls onto two roof prisms. Each roof prism splits its respective image into two beams which are reimaged by spherical mirrors onto a chopper and then are overlapped onto a detector. The detector thus sees the beams alternately. The system is nulled when the reimaged beams are of equal intensity.



### 5.1.2.1 Sunshield

Some of the time the instrument will operate with the optical axis within 30 degrees of the sun. To prevent stray light from entering the instrument, a sunshield is installed on the outer dewar shell. If the illumination due to scattered light were uniform, a level comparable to that of the detector photon noise level could be tolerated. If the illumination is not uniform, the error introduced must be less than  $5 \times 10^{-4}$  arc-seconds. This demands that the scattered light be less than 1/3000 of the target star's intensity. The required level is somewhere between these two numbers since there will be some nonuniformity. For this study, the nonuniformity was assumed severe. Thus, the sun shade is specified so that it attenuates sunlight at closest sun approach to 1/3000 of the target star intensity. The total required attenuation provided by the system is then

$$\text{Attenuation} = \frac{(3000)(\text{Sun Intensity})}{\text{Rigel Intensity}}$$

For stellar magnitudes  $m = 0.3$  for Rigel and  $m = 26.7$  for the sun we have

$$\text{Attenuation} = \frac{(3000)(2.512)^{26.7}}{(2.512)^{-0.3}} \cong 2 \times 10^{14}$$

To determine how much stray light attenuation is required in the sun shield, we will first calculate how much attenuation occurs within the telescope due to the small field of view. A portion of the light scattered by the sun shade will enter the telescope. It is assumed that this light is scattered uniformly in a hemisphere. The amount of this light that is in the 3 arc-minute field-of-view of the telescope is

$$\frac{\text{Acceptance Solid Angle}}{\text{Hemisphere}} = \frac{\frac{\pi}{4} \left( \frac{3}{3437} \right)^2}{2\pi} \sim 10^{-7}$$



of the total striking the plate.

Thus, the required attenuation for the sun shade alone is

$$\text{Attenuation}_{\text{Sun Shade}} = (2 \times 10^{14})(10^{-7}) \cong 2 \times 10^7$$

This requires a sophisticated baffle. The best solution is to use two truncated cones (see Fig. 5-1), which allow no direct sunlight to fall on the inner cone. The baffles on the inside of the outer cone are arranged so that no sunlit surface (other than the edges of these baffles) is seen by the inner baffle.

Figure 5-1 shows the rays used to design such a baffle. Ray 1 defines a cone slightly outside of the telescope field-of-view and hence defines the inner baffle cone angle. Ray 3 makes an angle of 30 degrees with the optical axis which is the nearest approach of the sun. Ray 2 defines the outer cone angle. The intersection of ray 2 with ray 3 is chosen to minimize the physical length and diameter of the assembly. The edge of baffle B1 is not illuminated except by light scattered from the other baffle edges. This is shown by rays 3 and 4, which defines the position of the baffles in the outer cone. Since B1 is outside the field-of-view, light scattered from it is not "seen" at the detector without additional scattering. The edges on the inside of the inner cone are arranged (see ray 5) to ensure that light scattered from B1 does not shine directly onto the edge of baffle B2. This baffle would suffice if Rigel is the target star.

At least three and usually many more reflections from the blackened, roughened surfaces are required for sunlight to get into the main optics. Calculations and measurements indicate a rejection ratio of  $10^9$  to  $10^{15}$  for a baffle of this type for the sun within  $30^\circ$ - $45^\circ$  of the optical axis. To our knowledge, no tests have been performed on baffles designed to operate within  $20^\circ$  of the sun.

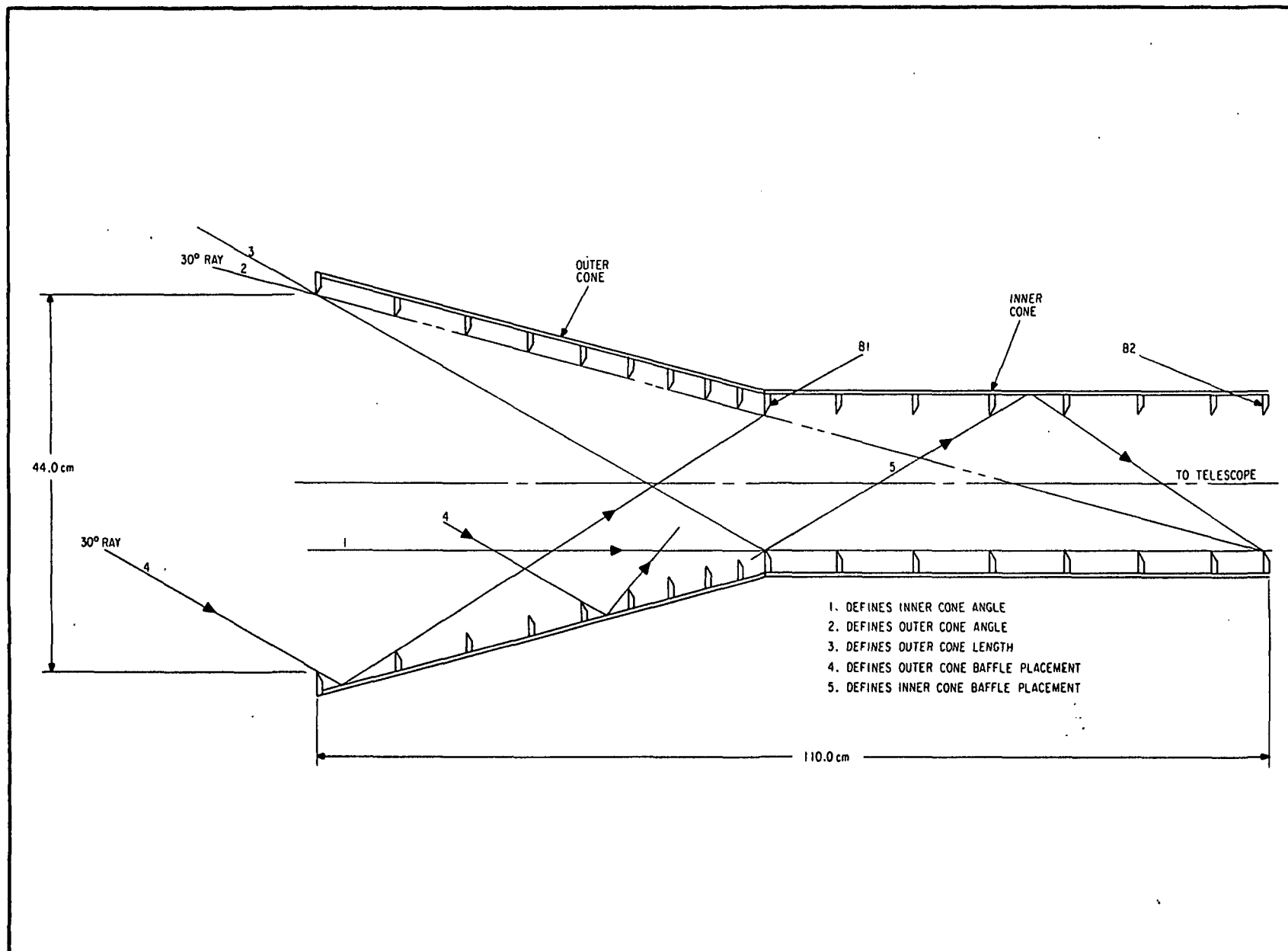


Fig. 5-1 Sun Shield, 30-Degree



The telescope also aids by discriminating between incident radiation at different angles with respect to the optical axis. Additional baffling is provided throughout the telescope to prevent specular reflections from being imaged in the field-of-view and to minimize multiple reflections (see Fig. 5-3). Figure 5-2 is a drawing of a  $22^\circ$  sunshield. This sunshield would be required if Procyon is the target star. Note that it is larger than the  $30^\circ$  sunshield. This  $22^\circ$  sunshield is shown on all the satellite drawings.

#### 5.1.2.2 Optics

The optics consist of the following items (also see Fig. 5-3):

- 3 front windows (not shown in Fig. 5-3, see Fig. 5-20)
- 3 spherical mirror telescopes with correction plate
- 1 beam splitter
- 2 roof prisms
- 1 relay system of either fiber optics or spherical mirrors

The three front windows are required to reduce heat flux into the dewar. One surface of each is coated with a dereflected gold film having transmission and reflectance properties shown in Fig. 5-4. The transmission peak can be moved around in the visible spectrum by changing the coating thicknesses, but this results in a loss in overall transmission with the blue cut-off remaining relatively unchanged. Of the coatings which are commercially available at the present time, this coating provides the highest visible transmission while preserving the low

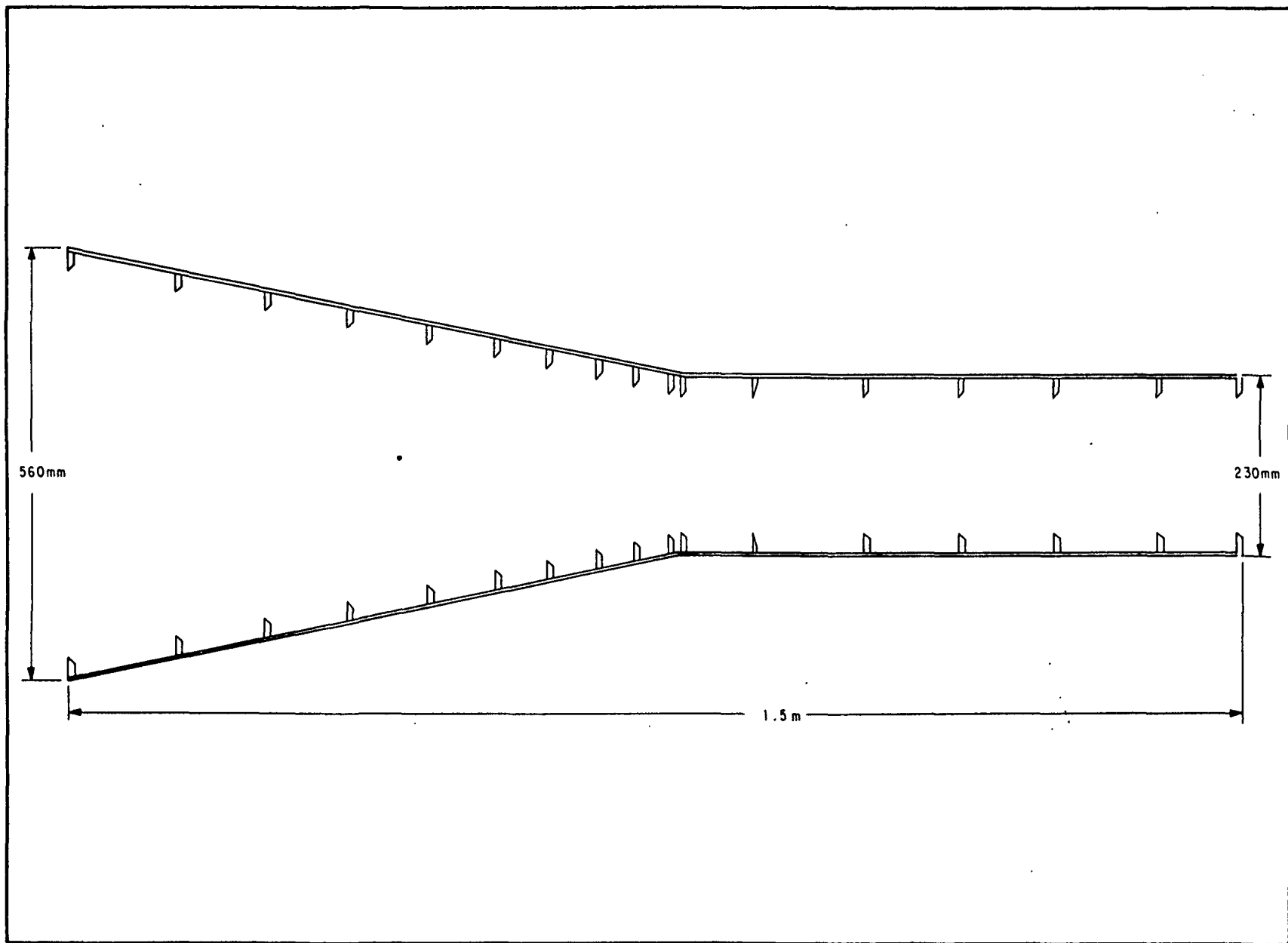


Fig. 5-2 Sun Shield, 22-Degree

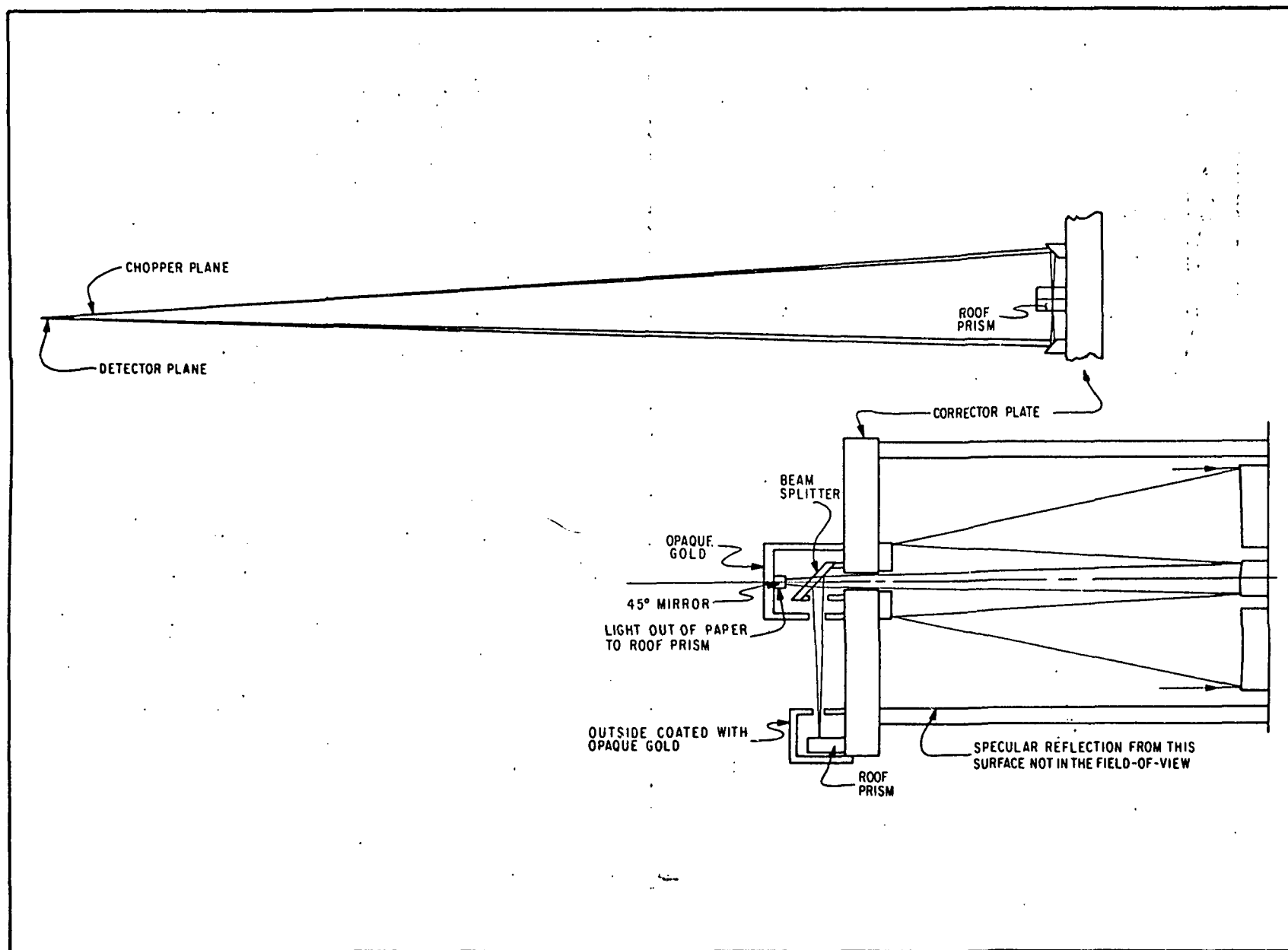


Fig. 5-3 Telescope Optical System

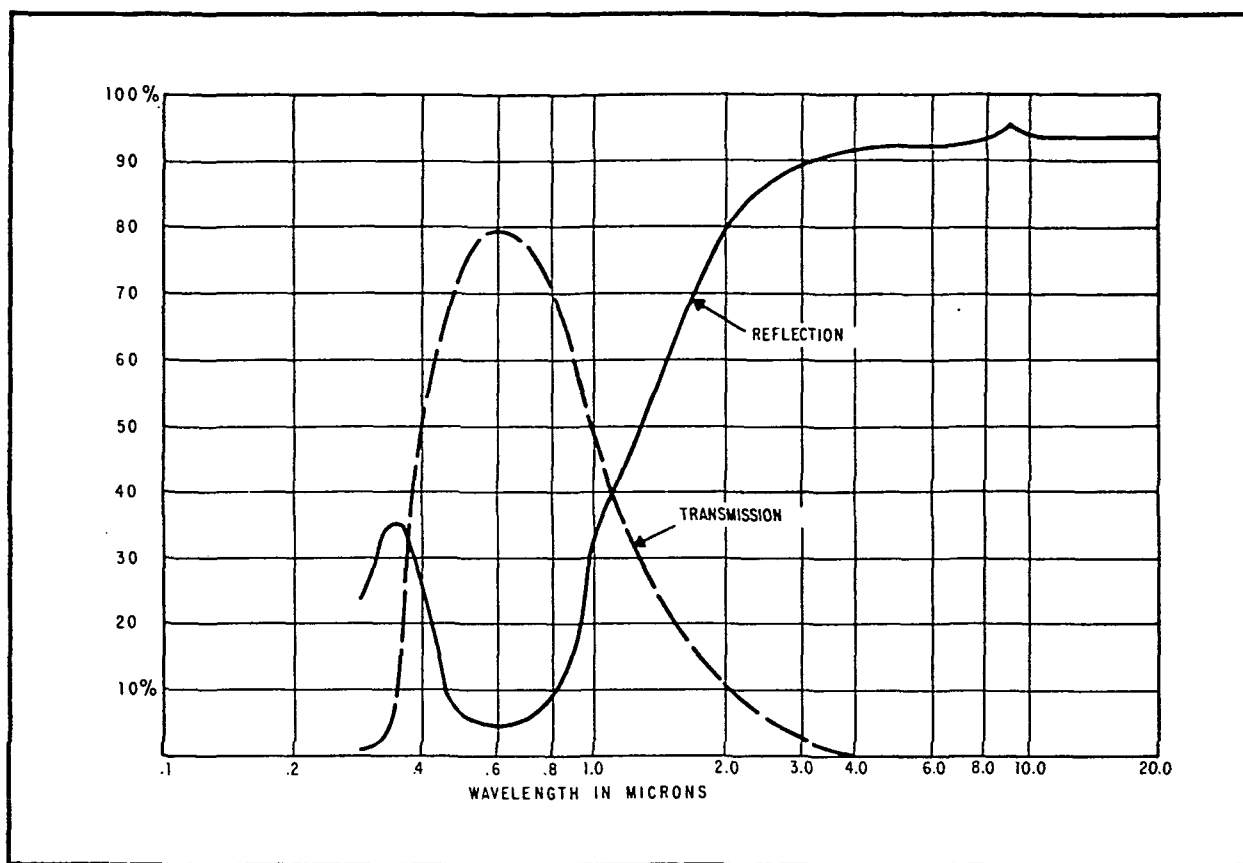


Fig. 5-4 Transmission and Reflectance of Derelected Gold

emissivity of gold in the 10  $\mu$  region. In addition, its blue cut-off of below 4000  $\text{\AA}$  makes maximum use of energy of Rigel which is approximated as a blackbody of temperature 13,000°K, peaking at about 2200  $\text{\AA}$ . This coating is expected to be stable at liquid helium temperatures, but its exact spectral characteristics are unknown there.

The other surfaces are coated, with a broadband antireflective coating like OCLI's HEA\*. The portion of the window inside the telescope's obscuration will be coated with opaque gold to improve the thermal characteristics of the assembly, and to remove

\*OCLI - Optical Coating Laboratory, Inc., Santa Rosa, California





stray light due to multiple reflections originating from light reflected from the box containing the beam splitter.

The windows will be of Schlieren grade fused silica, with prism angle of less than 1 arc-second, to keep chromatic aberrations to less than 0.1 arc-second. Their mutual alignment is not critical and they will be canted with respect to each other by about 5 arc-minutes to remove the ghosts due to multiple reflections from the field-of-view.

Telescope. During the study, a telescope design was developed for the purpose of analysis which is similar to the Davidson Optronics engineering model except that the focal length was reduced from 3880 mm to 2500 mm. This design is the basis for the analysis in the report.

The telescope consists of three spherical mirrors with a corrector plate. The corrector plate removes residual on-axis aberrations, primarily third order spherical aberration due to the three spherical mirror imaging system. As shown in the section on error analysis, the image intensity must approach that of an Airy disc and have a high degree of symmetry. The telescope parameters are given in Table 5-2.

The mirrors will be coated with the most efficient and stable coating available. At the present time, overcoated silver is the best choice; however, enhanced aluminum is also a possibility (see Figs. 5-5 and 5-6). The corrector plate will be coated with a broadband, anti-reflective coating like OCLI's HEA.

Beam Splitter. The beam splitter is at 45° nominal angle of incidence. It has a beam splitting film on one side and a broadband anti-reflective coating on the other side to minimize multiple reflections. The broadband dielectric coating has a nominal transmittance of 60 percent and reflectance of 40 percent across



Table 5-2  
TELESCOPE PARAMETERS

Overall Focal Length	$f = 2500 \text{ mm}$
Primary Focal Length	$f_1 = 337.5 \text{ mm}$ (concave)
Optical Obscuration Ratio, Secondary	$\beta_2 = 0.33$
Optical Obscuration Ratio, Tertiary	$\beta_3 = 0.15$
Secondary Magnification	$m_2 = 2.03$
Secondary Focal Length	$f_2 = 154.95 \text{ mm}$ (convex)
Primary to Secondary Distance	$d_1 = 225.0 \text{ mm}$
Secondary to Tertiary Distance	$d_2 = 225.0 \text{ mm}$
Tertiary Magnification	$m_3 = 2.03$
Tertiary Focal Length	$f_3 = 364.08 \text{ (convex)}$
Image Distance from Secondary Vertex	$e_3 = 150.0 \text{ mm}$
Primary Aperture Diameter	$D = 140.0 \text{ mm}$
Actual Obscuration Ratio	$\gamma \leq 0.4$
Total System Transmission	0.11 with beamsplitter in transmission 0.08 with beamsplitter in reflection
Diffraction Limit ( $\frac{1.22\lambda}{D}$ )	0.87 sec

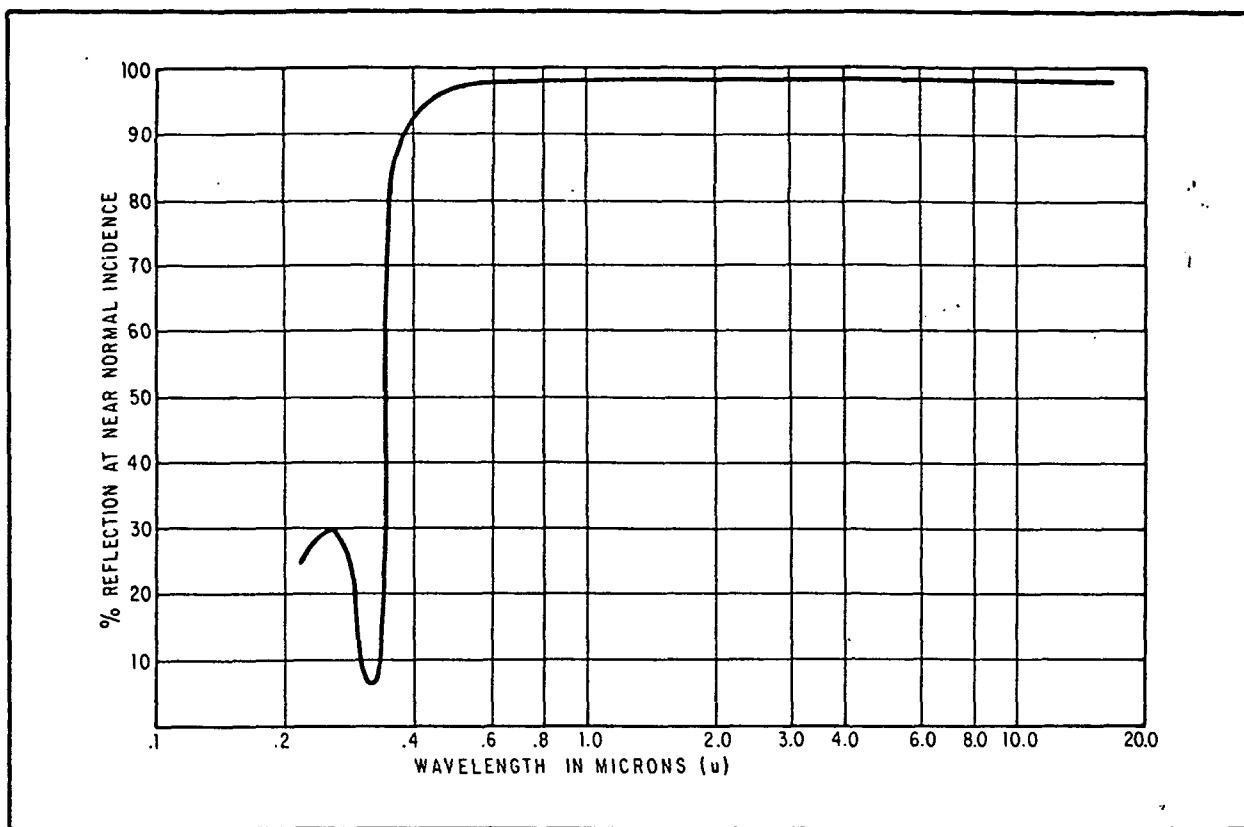


Fig. 5-5 Reflectance of Front-Surface Silver-Coated Mirror

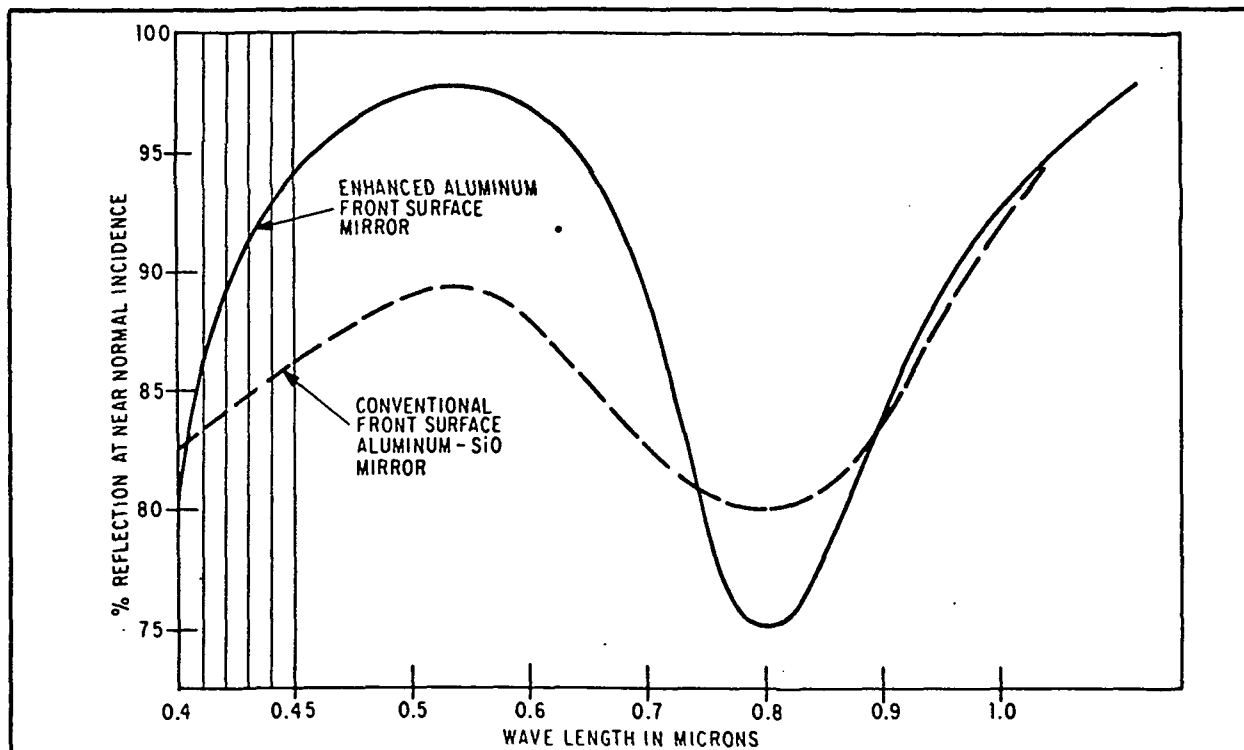


Fig. 5-6 Reflectance of Front-Surface Enhanced Aluminum Mirror



the visible spectrum. The prism angle will be less than 10 arc-seconds. The beam splitter surfaces are each plane to better than  $\lambda/10$ .

Roof Prisms. The roof prisms have two plane  $\lambda/10$  surfaces intersecting at  $90^\circ$ , coated with overcoated silver or enhanced aluminum. The intersecting edge must be very fine with an absence of nicks larger than  $7500 \text{ \AA}$  diameter. The width is not as critical a parameter as are nicks, as is shown in the error analysis section.

Relay System. Figures 5-3 and 5-7, respectively, show two possible relay systems. The reflective scheme shown in Fig. 5-3 is recommended because the transmission characteristics are more stable and therefore pointing errors due to changes in transmission are smaller than for the alternate (fiber optics) relay scheme.

In the fiber optics relay scheme the beam from each roof prism is collimated by a lens and directed toward the front of the satellite by plane mirrors which are optically contacted to the telescope structure as shown in Fig. 5-7. The two fibers for each axis are wound around the structure in front of the telescope and brought together at the chopper-detector assembly which is at a temperature of  $>210^\circ\text{K}$ . Some of the problems inherent in the use of fiber optics are:

- The fibers consist of a higher refractive index glass cylinder clad with a lower refractive index glass. The effects of differential thermal expansion would have to be tested. Corning Glass Works, Corning, New York, has no data on this but thought the fibers might shatter upon cooling to liquid helium temperatures.

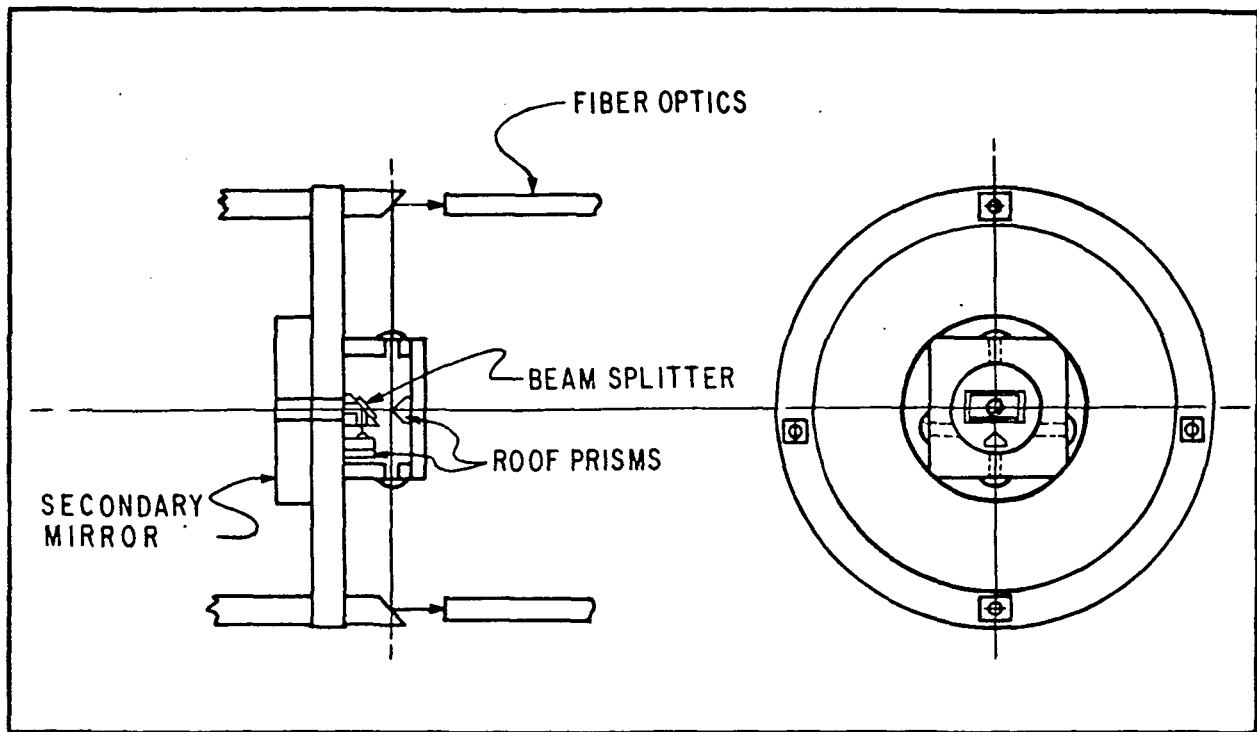


Fig. 5-7 Fiber Optics Relay

- The standard jacket is polyvinylchloride. This material stiffens upon cooling and will crack if bent. The stiffening would destroy the advantage of flexibility provided by fiber optics. A different jacket material would have to be used.
- The transmission for two feet of fiber optics is about 60 percent in the visible. The transmission of solid rod (0.075" to 3/16" diameter) is about 70-75 percent.

The transmission for the direct scheme using mirrors as the relay is at least 90 percent.

- Differential transmission changes due to radiation darkening would be read as direct pointing errors. Tests would have to be performed to determine the



magnitude of the problem (or at least data located). The problem should not be as bad in the reflective relay system for there is a wider choice of materials for the mirror coating and the differential mirrors can be coated together providing uniformity between the coatings.

- Contamination from the fiber optics would have to be investigated.

Corning recommended the use of solid rod in the coldest environment. The solid rod would relay the light to the flexible fiber which would remain in the warmer environment. This approach would destroy the advantages of using fiber optics.

The reflective relay scheme overcomes these problems. Spherical mirrors optically contacted to the quartz block relay the error signal beams to the detector and therefore the relative position of the two beams remains fixed as is required to minimize the effect of photocathode non-uniformities.

The chopper is a tuning fork, such as the Bulova L40, used in a scissors mode as shown in Fig. 5-8. It requires shock mounting since it would induce an acceleration of  $\sim 2 \times 10^{-4}$  g's at twice the chopper frequency into the satellite without it.

The image size at the chopper is about  $3.5 \times 10^{-3}$  mm. The images are placed 3 mm apart. Each chopper blade is 3 mm wide and one blade is centered between the images. The blades oscillate about this equilibrium position with amplitude of  $\pm 2$  mm at frequency of 50 Hz.

The major deficiency of a reflecting relay system is that it does not allow motion of the outer dewar shell and detector, with respect to the telescope.

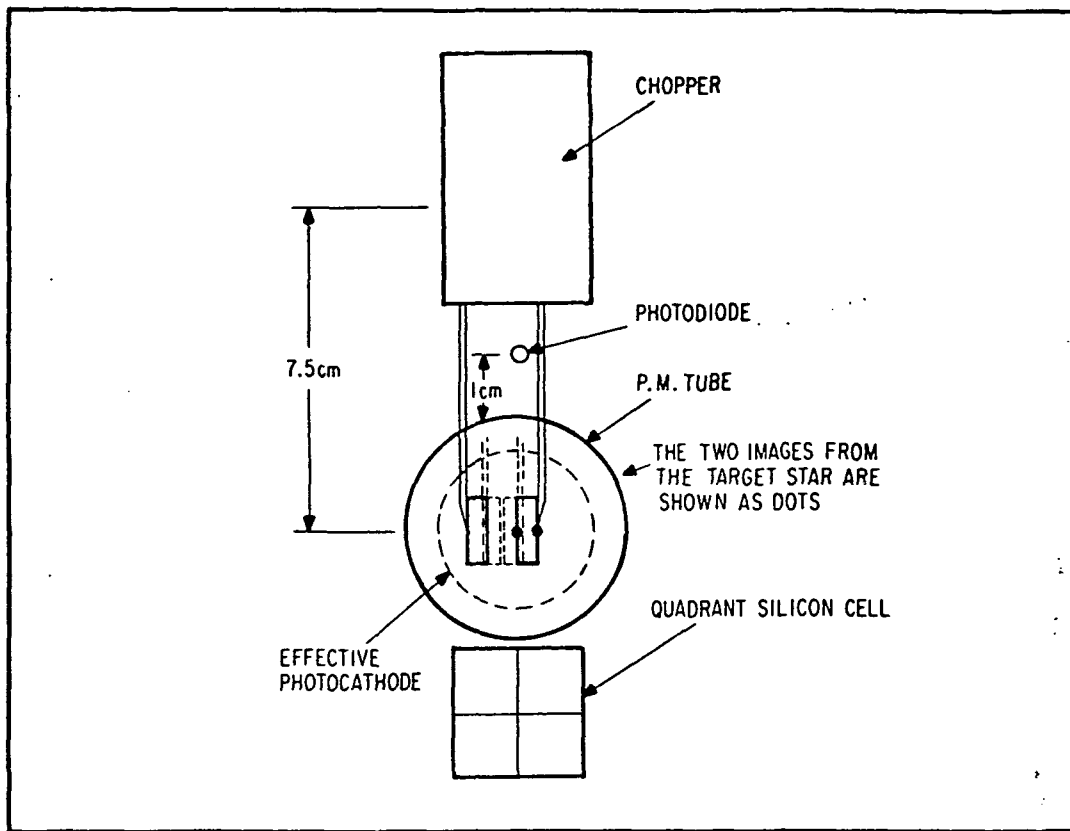


Fig. 5-8 Chopper Servo Schematic

In the section on Image Motion on the Photocathode, it is estimated that the overlapped error signal images must remain stable with respect to the detector to better than 0.2 mm. The detectors are mounted on the outer skin of the satellite. It is estimated that there will be about 1.5 arc-minutes motion of the outer skin of the satellite with respect to the optical axis. This corresponds to 0.3 mm of linear motion with respect to the relay mirrors. Hence, it may be necessary to mount the detectors and chopper on a two dimensional linear drive, although more data on photocathode uniformity and on the outer skin stability is required before a definite decision is made. If a drive system is required, one way to accomplish it is as follows.

The chopper blades are 1 cm long. The chopper-detector assembly must be translated in each of these two axes a maximum of  $\pm 1.0$  mm to re-center the chopper blades on the star image. This needs to be done to an accuracy of about  $\pm 0.1$  mm. One way to sense the



required motion is to mount a near-infrared (IR) photodiode and a quadrant silicon cell as shown in Fig. 5-7. One then autocollimates through the telescope, off the plane surface of the corrector plate, to the silicon cell nulling the silicon cell output. The chopper does not chop beam coming from the photodiodes and falling on the silicon cell. To increase the energy reflected from the corrector plate, it could be coated with a near IR reflector dichroic multi-layer coating. This coating has about 85 percent transmission across the visible and 95 percent reflectance in the vicinity of 8000-9000 Å. Preferably the motions of the outer shell relative to the telescope will be small enough during operation that one would not have to recorrect midway through the year. Photocathode nonuniformity errors could be totally eliminated by continually nulling this sensor.

In the High Altitude Observatory - ATM experiment the internal occulting disk drives in two axes in steps of 10 microns over  $\pm 5$  mm. The SRS telescope required two axes,  $\pm 1$  mm with about 100 $\mu$  steps.

### 5.1.3 Telescope Signal-to-Noise

The telescope motion due to jitter plus the dither must be small enough that the telescope always remains aligned to the star to 0.05 arc-second. The servo analysis shows that telescope noise is the predominant cause of jitter. Also, to limit the accelerations on the gyro by the control system and to keep the valves from being driven to a sizable part of their range, noise must be kept low. The requirement established for this study was 0.03 arc-second in a 100 radians per second bandwidth.





The output noise of a telescope referred to angular input is:

$$\phi_n = \frac{\text{noise current at cathode}}{\text{angular gain referred to cathode current}} = \frac{I_n}{2G}$$

$$2G \sim \frac{\text{peak current}}{0.7 \text{ image radius}} = \frac{I_s}{0.7 \frac{1.22\lambda}{D}} \sim 1.64 \cdot I_s$$

for the satellite telescope.

Combining the above equations gives:

$$\phi_n = \frac{I_n}{1.64 I_s}$$

The required noise current referred to the cathode is:

$$I_n = \phi_n (1.64 I_s) = 0.049 I_s$$

Since the noise is a function of the peak signal output, it is useful to use required signal-to-noise ratios to specify the noise of the telescope. This ratio is:

$$\frac{I_s}{I_n} = 20$$

The noise from the telescope is "shot noise" caused by the granularity of the electron released by the photon. The equation for this noise is:

$$S/N = \left[ \frac{I_s}{2Ke \Delta f} \right]^{1/2}$$



where

$K$  = ratio of anode to cathode noise ( $\sim 1.5$ )

$e$  = charge on the electron ( $1.6 \times 10^{-9}$  coulombs)

$\Delta f$  = bandwidth (100 rad/sec)

The following table gives the predicted results for a silicon cell and an S-20 photocathode:

Detector	S/N Ratio	
	<u>Rigel</u>	<u>Procyon</u>
Si ( $T = 100^\circ\text{K}$ )	87	75
S-20 ( $T = 210^\circ\text{K}$ )	250	190

Photon noise is the limiting noise source for the S-20 detector. Electronic noise is the limiting source for the Silicon cell. Silicon cell noise level is extrapolated from measurements made at BBRC of 0.1 picoamp at  $T = 300^\circ\text{K}$  and  $\Delta f = 160$  Hz. The S/N ratio for the Si detector is not appreciably above the requirement, and therefore we have selected the S-20 detector although the silicon detector should not at this moment be discounted. If the margin remains as the system becomes better defined, a silicon cell may be feasible.

The photon noise current for the S-20 detector is:

	<u>Rigel</u>	<u>Procyon</u>
S-20	$1.5 \cdot 10^{-15}$ ampere	$1.2 \cdot 10^{-15}$ ampere

Dark current at the cathode is about  $10^{-15}$  to  $10^{-16}$  ampere at  $20^\circ\text{C}$ ; at  $-40^\circ\text{C}$  to  $-55^\circ\text{C}$ , the dark current should be  $10^{-17}$  to  $10^{-18}$  ampere.



Albedo shining on the photocathode (high voltage off) would increase this to  $10^{-15}$  to  $10^{-16}$  ampere. Therefore, the other noise sources are not significant.

The angular error corresponding to the anticipated telescope noise is  $6 \times 10^{-3}$  arc-seconds for Rigel and  $10 \times 10^{-3}$  arc-seconds for Procyon in a bandwidth of 100 radians per second.

#### 5.1.4 Error Analysis

##### 5.1.4.1 Telescope Linearity Degradation

Figure 5-9 shows the linearity error as a function of pointing error for different obscuration ratios ( $\gamma$ ). Roof prism widths ( $\delta$ ) up to  $0.5\mu$  were tried and did not noticeably affect linearity. The telescope is assumed to have a focal length of 250 cm. These results and those of Fig. 5-12 were obtained through the following analysis performed on BBRC's IBM 1130 computer.

The polychromator Modulation Transfer Function (MTF) of the system is the weighted average of monochromatic coherent MTF's. Let  $R(\lambda)$ ,  $T(\lambda)$  and  $H(\lambda)$  be the relative spectral detector response; optics spectral transmission, and source spectral intensity, respectively.

$$M(f) = \frac{\int_0^\infty \tilde{M}(f, \lambda) R(\lambda) T(\lambda) H(\lambda) d\lambda}{\int_0^\infty R(\lambda) T(\lambda) H(\lambda) d\lambda}$$

where  $f$  is spatial frequency in line pair/rad.

It can be shown that

$$M(f, \lambda) = \frac{A(z, 1) + \gamma^2 A\left(\frac{z}{\gamma}, 1\right) - 2A(z, \gamma)}{1 - \gamma^2}$$

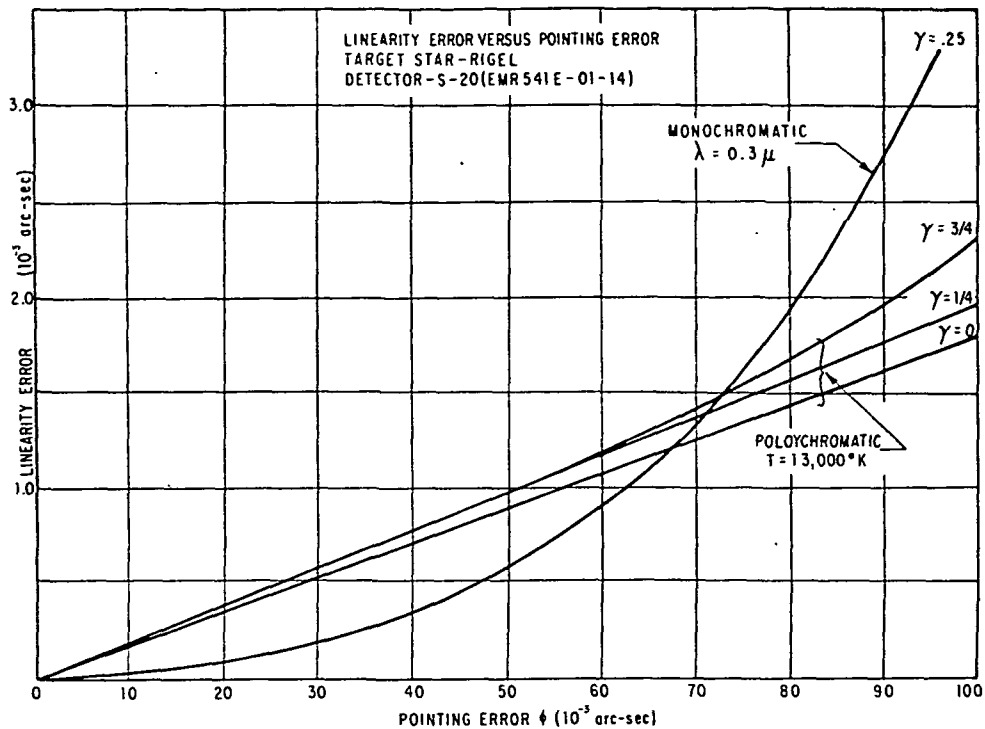


Fig. 5-9 Linearity Error Versus Pointing Error

where  $z = \frac{f\lambda}{2\pi D}$ ,  $D$  = aperture diameter,  $\lambda$  = wavelength,

and  $A(z, \gamma) = \gamma^2$  for  $0 \leq z^2 \leq (1-\gamma)^2/4$ ,

$$\begin{aligned}
 A(z, \gamma) = & \gamma^2 - \frac{2}{\pi} \sqrt{(z^2 - (1-\gamma)^2/4) \left( \frac{(1+\gamma)^2}{4} - z^2 \right)} \\
 & + \frac{1}{\pi} \cos^{-1} \left[ \frac{(1-\gamma^2)/4 + z^2}{|z|} \right] \\
 & - \frac{\gamma^2}{\pi} \cos^{-1} \left[ \frac{(1-\gamma^2)/4 - z^2}{\gamma|z|} \right]
 \end{aligned}$$



$$\text{for } \frac{(1-\gamma)^2}{4} \leq z^2 \leq \frac{(1+\gamma)^2}{4},$$

$$\text{and } A(z, \gamma) = 0 \text{ for } \frac{(1+\gamma)^2}{4} \leq z^2.$$

In these expressions  $\sqrt{\quad}$  is always positive and  $\cos^{-1}(\quad)$  is in the first or second quadrant.

Consider a roof prism of straight edges with a perfectly absorbing edge of width  $\delta$ . The angular output will be

$$y(\phi) = \frac{1}{\pi} \left[ \int_{-\infty}^{\phi-\delta/2} d\phi \int_0^{\infty} M(f) \cos(f\phi) df - \int_{\phi+\delta/2}^{\infty} d\phi \int_0^{\infty} M(f) \cos(f\phi) df \right]$$

Exchanging the order of integration and integrating over  $\phi$ :

$$y(\phi) = \lim_{t \rightarrow \infty} \frac{1}{\pi} \int_0^{\infty} \frac{M(f)}{f} \left[ \sin f\phi \Big|_{-t}^{\phi-\delta/2} - \sin f\phi \Big|_{\phi+\delta/2}^t \right] df$$

$$y(\phi) = \frac{2}{\pi} \int_0^{\infty} \frac{M(f)}{f} \sin f\phi \cos \frac{f\delta}{2} df$$

$$\frac{dy(\phi)}{d\phi} = \frac{2}{\pi} \int_0^{\infty} M(f) \cos f\phi \cos \frac{f\delta}{2} df$$

The error in linearity is given by

$$E(\phi) = \frac{\phi \left( \frac{dy(0)}{d\phi} \right) - y(\phi)}{\frac{dy(\phi)}{d\phi}}$$



As shown in Fig. 5-9, the effect of different  $\gamma$ 's (i.e., different MTF's) is reasonably small. In the computer program, an S-20 response and a dereflected gold coating were used to shape the spectrum.  $H(\lambda)$  was assumed to be a black body of temperature 13,000°K (i.e., Rigel).

Also shown is the linearity error for the monochromatic case in which the image spot is narrower than in the polychromatic case and therefore the response is more linear for small pointing errors and a less linear for large pointing errors.

To average pointing errors during data reduction, the inherent linearity must be less than 0.0005 arc-second over the allowed "linear" range. If the image and tracker are perfect (and stable), a linear range of  $\pm 0.050$  arc-second is achievable with nonlinearity less than 0.001 arc-second.

Since what really matters is the time averaged error, the 0.0005 arc-second is achievable because on the average the tracker will spend 67 percent of the time with pointing errors of less than 0.017 arc-second, and 32 percent of the time with pointing errors between 0.017 arc-second and 0.050 second. The average linearity error will be less than  $0.67$  (error at 0.017 arc-second)  $+ 0.32$  (error at 0.050 second)  $= 0.0005$  arc-second.

A detailed analysis of the data reduction scheme is required. If the system degrades to a very small degree (say for  $\gamma = 0.4$ , the null shifts  $5 \times 10^{-3}$  seconds), the linearity error will be greater than  $10^{-3}$  arc-second.



The linearity discussed above assumed no aberrations. This discussion shows this is a good assumption. Assuming a perfectly aligned telescope, coma is a possible limit to the usable range. The total tangential coma is approximately (this analysis assumes a telescope consisting of a paraboloidal primary and hyperboloidal secondary and tertiary mirrors)

$$C_t = \frac{3}{16(f\#)^2} \alpha$$

where  $\alpha$  is the field angle (angle between axis and star).

If  $D = 140$  mm,  $f = 2500$  mm

then  $f\# = 17.8$ , and

$$C_t = 5.9 \cdot 10^{-4} \alpha$$

If  $C_t < 1.0 \cdot 10^{-3}$  arc-second,  $\alpha$  must be  $< 1.7$  arc-seconds. (See the section on Telescope Tolerancing for a derivation of  $C_t = 1.0 \cdot 10^{-3}$  arc-second as being an allowable aberration.)

Since the proposed field angle  $\alpha < 0.05$  arc-second and the actual coma will not differ appreciably from the above derived result the telescope aberration will not limit the linear range of the system.



Nick in Roof Prism. Assume a nick which takes an energy fraction  $r$  of  $I_1$  and puts it in  $I_2$  where  $I_1$  and  $I_2$  are the opposing detector outputs if  $r = 0$ .

$$y_0 = I_1 - I_2$$

$$y = [1-r] I_1 - r I_1 - I_2$$

$$y = y_0 - 2r I_1$$

where  $r I_1$  is the detector output due to the energy intercepted by the nick.

Using  $G_1$  as a proportionality constant, assume

$$I_1 = G_1 \phi \text{ and } I_2 = -G_1 \phi$$

Therefore  $y_0 = 2G_1 \phi$

$$y = y_0 - 2rG_1 \phi = (1-r) G\phi \text{ with } G = 2G_1$$

$$\frac{dy}{d\phi} = G(1-r)$$

The effect is not strong if  $r \leq 10^{-2}$ . Now  $r \sim \frac{A_{\text{nick}}}{1/2\pi(0.5)^2}$  where

$A_{\text{nick}}$  = area of nick and  $1/2\pi(0.5)^2$  is roughly the area corresponding to  $I_1$ . The nick diameter is 0.06 arc-second. If  $f = 250$  cm the nick diameter is  $0.75\mu$ , which is the maximum tolerance nick size.

Image Non-uniformities and Instabilities. Assuming a perfectly uniform square image of side  $w$ , the output will be:

$y = 2 \times wK$  where  $x$  is the displacement from null and  $K$  is the gain constant depending on the transmission and the detector.



Assume there are voids and surpluses of area  $w^2 r$  as shown in Fig. 5-10,  $y(x) = 2Kw(x-rw)$ .

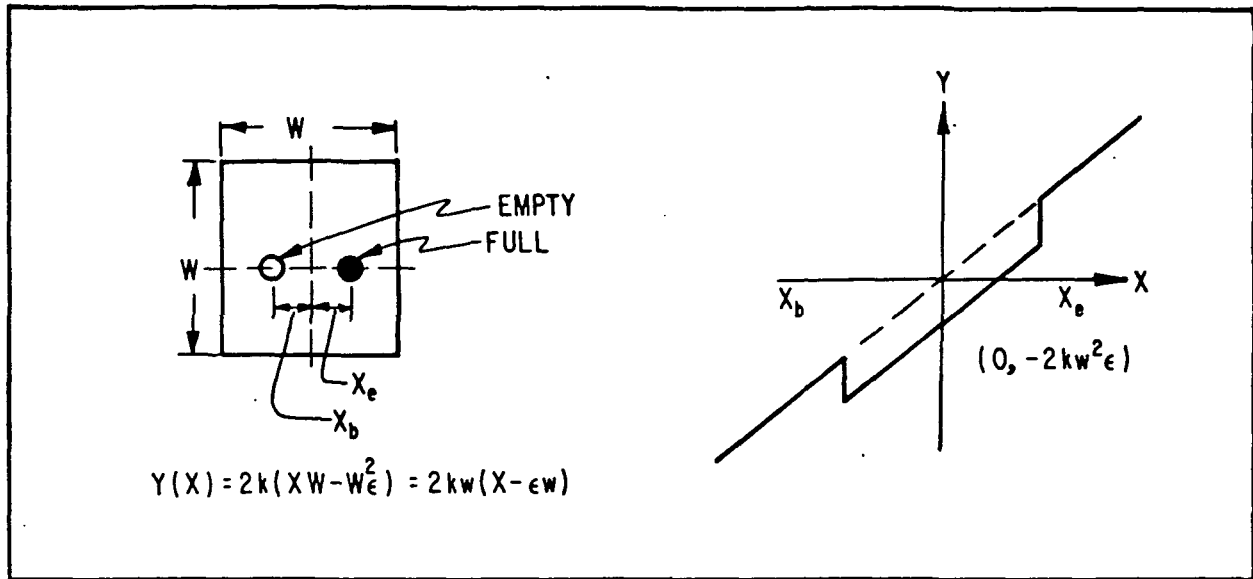


Fig. 5-10 Effects of Image Nonuniformity

If voids and surpluses are outside the  $3\sigma$  noise level, there is no problem. If they are in the linear range of excursion, the error in the data will depend on the time the image spends on them. If they are outside the  $1\sigma$  noise level, they should not cause too much trouble because little time will be spent in that region.

If  $x_b$  is greater than the  $3\sigma$  noise level and  $x_e = 0$  (assume the surplus came into being after alignment), approximately one-half of the data will have an error  $Krw^2$  in it. This would average with the other half of the data to give an error  $Krw^2/2$  and the zero would appear to be offset by a distance  $\delta = rw/2$  where  $r$  is the fraction of the total area which appears in the spot. If  $\delta < 1/2 \cdot 10^{-3}$  arc-second is allowed, with  $w \sim 1$  arc-second then,  $\epsilon < 10^{-3}$  is required or the total size of the defects must be less than  $125 \text{ \AA}$ . Fortunately, rolling of the satellite will relax this by at least an order of magnitude.



This implies that the image intensity centroid needs to be stable to about 50 Å. The optical elements must be stable, the optical path evacuated, and telescope "hot-dog" deformation due to creep and thermal effects must be small to accomplish this. For an image motion of  $0.3 \times 10^{-3}$  arc-second, the hot-dog angle allowed is about  $10^{-3}$  arc-second. The effect is given by  $\delta = \beta\phi$  where  $\delta$  is the lateral image motion and  $\phi$  is the hot-dog angle. For a tube 20 cm diameter and 30 cm long (tube between primary and secondary mirrors),  $\Delta L = 8(5 \times 10^{-6})(10^{-3}) = 40 \times 10^{-9}$  cm is allowed as the change in length of one side with respect to the other:

$$\frac{\Delta L}{L} \sim \frac{40 \cdot 10^{-9}}{12} \sim 3.3 \cdot 10^{-9} = 0.0033 \text{ ppm}$$

Corning reports the instability of fused silica at room temperature to be 0.10 ppm for one year. This may be a problem. It certainly requires further study to determine the magnitude and time constant of the effect at liquid helium temperatures. Also, its dependence on strain birefringence and material history requires investigation. Taking the linear thermal expansion coefficient to be  $3.3 \cdot 10^{-9}/^{\circ}\text{K}$ , (see Table 5-3) the allowable temperature differential is  $0.6^{\circ}\text{K}$  across the tube.

#### Differential Darkening of Opposed Channels

$$y_o = I_1 - I_2 = K(T_1 - T_2)$$

Let,

$$I_1 = KT_1$$

$$I_2 = K(T_1 - \delta)$$

where  $T_1$  and  $T_2$  are the system efficiencies (including the beam splitter and chopper).



$$\frac{K\delta}{KT_1} \approx \frac{5 \cdot 10^{-4}}{0.87}$$

since 0.87 arc-second would be roughly the diameter of the image if it were uniform. Therefore,

$$\delta \approx 5.6 \cdot 10^{-4} \approx \frac{1}{1800}$$

Table 5-3  
LINEAR EXPANSION COEFFICIENT FOR FUSED SILICA

Fictive Temperature - 1273°K

<u>Temp °K</u>	<u><math>\alpha - 1/^\circ\text{K}</math></u>	<u><math>\Delta L/L</math></u>
0	0	0
1	$-4.1 \times 10^{-10}$	---
2	$-33 \times 10^{-10}$	$-0.1 \times 10^{-8}$
3	$-111 \times 10^{-10}$	$-0.6 \times 10^{-8}$
4	$-263 \times 10^{-10}$	$-1.9 \times 10^{-8}$
5	$-513 \times 10^{-10}$	$-5.0 \times 10^{-8}$

Fictive Temperature - 1573°K

<u>Temp °K</u>	<u><math>\alpha - 1/^\circ\text{K}</math></u>	<u><math>\Delta L/L</math></u>
0	0	0
1	$-3.5 \times 10^{-10}$	---
2	$-28 \times 10^{-10}$	$-0.1 \times 10^{-8}$
3	$-95 \times 10^{-10}$	$-0.54 \times 10^{-8}$
4	$-224 \times 10^{-10}$	$-1.7 \times 10^{-8}$
5	$-438 \times 10^{-10}$	$-4.1 \times 10^{-8}$

$$\alpha = -(4.1 \pm 0.1) 10^{-10} T^3 \text{ for Fictive Temperature} = 1273^\circ\text{K}$$

$$\alpha = -(3.5 \pm 0.2) 10^{-10} T^3 \text{ for Fictive Temperature} = 1673^\circ\text{K}$$

T is in °K



If one fiber in a 200-fiber bundle broke,  $\delta$  would change by 10 times than this value. If the fiber rupture were intermittent, the problem would be more serious. The relay mirror system concept with mirrors coated at the same time should be sufficiently stable. Rolling the satellite will allow errors of this sort to be detected in the data analysis and removed.

Gain Decay Due to Cathode Aging. Measured data on EMR photo-multipliers shows photocathode efficiency decays to 50-60 percent of its original value after one year with a cathode load of  $J \approx 1 \mu\text{a}/\text{cm}^2$ . The photocathode decays exponentially with time to this value for the total time integrated charge corresponding to  $1 \mu\text{a}/\text{cm}^2$  for one year.

- Target Star Exposure

$$J \approx \frac{0.4 \cdot 10^{-12} \text{ amp}}{10^{-2} \text{ cm}^2} = 4 \cdot 10^{-5} \mu\text{amp}/\text{cm}^2$$

This is small compared to  $1 \mu\text{a}/\text{cm}^2$  so this effect will not cause appreciable degradation.

- Albedo (from the earth, moon or a planet) can be as high as 70 percent of the solar intensity, if bright local areas are extended over a hemisphere of viewing angle. The average flux over the earth and for the one year mission life is more like 10 percent. The moon and planets do not have appreciably higher surface brightnesses and are seen less often so the earth albedo is the important input. The albedo input to a 3 arc-minute diameter cone is

$$0.1 \frac{\pi \left( \frac{3}{3437} \right)^2}{2\pi} = 10^{-8}$$



of solar flux. This is 20.0 stellar magnitudes. Thus, this input produces  $-26.7 + 20.0 - 0.3 = 7.0$  magnitudes,  $\sim 600$  more current than the guide star; i.e.,  $0.02 \mu\text{a}/\text{cm}^2$ . If the detector saw the albedo for a full year, we would expect the sensitivity to approach a 50 percent decreased. Hence, the high voltage must be turned off when the albedo will be seen. If the moon or a planet flashed through the field of view there will be no noticeable decay.

S/N Decay Due to Anode Aging. The other phenomenon which causes a photomultiplier degradation is anode fatigue. The effect occurs quicker than cathode fatigue. It is a function of the current through the dynode string and appreciable fatigue occurs for anode currents of 10-20  $\mu\text{amp}$ . For anode currents less than 1  $\mu\text{a}$ , the fatigue is negligible. This effect can be totally eliminated by limiting the current in the dynode string.

- Target star exposure:

$I_{\text{anode}} \sim 0.4 \times 10^{-12} \times 10^6 = 0.4 \mu\text{a}$  where a gain of  $10^6$  is assumed, so the telescope will have no problem here.

- Albedo (high voltage on):

$$I_{\text{anode}} \sim 0.4 \times 10^{-10} (4 \times 10^3)(10^6) = 0.16 \text{ amp}$$

This also shows the high voltage should be turned off when exposed to earth albedo and the anode current must be limited.

Image Motion on Photocathode. Assume each beam has a total area  $A_0$  and an area  $A$  of it is not overlapped. Image motion on a non-uniform photocathode shifts the null.



Again this effect can be detected by satellite roll. The maximum allowable null shift is about 0.0005 arc-second for a non-rolling satellite. This implies that the difference in the output must be:

$$\Delta i < \frac{i_s}{2000}$$

For Rigel, the cathode current is  $i_s \sim 0.4$  pa and  $\Delta i < 0.4 \times 10^{-3}$  pa  
 $\Delta i = AK(\eta_{1av} - \eta_{2av}) = AK(\Delta\eta)_{av}$  where  $K$  is a gain constant and  $\eta_{iav}$  are the average quantum efficiencies in the non-overlapped regions of the  $i^{th}$  channel ( $i = 1, 2$ )

$$i_s \equiv A_o K \eta$$

$\Delta\eta_{av}$  must be such that the following is true:

$$AK \Delta\eta_{av} \leq \frac{A_o K \eta}{2000}$$

$$\Delta\eta_{av} \leq \frac{A_o \eta}{A(2000)} \sim \frac{A_o}{A} (5 \times 10^{-5}) \text{ with } \eta \approx 0.1$$

If  $A_o/A = 10$ ,  $\Delta\eta_{av} \leq 5 \times 10^{-4}$ . This case can be achieved optically with the reflective relay system and possibly with the fiber optic relay system.

If  $\frac{A_o}{A} = 100$ ,  $\Delta\eta_{av} \leq 5 \times 10^{-3}$ . At least a 99 percent overlap is desired.

More work needs to be done to determine if these average quantum efficiencies are achievable.



Errors caused by average cathode degradation can also cause errors. If a drive system kept the image centered within distance  $\delta$  as shown in Fig. 5-11, the allowable variation with time is derived as follows:

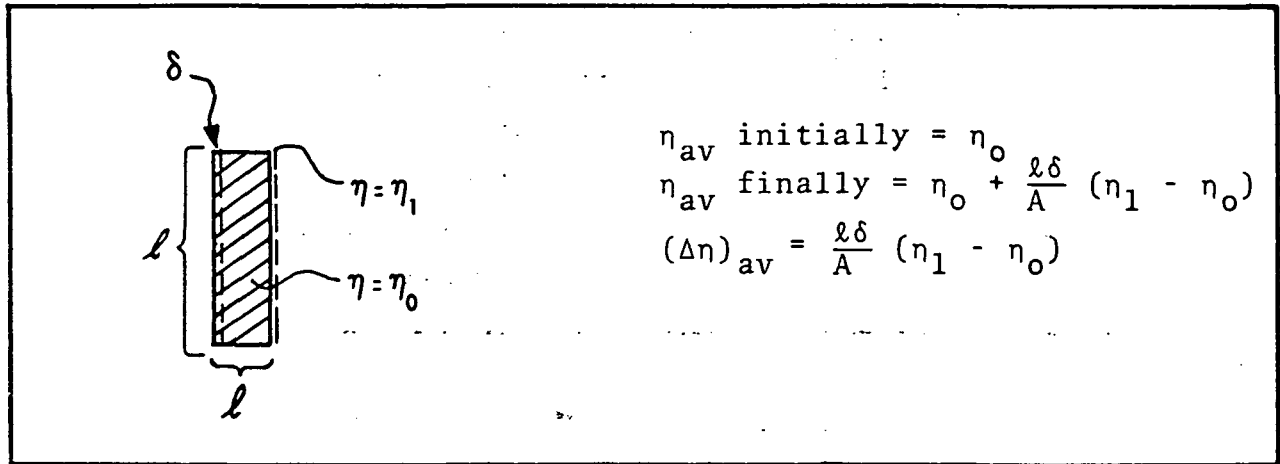


Fig. 5-11 Image Offset

If  $\ell$  is in mm and  $A$  is in  $\text{mm}^2$   $(\Delta \eta)_{av} = \delta (\eta_1 - \eta_0)$  since  $\ell = 1 \text{ mm}$  and  $A = 1 \text{ mm}^2$ . If  $\eta_0 = 0.1$  and  $\eta_1 = 0.095$ ,  $(\Delta \eta)_{av} = \delta (0.01) < 5 \times 10^{-3}$  assuming a 95% overlap. Thus  $\delta \leq 0.2 \text{ mm}$ .

Companion Star in Field-of-View. A companion star in the field-of-view has the effect of shifting the tracker null towards the companion. Hence two effects occur:

- There is a null offset which can be taken out during data reduction if the companion star parameters are known.
- The linear range is no longer divided equally about null. Here it is assumed that the Airy patterns from the two stars do not overlap appreciably.



If the target star is Rigel, the ratio of intensities between Rigel and its companion 9.4 arc-seconds away is roughly  $(2.512)^{6.4} = 590$ . Since the companion would not be divided by a roof prism, it would be equivalent to a source  $1/295$  as bright as the target star. From Fig. 5-12 this would be equivalent to an offset of about  $4 \times 10^{-3}$  arc-second. The linear range is effectively reduced by about  $4 \times 10^{-3}$  arc-second due to the companion star. The satellite will jump by  $\pm 4 \times 10^{-3}$  arc-second as this star crosses the roof prism during the roll cycle. Since the location of this companion is known and the step change takes place in the data, the effect of the companion can be satisfactorily accounted for.

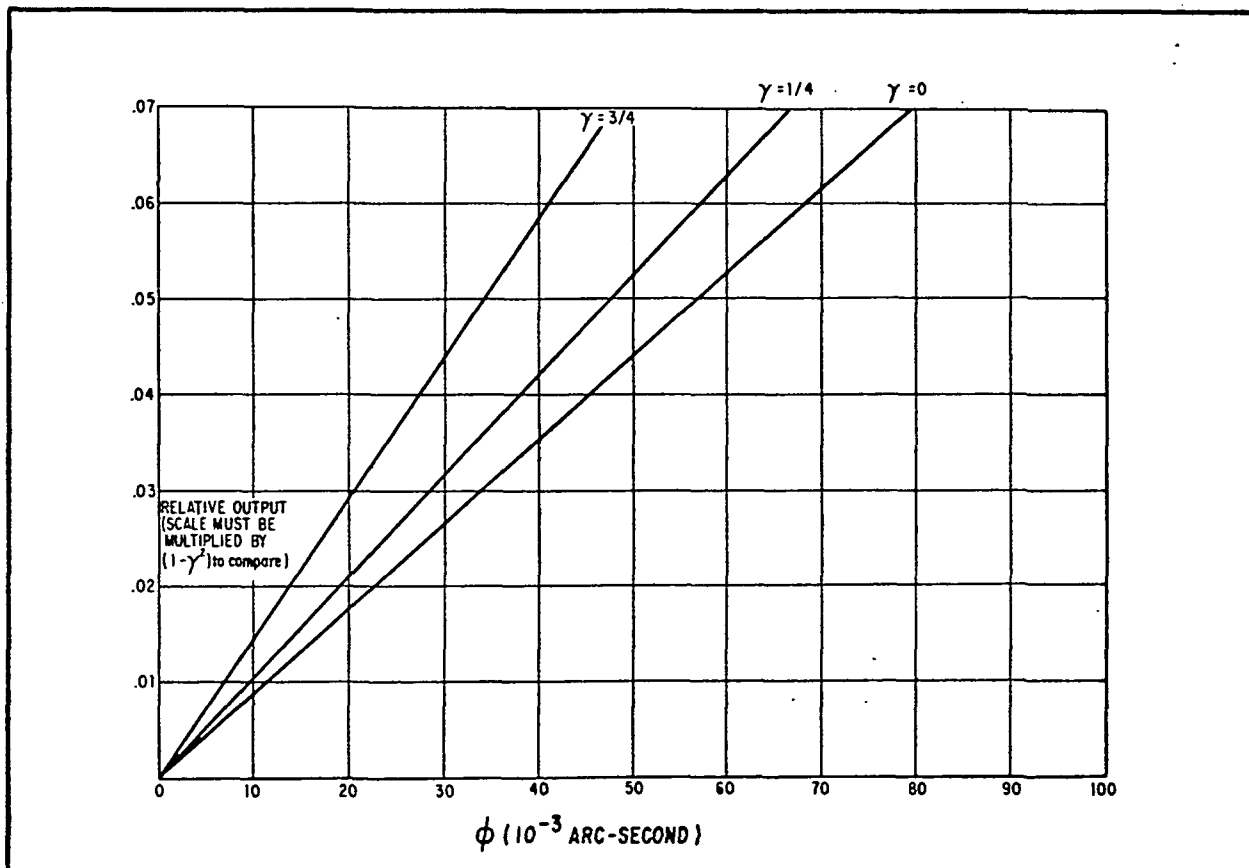


Fig. 5-12 Position Detector Angle Versus Error Angle





#### 5.1.4.2 Telescope Tolerances

In Para. 4.1.4.1, it was shown that the aberrations of an aligned telescope are small over the field-of-view which is used in the satellite telescope. This section derives the alignment tolerances which the components must meet or exceed in order that the telescope may be considered aligned. It also derives the allowable image blur which is in turn used to derive mirror element motion tolerance during operation and which was also used in Para. 4.1.4.1 to show that the operating field of the telescope is not limited by aberrations.

As in Para. 4.1.4.1 we will consider only third-order coma, which is linear with field angle, since third-order spherical aberration will be removed by figuring the corrector plate and third-order astigmatism will be small compared to coma since astigmatism varies with the square of the field angle.

The total angular length of the comatic pattern in the paraxial focal plane of the telescope due to a field angle at the secondary or tertiary mirrors is:

$$C_{t_i} = \frac{3a_i}{4} \left( \frac{1}{f_i^\#} \right)^2 \alpha_i \beta_i, \quad i = 2, 3$$

$\alpha_i$  = field angle at the appropriate mirror

$\beta_i$  = obscuration ratio

$a_i = -1/4 (m_i^2 - 1)$

$m_i$  = the mirror's magnification

$f_i^\#$  =  $f$ /number of beam leaving  $i^{\text{th}}$  mirror

$i = 2$ , secondary

$i = 3$ , tertiary



The secondary mirror's aberration is affected by the tertiary. The  $\beta_i$  and  $f_i^\#$  factor accounts for this in the secondary contribution  $C_{t_2}$  and also scales the tertiary contribution  $C_{t_3}$ .

The corresponding formula for the primary mirror is:

$$C_{t_1} = \frac{3 \alpha}{16 (f_1^\#)^2}$$

The applicable telescope parameters from Table 5-2 are

$$m_2 = 3.65, m_3 = 2.03, f_1 = -337.5 \text{ mm}, D = 140 \text{ mm}$$

$$f_1^\# = 2.41, \beta_2 = 0.33, \beta_3 = 0.15$$

Solving the above equations with these values gives:

#### COMATIC CONTRIBUTIONS

<u>Primary</u>	<u>Secondary</u>	<u>Tertiary</u>
0.032 $\alpha$	-0.010 $\alpha$	-0.0003 $\alpha$

Where  $\alpha$  is the angle of incidence with respect to the element in question (i.e., the tilt misalignment angle).

It is of interest that in the aligned telescope,  $\alpha_2 = -\frac{\alpha}{\gamma_2}$  and  $\alpha_3 = -\frac{\alpha_2}{\gamma_3}$ .

Initial Alignment. The Airy disk will have a diameter of about 1.9 seconds of arc. If we allow initial alignment aberrations to be 1/4 of this, then the allowed  $\alpha$  is ~14 arc-seconds for the primary,  $\alpha \sim 45$  arc-seconds for the secondary,  $\alpha \sim 1500$  arc-seconds for the tertiary. These effects will add (or cancel) but one can see that



the primary to secondary alignment is the most critical. However, 10 arc-seconds uncertainty in the primary optical axis (with respect to the telescope's optical axis) will suffice. This corresponds to  $1.3 \times 10^{-4}$  cm at the secondary. Ten arc-seconds is tight but achievable.

During Operation. The aberration allowed depends on the data analysis scheme (i.e., on the way the linearity error averages). Probably the worst case would be a delta function intensity spike on top of the Airy disk. This would put a step function into the telescope output versus error angle curve.

Aberrations would not add such a spike but would tend to smear the image in a manner which depends on the aberration present. Normally one applies Marechal's criteria, allowing the RMS deviation of the wavefront to be  $\lambda/14$ . This is usually stated as being  $\lambda/4$  peak-to-peak error in the wavefront with the assumption of randomness implied. The allowed tolerance of the wavefront depends on the type of aberration present, the maximum deviations from the Gaussian reference sphere being  $0.94\lambda$  for spherical aberration,  $0.60\lambda$  for coma, and  $0.35\lambda$  for astigmatism\*.

For imagery applications, these errors are allowable. For this application they are not allowable. In fact, Figure 9.8 of Born and Wolf\* shows the comatic result of a wavefront error of  $1/2$  the tolerance given by the Marechal criteria. A significant amount of energy is placed in a non-symmetrical moon-shaped region adjacent to the center spot. The comatic size and shape is roughly

---

\*Born, Max and Emil Wolf, Principles of Optics; Electromagnetic Theory of Propagation Interference and Diffraction of Light, 4th Ed. New York: Pergamon Press, 1969, Chapter 9.



approximated by the third order aberration size. Hence, to maintain the centroid of the energy to angles like 0.0005 arc-second, the third order aberration (tangential comatic length), should be constant to  $\sim 0.001$  arc-second. This implies alignment stability of the order of 0.030 arc-second. An angle of 0.030 arc-second over 20 cm (telescope diameter) corresponds to a displacement of roughly  $200 \text{ \AA}$ . This is much larger than the stability required between image position and the roof prisms, so aberrations should not cause a problem.

#### 5.1.5 Target Star

A guide star, close to the celestial equator and as far as possible from the ecliptic must be sought. This defines a region in the Northern hemisphere near a right ascension of 18h or in the Southern hemisphere near a right ascension of 6h.

The only bright star available near right ascension of 18h is  $\alpha$  Ophiuchus. Its proper motion, however, is rather large. This limits the choice to stars near or in the Southern part of Orion. Among these, Rigel stands out as having a very small proper motion, due to its large distance and being out of the Milky Way. Procyon was considered at one time but it is farther from 6 hours than desired, is in the Milky Way and is only about  $20^\circ$  from the ecliptic.

Therefore, Rigel is the most attractive star. Data for stars Procyon and Rigel are given below:



								Proper Motion		Standard	
								Deviation			
	R.A.				DEC.			R.A.	DEC.	R.A.	$\delta$
	m	h	m	s	°	'	"	arc-sec.	arc-sec.	arc-sec.	arc-sec.
Rigel	0.3	5	12	7.990	-8	15	28.65	-0.003	-0.002	0.001	0.001
Procyon	0.5*	7	36	41.117	5	21	16.81	-0.710	-1.029	0.000	0.001

Reference: Smithsonian Astrophysical Observatory Star Catalog

\*Combined magnitudes of component stars.

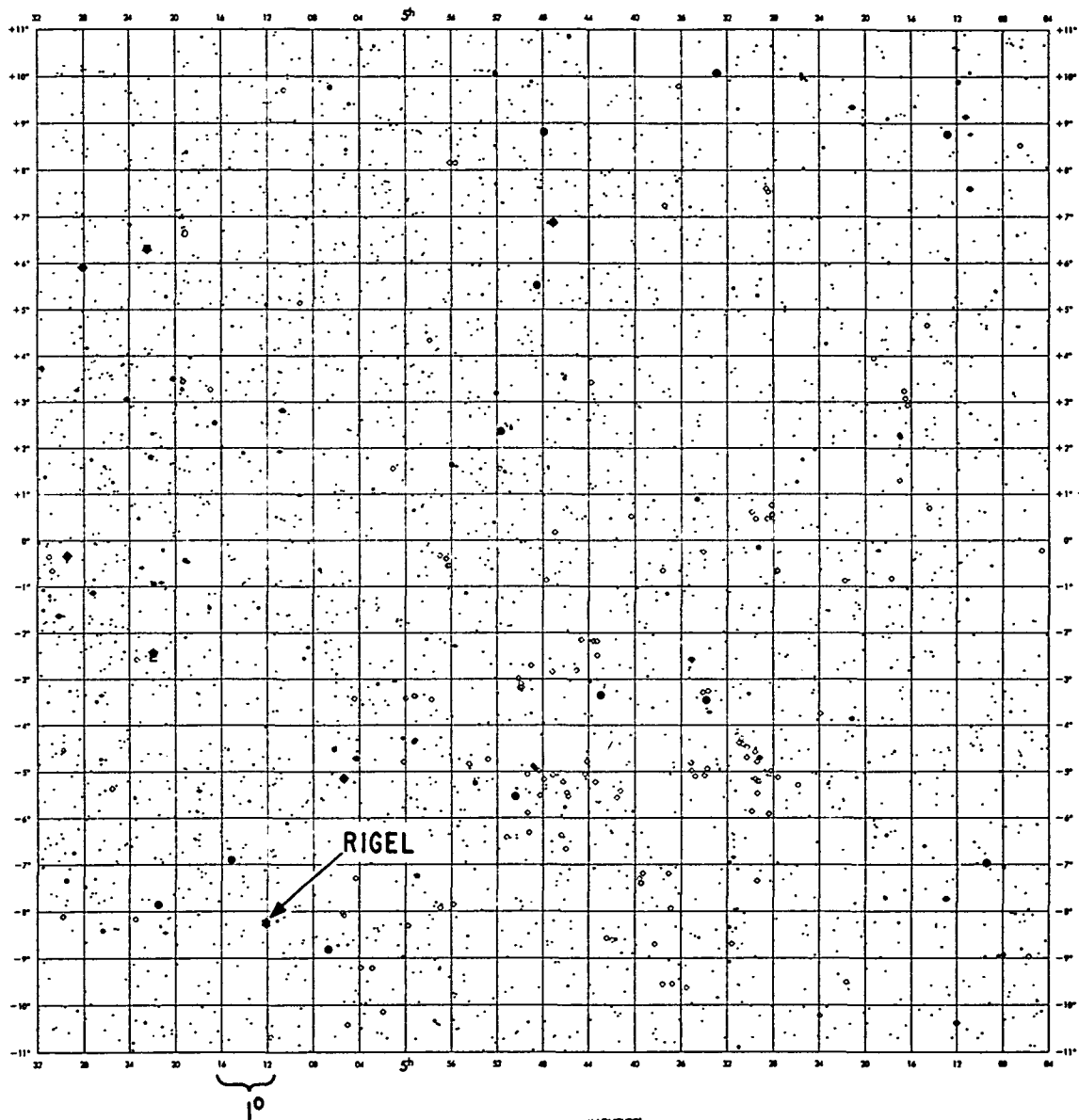
Note that Procyon has a large proper motion.

Rigel has a companion 9.4 arc-seconds away, of magnitude 6.7. The problem created by the companion star is treated in the section on error analysis and shows this will not cause a serious problem. The other nearly stars are shown in Fig. 5-13. The next closest star is of  $m \approx 6.2$  and is  $\sim 15'$  away from Rigel, well outside of the field-of-view of the telescope.

Procyon is a double star with a number of nearby neighbors (see Fig. 5-14).

## 5.2 GYROSCOPES

One of the ground rules for the study was that the gyroscopes were to be assumed operable to the required accuracy. The work performed concerning the gyroscopes was mostly aimed at determining the requirements that the gyroscopes put on other systems and in defining these systems in a way that satisfied these requirements.



INDEX		
12	11	10
71	71	70
19	19	18

MAGNITUDES									
1	2	3	4	5	6	7	8	9	10
11	12	13	14	15	16	17	18	19	20
21	22	23	24	25	26	27	28	29	30
31	32	33	34	35	36	37	38	39	40
41	42	43	44	45	46	47	48	49	50
51	52	53	54	55	56	57	58	59	60
61	62	63	64	65	66	67	68	69	70
71	72	73	74	75	76	77	78	79	80
81	82	83	84	85	86	87	88	89	90
91	92	93	94	95	96	97	98	99	100

SAO STAR CHART - 1967  
EQUINOX AND EPOCH 1950.0  
FK4 SYSTEM  
MERCATOR PROJECTION  
SCALE 6/93<sup>h</sup>  
BANDWIDTH 10" - 10"

Fig. 5-13 Rigel Location and Neighbors

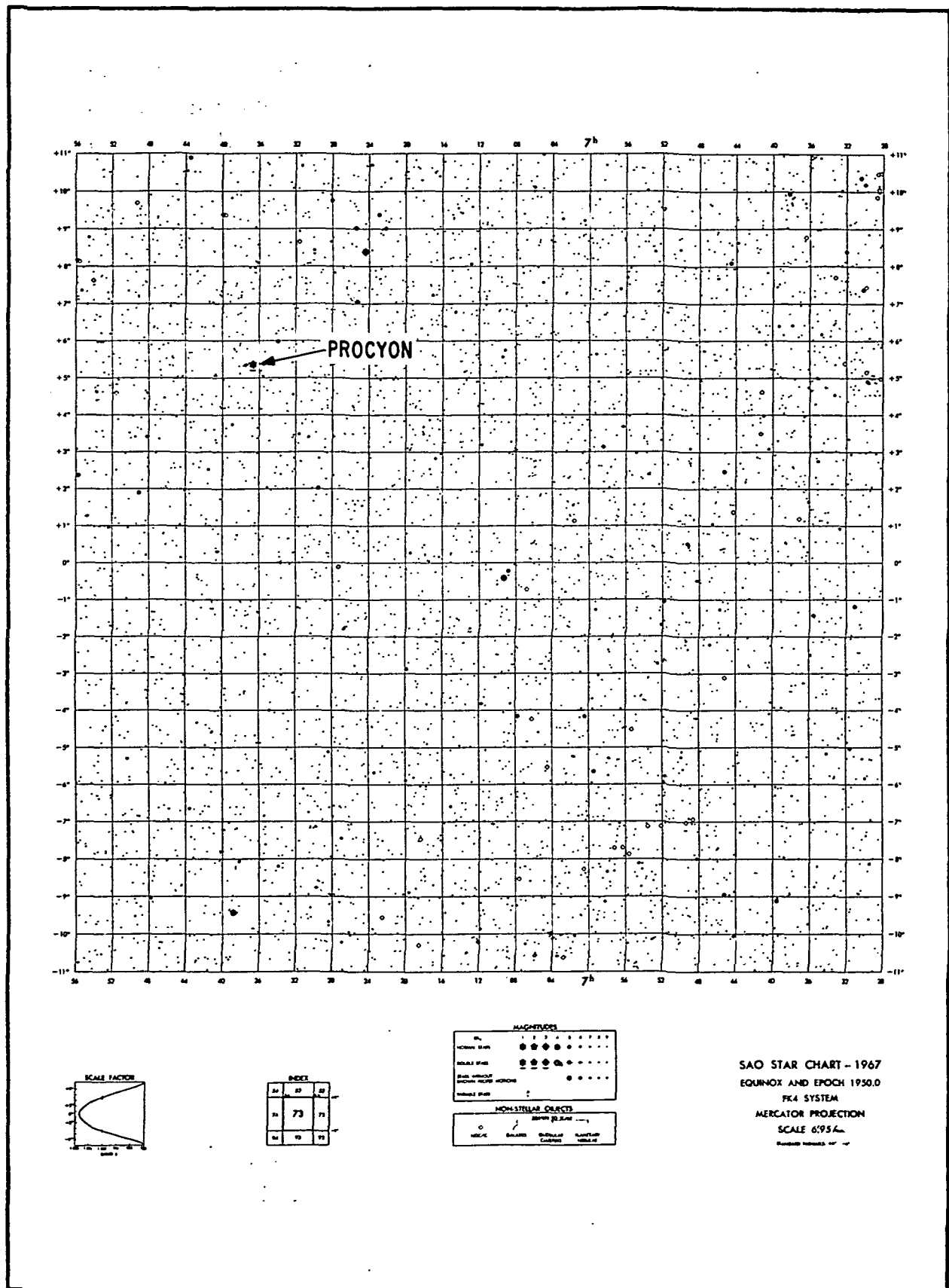


Fig. 5-14 Procyon Location and Neighbors



The error analysis and design of the gyroscopes was not addressed. Some work was done to lay out the plumbing and wiring to the gyroscopes and to determine how they might be located on the quartz block substrate. This resulted in a configuration concept which could be used as a basis for calculation of inertias and accelerations but is not sufficiently advanced to be considered anything more than that. It was known from the beginning that there were still some difficult development problems to be solved. These are described very briefly at the end of this section and are recommended for accelerated effort in the program plan for technology advancement.

#### 5.2.1 Requirements

The following table gives the performance and alignment requirements of the gyroscopes.

##### PERFORMANCE

Gyroscope drift and stability	}	<0.0006 arc-sec per year
Measurement drift and nonlinearity		
Linear range		±32 arc-sec

##### PARALLEL GYROSCOPE ALIGNMENT ACCURACY

Primary loop to telescope axis	±3 arc-sec
Secondary loop to telescope axis	±3 arc-sec
Tertiary loop to telescope axis	±10 arc-min
Spin axis to telescope axis	±3 arc-sec

##### PERPENDICULAR GYROSCOPE ALIGNMENT ACCURACY

Primary loop to telescope axis	±3 arc-sec
Secondary loop to telescope axis	±6 arc-sec
Tertiary loop to telescope axis	±6 arc-sec
Spin axis to telescope axis	0.6°





### 5.2.2 Gyroscope Description

The gyroscope design described here has been developed by Stanford in cooperation with Honeywell, Inc. It is described in considerable more detail along with a detailed discussion of errors in "The Stanford Gyroscope Experiment" by Dr. C. W. F. Everitt of Stanford University dated March 1971.

The gyroscope consists of three basic parts, a spherical rotor and two hemispherical shells comprising the housing, Fig. 5-15.

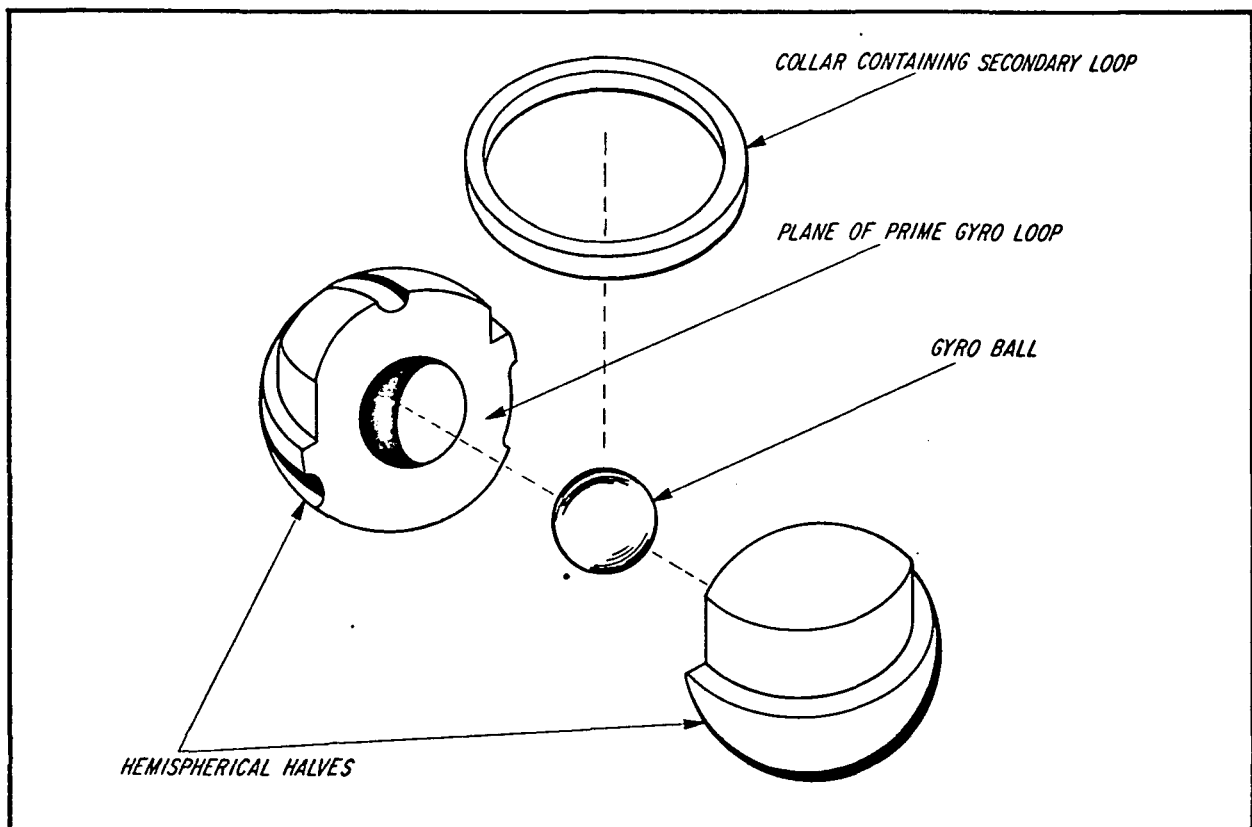


Fig. 5-15 Gyroscope Basic Parts



The 38.2 mm diameter rotor, made of fused quartz, is homogeneous to 1 part in  $10^6$  and spherical to  $2.5 \times 10^{-5}$  mm (1  $\mu$ in.). A thin niobium coating is placed on the ball to provide a metallic surface for the suspension system and to provide a superconducting surface to generate the London Moment field used to sense the orientation of the spin axis of the rotor.

The housing halves, also of fused quartz, have hemispherical cavities accurate to 20  $\mu$ in. On the inside of the housings, three pairs of mutually perpendicular suspension pads are located. Channels are machined into the inside surface of the housing to carry the spin up helium gas from its entrance port around the inside of the housing to the exhaust port. To prevent this gas from leaking into the area of the suspension pads during spin up, which could cause arcing, there are double raised ridges surrounding the suspension pads. The clearance between the ridges and the rotor is only  $3.8 \times 10^{-3}$  mm (150  $\mu$ in.). Multiple pumping ports between the pairs or ridges pull out any gas which passes the first ridge from the spin up channel, keeping the pressure below the arcing pressure. This low pressure gas is exhausted out of the gyroscope housing and its shield past the telescope to a large vent beside the telescope windows.

An alternate housing design is being developed at MSFC by Decher and Angele in which the spin-up channels are carried in a disk-shaped ring that is sandwiched between the two nearly hemispherical shells. This design avoids the very difficult task of machining the spin-up channels and the associated pumping grooves. Both designs are expected to be ready for a spin-up in the first quarter of 1972.



Three mutually perpendicular readout loops surround the gyroscope housing. On the Stanford design:

- The primary loop is deposited in a small groove on one of the faces of the hemispherical housing halves.
- The secondary loop is deposited on a ring that slides over the two hemispherical halves and seats on a reference surface. Its plane is perpendicular to the first loop.
- The third loop is perpendicular to the first two. Its method of attachment has not yet been determined.

The placement of the loops on the MSFC design has not yet been decided.

The loops and their performance are discussed in Section 5.3.2.1.

The gyroscope assembly is optically contacted, by pads in the plane of the primary loop, onto a fused quartz magnetic shield which consists of two hemispheres coated with a superconductor. This assembly is in turn optically contacted to the fused quartz block to which the telescope is contacted. The surface which is contacted is the one containing the primary loop.

The magnetic shields are a vital part of the gyroscope and present a severe design problem. The superconducting magnetic shield can be made to exclude the last quantum of flux, provided the shield is made superconducting while located within a field of less than  $10^{-6}$  gauss and provided there are no leakage paths in the shield. A



large facility for obtaining these low fields is being constructed at Stanford and would be used for this program. The problem of leakage paths is one which has not yet been solved completely. Where wires and spin up gas plumbing must penetrate the shield, a long, narrow superconducting tube can be used to surround the wire or pipe and act as a shield. A large cluster of these pipes is used for the low pressure gas venting. Where optical contacting takes place, there is a hole in the shield that cannot be protected in this way. The method shown in Fig. 5-16 and Fig. 5-17 uses small contacting pads with magnetic shields reaching around the pads. It is doubtful that this is a sufficient shield. This area needs much more work and is one of the areas recommended for accelerated effort during the technology advancement program.

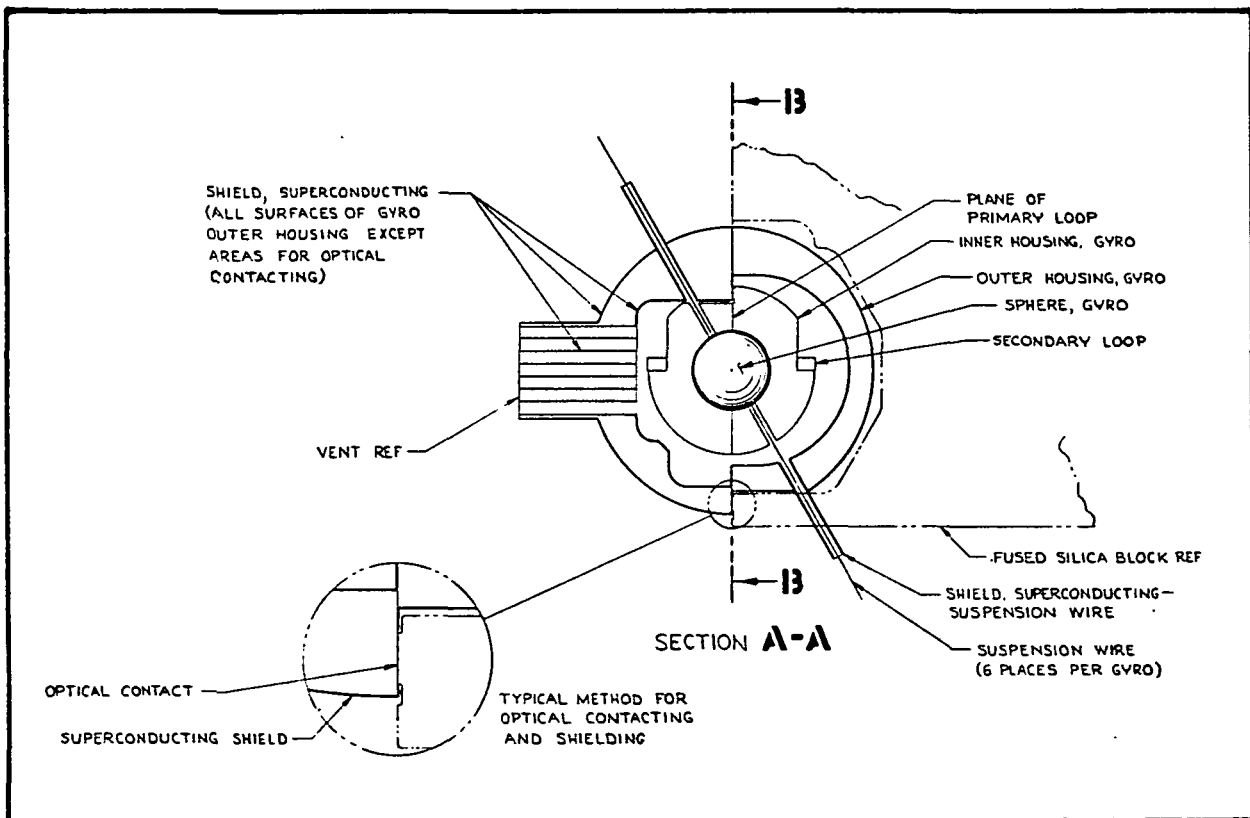


Fig. 5-16 Gyroscope Shielding Detail

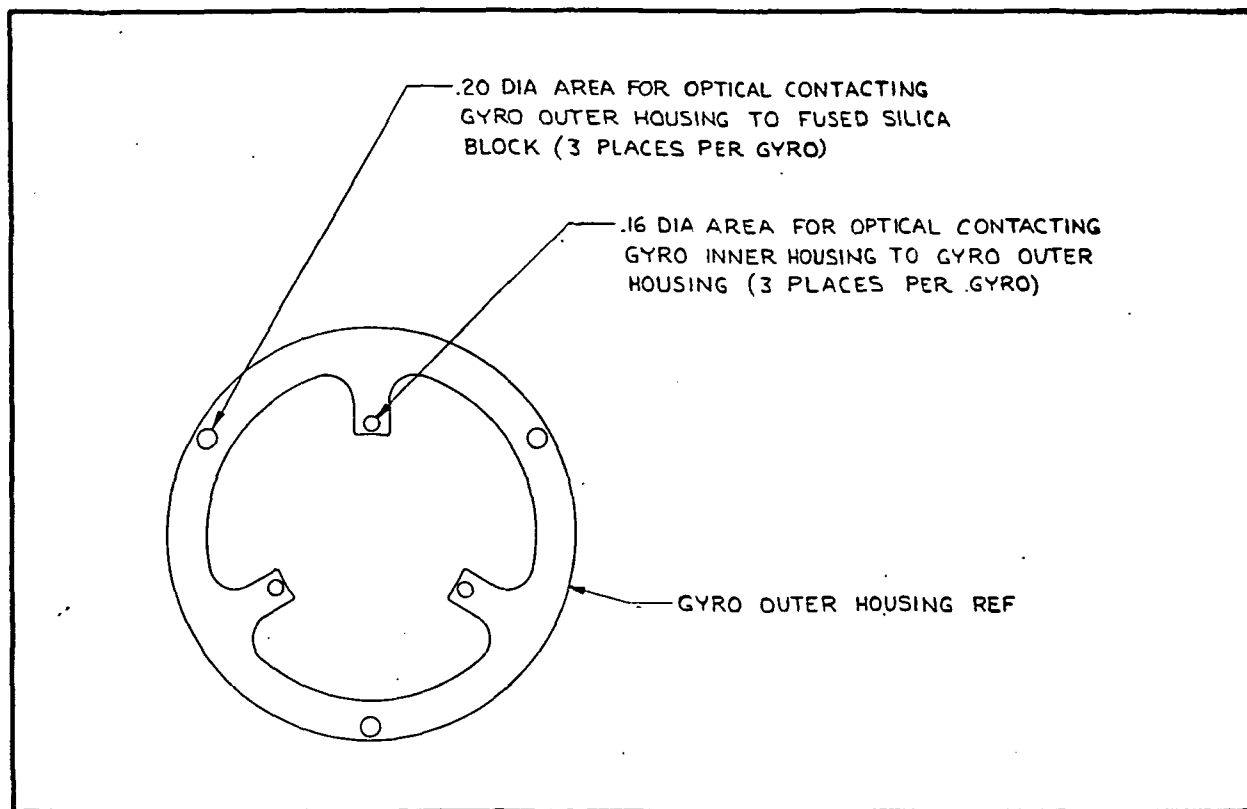


Fig. 5-17 Gyroscope Optical Contact

Tables 5-4 and 5-5 give a list and location of the wires and tubes which must penetrate the shield.

Figures 5-18 and 5-19 show the configuration of a quartz block used for the analysis with the gyroscopes mounted to it. An example of the plumbing complexity is shown.



Table 5-4  
WIRING PER GYROSCOPE

6	Suspension Wires -- Electrostatic bearing pads (special co-ax, center to electrode) shield to magnetic 10/1 shield.
1	Ground Wire -- Between electromatic pads connected to single ground wire out to room temperature.
1	Primary Loop -- Kapton strip to magnetometer
1	Secondary Loop -- Strip to magnetometer
1	Tertiary Loop -- Strip to magnetometer
3	Heater to null loops in gyro.

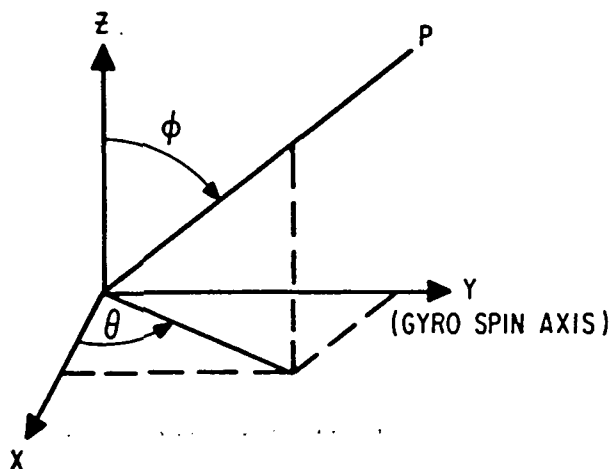
---

13



Table 5-5  
COORDINATES OF LEADS FORM GYROSCOPES

LEAD	SPHERICAL COORDINATES	
	$\theta$	$\phi$
Ground, between electrostatic bearing pads	110°	90°
Suspension Wire #1	0°	120°
Suspension Wire #2	120°	120°
Suspension Wire #3	240°	120°
Suspension Wire #4	60°	60°
Suspension Wire #5	180°	60°
Suspension Wire #6	300°	60°
Primary Coil Readout	290°	90°
Secondary Coil Readout	90°-100° or 260°-270°	90°
Tertiary Coil Readout	180°	90°
Super Conducting Shielded Vent		0°
		60°
Helium IN	20°	90°
Helium IN	160°	90°
Helium OUT	200°	90°
Helium OUT	340°	90°
Heater (for null or gyro)	280°	90°



Pri. Loop in XY Plane  
Sec. Loop in YZ Plane  
Ter. Loop in ZX Plane

Gyro Coordinate System

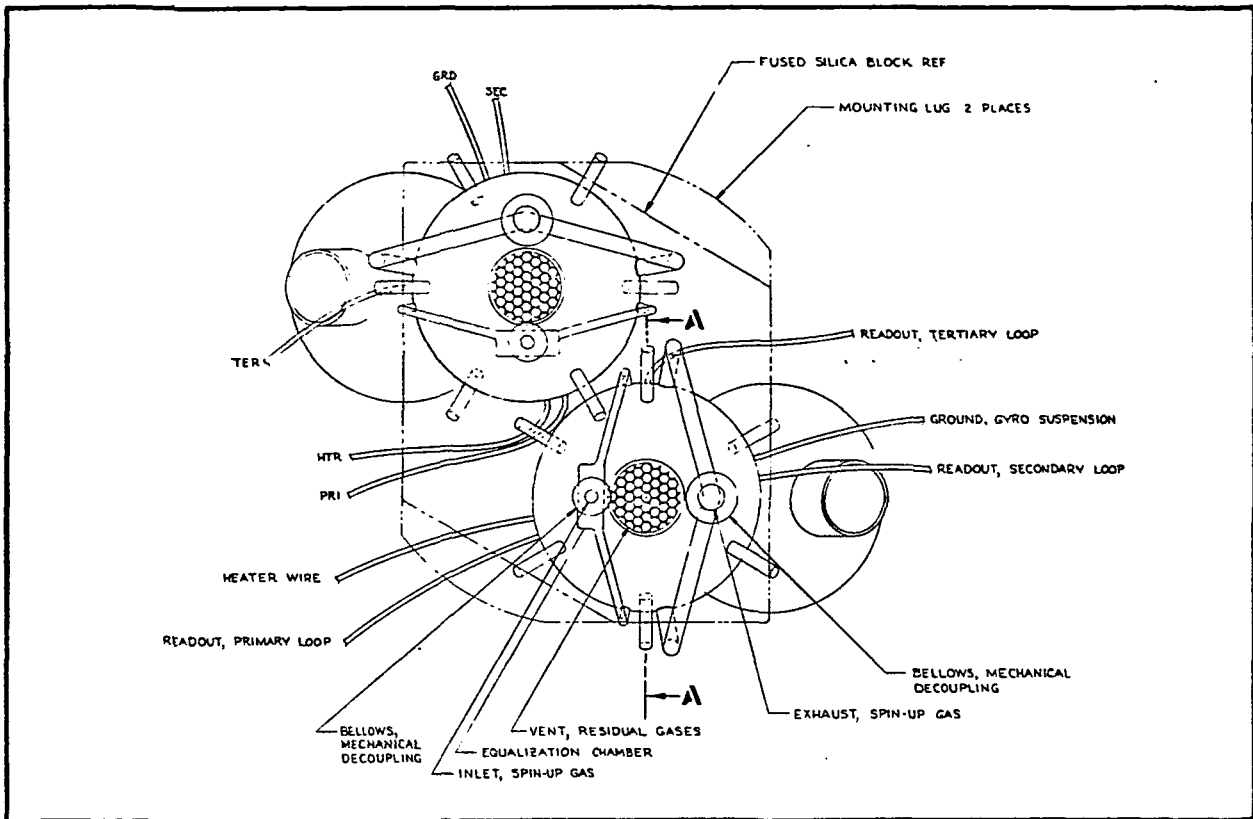


Fig. 5-18 End View of Quartz Block Assembly

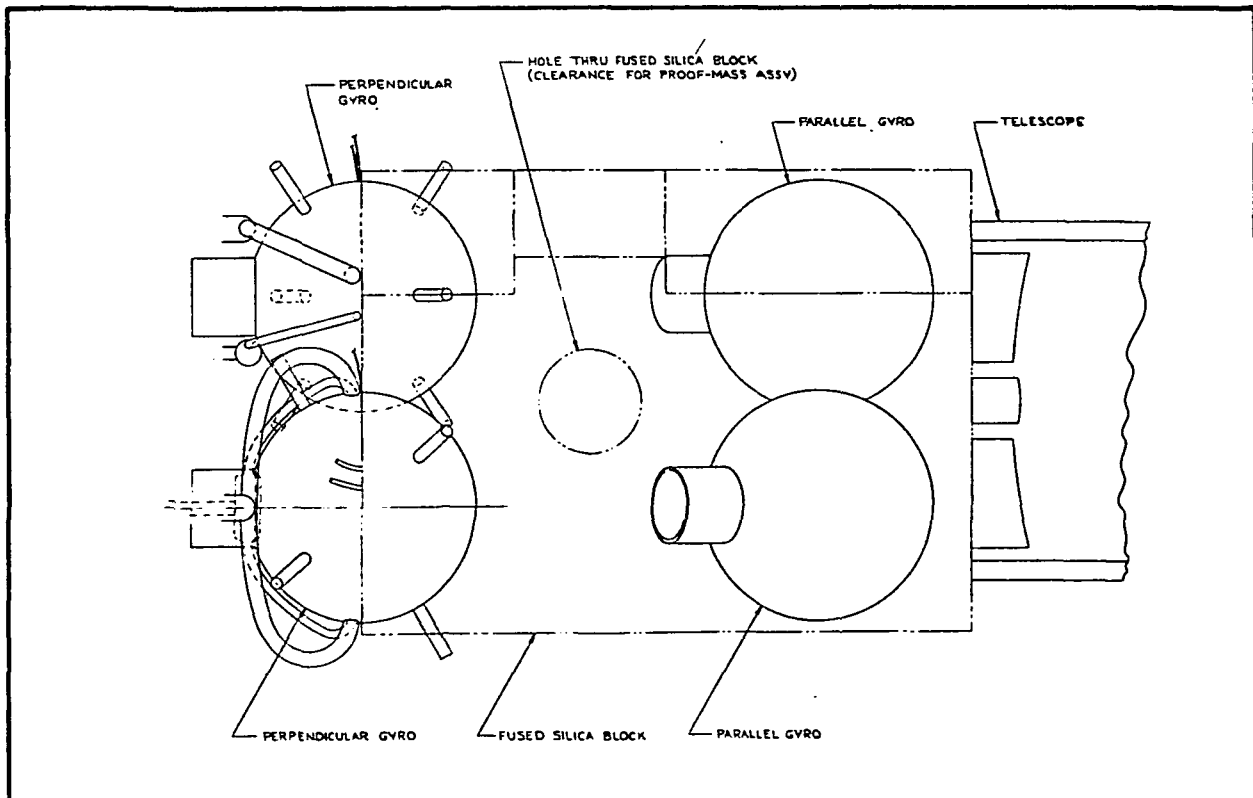


Fig. 5-19 Side View of Quartz Block Assembly





The shielded gyroscope assemblies are located on the instrument block as shown in Fig. 5-20. The arrow on each gyroscope shows its spin axis direction. In each case the primary loop vector (the vector perpendicular to the plane containing the primary loop) points either into or out of the block. In this manner, the primary loop can be initially aligned to the telescope axis to 3 arc-seconds by using sufficiently small manufacturing tolerances. It also makes use of the stability of the material and optical contact joint.

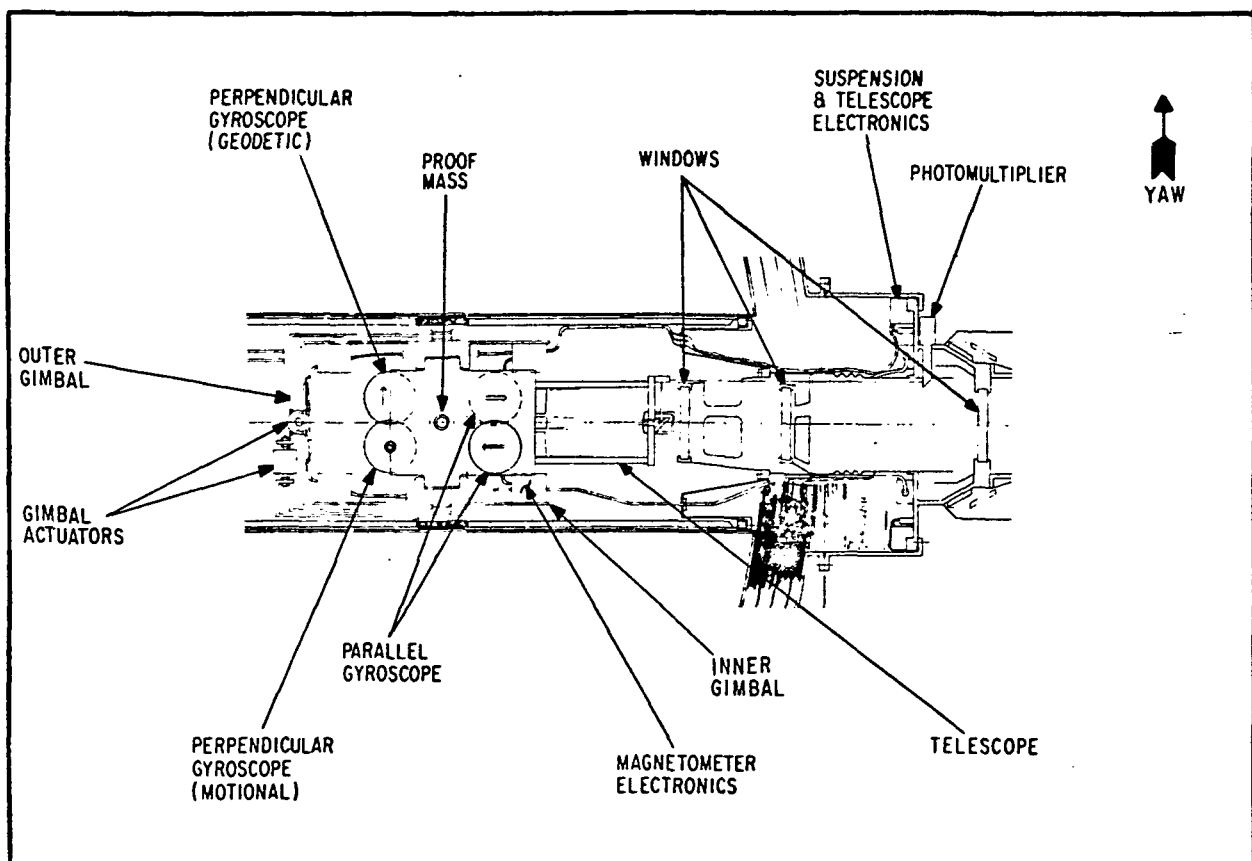


Fig. 5-20 Quartz Block and Window Portion of Dewar



To minimize the self-gravity effect on the perpendicular gyroscopes, fused quartz can be removed adjacent to the gyroscope and extra mass can be added to the Dewar adjacent to the gyroscope. The fused quartz would be removed by drilling holes in the block at the appropriate locations.

The proof mass assembly is located at the center of gravity of the satellite. It is attached to the gimbal ring. A hole is provided into the fused quartz block into which the proof mass assembly protrudes.

### 5.2.3 Optical Contacting

Optical contacting is a process by which two very flat, smooth and clean quartz surfaces fuse together. The surfaces are first placed together forming interference fringes. If the surfaces are sufficiently flat, smooth and clean, the fringes spread apart as the surfaces become more parallel. Finally no fringe remains and no demarcation line is visible. If at any time during the assembly of the quartz block an error is made, such as an inaccurate measurement or a shift in position as the contact joint is setting up, one may have to risk damaging the whole telescope in order to correct the error. Elaborate fixturing and great care are required to avoid this possibility.

If separation of the two pieces is required, it can sometimes be accomplished by heating (or cooling) one piece with respect to the other (as under running water). This technique will not be successful if the joint has sufficient strength for this application. If the joint will not separate under this thermal shock treatment, it is sometimes possible to separate it by rapping it with a soft hammer or if this fails by striking a razor blade placed along the joint. If this separates the two pieces along the joint, sometimes one will find chunks of one piece attached to the other piece, indicating the following:



- The pieces have not separated cleanly
- The optical contact joint is formed by the molecular transfer of material from one piece to the other piece across the demarcation line.
- The optical contact joint is not uniformly stressed.

BBRC has been unable to find any published literature on optical contacting. The theory of the process is not well understood. Certain optical manufacturing houses have been contacting pieces together for 10 years or so. By carefully controlling dimensions and angles, alignment accuracies of one second of arc can be held. The surfaces should be flat by  $\lambda/20$ , to reduce stresses in the final assembly, and have a very good optical polish. By this is meant the surface should be as smooth as can be achieved. Micro-ripple will probably be in the range of  $10\text{\AA} - 20\text{\AA}$  RMS with the present state-of-the-art. At this point one can begin to see the possible problem area concerning the stability of the joint. Small flats have been polished with microripple of  $7\text{\AA}$  RMS \*. The prime axes of the gyroscopes must be stable to better than  $0.5 \times 10^{-3}$  arc-second with respect to the telescope axis over one year. The required stability over one year is about  $1.7\text{\AA}$  as shown in the following table.

<u>Element</u>	<u>Typical Stability Tolerance (arc-sec)</u>	<u>Lever Arm (cm)</u>	<u>Tolerance in Linear Measure</u>
Prime gyroscope	$0.5 \times 10^{-3}$	7	$1.7\text{\AA}$
Primary mirror prism	$0.5 \times 10^{-3}$ at roof	14	$1.7\text{\AA}$

---

\*Applied Optics, Vol. 6, No. 7 (July 1967) page 1275.



Since it is only practical to achieve a  $10\text{-}20\text{ \AA}$  micro-ripple, the two surfaces will be undefined to a larger degree than is allowed for misalignment. It is not known whether this will cause excessive drift. The alignment must also be held through an environment of cooling to  $2^\circ\text{K}$  and through a launch environment which may tend to relieve stresses in portions of the joint and hence cause misalignments. Rolling the satellite reduces this stability requirement considerably but it will still be a difficult task.

Data must be either measured or found which would allow determination of the absolute stability of the contacted plane. Tensile and shear tests must be performed on optically contacted joints. We know of no such data at present. The accuracy required (parts of millisecond of arc or a few  $\text{\AA}$ ) would require an extremely well-controlled experiment and may indeed be beyond the state of the art. Recently the literature\* has reported a scheme for measuring length changes to 1 part in  $10^9$  using a Fabry-Perot etalon coupled with an extremely stable laser. Such a scheme might find application here.

The mechanical strength of optical contacted joints must be determined so that the quartz block assembly can be designed. Assembly process specifications and inspection methods must be developed so that flight hardware will have a high chance of passing acceptance tests. This is another area recommended for accelerated effort during the technology advancement program.

---

\*Applied Optics, Vol. 9, No. 11, (Nov. 1970) page 2477.

#### 5.2.4 Mounting

The assembled block consisting of the aligned telescope and the coaligned gyroscopes is mounted to an aluminum collar that contains the flexures and mounts inside the inner dewar. (See Figs. 5-20 and 5-21.) The pitch actuator acts between the inside of the dewar and the outer gimbal to pivot the assembly is as shown in Figs. 5-20 and 5-21.. The yaw actuator acts between the outer and inner gimbal. The fused quartz block is mounted to the gimbal by two lugs (Fig. 5-20), each spring loaded in the gimbal ring. The block rests against a material such as Vespel. The spring may also be a solid piece of a material like Vespel. A material and stress study must be completed before a choice of material and spring can be made.

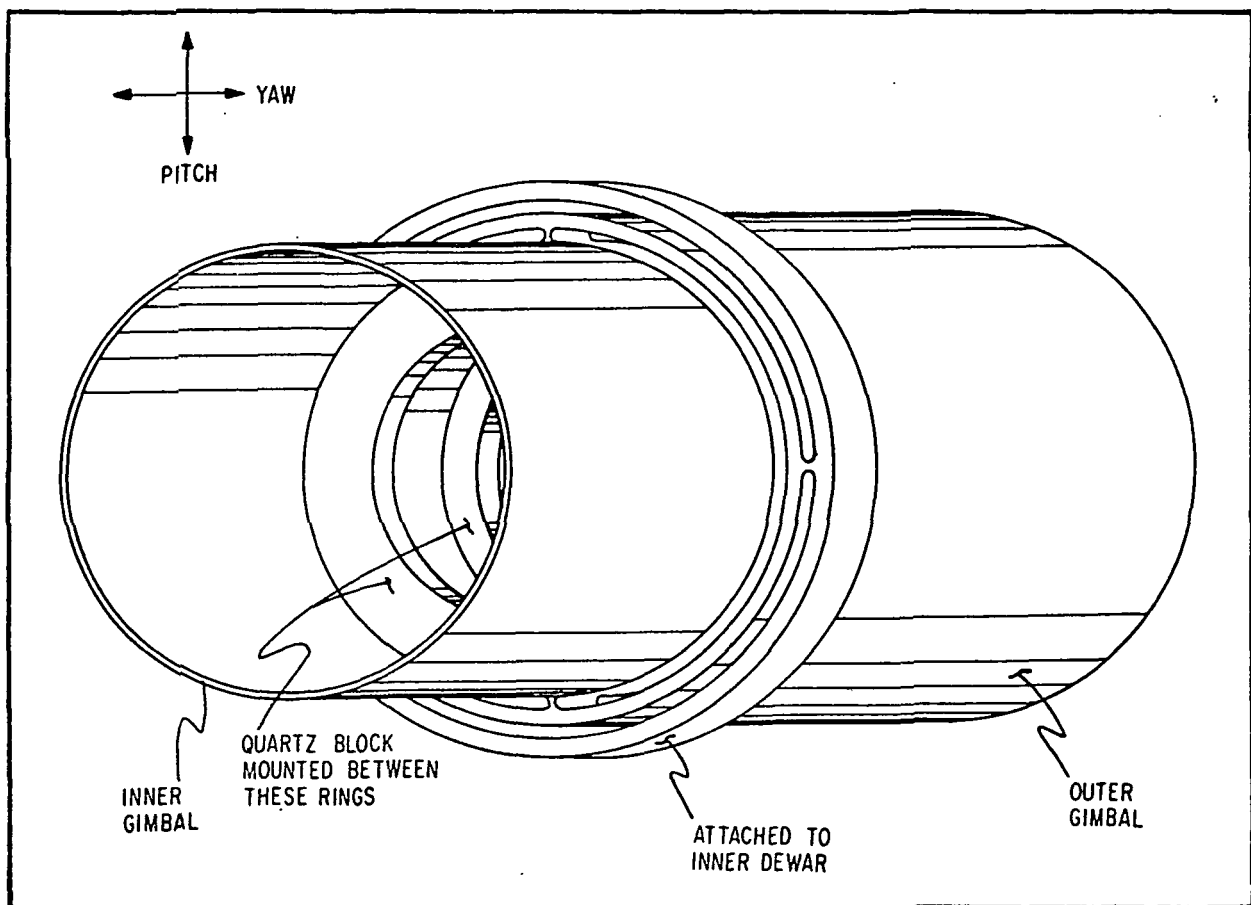


Fig. 5-21 Quartz Block Gimbal



An estimate of the anticipated vibration-induced load into the quartz block was made:

$$f_{\max} = \frac{6KPe}{wb^2} \approx (K)(1.38 \cdot 10^6) \text{N-m}^2$$

where  $K$  = amplification factor

$P$  = applied force  $\approx (20 \text{ g's})(27.3 \text{ kg}) = 545 \text{ kg}$

$e$  = height of fused quartz ear  $\approx 26 \text{ mm}$

$w$  = length of fused quartz ear perpendicular to optical axis  $\approx 102 \text{ mm}$

$b$  = length of fused quartz ear parallel to optical axis  $\approx 75 \text{ mm}$

$K$  is a function of the radius ( $r$ ) where the ear joins the remainder of the block.

$r$	$K$
5.1 mm	2.5
15.2 mm	2
51 mm	1.5

The rupture modulus of fused quartz at room temperature is about  $4.95 \cdot 10^7 \text{ Nm}^2$ ; hence, a 5.1 mm radius will give a stress of  $4.5 \cdot 10^6 \text{ Nm}^2$ . It is important that there are no fine scratches on the surface of the fused silica for they will act as stress risers. The surface should be etched with acid after manufacture to remove fine scratches.



### 5.2.5 Gyroscope Arrangement, Orientation and Alignment

This section describes the influence of arrangement and alignment of the gyroscopes on their performance. Ideally, each gyroscope and the drag-free proof mass would be located at the satellite center of mass. This is impossible and the gyroscopes experience added accelerations as a function of their C.G. offsets. The resulting gyroscope support forces cause gyroscope drift. To limit this drift the gyroscope locations must be constrained to limit acceleration components normal to the gyroscope spin axes to less than  $10^{-9}$  g bias steady state and  $3 \cdot 10^{-8}$  g sinusoidal (for periods shorter than a day). Somewhat larger spin axis acceleration components are tolerable because such torques are approximately averaged over every gyroscope rotor revolution.

For a polar orbit, the motional and geodetic relativity drifts are mutually orthogonal (along the earth's polar axis and the orbit normal respectively). Gyroscopes aligned with the drift axes would be acted on only by the relativity drift along the orthogonal axis. These orientations have been chosen for two of the four gyroscopes. These are referred to as the "perpendicular" gyroscopes, because they are aligned perpendicular to the telescope axes. These gyroscopes also provide satellite roll angle (about the guide star line) information.

A disadvantage to perpendicular gyroscope orientation is that the relativity drifts can only be detected by readout loops whose axes point at the guide star. These loops cannot be "turned over" to keep readout shift from looking like gyroscope drift. To get around this disadvantage, two other gyroscopes are pointed at the guide star. These "parallel" gyroscopes have readout loops perpendicular to the line to the guide star and their readout drifts can be reversed by rolling the satellite.



#### 5.2.5.1 Gyro Arrangement and Accelerations

The drift errors of the gyroscope must be less than 0.001 arc-sec per year. The sources of gyro drift error can be broadly categorized as resulting from support-dependent torque, and support-independent effects. In his analysis of gyro drift due to support-dependent torques\*, C. W. F. Everitt of Stanford concluded that, for realistic imperfections in the gyro balls, and in the suspension that the total residual acceleration of the gyro balls must be less than  $10^{-9}$  g bias, and  $3 \cdot 10^{-8}$  g sinusoidal to control the gyro drift error as desired.

The sources of gyro residual accelerations are summarized in Table 5-6. Because residual acceleration is contributed from a number of sources, individual contributions must be smaller than the total allowable residual acceleration. Individual acceleration contributions are broken into components in the orbit plane, and along the orbit normal. These components are combined statistically to find the probable total acceleration. About two-thirds of the total acceleration allocation is assigned to geogravity gradient, and about one-third to other sources.

Geogravity Gradient Effects. If the drag-free proof mass is located precisely at center of mass of the satellite, if the self gravitational attraction of the satellite on the proof mass is zero, and if no other forces act between the satellite and the proof mass, then the proof mass and the satellite follow purely gravitational orbits. For such an orbit the gyroscopes experience geogravity gradient accelerations proportional to their displacements from the satellite's center of mass.

---

\*"The Stanford Gyroscope Experiment", by C. W. F. Everitt, dated March 1971.





Table 5-6  
GYROSCOPE ACCELERATION SOURCES

Gravity Gradient	Vertical: $2.3 \cdot 10^{-9}$ g per cm offset (sinusoidal at orbit frequency) Horizontal: $1.2 \cdot 10^{-9}$ g per cm offset (sinusoidal in-plane component due to orbit motion--orbit normal component is sinusoidal only if the satellite rolls)
Self Gravity	$3 \cdot 10^{-11}$ (to $3 \cdot 10^{-9}$ ) g per cm offset "inside" a uniform quartz block 100 (to 20) cm "long". (roll-axis component is a bias--polar and orbit normal components are sinusoidal only if the satellite rolls.)
Centrifugal Acceleration caused by rolling	$\omega_R^2 (10^{-3})$ g per cm offset (sinusoidal at roll frequency)
Quartz-Block Rotations	$(\ddot{\theta} + \dot{\theta}^2) (10^{-3})$ g per cm offset (sinusoidal at quartz-block rotation frequencies)
Acceleration of the Satellite C.G. (and quartz-block)	$< 5 \cdot 10^{-10}$ g bias from perfect drag-free control (if the proof mass is located so it experiences $< 5 \cdot 10^{-10}$ g acceleration) $< 2 \cdot 10^{-9}$ g sinusoidal from proof-mass sensing noise for a 1 rad/sec control bandwidth.
Quartz-Block Acceleration caused by offset of the satellite cg from the quartz-block gimbal axes	$\dot{\theta}^2$ per cm offset at the outer body rotation frequency
Gyro Suspension Noise	$< 10^{-8}$ g for a linear suspension with a 6 rad/sec bandwidth and without a deadband.



In a "local horizontal" coordinate frame, defined by the radius vector from the satellite to the center of the earth and the orbit normal, the radial or vertical component of the gradient is twice as large as the horizontal component. The horizontal components (along the orbit normal and in the orbit plane) are equal. The gravity gradient acceleration components in the orbit plane rotate once for each orbital revolution of the satellite. The orbit normal component is fixed in both inertial and satellite body coordinates unless the satellite rolls.

Gyro acceleration estimates for the preliminary quartz block layout (see Fig. 5-18) are given in Table 5-7. Pitch, yaw and roll components of the estimated bias and sinusoidal acceleration are given for each identified source. The satellite pitch axis is nominally aligned with the orbit normal, and the yaw and roll axes lie in the orbit plane.

Two estimates are given for the geogravity gradient bias acceleration along the pitch axis. For a rolling satellite, the pitch acceleration is largely sinusoidal with a small bias proportional to the difference in right ascension angle between the orbit plane and the guide star. This misalignment is tentatively constrained to less than  $2^\circ$  which keeps this bias acceleration less than half the total allowable gyro bias acceleration. For a non-rolling satellite, the bias acceleration along the pitch axis exceeds the total allowable gyro bias acceleration by a factor of as much as 13, depending on the satellite roll attitude. If the satellite pitch axis is fixed, and aligned with the orbit normal, then the pitch axis bias acceleration is about 6 times as large as the total allowable.



Table 5-7  
GYROSCOPE ACCELERATION ESTIMATES

	<u>Pitch</u>	<u>Yaw</u>	<u>Roll</u>
<u>Bias (g's)</u>			
Geogravity Gradient (for the guide star 2° out of the orbit plane)	$5 \cdot 10^{-10}$ (or $6 \cdot 10^{-9}$ )*	0	0
Self Gravity Gradient	0 (or $5 \cdot 10^{-10}$ )*	0 (or $5 \cdot 10^{-10}$ )	$5 \cdot 10^{-10}$ **
Satellite CG Acceleration	$5 \cdot 10^{-10}$	$5 \cdot 10^{-10}$	$5 \cdot 10^{-10}$
Total (RSS) for a Rolling Satellite	$7 \cdot 10^{-10}$	$3 \cdot 10^{-10}$	$7 \cdot 10^{-10}$
<u>Sinusoidal (g's)</u>			
Geogravity Gradient	$1.3 \cdot 10^{-8}$	$2.6 \cdot 10^{-8}$	$2.6 \cdot 10^{-8}$
Self-Gravity Gradient	$5 \cdot 10^{-10}$	$5 \cdot 10^{-10}$	---
Roll Centrifugal Acceleration	$1.5 \cdot 10^{-9}$	$1.5 \cdot 10^{-9}$	---
Quartz-Block Rotations	$10^{-8}$	$10^{-8}$	$10^{-8}$
Satellite CG Acceleration	$2 \cdot 10^{-9}$	$2 \cdot 10^{-9}$	$2 \cdot 10^{-9}$
Telescope Gimbal Offset Acceleration	$5 \cdot 10^{-9}$	$5 \cdot 10^{-9}$	---
Gyro Suspension Noise	$10^{-8}$	$10^{-8}$	$10^{-8}$
TOTAL (RSS)	$2.2 \cdot 10^{-8}$	$3.1 \cdot 10^{-8}$	$3.1 \cdot 10^{-8}$

\* For a non-rolling satellite stabilized at "zero" roll angle  
(can be reduced to about  $10^{-9}$  g for all 4 gyros for a 30  
degree roll offset angle).

\*\* Requires careful mass compensation especially near the per-  
pendicular gyros.



This bias acceleration can be greatly reduced by rolling the satellite to an attitude, which approximately nulls the gyroscope offsets from the orbital plane. A  $25^\circ$  roll angle puts the parallel gyroscopes in the orbital plane while a  $45^\circ$  roll angle is required to bring the perpendicular gyros into the orbital plane. A compromise roll angle of  $30^\circ$  brings all four gyroscopes within about 1 cm of the orbital plane, and reduces the geogravity bias acceleration along the pitch axes to about  $10^{-9}$  g for all 4 gyroscopes.

Operating the satellite at a fixed roll attitude is only of interest as a backup mode at this time. If it is decided later that non-rolling operation is desirable for other reasons, then rearrangement of the gyroscopes to locate them in the nominal pitch plane should be considered.

Self-Gravity Effects. Other parts of the satellite exert a gravitational pull on the gyros and on the proof mass. If the satellite's self gravity acceleration of the gyros is the same as that of the proof mass, then the drag-free control jets accelerate the satellite to keep the gyro balls centered in their cavities without the need for gyro suspension control forces. Self gravity gradients in the quartz block cause the gyros to experience accelerations which differ from that of the proof mass. The self gravity gradient near the center of a uniform quartz block 100 cm long and 20 cm in diameter, is about  $3 \cdot 10^{-11}$  g's per centimeter axially and  $3 \cdot 10^{-9}$  g's per centimeter radially.

For the preliminary quartz block layout the uncompensated self-gravity acceleration of the perpendicular gyros is roughly  $3 \cdot 10^{-8}$  g's along the telescope axis, and about a third that large along the pitch and yaw axes. The self gravity acceleration of the parallel gyroscopes is roughly  $10^{-8}$  g's in all three axes. The uncompensated pitch and yaw axis accelerations of all four gyroscopes are acceptable because they are sinusoidal for a rolling



satellite. For a non-rolling satellite these accelerations, together with the roll axis acceleration, are biases.

If the total bias acceleration is to be less than  $10^{-9}$  g's, even if the satellite does not roll, the self gravity gradients in the quartz block must be greatly reduced from the above estimate. The roll axis bias acceleration of the perpendicular gyroscopes must be reduced substantially even if the satellite rolls.

Self gravity gradients can be reduced by either removing quartz on the inboard side of the gyroscopes or by adding compensating mass on the outboard side. If quartz is not removed on the inboard side of the perpendicular gyroscopes then a compensating mass of roughly 10 kilograms must be positioned outboard and very close to them. No serious problems with self gravity compensation are anticipated.

Roll Acceleration. The gyroscopes experience a centrifugal acceleration proportional to the product of the second power of the roll rate and their displacement from the roll axis. This acceleration is fixed in satellite body coordinates, but rotates with respect to inertial coordinates. For the tentatively selected roll rate of  $3 \cdot 10^{-4}$  radians per second this acceleration is about 1/10 as large as can be tolerated.

Quartz Block Control Rotations. The gyro suspensions accelerate the gyros to follow rotations of the quartz block. The gyro accelerations are proportional to the displacement of the gyroscopes from the quartz block gimbal axes. The principal source of quartz block rotational accelerations is the attitude control system.



The pitch/yaw, roll, and translation controllers and filters are constrained to produce rms quartz block accelerations no larger than  $10^{-8}$  g's. In each control mode, the principal problem is that of band limiting the controller-filter to achieve adequate sensor noise attenuation. The resulting attitude control systems have bandwidths of from 0.05 to 5 radians per second. Bandwidths this low should be acceptable because the principal disturbance torques are sinusoidal at 0.002 radians per second.

Accelerations From External Forces and Outer Body Control. Without drag-free control, the satellite would experience a bias acceleration due to solar radiation pressure of about  $5 \cdot 10^{-9}$  g's. Atmospheric drag would occasionally produce comparable acceleration levels. These accelerations can be reduced by an order of magnitude using drag-free control, if reasonable care is taken in self gravity gradient reduction near the proof mass and in controlling other forces between the proof mass and its cavity walls. Two other drag free satellites are being designed for launch in the next few years. They have bias acceleration goals 100 times tighter than that required for the mission. For a 1 radian per second translation control bandwidth, the expected noise in the proof mass position error signal should produce thrust noise that will accelerate the satellite at about  $2 \cdot 10^{-9}$  g's.

Pitch and yaw rotations of the outer satellite body are decoupled from the quartz block only if the quartz block gimbal axes pass through the satellite C.G. The quartz block experiences translational acceleration proportional to the offset between the gimbal axes and the satellite C.G. and to the amplitude and square of the frequency of sinusoidal outer body rotation components. These accelerations can be controlled to about  $5 \cdot 10^{-9}$  g's if the gimbal axes pass within 1 cm of the satellite C.G., if pitch and yaw jet control is band limited at about 1 radian per second, and if the rms pointing error of the outer satellite is constrained to about .1 arc-second.



A gyro suspension bandwidth of about 6 radians per second is desirable to provide a safety margin for meteoroid impacts and for control accelerations produced by the satellite attitude and translation control systems. The noise in the gyro position error signal produces gyro accelerations of about  $10^{-8}$  g's for the desired bandwidth.

The RSS total of individual sinusoidal amplitudes is slightly larger than desired. The total could be reduced if the gyroscopes can be more tightly clustered about the proof mass. This should be a goal in quartz-block design iterations as the program proceeds.

Gyroscope - Telescope Alignment and Orbital Attitude. The geodetic relativity drift is 140 times as large as the motional relativity drift. The motional perpendicular gyro must be aligned within about  $0.5^\circ$  of the orbit plane normal to keep the geodetic drift component it senses about the same size as the motional drift. If the motional gyro is aligned this well, and if its misalignment is determined to an accuracy of 10 arc seconds, then the motional drift measurement error caused by the geodetic drift is constrained to 0.0003 arc-second. If the motional gyroscope misalignment is as large as  $1^\circ$  then a 10 arc-second error in determining the misalignment corresponds to a 0.0007 arc-second error in the motional drift measurement.

A substantially larger misalignment error is tolerable between the geodetic perpendicular gyroscope and the orbit normal. Another factor makes it desirable to align both perpendicular gyroscopes within about 0.5 degrees of perpendicular to the telescope axis. Their relativity measurements contain errors proportional to the product of their roll angle misalignments with the telescope yaw pointing error (for the motional gyro) and pitch error (for the geodetic gyro). If these pointing errors varied linearly from +0.03 arc-second to -0.03 arc-second during a drift measuring



interval, then a 0.5 degree gyroscope misalignment would produce a 0.0005 arc-second error in the drift rate measurement.

Since the telescope pointing errors are expected to consist mainly of high frequency jitter as opposed to linear drift, it is unlikely that gyroscope misalignments somewhat larger than  $0.5^\circ$  would cause trouble. However, insurance against this potential error source is welcome.

The misalignment of both perpendicular gyroscopes must be determined to 10 arc-seconds to limit the corruption of their relativity drift measurements by starlight aberrations and to provide a sufficiently accurate roll angle reference for the relativity drift measurements by the parallel gyroscopes.

The parallel gyroscopes must be pointed within about 3 arc-seconds of the actual guide star (as opposed to the aberrated guide star image) to limit the linear range required in their readout loops.

A final factor which makes alignment of all four gyroscopes within  $0.5^\circ$  of the orbit plane (or its normal) desirable is the direct (as opposed to support-dependent) gravity gradient drift of the elliptically deformed gyroscopes. A gyroscope deformed 4 parts in  $10^6$  that is tipped  $45^\circ$  out of the orbit plane would drift over 0.03 arc-second per year. The gyroscopes must lie within  $1^\circ$  of the orbit plane (or its normal) to control this drift to 0.001 arc-second per year.

Rotation of the orbit plane also affects this alignment. This drift is largely predictable if the gyroscope shapes and orientations are known. It is preferable not to have to predict this drift and eliminate it from the data.





Gyroscope Problem Areas. The design difficulties associated with the magnetic shielding and optical contacting have been discussed. They impact very heavily on the detailed design of the entire quartz block assembly. Solutions are required before the initiation of the main program in order that the very tight satellite development program schedule can be met. We have recommended that special attention be given to these areas in the next year and a half.

The magnetometer used to read the gyroscope drift has not yet been developed to the necessary state. This is a very difficult development and must also have additional effort in the near term.

Testing of engineering model gyroscopes is expected to start in the first quarter of 1972. Spin-up tests will be performed first, followed by drift measurements. The drift characteristics and possibly the spin-up characteristics of the gyroscopes will be different in orbit from that measured on the ground in a 1 g field. Gyroscope drift is expected to be many millions of times worse on the ground than the 0.0005 arc-sec per year orbit performance. In Volume II, we have recommended an engineering flight test program to verify the orbital performance. This work must start in early 1972 to satisfy the schedule requirements.

### 5.3 EXPERIMENT ELECTRONICS

The function of the experiment electronics is indicated on the middle portion of the satellite systems diagram, bound in the back of this volume. This circuitry measures the orientation of the gyroscopes with respect to the quartz block and combines the measurement with the angular error signals from the telescope to produce difference signals.

The telescope and gyro signals are resolved into inertial coordinates and transformed into telemetry signals from which relativity data can be derived.



During stellar day the telescope signals are used by the control electronics to develop thruster signals for changing the attitude of the spacecraft, and actuator signals for varying the attitude of the quartz block and telescope. Two of the gyro relativity signals are used as pitch and yaw references for the attitude control system during the occulted or "night" portions of each orbit. During these intervals no telescope readouts are available for attitude control and no useful relativity data can be obtained. Attitude control is maintained by switching vehicle-oriented pitch and yaw gyro signals into the attitude control system in place of the telescope readouts.

The experiment electronic circuit functions are identical in many places and therefore basic circuitry modules are used in several applications. For example: The gyro loop readouts are all the same, six identical automatic gain control (AGC) modules are used to match the gains of the telescope and gyro signals and redundant parallel readout modules are used. Coordinate transformations are performed using a solid-state resolver. The roll-angle is calculated using a "two-speed" (coarse-vernier) solid state resolver.

#### 5.3.1 Typical Instrumentation Channel

Figure 5-22 shows a typical instrumentation channel which subtracts the telescope error signals from the gyro readout. To do this the scale factors of these two inputs must be equal. The gyro scale factor is established by extremely stable elements on the quartz block (at 1.2°K) plus the special feedback resistor (in a stable environment), and it is reasonable to assume that this scale factor will remain essentially invariant with time. The natural gyro spin-down should be very gradual and predictable.

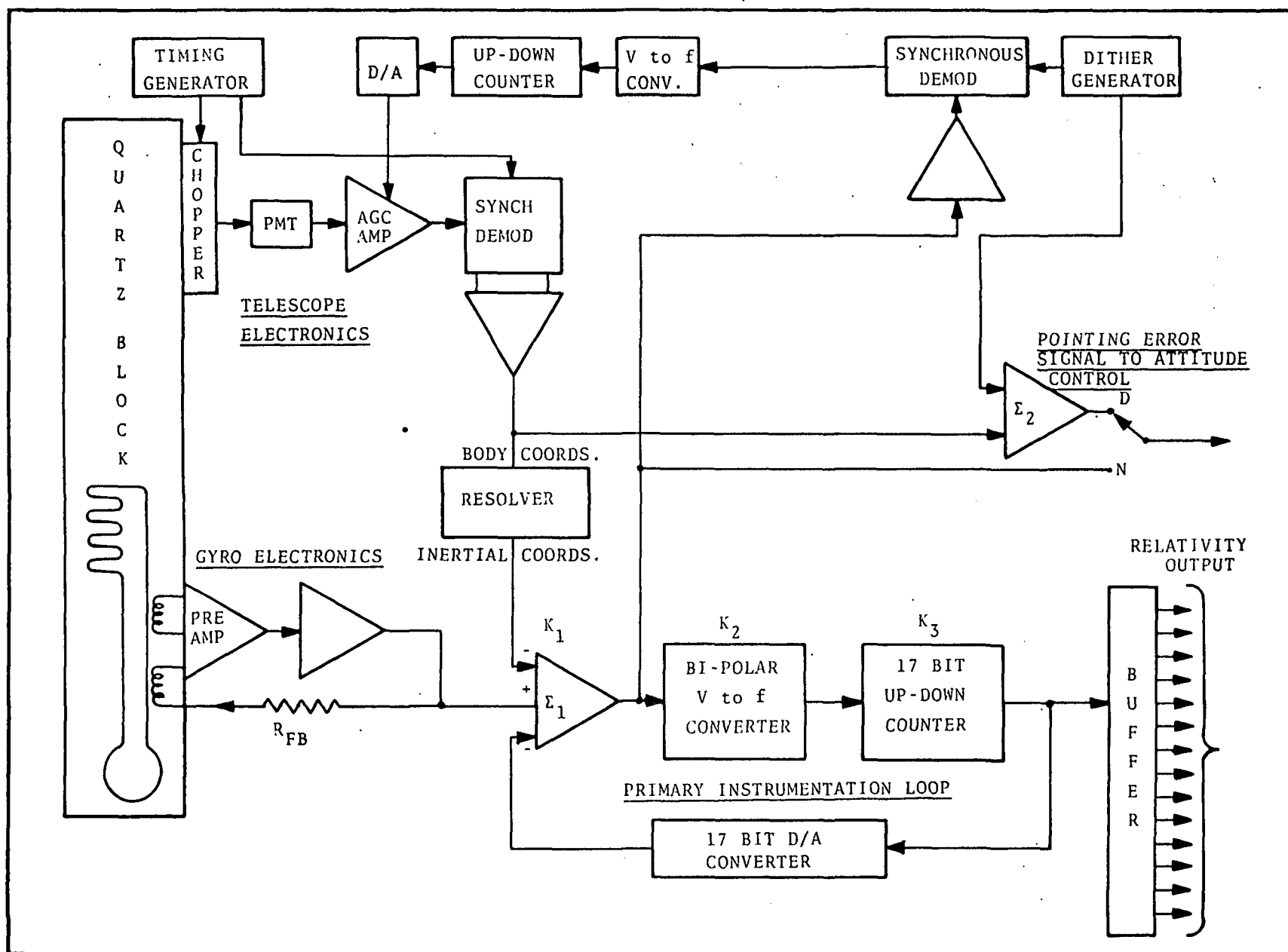


Fig. 5-22 Typical Instrumentation Channel and Signal Processing Loop





The telescope optics, roof-prism knife edges etc., are snugly contacted and thus an integral part of the quartz block, but the readout photodetectors degrade with time. Transmission of the optics also may eventually decline. Either of these effects, as well as any amplifier gain shifts, will result in telescope scale-factor variability with time.

For this reason an automatic gain control is necessary for each telescope readout signal chain prior to the point of subtraction from a gyro readout. This AGC is implemented by introducing a small amplitude, 0.1 radian per second "dither" signal into the control system, causing the telescope (quartz block) to oscillate about its center-pointing position. The amplitude of the excursion is restricted to the highly-linear region of telescope error-angle readout or about  $\pm 0.05$  arc-second to avoid compromising the accuracy.

Any mismatch in scaling between gyroscope and telescope readouts appears as a difference-signal input to the instrumentation loop at the dither frequency. This signal is in analog form at the output of the amplifier,  $\Sigma_1$ . It is amplified in a separate AGC signal chain, processed, and used to control the gain of an AGC amplifier in the appropriate telescope readout path. This AGC control signal must be integrated so that noise on the signal and other disturbances are reduced to a sufficiently low level. At the same time the DC gain of the AGC control loop must be high to enable matching readouts to one part in  $10^3$ . An integrator inside the loop provides the needed high gain at DC. The required settling time is about  $10^{+5}$  seconds.



### 5.3.2 Gyroscope Readout (Magnetometer)

#### 5.3.2.1 Development of the Gyroscope Readout Signal

The position of the gyroscope spin axis must be accurately measured. Conventional methods of position sensing are ruled out by the need to minimize all extraneous torques. The solution to this problem is provided by the unique properties of the cryogenic environment in which the gyroscopes are located.

Superconducting magnetic shields permit trapped magnetic flux to be reduced to zero (or to the one-or-two quantum levels). Once a spherical shield has been completely cooled, the enclosed flux is locked-in at the particular quantum level initially achieved.

A small magnetic dipole moment (London Moment) is generated by the spinning superconducting Niobium coating on the gyroscope balls along the direction of their spin axes. The moment is proportional to the spin rate. Superconducting planar pickup loops surround the spinning gyroscope balls. The reaction of these loops to the minute London Moment makes it possible to extract the gyroscope spin-axis component perpendicular to the plane of each loop.

A pickup loop is shown schematically at the left in Fig. 5-23. The resistance of a superconductor is zero and any change in flux through the (closed) loop produces a current which just cancels the flux increment. The component of spin perpendicular to the plane of the superconducting loop may be read out by measuring the current flow in the loop. To do this a second superconducting loop is in series with the primary detector loop but isolated from the London Moment. The second loop allows introduction of a modulated carrier and the use of a stable, narrowband, AC amplifier

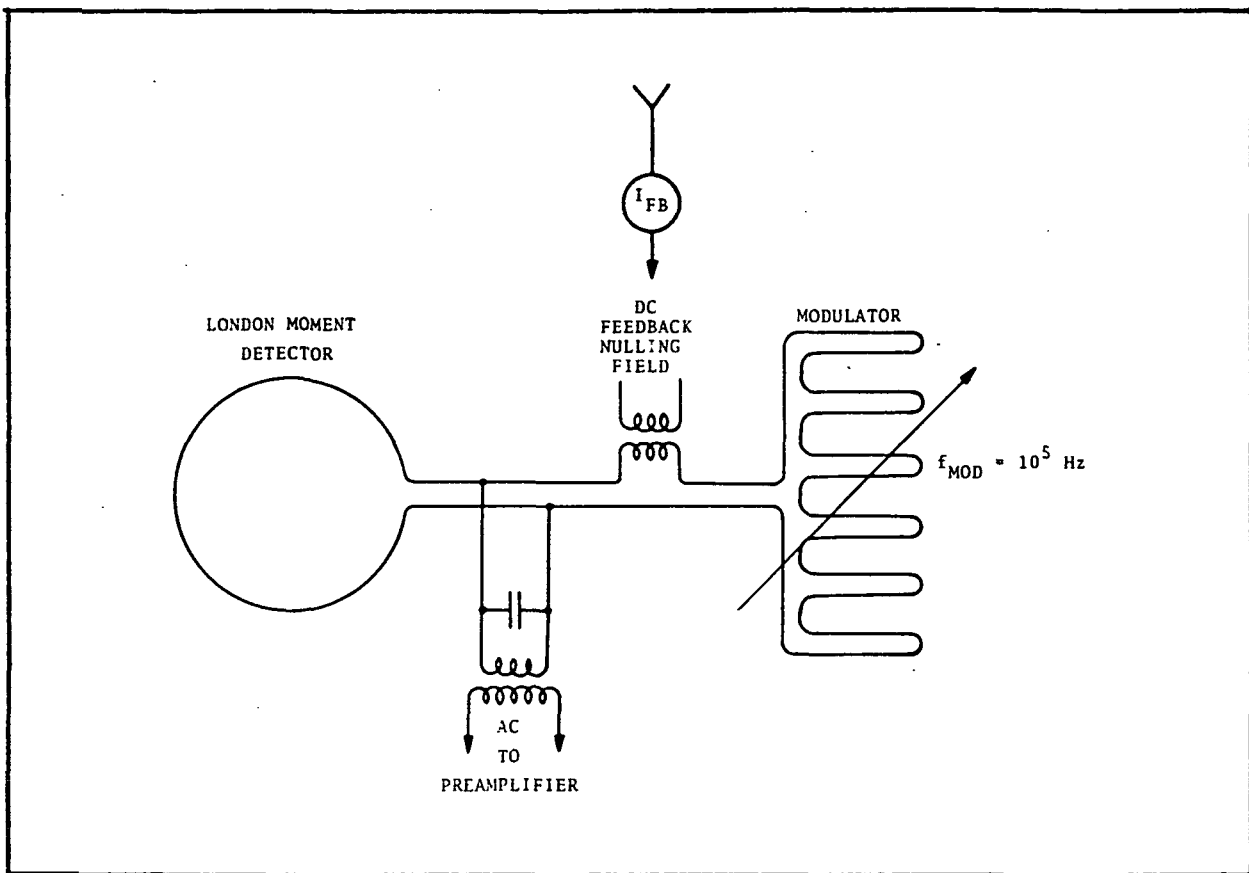


Fig. 5-23 Cryogenic Vibrating Plane Magnetometer

and synchronous detector in the readout. The modulation is introduced by a vibrating superconducting ground plane located parallel with and in close proximity to the second loop. This causes the inductance of the loop to vary at the driving frequency, pumping flux back and forth between the two loops and producing an AC current proportional to the London Moment. The position data is AC coupled, through a superconducting transformer, to the exterior where it is amplified as needed. A small capacitor is placed across the transformer, chosen to tune the circuit to the modulation frequency.



The extreme stability and accuracy requirement on the gyro readout can be realized only by using the detector in a continuously self-nulling mode of readout. After sufficient amplification, the output signal is integrated to produce a DC feedback current which is injected back into the detector circuit to keep the input (current in the superconducting loop) constant. The magnitude of this feedback current corresponds to the gyro position.

The DC current is transformer coupled to the magnetometer circuit by a second superconducting transformer as shown on Fig. 5-23. The ability to couple DC through the transformer comes about by virtue of the same principle of conservation-of-flux inside a superconducting shield. The DC field generated in the transformer primary winding by the feedback current couples into the superconducting loop to cancel any changes in flux distribution due to gyro precession.

The null stability of this configuration is dependent on components that are near absolute zero and protected by a superconducting magnetic shield and fabricated as an integral part of the quartz block. The scale factor of the readout is determined mostly by the spin rate and the current-feedback resistor. The decay of spin rate should be very gradual and the feedback resistor must be kept in a well controlled environment.

#### 5.3.2.2 Gyro Signal Amplification

A block diagram of the gyroscope readout loop is shown in Fig. 5-24. The cryogenic magnetometer is illustrated symbolically in the dashed block to the left. It interfaces with the gyroscope electronic amplifiers, demodulator, integrator and current feedback resistor depicted on the right.

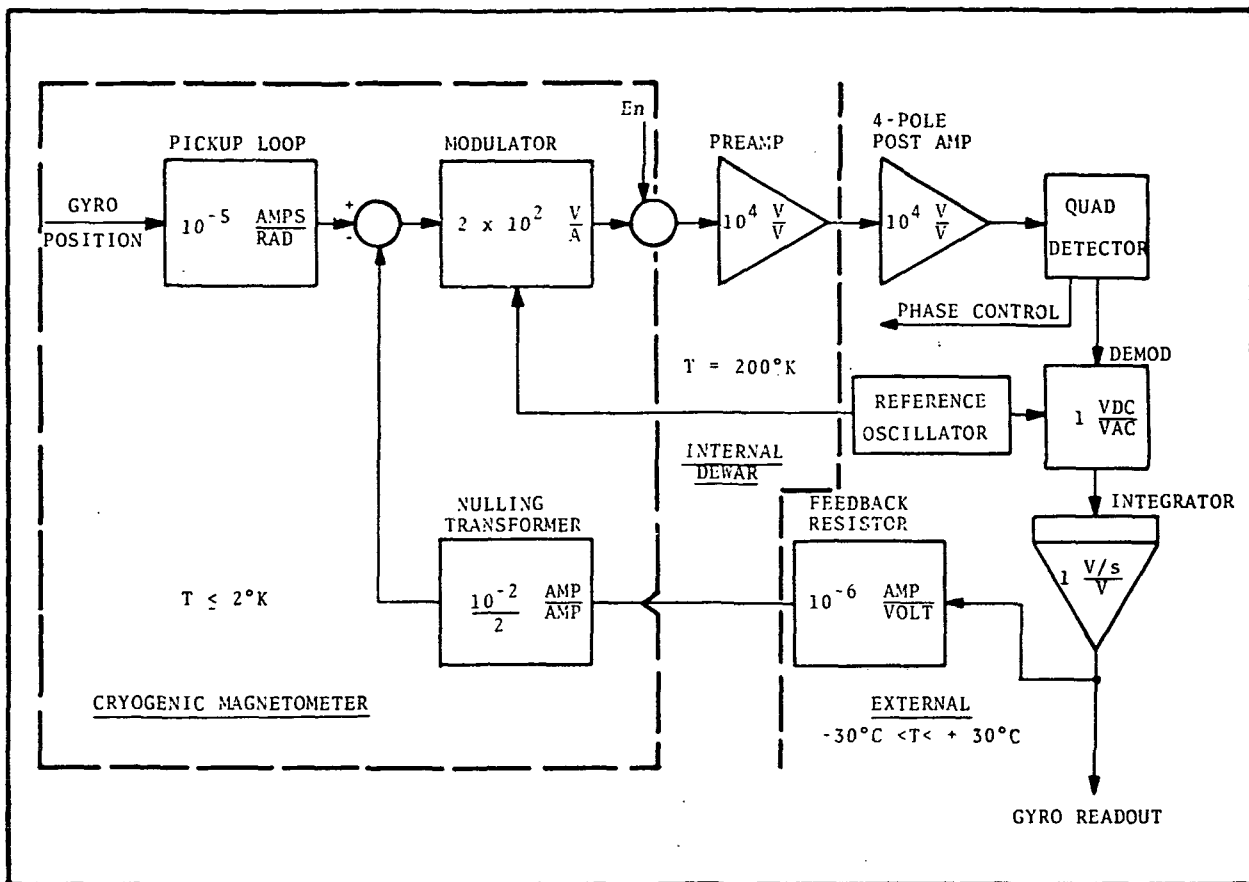


Fig. 5-24 Gyroscope Readout Loop

The entire magnetometer is immersed in a space where the temperature is within a degree or two of absolute zero and which is surrounded by a superconducting magnetic shield. Most of the electronics associated with the loop, however, are located outside of the dewar in an instrument compartment where the temperature is about 250°K. The important exception is the low-noise preamplifier. It is desired to operate this amplifier at a reduced temperature to minimize noise. Too low a temperature offsets the noise advantage because the gain of the amplifying devices also falls off. The preamplifier is therefore located as close as practical to the gyroscope but is in an insulated compartment where the heat balance with the one-milliwatt power dissipation keeps the preamplifier at about 200°K. The optimum temperature here will yield a maximum signal/noise ratio in the readout.





A large forward amplifier gain of  $10^8$  is needed to achieve a reasonable signal level at the output. This is distributed equally between the preamplifier and post amplifier. This gain is all put ahead of the synchronous detector in order to be free of DC drift and  $1/f$  noise problems. With such high gain a fourth-order bandpass filter centered on  $10^5$  Hz, is needed to decrease the noise so that it will not saturate the output of the amplifier.

The DC magnetometer signal is recovered in a synchronous demodulator driven from the same signal source which drives the vibrating plane in the magnetometer. The demodulator output drives an integrator having a typical  $1/s$  transfer characteristics (see Fig. 5-25). The integrator output is directly proportional to gyro angle if the feedback loop is closed through the  $10^6$  ohm feedback resistor to the magnetometer circuit. The presence of the integrator makes the loop gain extremely high for low frequencies.

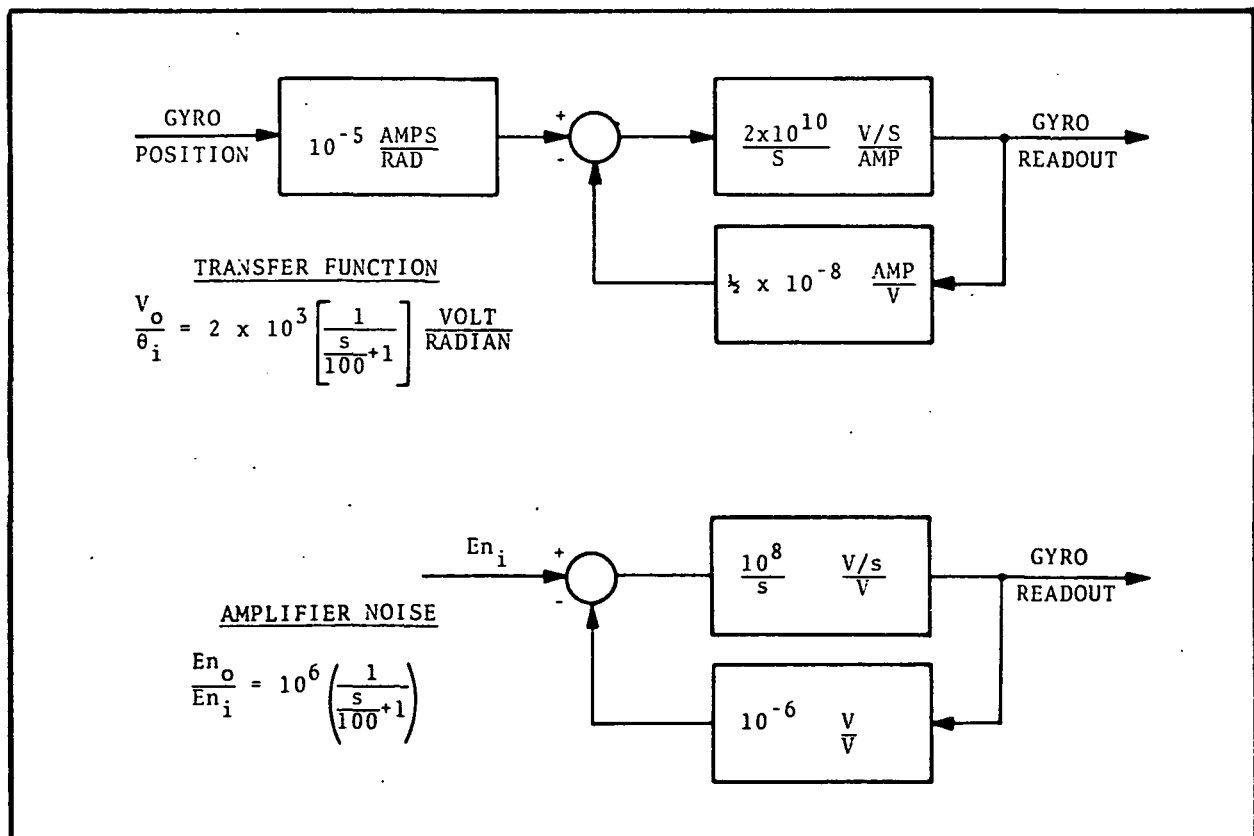


Fig. 5-25 Gyro Readout Loop Transfer Function and Noise Characteristics



The DC transfer characteristic of the gyro readout is thus established entirely by the feedback resistor in conjunction with the DC-field coupling-coefficient of the superconducting feedback transformer. On the other hand, the effective integrating time and the 3 dB bandwidth, is determined by the product of gain constants around the loop. The gain sets the 3 dB point of the entire gyro readout at 100 radians per second or about 16 Hz. The equivalent noise bandwidth could be  $\pi/2$  times greater or about 25 Hz.

One of the major problems with the gyro readout is maintaining the proper phase through the high gain amplifiers and 4th-order filter to assure satisfactory performance of the synchronous detector. High circuit Q's generate very steep phase versus frequency characteristics. Significant degradation of performance can result from very small component drifts or oscillator frequency changes. The AC amplification chain may need some type of active phase control to assure continued satisfactory performance for extended periods of time. A separate loop using a quadrature detector and continuous phase control loop may be needed.

#### 5.3.2.3 Gyro Readout Loop Performance and Problem Areas

The performance requirements on the gyro readout, given in Table 5-8, are predicated on a null stability being established by the cryogenic magnetometer itself and a scale factor established by the feedback resistor together with a superconducting transformer. The noise equivalent angle is determined by the first stage of the pre-amplifier and the system bandwidth as well as parameters of the cryogenic magnetometer.



Table 5-8  
GYRO READOUT PERFORMANCE

Magnetometer Circuit:

$\beta$	- Inductance Ratio	$= 1/2$
$Q$	- Quality of Resonant Circuit	$\geq 10^4$
$\alpha$	- Modulation Factor	$\geq 0.2$
$f_M$	- Modulation Frequency	$= 10^5$ Hz
$R_O$	- Output to Preamp	$= 2.5$ k $\Omega$ at 2°K
$W_O$	- Gyro Spin Rate	$\approx 200$ rps

Preamplifier:

$G_1$	- Voltage Gain at $10^5$ Hz	$= 10^4$
$G_{1s}$	- Voltage Gain at $f < 300$ Hz	$\leq 1$
$T_N$	- Noise Temperature	$\leq 20^\circ\text{K}$
$T_A$	- Ambient Temperature	$\approx 200^\circ\text{K}$
	Dynamic Range	$> \pm 100$ arc-sec
	Signal Line Shielding	$> 140$ dB

Entire Gyro Readout Loop:

Gain	$2 \times 10^3$ V/rad	$\equiv 10$ $\mu\text{V}$ /milli arc-sec
Bandwidth		$= 16$ Hz at 3 dB point
Noise Equivalent Angle		$\leq 1.4$ arc-sec
Dynamic Range		$> \pm 100$ arc-sec
Linearity Error		$< 5$ parts per million
Ambient Electronic Temperature Outside the Dewar		$-30^\circ$ to $+30^\circ\text{C}$



While the individual amplifier, demodulator and integrator gains are made as stable as possible, the required performance could not even be approached without using a self-nulling or servo-type of integrating feedback loop. In this manner, the gain changes and non-linearities in the amplifiers will not affect the result, provided that the overall gain remains sufficiently high. Careful phase-correction and shielding of the amplifiers is essential to assure freedom from any self-oscillatory instability in the presence of such high gains as  $10^8$ .

The four-pole bandpass filter helps prevent noise saturation of the last stages but it increases the complexity of stabilizing the entire loop. It is vital to keep all noise peaks well below any significant non-linearity in the later amplifier stages as well as the demodulator and integrator. This is dictated by the fundamental experiment requirement that nothing can be allowed to bias the mean of the noise probability distribution sufficiently to invalidate the 0.001 arc-second integrity of the primary relativity signals.

Not only are the bandpass characteristics in the immediate neighborhood of  $10^5$  Hz of concern but equally important is the off-band rejection from DC up to the highest frequencies that could conceivably be picked up from such other subsystems as proof-ball readout and gyroscope-suspension system. High rejection must be maintained in the 100-300 Hz region to prevent interference from spin-frequency signals due to trapped flux.

It is not sufficient to merely prevent spurious signals from appearing at the output. They must be suppressed earlier in the signal chain, well before they result in signal excursions into non-linear portions of amplifier transfer characteristics. This is essential not only to prevent bias of the mean of the noise distribution but also to avoid the formation of harmful modulation products. These must be scrupulously avoided to be certain that subsequent integration to reduce noise will truly yield an unbiased estimate of the relativity data.



If the above conditions are satisfied, the scale factor and linearity of the gyroscope readout should be independent of all parameters other than the spin rate, the nulling transformer and the feedback resistor. Therefore the transformer magnetization characteristic and DC coupling coefficient must be constant to 5 parts per million (PPM) over the full dynamic range. The feedback resistor must be carefully chosen, extremely stable, very well shielded and located where the temperature is constant.

### 5.3.3 Telescope Electronics

The function of the telescope electronics is to amplify and process the output of the telescope pointing sensor to provide a stellar reference, against which the relativistic gyro precession is measured. The nature of photo sensors makes it impossible to obtain the degree of accuracy, stability and dynamic range provided by the superconducting London Moment readout. Thus, the telescope readout is used in a null-seeking mode, generating pointing error-signals for the inner attitude control system. The latter cannot achieve an instantaneous position accuracy of 0.001 arc-sec. As a result, the instantaneous difference-signal between gyroscope and telescope must be used as the primary indication of relativistic precession, after long-term integration and auto-correlation.

This imposes requirements on the telescope signal chain more severe than that which would be required for a null-seeking device. In addition to needing a null-stability better than 0.001 arc-second, the off-null linearity must also be this good over the feasible attitude control error range of about  $\pm 0.05$  arc-second.



Further, the scale-factor changes from the photosensor must not be so large as to prevent subtraction of the gyroscope and telescope signal to 0.001 arc-sec accuracy. This requires gain control of the telescope signal chain. This is done by introducing a sinusoidal "dither signal" into the inner control loop as shown in Fig. 5-22 and discussed below in connection with the instrumentation loop.

A block diagram of the telescope electronics is shown in Fig. 5-26.

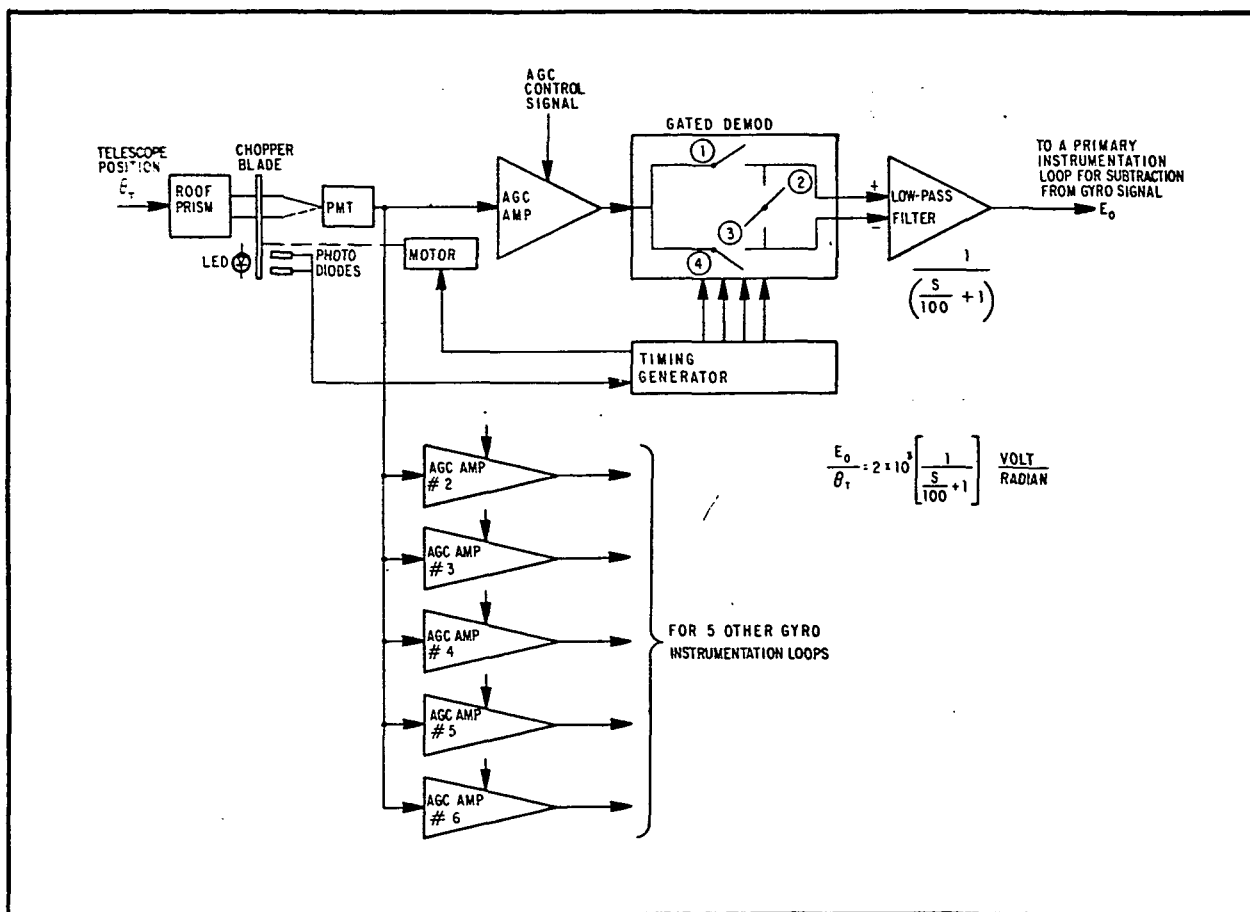


Fig. 5-26 Single Axis Telescope Electronics

The photomultiplier output signal, as established by the chopper blade, has a 50 Hz phase-sensitive square wave component proportional to pointing error plus a DC component. The square wave is amplified in the AGC amplifier while the DC component is rejected.



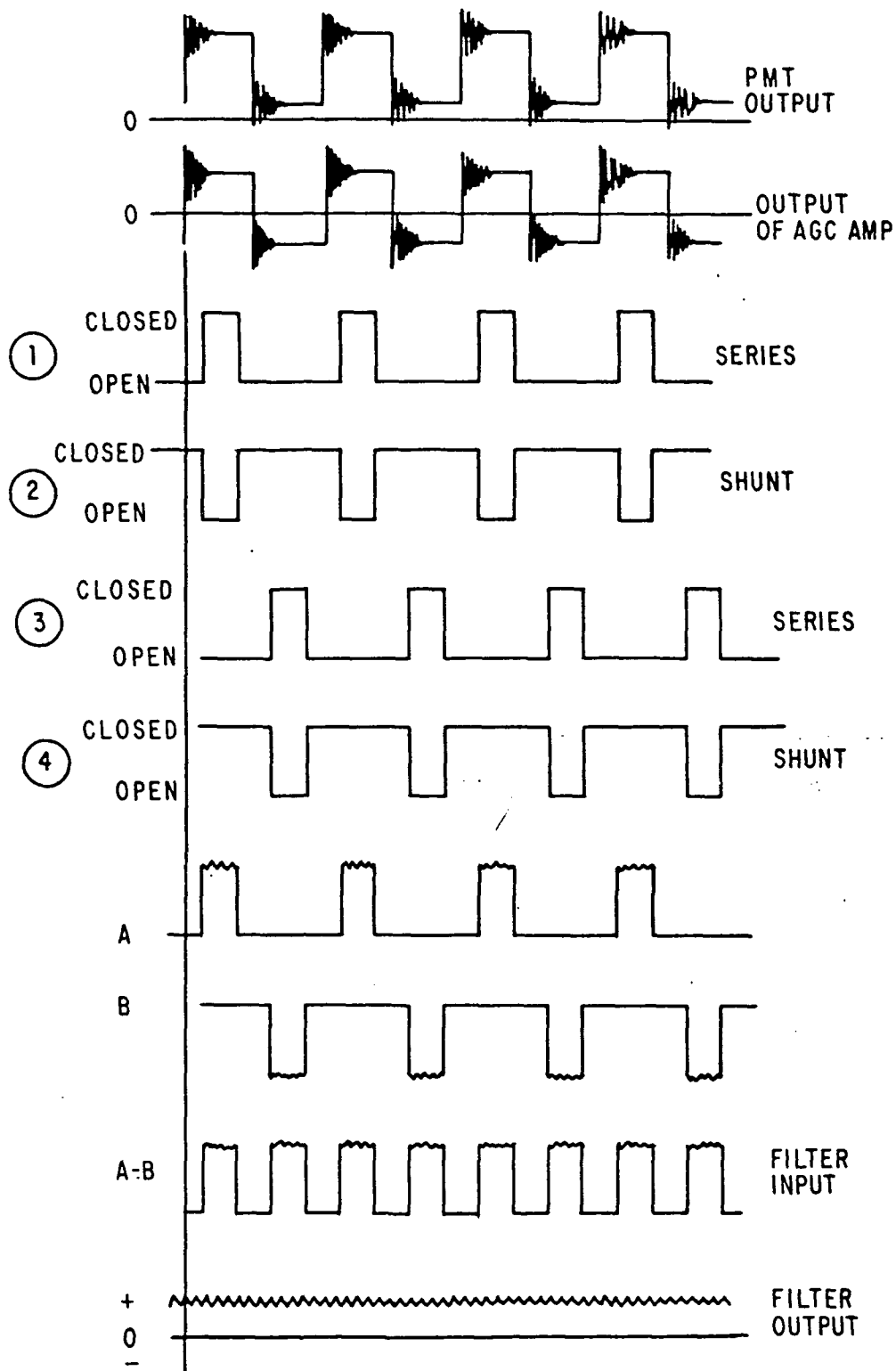
The square wave is amplified as much as needed to enable the overall scale factor of the telescope readout to be matched to that of the gyroscope readout. After amplification, phase-sensitive demodulation is performed by a special gating circuit which is insensitive to leading edge transients. The output is smoothed by the low-pass filter. The latter limits the bandwidth to 16 Hz to match that of the gyroscope electronics.

The AGC amplifier must have a voltage-controllable gain in its passband, so that the amplification of the 50 Hz square wave can be varied over a range of 4 to 1 by an external control voltage. The gain control must not perturb the symmetry or linearity of the transfer characteristic over the full useful range of telescope signals. That is, the gain must be adjustable without biasing the mean of any signal.

A major threat as a source of error resides in any non-ideal characteristics of the light chopping mechanism. For example, voltage spikes can result from imperfect overlap or underlap at the light-beam transitions. These can cause errors in the demodulated output if they are not appropriately gated-out at the synchronous detector.

The gating circuit is indicated in Fig. 5-26 and more detailed waveforms are shown in Fig. 5-27. It is seen that only the "flat" central portions of the modulated signal are used to regenerate the DC pointing error signal.

The demodulator is always kept synchronized by deriving the timing signals from the chopper itself via LED light sources and photodiodes. The sampling aperture for both halves of the modulated signal is timed by a simple monostable multivibrator to ensure equal weighting of each half when the signal is time-averaged in the low-pass output filter.



.05 ARC SEC NOISE, BW=100 RAD=16Hz  
 PHASE REVERSAL OF PMT CAUSES FILTER OUTPUT TO GO NEGATIVE.

Fig. 5-27 Telescope Electronics Waveform





#### 5.3.4 Signal Processing Instrumentation

The primary instrumentation loops perform the subtraction of the telescope error signals from the appropriate gyroscope readout signals and convert the difference signals from analog to 17 bit digital form for transfer to telemetry. In processing the difference signals additional data smoothing is performed to further reduce the noise.

The instrumentation also provides active matching of each telescope scale factor with that of its associated gyroscope readout. Appropriate telescope and gyroscope signals must also be furnished for day and night operation of the attitude control system.

##### 5.3.4.1 Feedback-Integrating A/D Converter

The basic signal-processing loop is shown in Fig. 5-28. The input is a highly stable operational amplifier which can accept either a single ended input or a differential pair such as the gyroscope and telescope signals. The amplifier output drives a bi-polar voltage-to-frequency (v to f) converter which is highly linear and whose transfer characteristic has no discontinuity at the origin. The v to f converter drives a 17-bit reversible counter, making this part of the loop a nearly ideal digital integrator. It has a  $1/s$  frequency characteristic and its output is the instantaneous 17-bit parallel number contained in the counter.

The heart of the instrumentation loop is the feedback path which establishes the overall input-output linearity and stability. The feedback path consists of a state-of-the-art 17-bit digital-to-analog converter, having a precision DC reference stable to 1 part in  $2 \times 10^5$ . It takes the 17-bit, parallel counter output word and converts this to analog form for completion of the feedback path

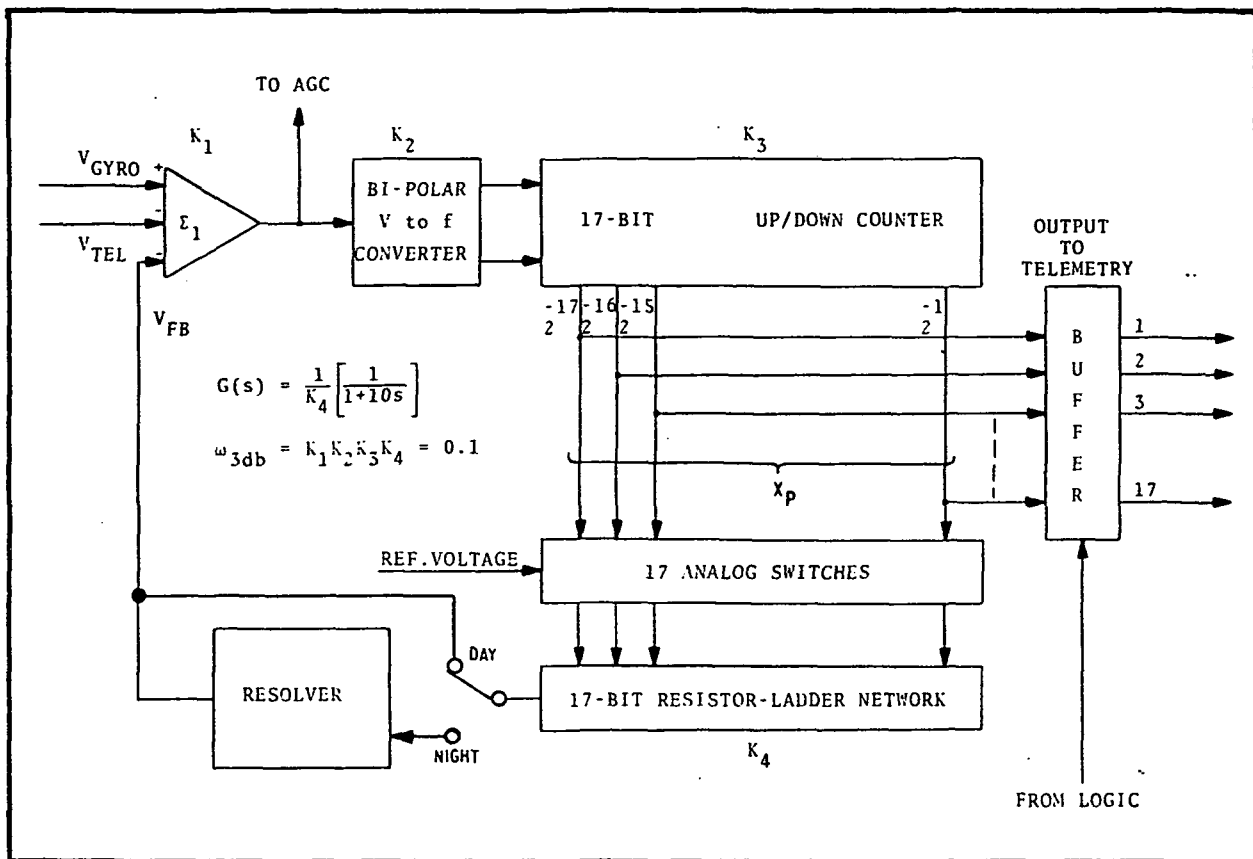


Fig. 5-28 Servo-Type Integrating Analog-Digital Converter

to the input of the loop. This forms a servo-type of parallel-feedback DC to digital converter, which behaves like a type "0" follow-up servo. When the feedback loop is closed, the  $1/s$  characteristic of the forward path results in an overall frequency transfer function of the form  $\frac{1}{1+sT}$ . Thus except for being a function of an integral variable, the external frequency function is identical to that of a simple RC low-pass filter. The integrator gives effectively infinite loop gain at DC, with the result that the A/D conversion accuracy is determined primarily by the D/A converter in the feedback path.



The effective bandwidth of the low-pass characteristic is determined by the product of gain constants around the loop. The gain factor is chosen to give a smoothing time constant of 10 seconds. This corresponds to a 3 dB bandwidth of 0.1 radian per second or 0.016 Hz. This choice represents a compromise between a long integration time desirable for noise reduction and a sufficiently fast response for signal dynamics and recovery from disturbances.

#### 5.3.4.2 Resolvers

Solid state circuitry is used in two different ways in the experiment circuitry to transform signals representing vector quantities or angles to coordinate transformation of signals and to solve for the position angle of a vector, given the orthogonal components.

Sine and cosine analog functions are generated in much the same way as a linear digital to analog transformation except an additional nonlinear ladder network is driven by the digital logic to produce the trigonometric function. If the reference voltage used for the resolver is a signal representing a vector component in one coordinate system and the angle of rotation (shaft position) controls the ladder logic, the output of the ladder will represent one component of the vector in the new coordinate system. Use of the resolver to solve for rotation angles is described in Para. 5.3.4.4.

#### 5.3.4.3 Instrumentation Loop Performance

Instrumentation loop performance requirements are given in Table 5-9. The instrumentation loop is similar to an integrating digital voltmeter with the input operational amplifier also computing the difference between the dual inputs from the gyro and telescope readout electronics. This type of loop is capable of very high accuracy. The corresponding slowness in conversion time is immaterial at the bandwidth of interest here.



Table 5-9  
INSTRUMENTATION LOOP PERFORMANCE

Summing Amplifier -  $\Sigma_1$ :

Chopper Stabilizer Op Amp	
Temperature Drift	< 0.1 $\mu\text{v}/^\circ\text{C}$
Stability	< 1 $\mu\text{v}/\text{mo}$ < 5 $\mu\text{v}/\text{yr}$
Input Bias	< $50 \times 10^{-12}$ amp
Input Offset	10 $\mu\text{v}$ - can be set to zero
Common Mode Rejection	> 80 dB, Bw 0.016 Hz
External Gain	2 v/v

Voltage-to-Frequency Converter:

Gain	$10^4$ pps/v
Linearity Error	< 0.01 percent
Drift	< 0.05 percent/week

Up-Down Counter:

Gain	1 count/count
Capacity	17 bit
Output	Parallel 17 bit word

D/A Converter:

Gain	$10^{-5}$ volt/count
Resolution	10 $\mu\text{v}$ or 1/2 milliarc-sec
Errors	$\leq$ 5 ppm $\leq$ 1 $\mu\text{v}$ from any source



Table 5-9 (Cont.)

Total Closed Loop:

Dynamic Range	$\pm 32$ arc-sec
Quantization of Readout	0.0005 arc-sec
Monotonic Transfer Characteristic	
Linearity Error	$< 0.0005$ arc-sec
Sine Wave Phase Lag Error	$< 100$ ppm
Short Term Drift	$< 5$ ppm
Long Term Drift Elim by Roll	
Gain	$10^5$ counts/volt
Phase Lag	$\tan^{-1} 10 \omega$

The accuracy is primarily a function of the precision with which the parallel binary output of the up-down counter,  $X_p$ , can be converted into the feedback signal,  $V_F$ , and on how well  $V_F$  can be subtracted from the input difference signal,  $V_G - V_T$ . See Fig. 5-28. With sufficiently high forward gain and input common-mode rejection, the conversion accuracy should be essentially that of the D/A converter in the feedback path.

The least significant bit of the 17 bit D/A network is  $10 \mu\text{v}$ . Therefore the offset in individual transistor switches, etc., must be restricted to the order of  $1 \mu\text{v}$  if their cumulative effect is to be safely less than  $5 \mu\text{v}$ . Precautions must be taken to eliminate leakage current through turned-off switches, capacitive feedthrough transients, finite resistance of closed switches etc. Thermal emf's are very serious at this level so all junctions of dissimilar metals must be eliminated. This applies to the DC portions of the gyro readout loop as well.



The reference voltage for the D/A network directly affects the absolute accuracy. A constant-temperature environment is needed to hold variations with time to the required 1 ppm. A relatively constant temperature environment is desirable for the critical resistors in the D/A network. The design of all the BJT and FET switches and selection of components will be very demanding in order to minimize the non-ideal "on" and "off" characteristics and their variation with time and temperature.

#### 5.3.4.4 Roll Encoder

Figure 5-29 is a schematic of an electro-mechanical resolver which solves for the rotation angle between two coordinate systems. The inputs to the resolver are voltages representing the orthogonal components of a vector in the "unrotated" system. Figure 5-29 shows how the vectors ( $\sin \theta$  and  $\cos \theta$ ) in the "unrotated" system (X-Y) can be used to develop an error signal ( $\epsilon$ ) of the proper phase to indicate when the shaft position(s) is just equal to the unknown angle  $\theta$ .

In Fig. 5-30 the error signal  $\sin \epsilon$  ( $\approx \epsilon$ ) is developed by summing the voltages developed by sine and cosine potentiometers. The motor drives the potentiometers until  $\epsilon = 0$ , and the shaft angle is equal to  $\theta$ .

To mechanize this system using solid state circuitry, the potentiometers are replaced by non-linear D/A function generators, the shaft-position is stored in a digital register which drives the function generators and the motor is replaced by a V/f counter. The content of the shaft position counter is the output or rotation angle.

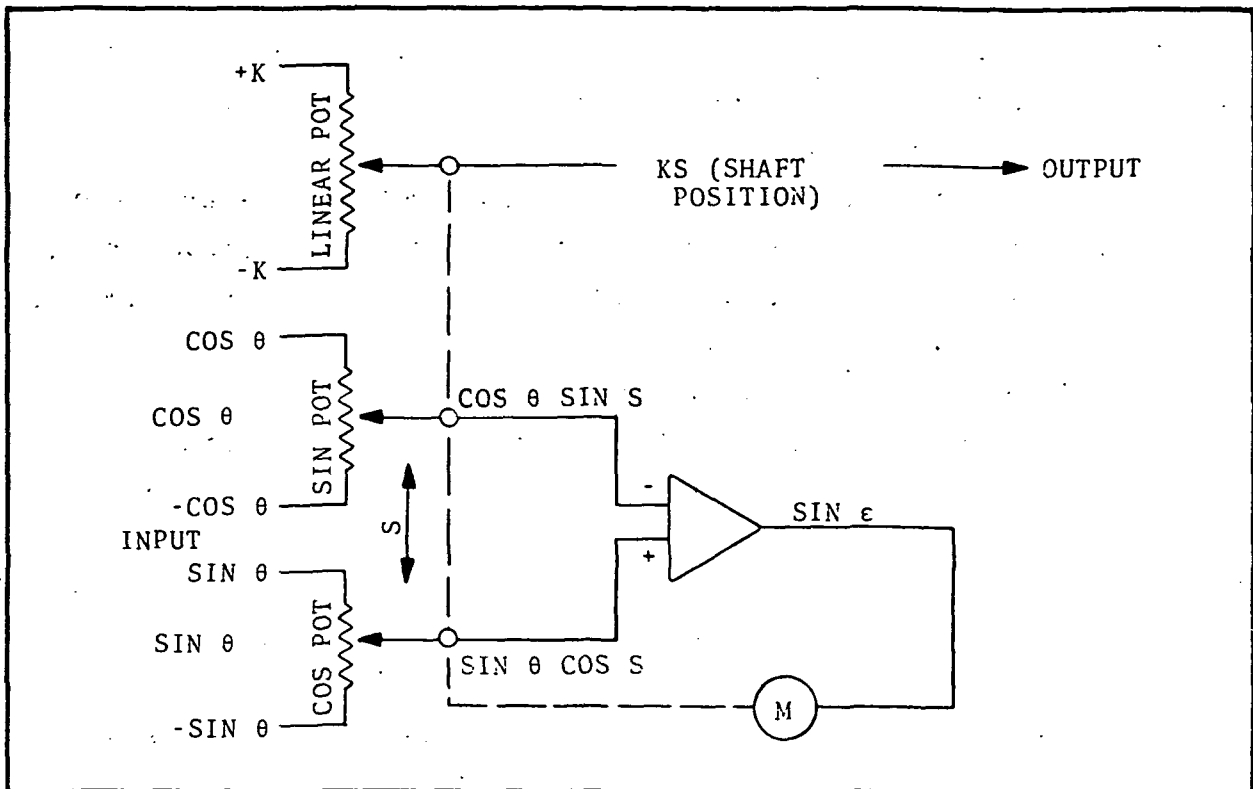


Fig. 5-29 Simplified Diagram of Electromechanical Resolver

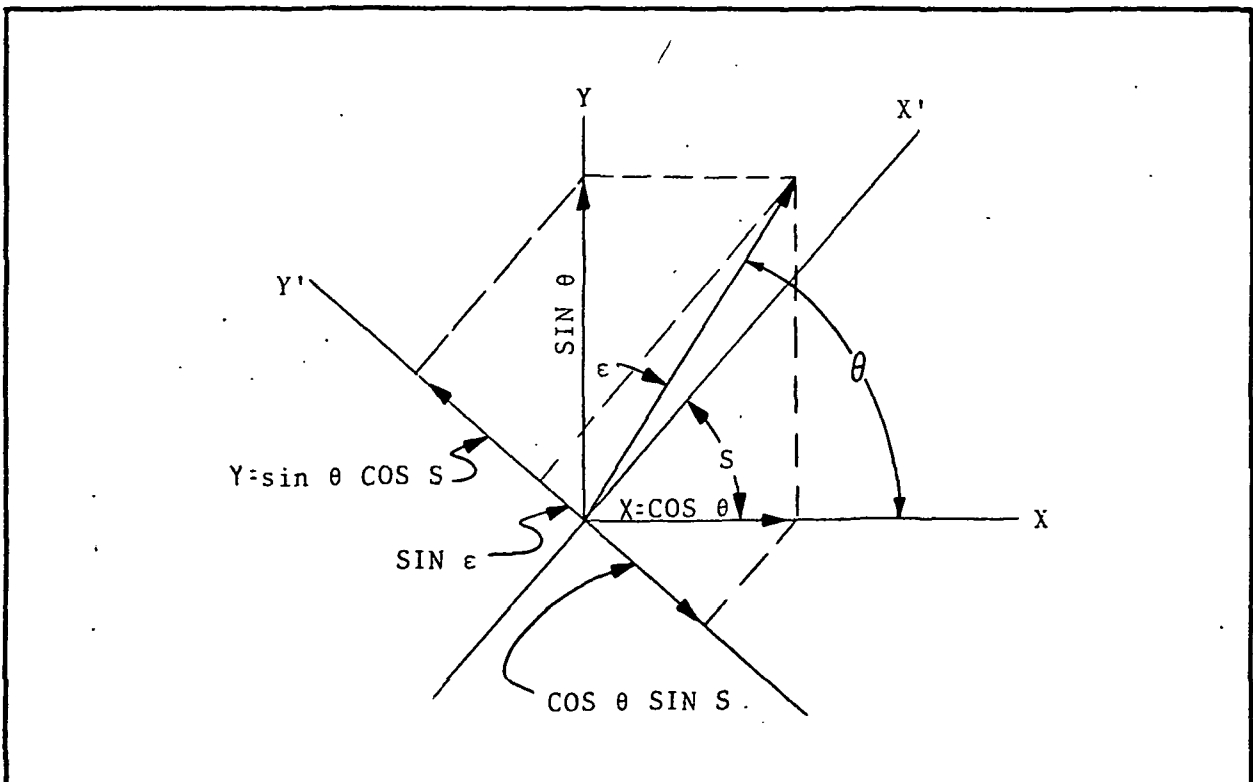


Fig. 5-30 Graphical Representation of Resolver Function

The roll encoder derives the instantaneous roll position of the quartz block using data from the perpendicular gyros.

The encoding function shown in Fig. 5-30 uses a "coarse" loop which is driven by the seven most significant bits of a "shaft position" register to generate an approximate value of the vector components.

A second "fine" loop uses derivative or "slope" function generators driven by the 12 least significant bits of "shaft position" to interpolate between the digital steps in the coarse function generators. This is shown in the inset where  $\sim \cos \theta \cos S$  is the value developed by the coarse generator,  $\Delta \theta$  is the contents of the 12 least significant bits, and  $m$  is the value of the slope at the position  $S$ .

The resolver error signal, derived by summing the signals developed by the function generators, drives the bidirectional (shaft position) counter through a V/f converter until the error is nulled.

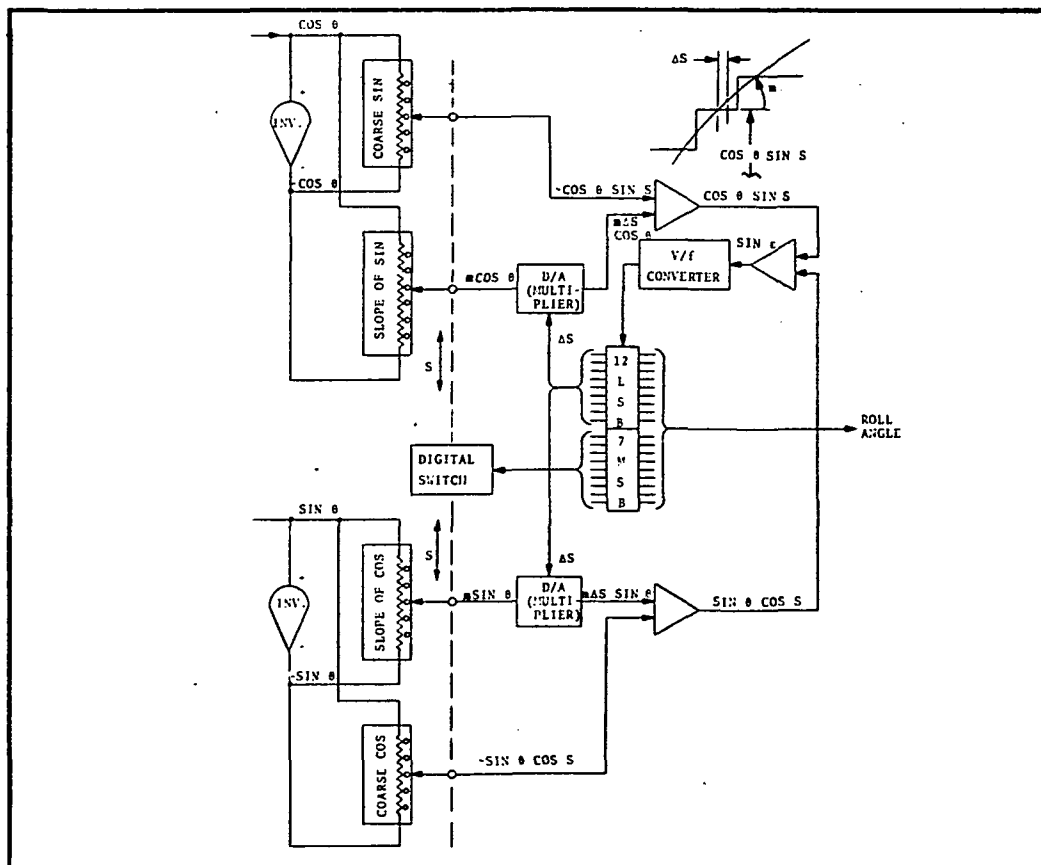


Fig. 5-31 Functional Diagram of Roll Encoder





#### 5.4 HELIUM DEWAR

Requirements placed on the helium dewar are quite severe due to the constraints of the experiment. Specifically, the experiment must be maintainable; it must have a viewing aperture for the telescope; and it must be capable of being cooled down initially in a low magnetic field. There is no known facility with a low enough field that can hold the full-size dewar. This magnetic field requirement dictates the use of a dewar within a dewar as described below. The inner dewar is also dictated because it is desirable to have a spare at this level of assembly. A lower level spare could not be maintained as a "ready to plug in" spare. Additional constraints for the dewar are the electrical wiring requirements for the experiment and the plumbing associated with gyro spin-up and subsequent evacuation of the cavity.

The outer shell of the dewar is the primary structure of the satellite and is discussed in section 5.1. The dewar must provide a load path from the external shell to the telescope/gyroscope package. This load path must be provided to support the instrument during the launch as well as for operation of the external control system during the orbital flight. To meet these structural requirements, the system should have strong retractable supports to handle the launch loads and smaller fixed supports to reduce heat input for orbital control. In addition, a structural and thermal tie is required between the inner dewar and outer main dewar. The final structure is the flex pivot required to gimbal the telescope/gyroscope package for internal fine pointing at the guide star. This gimbal must also provide a heat path from the experiment to the helium.



Most of the requirements noted above have conflicting thermal and structural impacts. However, a dewar system has been defined to meet these requirements. A description of the system, and a more detailed description of the major areas requiring definition, follows.

#### 5.4.1 System Description

A system to meet the requirements noted below consists of two dewars and a window neck area. The specific requirements are as follows:

- 1 year life
- Temperature of 1.6°K
- Provide support for the experiment
- Allow for gyroscope spin-up
- Provide for rapid pump-out of the gyroscope cavities
- Allow access for the experiment to be maintained
- Initial cooling in a magnetically clean environment
- Provisions for electrical components and leads
- Optical windows for the star tracking telescope
- Capable of being tested and supported for launch operations

The description of the system is broken into three sections, starting with the main dewar.



Main Dewar. An overall layout of the system is shown in Fig. 5-32. This drawing shows the main dewar with a center core for the experiment package which is contained in the inner dewar. The space between the pressure vessel and outer shell is a vacuum annulus filled with multi-layer insulation. This is evacuated to  $5 \times 10^{-6}$  torr and contains alternate layers of doubly aluminized mylar spaced with nylon or dacron netting. Also contained in this annular space is the support system and three vapor-cooled shields. The overall thermal protection system is a combination of the multi-layer insulation, low conductivity supports and the vapor-cooled shields. The latter, the vapor-cooled shields (VCS's) are incorporated to utilize the sensible heat of the helium gas to intercept heat flowing toward the pressure vessel. Heat is intercepted from the supports as well as from the plumbing and windows in the neck area. By using the refrigeration available in the gas effluent, the performance of the system is greatly improved.

Incorporated into the pressure vessel of the main dewar is a superfluid plug. The superfluid plug, Fig. 5-33, as described by the inventors\*, works because of the unique properties of extreme low viscosity and extreme high apparent thermal conductivity of superfluid helium (helium II). The operating temperature is (below the lambda transition for helium) at 16 mm Hg or about 1.6°K. The plug is a coil of tightly wrapped aluminum foil. Helium II can flow through the small paths between wraps. The pressure drop produced across the plug causes a decrease in plug temperature; and, because of the very high apparent thermal conductivity of Helium II, all heat entering the pressure vessel is caused to flow through the bulk liquid to the plug where evaporation takes place. The plug should work in zero-g because the body of liquid will be continuous and the heat transfer to the plug will be uninterrupted.

---

\*Advances in Cryogenic Engineering, Vol. 16, paper G-1, pp. 277.

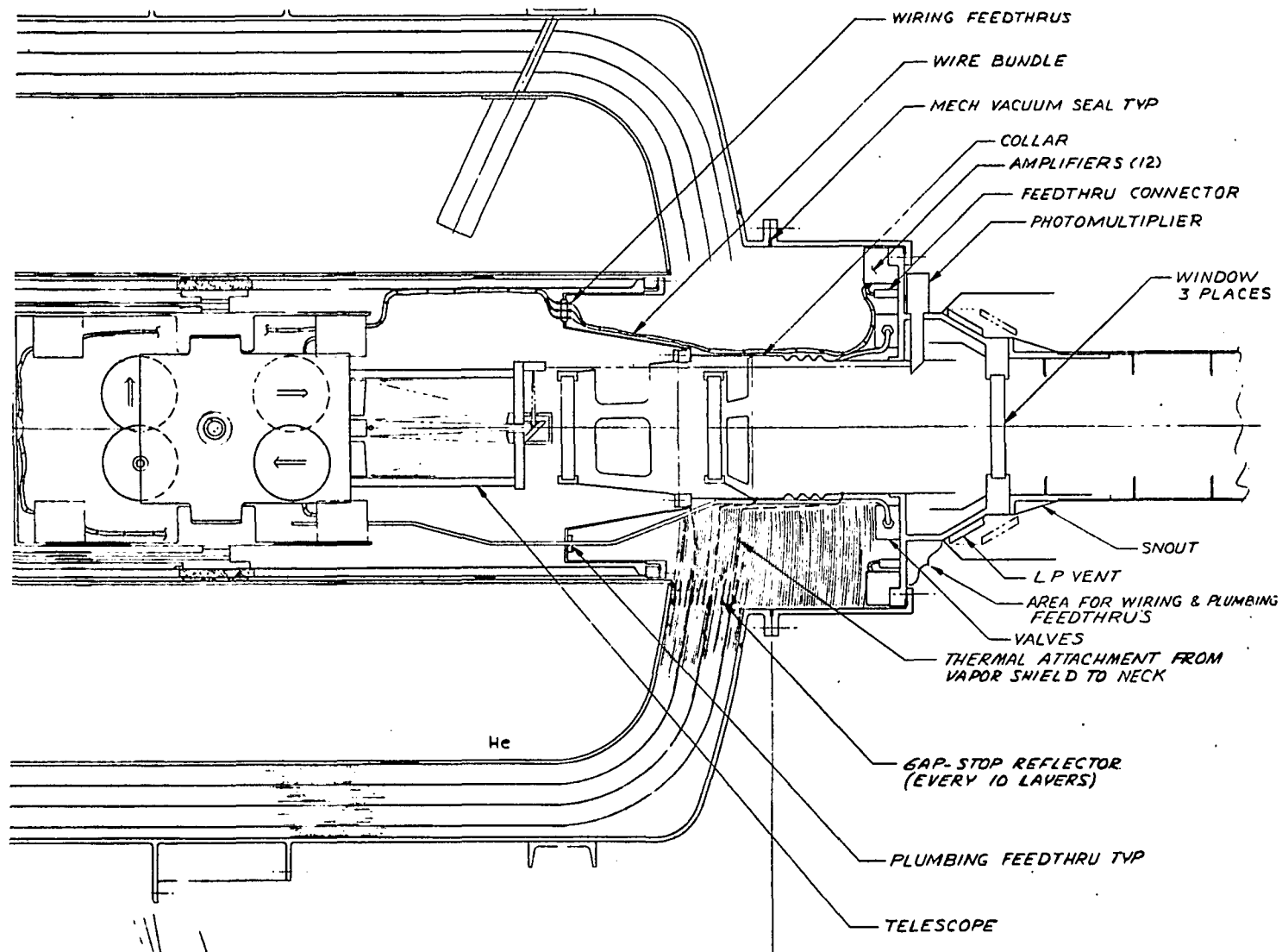


Fig. 5-32 Dewar Cross Section

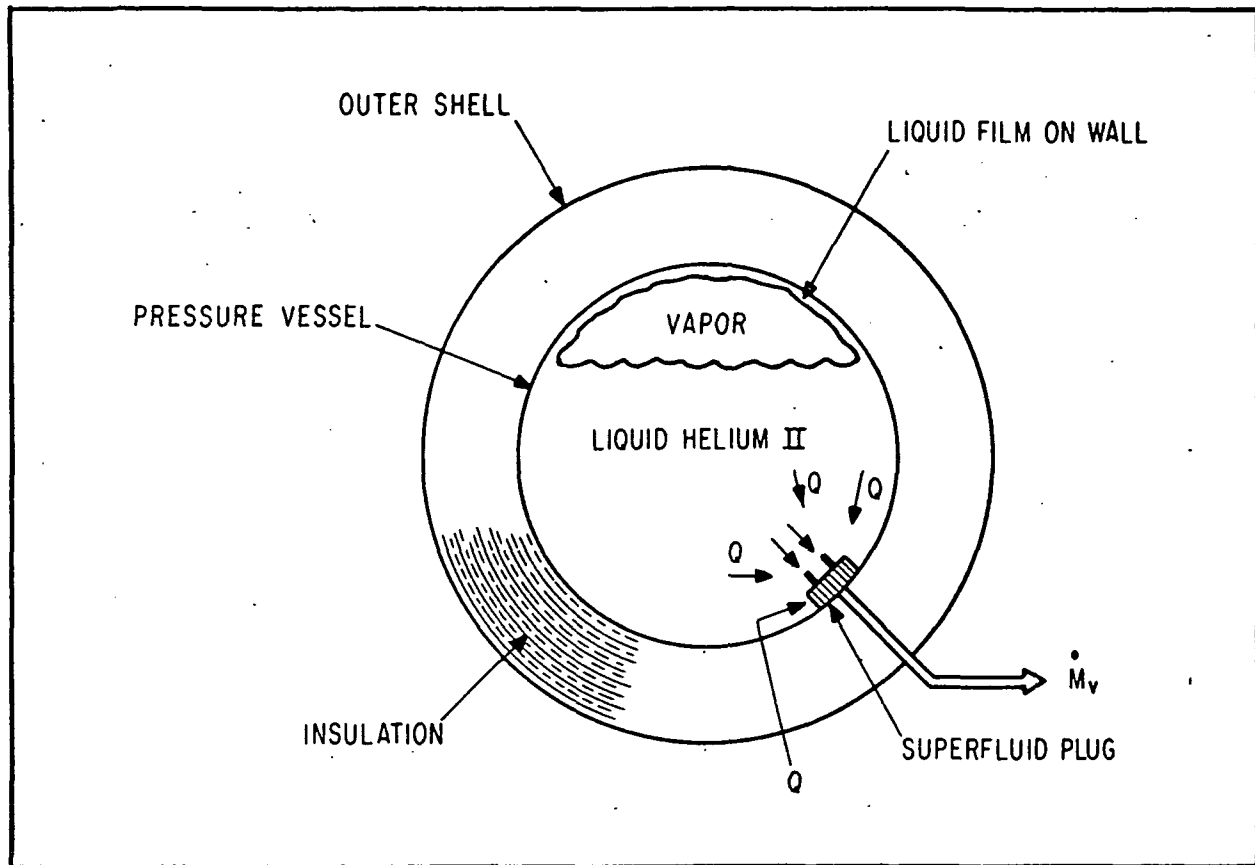


Fig. 5-33 Superfluid Plug

Advantages for the plug are that internally generated heat will be conducted to the plug by the high thermal conductivity of the liquid. Also, the gas exiting the plug leaves via the plumbing and exits directly to space without regulation. The plumbing required is a fill and vent line, wrapped around each shield to provide good heat transfer for the effluent. The shields in turn conduct the heat laterally to the plumbing and thus heat the exiting gas.

Other requirements for the main dewar are to provide for removal and replacement of the experiment and also to control the location of the helium within the dewar during orbital mission. Removal and replacement is mandatory because of the complexity of the experiment and the magnetic shielding requirements for the gyroscope. If the superconducting shields were to warm up for any



reason, the experiment and inner dewar would have to be removed to reattain the low flux field required. Control of the helium location is required to eliminate sloshing of the liquid and keep the center of gravity of the system centered in the quartz block throughout the mission.

Experiment Packages Dewar (Dewar Within a Dewar). The design contains a dewar within a dewar. Some of the advantages of such a configuration are:

- A smaller facility can be used to magnetically "flush" the experiment
- Magnetic material restrictions are less severe for the smaller dewar
- The separate dewar permits separate checkout and assembly of the experiment package and the main dewar
- There are some plumbing advantages to have the experiment self-contained
- One vacuum seal for experiment maintenance is eliminated

These advantages far outweigh the disadvantages of this arrangement. Primarily, these are engineering problems which can be readily solved. In particular, there must be a thermal switch to allow the inner dewar to be converted from an insulating container to a thermally conducting container. Also, the structure is somewhat more complex and some additional plumbing is required.

The design of the inner dewar is quite simple. An inner vessel is suspended by titanium rods within an outer shell and the space between is filled with multi-layer insulation and evacuated. The experiment package is suspended on a gimbal inside this dewar as shown in Fig. 5-34. Figure 5-32, the overall layout, shows the experiment's physical location within this inner dewar. Included with the inner dewar is a reservoir at the end opposite the window. This reservoir will be used to contain the required refrigeration when active cooling is not available and to supply the spin-up gas for the gyroscope.

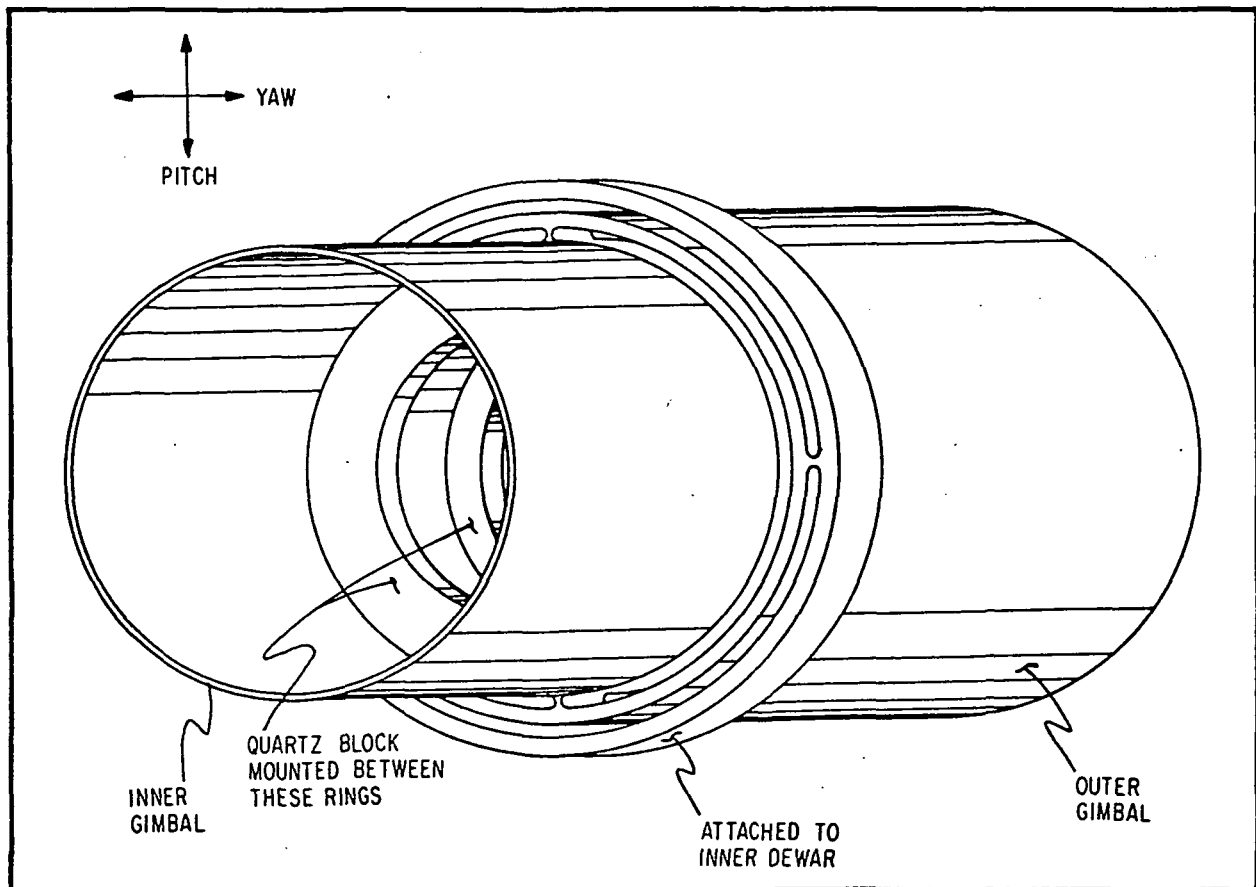


Fig. 5-34 Quartz Block Gimbal



In addition, the inner dewar has an active liquid helium cooling loop to provide refrigeration during operations when the inner dewar is separated from the main dewar. After installation in the main dewar, the larger dewar is filled with helium and the vacuum annulus of the inner dewar is filled with helium to provide the required thermal link between the experiment package and the main helium storage. The front end of the inner dewar is attached to the fiberglass collar which holds the three windows and also supports the plumbing and wiring.

Window Neck Assembly. Because the tracking telescope must be firmly attached and accurately aligned with the gyroscope, it is located in the 1.6K environment. This necessitates a window assembly for the viewing of the guide star. The window and neck assembly is made of three windows attached to a fiberglass tube which is connected to the inner dewar. Paths are provided for evacuation of the instrument cavity and the collar is used to mount the electrical wires required for operation and signal output. The neck assembly is expanded to allow better cooling of the windows and adequate routing of the plumbing required to control the gyro spin-up. All valves and amplifiers are attached to the outer flanges so that the inner dewar with the neck assembly will allow for full checkout of the experiment package. Details of the window neck assembly are given in Section 5.4.5.

#### 5.4.2 Main Dewar Design

Design considerations of a dewar vessel are derived from the experiment requirements, the launch environment and the orbital constraints. Actual design details are worked out for both thermal and structural parameters and the two mated and iterated to derive the final design. The performance characteristics are given in Table 5-10.





Table 5-10  
DEWAR PERFORMANCE CHARACTERISTICS

Dewar weight	204 kg
Fluid weight	136 kg
Total	340 kg
Calculated required helium	82 kg
Safety margin	166%
Size	126.7 cm diameter x 165.1 cm long
Center core	48.2 cm diameter
Frequencies	
<u>Linear</u>	
Launch supports	
Axial	102 Hz
Transverse	171 Hz
Orbital supports*	
Axial	9 Hz
Transverse	13 Hz
Gimbal	2-30 Hz
<u>Angular</u>	
Orbital supports*	
Around axis	2 Hz
Normal to axis	6 Hz
Gimbal	0.16 Hz

\* Minimum cross sectional area supports



#### 5.4.3 Thermal Design

The entire insulation, support system and thermal design must be solved concurrently to arrive at an optimum configuration. The problem is to reduce heat leak (or weight) to a minimum consistent with:

- The ability to fill the vessel
- The ability to operate during prelaunch and standby operations
- The ability to survive launch loads
- The ability to handle the zero-g venting problem
- The ability to provide sufficient gas for the attitude control and gyroscope spin-up systems
- Provide 10 times normal boil-off for emergency control purposes

##### 5.4.3.1 Thermal Analysis

The thermal analysis of a dewar can be divided into four steps: dewar sizing; calculation of plumbing, wiring, and penetration heat leaks; active shield location optimization; and iteration with structural, mechanical, and electrical designers. The first step has been completed and preliminary calculations have been made for the second.



The first step was done for a dewar with 1 cubic meter volume containing 135 kg helium surrounded by 30 kg of multilayer insulation and three active cooling shields, and internally supported by six fiberglass bands of 0.25 cm area each. All heat leaks which are small and/or not strong functions of temperature (such as plumbing, wiring, and penetrations) were assumed to be direct heat loads to the various shields and the dewar. These heat loads and the proper area-to-thickness and area-to-length ratios for the insulation system are input to a BBRC-developed computer program\* (HEL2 or HEL3) which computes the flow rate and the temperatures of the actively cooled shields. Equations for these programs are given in Appendix D. This flow rate multiplied by the desired life of the dewar and the desired safety factor should be less than or equal to the weight of helium initially assumed.

Heat Leak Breakdown. Results of the thermal calculations are shown in Table 5-11. The 135 kg capacity concept design is partially optimized in that the active shields are believed to be close to their optimum locations. The contribution of the multilayer insulation to total heat leak is very small, which means that either the overall insulation thickness is too great, or that there is a substantial margin of safety in the thermal conductivity assumption. The in-orbit fiberglass supports are larger than required for 1 g loads to simplify attitude control system design. The heat leak through the supports is still reasonable.

The two-window telescope viewing port which Stanford was considering at the start of the mission definition study was replaced by a three-window port because of the large preliminary heat leak estimates. The heat leak for the current design is quite low.

---

\*BBRC Final Report F70-14, "Study of Design Considerations for Maintenance of Space Experiments".



Table 5-11  
DEWAR HEAT LEAK SUMMARY

	<u>Orbit (Milliwatts)</u>	<u>Launch (Watts)</u>
Multilayer Insulation	0.3	negligible
Fiberglass Fixed Supports	8.6	negligible
Power Dissipation & Wiring	29.0	negligible
Albedo	2.0	negligible
Plumbing	16.4	negligible
Neck Sleeve Conduction	24.4	negligible
Window Stray Radiation	0.2	negligible
Neck Sleeve Radiation	0.1	negligible
Launch Supports	---	6.4
	<hr/> 81.0 mW	<hr/> 6.4 W

It is possible that a two-window design would be satisfactory with proper use of active cooling.

Multilayer Insulation. The best type of insulation must be chosen from the family of multilayer insulations to meet the required thermal performance. Various investigators have reported low "K" values for these materials:

1. Reflector

- a) aluminum foil
- b) metallized plastic film (usually aluminized mylar)



## 2. Spacer

- a) none (crinkled metallized plastic reflector)
- b) glass papers
- c) netting and screen
- d) fuzz attached to reflector
- e) foam

Almost all combinations of these reflectors and spacers have been tried. Most flat plate "K" factors for samples lie in the range from 7 to 40 ( $10^{-8}$ )  $\frac{\text{Watts}}{\text{cm}^2\text{C}}$  between temperatures of 300 and 77°K under  $10^{-5}$  Torr maximum interstitial gas pressure. The group of investigators shows no single combination consistently outstanding. Generally, some kind of spacer is desirable. Combinations using aluminum foil tend to have lower "K" factors.

The problem of selecting the best insulation falls back to secondary considerations such as its:

- Density or total weight
- Ability to be applied to shapes without performance degradation
- Ability to be attached
- Vibration sensitivity
- Lateral conductivity to penetrations
- Outgassing
- Availability



The proper weight of these factors depends entirely on application; for vessels of the type under consideration here, the selection was made as follows:

1. Film - netting: Selected. Its "K" factor is among the lowest. The strong netting provides a positive way to attach the insulation through the net holes; therefore vibration resistance is good. Density is low. Outgassing is much lower than glass papers.
2. Aluminum foil combinations: Rejected. Density of these combinations is too high to justify slightly lower "K" factors. "K" factor is degraded most by permanent set after acceleration. The lateral conduction is higher than others. Ability to resist slumping in vibration without detrimental precompression (or holding pressure) is questionable.
3. Film - glass paper: Rejected. Density is too high for the older "thick" glass paper. Newer papers are much better but strength at attachments is very low. Needs some kind of quilting or cross-tie scheme to prevent slumping in vibration. These schemes add to the conduction by precompression. The newer glass papers run a very close second to the selected configuration because of their lower lateral conduction properties around penetrations. Best use seems to be as special parts in these areas. Glass fibers, however, are inherently very difficult to dry out in vacuum acquisition.
4. Film - foam: Rejected. These are also close to the selection but fail on strength.



5. Film - fuzz: Rejected. Attachment is poor without some reinforcement, and fuzz needles may damage insulation during vibration. Therefore vibration resistance is questionable. Thermal test data are limited and material is not readily available.
6. Crinkled film: Rejected. "K" factor tends toward the high end. Has questionable vibration characteristics.

In the film-netting group, there are several choices. As a baseline we will use 6 $\mu$  (1/4-mil) mylar, aluminized on both sides and spaced by nylon netting with 1.5 mm holes. There may be some advantages for metallized films of silver or gold or for netting of dacron or silk. Mylar of 6 $\mu$  thickness is available and has been used.

Layer Density. Over the total temperature range from 300 to 77°K, test data show that the density which provides lowest "K" factors varies from about 10 to 30 layers per cm. As the lower boundary temperature decreases, this optimum density decreases although much less test data are available. Practically no test data are available for the entire range from 300 to  $\approx$  0°K. Various investigators have attempted to analytically split the components of radiation and conduction to provide a better basis for design. In this design, we have used the available data for temperature dependence of an arbitrary 50-layer-per-inch layup.

The practical aspects of making a good insulation layup tend to drive the optimum layer density to lower values. Any wrinkles, folds or stiffness of the insulation tend to increase the solid conduction component through lower contact resistance. On the other hand, lateral radiation at penetrations can increase seriously if the layer density becomes too low. Multilayer



insulation "K" factors increase very rapidly with compression and there is a significant permanent increase in the "K" factor when pressure is released. This fact tends to decrease the optimum layer density due to the pressure of upper layers on lower layers during acceleration.

The suspension system supports the vapor shields and prevents the shields from compressing insulation. This arrangement also allows tailoring of the optimum layer density through the separate temperature ranges between shields. Final analysis will probably dictate a very low density (2 to 4 layers per cm) between the pressure vessel and the first vapor shield, an intermediate density between the first, second, and third shields, and a high density (20 to 40 layers per cm) between the third vapor shield and outer shell. Aluminum foil and tissueglass will probably be used between the first shield and pressure vessel, and the rest of the insulation will be metallized film and net.

Vacuum Acquisition. Insulation reflectors are sometimes perforated to aid initial vacuum acquisition. This procedure increases heat leak somewhat, and the material is partly degraded by the perforation process. Also, the holes tend to snag on spacers during layup. Tearing is more likely to start during vibration. We have found that an adequate procedure is to use unperforated insulation and simply pump longer during vacuum acquisition. Perforated insulation seems to have its best application on systems which are to be evacuated by space during launch.

Support Insulation. Many kinds of insulating supports have been used on cryostats. The conventional approach found on most commercial laboratory dewars is to hang the pressure vessel from a neck and to use no side support. This design is entirely inadequate for spacecraft launch loading. Spacecraft dewars have





been supported by insulation pads or metal trusses. Existing designs are inadequate because they have high heat leaks. Fortunately, high-strength glass-reinforced epoxy composites have been developed for cryogenic service. These are the most desirable materials capable of satisfying the proposed requirements. A design must be developed from these composites which makes good use of the inherent high-strength, low-conductivity properties. Typical thermal conductivities of unidirectional composites are shown in Fig. 5-35. A very important controlling factor is that the design must be compatible with the multilayer insulation so that low penetration heat leak will result. The material may be used in pure tension, compression or in combination such as in bending. The advantage of a pure tension member is that the cross-section of the support is minimized. Other supports require larger cross-sections and the size of penetrations tends to be large, although there may be fewer penetrations. Overall optimization tends to favor the pure tension member. The particular design we have chosen is shown schematically on Fig. 5-36. Heat flows lengthwise down the support from the outer shell to the pressure vessel. Heat flows laterally from the support into the cooled shields at the shield attach points. Heat flows in and out of the support from the multilayer insulation. Details of the penetration treatment follow.

In the conceptual design, shields are attached to the supports at crossover points. This geometry is an expedient used during early thermal analysis and these attachment locations are not necessarily optimum. Figure 5-37 shows detail at the attachment. The two-legged supports are convenient for placement of this attachment and off-setting is possible, as shown in the small detail. Mechanical attachment is desirable because most adhesives are quite brittle at these temperatures. Bonding is necessary because the thermal contact area must be "wetted" to transfer heat well in vacuum.

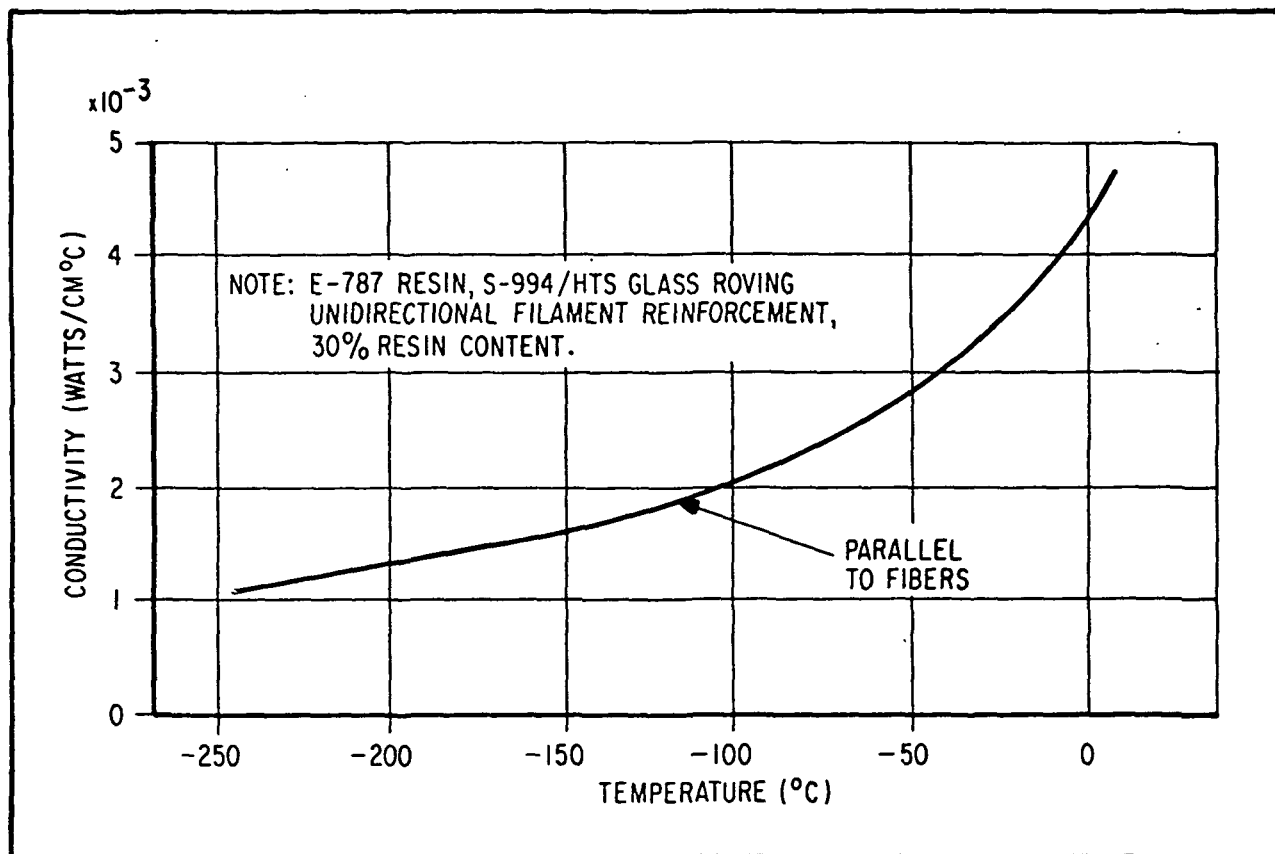


Fig. 5-35 Thermal Conductivity of Unidirectional Epoxy-Fiberglass Composite

Penetrations. The penalty associated with a penetration is defined as that heat leak in addition to separate unidirectional heat leaks of the insulation and penetrating member. Penetration heat leaks comprise a significant fraction of the total heat leak in high performance tanks and as such they must be studied and minimized throughout the design effort. Penetrations can be important enough to cause iterations in the entire design so as to minimize total heat leak.

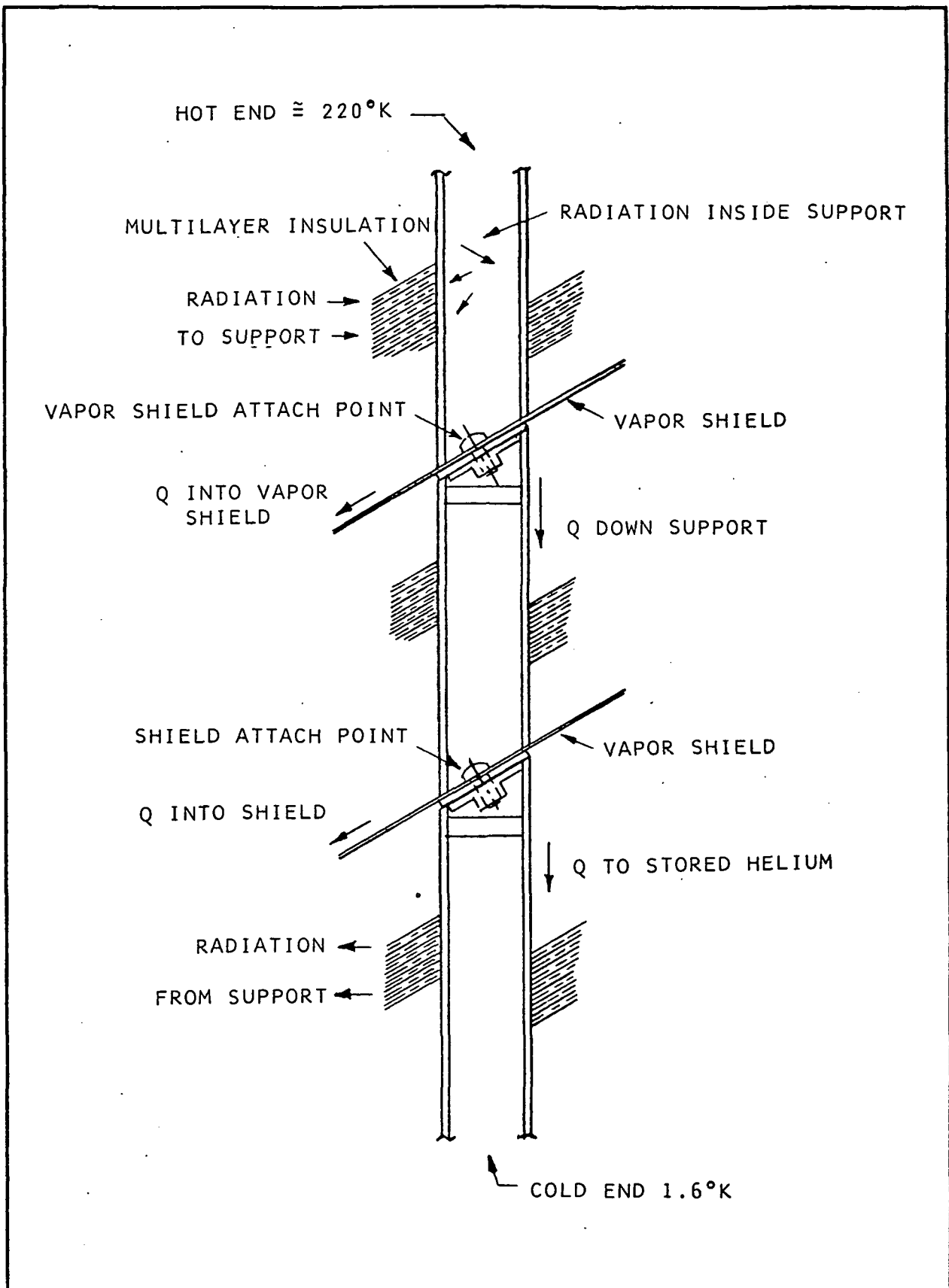


Fig. 5-36 Support Thermal Paths

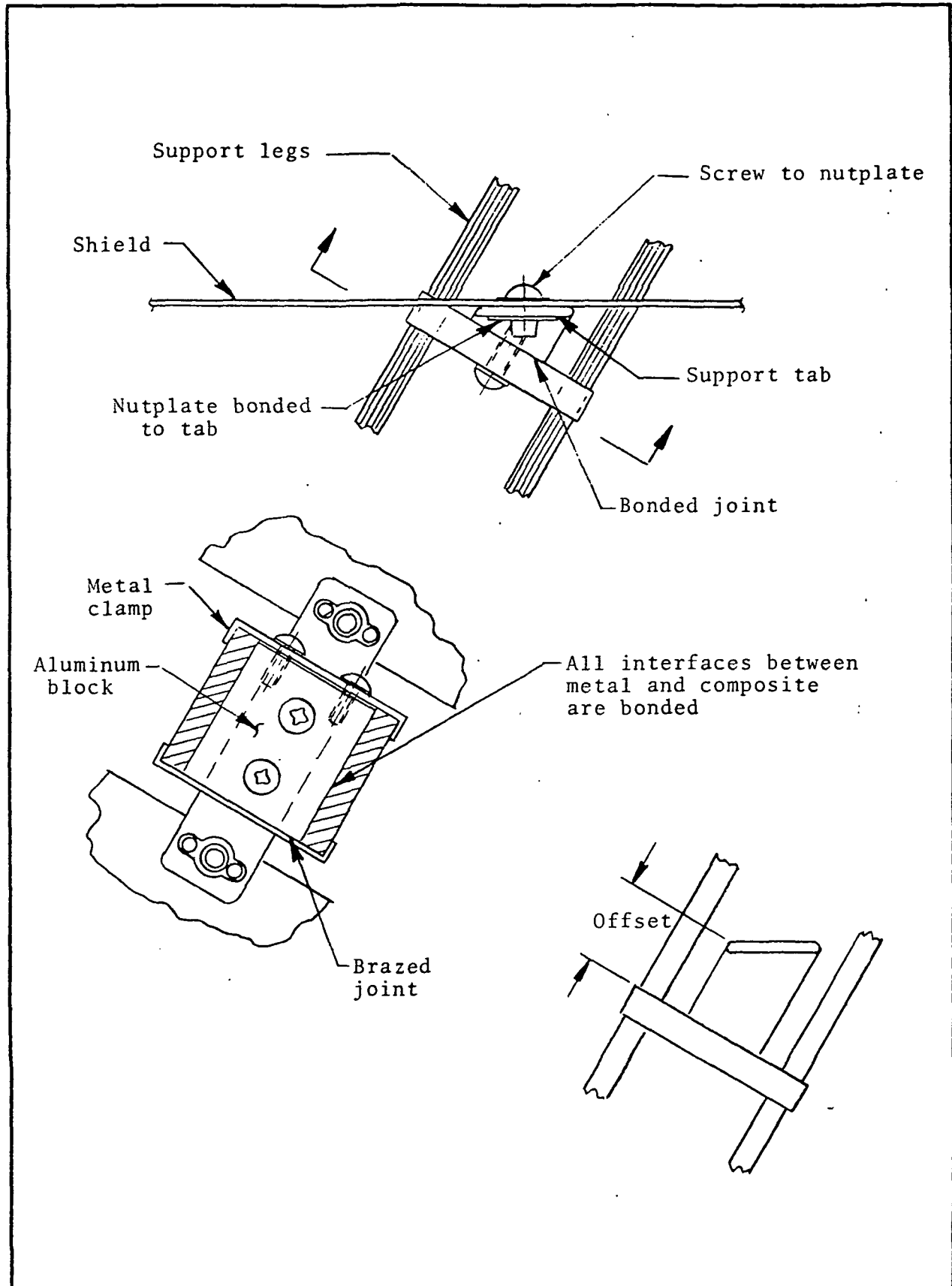


Fig. 5-37 Vapor Shield Support Heat Transfer Attachment



Penetration heat leak is caused by a mismatch of local temperatures between the penetrating member and the insulation. The outer containment and warmer layers may view colder layers and the inner vessel through the cut. The same is true for the penetrating member. Both radiation and solid conduction are present. Penetration heat leaks are minimized by providing an optimum treatment which attempts to match local temperatures, decouple the heat flow paths and minimize unnecessary gaps.

Penetration Treatment. If the edges of insulation layers are initially assumed to be in perfect thermal contact with the penetrating member, then the design concept of a thick, fibrous buffer zone will evolve. If the edges of insulation layers are assumed to be initially out of thermal contact with the penetrating member, other methods of treatment will appear to be better. While the fibrous buffer zone may seem to be an improvement over the first condition, it may be worse than the second. The real initial condition is between these extremes and certainly much closer to the second because a hole cut around a penetrating member will touch only on a small percentage of the edge and with greater than zero thermal resistance. Treatments and analyses presented hereafter are based on the zero contact assumption with due respect to the fact that this idea may be slightly less than conservative. When the complications of support cooling and assembly are considered, a purely radiative concept appears to be best.

Figure 5-38 shows the area around a fiberglass tension member. "U" shaped cutouts pass over the support as insulation cylinders are applied. At optimum spacings (every 3 to 5 layers) a punched aluminized mylar washer is passed over the support assembly. Depending on the results of further analysis, netting or glass paper spacer washers separating the mylar washers may be required. The fiberglass support is enclosed in a loose sectional sleeve of stiff aluminized mylar. These sleeve sections incorporate radiation dams which insulate the area inside the legs of the support.

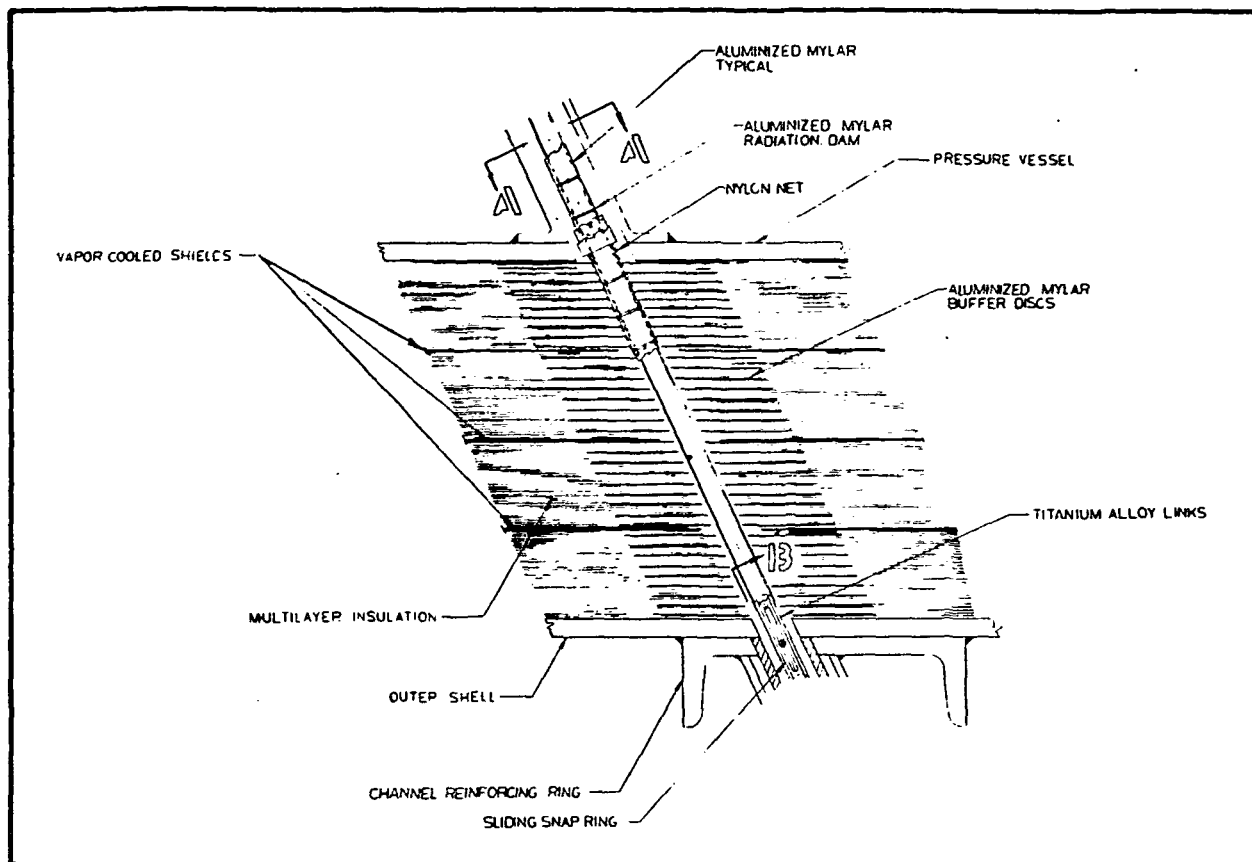


Fig. 5-38 Fixed Dewar Support

In the well at the cold end of the support, a stiff aluminized mylar collar "looks" at the sleeved support. Space is provided in this annulus for additional layers if these become necessary. The critical hot end radiation gap is covered by a gold-coated mylar cap. The hot end of the support is insulated after the outer shell is installed and before the support is attached. The end fittings are gold-coated and several concentric aluminized mylar cylinders are nested between netting or glass paper spacers around these ends.



There are six identical penetrations for supports. Tube penetrations are treated in the same manner. The two tubes penetrate each of the three insulation blankets in separate places. This arrangement provides insulation against all significant heat paths. Contact with the support is decoupled by the separate washers which are only used where necessary and not at every layer. The normally "grey" fiberglass is made externally reflective by the sleeves which are only weakly coupled by slight contact with the support. The view across the support inside is to aluminized mylar in one direction. Heat flow in the fiberglass-to-fiberglass direction is minimized by the sleeve dams which prevent heat flow across large temperature gradients. Heat flow in the "well" is easily resisted by aluminized mylar at the low temperatures found there. The cap on the hot end is intended to completely fill the gap around the support.

This conceptual design uses a minimum of parts and conservative emissivities are assumed. Improvements can be made by using gold-coated washers and sleeves. It would also be possible to aluminize the inside of the supports to further reduce penetration heat leaks.

Penetration Analysis. Penetrations are analyzed using the two computer programs discussed in Appendix D. The area is modeled as a closed-end set of concentric cylinders. Once geometry values are chosen, all view factors are calculated. Using emissivity and temperature inputs, a second program calculates the heat entering or leaving each of the surfaces. Once the heat entering or leaving the insulation and penetrant are first calculated, an iteration process starts which readjusts penetrant and insulation temperatures to calculate new unidirectional heat flows through these members.



The hardware being analyzed is inherently variable because of the loose tolerances required and the flexibility of insulation. It is imperative to analyze the geometry in its extremes to determine overall sensitivity of performance to these variations. To do this, maximum and minimum values are applied to gaps and areas. When a highly sensitive region is found, the geometry is improved to provide a design readily produced as analyzed.

Vapor Shields. Because of the high ratio between the sensible and latent heats of helium, multiple concentric vapor shields are desirable. It has been shown by analysis and test that the heat leak to liquid helium containers decreases significantly when up to 10 concentric shields are used. However, structural and practical limitations prevent the use of that many shields in space flight applications.

The design uses three main shields. Figure 5-32 shows how the shields are spaced within the insulation. These locations will undoubtedly change. Several factors enter into the optimization of these locations:

- Fluid properties
- Pressure vessel effluent condition (liquid, vapor or combination, and transients in the mixture)
- Temperature-dependent performance of multilayer insulation





- Overall geometry of container
- Support system cooling (geometry and thermal performance of supports)

The thermal system has been analyzed by computer, using the programs discussed in Appendix D. Refinements in the computer program to account for penetrations and the third shield have been added.

#### 5.4.3.2 Structures

The purpose of the structural analysis of this system is to ensure its structural integrity when acted upon by various forces. The forces which must be considered are the result of the following:

- Accelerations produced during ground handling and launch
- Fluid pressure of the cryogen or the atmosphere
- Temperature gradients and differences in contraction coefficients



The major structural problems are the pressure vessel, the supports, and the outer shell. Secondary problems are the shields and tubing. The general approach of the analysis will be as follows:

1. Analysis of the pressure vessel to the extent required to obtain approximate weights
2. Approximate analysis of the supports using the approximate inner vessel weight
3. Approximate analysis of the outer shell
4. Detailed analysis of the three major components
5. Analysis of the less critical parts such as shields and tubing

An iteration is required between the structural and thermal analysis in steps 1 and 2 since there is an interaction between structural and thermal requirements. The outer shell design is established almost entirely by structural requirements. Structural requirements of items such as the shields and tubing have little effect on their thermal performance.

A thorough structural analysis of this system is essential. The loading is far too complex to design using an "engineering sense." In addition, the thermal requirements are too demanding to allow other than a detailed structural analysis.



Supports. The function of the supports is to position the internal vessel within the insulation. The position must be maintained from the time of manufacture until the completion of the mission. Thermal and structural support requirements are opposites in a cryogenic tank. In order to maintain the required thermal resistance, a minimum amount of material must be used in the supports. The support system also must be relatively stiff so that excessive motion of the inner vessel will not damage the insulation, tubing, or electrical wiring, to keep transmissibilities low at the booster frequencies, and to keep mechanical frequencies high to simplify in-orbit attitude control.

During its times of use the cryogenic vessel must withstand a variety of accelerations with no degradation of the insulating qualities of the system. Typically, the resulting loads are moderate during ground handling, maximum during launch, and minimal while the unit is actually functioning. These environments suggest the use of two different supports in the design of the dewar.

Fixed Low Strength Supports. The low strength supports are used throughout the life of the vessel. The low strength supports are effective during orbital operations. As a result, the supports are less strong than required during launch. The in-orbit support must have high strength and low thermal conduction.

The best material for the supports is unidirectional fiberglass bound with cryogenic epoxy. This composite has strength comparable with high strength metals and thermal conductivity an order of magnitude below that of metals. The primary structural problem in using this material is the lack of ductility in the glass.



Stress concentrations are more critical than in a metal part since high local stresses cannot be relieved by yielding. This requires that the supports be thoroughly analyzed to minimize stress concentrations.

BBRC has performed extensive analyses of fiberglass parts of the proposed configuration. The finite element approach was followed. Anisotropy was included in the material properties. The study showed the effects of variations in the geometry of the parts. These general results provided the basis for the proposed configuration. The program will be utilized for a detailed investigation of the final support design. Additional information on the program and the findings of one study are given in Appendix D.

Retractable Supports. Since high-strength supports are not required in orbit, the thermal performance can be improved significantly by retracting a portion of the support system after launch; the remaining supports may have lower strength but better thermal properties. Under the assumption that greater heat leaks can be tolerated before and during launch, the retractable supports may be metal, for which the analysis is less critical and the design simpler than for glass supports. Details of a retractable support concept are shown in Fig. 5-39.

It is still desirable to use fiberglass supports while in orbit. The most severe loading on these supports would occur during ground testing. The supports must position the tank at this time with the primary supports retracted.

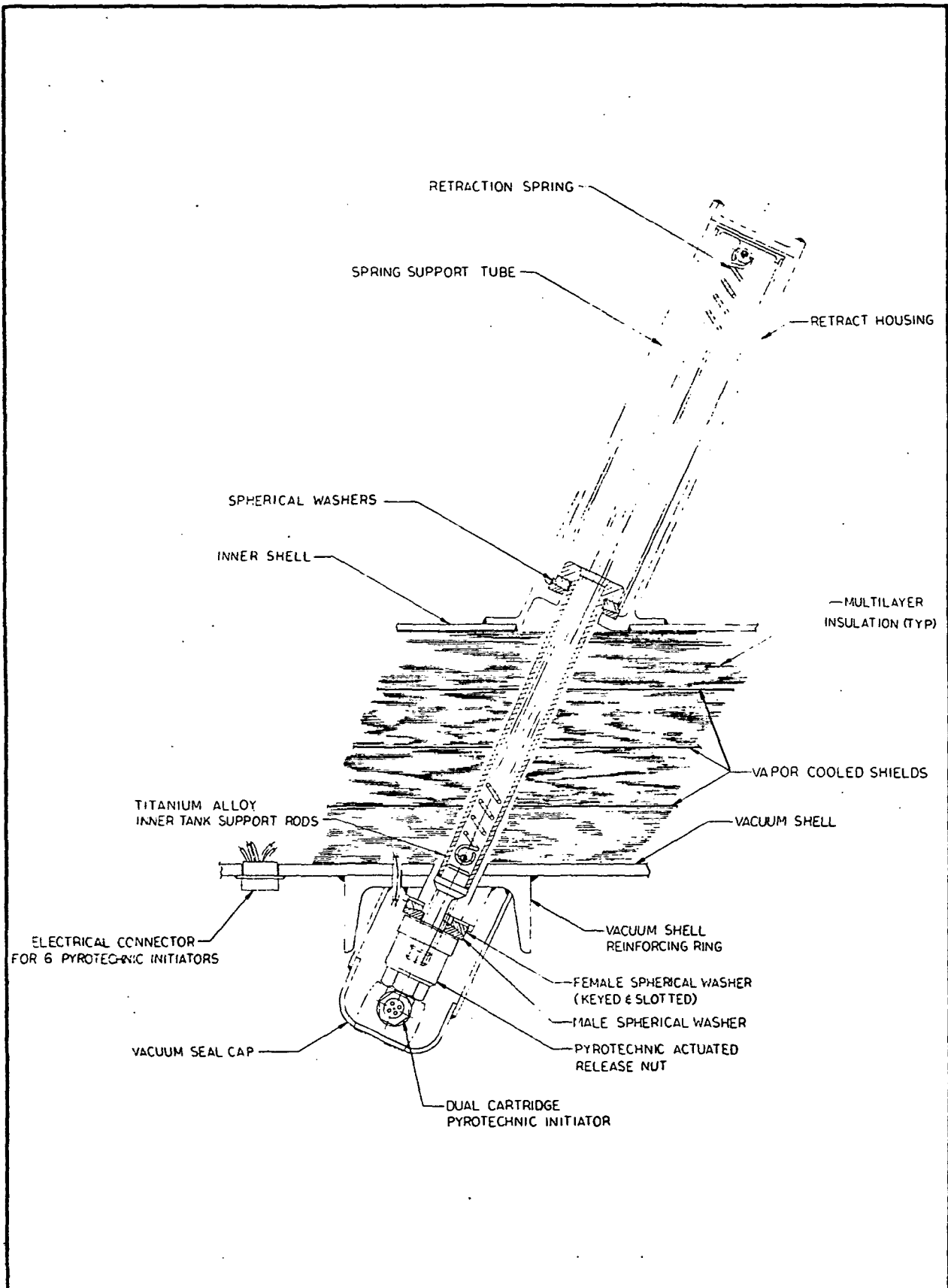


Fig. 5-39 Retractable Dewar Support



Performance of Support System. The support system uses fixed unidirectional filament, wound fiberglass supports. The configuration of these supports is such that a direct load path is provided to the end fittings. The support end attachments also are designed so that bending stresses are minimized in the supports.

The stress levels and rotational vibration frequencies depend on the angular position of the supports. The support angles chosen give equal stress for axial and transverse loads. The drawings show the supports "toed-in" toward the satellite center of mass. This direction is preferred for laying-up the multi-layer insulation. However, "toed-out" supports would give higher pitch and yaw rotational vibrations and this direction may become desirable because of the advantages it offers in attitude control. The supports are pre-tensioned to approximately one-half of the maximum expected load.

Since the supports are radial, the stiffness about the roll axis is proportional to the preload. Any rotation results in a restoring moment proportional to the rotation angle and preload. The preload must be high enough to produce the required roll vibration frequency.

Careful attention must be given to making the support system symmetrical. Symmetry minimizes the response of some potential modes of vibration and simplifies the structural analysis.

Inner Vessel. The function of the inner vessel is to contain the fluid, to provide a load path from the fluid and experiment to the vehicle structure, and to support the experiment. Loads



result from accelerations and fluid pressure. The loadings do not appear too critical at this time. Pressures are on the order of one atmosphere and the maximum vibration response is negligible for the fixed orbital supports.

The thickness of the vessel shell is dictated by a manufacturing requirement rather than some force encountered by the completed experiment. It is necessary that the inner vessel be subjected to one atmosphere of external pressure in order to check for leaks. Thickness calculations for the shell are discussed in Appendix D.

Outer Shell. The function of the outer shell is to maintain an internal vacuum and provide a load path for forces resulting from accelerations. Loading on the outer shell is more critical than with the pressure vessel since the outer shell can have no internal structure. All support loads must be transferred through the shell. Compression resulting from external pressure must be combined with the compression of the support loads since these conditions occur at the same time. A preliminary stress analysis was made using existing BBRC computer programs.

Methods of Analysis. The major portion of the shell analysis was performed with the aid of computer programs. These include:

- A program to determine stresses and deflections in a general structure by the finite element method
- A program to calculate vibration modes of a general structure modeled by finite elements



- A program to calculate the response of a general structure to sine vibration, random vibration, and shock
- A specialized program to calculate stresses in the fiberglass supports

We also used a program which analyzes shells of revolution. (This program was developed by Arturs Kalnins and was obtained from Wright-Patterson Air Force Base.)

To verify the accuracy of the Kalnins program, a simple structure was analyzed with the program and by using the methods of NASA TR R-103\* (for additional detail see Appendix D). The structure was a cylinder closed with a hemispherical head. Results are shown in Fig. 5-40. Obviously, the agreement is excellent.

#### 5.4.4 Dewar Within A Dewar

The dewar within a dewar design has evolved from the requirements of minimizing residual magnetic fields and for handling as described in Section 5.4.1.

Although this concept does add to the mechanical complexity of the system, certain simplifications of the overall dewar system result.

---

\* Johns, R. W. and Orange, T. W., "Theoretical Elastic Stress Distributions Arising from Discontinuities and Edge Loads in Several Shell Type Structures," NASA TR R-103, 1961.



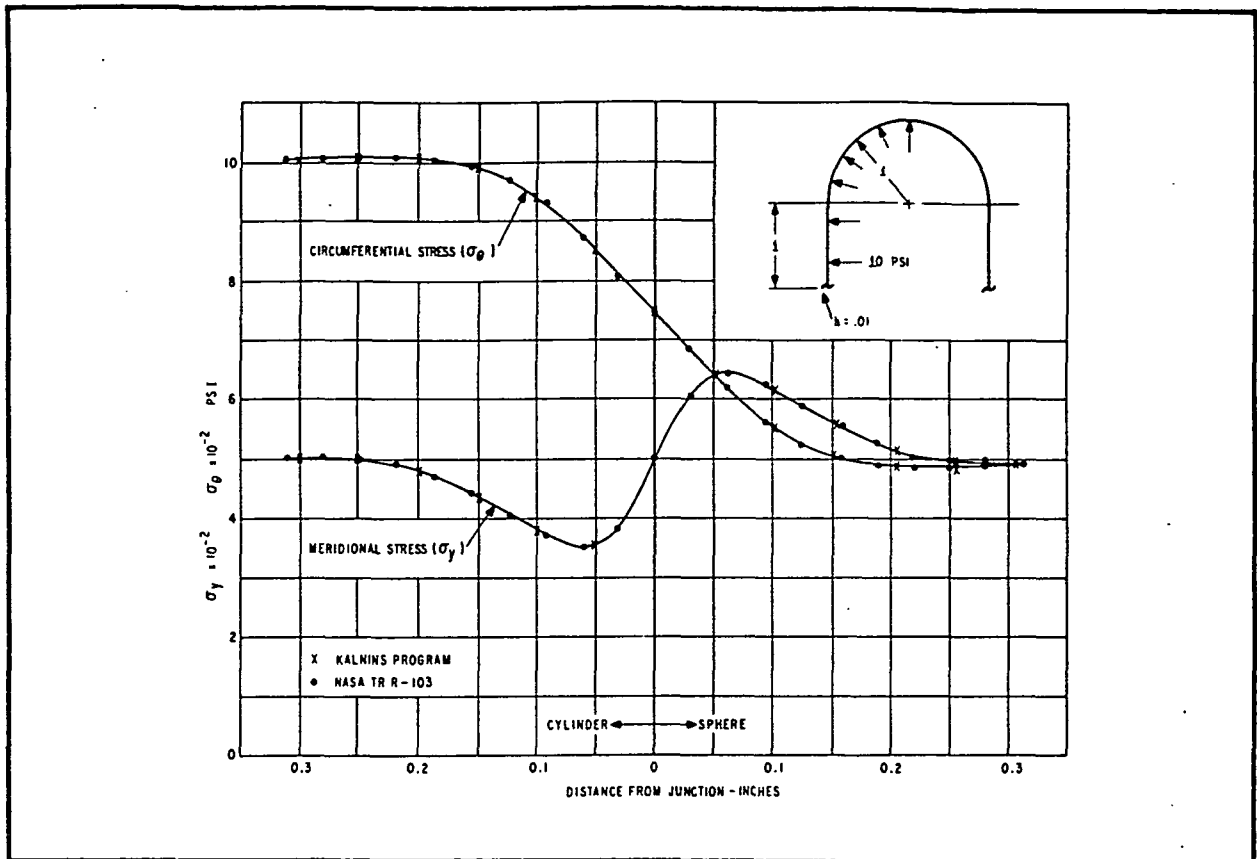


Fig. 5-40 Shell Stress Comparison

Figure 5-32 shows the cross section of the dewar. The central cavity consists of an aluminum tube about 19 inches in diameter. This cavity is connected to the insulation annulus and shares a common vacuum. The inner dewar is similar in construction to a stainless steel laboratory dewar; it consists of an inner and outer cylinder, welded to each other at the end closest to the window. A vacuum space is formed by this arrangement which serves as thermal insulation for the small helium reservoir and the experimental hardware during low-temperature work when the inner dewar is removed from the larger dewar. A valve is required to allow helium gas to fill this vacuum space after the



larger dewar is filled, so that its insulating quality will be destroyed. There must be a low thermal resistance here during normal operation for proper temperature equalization along the experiment.

About halfway along the length of the inner dewar, and just adjacent to the gimbal mount, fiberglass spacers act as low conductivity supports between the walls of the dewar. The entire inner dewar is held in place inside the cavity by the shrink fit of these dissimilar metal parts. Near the window end of the inner dewar, a mechanical seal is made to the neck assembly.

#### 5.4.5 Dewar Neck Area

The neck (or telescope viewing port) is complex because of all the requirements it must meet. The internal part of the neck is bolted and sealed to the inner dewar and stays with the experimental hardware when this equipment is being tested outside the main dewar. A fiberglass collar extends from the inner mechanical seal toward the gyroscope package until it reaches a ring through which all of the tubes and wires pass. The fiberglass collar extends back out of the assembly in a conical form until it reaches a constant diameter section. This straight section is sealed to the outer plate which is part of the outer shell of the larger dewar. A bellows flex section is required to absorb relative motion between the inner and outer main assemblies. This flex section is shown only schematically on the drawing.

Two of the three windows are supported by the assembly of fiberglass collars. The inner, and coldest, window is attached through a conical, highly conducting metal collar. The purpose of this



arrangement is to allow most of the heat which falls on this window to be conducted into the effluent vapor through thermal connections to the vapor shields. Likewise, the intermediate window is attached to the fiberglass collar about halfway along this assembly. Both cooled windows and the outer warm window are coated with gold in such a way that most infrared radiation is reflected but the desired visible light is transmitted to the telescope.

The inside surface of the collar assembly is selectively coated to minimize the amount of thermal radiation which arrives at the inner dewar. The optimum treatment consists of bands of absorbing and reflecting coatings which are placed according to the overall thermal balance which includes cooling stations attached to vapor shields. Thermal analysis results for this arrangement are described in Section 5.4.2. Structurally, the collars must withstand one atmosphere of external pressure because the inner space will be evacuated for tests while the experiment is removed from the larger dewar.

Thermal connections to vapor shields are made by attaching copper braid straps to metal rings on the outside of the collars. This operation must be done each time the inner dewar and experimental package are removed from the larger dewar. During this process, insulation layers must be replaced in the neck area. This is accomplished by placing split rings, consisting of several layers of insulation, around the neck. After each set of layers is installed, a circular gap will appear between the main dewar insulation and the rings. This gap is covered by one ring of stiff aluminized mylar which overlaps the gap and must be spliced into the main dewar insulation.



The interior of the collar assembly also serves as the low pressure vent path for gyroscope spinup gas. Large rectangular holes in the window support collars allow the gas to bypass the collars. The exhaust is vented in space vacuum through more rectangular holes around the circumference of a conical collar near the warm window. This collar is sealed by metal O-rings through all ground testing and launch. Once in space vacuum, the outer cover section is retracted by pyrotechnic devices to expose the large vent opening.

The four high pressure vent paths and the inner dewar fill and vent lines are routed close to the outside of the collar assembly. Sealed feedthroughs are located at the metal ring inside the inner dewar and again through the outer plate. Also shown in the neck area on Fig. 5-32 is the light path from the telescope to external phototubes. This path passes through the rectangular vent holes in the window support collars.

#### 5.4.6 Plumbing Arrangements

The gyroscope is shown schematically in Fig. 5-41. Two inlets are fed by a single line entering an equalization volume. Two high-pressure exhausts leave the gyroscope and are later connected to a single high pressure exhaust for each gyroscope. All of the area outside of the spinup channels is vented to the volume inside the inner dewar. Two basic arrangements are possible for the gyroscope spinup plumbing.

Figure 5-42 shows all gyroscope gas valves mounted in the cold area inside the inner dewar. There is an advantage in that there are four fewer lines than are required for the externally valved system shown in Fig. 5-43. The disadvantage of the internally

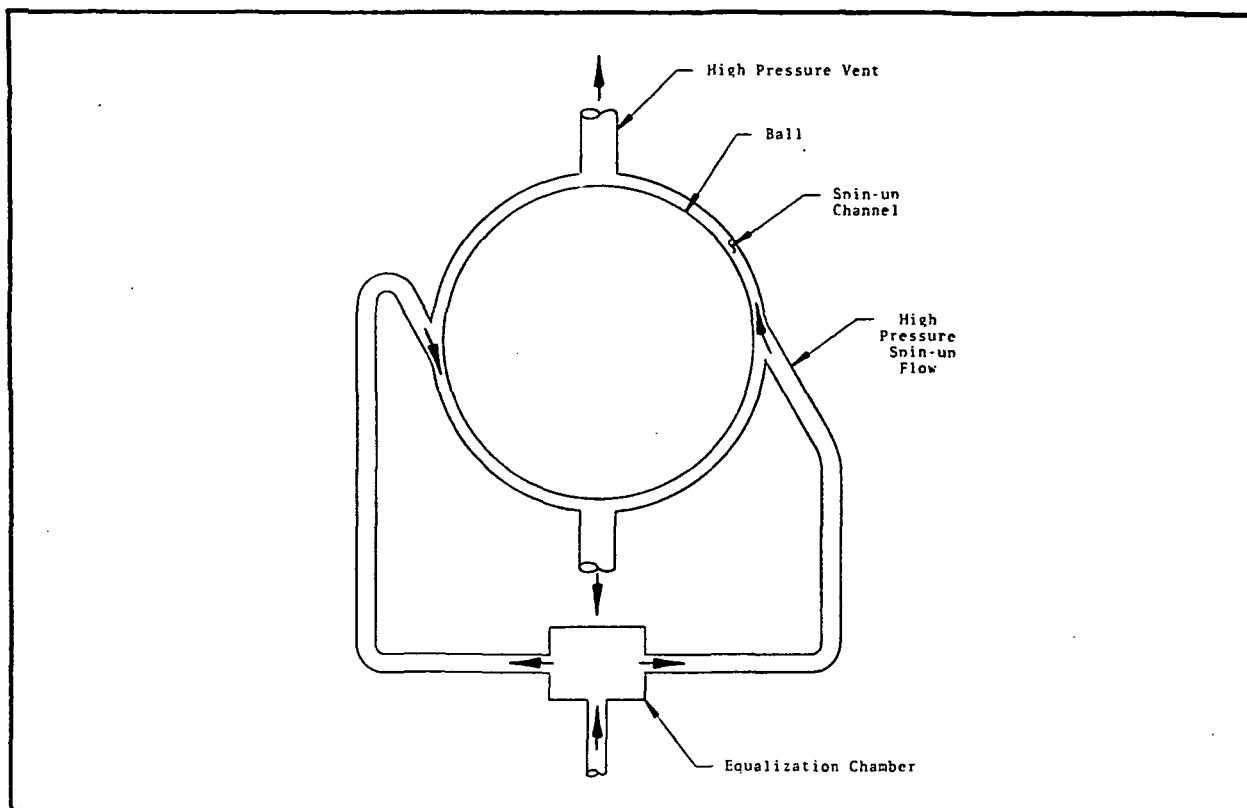


Fig. 5-41 Concept For Gyro Spinup

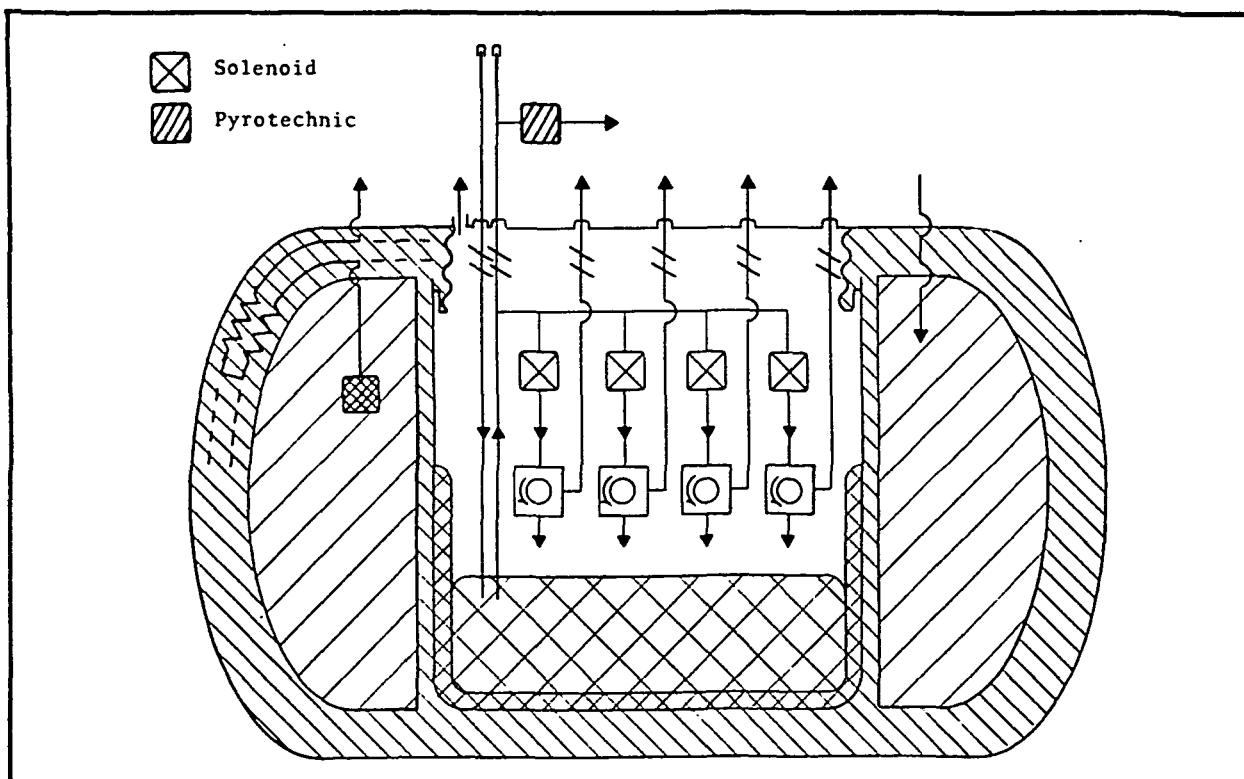


Fig. 5-42 Schematic For Inside Valving

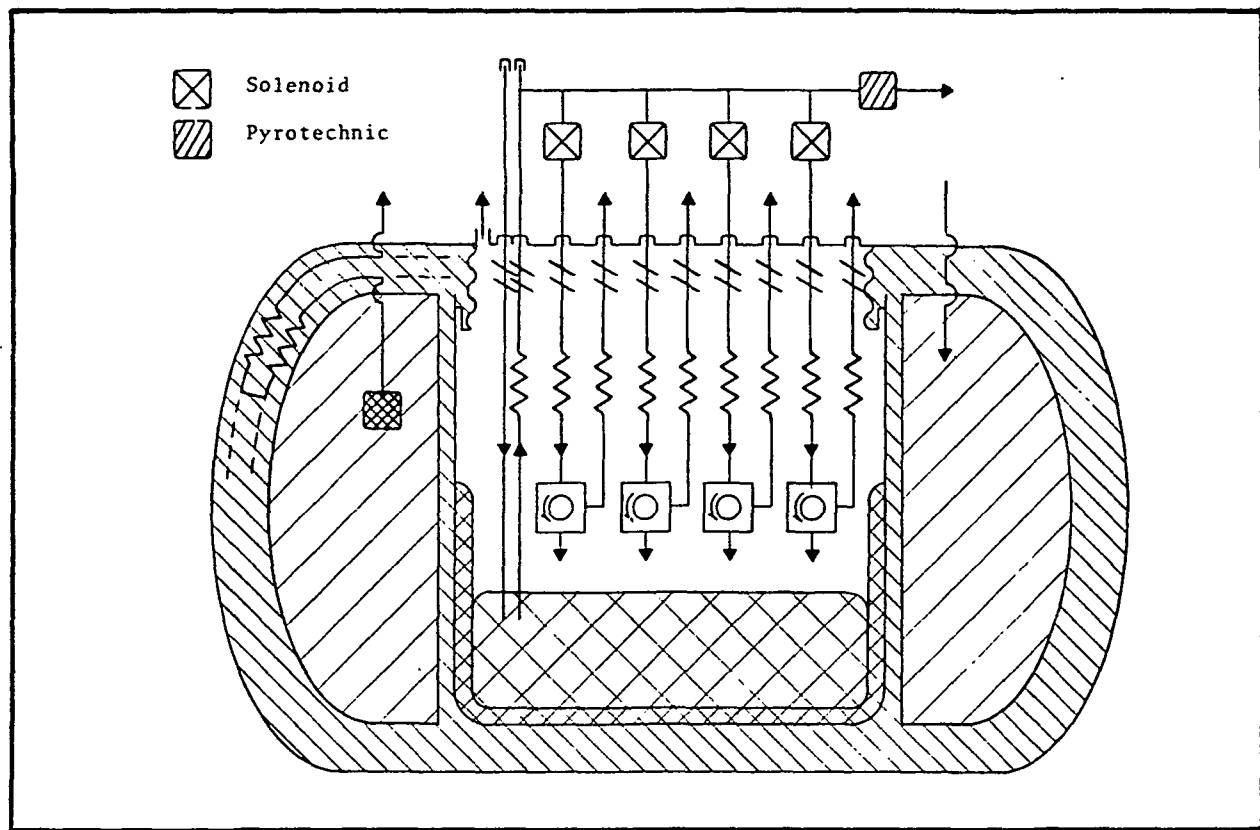


Fig. 5-43 Schematic For Outside Valving

valved system is that these valves must be designed to work in a lower temperature environment; and there are the problems of magnetic fields with the solenoids. The penalty for the externally valved system is the weight of extra helium required for the additional heat leak of the system. Further study is needed to determine which is the best arrangement.

Plumbing For Ground Testing. Figure 5-44 shows the vacuum unit required to support cryogenic testing on the ground. To keep the helium in the main dewar as a superfluid at 1.6°K a large capacity vacuum pump is required. This same system can be used to evacuate the gyros and inside of the inner dewar although all of these operations may not be possible simultaneously because of differences

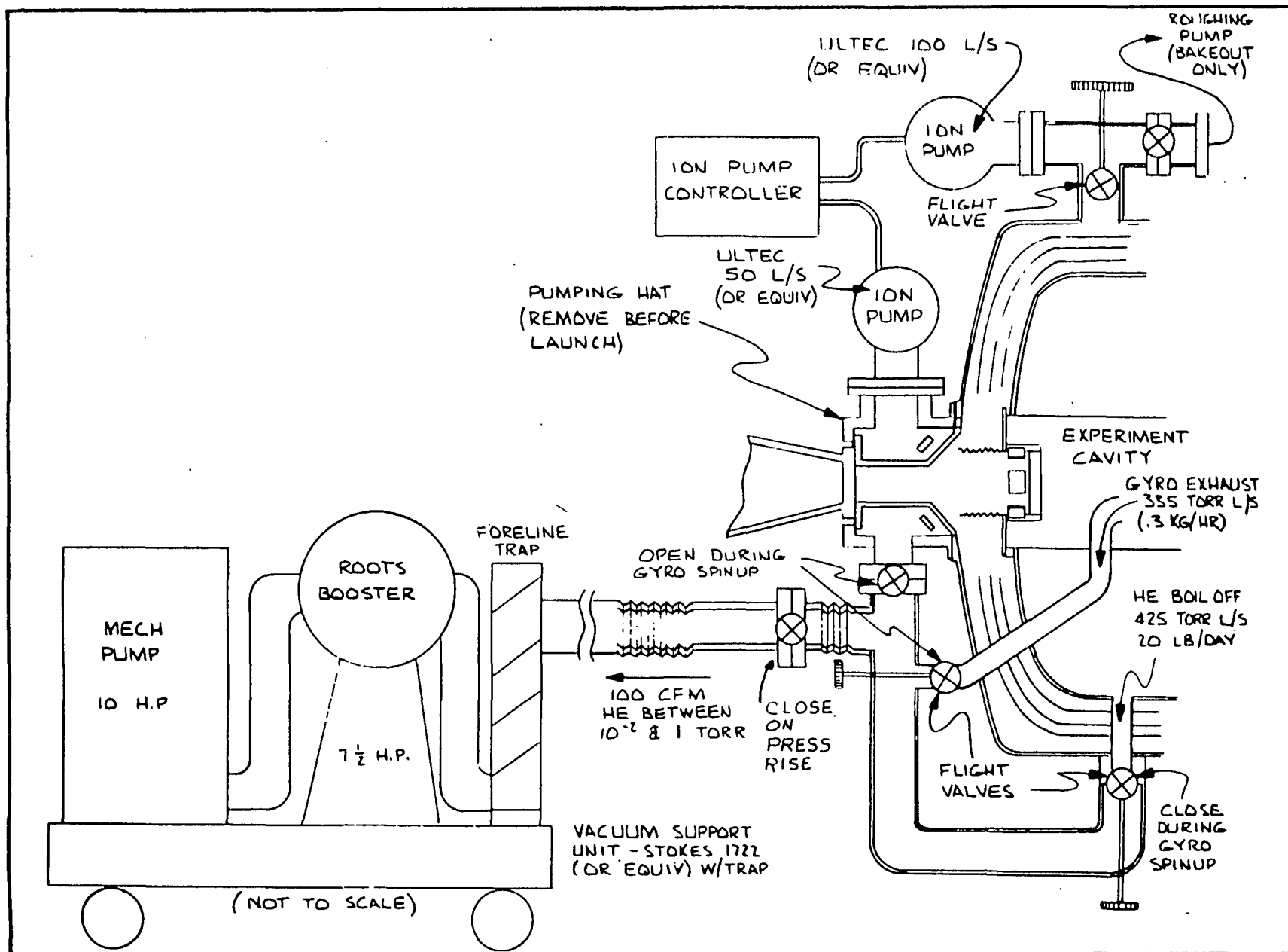


Fig. 5-44 Vacuum Support Unit



in the required vacuum levels. An ion pump is used to achieve the level of  $10^{-9}$  torr required in the gyros for slow spin down during extended tests.

The insulation annulus will be evacuated by a separate roughing pump system. High vacuum ( $<5 \cdot 10^{-6}$ ) torr will be maintained by another ion pump.

#### 5.4.7 Helium Management

Controlling the distribution and motion of the liquid helium is of critical importance due to the fine pointing requirements of the experiment. Uneven helium distribution and sloshing would impose severe requirements in the attitude control system and change the center of gravity. To manage the liquid helium, a cellular containment scheme has been devised which uses the surface tension of the liquid to control the location and flow of the fluid.

The proposed scheme is shown in concept in Fig. 5-45 as a series of rectangular cells connected to a common channel. This channel provides for flow of vapor or liquid to the superfluid plug which is the main outlet of the dewar. Flow into the channel is controlled by small orifices in the cells which is where bubble formation occurs. Surface tension of the vapor-liquid interface controls the movement of liquid. As a bubble begins to grow into the cell, the superfluid leaves the cell by film flow on the circumference of the orifice. This process continues until the bubble has fully grown into the cell. The last helium then leaves the cell by bulk flow. This sequence is shown in views a through d of the figure. The sequence of emptying for the various cells is



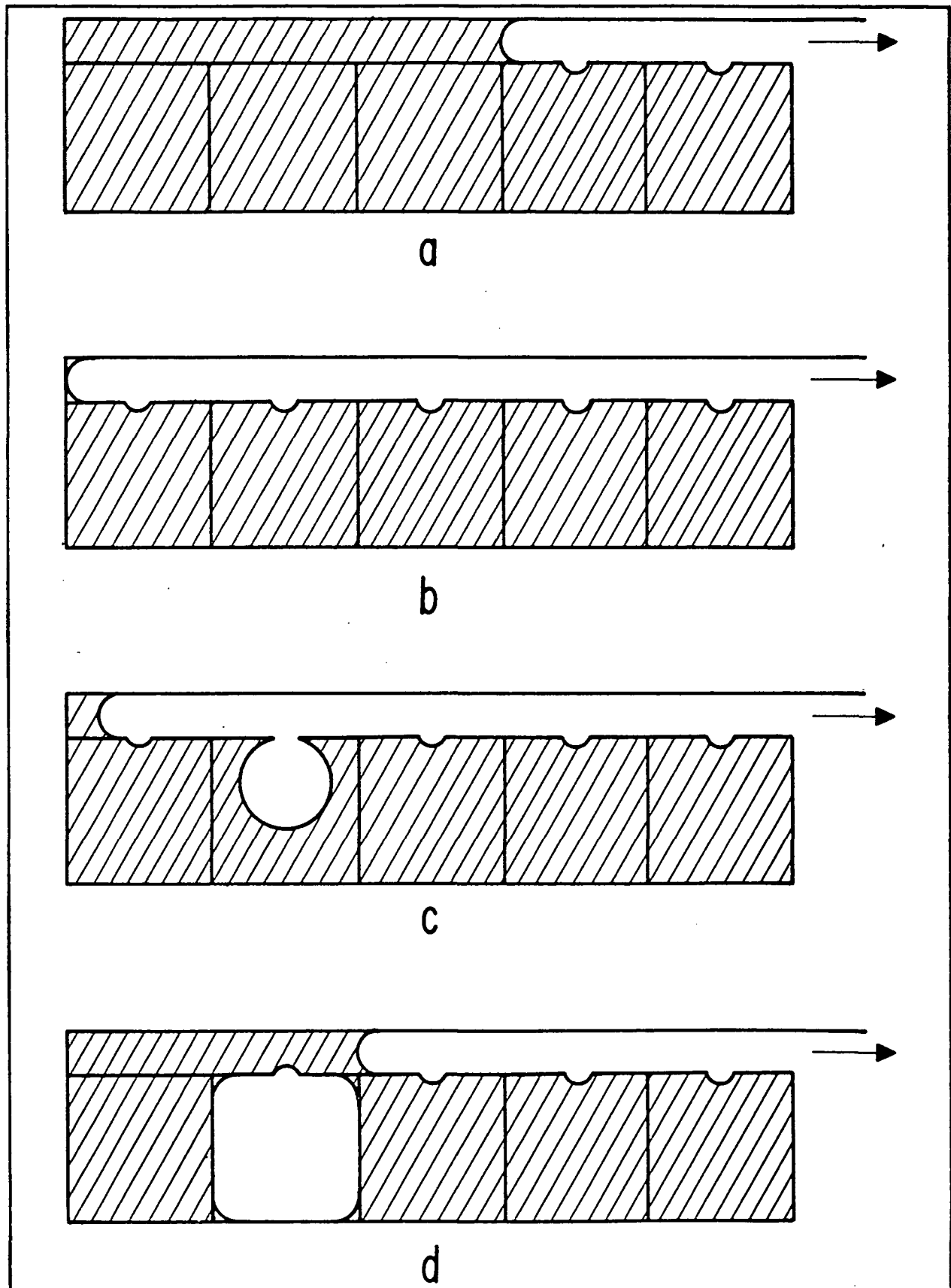


Fig. 5-45 Operation of Helium Management Scheme



controlled by varying the orifice sizes. The cells with larger holes empty first. By breaking the dewar into many cells with orifice sizes properly distributed, the center of gravity can be held nearly constant through the mission.

Application of this concept to the proposed dewar can be accomplished using layers of cells as depicted in Fig. 5-46. This concept uses a honeycomb disk, the cells of the honeycomb being drilled with different sized orifices. Many layers of these disks with spacing for the channels would provide the required mass control for the mission life. The tentatively selected orifice sizes would hold the helium in place for accelerations as high as  $10^{-4}$  g.

It might be necessary that each honeycomb cell have an orifice on each side of the disk for easier filling. If this does not work, the cells could be made of wire mesh. This would be a more delicate manufacturing problem but would provide the required control. As a third alternate, an additional cooling coil could be installed to condense the helium during filling.

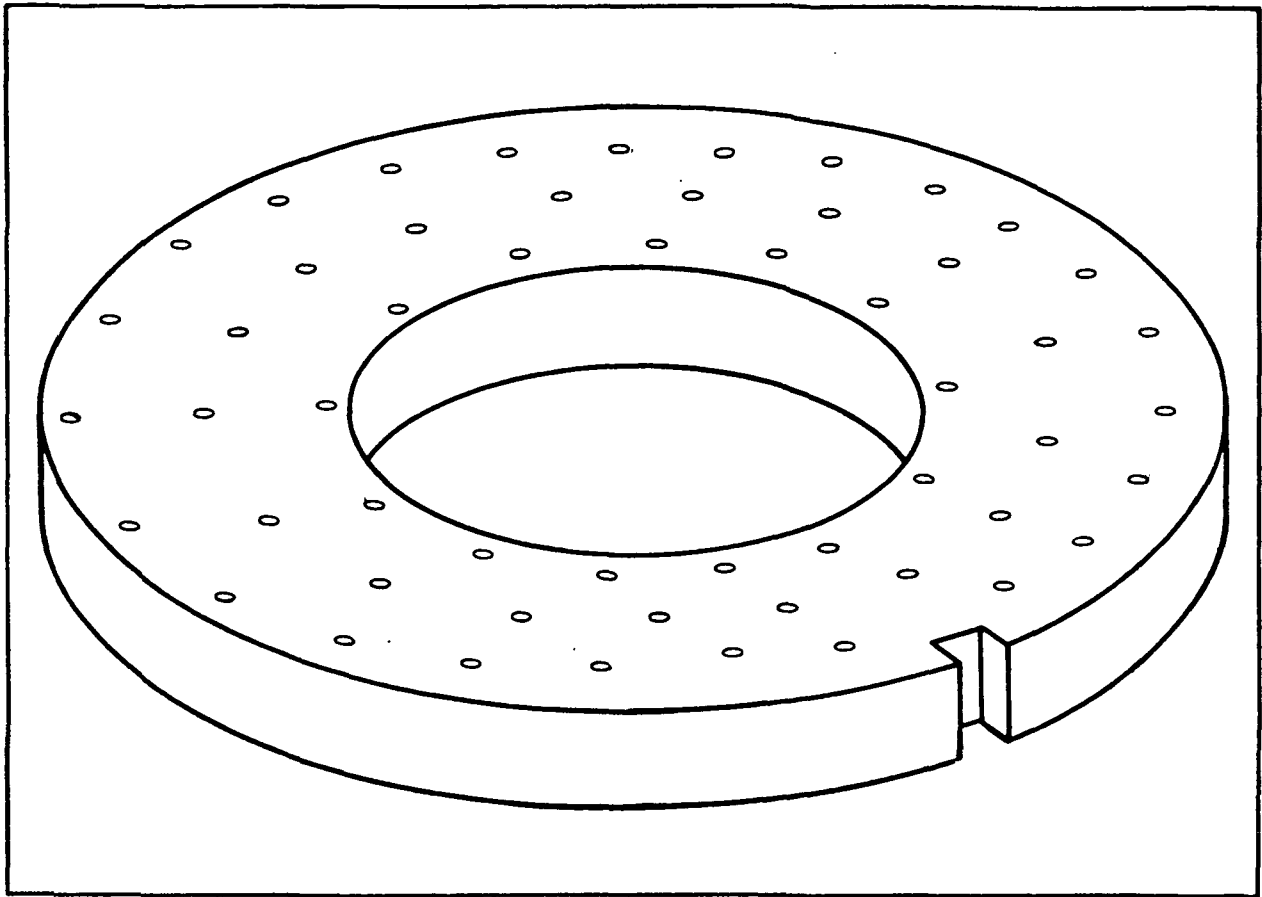


Fig. 5-46 Cell Assembly for Helium Management Scheme



## Section 6 SUBSYSTEMS

This section describes each of the five spacecraft subsystems. The requirements to which each subsystem was designed are given first, followed by a description of the chosen design, the performance of that design, and finally any analyses or important trade-offs that were made.

### 6.1 STRUCTURE

The structure is one of the areas where the experiment and the spacecraft overlap considerably. The outer shell of the dewar is the primary load carrying member of the satellite. The design of the dewar outer shell is discussed here while the details of the inner parts of the dewar are discussed as part of the experiment in Section 5.

#### 6.1.1 Requirements

Many items combined to shape and size the basic structural design. The major factors which contributed to the overall design, and the dynamic requirements which were used as a basis for the stress analysis are listed below. All of the requirements have been met.

#### BASIC REQUIREMENTS

- Dewar to hold 135 kg of liquid helium.
- Outer dewar shell to provide primary structural support.
- Total weight less than 900 kg.



## BASIC REQUIREMENTS (Cont.)

- Difference between moments of inertia of spin axis and transverse axes less than  $15 \text{ kg-m}^2$ .
- Dynamic imbalance less than  $0.4 \text{ kg-m}^2$ .
- Center of gravity of the spacecraft located less than 1 cm from experiment reference.
- Distance of the center of pressure from the center of gravity multiplied by the total projected area less than  $1.5 \text{ m}^3$ .
- Final design to fit within Delta firing.  
(2.18m dia)
- Solar array to stow for launch and deploy in orbit.
- Solar array to cause minimum shadowing between panels and minimum radiation blockage of the dewar.
- Provide  $0.18 \text{ m}^3$  electronics and equipment volume.
- Minimize the time for the electronics boxes to be in either total sunlight or total darkness.



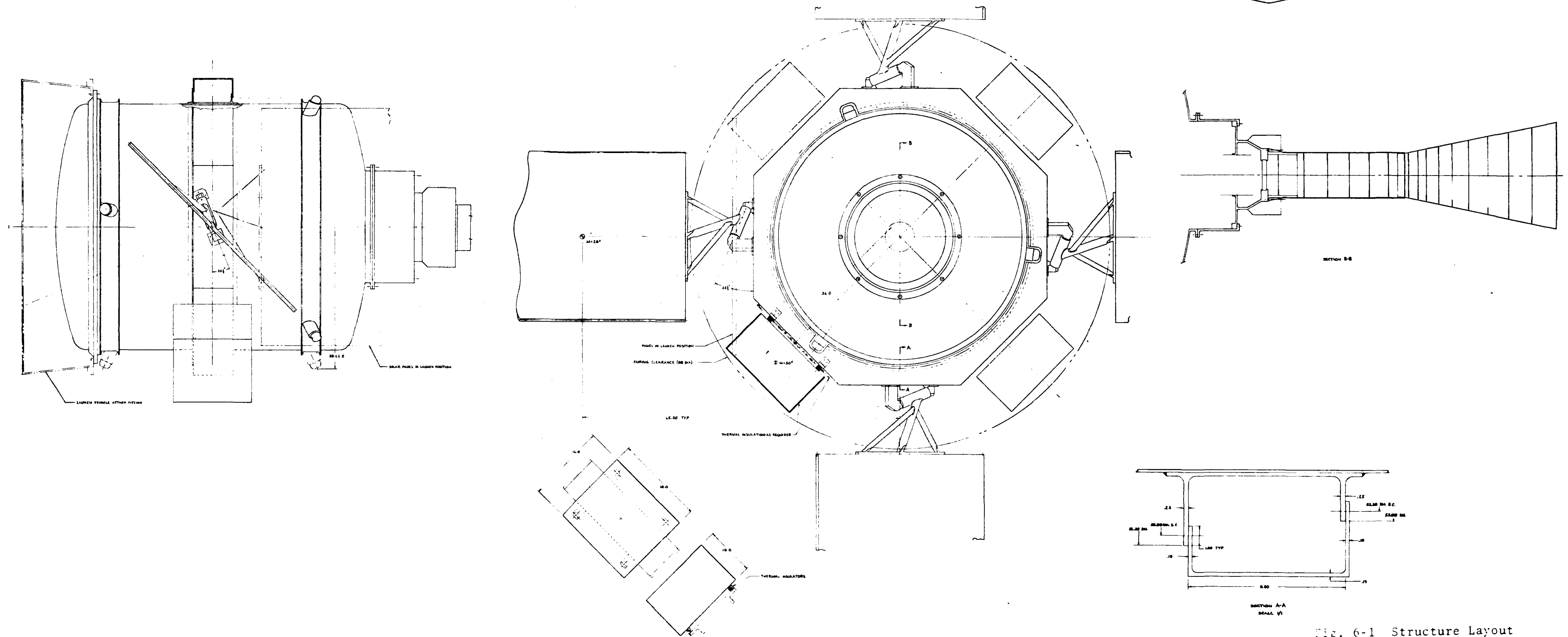
## DYNAMIC REQUIREMENTS

- LAUNCH - All structural resonant frequencies must be above 15 Hz
- ORBIT - In translation, all structural resonant frequencies must be at or above 10 Hz, except the inner to outer dewar shell resonance which is to be at or above 5 Hz

### 6.1.2 Description of the Structure

The design of the spacecraft is shown in Fig. 6-1 and the inner dewar is shown in Fig. 6-2. The design is simply a cryogenic dewar sized to contain approximately 135 kg of liquid helium, with a 0.47 meter diameter tube down the center. The outer shell of the dewar serves as the primary structure for the spacecraft. A girth ring, which is the mounting structure for the spacecraft equipment, attaches to flanges on the dewar (see Section A-A of Fig. 6-1). This allows easy removal of the support equipment for testing and allows subsystem checkout without the need for the helium-filled dewar.

Figure 6-3 shows an outline of the Delta fairing and Fig. 6-4 shows the launch configuration of the satellite as it would appear in the Delta fairing. Figure 6-5 shows it as it would appear in orbit and also gives overall size information. As shown in that illustration, there are four solar array panels and four electronic boxes. The electronic boxes provide a combined volume of about 0.2 cubic meter. These boxes will contain the instrumentation electronics for the experiment, power conditioning equipment, data storage, communication electronics, control electronics and other equipment as required. The budget for this volume is given in Table 6-1.



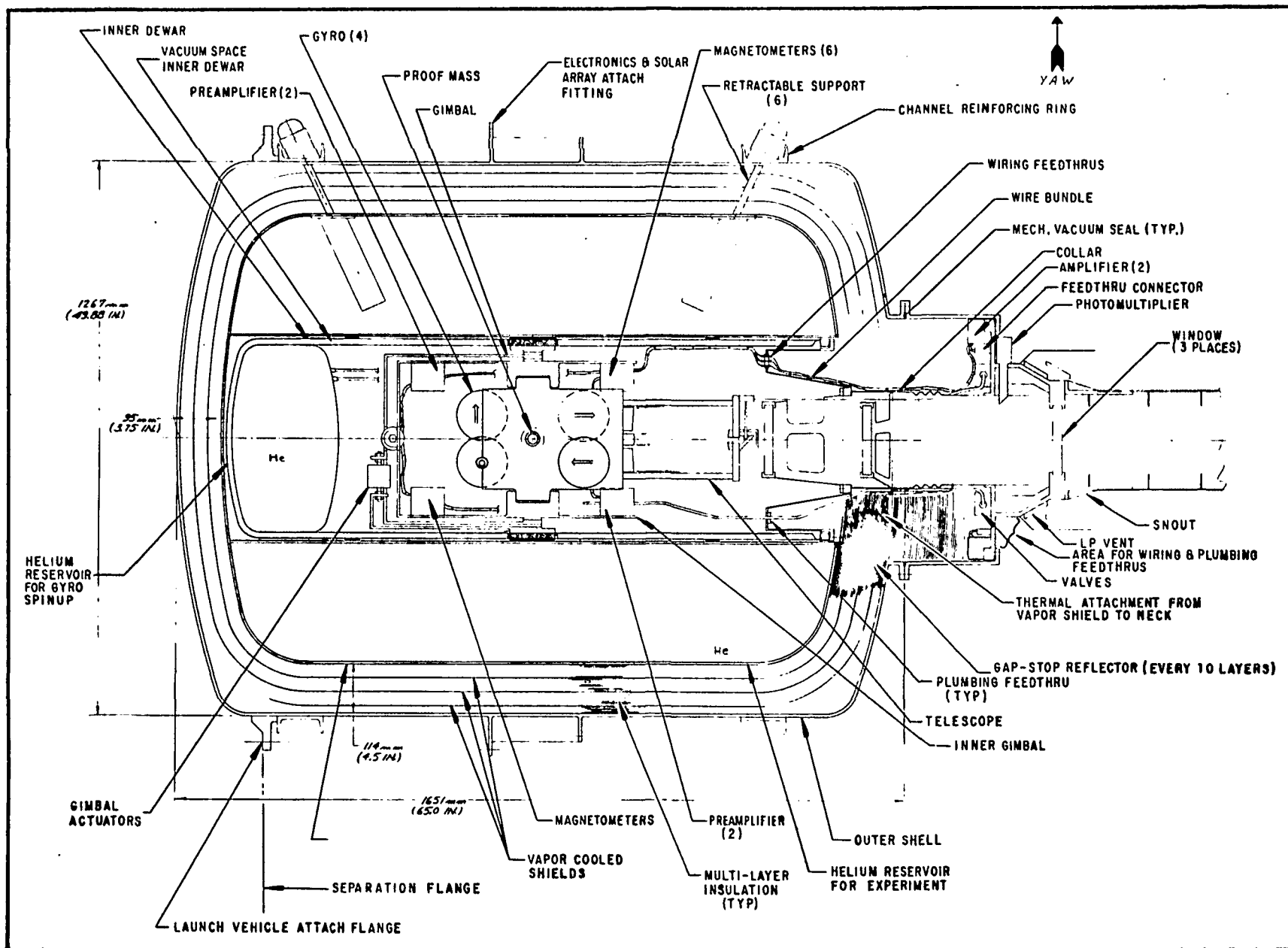


Fig. 6-2 Inner Dewar Layout, Bottom View



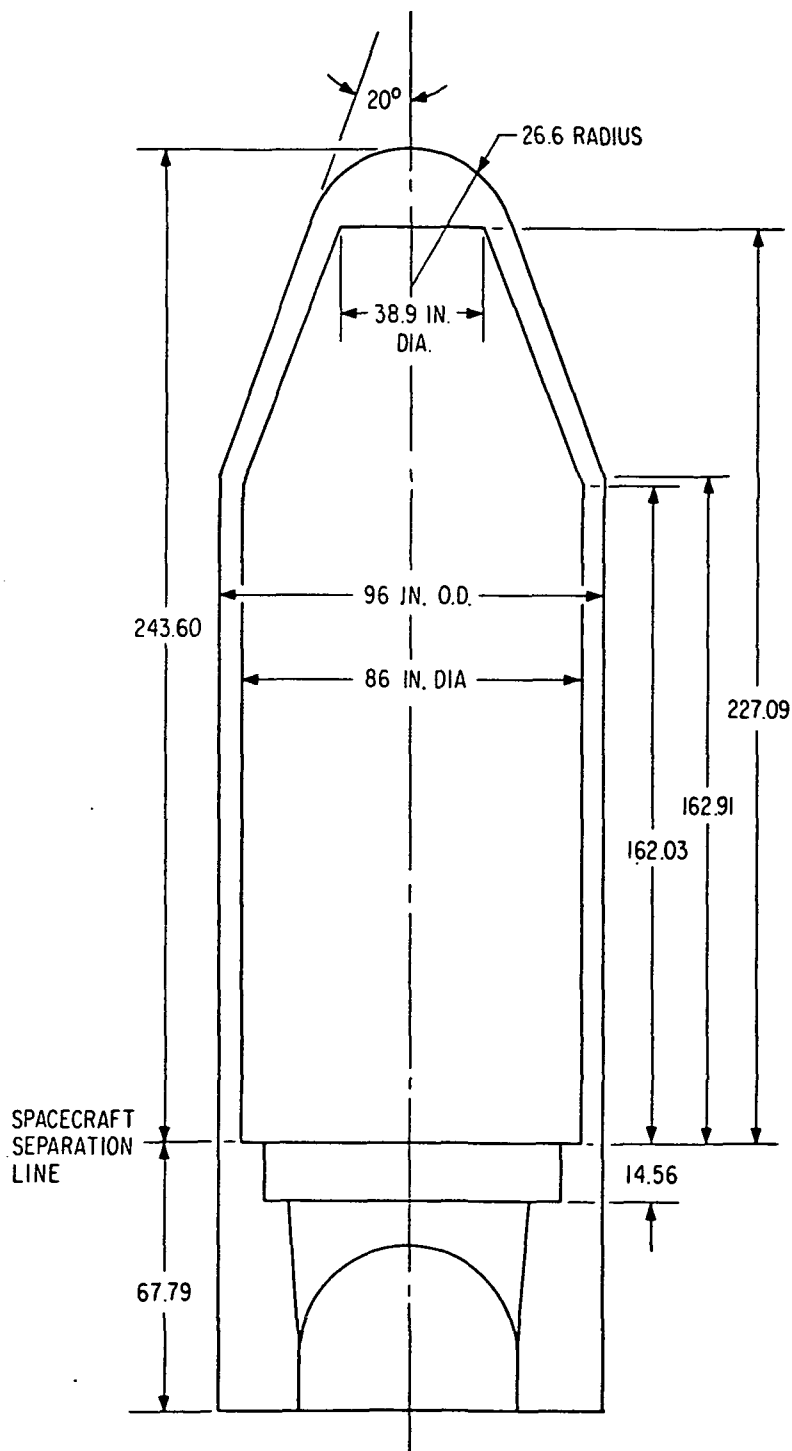


Fig. 6-3 Delta Fairing Outline

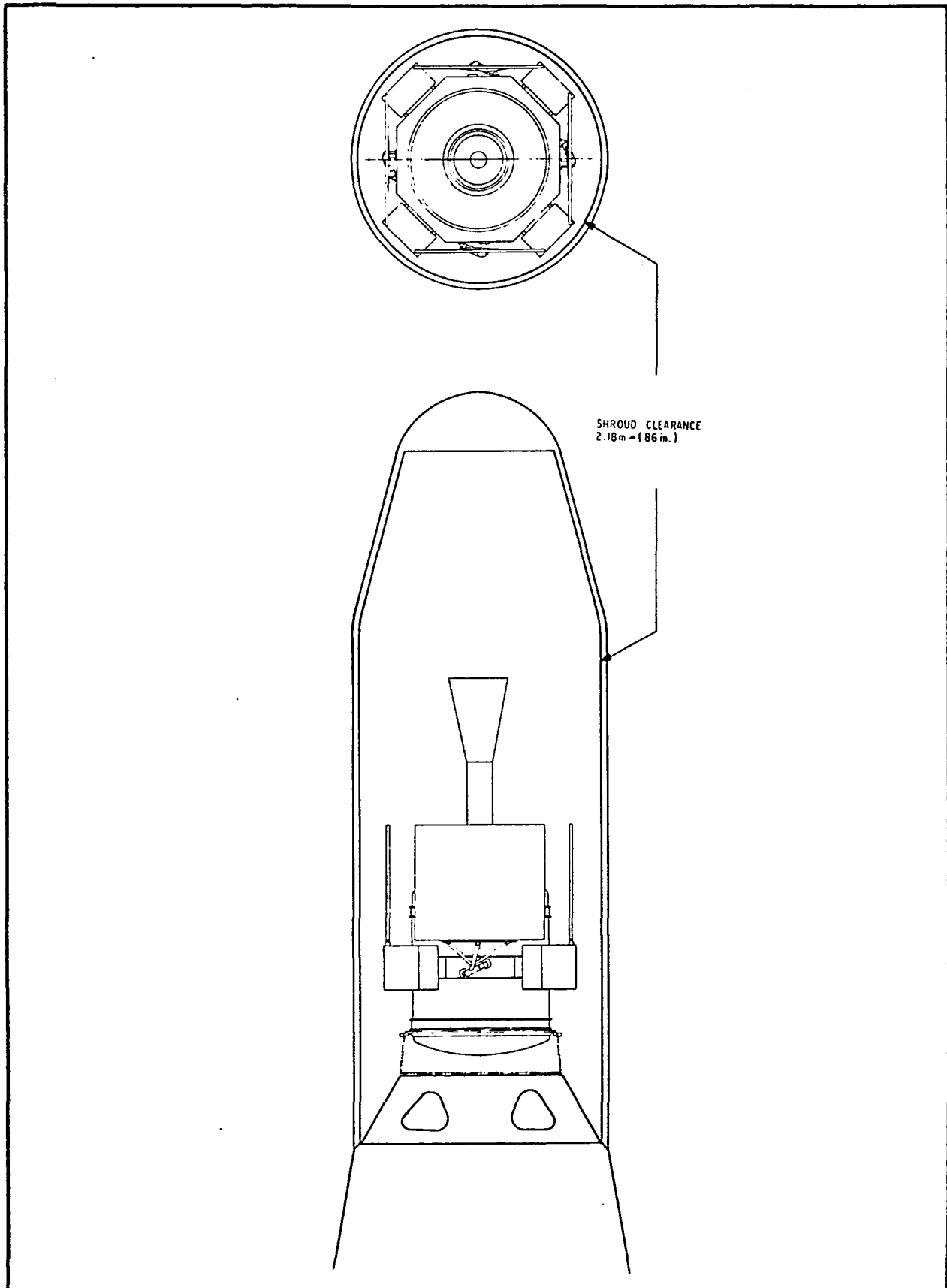


Fig. 6-4 Launch Configuration

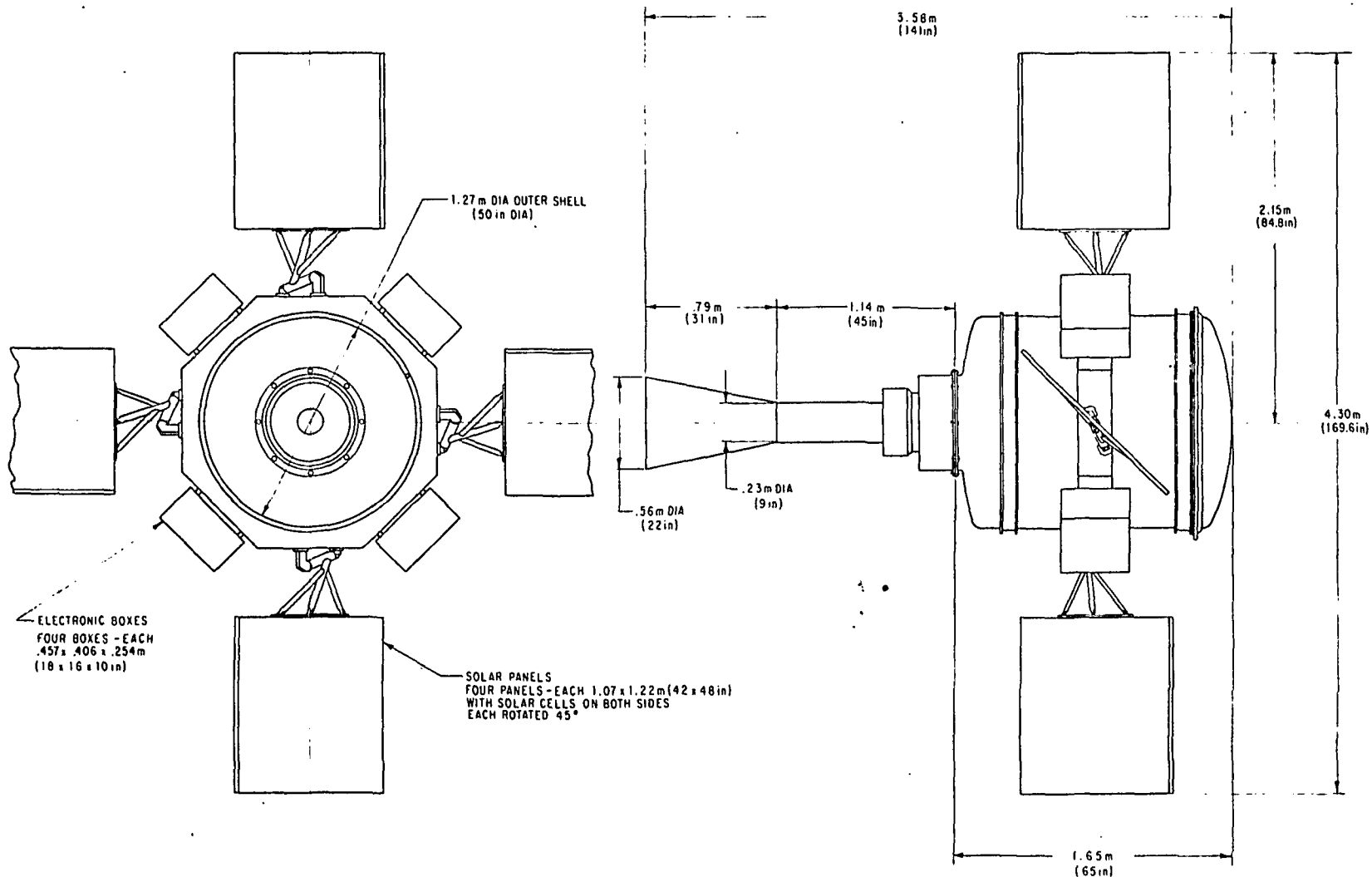


Fig. 6-5 Deployed Configuration



At this point in the design there is a 20 percent space margin. The boxes are structural in nature and are intended to provide housing for smaller, replaceable modules. They also provide thermal protection for the contents in that they are thermally insulated from the structure by special standoffs and covered with insulation. (See Section 6.2.)

Table 6-1  
ELECTRONICS ALLOCATIONS

ITEM	WEIGHT (kg.)	VOLUME (m <sup>3</sup> )
Batteries	18.1	0.011
Power Conditioning	6.8	0.014
Controls	13.6	0.028
Data Storage	4.5	0.009
Communications	13.6	0.028
Distribution	6.8	0.014
Experiment	18.1	0.046
TOTALS	81.5	0.150

Available volume = 0.19 m<sup>3</sup>

The solar panels are about 1.0 x 1.2 m in size and have solar cells on both sides. This gives a total solar cell area of approximately 10.4 square meters. (See Section 6.3 for power information.) The panels are folded up beside the dewar during launch and are deployed just before separation. Four tie points will be provided at the forward end of the dewar to secure the panels during launch. About halfway up their length, the panels will be attached to the tie points, to give the support necessary to survive launch. Release is effected through four pyrotechnic pin pullers. The hinges are designed so that as the panels move outward to become perpendicular to the spacecraft, they also



rotate 45°. This provides a nearly optimum orientation of the panels for the chosen orbit and satellite orientation. It should be noted that the 45° rotation is in opposite directions on alternate panels, to reduce windmill effects.

The panel substrate is 3/4-inch aluminum honeycomb with 0.020-inch aluminum face sheets. A square tube runs up the center of each panel to contain the RF cable that feeds the antennas. It will also be possible to run pneumatic lines through the same tubes if the control jets require a greater moment arm. Each panel is connected to its hinge mechanism by a 2-inch diameter torque tube. This tube determines the basic resonance of the array (refer to Table 6-2), and can be changed in size if it is necessary; however, the design as shown is compatible with all present satellite requirements.

Table 6-2  
RESONANT FREQUENCIES (HERTZ)

MASS	Translation (locked)			Translation (unlocked)			Rotation (unlocked)		
	X	Y	Z	X	Y	Z	$\phi$	$\psi$	$\theta$
ARRAY	high	16	16	10	10	10	10	10	10
INNER DEWAR	104	81	81	25	40	40	6	20	20
S/C FROM INTERFACE	high	81	81	--	--	--	--	--	--
SUN SHADE	277	43	43	277	43	43	high	43	43

A shock load of 1600 g's (1/2 sine at 0.8 msec) will produce less than a 3g load on the experiment as long as the inner dewar resonance is below 27 Hz. Above numbers are for a full dewar. Resonant frequencies will increase less than 30% when empty.



The sun shade is designed for stars as close as  $20^\circ$  to the sun. It could be significantly shorter for Rigel. It is a cylindrical section topped by a conical section. Both sections contain annular baffles. The design is such that no direct sunlight can reach the cylindrical section. The inner diameters of the baffles are optical knife edges and the entire inner surface is painted an optically flat black.

For launch, the satellite fits the standard Delta attach fitting shown in Fig. 6-6. Some adaptation may be required, but at present it appears that the adapter is acceptable as it exists.

#### 6.1.3 Performance of Design

Table 6-3 gives some of the general data of the mechanical design in summary form. A specific breakdown of the weight, and moments of inertia are listed in Table 6-4. As this table shows, the orbital weight is 570 kg at the start of the mission and about 430 kg at the end. As shown at the bottom of Table 6-3, there is a 45 kg allowance for launch structure (attachment and support structure that is not part of the satellite), so the launch weight would be about 615 kg. This is well within the capability of the Delta vehicle. Another point to note in Table 6-4 is the moment of inertia ratio. One of the requirements was that the difference between the roll and the transverse moments of inertia be less than  $15 \text{ kg-m}^2$ , and as the table shows, this has been accomplished. Note that the ratio is within tolerances at the beginning of the mission when the dewar is filled with helium and remains within tolerance as the helium is depleted.

The resonant modes of the satellite are of interest from two standpoints. The first is the launch environment which results in loads and stresses that size and shape the structural design. The second is the orbital condition which has a pronounced effect on the control system.

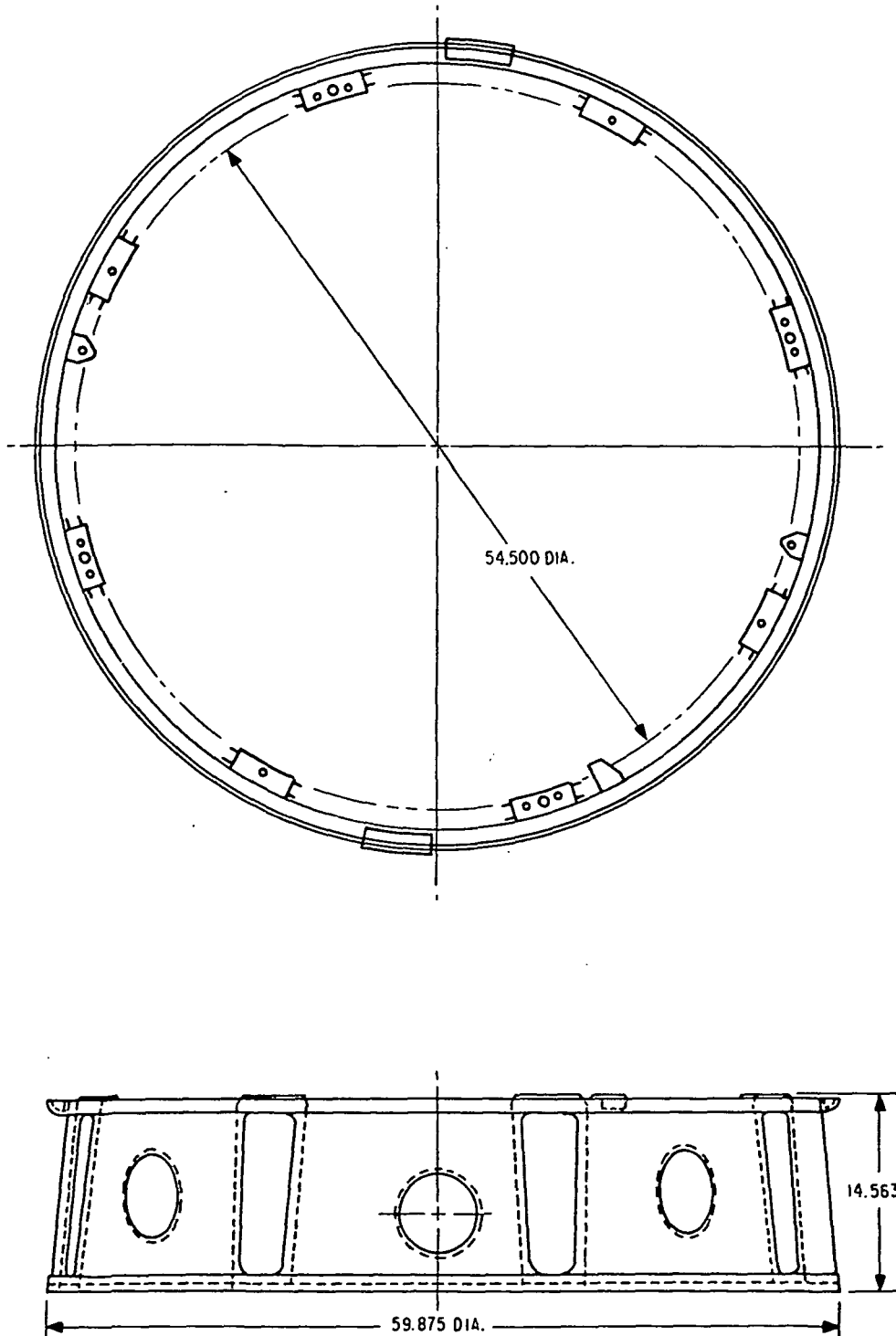


Fig. 6-6 Attachment Fitting



Table 6-3  
GENERAL INFORMATION

DEWAR: 1.27 m dia x 1.65 m (50 in. dia x 65 in.)  
contains 136 kg (300 lb) liquid Helium

SOLAR ARRAY:  $10.4 \text{ m}^2$  ( $112 \text{ ft}^2$ )  
Power output varies from 136 W to 220 W

ELECTRONICS:  $0.19 \text{ m}^3$  ( $6.7 \text{ ft}^3$ ) to hold 81.6 kg (180 lb)

DEPLOYED SIZE: 4.30 m (170 in) solar array span  
3.58 m (141 in) overall length

WEIGHT: 601 kg (1326 lb) at start of mission  
465 kg (1026 lb) at depletion of helium

MOMENTS OF INERTIA:  $I_{xx}$  317  $\text{kg}\cdot\text{m}^2$  (234 slug-ft<sup>2</sup>)  
 $I_T$  298  $\text{kg}\cdot\text{m}^2$  (220 slug-ft<sup>2</sup>)

CENTER OF PRESSURE:  $0.8 \text{ m}^3$  ( $28 \text{ ft}^3$ ) forward

LAUNCH STRUCTURE WEIGHT: 45.36 kg (100 lb)

Table 6-2 shows the predicted resonant frequencies for the more critical areas. During launch, the translation modes are of more interest so these were calculated with all launch locks in place. This means that the experiment is caged, the inner and outer dewar shells are locked together, and the solar arrays are folded and locked. In orbit, both modes are of interest and these frequencies occur with the solar panels deployed and all locks removed. A comparison of this table and the design requirements (Section 6.1.1) shows that the requirements have been met.





Table 6-4  
WEIGHTS AND MOMENTS OF INERTIA

ITEM	WEIGHT		$I_{XX}$		$I_T$	
	lb	kg	slug-ft <sup>2</sup>	kg-m <sup>2</sup>	slug-ft <sup>2</sup>	kg-m <sup>2</sup>
Instrument	120.0	54.4	0.5	0.7	2.9	3.9
Dewar	446.6	202.6	34.3	46.5	73.6	99.8
Helium	300.0	136.0	16.3	22.1	25.1	34.0
Solar Array	112.0	50.8	108.0	146.4	56.3	76.3
Electronics	180.0	81.6	51.7	70.1	26.7	36.2
Sun Shield	30.0	13.6	0.2	0.27	34.8	47.2
Girth Ring	80.2	36.3	14.8	20.1	7.6	10.3
Attach Fitting	57.5	26.0	8.7	11.8	11.5	15.6
TOTAL (WITH He)	1326.3	601.3	234.5	317.9	238.5	323.3
TOTAL (WITHOUT He)	1026.3	465.3	218.2	295.8	213.4	289.3

#### 6.1.4 Dynamic Analysis

From launch vibration and acceleration data, and ground handling and testing data, a dynamic analysis was performed to arrive at margins of safety of the satellite primary structure, and to develop proper vibration test specifications. The satellite resonant frequencies presented in the preceding section also results from this analysis.

Table 6-5 shows the predicted load factors and interface moments produced at the satellite during the boost phase. These were based on a computer model of the Delta booster and a model of OSO-7. Table 6-6 shows the margins of safety for the major parts of the satellite. These are the margins at ultimate loads; i.e., 1.5 times predicted 2 sigma flight loads. It should be noted that some of the maximum loads occur during non-vibration tests and not during any part of the flight. For example, the maximum load on the

Table 6-5  
SATELLITE LOAD FACTORS AND INTERFACE MOMENTS

Cond. #	Booster Frequencies Hz	Modal Definition	Event	Resultant Interface Moment * In-Lb	720.764 lbs Outer Shell			595.574 Pressure Vessel & Instrument			Outer Shell, Pressure Vessel & Instrument		
					N <sub>x</sub> g's	N <sub>y</sub> g's	N <sub>z</sub> g's	N <sub>x</sub> g's	N <sub>y</sub> g's	N <sub>z</sub> g's	$\ddot{\theta}_x$	$\ddot{\theta}_y$	$\ddot{\theta}_z$
1	2.5 & 9.9	1st & 3rd Bending Modes Excited	Liftoff	161,800	-3.375	0	2.688	-3.375	0	3.528	0	20.004	0
2	2.5 & 9.9	1st & 3rd Bending Modes Excited	Liftoff	161,800	-3.375	0	2.688	-3.375	0	3.528	0	20.004	0
3	5.6 & 12.0	2nd & 4th Bending Modes Excited	Liftoff	216,200	-3.375	0	-3.015	-3.375	0	-3.957	0	-36.515	0
4	5.6 & 12.0	2nd & 4th Bending Modes Excited	Liftoff	216,200	-0.375	0	-3.015	-0.375	0	-3.957	0	-36.515	0
5	6.9 & 12.0	Subsystem Resonance & 4th Bending Mode Excited	Liftoff	183,900	-3.375	0	-2.432	-3.375	0	-3.192	0	-33.296	0
6	6.9 & 12.0	Subsystem Resonance & 4th Bending Mode Excited	Liftoff	183,900	-0.375	0	-2.432	-0.375	0	-3.192	0	-33.296	0
7	2.5 & 9.7	1st & 3rd Bending Modes Excited	Liftoff	161,300	-3.375	2.638	0	-3.375	3.462	0	0	0	-20.651
8	2.5 & 9.7	1st & 3rd Bending Modes Excited	Liftoff	161,300	-0.375	2.638	0	-0.375	3.462	0	0	0	-20.651
9	5.6 & 11.7	2nd & 4th Bending Modes Excited	Liftoff	202,200	-3.375	-2.746	0	-3.375	-3.604	0	0	0	35.390
10	5.6 & 11.7	2nd & 4th Bending Modes Excited	Liftoff	202,200	-0.375	-2.746	0	-0.375	-3.604	0	0	0	35.390
11	22.9 & 56.2	POGO Mode Excited	POGO	24,680	-15.9**	0	0.750	-15.9**	0	0.750	0	0	0
12	22.9 & 56.2	POGO Mode Excited	POGO	24,680	-15.9**	0.750	0	-15.9**	0.750	0	0	0	0

\* Moments and Load Factors Shown Are Ultimate  
\*\*8.4g Steady State

F71-07



Vol. I



inner dewar shell occurs when it is pressure checked for leaks after welding. This is, however, a real part of making the satellite work so it is one of the high-stress conditions considered in the analysis.

Table 6-6  
MARGINS OF SAFETY

ITEM AND MODE OF FAILURE	g LEVEL	CONDITION	M.S.
Pressure Vessel, Tension	4200 psi*	Internal Press, (22.5 psig)	4.8
Outer Shell, Stability	3000 psi*	External Press, (22.5 psig)	0.53
Press. Vessel to Outer Shell Launch Locks, Tension	15.9	Launch (thrust)	3.70
Electronics Box Standoffs, Compression	3.015	Longitudinal Vibration	36.6
Outer Shell at Interface, Stability	15.9	Launch (thrust)	13.9
Sun Shield, Bending	9.6	Lateral Vibration	8.8
Solar Panel Tie Down, Bolt Tension	10.0	Lateral Vibration	19.9

\*Predicted Test Levels

$$M.S. = \frac{ALLOWABLE}{ACTUAL} - 1$$



The flight load factors and margins of safety were based predicted flight loads which are derived from the combined dynamic characteristics of the launch vehicle and the satellite. The suggested vibration test specifications are also derived from the analysis by notching the standard Delta vibration specification, so that flight loads are not exceeded at the satellite resonances.

The next section discusses the flight loads, the vibration specification, and the stress analysis.

#### 6.1.4.1 Flight Loads

While stresses caused by ground handling of the satellite must be taken into account, the structure design is primarily based on the vibration loading induced by the launch vehicle. Mechanical systems such as the outer dewar shell, the dewar fiberglass supports and the inner dewar shell must be designed to resonate far above the booster driving frequencies to prevent excessive transmissibilities.

Fortunately, the launch booster can only deliver high energy levels to the satellite at the primary resonance modes of the booster. These are the first several "free-free" bending modes of the booster, and the first several "free-free" compressional modes. These frequencies and the approximate "g" levels developed at the satellite are listed in Table 6-5. Note that the highest frequency is about 50 Hz. The vehicle does deliver vibration at frequencies up to about 200 cycles, but the energy at these other frequencies is low; i.e., the apparent impedance of the booster (considered as a source) is high. If the satellite has a resonance at one of these other frequencies, the effect is that the satellite damps or suppresses the input vibration. However, if small masses such as an electronic box resonates in this band, the booster does have sufficient energy to drive these small masses to appreciable g levels.



In order to get a realistic set of values for the predicted flight vibration environment at various places on the satellite, it is necessary to perform the combined satellite-booster dynamic analysis. This is usually done after the design is frozen. To get an approximate set of values at this early stage, we used a simplified dynamic model of the SRS and modified the input data obtained from the OSO-7 analysis.

Since the weights of this satellite and the OSO-7 are nearly the same and since the rigidity of the two structures is about the same, the OSO-7 data can be used to approximate the loads for the SRS. Because the SRS C.G. is farther from the attach fitting than the OSO-7, it was necessary to adjust the OSO-7 loads by a factor of  $r\ddot{\theta}$ , where  $r$  is the difference between the two C.G. locations and  $\ddot{\theta}$  is the corresponding OSO-7 angular acceleration. The g levels on the pressure vessel and instrument were based on the eigenvalues obtained from a modal analysis of the SRS.

These flight loads are used to obtain the vibration specifications given in Section 6.1.4.2 and also for the stress analysis given in 6.1.4.3.

#### 6.1.4.2 Vibration Specifications

As a result of flight load calculations, a specification was developed for vibration testing. Figures 6-7, 6-8, 6-9, and 6-10 show the recommended test input for various parts of the SRS satellite and following are the calculations which are the basis for the plots. Notching of the spacecraft vibration specification was based on not exceeding flight loads on the outer dewar shell. Notch widths were based on zero damping. Additional notching may be possible since the input levels for some components will result in flight loads being exceeded. The margins in Table 6-7 do not account for these high levels.

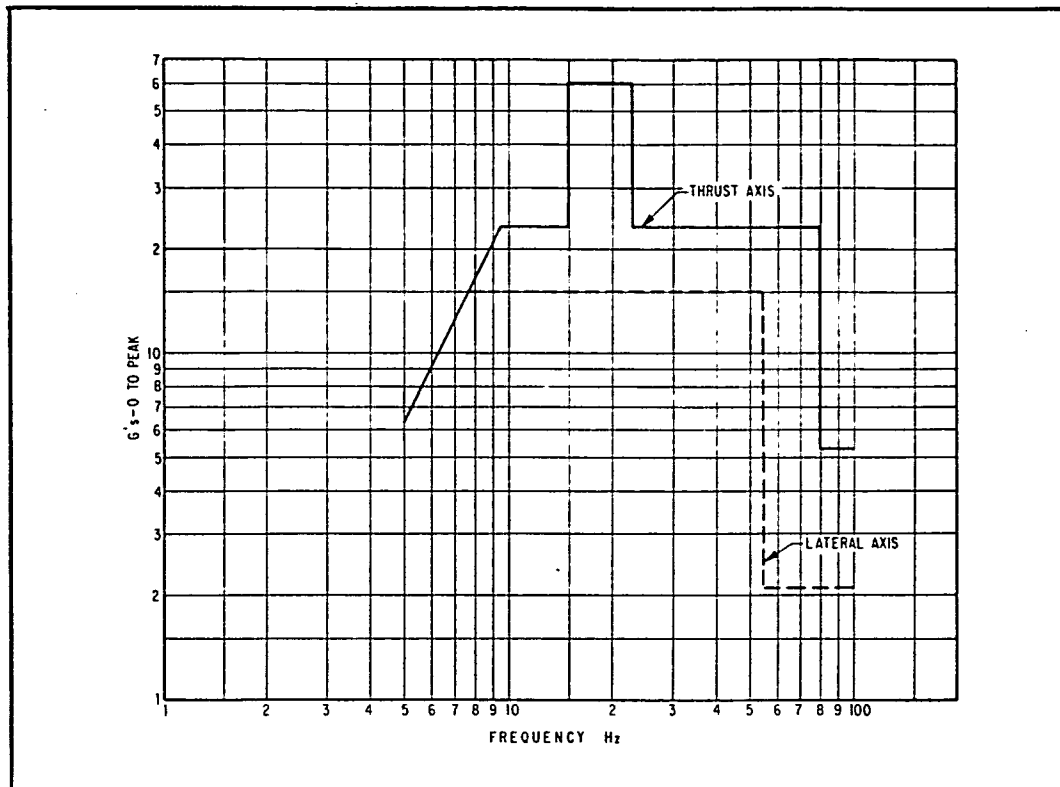


Fig. 6-7 Satellite Sine Vibration Input

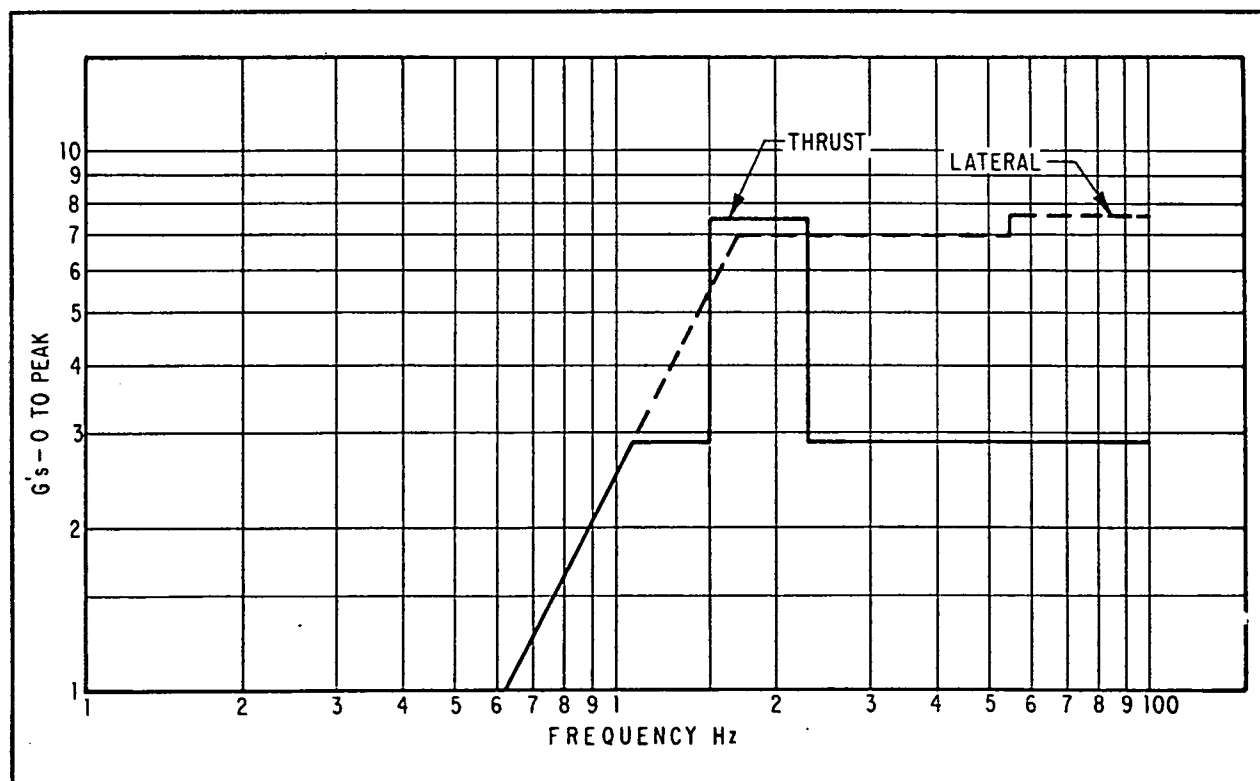


Fig. 6-8 Solar Panel and Sun Shield Sine Vibration Input

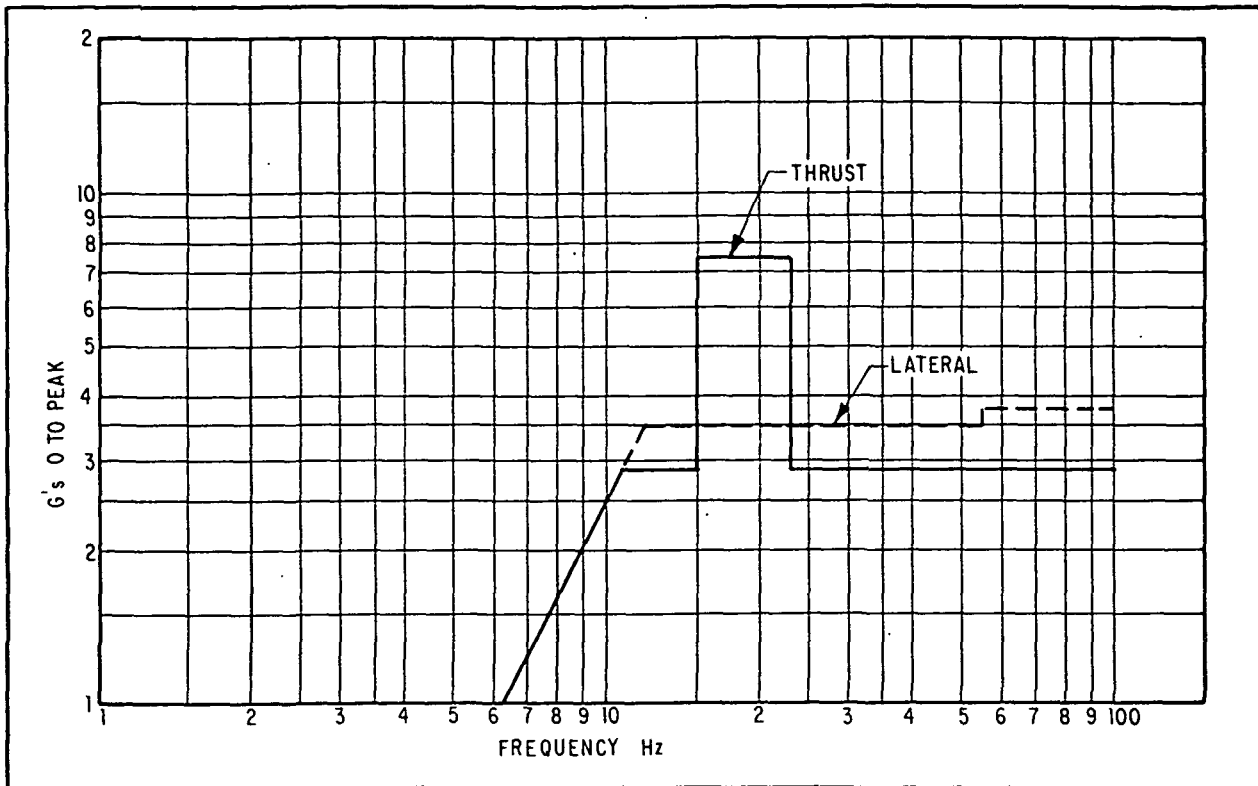


Fig. 6-9 Electronics Box Line Vibration Input

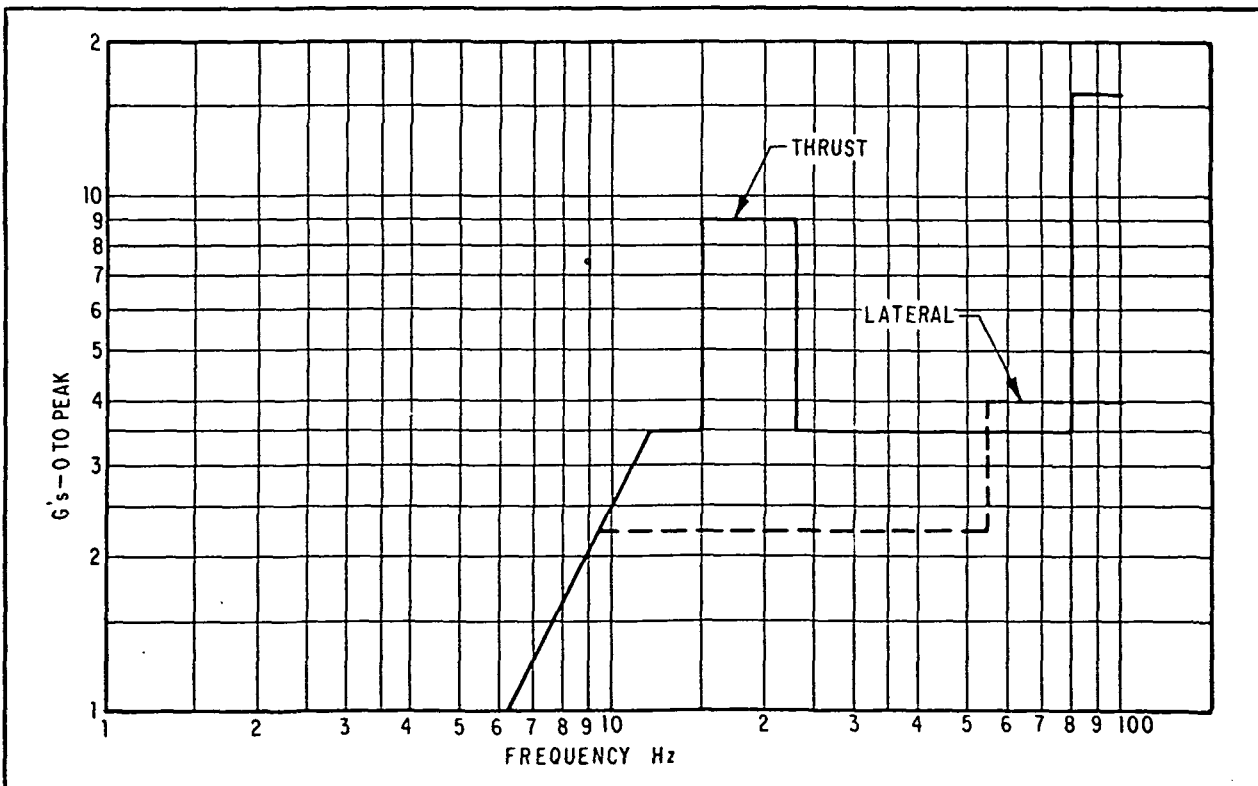


Fig. 6-10 Quartz Block Sine Vibration Input



- Lateral Level Calculations for Spacecraft

First lateral resonance is at 81.5 Hz with normalization at the sun shield. The eigenvalue for the C.G. of the outer shell is 0.48. Assuming a Q of 30 at resonance the g level at the outer shell C.G. would be

$$1.5(30)(0.48) = 21.6 \text{ g's}$$

Maximum g level based on OSO-7 data is 3.015 (lateral). Therefore, the input level must be notched to

$$1.5 \left( \frac{3.015}{21.6} \right) = 0.209 \text{ g's}$$

The eigenvalue for the pressure vessel and instrument for the 81.5 Hz resonance is 0.63. With the 0.209 notch the g level for the pressure vessel and instrument would be

$$0.209(30)(0.63) = 3.957$$

- Lateral Notch Width

Assuming no damping, determine the width of the 0.21 notch to allow return to the full input level of 1.5 g's.

$$\text{Allowable } T = \frac{3.015}{1.5} = 2.01$$





With zero damping:

$$T = \frac{1}{\sqrt{\left[1 - \left(\frac{\omega}{\omega_n}\right)^2\right]^2}} = 2.01$$

$$\left(\frac{\omega}{81.5}\right)^2 = 1 - \frac{1}{2.01} = 0.502$$

$$\omega = 57.8$$

- Longitudinal Level Calculations for Spacecraft

The first longitudinal resonance is at 104.1 Hz with normalization on the instrument and an eigenvalue of 0.98 on the pressure vessel. Assuming a Q of 30 at 100 Hz the g level at the instrument C.G. would be

$$2.3(30) = 69 \text{ g's}$$

Maximum g-level based on OSO-7 data is 15.9. Therefore, the input level must be notched to:

$$2.3\left(\frac{15.9}{69}\right) = 0.53$$

The g-level at the pressure vessel C.G. would be

$$15.9(0.98) = 15.6$$



- Longitudinal Notch Width

Assuming no damping, determine the width of the 0.53 notch to allow return to the full input level of 2.3 g's.

$$\text{Allowable } T = \frac{15.9}{2.3} = 6.913$$

With zero damping:

$$T = \frac{1}{\sqrt{\left[1 - \left(\frac{\omega}{\omega_n}\right)^2\right]^2}} = 6.913$$

$$\left(\frac{\omega}{104.1}\right)^2 = 1 - \frac{1}{6.913} = 0.8553$$

$$\omega = 96.1$$

- Lateral Level Calculations for Components

At 81.5 Hz the input to the spacecraft is notched to produce 3.015 g's at the outer shell C.G. The electronic boxes are located at approximately the same level as the outer shell C.G. Therefore, the boxes would have the same g level assuming  $T = 1$  through the box support structure. Assuming  $T = 1.25$  through the support structure, the input level to the boxes would be:

$$1.25(3.015) = 3.77 \quad \text{Use 3.8 at 81.5 Hz}$$

At 55 Hz the input to the spacecraft is 1.5 g's.  
With zero damping:

$$T = \frac{1}{\sqrt{\left[1 - \left(\frac{55}{81.5}\right)^2\right]^2}} = 1.836$$

6-23



The g level at outer shell C.G. =  $1.836(1.5) = 2.754$ .  
Input level to boxes would be:

$$1.25(2.754) = 3.44. \quad \text{Use 3.5 at 55 Hz}$$

The stowed arrays and the base of the sun shield are approximately twice as far from the spacecraft interface as the electronic boxes. Using the same criteria as used for the boxes and including the effect of location, the input levels for the arrays and sun shield would be twice the input levels for the boxes; i.e.,

$$7.6 \text{ g's at } 81.5 \text{ Hz}$$

$$7.0 \text{ g's at } 55 \text{ Hz}$$

- Longitudinal Level Calculations for Components

Assume  $T = 1.25$  for all components. Thus the vibration level will be 1.25 times that of the satellite input.

- Levels for Instrument (Quartz Block)

The quartz block is considered part of the primary structure; therefore, input will be limited to flight loads at resonances of the spacecraft. A 1.5 transmissibility will be assumed at all other frequencies.



### 6.1.4.3 Stress Analysis

- Ultimate Flight Loads

Ultimate load factors for the spacecraft are shown in Table 5-5. The load factors are to be applied at the C.G. of the spacecraft.

Calculations of these load factors use the following equation:

$$n = Tg_0 + \frac{l\ddot{\theta}}{g}$$

where  $n$  = number of g's seen at item in question (flight load)  
 $g_0$  = g level at C.G. of spacecraft  
 $T$  = transmissibility factor  
 $l$  = distance from spacecraft C.G. to subsystem C.G. (ft.)  
 $\ddot{\theta}$  = angular acceleration of subsystem C.G. (rad/sec<sup>2</sup>)  
 $g = 32.2 \text{ ft/sec}^2$

#### Sun Shield

Lateral load factor at C.G.

$$n = (1.05)(3.015) + \frac{(72 - 3.8)(36.515)}{12(32.2)} = 9.61 \text{ g's}$$

#### Stowed Solar Array

Lateral load factor at C.G.

$$n = (2.4)(3.015) + \frac{(32.7 - 3.8)(36.515)}{12(32.2)} = 9.96 \text{ g's}$$

#### Electronic Boxes

The electronic boxes are at approximately the C.G. of the spacecraft, therefore the lateral load factor is 3.015 g's.



- Stress on Outer Shell at Interface

The stress level at the interface is given by

$$f_c = \frac{P}{A} + \frac{Mc}{I}$$

where  $f_c$  = combined stress

$P$  = applied load

$A$  = area over which load is applied

$M$  = bending moment

$c$  = distance from neutral axis to max. stress

$I$  = moment of inertia

From the geometry and inputs to the spacecraft:

Thrust loading = 15.9 g's

Lateral loading = 0.75 g's

Cylinder diameter = 50 in.

Cylinder wall = 0.125 in.

Satellite weight = 1326 lb.

$$\text{So; } f_c = \frac{(15.9)(1326)}{2\pi(25)(0.125)} + \frac{(0.75)(1326)(25)(25)}{\pi(25)^3(0.125)} = 1175 \text{ psi}$$

From NACA Technical Note 3783

$$\sigma_{CR} = \frac{CEt}{r}$$

where  $\sigma_{CR}$  = Critical (allowable) stress

$C = 0.35$  [NACA 3783 Fig. 7]

$E = 10^7$

$t/r = 200$



$$\text{So; } \sigma_{CR} = 17,500 \text{ psi}$$

And the margin of safety is:

$$\text{M.S.} = \frac{17,500}{1175} - 1 = 13.9$$

• Bending Stress on Sun Shield

The maximum stress on the sun shield occurs due to bending which takes place during lateral vibration.

The moment is the product of the g load, the weight of the shade and the moment arm out to the C.G. of the shade.

$$M = 9.61(30)(45) = 12,974 \text{ in. lb.}$$

$$f_b = \frac{Mc}{I} = \frac{12,950 (4.5)}{\pi (4.5)^3 (0.05)} = 4079 \text{ psi}$$

From NACA Technical Note 3783

$$\sigma_{CR} = \frac{CEt}{r}$$

where  $C = 0.5$  [NACA 3783 Fig. 16]

$$E = 10^7$$

$$t/r = 90$$

$$\sigma_{CR} = 55,000 \text{ psi}$$

Since this is greater than the compressive yield strength of the material we use  $f_{cy} = 40,000 \text{ psi}$

$$\text{M.S.} = \frac{40000}{4079} - 1 = 8.8$$



- Stress on Solar Panel Tie-Down Bolts

The solar panels are secured for launch with two 0.188 diameter bolts made of A-286 steel or an equivalent material.

$$\begin{aligned}\text{Load per bolt} &= \frac{\text{g level} \times \text{weight}}{2 \text{ bolts}} \\ &= \frac{9.96(28)}{2} = 139.4 \text{ lb.}\end{aligned}$$

$$\text{Bolt tension allowable} = 2913 \text{ lb.}$$

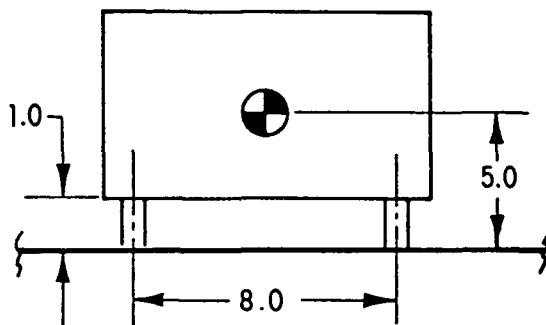
$$\text{M.S.} = \frac{2913}{139.4} - 1 = 19.89$$

- Stress on Mounting Bolts of Electronics Boxes

The electronics boxes are supported on four titanium tubes one inch diameter by 0.049 wall thickness and one inch in length.

The geometry of the box mounting is as shown here.

$$\text{Wt.} = 45 \text{ lb.}$$





The tension loads in the mounts are:

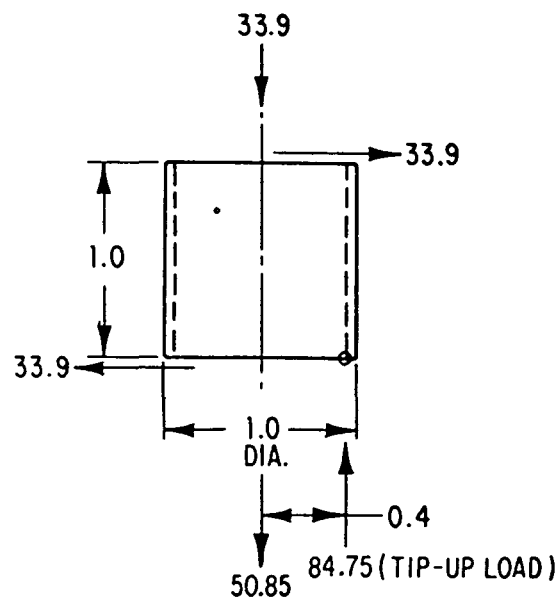
$$\begin{aligned}
 P_t &= \frac{\text{weight} \times \text{moment arm} \times g \text{ level}}{\text{distance between legs} \times \text{number of mounts}} \\
 &= \frac{45(4)(3.015)}{8(2)} = 33.9 \text{ lb.}
 \end{aligned}$$

Compression loads are the same.

The shear loads are:

$$\begin{aligned}
 P_s &= \frac{\text{weight} \times g \text{ level}}{\text{number of mounts}} \\
 &= \frac{45(3.015)}{4} = 33.9 \text{ lb.}
 \end{aligned}$$

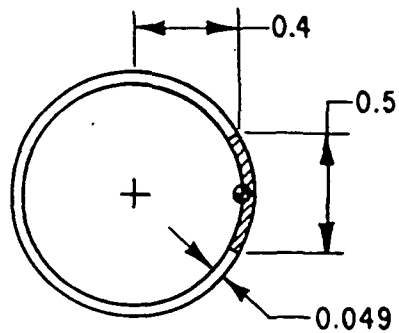
A free-body diagram of one mount, showing all load vectors would appear like this.







The approximate area in bearing on the cylinder when the "tip-up" load is present is:



$$A = 0.5(0.049) = 0.0245$$

$$S_c = \frac{84.75}{0.0245} = 3459$$

$$M.S. = \frac{130,000 \text{ (allowable)}}{3459} - 1 = 36.6$$

## 6.2 THERMAL DESIGN

### 6.2.1 Requirements

The design of the thermal subsystem is governed by the temperature limits of the experiment and components, the orbital environments, the satellite configuration and the power dissipation characteristics. The final design results from compromises between what is desired and what can be provided. The thermal requirements are given in Table 6-7.

Table 6-7  
SPACECRAFT THERMAL DESIGN REQUIREMENTS

• Dewar Exterior Temperature ( $T^3$ Avg.)	<240°K
• Electronic Boxes Temperatures	-10 to +30°C
• Battery Temperatures	0 to 25°C
• Solar Cell Array Temperatures	-100°C to +90°C
• Infrared Heating to LHe	<40 mw
• Albedo Heating of Experiment	<4 mw (annual average) <30 mw (peak)

The exterior of the dewar must be kept cold to minimize the liquid helium boil-off rate. The electronic box temperature range is set to keep design costs low. The batteries require tight temperature control to keep efficiency and life within the required limits. The temperature of the solar cell array is kept as low as possible since power output decreases by 0.7 percent per degree C rise. Also there is a materials problem when temperatures exceed about +110°C and when temperature cycles are larger than 150°C.

### 6.2.2 Thermal Design Description

The thermal design uses passive methods as the primary means to control the heat flow into and out of the satellite components



to obtain the desired temperatures. These methods involve the use of finishes and insulation as shown in Figs. 6-11 and 6-12. Active thermal control methods considered, but not used, included thermostatic electrical heaters, louvers, and thermal switches. Passive methods are preferred because of their simplicity and reliability. Active methods are used only if passive methods will not produce the required temperature control.

The use of surface finishes for thermal design involves controlling the optical properties of the surfaces. The two surface properties of interest are the absorptance of radiant energy in the solar spectrum ( $\alpha$ ), and the emittance of radiant energy in the spectrum corresponding to the black body temperatures of the satellite and of the surface and atmosphere of the earth ( $\epsilon$ ). Most of the solar energy is short wavelength (visible), whereas most of the energy from the satellite and earth is long wavelength (infrared, I.R.). Kirchoff's law states that when a body is in thermal equilibrium with another body in a two-body system, the emittance and absorptance of the body are equal. Since the satellite surfaces and the earth are close to the same temperature, the absorptance to the incoming earth radiation and the emittance for radiation from the satellite will be essentially equal. However, the sun is much hotter than the satellite, and the absorptance to the incoming solar radiation may be quite different from that for the incident earth radiation. It is customary to use absorptance ( $\alpha$ ) in reference to solar energy and emittance ( $\epsilon$ ) for both absorptance and emittance when dealing with earth and satellite radiation.

Finishes are available that have widely different values of  $\alpha$  and  $\epsilon$ . For satellite flights, the thermal optical properties must be stable throughout the mission. Ultraviolet and particle radiation will change the properties of many finish materials. Some of the more stable finishes are shown in Table 6-8.

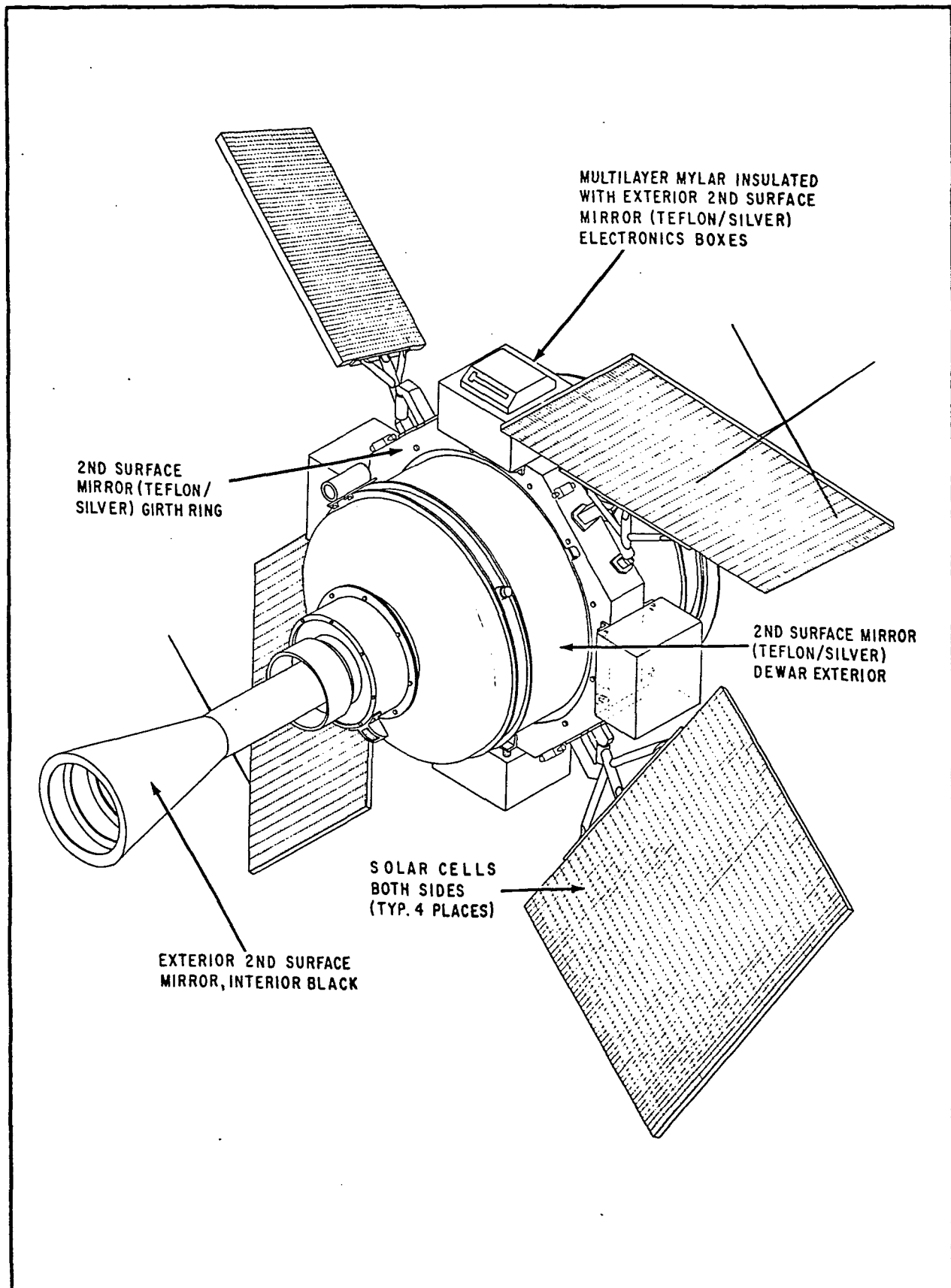


Fig. 6-11 Spacecraft Exterior Finishes

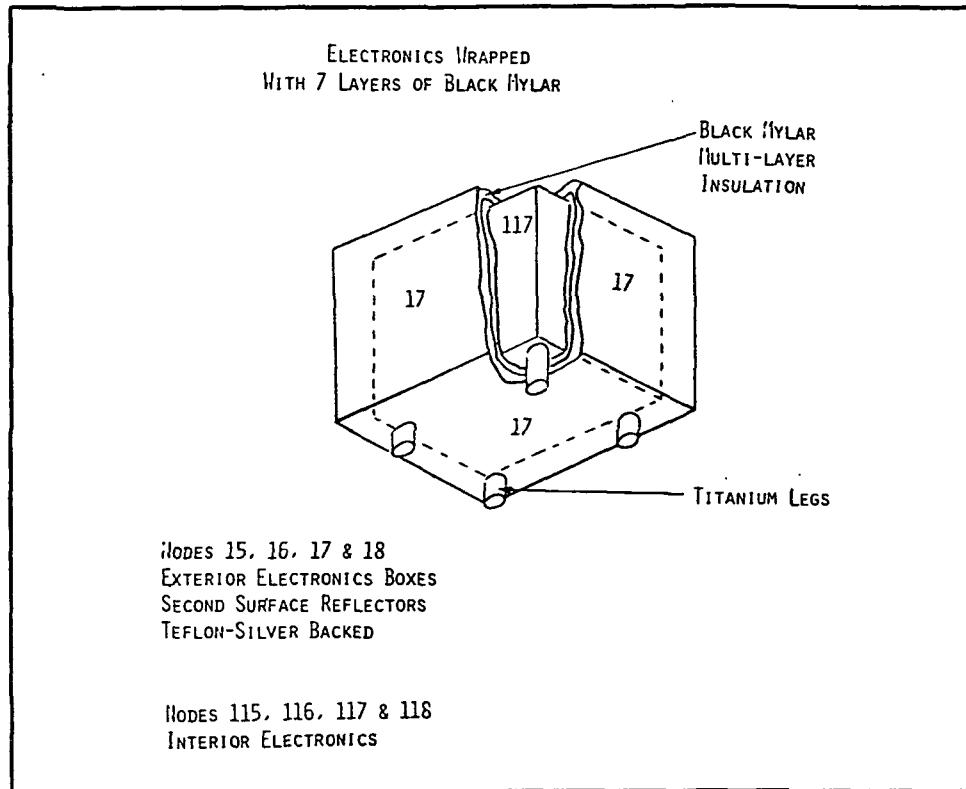


Fig. 6-12 Electronic Boxes Thermal Design

Table 6-8

## SOME STABLE THERMAL CONTROL FINISHES

<u>Finish</u>	<u><math>\alpha</math></u>	<u><math>\epsilon</math></u>	<u><math>\alpha/\epsilon</math></u>
Black paint (Cat-a-lac)	0.95	0.85	1.12
Bright gold	0.28	0.03	9.35
Aluminum - light chromicoat	0.45	0.05	9.00
Leafing Aluminum Paint (BBRC 80-U)	0.24	0.34	0.706
White Paint (BBRC 63-W)	0.20	0.80	0.25
FEP over Vacuum-deposited Aluminum (0.13mm) (Second surface mirror)	0.18	0.80	0.23
FEP over vacuum-deposited Silver over vacuum-deposited			
Inconel (Second surface mirror) (0.13mm)	0.09	0.80	0.113
(0.05mm)	0.06	0.50	0.12



Table 6-8 (Cont.)  
SOME STABLE THERMAL CONTROL FINISHES

<u>Finish</u>	<u><math>\alpha</math></u>	<u><math>\epsilon</math></u>	<u><math>\alpha/\epsilon</math></u>
Silver over vacuum-deposited (0.13mm) Inconel (Second surface mirror)	0.05	0.76	0.066
Solar cell array	0.79	0.78	1.01

A simple example will serve to illustrate how temperatures are controlled passively using surface finishes. Consider an isolated plane surface on a satellite that is normal to the sun's rays and views only space. The absorbed solar energy is radiated to space.

The energy balance equation becomes

$$S\alpha A = A\sigma\epsilon T^4 \quad (1)$$

where S is the solar constant ( $\text{w/m}^2$ )

$\alpha$  is the solar absorptance of the surface

A is the area of the surface ( $\text{m}^2$ )

$\sigma$  is the Stephan-Boltzmann constant ( $\text{w/m}^2 - \text{K}^4$ )

$\epsilon$  is the infrared emittance

and T is the surface absolute temperature ( $\text{K}^\circ$ ).

Solution for T yields

$$T = \left[ \frac{S}{\sigma} \frac{\alpha}{\epsilon} \right]^{1/4} \quad (2)$$

which demonstrates that small values of  $\alpha/\epsilon$  produce cold temperatures and large values of  $\alpha/\epsilon$  produce hot temperatures. Fig. 6-13 is a plot of equation 2.

The analysis of the satellite is more complex than this example since such things as absorbed earth radiation (I.R.), solar



radiation reflected from the earth (albedo), radiation interchange with other parts of the satellite, conduction between satellite parts, and electrical heating must be considered. Appendix B describes the BBRC thermal analysis methods used for this study.

It is evident that a stable, low  $\alpha/\epsilon$  surface is required on the exterior of the dewar to maintain a cold temperature. The family of second surface mirror systems has the most stable properties in space environment. The principle of operation is an interesting combination of optical effects. Figure 6-14 is a schematic drawing of the laminate. The sun-facing layer is transparent to most of the energy in the solar spectrum but opaque to the long-wavelength radiation corresponding to most of the energy in the spectrum from a black body at the temperature of the satellite surface. The vacuum-deposited silver has a high reflectance (low absorptance,  $\alpha$ ) in the solar spectrum, and therefore almost all (more than 90%) of the incident direct solar radiation and reflected solar radiation from the earth (albedo) is reflected from the mirror and not absorbed. However, because the outer layer is opaque to infrared, the radiation emitted to space is from the outer surface rather than from the silver through the layer. Therefore the laminate has a high emittance ( $\epsilon \approx 0.8$ ), characteristic of fused silica or FEP, rather than a low value ( $\epsilon \approx 0.05$ ), characteristic of vacuum-deposited metals. The effective emittance is a function of the thickness of the outer layer as shown in Table 6-8. This is due to the increase in transparency to infrared wavelengths when the thickness decreases below 0.13 mm (0.005 in). The thick layer is appropriate for this application to produce cold temperatures.

Dewar, Sun Shield and Girth Ring. The performance of second-surface mirrors on the dewar, sun shield and girth ring exteriors is such that the direct solar and albedo energy absorbed is minimized and the absorbed infrared radiation from the earth is more

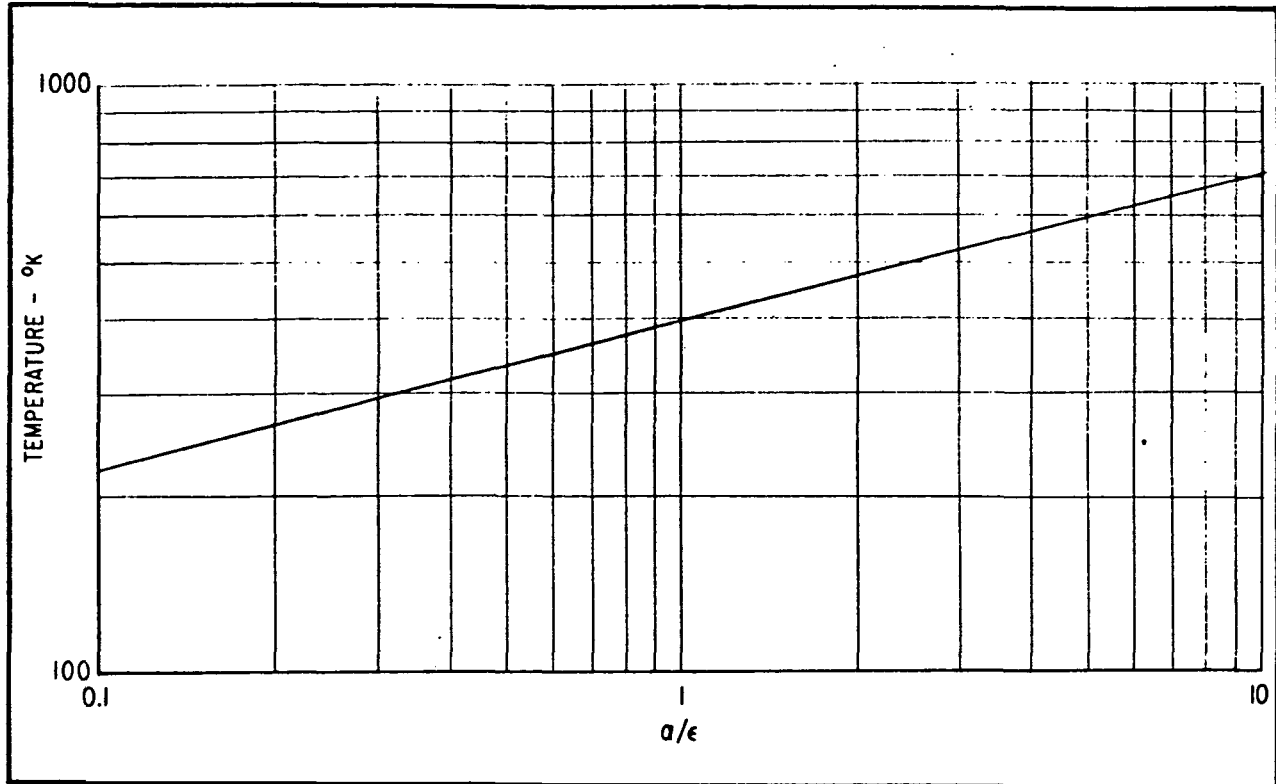


Fig. 6-13 Temperatures of Sun-Facing Surfaces at One Astronomical Unit

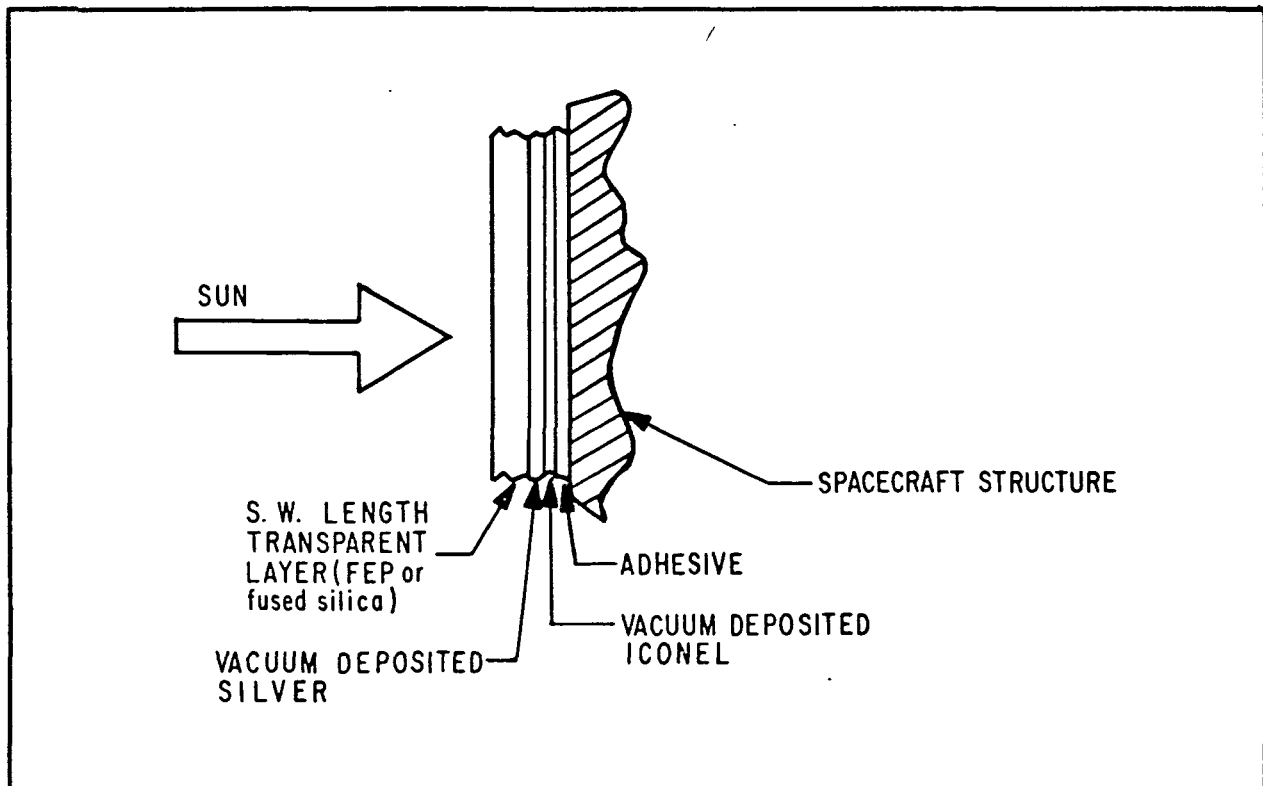


Fig. 6-14 Second-Surface Mirror Assembly





predominant. With a polar orbit of an inertially fixed satellite, the average incident earth radiation is nearly constant during a year, but the direct solar and albedo radiation incident on the satellite changes considerably as the sun position changes relative to the satellite in its orbit. Temperature gradients in the dewar outer shell are minimized by the thermal conductivity of the shell and because the satellite rolls about the star line as the satellite orbits the earth. The slow roll of the satellite helps reduce temperature extremes particularly near the spring and fall equinoxes when the sun is normal to the orbit plane.

Electronic Boxes. The slow relative movement of the sun about the satellite and the very slow roll rate required special measures to reduce the spread between the maximum and minimum temperatures of the electronics boxes. The passive system shown in Fig. 6-12 was shown to be feasible during the study. A thermal network of the design is shown in Fig. 6-15. Even a cursory analysis shows that

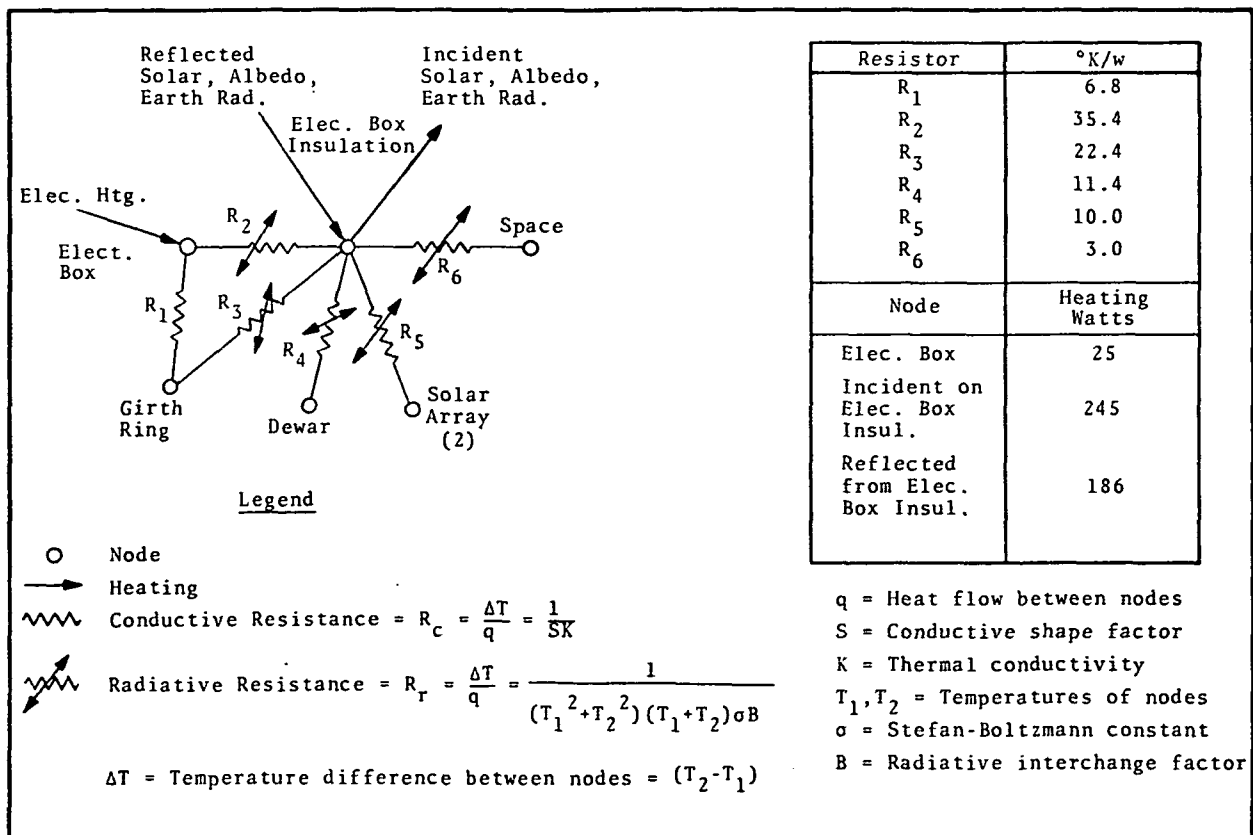


Fig. 6-15 Thermal Network for Electronic Boxes



the largest variation in heating is caused by changes in shadowing of the sun and albedo. We reduce this effect by the use of an outer surface with a small solar absorptance. The second-surface mirror finish chosen produces an average temperature that is too cold. Since the electrical dissipation in each box is nearly constant, it is possible to select the proper amount of insulation to raise the temperature of the internal components to the desired level and still retain the stability produced by the second surface mirror. Insulating thermal supports are used to isolate each box from the cold, but relatively stable, girth ring. In this way, the electronics are coupled through a fixed thermal resistance to cold but relatively constant heat sinks, the exterior of the insulation and the girth ring. Closer control can be obtained by using small thermostatic electrical heaters. Further refinements in the design of the satellite may dictate active heating of some of the boxes, particularly the one containing the batteries. In all cases, dummy heaters with the same dissipation as the electronics will be activated when the electronics are turned off.

Batteries. The thermal design of the nickel-cadmium batteries will require special consideration during the detailed design--as usual. During discharge, the cells undergo a chemical reaction that is exothermic. During charge, the chemical reaction is endothermic until the cells are charged; during overcharge, the reaction is highly exothermic. The power system design uses the third electrode system of charge-control which effectively eliminates the overcharge process and reduces the complexity of the battery thermal design. Even so, to make the system work, the battery assembly of cells must be designed so that temperature gradients are minimized between the individual cells in each battery string, and between the strings. The solution is to provide high thermal conduction paths between all cells without a great sacrifice in excess weight and electrical isolation. Several workable designs are available which can be chosen during the electronics package



design phase. All the batteries should be located in the same box to achieve uniform temperatures between all cells.

Inspection of the results of the steady-state analyses shown in Section 6.2.3 shows that the range of electronic box temperatures is essentially between 0 and 25°C. The insulation, external finish and power dissipation was identical for each box in the analysis, so that each computer run produces representative results for four box positions. The design of each box will be tailored to the particular power dissipation and requirements of the box. Therefore, it will be possible to design the battery box slightly colder and provide a small amount of thermostatically controlled electrical heating to reduce the temperature excursion. This is practical since it appears that the coldest environment does not occur when the available power is at a minimum.

Solar Cell Array. There is little latitude in the thermal design of the solar cell array panels since cells must be mounted on both faces of the panels. The resulting temperatures have been shown by the analysis to be within acceptable limits. A movable array that remains pointed close to the sun could be designed to have a smaller temperature excursion and a lower maximum temperature, but the added complexity and disturbance torques associated with a movable array are considered less desirable than the temperatures that result from the chosen configuration.

The panels provide adequate area for dissipation of the heat generated by the battery charge control system. As a matter of fact, the resulting increase in temperature of the array decreases the amount of power generated and therefore the excess that must be dissipated while the batteries are charged. In the final design, any area not covered with cells (including the edges) will be painted white to help reduce the maximum array temperature during the critical power system orbits.



### 6.2.3 Analysis and Performance

The analysis of the performance of the thermal design was performed in two stages. The first involved simplified calculations to evaluate configuration concepts, establish preliminary thermal design concepts, and establish realistic thermal requirements and temperature ranges for the other subsystems. The second stage involved a comprehensive thermal analysis to establish the thermal performance in greater detail. The satellite was subdivided into thirty-four nodes and the BBRC thermal analysis computer programs were used to calculate the temperatures of each node for three orbital conditions which cover the conditions that will produce the expected extremes in temperature during a year in orbit.

Nodal Model. The satellite was subdivided into the thirty-four nodes shown in Figs. 6-16 and 6-12. The values of solar absorptance ( $\alpha$ ) and infrared emittance ( $\epsilon$ ) of the exterior surfaces used in the analysis are given in Table 6-9. The value of solar absorptance used for the FEP/silver mirror surfaces (0.15) represents the degraded value after exposure to ultraviolet and particle radiation in orbit.

The three orbital conditions analyzed during the study are defined using the beta ( $\beta$ ) angle and the roll ( $\phi$ ) angle. The beta angle is the angle between the solar vector and the orbit plane (the complement of the angle between the solar vector and the orbit normal). When  $\beta = 0$ , the sun lies in the orbit plane. Under this condition the satellite experiences the maximum fraction of the orbital period in the shadow of the earth. Thus the greatest environmental cycling results and the greatest orbital temperature variations occur. This condition will exist at the summer and winter solstices.

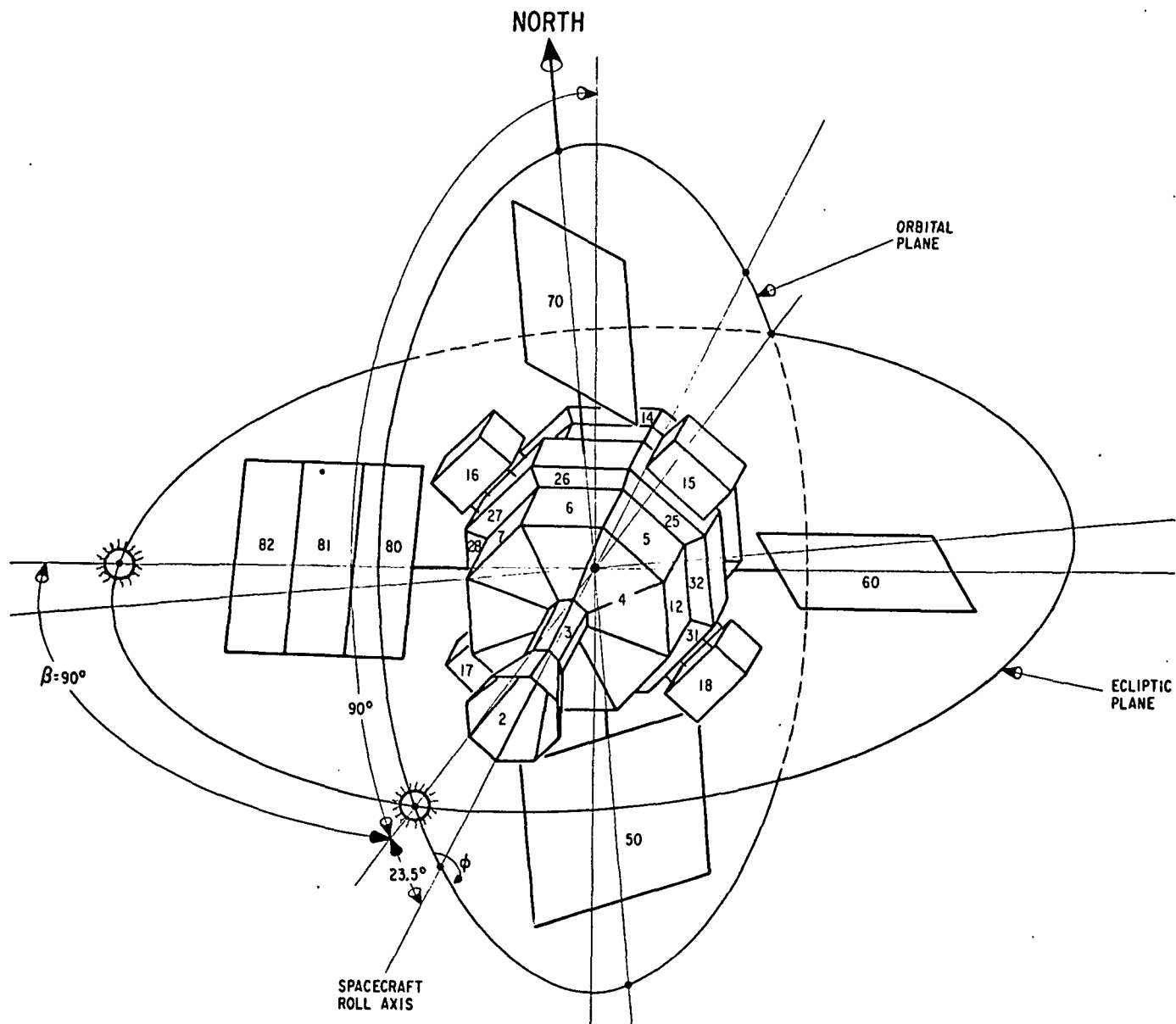


Fig. 6-16 Thermal Nodes



Table 6-9  
THERMAL MODEL OF EXTERIOR FINISHES

<u>Node No.</u>	<u>Description</u>	<u>Solar Absorptance <math>\alpha</math></u>	<u>Infrared Emittance <math>\epsilon</math></u>
2	Sunshade Cone	0.15	0.83
3	Sunshade Cylinder	0.15	0.83
4	Dewar Forward Head	0.15	0.83
14	Dewar Aft Head and Attachment Ring		
5	Dewar Shell		
6			
7			
8			
9			
10			
11			
12			
15	Electronic Box Insulation		
16			
17			
18			
25	Girth Ring		
26			
27			
28			
29			
30			
31			
32			
50	Solar Array Panel	0.79	0.78
60			
70			
80			
81			
82			
115	Electronic Box and Contents	0.83	0.83
116			
117			
118			



When  $\beta = 90^\circ$ , the satellite is in a full sunlit orbit. Because the roll rate is slow, the largest variations in the temperatures of the individual electronic boxes and solar array panels result. Only steady state results were computed since they differ little from the ones that result from the slow roll conditions, and are more severe.

The roll angle ( $\phi$ ) defines the angular orientation of the satellite about its spin axis. For this analysis,  $\phi = 0$  when solar panel node 70 is on the north side of the satellite. For  $\phi = 45$  degrees, electronic box nodes 16 and 116 are on the north side of the satellite. The spin axis was kept parallel to the equatorial plane and pointing near the summer solstice during all orbits. Therefore the sun was  $23.5^\circ$  north of the line of sight at the summer solstice and  $23.5^\circ$  south and behind it at the winter solstice, since the ecliptic makes a  $23.5^\circ$  angle with the equatorial plane.

The roll angle has little effect on the satellite temperatures when  $\beta = 0$  except for the solar array panels. The roll position  $\phi = 0$  gives the maximum temperature spread at this  $\beta$  angle and was selected for the analysis. For  $\beta = 90^\circ$ , the roll angle affects the temperature of the electronic boxes and the solar array panels. Therefore, analyses were made at both  $\phi = 0$  and  $\phi = 45^\circ$ .

Only one transient analysis was required to determine the maximum temperature variations during an orbit. Since the maximum variations occur when  $\beta = 0$ , the transient analysis was performed for the  $\beta = 0$ ,  $\phi = 0$  condition.

Thermal Performance. The results of the three steady state analyses are given in Appendix B for all nodes. Table 6-10 gives the results for the nodes of maximum interest. By comparison with the requirements set forth in Table 6-7 it is evident that the requirements are met with the passive thermal design. Since the power dissipated in the batteries may vary an appreciable amount, it may be necessary to adjust the insulation on the electronics box containing the batteries and include a small thermostatic electric heater



Table 6-10  
STEADY STATE TEMPERATURES OF SELECTED NODES

Node No.	Temperature - °C					
	$\beta$	$\phi$	$\beta$	$\phi$	$\beta$	$\phi$
	0	0	90	0	90	45
<b>Electronics</b>						
115	15.3		2.5		-0.5	
116	14.7		24.3		4.3	
117	9.4		24.3		23.3	
118	9.8		2.6		5.5	
<b>Array</b>						
50	15.6		45.2		28.0	
60	-4.0		-83.3		-87.2	
70	20.9		44.2		-87.4	
80	45.5		-55.0		30.1	
81	45.0		-75.6		23.1	
82	44.6		-81.0		21.7	
<b>Dewar</b>						
5	-53.3		-63.5		-68.7	
6	-50.0		-53.7		-66.8	
7	-53.1		-36.7		-57.1	
8	-58.4		-29.5		-39.2	
9	-60.7		-36.9		-32.3	
10	-60.9		-53.6		-38.2	
11	-60.8		-63.5		-56.6	
12	-59.1		-67.7		-66.7	
4	-42.6		-63.2		-64.7	
14	-60.1		-59.3		-60.5	
T <sup>3</sup> Surface Av.	217 °K		221 °K		219 °K	

in this box. This design is straightforward during the detailed design phase.

The significant results of the transient analysis of the  $\beta = 0$  orbit are shown in Figs. 6-17 through 6-20. The results from the transient analysis are given in Appendix B for all nodes.



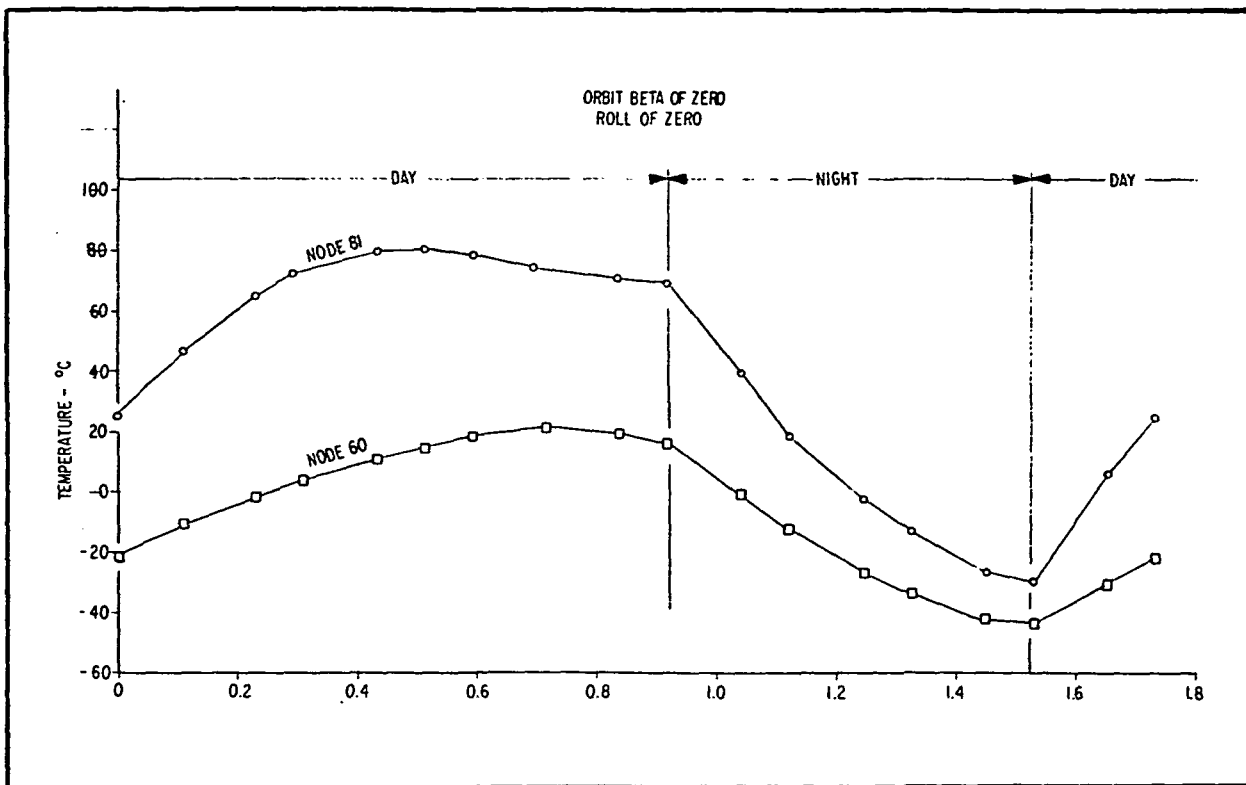


Fig. 6-17 Solar Array Transient Temperatures

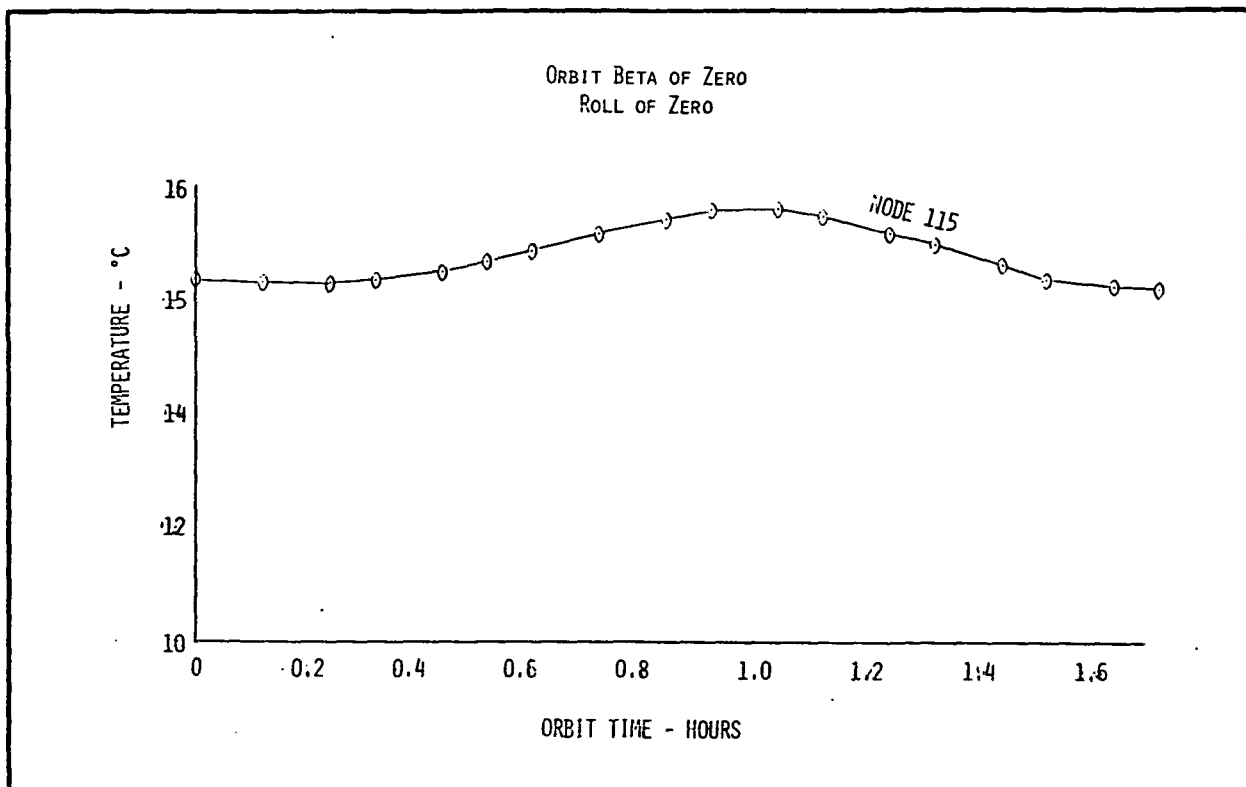


Fig. 6-18 Typical Electronics Transient Temperatures

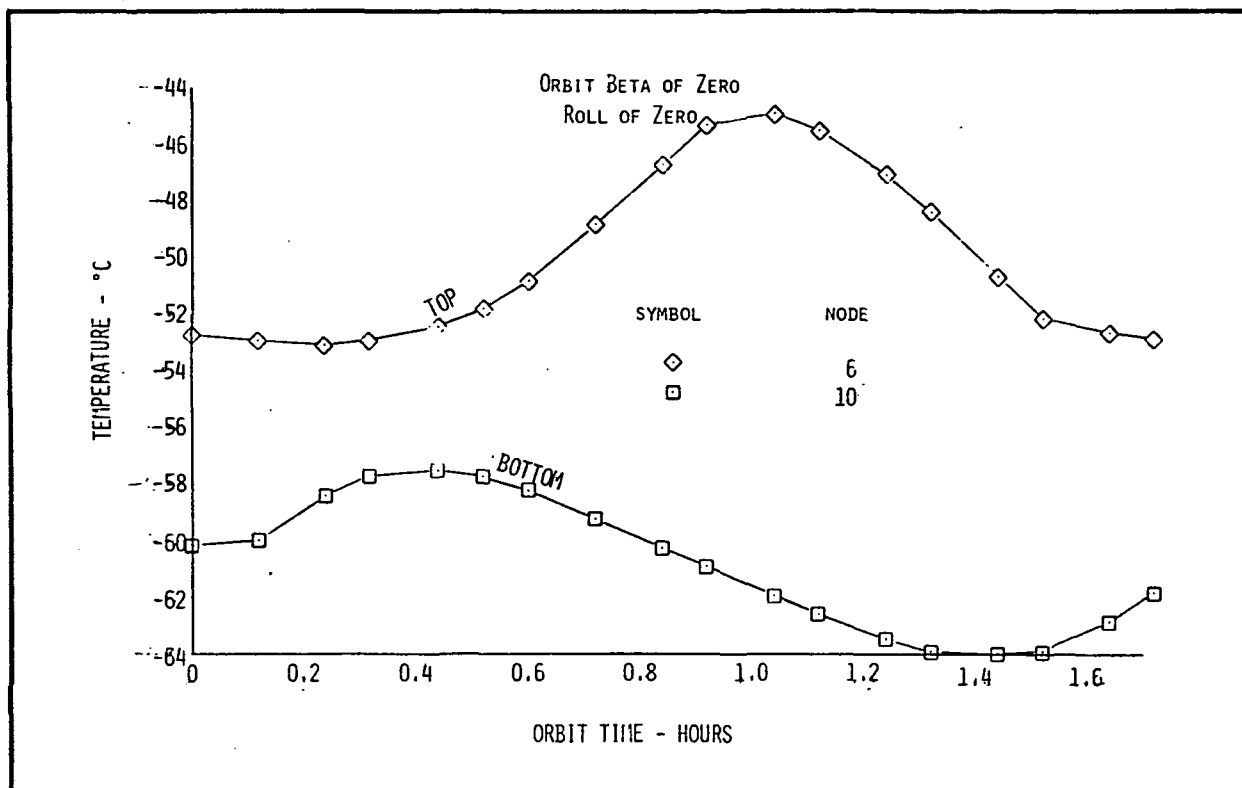


Fig. 6-19 Dewar Top and Bottom Transient Temperatures

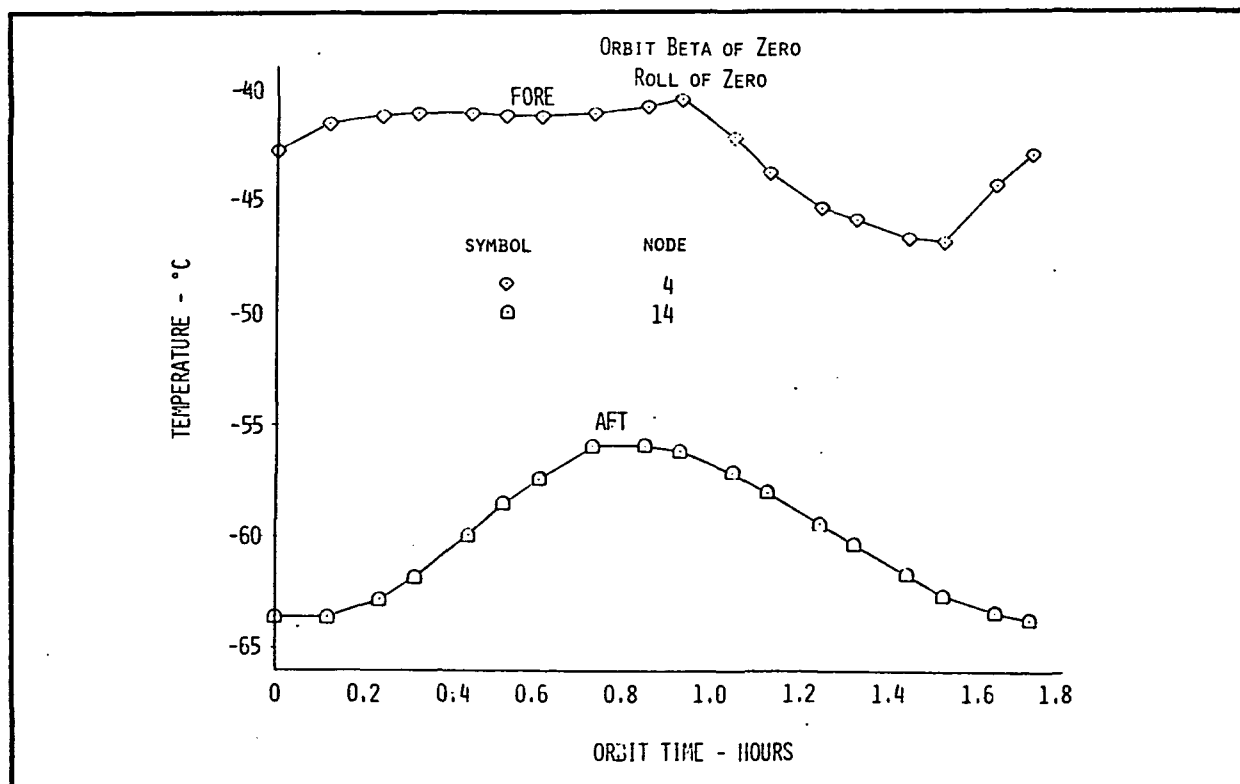


Fig. 6-20 Dewar Fore and Aft Transient Temperatures



## 6.3 POWER

### 6.3.1 Requirements

Listed below are the requirements to which this subsystem was designed:

- Generated System Power >100 watts
- Unregulated Voltage +28  $\pm$  4 VDC continuous
- Regulated Voltages
  - a) +28 VDC  $\pm$ 5%
  - b)  $\pm$ 15 VDC  $\pm$ 2%
  - c) +5 VDC  $\pm$ 5%
- Solar Array Temperatures -100°C to +90°C
- Number of Day-Night Cycles 3500 per year
- Life 1 year
- Environment 500 nmi polar orbit
- Battery Temperatures 0°C to +25°C
- Electronics Temperatures -10°C to +30°C
- System Commands
  - a) Satellite load control
  - b) Battery charge control
- System Telemetry
  - a) Operating temperatures
  - b) Voltage and current measurements
  - c) Operating mode confirmations



The temperature ranges mentioned above are maximum flight temperatures. Power system components will meet their performance requirements throughout these ranges. The components will survive temperature extremes of  $10^{\circ}\text{C}$  on both ends of the normal ranges; however, system performance may be degraded.

### 6.3.2 Power System Description

A power system block diagram is shown in Fig. 6-21. The system is made up of the following major components: solar array, nickel-cadmium batteries, charge control electronics, shunt regulator and shunt loads, undervoltage switch (UVS), and master regulator. Briefly, the systems work as follows: The solar array supplies sufficient power, during orbit day, for the spacecraft loads and battery charge requirements. During orbit night, the batteries power the loads. The orbit day battery charge rate

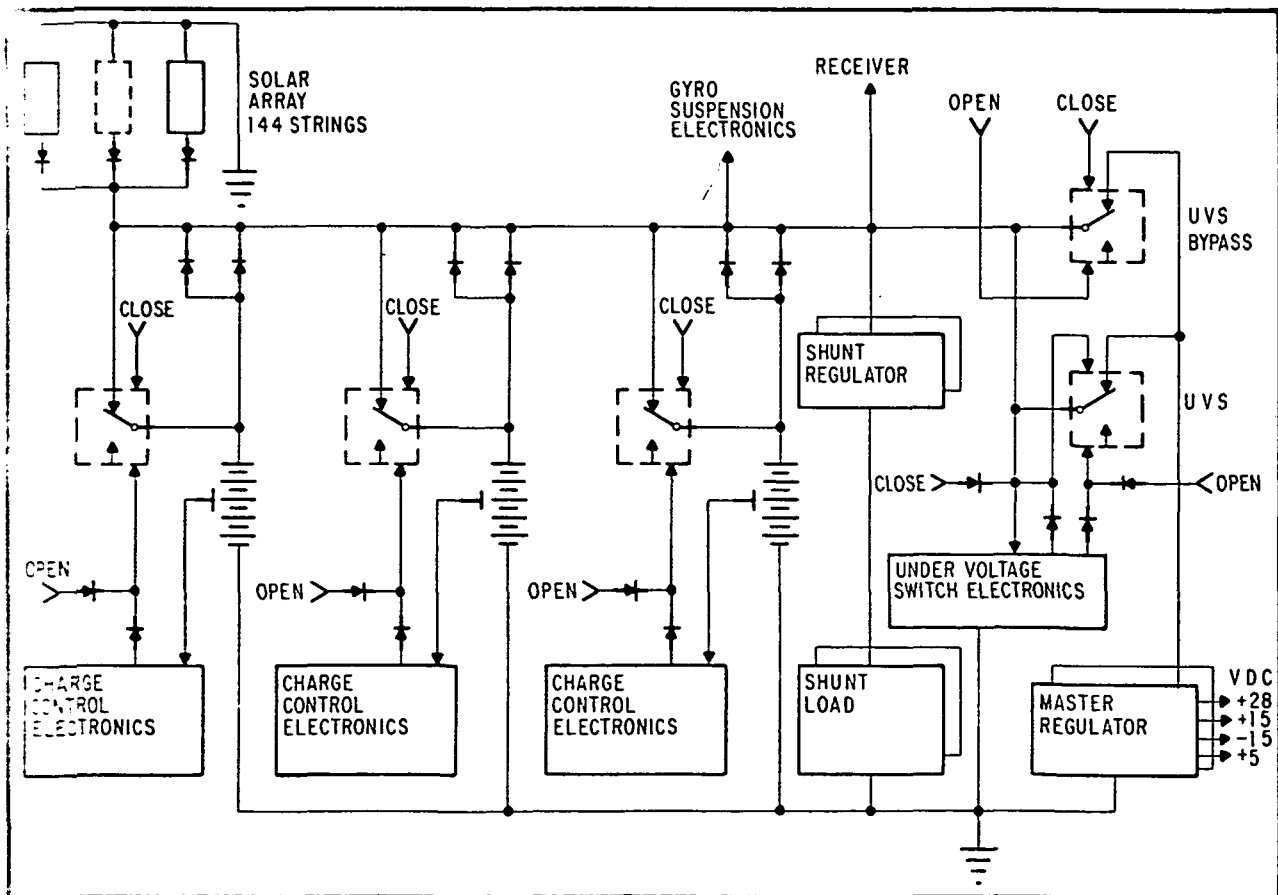


Fig. 6-21 Power System Block Diagram



is controlled by the charge control electronics. The shunt regulator maintains a constant bus voltage after the batteries are fully charged and the shunt load dissipates the extra power generated by the solar array. Several different regulated voltages are supplied by the master regulator for use by the various spacecraft electronic subassemblies.

Solar Array. The solar array consists of four identical 107 x 122 cm aluminum honeycomb paddles with solar cells mounted on both sides. Each solar cell is approximately 1.9 x 3.8 cm in size with an active area of about 7.1 cm<sup>2</sup>. The cell type is N on P with 2 ohm/cm base resistivity. In order to produce sufficient voltage at the maximum array temperature, 94 solar cells connected in series are required. Each side of each paddle provides enough area for 18 strings for a total of 144 strings for the total solar array. The area on each paddle not covered by solar cells is used for mounting isolation power diodes and the shunt load zener diodes. Each of the solar cell series strings is connected in parallel as shown in Fig. 6-22. The total effective array area is reduced to about 9.6 m<sup>2</sup> after allowing for the mounting of diodes and zener diodes and fabrication loss. The solar cell interconnections are made with silver-plated covar, rather than copper, to withstand the extreme temperature cycling requirements. Radiation protection for the solar cells is provided by 12 mil cover slips made of fused silica coated with an anti-reflection coating.

The solar array produces about 340 watts of end-of-life power at a temperature of 90°C during the daytime portion of the maximum power orbit. The available power reduces to about 193 watts during the minimum power orbit. These end-of-life power figures allow for radiation degradation of about 15 percent and seasonal change of sun intensity of 3.5 percent. The amount of radiation degradation was arrived at by increasing the observed OSO-III

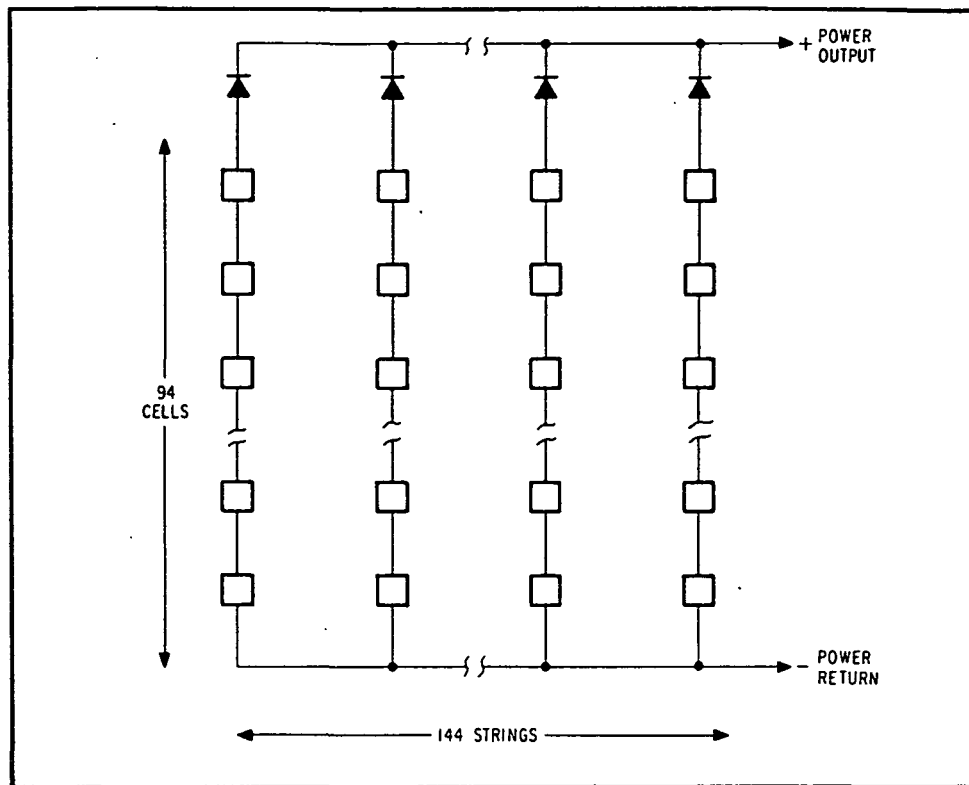


Fig. 6-22 Solar Array Cell Configuration

degradation of 1 percent (30 mil cover slips) to 1.5 percent for our 12 mil slips and then increasing that by a factor of 10 to allow for the change from an OSO 300 nautical mile orbit to a 500 nautical mile orbit. The factor of 10 was obtained from the report NASA SP-3024, "Models of the Trapped Radiation Environment, Vol. 1."

The effective array area for various sun angles and roll positions was obtained by using a digital computer modeling program and scaling techniques. The computer program accepts the satellite model and attitude with respect to the sun then plots a projection of the satellite at whatever sun angle or roll position is desired. Shadowed portions of the array are readily apparent. By measuring the dimensions of the unshadowed portions of the



array the effective array area was calculated, at the worst roll position, for many different sun angles. The sun angle is the angle between the satellite roll axis and the sun. This angle changes through  $180^\circ$  during six months. Figure 6-23 is a plot of the array gain factor vs. sun angles from  $0^\circ$  to  $120^\circ$ . A plot of orbit shadowing showing the percent of orbit in shadow vs. sun angle is presented in Fig. 6-24. By combining the curves in Figs. 6-23 and 6-24, a composite curve of total solar array power gain is shown in Fig. 6-25.

By observing Fig. 6-25, it can be seen that the lowest total array power gain occurs during the orbit where the angle between the spacecraft roll axis and the sun is equal to about 45 degrees. The maximum total array power per orbit occurs at an angle of 0 degrees. With a load power requirement of 100 watts, there is a power margin of about 10 watts during the minimum power orbit. With the present identifiable load of 91.9 watts, we have the capability of supplying an additional 18 watts of regulated power during the minimum power orbit.

Batteries. The power system energy storage is provided by three parallel battery strings, each made up of 21 series-connected nickel-cadmium cells. Each string produces a nominal +28 VDC and supplies 4 ampere-hours for a total capacity of 12 ampere-hours. This capacity is sufficient to allow the loss of one string, with enough capacity remaining to complete a normal spacecraft mission. A brief description of the battery thermal characteristics can be found in section 6.2.2.

Two cells in each string have a third electrode which produces a voltage signal when the cell is fully charged. This voltage signal is used to terminate the battery string charging current by opening a set of relay contacts as shown in Fig. 6-21, thus eliminating the possibility of battery damage due to overcharging.

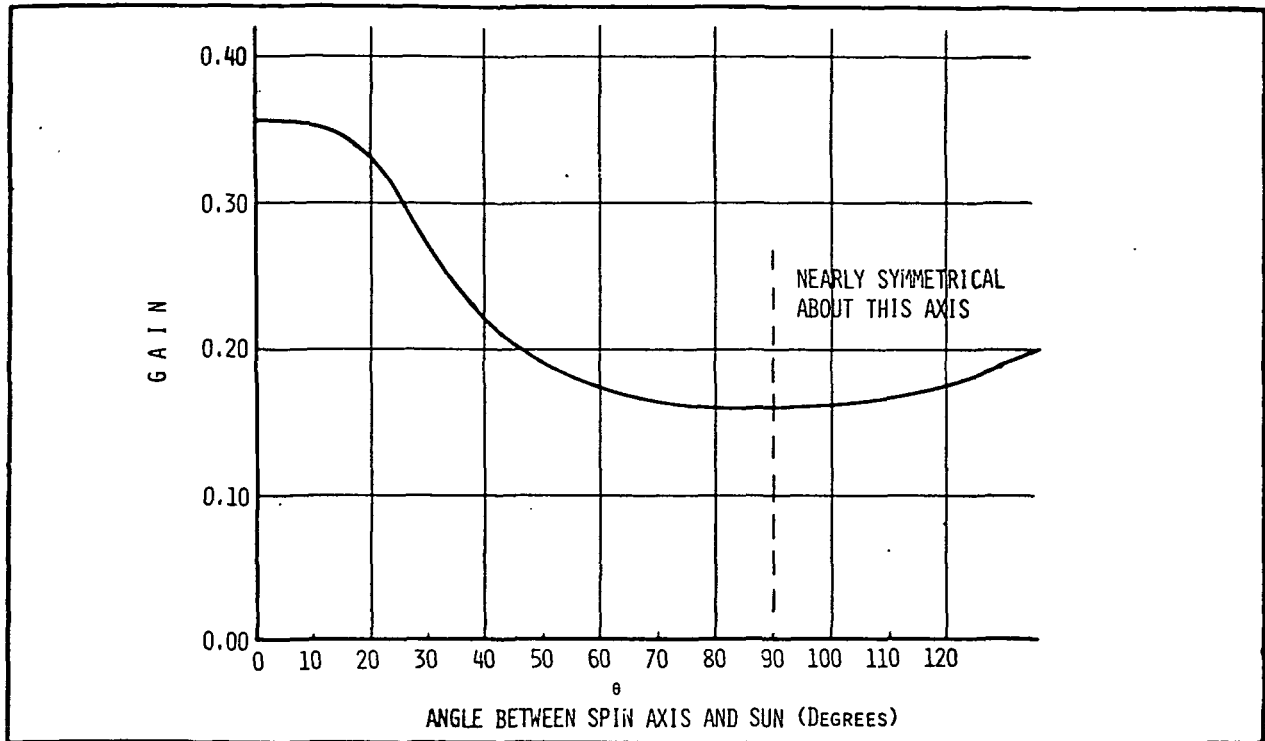


Fig. 6-23 Solar Array Power Gain Due to Angular Sunlight Incidence and Shadowing

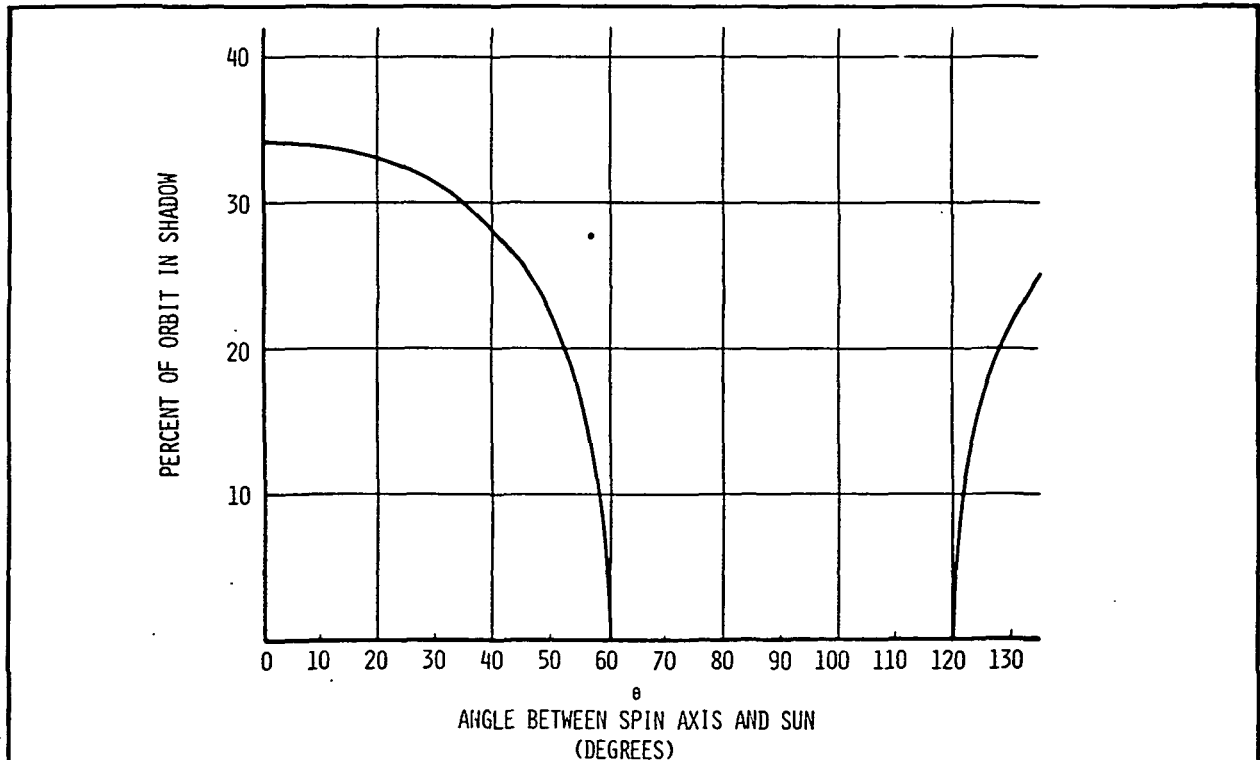


Fig. 6-24 Orbit Shadowing



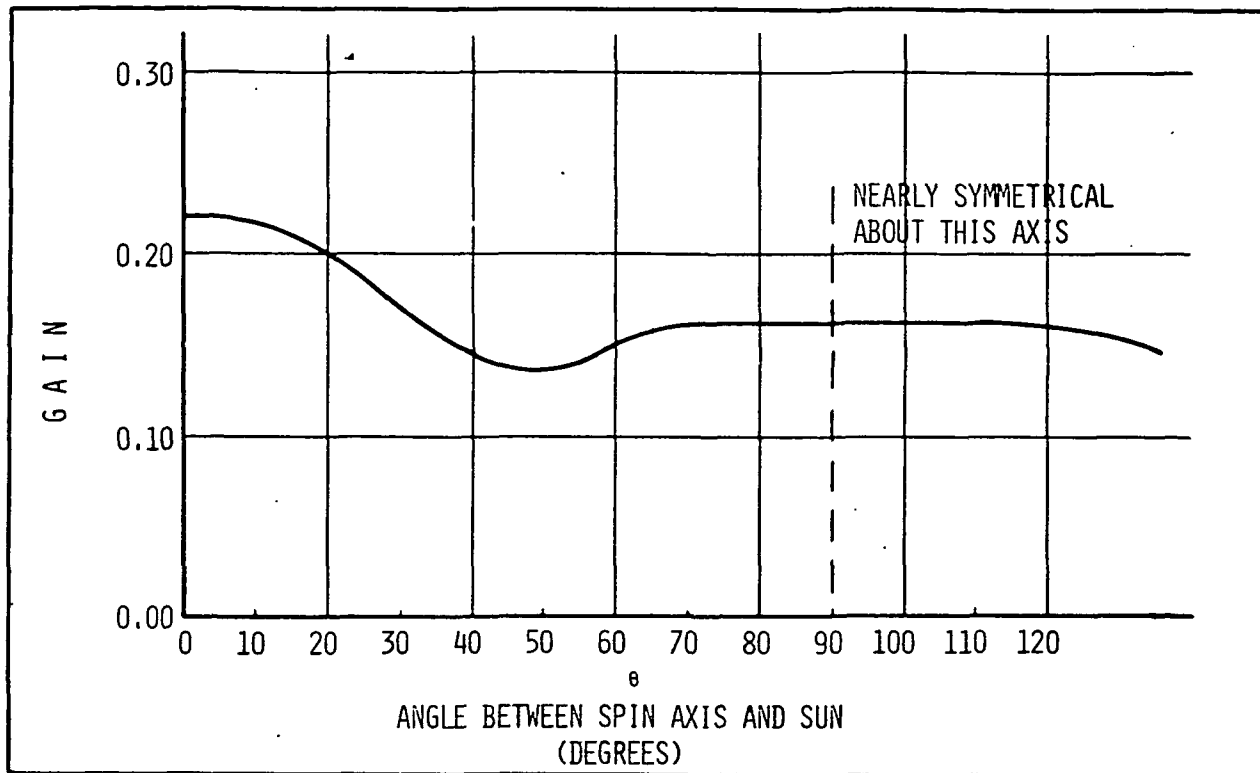


Fig. 6-25 Total Solar Array Power Gain

This type of charge control was successfully used on the OAO spacecraft backup power system and is also being used in the ATM primary power system. The batteries are automatically reconnected to the main power bus at the start of orbit night. Battery strings can also be connected or disconnected to the main voltage bus by command.

Shunt Regulator and Shunt Loads. The shunt regulator controls battery overcharge by limiting charge voltage. This is accomplished by drawing more or less current from the solar array to clamp its output voltage. The shunt regulator can be removed from the system by command, also the regulation voltage level could be made to change as a function of battery temperature and/or adjustable by command, if so desired. The shunt regulator



voltage set point is nominally 31 volts DC. A redundant shunt regulator can be switched in by command, if the primary regulator should fail.

The excess solar array power is dissipated in 4 shunt load banks which are made up of series strings of power zener diodes whose combined breakdown voltage is about 27 volts. The system is sized to dissipate the maximum amount of power the array can generate which is about 340 watts. This feature prevents possible damage to the batteries in the event that most loads are turned off and the spacecraft attitude is such that maximum power is being generated such as might be the case during initial acquisition. There are four identical load banks with one bank in each solar panel. The power dissipation capability of each bank is sufficiently large to allow the failure of one bank and still be able to dissipate the maximum array power in the remaining three banks.

Undervoltage Switch. The undervoltage switch controls a latching relay which connects all the spacecraft loads except the receiver, decoder and gyro suspension electronics to the unregulated bus. The undervoltage switch provides protection against excessive discharge of the batteries to the point where the command system will not work. The switch opens when the unregulated bus falls to 24.3 volts for more than three seconds or 20 volts for more than 10 ms, and resets when the batteries have charged up to 29.8 volts. The first voltage level is for general slow discharge and the second level is to protect the wiring harness and assure the undervoltage switch will work with a direct short.

In an emergency, the undervoltage switch relay can be commanded to either position regardless of bus voltage, without losing protection. There is also a command bypass around the relay in case it fails to operate.



Master Regulator. The master regulator provides four regulated output voltages: +28 VDC, +15 VDC, -15 VDC and +5 VDC. A simplified block diagram is shown in Fig. 6-26. The regulator is comprised of two main parts: a switching regulator, followed by a DC to DC converter with multiple outputs off the transformer secondary. The +15 volt output is fed back to the switching regulator to provide closed-loop feedback. The other output voltages will essentially track the feedback voltage. Their regulation will not be as good, but should be sufficient for most typical spacecraft loads. The regulator is short-circuit-proof and is also protected from power overloads by employing foldback current limiting.

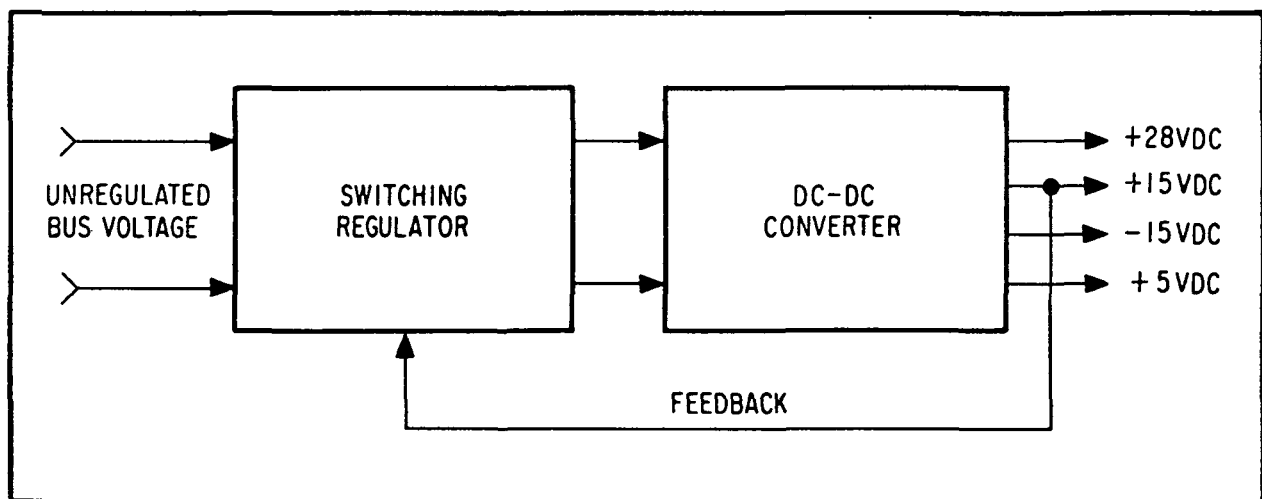


Fig. 6-26 Master Regulator Simplified Block Diagram

The +28 VDC output is provided for purchased standard spacecraft equipment. Analog circuitry such as operational amplifiers use the  $\pm 15$  VDC. The +5 VDC bus supplies power for logic circuits.

A redundant master regulator is included in the power system. The two regulators are identical and either one can be selected for use by command. Regulator inputs and outputs are switched by latching relays.



System Commands and Telemetry. The operation of the following power system major components can be partially controlled by commands:

- Battery charge control electronics
- Shunt regulator and shunt loads
- Undervoltage switch
- Master regulator

A list of the available commands can be found in Table 6-23. A listing of all the telemetry monitors such as temperatures, voltage levels, array current and relay status monitors are also found in Table 6-22.

System Power Budget. Table 6-11 is a tabulation of all the continuous power system loads.

### 6.3.3 Performance

Significant power system performance numbers are as follows:

- Solar Array:
 

Maximum power output	340 watts
Minimum power output	193 watts
Power margin at minimum power output (100 W load)	12 watts
- Batteries:
 

Capacity	12 amp-hrs
Charging voltage	30 VDC (nominal)
Discharging voltage	27 VDC (nominal)
Amp-hr charging efficiency	90% (nominal)
Depth of discharge	25%
Charging rates	$\frac{C}{5.7}$ to $\frac{C}{4}$ amp-hrs
Third electrode output voltage at 15 psi pressure	150 mV



Table 6-11  
POWER BUDGET

<u>Item</u>	<u>Average Power/ Orbit (Watts)</u>
Proof Ball (Drag Free) Electronics	2.0
Control System Electronics	5.0
Gyro Suspension Electronics	10.0
Gyro Readout Electronics	7.2
Telescope Electronics	3.0
Gyro Instrumentation Loop Electronics (Includes Three Electronic Resolvers)	41.2
AGC Electronics	1.2
Roll Encoder	4.0
Roll Control Electronics	1.5
Control Signal Processing Electronics	0.8
Cryo Actuator	0.2
VHF Transmitter	2.0
VHF Receiver	0.5
Decoders	0.3
Memory	6.0
PCM System	2.0
Housekeeping Electronics	2.0
Valve Electronics	3.0
	<hr/> 91.9

- Shunt Regulator and Shunt Loads:

Regulating voltage	31 VDC (nominal)
Shunt load maximum power dissipation capability	340 watts
Shunt load normal power dissipation range	12 to 78 watts

- Undervoltage Switch:

Switch open voltage	24.3 $\pm$ 0.2 VDC @ 3 sec 20.0 $\pm$ 0.2 VDC @ 0.01 sec
Switch close voltage	29.8 $\pm$ 0.2 VDC



- Master Regulator:

Output voltages	+28 VDC $\pm 5\%$
	+15 VDC $\pm 2\%$
	-15 VDC $\pm 2\%$
	+5 VDC $\pm 5\%$
Maximum power capability	100 watts
Overall efficiency	80%
Output impedance	$<0.5 \Omega$ from 0 to 100 kHz

Table 6-12 lists several performance numbers for three different orbits.

Table 6-12  
ORBIT PERFORMANCE DATA

	Orbit		
	Minimum Power	Maximum Power	90° Sun Angle
Orbit Day (Minutes)	75.0	65.0	100.0
Day Power Requirements (Watt-Hours)	156.2	135.4	208.3
Night Power Requirements (Watt-Hours)	52.0	72.9	0.0
Battery Charge Requirements (Watt-Hours)	64.3	90.0	0.0
Total Required Array Output (Watt-Hours)	220.5	225.4	208.3
Total Available Array Output (Watt-Hours)	242.0	367.0	258.0
Extra Available Regulated Power (Watts)	9.7	62.7	23.8

NOTE: Assuming 100-watt load.



#### 6.3.4 Design Trade-Offs

Considerable thought was given to deciding what method of solar cell hookup should be used. Most solar arrays are made up of series-parallel connections of solar cells. However, because of the complex shadowing experienced by the SRS array, it was decided to use simple series strings with diode isolation between strings.

The problem with series-parallel connections occurs when one or more parallel cells is shadowed. The operating point on the I-V characteristic curve shifts for all the series elements in the string, with the shadowed element being driven into the negative voltage region and the normal elements moving to higher positive voltage operating points. The total voltage across the string remains essentially constant because of the other parallel strings and the batteries. Power, equal to the product of the reversed voltage and the new string current, is dissipated across the remaining unshadowed parallel elements. If the power dissipation is high, causing excessive temperatures, the operating cells may be damaged or the solder connections may melt.

This shadowing problem may be solved by placing diodes in parallel with each parallel group of solar cells. However, this solution requires a huge quantity of power diodes.

When a single cell in a series string is shadowed, the string stops producing any current, provided that the cell reverse breakdown voltage plus the battery voltage is less than the string open-circuit voltage. If the cell should break down (zener) in the reverse direction, it could dissipate an excessive amount of power. It appears that an array temperature of about  $+10^{\circ}\text{C}$  is the most critical temperature for this mode of failure. At  $10^{\circ}\text{C}$  the array open-circuit voltage is about 56 VDC and the maximum power point



voltage is about 48 VDC. Assuming a cell zener voltage of 20 volts, a battery voltage of 28 VDC, and a string current of 250 mA, the power dissipated in the cell is about 5 watts. Thermal calculations show that this amount of power dissipation will result in a 58°C temperature rise, which will not cause an excessive temperature.

The problems associated with shadowing of the solar array can probably be solved in the near future with a newly developed cell produced by Spectrolab, a Division of Textron Inc. This device, called an "Integral Diode Solar Cell", is a combined solar cell and diode fabricated on a single wafer during cell production. This process eliminates the need for any external diodes and arrays fabricated with these cells will produce more total power during shadowing than the conventional cells in either the series or series-parallel connections.

#### 6.3.5 System Reliability

The reliability allocation for the electrical power system is 0.96000. The predicted reliability for the system is 0.99176. Figure 6-27 shows a reliability diagram of the system with the calculated reliability numbers listed below each functional grouping. A brief explanation of the way the predicted reliability numbers were obtained follows:

- Solar Array
  - 94 solar cells and 1 diode per series string
  - 144 strings
  - $\lambda = 144$  failures per string per  $10^9$  hours (from previous spacecraft reliability analysis)
  - $t = 1580$  hours (takes into account shadowed portions of the array and orbit)
  - Allowing for one failure out of 144 strings:





$$R_{SA} = 1 - \frac{144!}{142! \times 2!} (\lambda t)^2$$

$$R_{SA} = 0.99966$$

- Battery

$$\lambda_{Batt} = 1400 \text{ failures per } 10^9 \text{ hours (from AVCO Failure Rates, April 1962, by Earles and Eddins)}$$

$$t = 8760 \text{ hours (1 year mission)}$$

$$R_{BA} = e^{-\lambda t}$$

$$R_{BA} = 0.98774$$

- Third Electrode Electronics

$$\lambda_{Elec} = 370 \text{ failures per } 10^9 \text{ hours (from previous spacecraft reliability analysis)}$$

$$t = 8760 \text{ hours}$$

$$R_{EL} = e^{-\lambda t}$$

$$R_{EL} = 0.99686$$

- Battery and Electronics

Only two of the three battery-electronics combinations are required.

$$R_{BE} = R_{BA} \times R_{EL}$$

$$R_{BE} = 0.98463$$

$$R_{ES} = R_{BE}^3 + 3R_{BE}^2(1-R_{BE})$$

$$R_{ES} = 0.99929$$

- Shunt Regulator

Two shunt regulators are in standby redundancy.

$$\lambda_{Shunt Reg} = 253 \text{ failures per } 10^9 \text{ hours (from previous spacecraft reliability analysis)}$$

$$t = 8760 \text{ hours}$$

$$R_{SR} = e^{-\lambda t}(1+\lambda t)$$

$$R_{SR} = 0.99999$$



- Shunt Loads

Only three out of four shunt loads are required.

$\lambda_{\text{Shunt Load}} = 2408$  failures per  $10^9$  hours (from previous spacecraft reliability analysis)

$t = 6000$  hours

$$R_{\text{SL}} = 4e^{-3\lambda t} - 3e^{-4\lambda t}$$

$$R_{\text{SL}} = 0.99894$$

- Undervoltage Switch and Bypass

$\lambda_{\text{UVS}} = 563$  failures per  $10^9$  hours (from previous spacecraft reliability analysis)

$t = 8760$  hours

$$R_{\text{UV}} = e^{-\lambda t}$$

$$R_{\text{UV}} = 0.99511$$

Reliability of UVS bypass ( $R_{\text{BP}}$ ) from previous spacecraft reliability analysis = 0.99999. The total reliability of the combined UVS and UVS bypass in standby redundancy can be considered to be:

$$R_{\text{DC}} = 0.99511$$

- Master Regulator

Two master regulators are in standby redundancy.

$\lambda_{\text{MR}} = 5683$  failures per  $10^9$  hours (from previous spacecraft reliability analysis)

$t = 8760$  hours

$$R_{\text{MR}} = e^{-\lambda t}(1 + \lambda t)$$

$$R_{\text{MR}} = 0.99876$$



• Total System Reliability

$$R_T = R_{SA} \times R_{ES} \times R_{SR} \times R_{SL} \times R_{DC} \times R_{MR}$$

$$R_T = (0.99966)(0.99929)(0.99999)(0.99894)(0.99511)(0.99876)$$

$$R_T = 0.99176$$

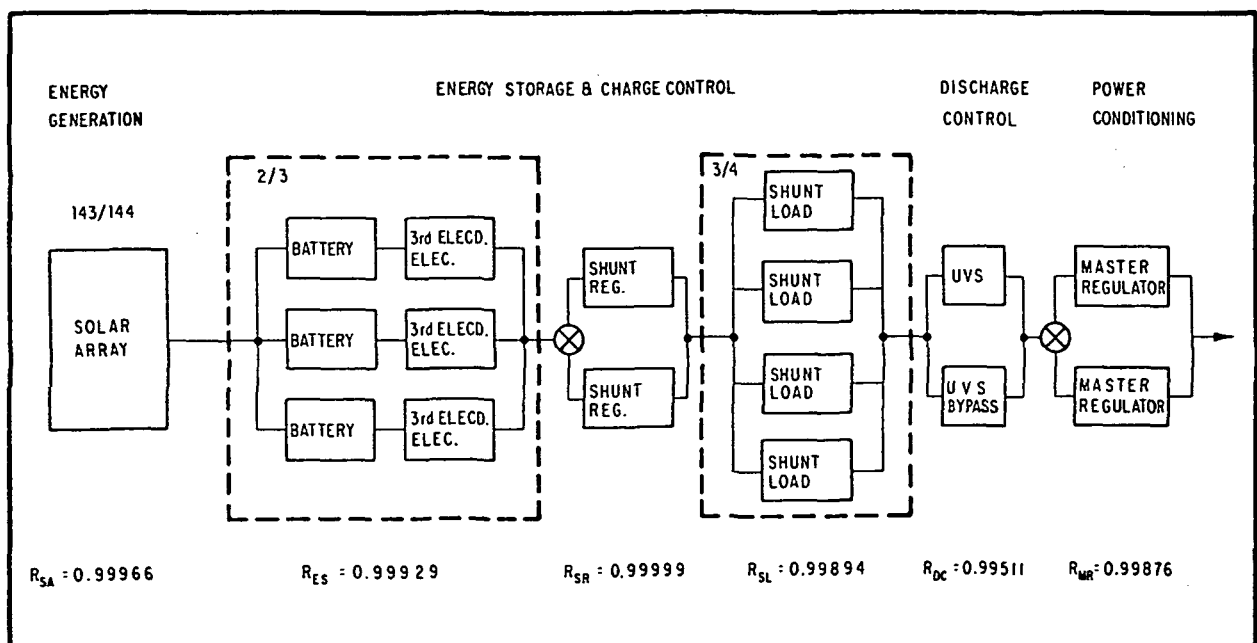


Fig. 6-27 Reliability Diagram



#### 6.4 CONTROL SYSTEM

Stanford has conducted a number of control system design studies since the inception of the gyro relativity program in 1962. Emphasis has been on translation control, pitch-yaw control, and gyroscope suspensions. The translation control analysis (including air table simulations) is well advanced because of Stanford's work on a drag-free control system for a Navy navigation satellite. However, this system is more accurate and complex than is required for the relativity satellite.

At the time the study began, Stanford's pitch-yaw control system concept had been defined as a two-stage modern control system using a state variable estimator and optimal state variable feedback to control an "inner" actuator and "outer" helium jets. The inner actuator acts directly on the quartz block assembly carrying the telescope while the jets act on the outer shell of the helium dewar. The telescope is the only source of error signals for the system, all other necessary signals being derived by the estimator.

During the study BBRC and Stanford worked jointly to refine this design as well as look for possible other, simpler systems. One simplification which is discussed is the complete elimination of the inner actuator because of the greatly increased stiffness of the inner dewar supports over what was previously considered reasonable. However, at the end of the study, the two-stage system is still the favored design.

Analog and digital computer runs were made to determine the response to disturbances with various changes of gain, damping, etc. The system that was finally arrived at satisfies all the



pitch-yaw control requirements, although it is uncomfortably close in some areas. The area of particular difficulty is in coming up with a pitch-yaw control system which is fast enough to respond to the disturbances but gentle enough to avoid excessive acceleration of the gyroscopes because of sensor and other noise.

The study also established design concepts to be used in initial acquisition, reacquisition in case of temporary loss of control, and roll control. No simulations in these areas were done and further work needs to be done to establish the detailed characteristics of the systems. Special attention needs to be given to the acquisition of the star by the pitch-yaw system when there is a sizable initial error; i.e.,  $>10$  arc-seconds.

The gyroscope suspension system is treated in this section since it is a control problem and one very closely allied with the rest of the control system. Its design is one of those that at this stage of conception barely meets its requirements. The problem here again is that the sensor noise creates accelerations which are very close to the allowable limit.

In spite of these difficulties and the fact that much additional work needs to be done, the general conclusion is that the control system can be designed and built to perform as required.

This section of the report first presents the requirements of the control system, then describes the individual control loops needed to satisfy these requirements. This is followed by the analysis establishing the disturbance forces and torques affecting the control system and finally by the analysis of the system performance in the presence of the disturbances.



#### 6.4.1 System Requirements

The following requirements apply to the entire control system, consisting of translation and pitch-yaw and roll attitude control:

##### SUBSYSTEM

Item	Requirement
Weight	9.1 Kg maximum
Power	28 watts, maximum
Volume	0.016 cubic meters, maximum
Commands	20 (maximum) required
Telemetry	20 analog channels maximum and 20 telltales maximum required.
Helium Availability	Average boil-off 135 kg/year. Normal variation, -50 to +100 percent; commandable maximum +1000 percent
Disturbances	Disturbance Budget (Table 6-15)
Acceleration of Quartz Block	Gyro acceleration budget (Table 3-3) Short Duration $<10^{-5}$ g (total impulse $<1$ m/sec during year)

##### ACQUISITION

Item	Requirement
Initial	Acquire with $1^{\circ}$ attitude error and 1 deg/sec rates.
Backup, Initial	Stop rates of $20^{\circ}/\text{sec}$ in 3 axes. Acquire from arbitrary attitudes.
During Orbit	Reacquire from arbitrary positions anytime during orbital life.



## PITCH-YAW

Item	Requirement
Accuracy	Point telescope continuously at the guide star within 0.05 arc-sec (including dither signal) during 50 percent of most orbits.  Point the outer body within 1 arc-sec of the guide star.
Sensor Noise	Telescope noise is 0.03 arc-sec in a 100 rad/sec bandwidth; gyro noise is 1.4 arc-sec in a 100 rad/sec bandwidth.
Day/Night Pointing	Switch to and reacquire from gyro control during loss of guide star in telescope.

## ROLL

Item	Requirement
Accuracy	3 arc-sec bias error and 4 arc-sec (rms) jitter with respect to desired roll angle program.
Roll Programs	Constant at commanded angle, 1 revolution in $\pi$ orbits, or 1 revolution in 5 minutes
Sensor Noise	Gyro noise is 1.4 arc-sec in a 100 rad/sec bandwidth.

## TRANSLATION

Item	Requirement
Accuracy	Keep proof mass in linear range of readout for expected disturbances
Sensor Noise	Capacitive pick-off noise is $2 \cdot 10^{-5}$ m in a 2000 rad/sec bandwidth.



#### 6.4.2 Control System Normal Operation

Four separate control systems are needed for normal operation. A pitch-yaw system is required to keep the telescope oriented at the reference star throughout the mission. A roll system is required to roll the satellite slowly about the telescope axis to reduce the effect of some sources of experiment error. A translation control system is needed to provide a drag-free environment to reduce gyroscope drift. In addition, each gyroscope has an electrical suspension system which must center the rotor for proper operation of the London Moment readout.

Normal operation of the control system is considered that portion of the mission where day-to-day relativity data is taken. It includes the operation when the reference star is in view (day) and when it is occulted (night). It does not include any acquisition or emergency modes. The discussion frequently refers to the overall system diagram in the back of this volume.

Signal Sources. All control signals for normal operation originate on the quartz block assembly. (Zone 9 of the diagram)

The reference telescope provides the error signals for pitch and yaw control during day. Starlight is passed through a beam splitter near the focal plane to generate a pitch and yaw beam. These beams fall on the knife edges of roof prisms located at the focal planes of the respective beams. Each knife edge divides the star image into two beams whose relative intensity forms the error signal. These two pairs of beams are relayed out of the cold environment for further processing.





The night control error signals for pitch and yaw are derived from the  $H_1$  gyroscope. The signal source is the same as that taken from readout loops L1 and L3 for relativity data. After being amplified, they are sent out of the cold environment for the special processing required to generate night pitch and yaw error signals.

Translational control error signals are generated by the proof ball assembly. Three mutually orthogonal pairs of capacitive pickoffs determine the relative location of the proof mass within its cavity. These signals are sent from the cold environment to be processed into the error signals for x, y, and z translation control systems.

Roll control error signals are derived from readout loops L1 and L3 of the perpendicular gyroscopes  $H_3$ . Loop L1 gives a signal proportional to the cosine of the roll angle and loop L3 gives a signal proportional to the sine of the roll angle. These signals are sent to the warm environment for processing into the roll error signal.

Actuators. Two sets of actuators are provided for normal operation.

The inner actuators, which are essentially superconducting solenoids, act directly on the quartz block to deflect it in pitch and yaw in its gimbals. The total motion is only a few arc-seconds. These actuators must keep the telescope aimed at the star within its linear range of  $\pm 0.05$  arc-seconds. The actuator shown schematically in Fig. 6-28 is in the conceptual stage and requires development and test:

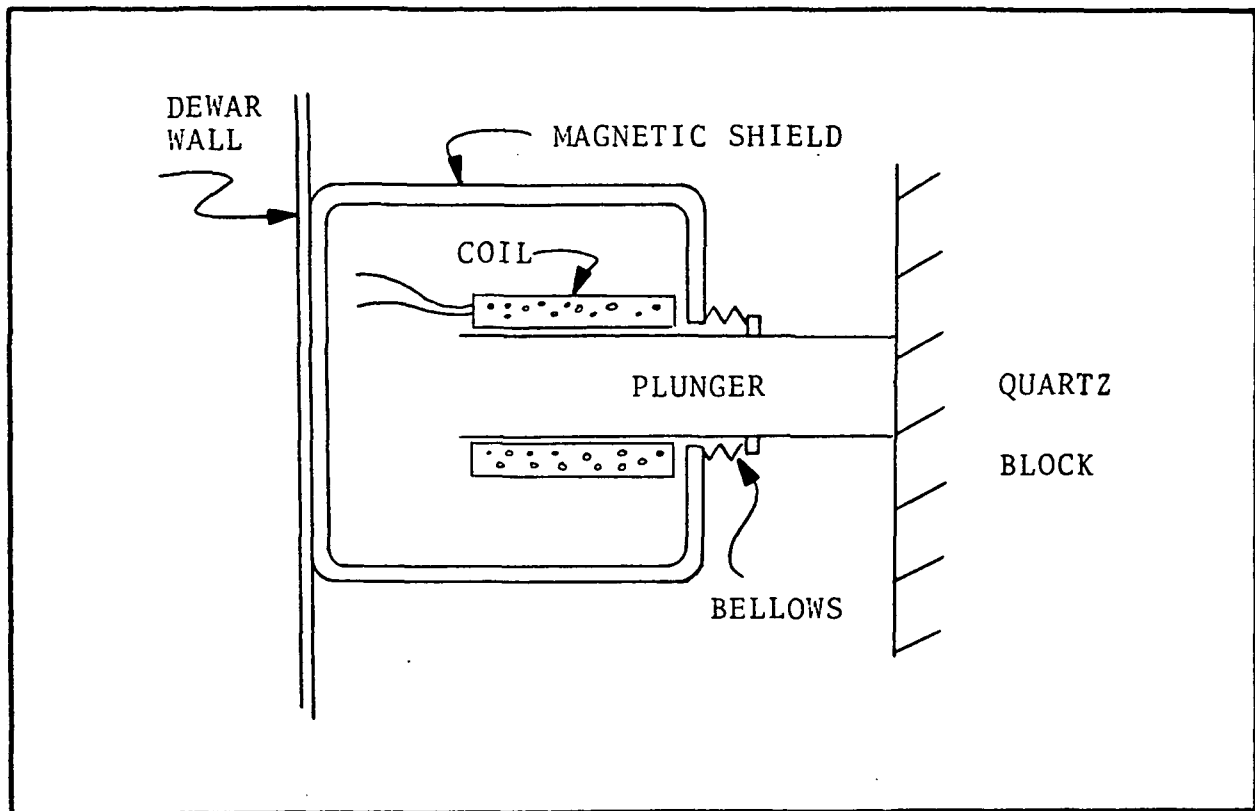


Fig. 6-28 Cryogenic Actuator, Section View

The actuator plunger is diamagnetic at cryogenic temperatures. When the magnetic field increases, the plunger is pushed out of the coil, exerting a force on the quartz block. The actuator operates at near 100 percent efficiency because the coil resistance is near zero at the operating temperature. The power used is only that required to move the plunger and quartz block. Since the actuator operates inside the dewar, magnetic shielding is important to keep fields away from the experiment.

The following development must be completed successfully during the development phase:

- Design and develop an engineering model actuator.



- Perform development testing to demonstrate scale factor, gain stability, null offsets, friction or drag, power-torque relationship, etc.
- Produce a prototype and test it to qualification environmental levels.
- Complete life and reliability analyses on the design.

The outer actuators (thrusters) consist of six pairs of proportional valves and nozzles which continually exhaust the boil-off helium in a controlled way. These thrusters are used to control the satellite body in the pitch yaw and roll rotational direction as well as in the x, y, and z translation directions. The outer satellite must be controlled to a few arc-seconds in rotation to keep the telescope within the range of its gimbals while looking at the star. The quartz block must be centered around the proof ball to an accuracy of 2.5 millimeters to keep the proof ball from touching its walls.

The helium thrusters are proportional, bidirectional units which operate as shown schematically in Fig. 6-29.

The plunger is held on flexures so that the helium flows past the flexures to the nozzles. At the relaxed position of the flexure, helium flow is equal in both directions. Flow cannot be stopped through the thruster and the helium will always be boiling off. The plunger is moved as a solenoid to control the net thruster force. Coil No. 2 is energized full time to maintain a partial solenoid field. Coils No. 1 and No. 3 are

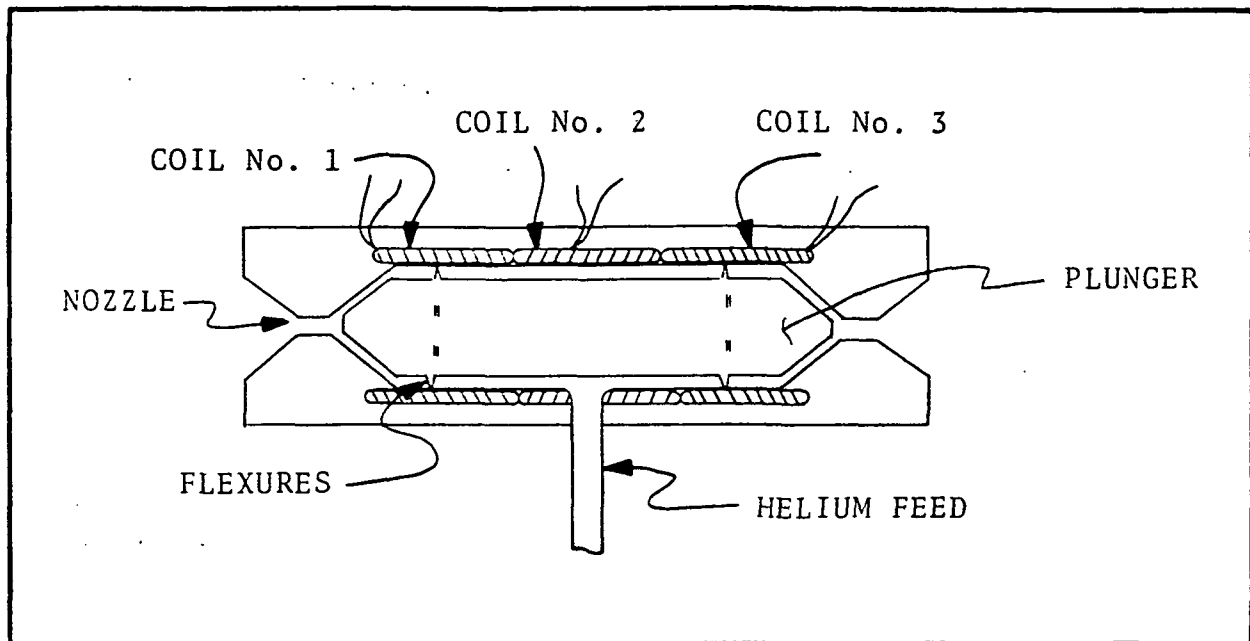


Fig. 6-29 Thruster, Cross-Section View

control coils. When the magnetic field produced by coil No. 1 exceeds that produced by No. 3, the plunger is forced to the left and helium flow increases to the right. The converse is true when field No. 3 is larger.

Thrusters for this application are not available commercially, so development and qualification are necessary during the development phase. Stanford University has completed sufficient development work in their guidance and control laboratory to demonstrate that the concept is feasible, but the following must be accomplished:

- Demonstrate hysteresis, gain stability, null offset characteristics, etc.
- Test to qualification environmental levels.



- Generate life and reliability data
- Design-in redundancy wherever possible

Normal Pitch-Yaw Controller/Estimator. The pitch-yaw controller uses a state estimator and an optimal controller to point the telescope to within 0.05 arc-second of the guide star. A simplified block diagram is shown in Fig. 6-30. The BBRC simulation studies are described in Appendix G.

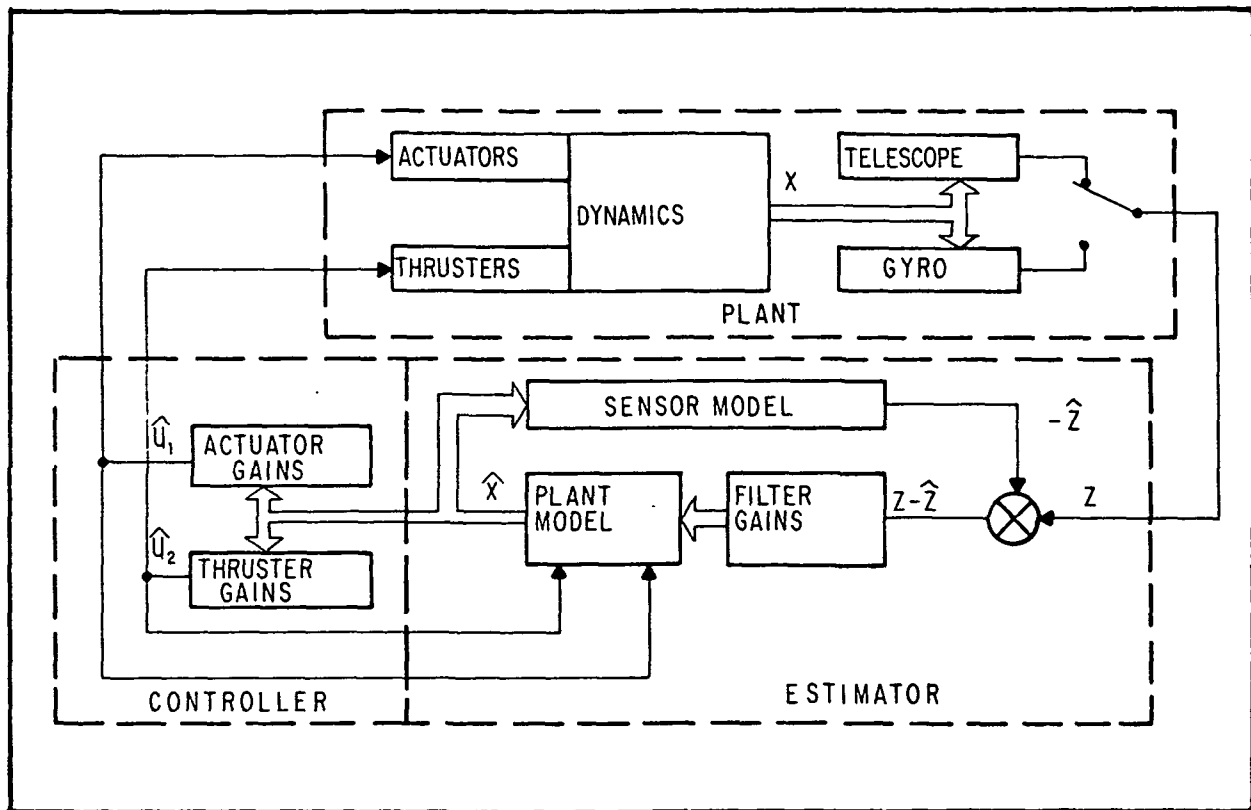


Fig. 6-30 Pitch-Yaw Pointing Controls

The plant to be controlled has two actuator systems. The quartz block is fine-pointed in pitch and yaw by cryogenic actuators located between the block and the inner support tube. The



satellite outer body attitude is controlled by helium thrusters located on the outer equipment support ring. The pointing control uses signals from the telescope when the guide star is visible and the experiment gyroscopes during star occult.

Now referring to the overall system diagram, the two pairs of split light beams in the telescope which represent the pitch and yaw error signals are processed identically from here on. We will only follow the path of the pitch signal labeled  $\psi$ .

The two halves of the split star image are focused on the same portion of the photocathode of a photomultiplier tube (PMT). A mechanical chopper, consisting of a tuning fork or rotating disc, alternately chops the two beams to produce a symmetrical square wave whose amplitude is the error magnitude and whose phase gives the error direction. This signal is examined by the star intensity electronics to develop a "star present" signal for control switching and to develop a telemetry signal to monitor star signal level. The square wave is also sent to the AGC card for AGC action and synchronous demodulation.

For relativity data processing, it is necessary that the telescope and gyroscope gains be matched very accurately. Although this is not necessary for the control system, it automatically compensates for photomultiplier sensitivity decay and will keep the gain constant to approximately 1 percent over the year. The AGC control signal is derived by introducing a small dither (0.03 arc-second) into the control loop and comparing the telescope and gyroscope output signals at the dither frequency (0.1 rad/sec). The comparison loop is described in Section 5 under Instrumentation.



The telescope signal used for pitch control is processed on the AGC card labeled  $H_1\psi$  which is identical to the card on top labeled  $H_3$  and  $H_4\psi$ . After gain adjustment, the signal is synchronously demodulated. The resulting signal is then filtered to remove the effects of chopping and to reduce the noise bandwidth. Details of this process are discussed in Section 5 (Telescope Electronics).

The telescope error signal, now in useful control form appears on bus  $\diamond B$ . Bus  $\diamond B$  can switch between this signal and an identical one derived from a redundant set of electronics. The signal noise corresponds to 0.03 arc-second with a 100 radians per second bandwidth.

The telescope error signal now reappears on the diagram in zone 5 as  $\diamond B$  where it is summed with the dither signal, a 0.1 radian per second sinusoidal of 0.03 arc-second amplitude. With the "day-night" switch in "day" and the "spin-up-normal" switch in "normal" the combined dither and error signal enters the Pitch Fine Pointing (PFP) electronics.

In the PFP electronics section, the single pitch error signal must be processed to provide drive signals for both the pitch jets and the pitch gimbal actuators. These signals must always keep the telescope pointing within its linear range of 0.05 arc-second (including the superimposed 0.03 arc-second dither displacement) and must keep the outer body of the satellite positioned in such a way that the telescope is within its gimbal travel of a few arc-seconds. Further, control forces must be restrained to limit the acceleration delivered to the gyroscopes to be less than  $10^{-8}$  g's. This requires angular acceleration of



the quartz block no greater than  $8 \cdot 10^{-7}$  radians per second<sup>2</sup>. Thus, precision and smoothness are both required. This is a challenging problem considering the noise level in the telescope signal and the high precision required.

The system concept shown here is that established by Stanford at the beginning of the study. It is a "modern" control system using a state estimator and an optimal controller to generate and process the necessary signals to drive both sets of actuators. The estimator contains an analog computer model of the entire physical system consisting of the quartz block and its flex pivot-gimbal arrangement, the dewar and outer satellite inertias, the sensor, the actuator, and the controller logic. With a sufficiently accurate model, it is possible to derive within the model what is happening in the whole satellite. In the model chosen, five signals (state variables) are derived for each axis:

1.  $\psi$ , the pitch angle between the telescope axis and the reference star.
2.  $\dot{\psi}$ , the rate of change of  $\psi$ .
3.  $\gamma$ , the angle between the telescope and the inner dewar, across the actuator.
4.  $\dot{\gamma}$ , the rate of change of  $\gamma$ .
5.  $\int \psi$ , the integral of  $\psi$ .





These five state variables are continuously updated as the system and the model respond to disturbance and control torques. Thus,  $\dot{\psi}$ ,  $\gamma$ ,  $\dot{\gamma}$  and  $\int \psi$  are generated using only the telescope error signal. These five signals are sent to the optimal controller where they are weighted according to preset gains and summed to derive the signals for the inner actuators and thrusters.

If major changes in system parameters occur, it is necessary to change the value of the gains in the controller or estimator. Such conditions occur routinely when control is switched at night to gyroscope control and in case of difficulty such as temporary failure of a thruster or actuator or when extra control gas is being used. The choice of gains is an important part of the detailed control system design.

The signal from the controller to the helium thruster is shown in the diagram by the symbol  $\langle N \rangle$ . It appears as an input to a summing amplifier in the Low Pressure Pneumatics section of the diagram in zone 2. The pitch drive signal is summed with appropriate gain with the Z translation signal to drive two pairs of thrusters. The pitch signal drives the thrusters differentially to generate torque while the translation signal drives them in parallel to generate thrust. Since it is more important to maintain attitude control than a zero-drag condition, the signals are scaled to allow the rotational signal to override the translation signal if necessary.

The signal from the controller to the gimbal actuator is shown by the symbol  $\langle 0 \rangle$ . It directly drives the cryogenic actuator to rotate the quartz block in its gimbal.



Night Pitch-Yaw Control. The input signals to the pitch-yaw controls are switched between the telescope and the gyro for day and night operation as shown in Fig. 6-31.

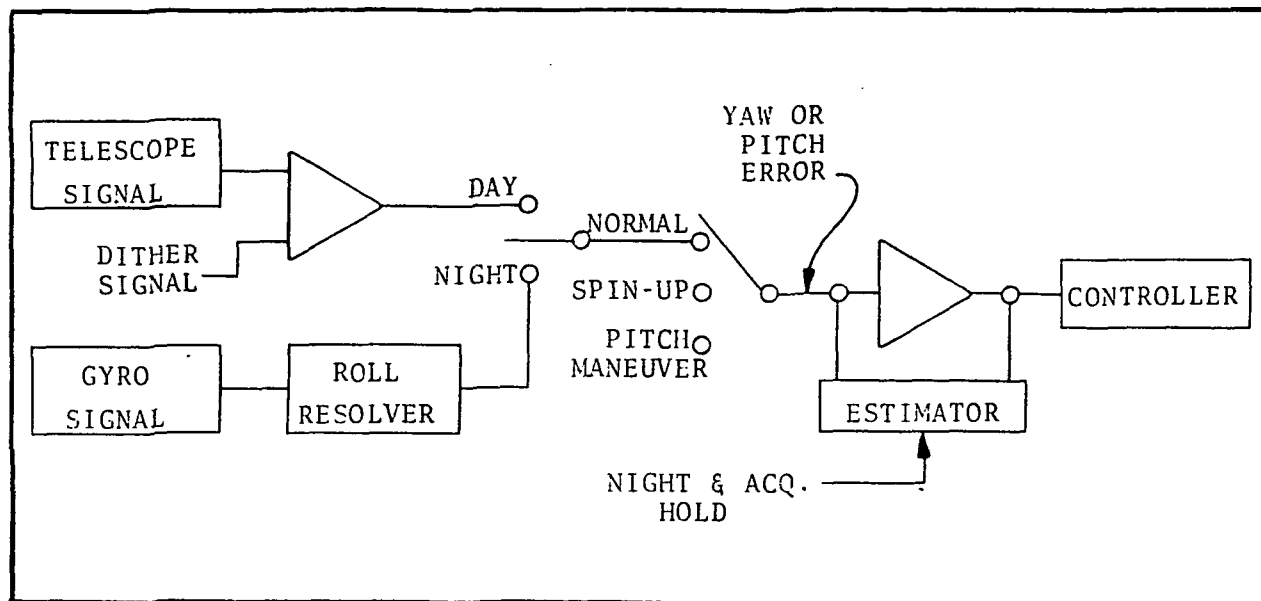


Fig. 6-31 Day-Night Operation

The gyro holds the experiment in the same attitude during the star-occulted part of the orbit that the telescope does during star presence.

Referring to the system diagram, the pitch and yaw error signals are derived from readout loops L1 and L3 of relativity gyroscope H1. Again we will follow only the  $\psi$  (pitch) signal as the yaw signal is treated identically.

When the earth occults the star, the telescope axis must be held nearly fixed inertially, so that when the star reappears next dawn, it is less than an arc-second from the telescope null.



The signal out of the readout loops cannot be used directly since the gyroscope spin axis can be as far as 30 arc-seconds away from the telescope and the telescope should be held to within  $\pm 0.5$  arc-second to have a well-damped reacquisition. However, there is a signal generated in the experiment instrumentation loop that can be processed into the error signal after compensating for the satellite roll.

The instrumentation loop is described in detail in Section 5. We will review it only briefly here.

The signal from readout loop L1 of gyroscope H1 comes to a summing amplifier on the Parallel Readout Card (zone 8 of the diagram) where it is subtracted from the telescope error signal during normal day operation. The difference signal drives a voltage-to-frequency converter which produces a frequency proportional to the magnitude of the difference signal. The frequency is counted in a 17-bit, bidirectional counter, counting up or down depending on the sense of the error signal. The accumulated count is converted to an analog voltage in the A/D converter and fed back directly to the summing amplifier under normal day operation. When the converted accumulated count signal equals the gyroscope-telescope difference signal, the voltage-to-frequency converter stops and the system is nulled. Because the telescope signal is always small ( $< 0.05$  arc-second), the converted accumulated count signal represents the gyroscope readout signal very closely. If we now freeze the counter and shut off the telescope signal, the signal appearing at  $\langle E \rangle$  represents the change in the gyroscope readout from the instant of the freeze. If the satellite were not rolling, this would be the control signal needed to hold the body fixed during the stellar night. (The absence of the star inhibits the counter by means of signal  $\langle Y \rangle$ .)



The problem is complicated by the roll of the satellite. At night, the roll must continue to take place about the telescope axis, not an offset gyroscope axis. We must now look at the signals from both the pitch and yaw readout loops. The gyroscope momentum vector remains fixed inertially while the body-fixed readout loops roll with the satellite. If we start with an arbitrary roll angle,  $\phi$ , the signals that appear on the two gyroscope readout loops are:

$$\left. \begin{array}{l} \text{For loop L1} \quad E_1 = \psi \cos \phi + \theta \sin \phi \\ \text{For loop L3} \quad E_3 = \theta \cos \phi + \psi \sin \phi \end{array} \right\} \quad a$$

where  $\psi$  and  $\theta$  represent the pitch and yaw components of the gyroscope momentum vector at  $\phi = 0$ .

At dusk, when the counters are stopped, the signals stored in them are the inertially fixed angles,  $\psi$  and  $\theta$ , corresponding to the gyroscope momentum vector angles at the arbitrary roll position of  $\phi = 0$ . These must be converted to represent body-fixed angles as the satellite rolls to provide the attitude control reference.

This is accomplished by processing the signals through a digital electronic resolver which rotates at the satellite roll rate. Each dusk occurs at a new arbitrary roll angle. The resolver always starts at zero at dusk, to remember that roll angle. The satellite rolls at a rate in synchronism with a clock, signal  $\langle K \rangle$ . This signal then drives the resolver through a counter at the satellite roll rate.



The feedback signal appearing at the pitch summing amplifier is then  $\psi \cos \phi + \theta \sin \phi$ , and that at the yaw summing amplifier is,  $\theta \cos \phi + \psi \sin \phi$ . These reference signals, when differenced with the gyroscope pitch and yaw readout signals, provide the control system error signals.

The requirements on this resolver are modest in that the maximum values of  $\psi$  or  $\theta$  are expected to be 30 arc-seconds and we only need to control to about 0.5 arc-second. Further, the expected roll angle is  $36^\circ$  for a typical 30-minute night period.

We can now continue to follow the gyro pitch error signal through the system. This signal, shown at  $\langle E \rangle$ , reappears at zone 5 of the diagram as an input to the Control Signal Processor. It passes through the "Day-Night" switch and the "Normal-Spinup" switch to the same set of Pitch Fine Pointing Electronics as the telescope signal did for day operation.

The operation here is the same as for the day operation except the estimator and controller gains must be changed. It appears that it is only necessary to change a few of the 15 controller/estimator gains. The gyroscope signals are about 50 times noisier than the telescope signals. This much noise would saturate the control system and put excessive acceleration on the gyroscopes. The system bandwidth must therefore be reduced.

Once the signal leaves the Fine Pointing Electronics, the operation is the same as for daytime.

Roll Controller. The purpose of the roll control system is to hold the satellite at a fixed angle or to roll it at a steady enough rate to allow gyroscope drift to be determined from



telemetered gyroscope readout loop data and for the drift to be distinguished from readout drifts. When not rolling, the roll orientation need only be within about  $0.5^\circ$  of that commanded. When rolling, the roll rate need only be steady to 1 percent. However, in both cases the roll orientation must be determined to 10 arc-seconds. The ground data reduction task is simplified if the roll orientation is held (or controlled while rolling) within 10 arc-seconds of the commanded value (ramp).

In the normal mode of operation, the satellite rolls with a period equal to  $\pi$  times the orbit period or about 300 minutes. The roll rate is then 72 arc seconds per second. Various acquisition maneuvers and possible data taking modes require roll to be stabilized. Establishment of an absolute roll reference will also be discussed under acquisition.

The roll controller is a conventional system which operates from an error signal developed as shown in Fig. 6-32.

The satellite roll angle is derived from readout loops L1 and L3 of gyroscope H3. These loops contain the telescope axis. The H3 gyroscope spin axis is perpendicular to the telescope axis. As the satellite rolls about the telescope axis, loop L1 generates a signal proportional to  $\cos \phi$  while loop L3 generates a signal proportional to  $\sin \phi$ . These signals are processed in the roll angle digital encoder (zone 6). This device is described in Section 5 under instrumentation. The output of the encoder is a 19-bit binary word representing the roll angle as derived from the gyroscope readout. The resolution of the encoder is 2.5 arc-seconds and represents a design problem comparable to the 17-bit conversion in the instrumentation loop.

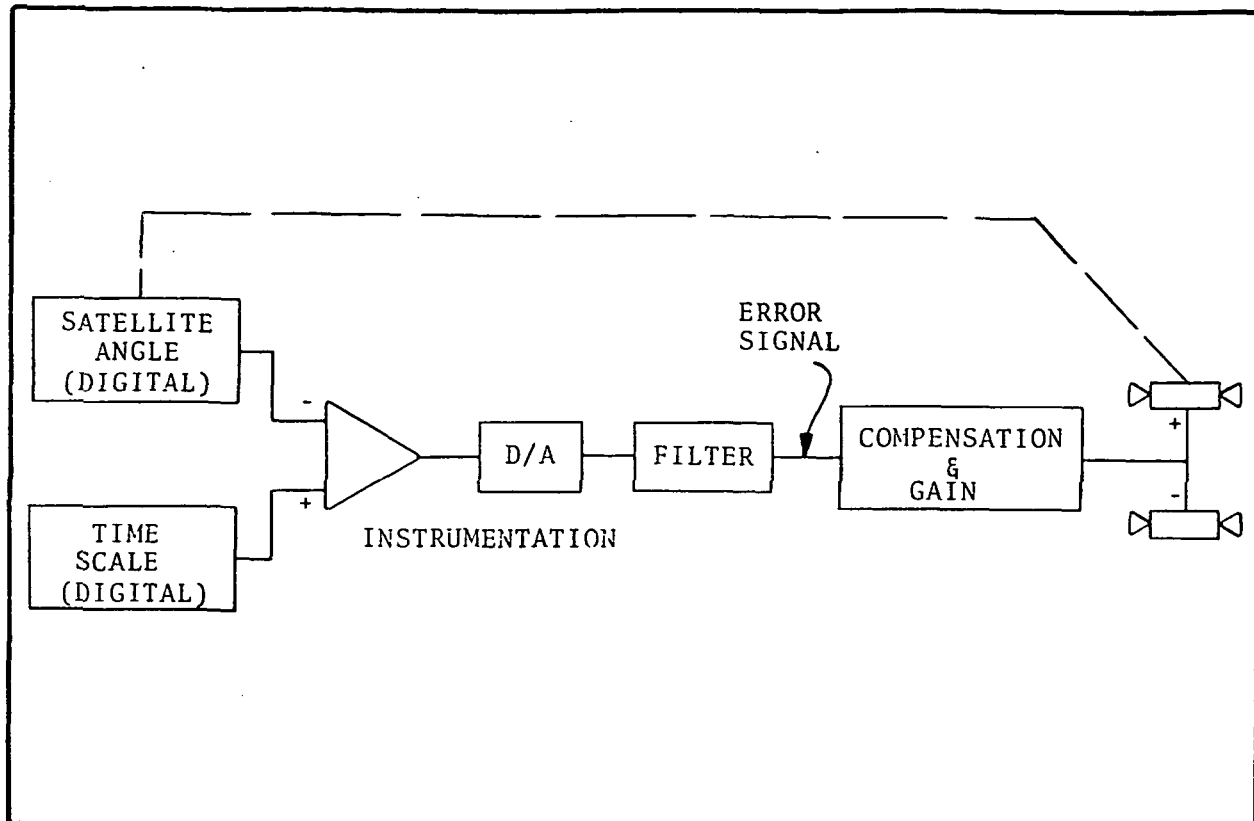


Fig. 6-32 Roll Control System

The 19-bit roll angle is in the form of a binary number which increases as the roll angle increases. This signal disappears at  $\diamond A$  and reappears again in zone 5 as an input to the roll control electronics. Here it is compared in digital form to a 19-bit binary number which is generated by counting the telemetry clock (appropriately divided down). The difference between the digital ramp representing the desired roll position of the satellite and the ramp from the roll encoder representing the roll angle, is the error signal. This digital signal is converted to an analog signal and filtered. The count rate of 29 counts per second results in an easy filter problem.



The roll control servo loop is a simple second-order linear system with lead-lag-lag compensation. The roll error angle is expected to be less than 0.5 arc-second.

#### 6.4.3 Translation Control

The translation controller keeps the satellite positioned about the proof mass so that the satellite behaves as if it were drag-free. This limits the suspension forces required to keep the gyros in the centers of their cavities. It is accomplished by monitoring the position of a proof-mass located inside a hollow cavity in the quartz block and driving the helium thrusters to make the satellite "follow" the proof-mass. This approximately matches the satellite acceleration to that of the proof-mass and the gyroscope support accelerations are reduced to the difference between the inertial accelerations of the gyroscopes and the proof-mass. These acceleration differences are made acceptably small by clustering the gyroscopes close to the proof-mass, by carefully compensating the self-gravity attraction of the gyroscopes and proof-mass by the satellite, and by limiting the forces applied to the gyroscopes and proof-mass by their capacitive position readouts.

The proof-mass is located at the nominal satellite center of mass and its acceleration is nominally the same as that of the center of mass. Under these conditions, the proof-mass and satellite nominally follow a drag-free (or geodetic) orbit. Orbit determination is simplified for such an orbit because the solar pressure and atmospheric drag perturbations (which cannot be accurately predicted) are virtually eliminated. Centering the proof-mass on the quartz block gimbal axes also limits cross-coupling between attitude and translation control.





The translation control system senses the proof-mass position along three axes. The elements of one axis of control are shown in the block diagram, Fig. 6-33.

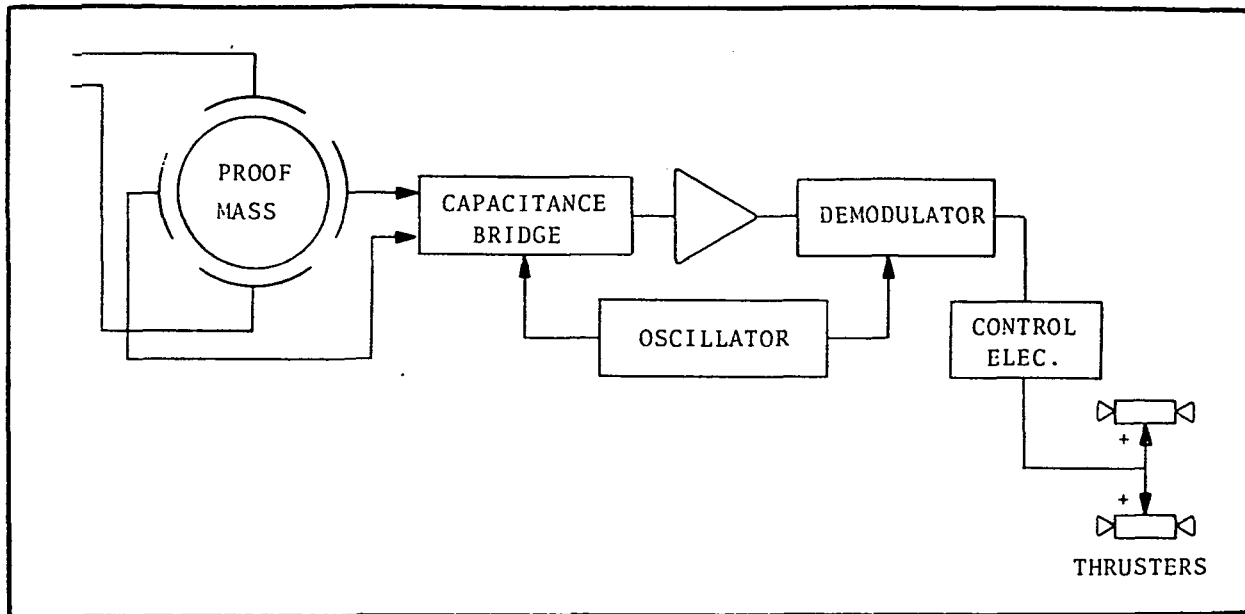


Fig. 6-33 Translation Control System

The proof-mass position is sensed by a resonant capacitance bridge. The bridge output amplitude varies with the mass position and is demodulated to create a DC signal proportional to the mass displacement. The control electronics provide gain and compensation in a conventional manner and drive the thruster. The thrusters are the same helium units used in the pointing control system. The translation and attitude control signals are summed to control both functions simultaneously.

The proof ball, zone 10 of the overall system diagram, is a relatively dense metallic sphere 1.5 cm in diameter, located in a 2 cm diameter spherical cavity. Three mutually perpendicular



sets of capacitive pickoffs, sensing in the satellite x, y and z directions, are located on the inner walls of the cavity. These pickoffs are part of three separate resonant capacitive bridges driven in synchronism by a three-phase oscillator at a frequency of about 1 MHz.

The signals from the pickoffs go to the Proof Mass Readout and Control Electronics, zone 10 of the diagram. The output of each bridge is amplified and synchronously demodulated to provide the error signals for x, y and z control.

The translation controller is a conventional second-order linear system with lead-lag-lag compensation. The resonant frequency of the control system can be as low as 0.05 radian/second since the disturbance forces are relatively weak. The sensor noise is negligible at this bandwidth. Thus, the controller has relatively modest requirements.

The output signals of the controller are at  $\langle k \rangle$ ,  $\langle l \rangle$ , and  $\langle m \rangle$ . They reappear at zone 2 of the diagram, where they are summed with the pitch, yaw and roll signals to drive the thrusters.

#### 6.4.4 Acquisition

There are three systems that acquire the guide star, establish proper roll rate and position, initiate drag-free control, and prepare for data-taking. The first uses the attitude of the launch vehicle as the initial condition. The second is a backup mode for use if an anomaly or failure prevents proper function of the primary system. The third is for reacquisition during normal operation if the star is lost.



Signal Sources. Additional signal sources are needed for acquisition and acquisition backup.

In the primary initial acquisition system, the Delta vehicle guidance package orients the second stage so that the reference star (Rigel) is in the field of view of a wide angle ( $8^\circ$ ) auxiliary star tracker mounted on the satellite and aligned to the experiment telescope axis. It does this without reference to the star tracker or any of the satellite systems.

The auxiliary star tracker has an accuracy of 0.5 arc-minute and is aligned with the reference telescope to an accuracy of 5 arc-minutes. It is a scanned-raster tracker with requirements identical to present-day space-qualified trackers. It provides pitch and yaw error signals to allow transfer of the star from its control to the reference telescope control.

Three non-floated rate-integrating gyroscopes equivalent to the Northrop GI-GG are required. A drift rate of about 1 hour can be achieved with such a gyroscope. The purpose of these gyroscopes is to provide rate damping during acquisition maneuvers and modest position holding reference when the celestial sources are hidden by the earth.

A sun sensor with a field of view as shown in Fig. 6-34 is required as part of the backup acquisition system. The digital angular output in pitch is incremented in  $0.5^\circ$  steps and covers  $180^\circ$ . The roll output is linear over  $2^\circ$ . The ground-programmable electronic package associated with this detector allows pointing to any of the digital pitch increments.

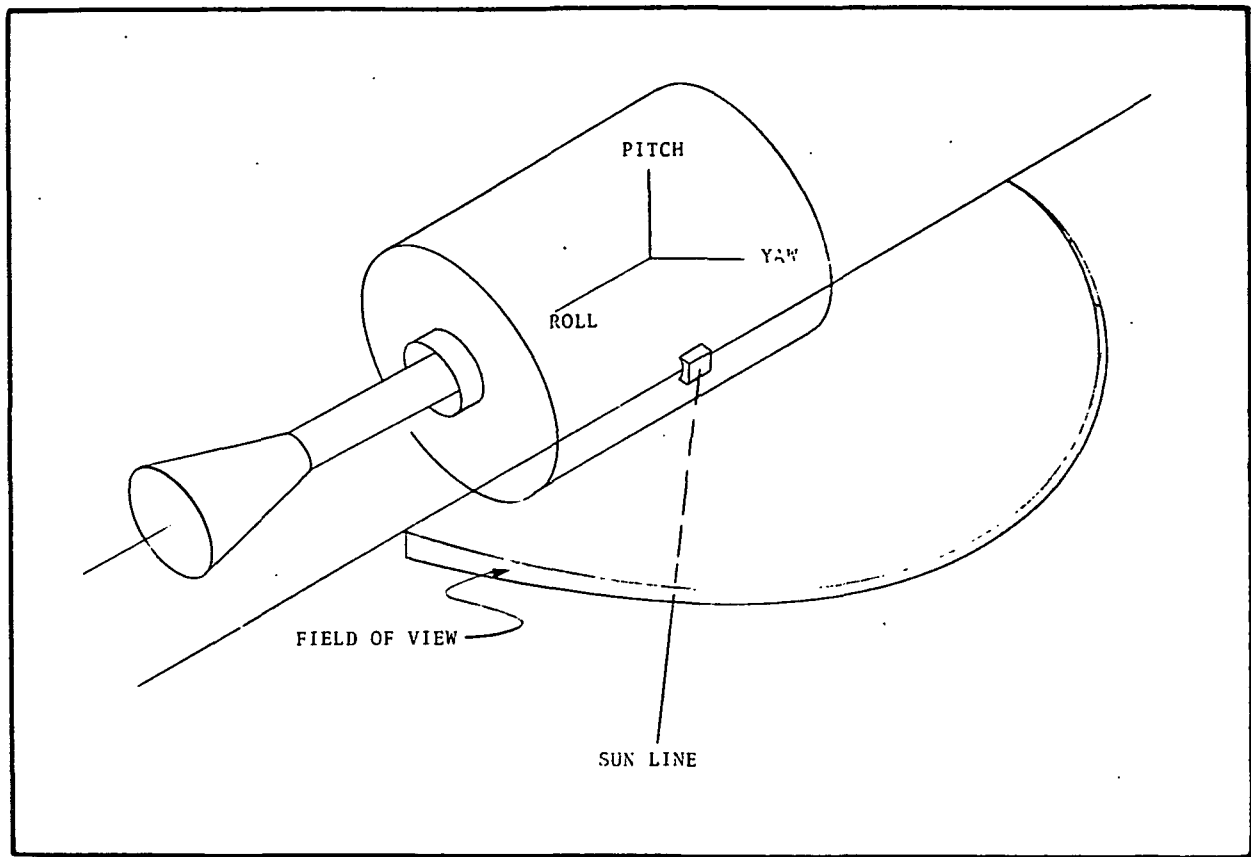


Fig. 6-34 Sun Sensor Position and Field of View

The readout loops of the perpendicular gyroscopes H3 and H4 are used for pitch, yaw and roll references during various acquisition maneuvers.

Actuators. An auxiliary set of 6 or 12 thrusters is required to back up attitude control by the helium thrusters with higher thrust levels for acquisition and during spin-up of the experiment gyroscopes. The system consists of nitrogen, regulators, tanks, manifold, solenoids, and thrusters for three-axis attitude control. Nitrogen storage for this system will be in two toroidal tanks placed in the girth ring channel. The pneumatic components will be installed in the electronic boxes.



## 6.4.4.1 Normal Initial Acquisition.

Table 6-13 gives the normal initial acquisition steps.

Table 6-13  
INITIAL ACQUISITION STEPS

<u>TIME FROM LIFT-OFF</u>	<u>STEP</u>
	Pre-separation Functions
1 hr. 45 min.	Separation
1 hr. 55 min.	Guide star acquisition by star tracker
3 1/2 hrs.	Guide star acquisition by telescope
7 1/2 hrs.	Roll star acquisition by telescope
12 1/2 hrs.	Guide star real position acquisition by telescope
16 hrs.	Parallel gyro spin-up
17 3/4 hrs.	Zero drag initiation
17 3/4 hrs.	Normal pointing operation

These steps are discussed in detail in the following paragraphs, referring to the overall system diagram.

Pre-Separation Functions. The Delta vehicle positions the second stage with the satellite attached, with the roll axis pointed within  $0.5^\circ$  of the guide star and the pitch axes within  $0.5^\circ$  of the orbit normal. The Delta pointing accuracy is  $0.6^\circ$  at lift-off, but  $0.3^\circ$  can be achieved. The satellite must be pointed at



the guide star for approximately one hour after orbit injection. The Delta operating time must be increased by about one half hour by adding battery capacity and nitrogen supply, and increasing the computer cooling capability. During two hours the Delta gyroscopes can drift by as much as  $0.5^\circ$ . The experiment perpendicular gyroscopes can be spun up so the spin axes are pointed with an accuracy of  $0.17^\circ$ . The RSS of the initial Delta error and gyroscope drift and of the experiment gyroscopes spin-up accuracy yields a total pointing accuracy for the experiment gyroscope spin axis of  $0.6^\circ$ . This is used as the allowed error for proper acquisition.

While the guide star is within the field of view of the auxiliary star tracker, the satellite must perform a number of functions prior to separation from the Delta second stage:

- Unseal the dewar. Before launch the dewar was filled and sealed. It is now unsealed and connected to the low pressure pneumatic system.
- The solar arrays are moved to their orbit positions.
- The dewar launch supports are retracted.
- System checkout: During the Tananarive pass (after final burn) the following will be checked: Delta pointing performance with reference to the auxiliary tracker, along with the condition of expendables, gyro suspension voltages, status of dewar supports, and solar array positions. If these are incorrect, commands will be sent to either correct the problem or inhibit perpendicular gyro spin-up.



- Spin-up the perpendicular gyroscopes. The two gyroscopes are spun up simultaneously to speeds of 200-250 rps. This will take approximately 40 minutes.

Separation. The satellite is now ready to be separated. Pitch and yaw control signal will be obtained from the 6 loops of the perpendicular gyroscopes. These signals, originating on the quartz block assembly (zone 9 of the overall system diagram) are directed to the acquisition electronics (zone 5). The "Acquisition Spin-up" switches are in "Acquisition" and the offset generator is turned off. These signals pass directly through the roll resolver unmodified since the roll resolver is at its zero shaft angle condition. The signals then go to the pitch and yaw coarse control electronics. Although shown as a separate block the coarse controller may be the same as the stellar night portion of the fine pointing electronics. Additional band-limiting may be desirable to avoid saturation for large errors. The coarse system probably should be capable of using the telescope position error signal while rate damping is derived from the gyroscope signals. During acquisition, the nitrogen thrusters are driven by the electronics output at symbols  $\diamond U$  and  $\diamond V$ .

The roll error signal comes from the normal roll output of the H3 gyroscope, as in normal operation. The roll angle is encoded in the roll angle encoder (zone 6) and sent to the roll control electronics (zone 5) as signal  $\diamond A$ . Since the roll angle should be held fixed, the roll command counter is set to zero. From this point on, the system is similar to the pitch and yaw coarse control using the nitrogen system.



Separation rates of  $<1^\circ/\text{second}$  are specified to allow acquisition in a small fraction of an orbit.

Coarse Acquisition By Tracker. Using the nitrogen system and the error signals described above, the satellite rates are stopped and the gyroscope readout loops are brought to null by the control system. The reference star is now in the field of view of the auxiliary star tracker. Control is now transferred to the star tracker by changing the acquisition switch position (zone 4) to the star tracker position. The star tracker then drives the pitch and yaw control electronics to null its output.

Guide Star Acquisition. Once the star tracker is nulled, a scan pattern is started by ground command to move the satellite in a raster pattern about the guide star until the star appears in the field of view of the experiment telescope as determined by a star-present signal. The misalignment of the telescope and the star tracker is not expected to be greater than  $\pm 5$  arc-minutes. Using a 10 arc-minute square uncertainty, a 3 arc-minute telescope field of view, a 1 arc-minute scan pattern overlap (2 arc-minute line spacing) and a scan rate of 8 arc-seconds per second, a complete search will take 6.25 minutes. When the star is in the field of view of the telescope, control is transferred to it by switching to the "normal" mode for pitch and yaw. When this control mode has settled down, the pitch loop of H3 (loop L2) and the yaw loop of H4 (loop L2) are read to determine the initial spin axis orientation of these two gyroscopes in these directions.

Roll Reference Star Acquisition. In order to establish a roll reference, the satellite is pitched to a new reference star which is approximately in the orbit plane. Polaris would be a





good candidate. The pitch maneuver is accomplished using gyroscope control and the coarse control electronic and gas systems. During the pitch maneuver, yaw control is maintained using an error signal from loop L2 of gyroscope H4. Roll control is obtained using the error signal from loop L1 of gyroscope H4,  $\diamond$ .

In the pitch axis readout, loops L1 and L2 of gyroscope H3 are used to generate  $\sin \delta$  and  $\cos \delta$ .  $\delta$  is the angle in declination of the satellite to the guide star. The pitch programmer (zone 4) generates  $\lambda$ , the desired pitch angle, and feeds it to the resolver as the "shaft input." This input is a 10-bit word which divides the approximately  $90^\circ$  swing into 1028 steps of about 5 arc-minutes each. The resolver output is  $\sin (\delta - \lambda)$ . The control system drives this error to null and in so doing makes the satellite track the pitch program. When the pitch-up program ends, the roll reference star is in the field of view of the auxiliary star tracker. The acquisition of this star by the reference telescope takes place in the same manner as for the regular guide star.

Once the reference telescope is locked on the roll reference star, H3 gyroscope loop L3 is in a position to be sensitive only to the roll angle (in inertial coordinates) of the H3 gyroscope. Thus, its angle with respect to the roll reference star can be measured to an accuracy of about 1 arc-second. Loop L2 of the H4 gyroscope provides similar information about the roll angle of gyroscope H4.

After the measurements are made, the system reverts to gyroscope control and the pitch programmer generates a reverse pitch program to return the satellite to orientation on the guide star, Rigel, and operating in the normal acquisition mode.



Guide Star True Position Acquisition. In order to minimize the dynamic range required in the relativity readout, it is necessary to have the parallel gyroscope spin axes aligned to the true position of the guide star as opposed to the aberrated position. To accomplish this, the satellite is biased off the apparent star position during the time these gyroscopes are spun up. This offset is entered in the offset generator (zone 5) by ground command based on calculation of the aberration at that time of year, the position in the orbit, and the roll misalignments of the perpendicular gyroscopes. This offset is then added to the pitch and yaw signals generated by the L2 loops of gyroscopes H3 and H4.

Parallel Gyroscope Spin-up. The parallel gyroscopes are spun up while the satellite is pointed at the true star position. To average spin-up cross-torques, the satellite is rotated about the true star line at a rate of about 0.2 rpm during spin-up. Roll control is the same as normal operation roll control, except the rate is increased. By ground command, the roll rate counter changes the clock division rate to give a roll rate of 0.2 rpm. The roll angle encoder operates normally to provide the roll reference signal.

Pitch and yaw control signals come from the offset pitch and yaw signals mentioned above. These are inertial signals and must be resolved into body coordination as the satellite rolls. This occurs in resolver No. 2 (zone 5). These resolved signals are fed to the Fine Pointing Control Electronics, where they are processed normally.



When the gyroscopes are at operating speed, the roll rate is reduced to the mission roll rate. The parallel gyroscopes now become the primary reference for night pitch and yaw control and to develop relativity data.

While the two gyroscopes are being spun up, 0.25 kg of helium is used during 40 minutes. The satellite will exhaust the helium in a balanced manner, so that minimum unbalance torque will result. If the exhaust ports are unbalanced by 10 percent,  $7 \times 10^{-3}$  N-m of disturbance torque results. This is approximately 10 times the control torque of the normal helium jets, so the nitrogen thruster system or an accelerated helium boil-off must be used for control during gyroscope spin-up.

Zero Drag Initiation. With the experiment gyroscopes spinning, the satellite can be commanded to zero drag operation. Prior to this time, all available helium is used for attitude control.

Normal Pointing Operation. The aberrated guide star is reacquired, a roll rate of  $1/\pi$  revolution per orbit is established, and the experiment is ready to measure relativity drift.

#### 6.4.4.2 Backup Acquisition

In case the Delta is unable to point the satellite while the perpendicular gyroscopes are spun-up, a backup system is available. The assumed condition is a Delta control system failure resulting in a usable orbit, but with an arbitrary attitude and with attitude rates up to  $20^\circ$  per second.

The backup acquisition sequence is shown in Table 6-14.



Table 6-14  
BACKUP ACQUISITION STEPS

<u>COMPLETION TIME</u>	<u>STEP</u>
1 hr. 30 min.	Failure recognition
1 hr. 45 min.	Orbit setup
2 hrs.	Arrest rates
2 hrs. 30 min.	Sun sensor acquisition
5 hrs.	Star acquisition
7 hrs.	Roll-offset using auxiliary gyroscope
7 hrs.	Spin up perpendicular gyroscope
10 hrs.	Continue Normal Acquisition

The backup system operates as follows:

Failure Recognition. Failure or out-of-specification operation must be detected prior to spinning up the perpendicular gyros, for a fully successful mission. When a failure is detected, the automatic sequence is inhibited by command, probably at Tananarive. The control electronics are switched to the back-up mode.

Orbit Setup. The dewar is uncapped, solar arrays deployed, dewar launch supports retracted, and the backup sequence initiated by command.



Separation. Separation is allowed to occur at the programmed time. Further action then comes from the ground controllers.

Arrest Rates. Using signals from the rate gyroscopes (zone 6) placed to sense rates about the three major axes, the satellite rates are reduced to less than 0.1 degree per second, using the coarse pointing electronics and the high pressure gas system.

Sun Sensor Acquisition. The sun sensor with a field-of-view as shown in Fig. 6-34 is located on the satellite. An acquisition roll rate (0.2 rpm) is started and held until the sun is in the sensor field-of-view. The satellite is oriented to the sun in roll and an offset pitch angle and held there.

Star Acquisition. While controlling the satellite to the sun in pitch and roll, the yaw jets are fired for a predetermined time. Since the pitch and roll jets will be activated by the control system to maintain sun alignment, a rotation about the sun line will take place. The offset pitch angle of the sun sensor is set by ground command so that the angle between the sun sensor null axis and the star tracker is the same as the angle between the sun and the star. In a full revolution of the satellite about the sun line, the star and star tracker must become aligned. Star acquisition from the tracker to the telescope is as described previously.

Correct Roll Attitude. After fine acquisition of the guide star, the satellite roll attitude is the angle between the North polar axis and the line containing the sun and guide star. A roll offset angle based on this angle is calculated on the ground and loaded into the offset timer (zone 5). The timer torques the roll gyro through that angle to position the satellite to the zero roll angle position.



Perpendicular Gyro Spin-up. After the roll offset timer times out, the satellite reverts to the attitude-hold mode and the perpendicular gyros are spun up.

Continue Normal Acquisition. From this point the acquisition is the same as in the primary method.

#### 6.4.4.3 Reacquisition

During normal pointing, the guide star can be lost from the telescope field-of-view because of meteorite hits or a failure in a control system. Under these conditions, we can assume that enough experiment gyroscopes are properly operating to use their outputs in reorienting the satellite and that control system failures have been isolated and replaced by redundant controls. Reacquisition is performed using equipment already available in the primary system. The reacquisition procedure is:

- Arrest rates: The three rates gyroscopes are turned on and the rates reduced to zero.
- Reacquisition: Using the experiment gyroscopes as position sensors and the rate gyroscopes for rate control, the satellite reacquires the guide star.

#### 6.4.5 Control System Redundancy

The required reliability of the control system is 0.93. Since no severe design problems are known, this can be attained by sufficient redundancy.



Acquisition System Redundancy: The system for initial acquisition is completely redundant, as described above.

For reacquisition during the mission, the experiment gyroscopes are used as position sensors. Redundancy can be provided by switching to different gyroscope readout loops if a gyroscope fails. The only redundancy hardware required is the switching equipment.

Pitch and Yaw Pointing Control Electronics. Since the mission data depends upon the pointing capability, the control electronics are fully redundant in both pitch and yaw. The determination of the level at which the switching takes place should be determined in the detail design.

#### 6.4.6 Disturbance Forces and Torques

The attitude control system must point the telescope and the outer satellite body to the required accuracies in spite of external and interbody disturbance torques. The translation control system must prevent external forces from accelerating the quartz block to levels that exceed  $10^{-9}$  g's. The disturbance forces and torques that the control system must be designed to handle are estimated here.

In Section 6.4.6.1 the external forces and torques that act on the outer satellite are estimated. In making these estimates, it is assumed that the satellite is a single, rigid body. Slowly varying external forces and torques can only be reacted by the expenditure of helium control gas. Estimates are combined in a worst case manner in Table 6-15 to arrive at a pessimistic total disturbance estimate for normal operation.



Table 6-15  
OUTER SATELLITE PEAK DISTURBANCE (GAS) BUDGET  
(Normal Operation)

<u>ITEM</u>	<u>CRITICAL PARAMETER VALUES</u>	<u>FORCE (NEWTONS)</u>	<u>TORQUE (N-m)</u>
Solar Pressure	$A = 5\text{m}^2, \ell = 0.3\text{m}$	$3 \cdot 10^{-5}$	$10^{-5}$
Atmospheric Drag	$A = 5\text{m}^2, \ell = 0.3\text{m}$	$3 \cdot 10^{-5*}$	$10^{-5*}$
Magnetic Interaction	$D = 500 \cdot \text{pole} - \text{cm}^3$	----	$2 \cdot 10^{-5}$
Gravity Gradient	$\Delta I = 15 \text{ kg-m}^2$	----	$2 \cdot 10^{-5}$
Static Roll Imbalance	$\omega_R = 3.5 \cdot 10^{-4} \text{ rad/sec}$ $U_S = 6 \text{ kg-m}$	$7 \cdot 10^{-7}$	----
Dynamic Roll Imbalance	$\omega_R = 3.5 \cdot 10^{-4} \text{ rad/sec}$ $U_D = 0.4 \text{ kg-m}^2$	----	$5 \cdot 10^{-8}$
Slewing While Rolling	$\dot{\theta} = 0.1 \text{ arc sec/sec}$ $\omega_R = 3 \cdot 10^{-4}$	----	$5 \cdot 10^{-8}$
Probable Worst Case Sum	Per axis during normal operation	$5 \cdot 10^{-5}$	$5 \cdot 10^{-5}$
Control Gas Available (per axis)	$\dot{m} = 135 \text{ kg/year}^{**}$ $I_{sp} = 100 \text{ sec}$	$5 \cdot 10^{-4}$	$5 \cdot 10^{-4}$

\* Air drag averages about 1/30 this large so its total impulse is small.

\*\* About 1/2 kg of helium is required for spinning up four gyros and about 2 kg will be lost during the 3-hour final built-in hold and the launch sequence. Also, system noise and cross-coupling between axes cause about a 10 percent reduction in linear range.





However, in a sense, the resulting budget is optimistic, since relatively high frequency disturbances, thruster imperfections and interbody disturbances have been ignored.

The system performance in the presence of high frequency disturbances and sensor noise is discussed in Section 6.4.7. External disturbances during acquisition and gyro spin-up are treated in Section 6.4.6.3. Thruster imperfections are discussed in Section 6.4.6.3. Interbody disturbances are discussed in Section 6.4.6.5 where it is explained that these disturbances are generally smaller than the external disturbances.

#### 6.4.6.1 Outer Satellite Disturbances (Normal Operation)

Peak disturbance force and torque estimates for the outer satellite are summarized in Table 6-15. For normal operation, the estimates include the peak values of the fundamental frequency (1 or 2 cycles per orbit) of the cyclical disturbance components. Peak values are of interest because the satellite has no ability to store the momentum induced by low-frequency disturbances. The satellite control gas capability must continuously exceed the instantaneous disturbance forces and torques to prevent temporary loss of control.

Solar Radiation Pressure Force. The solar photon pressure on a flat mirror aimed at the sun is just less than  $10^{-5}$  Newtons per square meter when the sun is closest to earth\*. The pressure is about half as large if the plate is thin and black, and about two-thirds as large for a shiny cylinder with its axis perpendicular to the sun line. We will use  $P_s = 7 \cdot 10^{-6} \text{ N/m}^2$

---

\* NASA-CR-831



for our preliminary satellite estimate. The preliminary configuration has a projected area of less than  $5 \text{ m}^2$ . The resulting "solar pressure" force is about

$$F_s = 3 \cdot 10^{-5} \text{ N}$$

This estimate is good to about  $\pm 50$  percent. When the satellite is in sunlight, the force will change about  $\pm 30$  percent due to changes in area projected at the sun (especially those caused by rolling) and by changes in the distance to the sun. The force-impulse per orbit will vary by about  $\pm 50$  percent since the earth will shadow parts of the orbit during two seasons of the year. The solar pressure acceleration is largely secular (cumulative from orbit to orbit) and, in absence of drag-free control, would accelerate the satellite an average of something less than

$$a_s = \frac{3 \cdot 10^{-5} \text{ Newtons-g}}{(600 \text{ kg}) \cdot (10 \text{ m/sec}^2)} = 5 \cdot 10^{-9} \text{ g}$$

This acceleration is 5 times larger than is acceptable to the gyroscopes. However, since there is some pessimism in the estimate, solar pressure alone barely dictates the use of drag-free control.

Atmospheric Drag Force. The air drag pressure is far more variable and unpredictable than is solar pressure. Density variations are caused by variations in solar activity and are catalogued against exospheric temperature (see Fig. 7-1). Over many years the exospheric temperature has been observed to



fluctuate between about 600 and 2100°K. Near a solar maximum, the temperature should average about 1000°K with several peak excursions during a year to near 2000°K for several successive orbits\*. The corresponding range of air density is from  $2 \cdot 10^{-14}$  to  $8 \cdot 10^{-13}$  kg/m<sup>3</sup> at 740 km and  $5 \cdot 10^{-15}$  to  $2 \cdot 10^{-13}$  kg/m<sup>3</sup> at 925 km. We plan to constrain the orbit perigee altitude so that the peak air pressure seldom exceeds the solar pressure.

The air drag pressure is given by

$$P_A = 1/2 C_D \rho V^2$$

where  $C_D \approx 2.4$  is a drag coefficient,  $\rho$  is air density and  $V = 7.3 \cdot 10^3$  meters per second is the satellite orbital velocity. To find the density that will give an air drag pressure equal to solar pressure, we equate

$$P_A = (1.2)(\rho)(5.4)(10^7) = P_s = 7 \cdot 10^{-6}$$

This gives  $\rho = 1.1 \cdot 10^{-13}$  kg/m<sup>3</sup>. This density corresponds to a 2-sigma peak density at just under 925 km altitude.

The density (and air drag pressure) will change about a factor of 1/2 to 2 with  $\pm 90$  km changes in altitude. Orbit injection errors and orbit distortion by the earth's equatorial bulge must be accommodated. Even for an orbit that is circular within  $\pm 10$  km, the density can vary by a factor of 2 to 5

---

\* U.S. Standard Atmospheric Supplements, 1966. Note - we are actually interested in peak density excursions with durations as short as a few minutes. Little data is currently available on such excursions although some in situ measurements have been made and more are planned in the near future.



because of an atmospheric bulge created by "local" solar heating. Thus, although the air drag acceleration rotates once per orbit, the acceleration has a secular component that is  $1/5$  to  $1/2$  the peak value.

The average air density over the year should be a factor of 20 to 50 less than the peak. The average air drag force should be around  $10^{-6}$  Newtons which continually decelerates a 600 kg satellite just under  $2 \cdot 10^{-10} g$ . Over a year the accumulated velocity loss should be about

$$\Delta V = (2 \cdot 10^{-9} \text{ m/sec}^2) (3 \cdot 10^7 \text{ sec}) \approx 0.06 \text{ m/sec}$$

This shows there need be no concern about orbit decay or frequent redetermination of orbit period or semi-major axis even without drag-free control (solar pressure perturbations would be more important but they mainly affect the orbit's shape and orientation).

Static Mass Imbalance Forces. If the satellite center of mass is  $r = 1$  cm off the intended roll axis (that is, the axis through the center of the drag-free proof-ball), and if we roll at a rate  $\omega_R$  then the control system must supply the centripetal force required to make the satellite center of mass "orbit the proof-ball".\* This force is

$$F_{su} = M r \omega_R^2$$

For the normal roll rate of  $3.5 \cdot 10^{-4}$  radians per second and a 1 cm center of mass offset, we have  $F_{su} = 7 \cdot 10^{-7} \text{ N}$ .

---

\* If necessary, this force can be reduced by estimating the imbalance and electrically offsetting the proof mass null or by in-orbit rebalancing of the satellite.



Available Translation Control Force. If 135 kg of helium is boiled-off during a year, and the gas is allotted equally among the three translation and three attitude axes, then the "average" control force capacity per axis is

$$F_C = \left(\frac{1}{6}\right)(135 \text{ kg})(1000 \text{ m/sec})\left(\frac{1}{3 \cdot 10^7 \text{ sec}}\right)(0.7) = 5 \cdot 10^{-4} \text{ N}$$

This assumes a specific impulse of 100 seconds (initial thruster test results at Stanford suggest that a 20 to 30 percent higher specific impulse may be feasible). A factor of 0.7 reduction is used to account for the fact that the control jets cannot divert all the gas in the desired direction, there is noise in the control signals, and there is cross coupling between axes. A discussion of these effects is given in Section 6.4.6.2. The average control force is 15 times larger than the expected solar pressure force and about 10 times the expected 2-sigma peak sum of solar and air pressure forces.

Solar Pressure Torque. The peak solar pressure torque should be no larger than

$$\begin{aligned} M_S &= F_S \ell = (3)(10^{-5})(0.3) \\ &\approx 10^{-5} \text{ N-m (100 dyne-cm)} \end{aligned}$$

where  $\ell = 0.3 \text{ m}$  is the expected maximum offset between the center of mass and center of pressure.



If the solar paddles were canted in the same sense (to give a "windmill" roll axis torque), the windmill torque would be

$$M_B^R = P_s A \sin \theta \cos \theta L$$

where  $P_s$  is the solar pressure for a surface perpendicular to the sunline,  $A$  is the area of four solar paddles projected at the sun,  $\theta$  is the paddle cant angle to the satellite roll axis, and  $L$  is the paddle lever arm about satellite center of mass. Maximum torque occurs for  $\theta = 45^\circ$ . For  $P_s = 5 \cdot 10^{-6} \text{ N/m}^2$  (the paddles are rather thin and black),  $A = 1.5 \text{ m}^2$ ,  $L = 2\text{m}$ , and  $\theta = 45^\circ$ , we have

$$M_S^R = (5 \cdot 10^{-6})(1.5)(0.7)(2) \approx 10^{-5} \text{ N-m (100 dyne-cm)}$$

Care has been taken to make sure the roll axis torque is smaller than this by canting the paddles in opposite axes to avoid a windmill configuration. Pitch and yaw axis "windmill" torques are half this large for the worst case solar angle and are cyclical at the roll frequency.

The solar pressure torques will have a  $\pm 20$  percent variation at the satellite roll rate and a  $\pm 20$  percent annual variation, and they appear and reappear rather abruptly at satellite dawn and dusk.

Air Drag Torque. The air drag torque will seldom exceed the solar pressure torque,

$$M_A = M_S \approx 10^{-5} \text{ N-m (100 dyne-cm)}$$



The air drag torque rotates once per orbit and its magnitude fluctuates (below the above value) by a factor of up to 30.

Magnetic Interaction Torque. Residual magnetic dipole moments on a non-rolling satellite react with the geomagnetic field to produce a torque which rotates twice per orbit (for a polar orbit) and with a magnitude change of a factor of about 2 as the satellite moves from the equatorial to the polar regions. The earth's field is no larger than 0.4 gauss in a 925 km polar orbit. Thus, we can control the peak magnetic torque to

$$M_M = 2 \cdot 10^{-5} \text{ N-m (200 dyne-cm)}$$

if we can keep the dipole moment under 500 pole-cm<sup>3</sup>. This is not easy but we do about twice this well on OSO. One dipole moment contributor which is quite different from those on OSO is that due to currents induced in the superconducting shields in the quartz block. Rough calculations show that this dipole moment can be compensated by "bucking" superconducting loops. This tentative conclusion should be verified later in the satellite program.

Gravity Gradient Torque. The greater geogravitational pull on parts of a satellite closer to the earth produce a torque proportional to differences between the satellite's principal moments of inertia. The torque rotates twice-per-orbit (and twice per satellite roll revolution) with a peak value at 925 Km of about

$$M_G = 1.5 \Delta I \cdot 10^{-6} \text{ N-m} *$$

For the tentative constraint  $\Delta I \leq 15 \text{ kg-m}^2$  the gravity gradient torque is

---

\* NASA CR-831



$$M_G \leq 2 \cdot 10^{-5} \text{ N-m (200 dyne-cm)}$$

Dynamic Imbalance Torque. The torque required to cause the satellite to spin about an axis other than a principal axis is given by

$$M_{DU} = U_D \omega_R^2$$

where  $U_D$  is the dynamic mass imbalance about the desired roll axis and  $\omega_R$  is the roll rate. The dynamic imbalance caused if two opposite solar paddles are rotated about a transverse axis so their mass centers are each displaced 1 cm is about

$$U_D = 2 \cdot 10 \text{ kg} \cdot 2 \text{ m} \cdot 0.01 \text{ m} = 0.4 \text{ kg-m}^2$$

It appears that we can control the distribution of the helium so that its contribution is small compared to this. Therefore, we are setting  $0.4 \text{ kg-m}^2$  as the dynamic imbalance specification.

For this imbalance and for the normal roll rate of  $3.5 \cdot 10^{-4}$  radians/per second we find

$$M_{DU} = 5 \cdot 10^{-8} \text{ N-m (0.5 dyne-cm)}$$

Gyroscopic Slewing Resistance Torque. The telescope must be slewed 5 arc-seconds in 1400 seconds to follow the orbital aberration of starlight. The control system must slew considerably faster during dawn acquisition (0.1 arc second per second may be enough). The gyroscopic resistance to slewing is given by

$$M_g = H_R \dot{\theta} = I \omega_r \dot{\theta}$$





For  $I = 300 \text{ kg-m}^2$ ,  $\dot{\theta} = 5 \cdot 10^{-7} \text{ rad/sec}$  (0.1 arc sec/sec) and for  $\omega_R = 3.5 \cdot 10^{-4} \text{ rad/sec}$  we have

$$M_g = (300) (3.5 \cdot 10^{-4}) (5 \cdot 10^{-7}) = 5 \cdot 10^{-8} \text{ N-m (0.5 dyne-cm)}.$$

This shows that reasonable slewing rates are no problem.

Attitude Control Torque. If the control jets can be positioned to give a 1 meter lever arm, the average control torque per axis is about

$$M_C = 5 \cdot 10^{-3} \text{ N-m (5,000 dyne-cm)}$$

This estimate exceeds the worst case sum of disturbance torques (for  $\omega_R < 3.5 \cdot 10^{-3} \text{ rad/sec}$ ) by a factor of about 10.

The quartz block actuator's maximum torque is  $10^{-3}$  to  $10^{-2} \text{ N-m}$ . The  $3 \text{ kg-m}^2$  block can thus be accelerated much faster by the inner actuator than by the helium thrusters. The peak gimbal angular velocities are rather low because the gimbals have only about 2 arc-seconds freedom of rotation.

#### 6.4.6.2 Outer Satellite Disturbances (Acquisition and Gyroscope Spin-Up)

During gyroscope spin-up, the spin gas exhaust produces additional disturbance forces and torques. The higher roll rate desired for gyroscope spin up increases the mass imbalance forces and torques.



Gyroscope Spin-Up Gas Disturbance Force. The gyroscopes are spun-up in pairs. Two liters (about 0.2 kg) of helium must be applied for about 40 minutes to spin up two gyros. This gas cannot be vented through the normal control thrusters. About 98 percent is vented through a 1 cm diameter "high pressure line," and the remainder through a 10 cm line. For an assumed specific impulse of 100 seconds, the force impulse for 0.2 kg of helium is 200 Newton-seconds (the specific impulse may be somewhat lower if the exit velocity can be limited to thermal velocity of the molecules and if the exit ports can be made colder than the satellite skin). If all this impulse is applied in a fixed direction along an axis passing through the satellite center of mass, the resulting velocity change is 0.3 meters per second. The resulting orbit perturbation is acceptable, so it is not necessary that the translation control system operate and cancel this disturbance during gyroscope spin-up.

If the spin-up gas was exhausted along an axis passing through the satellite center-of-mass, the disturbance force would be about 0.08 Newton. The high pressure spin-up exhaust gas will be deflected to largely cancel the resultant force. (Deflection is necessary to reduce the disturbance torque as is explained below.) The resultant should be  $10^{-3}$  to  $10^{-2}$  Newton. It is not intended that this force be opposed. (If unopposed, the satellite acceleration of less than  $2 \cdot 10^{-6}g$  is negligible compared to the gyro spin-up suspension capability). If, for any reason, translation control must be maintained, then 2 to 20 times the "average" helium boil-off rate (or higher force nitrogen thrusters) will be required.



Static Imbalance Force. To largely cancel the gyro spin axis misalignment caused by cross-axis spin gas torques, it is desirable to roll many cycles during spin-up of the parallel gyroscopes. The minimum acceptable roll rate is estimated to be  $\omega_R = 2 \cdot 10^{-2}$  rad/sec<sup>2</sup>. For this roll rate and the estimated static imbalance of  $u_s = 6$  kg-m, the transverse disturbance force amplitude is

$$F_{su} = u_s \omega_R^2 = 6 \cdot 4 \cdot 10^{-4} = 2.4 \cdot 10^{-3} \text{ N}$$

It is not necessary to react this force. If it was necessary, a helium boil-off rate of about five times the average rate would be required.

Available Translation Control Force. It is intended that translation control be inactive during attitude acquisition and gyro spin-up. This roughly doubles the available control torque.

Spin-Up Gas Disturbance Torque. Gyro spin-up gas is exhausted from ports that are no more than a meter away from the satellite cg. If all the gas was diverted at right angles to the radius vector from the cg then a disturbance torque of  $8 \cdot 10^{-2}$  Newton-m and a torque impulse of 200 Newton-m-sec would be applied to the satellite. This is over 100 times the normal control torque capability and would accelerate the satellite to a rate of 40° per second if unopposed. Attitude control must be maintained or the parallel gyroscopes will not be properly oriented. To avoid losing control, this disturbance torque must be reduced or control capability must be increased. We have tentatively constrained the residual disturbance torque to  $5 \cdot 10^{-3}$  N-m and



plan to increase the normal helium boil-off rate by a factor of 10 during gyro spin-up to increase control capability. A higher pressure nitrogen system backs up the helium system. To constrain the spin gas disturbance as desired, the high pressure spin-gas discharge must be balanced to about 6 percent. Active balancing may be required.

Dynamic Imbalance Torque. For the minimum acceptable gyro spin-up roll rate of  $\omega_R = 2 \cdot 10^{-2}$  radians per second and the expected dynamic imbalance of  $u_D = 0.4 \text{ kg-m}^2$  the transverse axis disturbance torque is

$$M_{Du} = u_D \omega_R^2 = (0.4)(4 \cdot 10^{-4}) = 1.6 \cdot 10^{-4} \text{ N-m}$$

This is small compared to the goal of  $5 \cdot 10^{-3} \text{ N-m}$  for the gyro spin gas exhaust disturbance torque.

Available Control Torque. If all the helium boil-off gas is used for attitude control (i.e., if translation control is disabled), the nominal control torque capability per axis is  $10^{-3} \text{ N-m}$ . An accelerated boil-off rate of 10 times nominal is planned during spin-up of the parallel gyros. This exceeds the spin-up exhaust gas torque goal by a factor of 2. A higher boil off rate or a separate nitrogen system can provide 0.02 to 0.1 N-m if future disturbance estimates show that control levels this large are required.

#### 6.4.6.3 Control Gas Disturbance Forces.

A number of factors prevent the helium thrusters from precisely producing the commanded control forces. Some of the deviations from perfect performance degrade pointing accuracy but do not



require additional gas usage. A  $10^{-5}$  Newton allocation is recommended on top of the gas budget to cover thruster noise and time-varying cross-coupling disturbances. The largest contributor is sensor noise and the  $10^{-5}$  Newtons allocation is for the normal helium boil-off rate. Thrust imperfections are discussed in the following paragraphs.

Null Biases. Discrepancies between the electrical null of the actuator and the error signal which gives balanced thrust from its opposing thrusters affect pointing errors like a bias disturbance force (for identical thruster pairs). Gas usage is not affected, but the linear range of the thrusters is reduced. It is desirable to constrain thruster null biases to 1 to 5 percent of full scale so the resulting pointing error contribution is smaller than for the environmental disturbances. It would be undesirable to allow null biases larger than this because of the reduction in thruster linear range. Differences in null biases between two thruster pairs cause cross-coupling between attitude and translation control. Cross-coupling disturbances are discussed under "Unequal Thrust."

Gain Deviations. Thruster gain varies directly with the helium boil-off rate. For identical thruster pairs, this produces a change in the closed-loop control gains. The effect of control gain variations is described in Appendix G. Differences in gain between thruster pairs cause cross-coupling between attitude and translation control proportional to the level of control activity. Rapid variations in control levels can disturb the cross-axis in a way that requires gas usage in addition to using up the pointing error and linear range budgets.



Unequal Thrust. Unequal thrust between thruster pairs is caused by unequal null biases and gain. These discrepancies are caused by differences in thruster, actuator, and gas feed line geometries and by temperature differences. Unequal thrust from opposing thruster pairs causes cross-coupling between attitude and translation control. It is desirable to constrain thrust differences so that the resulting cross-coupled disturbances do not exceed environmental disturbances. This can be accomplished by constraining the thrust differences to 1 to 5 percent. This in turn requires that null biases be constrained to 1 to 5 percent and that gain deviations (including those caused by temperature) be constrained to 1 to 5 or 10 to 50 percent. The tighter gain difference constraint applies if full thrust is assumed in the cross-axis. The looser gain requirement applies for expected control levels. We tentatively require less than 10 percent gain deviation.

Thrust Noise. The noise associated with the statistics of departure of helium molecules from the thrusters and the thruster response to sensor noise act like white noise disturbances on the outer satellite (the component due to sensor noise is band limited by the controller/estimator). Thruster noise performance will be determined in tests now being conducted by Stanford. Rough analysis suggests that for a 0.05 radian per second translation control bandwidth, the rms noise amplitude will be under  $10^{-5}$  Newtons. The main contributor is sensor noise. This component is proportional to the helium boil-off rate. The absolute level may exceed  $10^{-5}$  Newtons for faster than normal boil-off, but 5 times the budget entry is acceptable.



Irregular Thrust. Thrust irregularities such as would be caused by a "sticky" actuator introduces thrust "dead spots" that degrade the pointing accuracy of the helium jet system. These disturbances from linear operation should be constrained to a few percent of the full-scale actuator deflection.

Thrust Lag. The first order lag in thrust build-up must be short enough that it does not band-limit the attitude and translation controllers below the desired rates.

Control Gas Disturbance Torques. Preliminary estimates show that most of the gas control torque noise is due to attitude control sensor noise. Pitch/yaw sensor noise drives both the helium thrusters and the quartz-block actuators. The "inner" control loop has a higher bandwidth than does the thruster control loop. The pacing requirement on pitch/yaw sensor noise attenuation is based on limiting quartz-block acceleration by the inner actuator. The selected controller/estimator gains limits pitch/yaw thruster noise to less than  $10^{-5}$  N-m.

A roll-axis rms thruster noise of  $1.5 \cdot 10^{-4}$  N-m would be acceptable from the standpoint of gyro accelerations. It is desirable to limit this noise to  $3 \cdot 10^{-5}$  N-m to limit thruster linear range degradation to about 5 percent. This is accomplished by limiting the roll control system bandwidth to less than 0.5 radian per second.

#### 6.4.6.4 Meteoroid Impact Force

The satellite will be constantly bombarded by cosmic dust. The probability of being hit by a particle above a given size decreases rapidly as the threshold size is increased. NASA SP-8038 gives



less than 1 percent probability that a 5 square meter satellite will be hit in a one year period by a meteoroid weighing as much as  $10^{-3}$  g. A failure rate contribution in this range is acceptable. NASA SP-8038 and NASA SP-33 give the probable velocity of  $10^{-3}$  g meteoroid as less than  $3 \cdot 10^4$  meters per second (velocities over twice this value are possible but extremely unlikely). The corresponding probable force-impulse is less than  $3 \cdot 10^{-2}$  Newtons since meteoroid impacts are inelastic collisions. This force impulse would change the velocity of the 600 kg satellite by  $5 \cdot 10^{-5}$  meters per second. The gyroscope suspensions must be designed to protect the gyroscopes for impulses that are roughly this large.

Meteoroid Impact Torques. A  $10^{-3}$  gm meteoroid moving  $3 \cdot 10^4$  meters per second produces a force impulse of  $3 \cdot 10^{-2}$  Newtons. The torque impulse from a meteoroid hit produces a translational gyro acceleration proportional to the distance  $d$  from the gyro to the satellite center of mass. For a satellite radius of gyration  $\rho$  and a meteoroid hit lever arm  $D$  the linear velocity of the gyro case  $\Delta V'$  can be expressed in terms of the "equivalent" direct translation velocity change  $\Delta V$  as

$$\Delta V' = \frac{dD}{\rho^2} \Delta V$$

Since  $dD < \rho^2$  the direct translational velocity, which was treated as a meteoroid disturbance force, is of greater concern in gyro-suspension design than this rotational counterpart.





#### 6.4.6.5 Inner Body Disturbances

Except for the geogravity gradient, the outer satellite shell largely shields the quartz block from the outside environmental disturbances. Because the quartz block is smaller than the outer body, the geogravity gradient torque on the quartz block is only 2 to 5 x 10<sup>-6</sup> N-m.

The geomagnetic field cannot reach through to the quartz block because of the superconducting shield which is part of the "dewar within a dewar" design. If this superconducting shield was not present, it would be necessary to very carefully compensate for the induced dipole moments in the four smaller superconducting shields which surround each gyroscope.

In addition to the external disturbance torques applied to the quartz block, there are a number of interbody disturbance sources. These include:

- Thermal expansion and contraction of the dewar fiberglass supports.
- Erratic stress relief in the dewar supports.
- Thermally induced deflection of the solar array paddles.
- Helium motion.
- Organ pipe modes in the helium boil-off lines.
- Random "twitching" of super insulation in the dewar walls and of the vapor shields.



- Random "twitching" of leadout wires and pipes and of the telescope scaffolding.
- Motion of the telescope light choppers.
- Electrical noise applied to the quartz block actuators.
- Electrical noise applied to the helium thrusters.
- Offset of the quartz block gimbal from the satellite C.G. which causes cross-coupling between rotational and translation motion.

Preliminary estimates show that interbody disturbances are substantially smaller than the external disturbances, but the uncertainty in the estimates is large.

The uncertainty in disturbance estimates in the dewar wall can be greatly reduced by using sufficiently large fiberglass orbit supports. The cross-sectional area of 0.25 cm for each of six supports (about 10 times larger than is required for other reasons) is large enough that the supports should dominate other disturbances. If tension in the supports is sufficiently low, thermal deflection of the supports should produce the largest disturbance force.

The thermal analysis give a worst-case temperature variation of the warm end of the supports of  $\pm 5^{\circ}\text{C}$  which is sinusoidal at one cycle per orbit. Even if this difference was across the entire 0.25 m length of a support the total variation in support



length is only  $4 \cdot 10^{-6}$  m. The peak acceleration in support length is  $4 \cdot 10^{-12}$  m/sec<sup>2</sup>. If the helium vessel follows this displacement, then its angular acceleration is:

$$\ddot{\theta} = \frac{\ddot{x}}{\ell} = 10^{-12} \text{ rad/sec}^2$$

where  $\ell \geq 0.4$  meter is the support's lever arm about the satellite cg. The equivalent disturbance torque on the helium vessel is:

$$M_D = I \ddot{\theta} \approx (50)(10^{-12}) = 5 \cdot 10^{-11} \text{ N-m}$$

and is negligible.

The deflection of the tip of a solar array panel exposed to sunlight is 1 cm. The solar panels have thermal time constants of about 1000 sec. The peak angular acceleration of the satellite when a single panel is suddenly exposed to sunlight is less than  $5 \cdot 10^{-10}$  rad/sec<sup>2</sup>. The equivalent torque on the outer satellite shell is less than  $1.5 \cdot 10^{-7}$  N-m, and is negligible.

A worst-case estimate for the disturbance due to helium motion was made assuming surface tension acts to empty the dewar cell with the largest part. The reaction force is less than  $7 \cdot 10^{-6}$  Newtons. The corresponding disturbance torque is less than  $5 \cdot 10^{-6}$  N-m.

Disturbances within the dewar cavity should be small because of the uniform thermal environment. Organ pipe vibrations are relatively high frequency but should cause very small accelerations. The telescope light chopper design must be constrained to deliver small quartz block accelerations. A quiet electrical drive signal is required for the inner actuator but no serious problem is foreseen in meeting this requirement.



The electrical drive signal to the helium thrusters must also be quiet. The direct reaction forces and torques which occur when the thruster solenoids drive the gas diverting armatures must be considered along with the resulting helium gas disturbance noise (which was discussed in Section 6.4.6.2). The armatures are estimated to weigh  $m = 5$  gm each and full-scale deflection is about  $\chi = \pm 2$  mm. If the drive signal noise is limited to  $\pm 10$  percent of full scale (as recommended in Section 6.4.6.2), then the disturbance force noise from a pair of armatures driven at a frequency  $\omega = 5$  rad/sec is

$$F_D = 2m\ddot{\chi} = 2m(0.1)\times\omega^2 = (10^{-2})(10^{-1})(2\cdot 10^{-3})(25) = 5\cdot 10^{-5}N$$

This is five times the helium gas thrust noise and makes it even more important to constrain the amplitude and frequency response of the thruster drive. The calculated noise accelerates the gyroscope at  $10^{-8}g$  so it is important to keep the drive bandwidth below 5 rad/sec.

The presence of a highly compliant inner gimbal for the quartz-block reduces the pointing errors caused by high frequency angular motions of the helium vessel. On the other hand, decoupling the quartz-block's inertia from that of the satellite greatly increases the error caused by high frequency torques applied directly to the quartz-block. At this time we don't know whether the inner gimbal improves or degrades quartz-block motion due to mechanical noise.

#### 6.4.7 Control Systems Design and Performance

In this section, simplified analyses are applied for each controller to roughly establish the required characteristics and to draw attention to the more difficult design problems. In these analyses, the satellite is treated as one or two rigid bodies with linear control forcers or torquers. More realistic



control simulations were performed to verify the conclusions of this section. The results of these analog computer simulations are given in Appendix G.

Each of the control loops to be examined has similar problems in that a trade-off must be made between the system static error that is developed due to low-frequency disturbances and the acceleration that the system applies to the gyroscopes due to the sensor noise. Constraints on the undamped natural frequency of the system are developed first, to meet the static error and the gyroscope acceleration requirements. First, a lower constraint on the system's undamped natural frequency is calculated (to meet the static error requirement). Next, an upper constraint is calculated (to meet the gyro acceleration requirement).

The lower constraint is based on the assumption that integral feedback is not used. This constraint can be reduced by a factor of roughly 10 by using integral feedback. The upper constraint is based on the intended control torque of the inner actuators and helium thrusters. This constraint ignores the acceleration produced when the thruster solenoids drive the gas diverting armatures. If the armature mass is large enough, this constraint will have to be reduced.

These constraints are calculated for each loop to determine if a simple second-order linear controller with roll-off (position feedback with lead-lag-lag compensation) is feasible.

The gyroscope acceleration requirements dictate the required "smoothness" of control and a double lag is required to attenuate the acceleration noise due to sensor noise. A linear controller with position feedback gain  $K$ , and a lead time constant  $\tau$  produces acceleration noise less than

$$a = \left(\frac{K}{M}\right)x_R + \left(\frac{K\tau}{M}\right)\dot{x}_R$$



where  $X_R$  is the sensor noise amplitude (reduced from the noise bandwidth  $\omega$  to the double-lag break frequency\*), and  $M$  is the satellite mass (or inertia). For a less than critically damped controller, the control resonant frequency is approximately the undamped natural frequency

$$\omega_c = \sqrt{\frac{K}{M}}$$

A moderate gain margin can be retained for a double-lag break as low as  $5 \omega_c$ . For white noise, the noise amplitude "reduced" to the controller roll-off frequency of  $5 \omega_c$  is

$$X_R = \sqrt{\frac{5\omega_c}{\omega}} X$$

The acceleration noise of the controller to white noise band-limited to the roll-off frequency is lower than for a noise sinusoid at the roll-off frequency with rms amplitude equal to the reduced rms white noise amplitude. (The amplitude noise, or jitter, is lower than for a noise sinusoid at the controller resonant frequency of rms amplitude equal to the sensor noise amplitude reduced to the resonant frequency.)

For a noise sinusoid,  $X_R \sin 5 \omega_c t$ , the controller accelerates the satellite less than

$$a = \left(\frac{K}{M}\right) X_R \sin 5 \omega_c t + 5 \left(\frac{K\tau}{M}\right) \omega_c X_R \cos 5 \omega_c t = (\sin 5 \omega_c t + 5 \tau \omega_c \cos 5 \omega_c t) \frac{K}{M} X_R = \sqrt{5} (\sin 5 \omega_c t + 5 \tau \omega_c \cos 5 \omega_c t) \omega_c^2 \sqrt{\frac{\omega_c}{\omega}} X$$

(a)

\*See Appendix G for more information on the acceleration response of a controller and on the frequency domain equivalent to these equations.



For damping 0.5 times critical,  $\tau\omega_c \approx 1$  and the first two factors have an rms amplitude of about 10. We can solve for the maximum allowable control resonant frequency for a given allowable acceleration,  $a$ , as

$$\omega_c = \left( \frac{\sqrt{\omega} a}{10 X} \right)^{2/5} \quad (b)$$

where  $X$  is the input noise amplitude and  $\omega$  is its bandwidth.

For a second order linear controller (without integral feedback) the minimum allowable control resonant frequency can be determined from the required dc gain. The error  $\Delta X$  caused by a steady disturbance force (or torque)  $F_D$  is

$$\Delta X = \frac{F_D}{K} = \frac{F_D}{M\omega_c^2} \quad (c)$$

and we have

$$\omega_c = \sqrt{\frac{K}{M}} = \sqrt{\frac{F_D}{M\Delta X}} \quad (d)$$

Pitch-Yaw Controller. The purpose of the pitch-yaw control system is to point the telescope at the guide star well enough that the image remains within the usable linear telescope range of 0.05 arc-seconds continuously for 50 percent of most orbits. This is the fundamental requirement that must be met to read out the gyroscope drifts to the desired accuracy. The telescope pointing error with respect to the guide star must include a 0.03 arc-second sinusoidal dither component at about 0.1 radian



per second that is required to calibrate the telescope and gyroscope readout gains. The telescope pointing error signal is used for pitch-yaw control except when the guide star is occulted by the earth. During occulted periods pitch and yaw errors are taken from one of the parallel gyroscopes. During these periods, pitch and yaw errors need be controlled only well enough that guide star reacquisition can occur a few minutes after the star reappears. The pitch-yaw controller must also be able to null initial errors as large as 1.5 arc-minutes in less than 30 minutes even though the telescope output contains no rate information for errors larger than 0.5 arc-second.

The required pitch-yaw pointing accuracy is substantially better than that achieved by any satellite to date. Probably the most dramatic improvement over existing designs will be in the telescope, made possible by the cryogenic environment. Pointing the satellite within 0.03 arc-second of the desired point as defined by the telescope is also a challenging problem. The solution to this problem depends on delivering sufficiently large and smooth control torques in response to sufficiently small and smooth disturbance torques. (The pointed experiments on OSO-VI are pointed within  $\pm 1$  arc-second of the solar sensor null, but this jitter amplitude would be a factor of more than 20 smaller if there was less friction in the experiment gimbal.)

The worst-case peak disturbance torques on the outer shell of the satellite are estimated to be less than  $5 \cdot 10^{-5}$  N-m. A major portion of the overall control problem is constraining the configuration and magnetic cleanliness to assure that this estimate is not exceeded. Most of the disturbance can be represented as a sum of one and two cycle per orbit sinusoids, which means the disturbance is relatively smooth. (By contrast,





the gimbal friction torque on OSO-VI is about 0.1 N-m and it has a "slip-stick" character).

We can get an idea of how fast the pitch-yaw controller has to be by calculating how long it takes a step change from zero to the worst-case disturbance torque to drive the satellite through an angle  $\Delta\theta = 0.05$  arc-sec  $= 2.5 \cdot 10^{-7}$  radian. The peak disturbance acceleration is

$$\ddot{\theta} = \frac{M_D}{I} = \frac{5 \cdot 10^{-5} \text{ N-m}}{300 \text{ kg-m}^2} = 1.6 \cdot 10^{-7} \text{ rad/sec}^2$$

and we have

$$\Delta t = \sqrt{\frac{2\Delta\theta}{\ddot{\theta}}} = \sqrt{\frac{5 \cdot 10^{-7}}{1.6 \cdot 10^{-7}}} \approx 1.7 \text{ seconds}$$

This shows that the pitch-yaw controller and its torquers need not respond rapidly, even to counter unexpectedly large step changes in the outer satellite disturbance torque.

Prior to this study, it was estimated that the mechanical vibration frequency of the helium vessel would have to be lower than 1 radian per second to adequately control the heat leak through its supports. For a compliance this high, the telescope error signal lags disturbances too much for effective control. In addition to the problem of precisely controlling the telescope by pushing through a weak spring, it was feared that the weak spring would allow the helium vessel to "twitch" at relatively high frequencies (especially in view of the 200°C temperature differential between the helium vessel and satellite



shell). To get around these difficulties, a "fine" control actuator was added between the quartz block and helium vessel to supplement coarse control by the helium thrusters.

A two-stage pitch-yaw control system is retained in the current preliminary design although it is now estimated that the pitch-yaw dewar vibration frequencies can be made greater than 100 radians per second. The fine (inner) loop should be retained until tests can be made that demonstrate that helium thruster performance is adequate for single-loop control and that disturbances within the dewar wall are small enough that rotational (and possibly even translational) decoupling of the quartz block is not required. Elimination of the inner gimbals and control loops would greatly simplify the design and therefore is a very attractive option. However, it is easier to remove the gimbals at a point further down stream in the program than to introduce them if it becomes clear that they are necessary.

Before describing the two-stage optimal controller-estimator (which operates with five state variables) we calculate the resonant frequency constraints that would apply to a single-stage linear second-order controller using only the helium jets. For an allowable static error of  $\Delta\theta = 0.03$  arc-second  $= 1.7 \cdot 10^{-7}$  radian in the presence of a worst-case peak disturbance torque of  $M_D = 5 \cdot 10^{-5}$  N-m, the required position feedback gain is

$$K = \frac{M_D}{\Delta\theta} = \frac{5 \cdot 10^{-5}}{1.7 \cdot 10^{-7}} \approx 300 \frac{\text{N-m}}{\text{rad}}$$

For appropriate lead-lag-lag compensation, equation (d) gives the minimum allowable controller resonant frequency as



$$\omega_c = \sqrt{\frac{K}{I}} = \sqrt{\frac{300}{300}} = 1 \text{ rad/sec.}$$

where  $I = 300 \text{ kg-m}^2$  is the satellite pitch-yaw inertia.

To meet the gyro acceleration budget, pitch-yaw jitter acceleration of the quartz-block must be limited to about  $\ddot{\theta} = 8 \cdot 10^{-7} \text{ rad/sec}^2$ . When the telescope provides the error signals the noise level is less than  $\theta = 0.03 \text{ arc-second} = 1.5 \cdot 10^{-7} \text{ radian}$  below  $\omega = 100 \text{ radians per second}$ . (When the gyroscope readouts are used during guide-star occultation for pitch-yaw control, the noise amplitude is larger and additional bandlimiting is required.) For the telescope noise the maximum acceptable resonant frequency is given by equation (b) as

$$\omega_c = \left( \frac{\sqrt{\omega} \ddot{\theta}}{10^{\theta}} \right)^{2/5} \approx 2 \text{ radians per second}$$

A control frequency of 1.5 radians per second would give a factor of about 2 margin for disturbance torques and a factor of about 2 margin for quartz-block acceleration from sensor noise. These margins may not be adequate because they would be largely used up by expected gain changes with changing helium boil-off rate.

The estimated margins are pessimistic because the telescope noise may be one-fifth of the design value (see Section 5.1.3). Even if the noise is as large as the design value, the margins could be substantially increased by (a) adding integral theta feedback to increase the low frequency gain, and (b) by reducing the controller resonant frequency to less than 1 radian per



second. Another option is to switch to a lower controller gain when an accelerated helium boil-off rate is commanded. The controller frequency is a factor of about 50 lower than the lowest pitch-yaw rotational mechanical mode so control interaction with the structure should be small.

The characteristics of this single-stage linear second order controller are summarized in Table 6-16.

Two-Stage Modern Pitch-Yaw Controller. Pitch and yaw gimbals rotationally decouple the quartz block from the rest of the satellite. This largely isolates the block from high-frequency disturbances which are applied to the outer shell or which originate in the dewar walls. The block is rotated with respect to the rest of the satellite by electromagnetic cryogenic actuators which overcome gimbal flexures. This makes quiet, fast and linear control feasible even if the helium thrusters are noisy, slow and nonlinear. Of course, the helium jets still must be driven to coarsely control the attitude of the rest of the satellite and quartz block control is only as quiet, fast and linear as are the inner actuators.

If the telescope or gyro outputs are the only pitch-yaw error signals, the controller is single input/double output and the standard "classical" control methods are not applicable. If the coarse star tracker output or gimbal angle pick-off signals were added as inputs and if the inner and outer control frequencies could be widely separated, lightly coupled inner and outer single input/single output controllers could be designed by standard classical methods. The "modern" control methods which Stanford has applied permit the use of an efficient, highly



Table 6-16

SINGLE-STAGE LINEAR  
SECOND ORDER PITCH-YAW CONTROLLER,

Error Signal	Telescope (gyros during occultation)
Usable range for relativity data	0.05 arc-sec
Noise	0.03 arc-sec in 100 rad/sec.
Torquers	Helium thrusters
Controller	Position feedback with lead-lag-lag compensation
Resonant frequency	1.5 rad/sec
Lead break	1.5 rad/sec
Lag-lag-break	7.5 rad/sec
Damping	>0.3 times critical for nominal gain
	>0.2 times critical for $\pm 50$ percent gain change
Static error	0.015 arc-sec
Quartz block jitter displacement (for worst expected disturbance)	0.005 arc-sec (rms)
Quartz block jitter acceleration (for expected telescope noise)	$5 \cdot 10^{-7}$ rad/sec <sup>2</sup> (rms)
Ratio of control resonant frequency to lowest satellite pitch-yaw frequency	1/50



coupled two-stage controller/estimator which uses constant gains and requires no outer body attitude sensor.

For each control axis (pitch and yaw), five state variables are defined which describe the attitude behavior of the quartz block and outer body. Four variables determine the instantaneous attitudes and rates and the fifth is the integral of the quartz block attitude error. Figure 6-35 shows the important elements and signal flow within the system. The upper half of the diagram is the plant (complete with sensor and torquers). The equation of motion of the satellite is  $\dot{X} = FX + GU + w$  where  $X$  is the five-element state vector,  $U$  a two-element control vector,  $w$  an external disturbance noise vector, and  $F$  and  $G$  are treated as constant matrices. (Actually the elements of  $F$  and  $G$  vary slowly as the satellite inertia changes because of helium depletion.) The control vector is generated by electromagnetic actuators which drive the quartz block gimbals and the helium thrusters in response to command signals  $\hat{u}_1$  and  $\hat{u}_2$  from the controller/estimator.

The satellite sensor is either the telescope or a gyroscope read-out loop (the rms sensor noise level  $v$  is about 50 times larger when the gyroscope is used). The sensor's only direct output is the pitch (or yaw) angle of the quartz block plus noise. Thus, the matrix  $H$  in the equation  $Z = HX + v$  is a constant row vector which picks the pitch (or yaw) angle out of the state vector.

The estimator, or Wiener filter, is a special form of the highly publicized Kalman filter. The optimal filter gains  $K$  are constant in the Wiener filter. The filter (or estimator) is optimal in the sense that it is a maximum likelihood filter. The filter

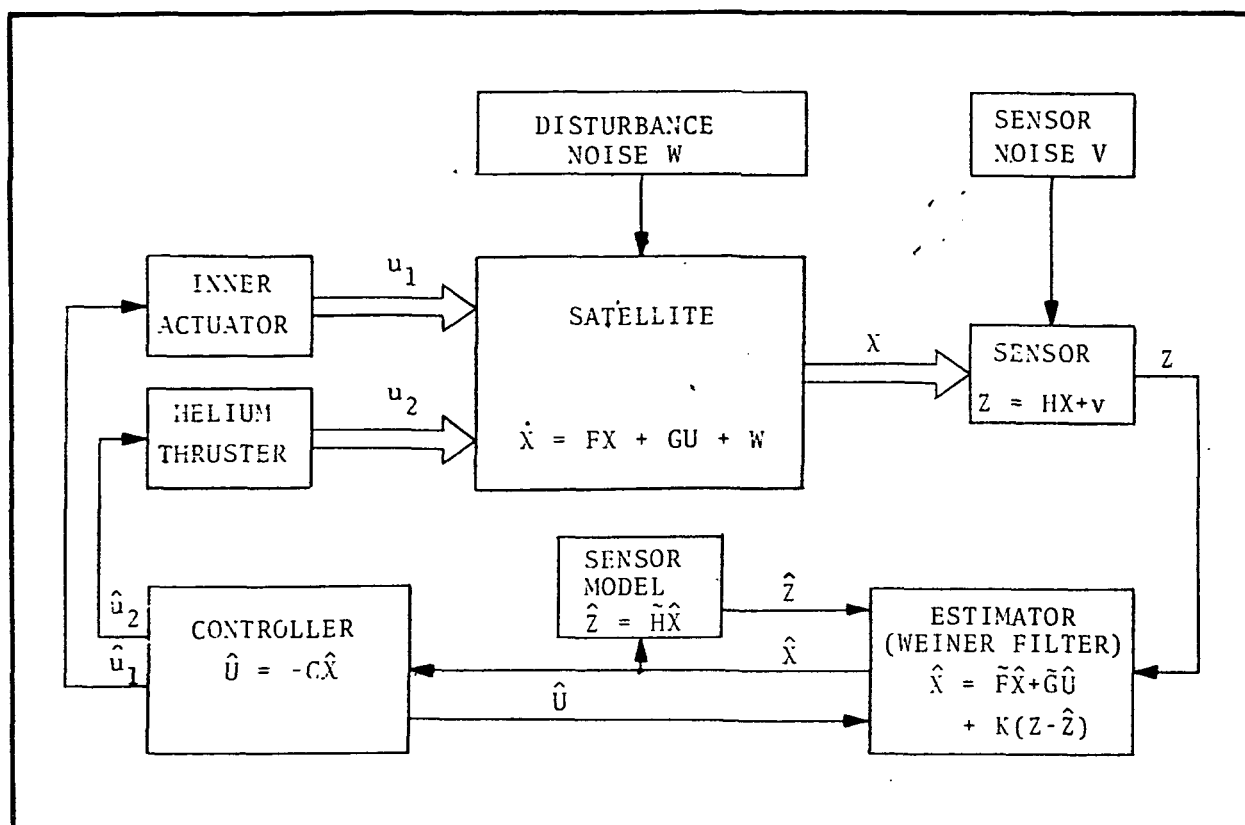


Fig. 6-35. Two-Stage Modern Pitch-Yaw Controller/Estimator

gains are functions of the flexure stiffness between the two bodies and the expected disturbance and sensor noise levels. The state variable residuals are weighted by the inverse square of their variances in a maximum likelihood estimate.

The filter contains an analog computer simulation of the plant. This allows the filter to estimate state variables which are not measured by the sensor. The equation simulated is  $\dot{\hat{\hat{X}}} = \tilde{F}\hat{\hat{X}} + \tilde{G}\hat{U} + K(Z - \hat{\hat{Z}})$  where  $\hat{\hat{X}}$  is the state estimate,  $\hat{U}$  is the control command vector (which also drives the satellite control torquers),  $\hat{\hat{Z}}$  is the estimated pitch (or yaw) angle of the quartz block, and  $\tilde{F}$  and  $\tilde{G}$  are constant matrices which approximate  $F$  and  $G$  as well as is practical.



The controller provides optimal state variable feedback through ten constant gains (per control axis). The controller is optimal in the sense that the sum of the weighed squares, of the state errors and control levels are minimized. The quadratic performance criterion gives rise to a linear controller. The chosen weighing factors are inverse squares of the desired value of the state and of the control levels. The magnitudes of the position weighing factors determine the bandwidths of the inner and outer control loops. The relative magnitudes of the position, rate and control level weighing factors determine the dominate control frequencies and damping characteristics. The gain matrix C is a constant 2 by 5 matrix, some of whose elements are switched to new values when control is transferred from the telescope to the gyroscopes and when accelerated helium boil-off is commanded.

Stanford has developed digital computer programs which solve for the five filter gains K and the ten control gains C for each axis as a function of the plant (as described by the F, G and H matrices), the expected disturbance and sensor noise levels, and desired state variable errors and control levels. A number of gain iterations have occurred during the mission definition study and important changes in control philosophy have occurred. These changes are largely the result of the large increase in the expected mechanical vibration frequency of the dewar.

The analog computer simulation described in Appendix G has shown that another gain iteration is desirable. Further iterations should be expected as the control systems analysis proceeds.

An important change in philosophy made during the study is that the control system is not required to damp dewar wall vibrations.





Damping must be achieved by other methods and the control system design must be constrained to avoid instabilities. Other possible damping methods are:

- Provide direct damping in the fiberglass bands by using many rough strands or a lossy sheath.
- Tune the solar array paddles and damp them well to make them function as vibration absorbers.
- Use an active electro-mechanical damper in the dewar wall.

The characteristics of the modern controller/estimator can be conveniently described in terms of the two sets of closed-loop poles. If the filter has a perfect model of the plant (i.e.,  $\tilde{F} = F$ ,  $\tilde{G} = G$ ,  $\tilde{H} = H$ ) then the system's characteristic equation can be factored. One factor contains the poles associated with  $(F - GC)$  and the other with  $(F - KH)$ . We can label these as control and filter poles respectively. An important aspect of the modern control approach is this decoupling of control and filter poles. For perfect modeling, it is possible to design the filter and controller independently. Modeling errors produce interactions which may require adjustments in the combined design.

The last set of filter and controller gains Stanford provided for the analog simulation in Appendix G are:

$$K = \begin{bmatrix} 1.9 \\ 9.5 \\ 45 \\ 52 \\ -5.6 \end{bmatrix}$$



$$C = \begin{bmatrix} 1.0 & 21 & 14 & 2.8 & -0.34 \\ 6.5 & 86 & 246 & 86 & 244 \end{bmatrix}$$

where the state variables are the integral of the quartz block inertial angle, the quartz block inertial angle relative to the guide star, the quartz block inertial rate, minus the quartz block gimbal angle, minus the quartz block gimbal rate. The controller/estimator pole locations are:

F - KH	F - GC
0	-0.1
$-4 \pm 4.1j$	$-1.7 \pm 1.5j$
$-0.78 \pm 0.78j$	$-0.37 \pm 0.35j$

The characteristics of the modern pitch-yaw controller are summarized in Table 6-17. The association of one filter pole with the inner and the other with the outer body is misleading because the highest frequencies in the state estimate  $\hat{X}$  drive both the helium thrusters and the inner actuators (but through different gains).

There is much more design freedom in the two-stage modern controller than in a single-stage second order controller. One free element is the relative location of the inner and outer loop bandwidths. Another is the relative location of the filter and control poles. For the current design the filter is "faster" than the controller. An undesirable effect is that the actuators and thrusters are driven at relatively large amplitudes by relatively high-frequency sensor noise components. For example, the peak thruster torque excursions are  $3 \cdot 10^{-4}$  N-m which corresponds to over 20 percent of the full scale thruster actuator deflection at the normal helium boil-off rate. Furthermore, this excludes



Table 6-17  
TWO-STAGE MODERN PITCH-YAW CONTROLLER

Error Signal	Telescope (gyrós during occultation)	
Usable range for relativity data	0.05 arc-sec	
Noise	0.03 arc-sec in a 100 rad/sec bandwidth	
Torquers	Inner actuator and helium thrusters	
Allowable pointing error	0.03 arc-sec	
Controller	Linear 5-state feedback to two torquers	
Dominant frequencies (rad/sec)	<u>Inner Body</u>	<u>Outer Body</u>
Filter	5.7	1.1
Control	2.2	.52
Damping	0.7 times critical	
Static error for expected disturbance	0	0.25 arc-sec
Jitter displacement from telescope noise (rms)	0.01 arc-sec	0.04 arc-sec
Jitter acceleration from telescope noise (rms)	$1 \cdot 10^{-6}$ rad/sec <sup>2</sup>	$2.5 \cdot 10^{-7}$ rad/sec <sup>2</sup>
Torquer noise from telescope noise (rms)	$4 \cdot 10^{-6}$ N-m	$7 \cdot 10^{-5}$ N-m



the direct mechanical reaction disturbance caused by the thruster solenoid driving the helium diverting armatures. This is an unnecessary reduction in the thruster linear range and can conceivably cause gyroscope acceleration problems in spite of the quartz block decoupling gimbal. The quartz block cannot be driven at these relatively high frequencies (because of its inertia), so there is little point in passing them. Stanford and BBRC agree that the filter should be slower than it was for the last gain iteration in the current study. This would reduce the jitter acceleration from the  $10^{-6}$  rad/sec<sup>2</sup> given in Table 6-17. (Gyroscope acceleration for  $10^{-6}$  rad/sec<sup>2</sup> is slightly larger than desired.)

The greater design freedom in the modern controller should give superior performance for this more sophisticated design. Additional work is required to get the most from the powerful modern control tools.

Roll Controller. The purpose of the roll control system is to hold the satellite at a fixed roll angle or to roll it at a steady enough rate to allow gyroscope drift to be determined from telemetered gyroscope readout loop data and to be distinguished from readout drifts. When not rolling, the roll orientation need be only within about  $0.5^\circ$  of that commanded. When rolling, the roll rate need be only steady to 1 percent. However, in both cases the roll orientation must be determined to 10 arc-seconds. The ground data reduction task is simplified if the roll orientation is held (or controlled while rolling) within 10 arc-seconds of the commanded value (ramp). This approach has been taken.



The roll error signal is formed by resolving the outputs of two readout loops on one of the perpendicular gyros. The roll orientation of the perpendicular gyros is determined to a small fraction of an arc-second by reading out the gyros while the telescope is pointed at the roll reference star. The roll error is allocated among system components in Table 3-6. The roll controller must keep the roll bias pointing error less than 3 arc-seconds. For a linear second-order controller and for a worst-case roll disturbance torque of  $5 \cdot 10^{-5} \text{ N-m}$ , the required position feedback gain is

$$K = \frac{M_D}{D\phi} = \frac{5 \cdot 10^{-5} \text{ N-m}}{1.7 \cdot 10^{-5} \text{ rad}} \approx 3 \frac{\text{N-m}}{\text{rad}}$$

For appropriate lead-lag-lag compensation, this gives a minimum controller resonant frequency of

$$\omega_c = \sqrt{\frac{K}{I}} = \sqrt{\frac{3}{300}} = 0.1 \text{ radian per second}$$

where  $I = 300 \text{ kg-m}^2$  is the satellite roll-axis moment of inertia.

The roll controller must also attenuate the roll error signal noise to keep gyroscope acceleration under  $10^{-8} \text{ g}$ . This requires that quartz block jitter acceleration be limited to about  $8 \cdot 10^{-7} \text{ rad/sec}^2$ . The roll error signal noise is equal to the gyroscope readout noise of  $\phi = 1.4 \text{ arc-seconds}$  ( $7 \cdot 10^{-6} \text{ rad}$ ) in a bandwidth of  $\omega = 100 \text{ radians per second}$ . The maximum allowed controller resonant frequency for a jitter acceleration of  $\ddot{\phi} = 8 \cdot 10^{-7} \text{ rad/sec}^2$  is

$$\omega_c = \left( \frac{\sqrt{\omega \ddot{\phi}}}{10\phi} \right)^{2/5} \approx 0.5 \text{ radian per second}$$



The selected roll control resonant frequency of 0.3 radian per second gives a factor of 9 margin for disturbance torque and a factor of about 3 margin for sensor noise or quartz-block acceleration levels. The selected frequency is a factor of 100 lower than the lowest expected roll mechanical vibration frequency. Control interaction with this mode should be small. Roll controller characteristics are summarized in Table 6-18.

Roll attitude control is straightforward compared to pitch-yaw control. Alternatives to the selected approach were not considered because no important potential drawbacks were recognized in the recommended system.

Translation Controller. The purpose of the translation control system is to limit the support forces required to keep the gyroscopes in the centers of their cavities. This is accomplished by making the satellite follow a proof-mass inside a hollow cavity in the quartz block. This approximately matches the satellite acceleration to that of the proof-mass. If matching is perfect, the gyroscope support accelerations are reduced to the difference between the inertial accelerations of the gyroscopes and the proof-mass. These acceleration differences are made acceptably small by clustering the gyroscopes close to the proof-mass, by carefully compensating the self-gravity attraction of the gyroscopes and proof-mass by the satellite and by limiting the forces applied to the gyroscopes and proof-mass by their capacitive position readouts.

The gyro acceleration budget (Table 3-3) allocates a  $5 \cdot 10^{-10} g$  bias to acceleration of the satellite center of mass. To meet this requirement the self-gravitational attraction of the proof-mass must be less than  $4 \cdot 10^{-10} g$  and other forces on the proof-mass (such as that produced by its readout) must be less than  $3 \cdot 10^{-10} g$ .



Table 6-18  
ROLL CONTROL SYSTEM CHARACTERISTICS

Error Signal	Two secondary loops from a perpendicular gyroscope and a roll encoder
Noise	1.4 arc-sec. in 100 rad/sec.
Allowable static error	3 arc-sec
Torques	Helium thrusters
Controller	Position feedback with lead-lag compensation
Resonant frequency	0.3 rad/sec
Lead break	0.3 rad/sec
Lag-lag break	1.5 rad/sec
Damping	>0.3 times critical for nominal gain >0.2 for $\pm 50$ percent gain change
Static error (for worst expected disturbances)	0.3 arc-sec
Jitter displacement	0.1 arc-sec (rms)
Jitter acceleration (for expected sensor noise)	$3 \cdot 10^{-7} \text{ rad/sec}^2$ (rms) ( $4 \cdot 10^{-9} \text{ g}$ on the parallel and $3 \cdot 10^{-9} \text{ g}$ on the perpendicular gyroscopes)
Ratio of control bandwidth to lowest satellite roll natural frequency	1/100



The bias (over periods of many orbits) acceleration error in chasing the proof-mass will be extremely small if the proof-mass is kept away from its cavity walls.

For the selected 0.25 cm gap between the proof-mass and its cavity, the one and two cycle per orbit sinusoidal proof-mass chasing acceleration errors will be small compared to the allocated amplitude of  $10^{-8}g$ . If the amplitude of the sinusoidal chasing error is  $A = 2.5 \cdot 10^{-3}$  meter and the frequency is twice per orbit ( $\omega = 2 \cdot 10^{-3}$  radian per second), then the acceleration amplitude is  $A\omega^2 = 10^{-8} \text{ m/sec}^2 = 10^{-9}g$ . The satellite self-gravity gradient inside the proof-mass cavity probably will be well under  $10^{-9}g$  per cm so there is no requirement to keep the proof-mass near the center of its cavity. However, it is desirable to keep the proof-mass well centered for the expected disturbance forces to provide a linear control margin for higher forces. This might allow the drag-free control objectives to be met even if the launch vehicle failed to achieve the required perigee altitude. Mission success would then be contingent on control gas availability rather than on the translation controller gain.

High-frequency acceleration or jitter is the main source of sinusoidal gyroscope acceleration. Most of the jitter is expected to result from proof-mass position sensor noise. The translation controller bandwidth must be low enough to attenuate accelerations due to sensor noise to less than  $a = 10^{-7} \text{ m/sec}^2 = 10^{-8}g$ .

For a 1.5 cm diameter proof-mass in a 2 cm cavity, the capacitive position pick-off noise level is estimated at  $X = 2 \cdot 10^{-5} \text{ m}$  in a





bandwidth of  $\omega = 2000$  radians per second. The maximum allowable controller resonant frequency is given by equation (b) as

$$\omega_c = \left( \frac{\sqrt{\omega} a}{10X} \right)^{2/5} \approx 0.2 \text{ radian per second}$$

For  $M = 600$  kg, for the maximum permissible resonant frequency,  $\omega_c = 0.2$  radian per second and for the largest expected disturbance torque of  $5 \cdot 10^{-5}$  Newtons equation (c) gives a static error of about  $2 \cdot 10^{-6}$  m. This is 1200 times smaller than the chosen proof-mass gap of 2.5mm. A disturbance/force margin greater than about 100 is not useful because control forces would already be limited by gas availability.

The recommended translation control resonant frequency of 0.05 radian per second divides the margin in the system between disturbance forces and sensor noise. For a given control resonant frequency, the allowable disturbance force and sensor noise amplitudes can be calculated by rearranging equations (c) and (b). These allowables are divided by the expected values to give the system margins for disturbance forces and sensor noise (or quartz block acceleration levels).

The allowable disturbance force is obtained from equation (b) as

$$F_D = M \omega_c^2 \Delta X_{\text{Allowable}}$$

Since  $M = 600$  kg,  $\omega_c = 0.05$  radian per second and  $\Delta X_{\text{Allowable}} = 25$  mm (the proof-mass clearance) we find

$$F_D = 4 \cdot 10^{-3} \text{ N-m}$$



Thus, the disturbance force margin is nearly 100.

The allowable sensor noise is obtained from equation (a) as

$$X = \frac{\sqrt{\omega}}{10 (\omega_c)^{5/2}} a_{\text{Allowable}}$$

For  $\omega = 2000$  radians per second and  $a_{\text{Allowable}} = 10^{-7} \text{ m/sec}^2$ , we find

$$X \approx 10^{-3} \text{ m}$$

This is 50 times the expected sensor noise of  $2 \cdot 10^{-5} \text{ m}$ .

The chosen control resonant frequency is a factor of more than 1000 lower than the lowest satellite mechanical translational frequency. For this ratio, control interaction with the satellite structure is virtually nonexistent. A substantially higher frequency could be used and might be desirable if the proof-mass clearance was decreased.

The translation control system characteristics are summarized in Table 6-19.

The translation control options considered involve the proof-mass. The first option is to reduce the gap between the proof-mass and its cavity by a factor of 10 to 100. The objective is to avoid having to cage the proof-mass during launch. This option is recommended if future analysis and tests show that an uncaged proof-mass of appropriate material (and its cavity) can survive launch vibration for cavity gaps of 0.002 to 0.05 cm and



Table 6-19  
TRANSLATION CONTROL SYSTEM CHARACTERISTICS

## Proof-Mass

Proof-mass diameter	1.5 cm
Cavity diameter	2 cm
Launch protection	Mechanically caged
Position sensor	Capacitive pick-off
Sensor noise	$2 \cdot 10^{-5}$ m in 2000 rad/sec.

## Force

Helium thrusters

## Controller

Position feedback with  
lead-lag-lag compensation

Resonant frequency	0.05 rad/sec
Lead break	0.05 rad/sec
Lag-lag break	0.25 rad/sec
Damping	>0.3 times critical for nominal gain
	>0.2 times critical for $\pm 50$ percent gain change
Static error (for expected disturbances)	$3 \cdot 10^{-5}$ m
Jitter displacement	$1.5 \cdot 10^{-7}$ m (rms)
Jitter acceleration (for expected sensor noise)	$2 \cdot 10^{-10}$ g (rms)
Disturbance force required to "bottom" the proof-mass	$4 \cdot 10^{-3}$ Newtons



that it continues to appear that a cryogenic caging mechanism is a non-trivial addition to the design. The cost of this option is reduction of the margins for disturbance forces and sensor noise. These margins are large enough for the recommended system that this cost is reasonable.

A second option is to use an electrostatically supported accelerometer instead of a free proof-mass. Currently available accelerometers do not have the required accuracy but several designs are being tested. An acceptable unit might be built using a gyroscope housing and suspension and a non-spinning ball. It is even possible that error signals from one of the four gyroscopes could be used for translation control. This would eliminate the need for a separate translation sensor. This option should be reviewed as the program progresses.

Gyroscope Suspension. The gyroscope suspensions must keep the rotors near the center of their cavities. The balls must be centered to an accuracy of  $2.5 \cdot 10^{-7}$  meters for proper operation of the gyroscope readout loops. The suspensions must also have sufficient gain and dynamic range to keep the balls away from their cavity walls during control activity, meteoroid hits, and other disturbances. The suspensions must be quiet enough to accelerate the gyroscopes no more than  $10^{-8}g$  (rms) as required in the gyroscope acceleration budget in Table 3-3.

During normal pointing, gyroscope accelerations with respect to the quartz block are no larger than  $\ddot{x} = 3 \cdot 10^{-8}g = 3 \cdot 10^{-7}m/sec^2$  (rms). For a linear second-order suspension, the resonant frequency required to limit ball excursions to  $\Delta X = 2.5 \cdot 10^{-7}m$  is



$$\omega_c = \sqrt{\frac{\ddot{x}}{\Delta x}} = \sqrt{\frac{3 \cdot 10^{-7}}{2.5 \cdot 10^{-7}}} \approx 1 \text{ radian per second}$$

The control systems can produce transient accelerations larger than  $3 \cdot 10^{-8} g$ . However, the gyro excursions can exceed  $2.5 \cdot 10^{-7} m$  during periodic brief transients since relativity data can be ignored during these periods. To limit these excursions and to greatly reduce the chance of "bottoming" a gyro during control activity, it is desirable to place the suspension bandwidth above the highest control bandwidth. The highest control bandwidth for nominal gains is 3 to 5 radians per second in pitch-yaw. (The controller electrical gains would have to be reduced for accelerated helium boil-off rates to avoid large increases in bandwidth.)

The gyro suspensions must keep the gyros from bottoming for relatively likely meteoroid impacts. A failure probability contribution of less than 0.01 per year is acceptable. NASA SP-8038 gives a meteoroid size of  $10^{-3} gm$  for this hit probability on a 5 square meter satellite. The probable velocity for such a meteoroid is less than  $3 \cdot 10^4$  meters per second, and for an inelastic impact the probable force impulse is less than  $3 \cdot 10^{-2}$  Newton-second. This impulse accelerates the 600 kg satellite to a velocity of  $5 \cdot 10^{-5}$  meters per second. The gyroscopes must be accelerated by their suspensions to catch up. Without suspension forces, the quartz block would move  $4 \cdot 10^{-6} m$  and hit the gyros in only 0.08 second.

The position feedback alone (ignoring the help given by lead compensation) of a second order linear suspension would limit the gyro excursions to



$$\delta = \frac{\Delta V}{\omega_c}$$

where  $\omega_c$  is the suspension resonant frequency. For  $\Delta V = 5 \cdot 10^{-5}$  m/sec and  $\delta = 4 \cdot 10^{-6}$  m (the gyroscope clearance) we find a resonant frequency as high as 12 radians per second is required to prevent bottoming. For a 0.7 times critically damped gyroscope suspension, the lead compensation reduces the gyroscope displacement by a factor of about 1/2. This reduces the required minimum gyroscope suspension resonant frequency to about 6 radians per second.

The gyro suspension resonant frequency must be low enough that noise in the gyro position sensor causes accelerations no larger than  $10^{-8}$  g. The noise in the capacitive position sensor is estimated at less than  $X = 3 \cdot 10^{-9}$  m in a bandwidth of  $\omega = 2000$  radians per second. (This is one-tenth of the amplitude that has been measured for the high voltage suspension with an electrical gap of  $4 \cdot 10^{-5}$  m.) The maximum allowable suspension resonant frequency for an allowable gyro acceleration  $a = 10^{-7}$  m/sec<sup>2</sup>, and for 0.7 times critical damping in the suspension is

$$\omega_c \approx \left( \frac{\sqrt{\omega} a}{15X} \right)^{2/5} \approx 6 \text{ radians per second}$$

Since the calculated maximum and minimum allowable gyro suspension resonant frequencies are equal, the only margin for abnormal accelerations and sensor noise is associated with the conservative assumptions in the calculations. However, a 6 radian per second resonant frequency gives a margin of 36 for gyroscope displacements during normal accelerations. This margin is adequate



and there is no need to add integral feedback to increase the DC gain. The design problems in the gyroscope suspensions is fundamentally different from the other controllers. Transient response speed is crucial to protect the gyroscopes against quartz-block velocity steps caused by meteoroid impacts. The other controllers only need to respond in a small fraction of an orbit (several minutes). Their static gain requirements set their response speeds. Gyroscope suspension characteristics are given in Table 6-20.

It is desirable to provide a larger margin for abnormal accelerations and for gyroscope position sensing noise. This might be accomplished by introducing a control dead zone of about  $10^{-7}$  m. This dead zone would reduce the rms gyroscope acceleration due to gyroscope position sensing noise and would permit the use of a higher suspension resonant frequency. However, there are potential disadvantages to using a dead zone. The margins could also be increased if the suspension were made nonlinear in the sense that the gain increases with gyroscope displacement. This may be difficult to mechanize. Finally, the margins could be increased if the gyroscope position sensor noise could be reduced from the estimated value. The performance of the high voltage system should be carefully measured and extrapolated for the orbital system. All these options should be investigated.

## 6.5 COMMUNICATIONS

### 6.5.1 Requirements

Communications requirements have been derived and are listed below:



Table 6-20

## GYROSCOPE SUSPENSION SYSTEM CHARACTERISTICS

Error signal	Capacitive pick-off
Noise	$3 \cdot 10^{-9}$ meters in 2000 rad/sec
Clearance of Gyroscope	$4 \cdot 10^{-6}$ m
Allowable centering error	$2.5 \cdot 10^{-7}$ m
Forces	Capacitive plates
Controller	Position feedback with lead-lag-lag compensation
Resonant frequency	6 rad/sec
Lead break	4 rad/sec
Lag-lag break	20 rad/sec
Damping	>0.5 times critical
Static error for $3 \cdot 10^{-8}$ g low frequency acceleration	$8 \cdot 10^{-9}$ m
Jitter displacement from sensor noise	$4 \cdot 10^{-9}$ m (rms)
Jitter acceleration from sensor noise	$10^{-8}$ g (rms)
Gyro displacement for $10^{-3}$ gm meteoroid impact (once in 300 years)	$4 \cdot 10^{-6}$ m



Telemetry

## ● Digital Channels:

<u>Word length</u>	<u>No. of Words</u>	<u>Word Rate</u>	<u>Function</u>
19 bits	1	20/min	Roll position
17 bits	6	20/min	Relativity data
12 bits	16	1/min	Gyro axis & spin rate
8 bits	3	3/min	Proof mass position

- Telltales: 160 channels at approximately 1 sample per minute

- Analog: 180 channels at approximately 1 sample per minute

0 to 5 volts

0.5% accuracy

- Bit Error Rate:  $<10^{-6}$
- Time correlation with GMT:  $<0.1$  sec.
- Time correlation between data words:  $<15$  msec.
- Data Storage: Capability to store data for 110 minutes.
- STADAN compatibility including minitrack.



- Data Dump time:  $\leq 4$  minutes

#### Command

- Commands 140 discrete commands  
30 digital commands  
(12-bits ea.)
- Missed Commands  $< 1$  in 100
- Misinterpreted Commands  $< 1$  in 1000
- Spurious Command  $< 5$  in 1 year
- Operating Voltage  $< 20$  volts
- STADAN Compatible

#### 6.5.2 Subsystem Description

A block diagram of the communications subsystem which will meet the requirements given in paragraph 6.5.1 is shown in Fig. 6-37. The subsystem transmits at 136 MHz and receives at 150 MHz. Both of these frequencies are STADAN compatible.

#### Antenna

The antenna needs to be omnidirectional at both the command and telemetry frequencies because the spacecraft is not oriented with respect to the earth. Two turnstile antennas are used for command while only one is used for telemetry. The turnstiles are mounted on the end of two of the solar panels as shown on frontispiece. This is done to reduce the effect on the radiation pattern by the spacecraft body. The antennas are fed so that



each turnstile provides right circular (RC) and left circular (LC) polarized radiation patterns as shown by Fig. 6-36.

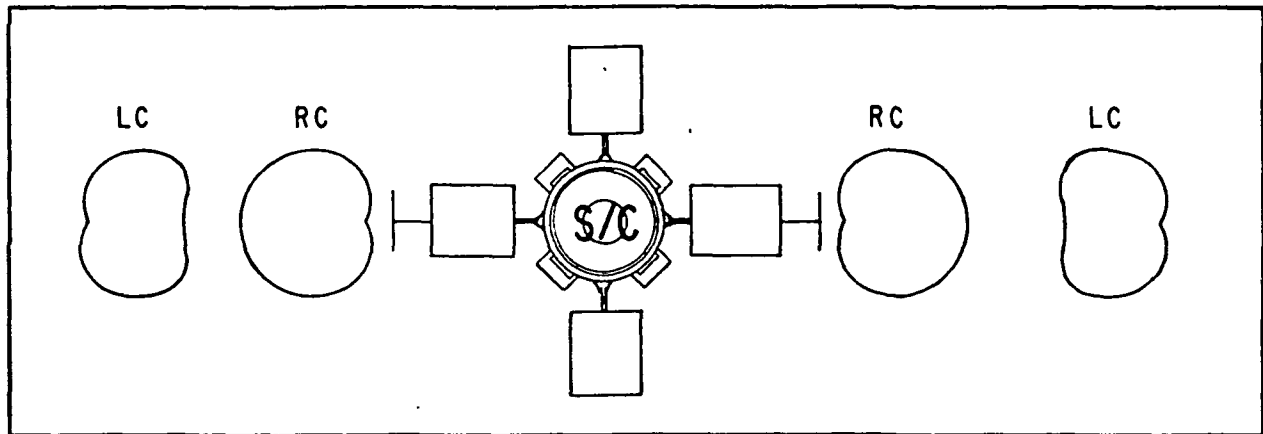


Fig. 6-36 Antenna Pattern

Only the RC radiation patterns are used for command. The antenna patterns complement one another since the null of one antenna is "filled-in" by the peak of the other. Each turnstile is connected to a command receiver. The output of each command receiver is connected to both demodulators. Commands are transmitted from the ground with a right hand circular antenna. This arrangement results in an elementary diversity system which gives spacecraft commanding capability for 100 percent of all aspect angles. The minimum antenna gain for receiving will be -10 dB. If one spacecraft receiver fails in orbit, command capability will be reduced because only one turnstile will be effective. With only one turnstile it is possible to have a null pointed at the earth. The portion of an imaginary sphere where the link margin is less than zero is about 0.5%.

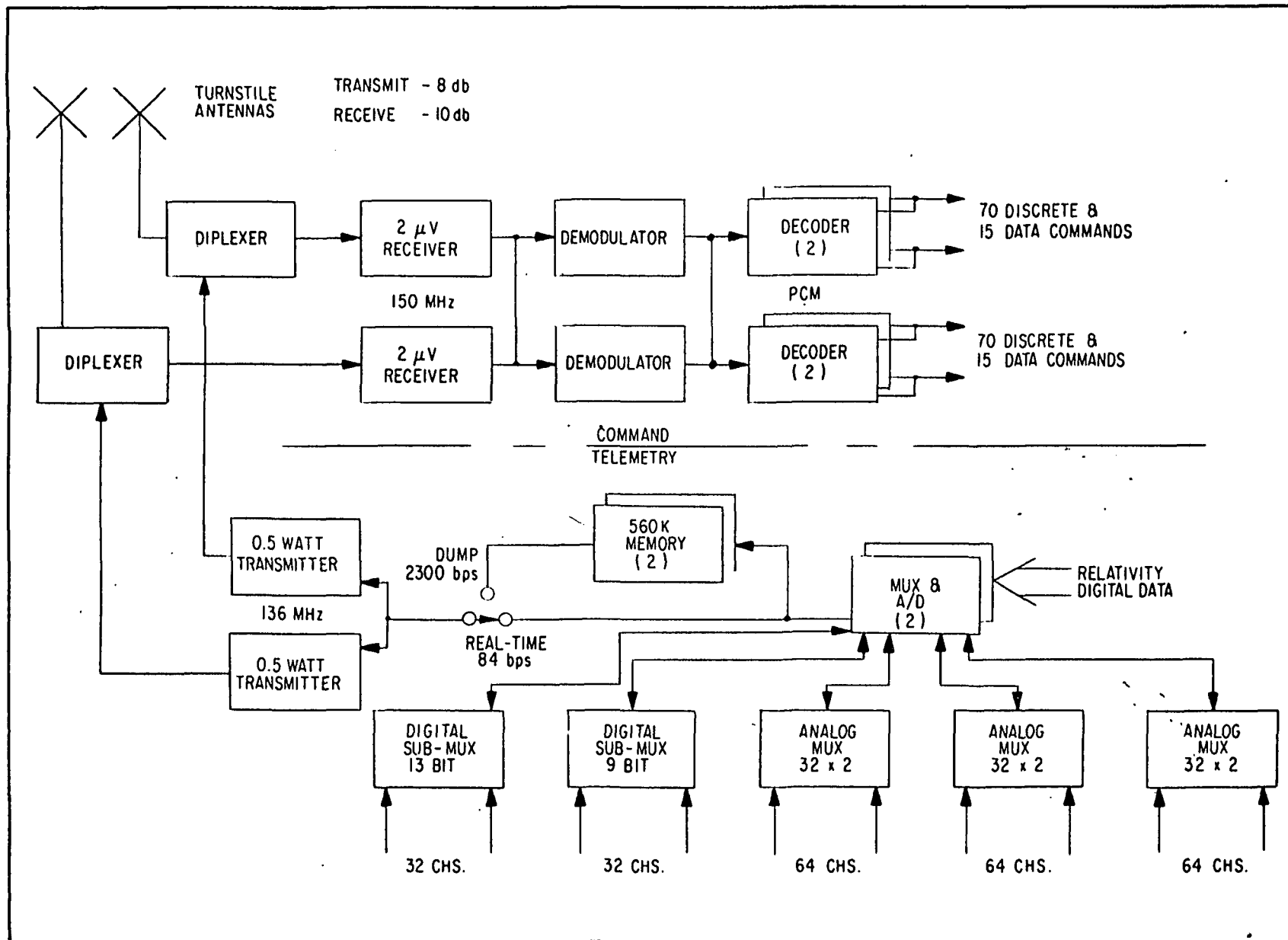


Fig. 6-37 Communication Concept



When transmitting from the spacecraft only one turnstile is used depending on which transmitter is turned "on." Both the RC and LC radiation pattern of the turnstiles are used. Telemetry transmission will be possible for 100 percent of all aspect angles because the ground station uses polarization diversity, that is, it can receive both right hand and left hand polarization. One turnstile provides omnidirectional coverage with a minimum gain of -8 dB when polarization diversity is used on the ground.

The diplexers shown on Fig. 6-37 are passive filters which allow the transmitters and receivers to use the turnstile antennas simultaneously.

Telemetry. The telemetry section shown on Fig. 6-37 consists of a 1/2 watt PM transmitter, a 560 k bit memory, a main PCM multiplexer and Analog to Digital Converter and eight submultiplexers. The transmitters, memory and main MUX and A/D are black box redundant while the submultiplexers are not. Telemetry data is transmitted at 84 bps in real-time and 2300 bps during memory dump.

The transmitters are a solid state design typical of many flown on previous NASA satellites. An isolator will be used on the output of each transmitter to provide an impedance match to the diplexers whether the transmitters are "ON" or "OFF." This is necessary for proper operation of the diplexer. This method is chosen over a coaxial relay because it is more reliable. A premodulation filter will be used at the modulation input of the transmitter to assure that RF channel bandwidth utilization is within the GSFC Aerospace Data Systems Standards. The telemetry transmitter whether transmitting at 84 bps or 2300 bps will provide enough power in its carrier frequency to do mini-track tracking.



The main multiplexer and analog to digital converter generates all of the timing signals to multiplex all data and includes an 8-bit analog to digital converter. The oscillator from which these timing signals are derived is accurate to 1 part in  $10^5$ . Primary digital data (data which occurs in every minor frame) is fed directly to this main MUX. The telemetry format is shown by Fig. 6-38. Table 6-21 gives the preliminary submultiplexer channel assignments. The minor frame length is 252 bits consisting of twenty-eight 9-bit words. The primary digital data is 17 or 19-bits in length. Two 9-bit words will be used for the 17-bit data and three 9-bit words will be used for the 19-bit data. Two 9-bit words are used for an 18-bit frame synchronization code. A high real time bit rate mode is provided to increase sample rates. The bit rate will be increased by 32 times with a discrete command. This mode would only be used for spacecraft analysis from the ground in the event a problem should occur. Storage of data during this mode would not be done.

There are two digital submultiplexers each having a length of 32. Two 9-bit minor frame words are used for one of the multiplexers. It is actually a 13-bit multiplexer because 5-bits are used to identify the sub-frame number. The remaining 13-bits are used to multiplex digital data that requires sampling at rates which are slow compared to the minor frame sample rate. Sixteen of the 32 words are used for 208 telltales. This multiplexer also includes a major frame counter. This count will occur in one of the 32 words of the sub-frame. The frame count along with the 5-bit sub-frame identification word gives a spacecraft clock which can be used to correlate spacecraft time with GMT. The other digital submultiplexer is 9-bits by 32 words in length. It is also used to multiplex slow data. Each word in the two digital submultiplexers is sampled every 96 seconds.

FRAME SYNC (18B)	L1 PITCH (18B)	L2 PITCH (18B)	L1 YAW (18B)	L2 YAW (18B)	L3 GEODETIC (18B)	L4 MOTIONAL (18B)	SPARE (18B)	ROLL POSITION (27B)	SB ID (18B)	I3B SUB MUX (9B)	SUB MUX (9B)	ANALOG SUB (9B)	ANALOG SUB (9B)	ANALOG SUB (9B)	ANALOG SUB (9B)	ANALOG SUB (9B)	ANALOG SUB (9B)
<p>NOTES:</p> <ol style="list-style-type: none"> <li>1. MINOR FRAME - 252 BITS (3 SEC.)</li> <li>2. MAJOR FRAME - 32 MINOR FRAMES (96 SEC.)</li> <li>3. BIT RATE = 84 BPS</li> </ol> <p>SUMMARY:</p> <ol style="list-style-type: none"> <li>1. RELATIVITY AND ROLL POSITION WORDS READ ONCE EVERY 3 SEC.</li> <li>2. EACH GYRO AXIS READ ONCE EVERY 96 SEC.</li> <li>3. EACH PROOF MASS AXIS READ ONCE EVERY 24 SEC.</li> <li>4. GYRO SPIN RATE READ ONCE EVERY 96 SEC.</li> </ol> <p>KEYS:</p> <p>T<sub>a</sub> = 13 TELL TALES  L<sub>a</sub> = GYRO NO. a  S = SPARE  L<sub>ab</sub> = GYRO NO. a, AXIS b  P<sub>a</sub> = PROOF MASS POSITION, AXIS a  B = BITS  FC = FRAME COUNT</p>									1	T <sub>13</sub>	L <sub>11</sub>	1	1	1	1	1	1
									2	L <sub>1</sub> SPIN	L <sub>12</sub>	↓	↓	↓	↓	↓	↓
									3	T <sub>26</sub>	L <sub>13</sub>	↓	↓	↓	↓	↓	↓
									4	L <sub>2</sub> SPIN	P <sub>a</sub>	↓	↓	↓	↓	↓	↓
									5	T <sub>39</sub>	P <sub>b</sub>	↓	↓	↓	↓	↓	↓
									6	L <sub>3</sub> SPIN	P <sub>c</sub>	↓	↓	↓	↓	↓	↓
									7	T <sub>52</sub>	S	↓	↓	↓	↓	↓	↓
									8	L <sub>4</sub> SPIN	S	32	32	32	32	32	32
									9	T <sub>65</sub>	L <sub>21</sub>						
									10	S	L <sub>22</sub>						
									11	T <sub>78</sub>	L <sub>23</sub>						
									12	S	P <sub>a</sub>						
									13	T <sub>91</sub>	P <sub>b</sub>						
									14	S	P <sub>c</sub>						
									15	T <sub>104</sub>	S						
									16	S	S						
									17	T <sub>117</sub>	L <sub>31</sub>						
									18	S	L <sub>32</sub>						
									19	T <sub>130</sub>	L <sub>33</sub>						
									20	S	P <sub>a</sub>						
									21	T <sub>143</sub>	P <sub>b</sub>						
									22	S	P <sub>c</sub>						
									23	T <sub>156</sub>	S						
									24	S	S						
									25	T <sub>169</sub>	L <sub>41</sub>						
									26	S	L <sub>42</sub>						
									27	T <sub>182</sub>	L <sub>43</sub>						
									28	S	P <sub>a</sub>						
									29	T <sub>195</sub>	P <sub>b</sub>						
									30	S	P <sub>c</sub>						
									31	T <sub>208</sub>	S						
									32	FC	S						

Fig. 6-38 Telemetry Format





Table 6-21

## SUBMULTIPLEXER CHANNEL LIST

<u>FUNCTION</u>	<u>NO. OF CHANNELS</u>
<u>Analog Channels</u>	
Solar Array Output Current	1
Unregulated Bus Voltage	1
Regulated Voltage, +28, +15, +5 VDC	4
Battery String Voltage, No. 1, 2 and 3	3
Battery String 3rd Electrode Signal	2
Solar Array Temperature	8
Battery Temperature	2
Shunt and Master Regulator Current	2
Shunt and Master Regulator Temperature	2
Command Receiver AGC	14
Electronics Box Temperature	5
Sun Shade Temperature	4
Dewar Exterior Temperature	6
Receiver/Demodulator Signal Presence Gate	2
Dewar Temperature	6
Helium Level	3
Suspension Force Status	4
Telescope Error Signal	2
Gyro Loop Heater Status	8
Spin-Rate Readout (initial)	4
Telescope Light Chopper Status	2
Electronics Turn-On Status	4
Critical Electronics Temperature	8
Critical Telescope Temperature	8
Telescope Pitch & Yaw Control Signals	2
Thruster Valve Positions	6
Gyro Pitch & Yaw Errors (night)	2
Roll Position (encoder output)	1
Servo Electronic Test Points	8
Electronic Temperatures	2
Proof Mass Position	3
Spares	63
TOTAL	192





Table 6-21 (Con't)  
SUBMULTIPLEXER CHANNEL LIST

<u>FUNCTION.</u>	<u>NO. OF CHANNELS</u>
<u>Telltale Channels</u>	
Undervoltage Switch and Bypass Position	2
Master and Shunt Regulator ON, OFF	2
Experiment Power ON, OFF	1
Battery String Open, Close; No. 1, 2 and 3	3
Transmitter ON, OFF; No. 1 and 2	2
Memory ON, OFF, record, dump; No. 1 and 2	6
PCM ON, OFF; No. 1 and 2	2
Attach Fitting Release	1
Solar Panel Release, Lock; No. 1, 2, 3 and 4	8
Liquid Level	3
Gyro Spin-up Status	4
Spin-up Pump Out Status	4
Proof Ball Release Status	1
PMT High Voltage Status	2
Star-Occulted Indicator	2
Telescope Cover Removed	2
Day-Night	1
High Pressure Pneumatics OFF-ON	1
Mode Control Switch Position	8
Star Tracker - ON-OFF	1
Rate Gyros - ON-OFF	1
Offset Generator	1
Telescope - Star Presence	1
Rate Gyros Rate-Integrating	3
Roll Rate High-Low	1
Zero-Drag ON-OFF	1
Spares	144
TOTAL	208



Six analog multiplexers having 32 channels each are provided. They will accept inputs between 0 and 5 volts. The sample rate for each channel is once every 96 seconds. An 8-bit analog to digital converter is planned in the main multiplexer even though nine bits are allocated in the minor frame. Nine-bit word lengths are chosen for two reasons: 1) GSFC Data Systems Standards prefers to use equal length words throughout the frame; and 2) nine bits turns out to be a good choice to minimize data bandwidth. If the accuracy given by a 9-bit A/D turns out to be necessary, the extra bit is available. All submultiplexers are capable of being stopped on a selected channel by ground command to effectively increase the sample rate by 32 times. The high bit rate mode will increase the sample rate an additional 32 times.

Each of the two redundant solid state memories has a capacity of 560 k bits. This is the only black box in the communications subsystem that will require significant development. A 560 k bit memory is adequate to store data for 110 minutes at the real-time bit rate of 84 bps. The dump rate is 2300 bps which means the entire memory can be dumped in 4 minutes. A random access type memory is planned for reasons given in Section 6.5.4. This mission does not require the random access capability so we will allow the memory to sequence through in a predetermined fashion. The memory would normally input and output data in parallel, so we will convert from serial to parallel at the input and parallel to serial at the output. The two memories will be alternately used so no data is lost; that is, when one memory is commanded to dump, the other memory will simultaneously be commanded to begin taking data.



The reliability allocation for the telemetry section is 0.97 for one year. The predicted reliability is 0.9659 if the non-redundant analog and digital submultiplexers are not included in the calculation. This is valid if the submultiplexer data is not critical to the mission. A complete failure of any one submultiplexer would not result in a mission failure, but could place some uncertainties on the results. For example, if the 13-bit digital submultiplexer failed, we would not have a frame counter for time correlation between GMT and spacecraft time. Instead of a complete failure, it is more likely that a submultiplexer would partially fail by losing some of the channels. Words of secondary importance such as the frame count could be multiplexed more than once in the sub-frame to improve reliability.

Command. The command section shown in Fig. 6-37 consists of two VHF-AM receivers, two demodulators, and two redundant pairs of decoders. The receivers are typical of many flown on other NASA spacecraft. They have a sensitivity of 2 microvolts for an output signal plus noise to noise ratio of greater than 10 dB. The receivers have an AGC and squelch system so the audio output will be suppressed until the received signal strength is adequate for reliable detection of the data.

The command signal is categorized as PCM/FSK - AM/AM and is consistent with the GSFC PCM/FSK Command System Standard. The initial bit modulation is PCM-NRZ. The pulse code frequency modulates a subcarrier oscillator by coherently switching this oscillator between two assigned frequencies in the 7 to 12 kHz band. A sinusoidal bit synchronization signal is 50 percent amplitude modulated onto these subcarriers. The composite signal amplitude modulates the RF carrier to a nominal 80 percent.



A complete command message for transmitting one command consists of 52 bits. Figure 6-39 shows the message format.

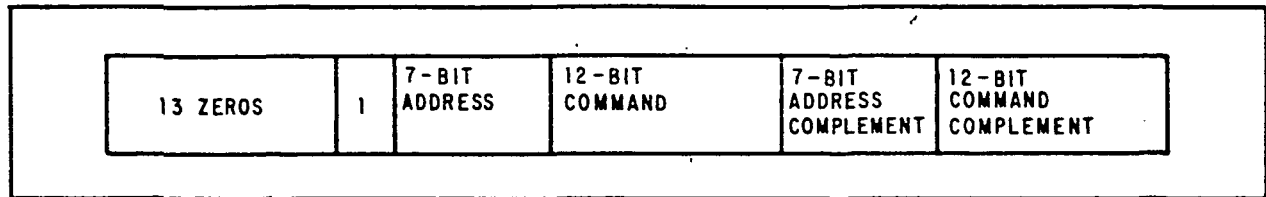


Fig. 6-39 Command Message Format

The first 14 bits of the command message are synchronizing bits. The next 19 bits are the decoder address, followed by a command word. The last 19 bits are the complement of the address and command. A valid comparison of the message and message complement is required before a command is issued by a decoder.

The two receiver outputs are cross-strapped to both demodulators in a fail-safe manner. The demodulators provide to the PCM decoders a PCM command word, a clock signal and a signal presence gate.

The decoders are quiescent until a signal presence gate is received. Each decoder is assigned an address which is contained in the command word. Each decoder will provide 70 discrete commands and 15 data commands (12 bits each). A preliminary command list is given in Table 6-22.

It is necessary that the command system be secure so that ground transmitted commands are neither missed or misinterpreted. Also spurious commands should not occur. Listed below are several features of the command system which assure command security:



Table 6-22  
COMMAND LIST

	<u>NO. OF COMMANDS</u>	
	<u>Discrete</u>	<u>Instruction</u>
Solar Panel Release Backup	1	
Transmitter ON, OFF; No. 1 and 2	4	
Memory ON, OFF, record, dump; No. 1 & 2	6	
PCM ON, OFF; No. 1 and 2	4	
Undervoltage Switch Bypass Open, Close, Set, Reset, Backup Open	5	
Master and Shunt Regulator ON, OFF	4	
Experiment power ON, OFF	2	
Battery String Open, Close; No. 1, 2 & 3	6	
Gyro Suspension Force Change	4	4
Gyro Spin-up	4	
Heat Gyro Loops		8
Spin Rate Readout Mode	4	
Proof Ball Release	2	
Pump-out Spin Gas	4	
Telescope Light Chopper Turn-on	2	
Light Shield Deploy	2	
PMT High Voltage Turn-on	2	
Amplifier and Readout Loop Turn-on	2	
Helium Heaters (Fine Control)		3
Backup Acquisition Mode	1	
Pitch Maneuver	1	
Offset Gyro Loops		8
Control System Redundancy Switching	10	
Roll Maneuver, Start, Stop	2	
Spin Rate Gain Change	1	
Spares	<u>67</u>	<u>7</u>
TOTAL	140	30



- An assigned RF channel.
- An assigned subcarrier channel.
- A 7-bit address code assigned to the satellite.
- AGC and squelch system on airborne receivers.
- Narrow bandpass of airborne receivers.
- Ground verification of command message before transmitting.
- Airborne bit by bit check of a true and complemented command word.
- Fourteen synchronizing bits at the beginning of a command message.

Further security will be provided on commands which are considered critical to the mission. One such command is the Under Voltage Switch Bypass Command (UVS-BP). We will require that two commands be sent and verified before the UVS is bypassed. To open the bypass, we will use quad-redundant commands. Figure 6-40 is a sketch showing how this is done.

The reliability allocation for the command section is 0.98 for one year. The predicted reliability is 0.9878 when redundant decoders are used.

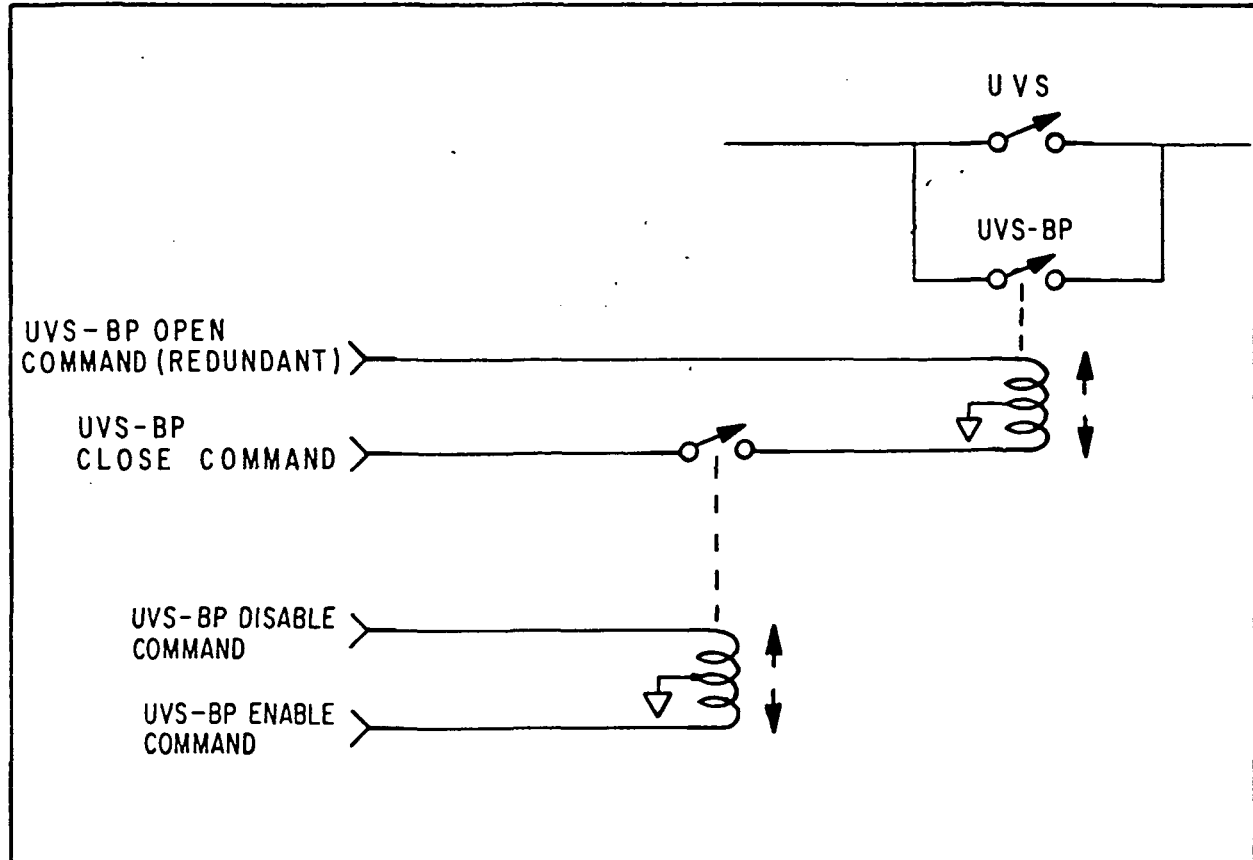


Fig. 6-40 Critical Command Method

### 6.5.3 Subsystem Performance

The performance of the communications subsystem is summarized in Table 6-23.

#### 6.5.4 Subsystem Tradeoffs

Trade-offs which were used in designing the subsystem are given below:

Memory Considerations. The memory size required is 560 K bits. This memory size is derived from the real-time bit rate of 84 bps,



Table 6-23

## COMMUNICATIONS PERFORMANCE

Telemetry

1. Frequency and channel bandwidth	136 to 137 MHz band 30 kHz channel bandwidth
2. Modulation and bit rate	PCM-PM 84 bps real-time 2300 bps dump
3. Transmitter output pwr and oscillator stability	500 milliwatts minimum 0.005 percent
4. Antenna	>-8 dB gain for all aspect angles when using right circular and left circular polarization diversity on the ground
5. Minor Frame	252 bits 3 seconds
6. Major Frame	32 minor frames 96 seconds
7. Frame Synchronization	18-bit code in minor frame
8. Digital Data Handling Capability	7 - 18 bit words at 20 words per minute  1 - 27 bit words at 20 words/min  15 - 13 bit words at 0.625 words per minute  32 - 9 bit words at 0.625 words per minute
9. Telltale Monitors	208 channels at 0.625 samples per minute





Table 6-23 (Cont)

Telemetry

10. Analog Monitors	192 channels at 0.625 samples per minute 8 bit A/D - 0.5 percent accuracy 0 to 5 volt
11. Clock Accuracy	0.001 percent
12. Clock Counter	13 bit major frame counter (218 minute recycle time)
13. Sub-frame Identification	5 bit word
14. Data Storage	110 minute storage on each memory 4 minute dump time on each memory

Command

1. Frequency	148.2 to 154.2 MHz band
2. Modulation	PCM/FSK - AM/AM
3. Subcarrier frequency	7 to 12 kHz band
4. Receiver sensitivity	2 $\mu$ V for output signal plus noise to noise ratio of 10 dB
5. Antenna	> -10 dB gain for all aspect angles when using right circular polarization ground antenna
6. Commands	140 discrete relay driving commands, 30 digital commands of 12 bits each
7. Missed Commands	less than 1 in 1000
8. Misinterpreted Commands	less than 1 in 10,000



Table 6-23 (Cont)

Telemetry

9. Spurious Commands	less than 1 in 1 year
10. Command Message	14 synchronizing bits
	7 bit address
	12 bit command
	7 bit address complement
	12 bit command complement

Power and Weight

<u>Unit</u>	<u>Ave. Power/Orbit</u>	<u>Kilograms</u>
Transmitters	2	0.9
Receivers	0.5	0.9
Decoders	0.3	3.6
Memory	6	3.6
PCM	2	2.7
Antennas	---	0.3
RF Couplers	---	1.2
TOTAL	_____	
TOTAL	10.8 Watts	13.2 Kg



the maximum time between memory dumps of 110 minutes, and a requirement that all data should be stored.

Tape recorders are usually used in satellites for bulk storage. They were not considered for this mission because of the unusually tight requirement to minimize torques on the spacecraft. Memories considered were solid state random access and sequential, plated wire random access and sequential, and cores.

A study was performed by Bellcomm Inc. for NASA concerning spaceborne memories <sup>1</sup>. Table 6-24 shows data taken from this study.

Table 6-24

560 K BIT MEMORY COMPARISON

<u>TYPE</u>	<u>Power (Watts)</u>	<u>Weight (Kg)</u>	<u>Volume (cm<sup>3</sup>)</u>
MOS Shift Register, 1 MHz	60	0.2	8
MOS Random Access, <200 $\mu$ s Cycle	5.5	0.9	165
Plated Wire Sequential, 100 kHz	0.6	3.6	635
Plated Wire Random Access, 1 $\mu$ s Cycle	25	6.8	760
Core, 2 $\mu$ s Cycle	100	9.1	1270

Cores and plated wire, random access memories are immediately discounted because of high power, weight and volume. A plated wire sequential memory consumes the least power and has reasonable weight and volume. This memory was not chosen because we

<sup>1</sup> "Future Spaceborne Memories with  $10^3$  -  $10^7$  bit Capacities,"  
B. W. Kim, Bellcomm Inc., TM-68-1031-4, July 26, 1968.



are concerned about the reliability of a sequential memory. The power requirements of an MOS shift register are high but probably could be reduced significantly because a speed of 1 MHz is not required for this mission. This leaves an MOS random access memory as our first choice. The MOS memory will have to be shielded to protect against radiation damage in-orbit. Six-tenths cm of aluminum will be adequate. This will add only about 1.4 Kg to the spacecraft, so weight is not considered a problem.

Stored Commands. The BBRC proposal for this study indicated that the need to store commands for later execution would be investigated. Our investigation has revealed that there is no requirement for stored commands. As will be seen in Section 7.2 of this report, the ground station coverage is quite good. There will be a ground station pass at least every 108 minutes. There is no requirement to command the spacecraft between these passes.

Data Compression. The BBRC proposal indicated that on-board data compression would be examined. The relativity data is integrated on board for 10 seconds which results in a real-time transmitted bit rate of only 84 bps. Since this bit rate is already so low, we do not feel that the additional system complexity which would be added by further data compression is warranted. Another reason for not considering further data compression, is the complications in the RF system that very low bit rates can cause. A very low bit rate results in modulation components falling in the loop bandwidth of the ground-based phase-locked receivers. These same modulation components can fall into the narrow bandwidth minitrack receivers. Both of these problems could be overcome but would result in additional complexity in the RF system.



Data compression could have the advantage of reducing the size of the memory. If data compression was used on the stored data, and not on the real-time data, the stored data format would differ from the real-time data format. This would make it more difficult to correlate spacecraft time with GMT. A reduced memory size is not a significant advantage unless it could be reduced to less than about 100 K bits. A reduction by this amount does not seem likely.



## Section 7 MISSION SUPPORT

In this section are discussed all phases of the satellite mission except the orbiting hardware. The main topics covered are as follows:

- Orbit and booster
- Tracking and data support
- Operations from fabrication to data reduction.

### 7.1 ORBIT AND BOOSTER

This section deals with two mission subsystems, the orbit and the booster. The orbit is treated first. Two levels of orbit requirements are treated. The general orbit requirements are those that led us to choose a 925 km circular polar orbit for this mission. Detailed orbit achievement requirements for the chosen orbit are given next. Orbit determination requirements are given in Section 7.2.4. The performance (or characteristics) of the chosen polar orbit are described in Section 7.1.3 followed by a discussion of the trade-offs which led to the selection of a polar orbit. Sections 7.1.5, 7.1.6 and 7.1.7 deal with requirements on the launch vehicle, the performance of the chosen Thor-Delta vehicle, and the trade-off considerations which led to its selection.

#### 7.1.1 General Orbit Requirements

The general orbit requirements, summarized in Table 7-1 are more in the nature of design goals for the orbit than hard require-



Table 7-1  
GENERAL ORBIT REQUIREMENTS

<u>ITEM</u>	<u>REQUIREMENTS</u>	<u>JUSTIFICATION</u>
Minimum Perigee Altitude	875 km	Limit atmospheric drag force and torque.
Maximum Apogee Altitude	1000 km	Limit trapped particle radiation dosage, limit characteristic velocity required of the booster and provide large enough relativity drift rates.
Maximum Eccentricity	$10^{-2}$	Allow relativity drift to be computed from first order perturbation of a reference circular orbit.
Inclination and Ascending Node Angles and Drift Rates	To be chosen to maximize the probability of determining the relativity drifts to the required accuracy with reasonable data reduction effort	

ments. The minimum perigee altitude is specified as 875 km. This limits the atmospheric drag force and torque to values which almost never exceed the other environmental disturbance forces and torques. The long-term average values of atmospheric drag force and torque should be as much as 30 times smaller than the solar radiation pressure force and torque. The requirement for minimum perigee altitude might be reduced to as little as 700 km before the atmospheric drag disturbance becomes comparable to other disturbances on nearly every orbit. However, for a 700 km perigee, the peak atmospheric drag disturbance during periods of high solar activity should dominate the other disturbances and might occasionally exceed the control capability provided by the normal helium boil-off rate. The advantages of a lower



perigee altitude are a slight increase in the payload capability of a given booster, a slight increase in the relativity drift rates and less radiation shielding. None of these improvements is large enough to justify lowering the minimum perigee altitude by 100 or 200 km.

The maximum apogee altitude is specified as 1000 km. This limits the radiation dosage from trapped electrons and protons to levels which do not require unusual shielding of electronic components or an unusual allowance for solar array degradation. With careful attention to shielding, the apogee altitude requirement might be relaxed to as much as 2000 km. At 2000 km, the increase in characteristic velocity required of the booster and the reduction in the amplitude of the relativity drift rates would become significant problems.

The maximum orbit eccentricity is specified as  $10^{-2}$ . This allows the relativity drift rate calculations to be based on a first-order perturbation analysis using a reference circular orbit. This is a welcomed reduction in the data processing load; however, it is not a firm requirement.

The requirement on orbit orientation and its consequent rate of change is a qualitative one. The desired orbit orientation is the one that maximizes the probability of determining the relativity drift rates to the required accuracy with reasonable data reduction effort. The orbit inclination to the equatorial plane, which should remain essentially constant throughout the mission, is the key parameter. The inclination angle determines the nodal drift rates, or rate of rotation of the orbit plane about the earth's polar axes. Nodal drift is caused by the ellipsoidal shape of the earth. No nodal drift occurs for polar orbits (those inclined  $90^\circ$  to the Equator). The nodal drift rate increases for lower inclination angles, approaching a rate of 10 revolutions





per year for orbits which are nearly equatorial. An inclination deviation of only 5 to 10 degrees (depending on orbit altitude) from polar produces a nodal drift rate of one revolution per year. A very precise polar orbit has been tentatively selected for this mission. The main reason for selecting the polar orbit is that with this orbit the motional relativity drift is at right angles to, and therefore easily separated from, the much larger geodetic relativity drift.

#### 7.1.2 Detailed Orbit Achievement Requirements for the Chosen Polar Orbit

The altitude and shape requirements of the chosen polar orbit are listed as general orbit requirements in Table 7-1. Requirements for the precision of inclination angle, and the ascending node angle, and for the allowable nodal drift are given here. Since the geodetic relativity drift is along the orbit normal and since gyroscope drift measurements can only be made at right angles to the line-of-sight to the guide-star, the orbit ascending node must be chosen to roughly align the orbit normal at  $90^\circ$  to the line-of-sight to the guide star. Crude alignment to  $10^\circ$  or so would adequately control the geodetic drift measurement error because the error is proportional to 1 minus the cosine of the misalignment angle. However, the pacing requirement on orbit plane alignment is derived from the requirement that the inertially fixed geogravity gradient accelerations of the gyroscope balls must be less than  $10^{-9}$  g. To keep the orbit-normal component of the geogravity-gradient acceleration of the gyroscopes this small, the average displacement of each gyroscope must be less than 1 cm. Since at least two gyroscopes have roll axis offsets from the satellite center of mass of at least 20 cm, the satellite roll axis (that is, the guide-star axis) must remain within about  $\pm 2^\circ$  of the orbit plane throughout the mission. To accomplish this, it is necessary to align the orbit initially



within about  $0.5^\circ$  of the line of sight to the guide star, and further, to ensure that the nodal drift during the mission does not exceed  $1.5^\circ$ . To control the nodal drift to  $1.5^\circ$  in a year, the orbit inclination must be within  $0.04^\circ$  of polar.

In addition to the gyroscope drift due to acceleration of the gyroscopes, the geogravity gradient causes a direct torque on an ellipsoidally deformed ball. This drift amounts to 0.001 arc-second per year for the expected spin-induced ball deformation and for a  $1^\circ$  offset of the gyroscope spin axis from the orbit plane. This drift is partly predictable but it is preferable to constrain the drift to a level which can be ignored. To accomplish this, the nodal drift rate must be constrained to less than  $0.5^\circ$  per year, which is difficult to achieve.

### 7.1.3 Characteristics of the Chosen Polar Orbit

Important characteristics of the chosen polar orbit are summarized in Table 7-2. The semi-major axis corresponds to an orbit altitude of 925 km. The allowable deviations in semi-major axes and eccentricity roughly constrain the orbit altitude to lie between 875 and 1000 km, as listed in Table 7-1. The eccentricity constraint further guarantees, that orbit-by-orbit application of the first order perturbation analysis derived by D. C. Wilkins of Stanford gives suitable estimates of the relativity drift. The inclination requirement is consistent with the nodal drift requirement. The apsidal drift rate (that is, the advance of the perigee of a slightly eccentric orbit) of 3 revolutions per year is primarily of academic interest. The geodetic and motional relativity drifts are approximately ramps and are approximately at right angles to each other throughout the mission. Orbit determination requirements which must be met to permit calculation of the relativity drifts to the desired accuracy are discussed in Section 7.2.



Table 7-2  
ORBIT DESCRIPTION

<u>PARAMETER</u>	<u>NOMINAL VALUE</u>	<u>ALLOWABLE DEVIATION</u>
Semimajor Axis	7300 km	±30 km
Eccentricity	0	0.009
Ascending Node	78.3° (or 258.3°)	±0.5° (initially)
Inclination	90°	±0.04°
Nodal Drift	0	±1.5° per/year
Apsidal Drift (for eccentricity ≠ 0)	3 revolutions per year	----
Geodetic Relativity Drift	6.3 arc-seconds per year along the orbit normal.	
Motional Drift	0.05 arc-second per year along the Earth's polar axis.	
Annual Starlight Aberration:		
(Earth's Polar Component)	20 arc-seconds amplitude sinusoid, once per year.	
(Orbit Normal Component)	10 arc-seconds amplitude sinusoid, once per year.	
Orbital Starlight Aberration	5 arc-seconds amplitude sinusoidal, once per orbit with the positive (or negative) 40 percent missing due to guide star occultation.	
Solar Geometry	Two seasons of "continuous" side illumination and two seasons of partly occulted front and rear illumination.	
Geomagnetic Field Geometry	Geomagnetic field vector rotates twice per orbit with polar magnitude roughly twice that at the equator.	
Geogravity Field Geometry	Geogravitational acceleration rotates once per orbit in the orbit plane which is approximately inertially fixed.	
Communication Geometry	Most orbits have usable passes over Fairbanks, Alaska with Santiago, Chile, and Ororal, Australia filling in.	
Disturbance Torques and Forces	Worst case sum nearly always less than $5 \cdot 10^{-5}$ n-m and $5 \cdot 10^{-5}$ n, respectively (about 1/10 as large as control forces and torques for average helium boil-off rate).	



The Earth's motion about the sun and the satellite's orbital motion produce starlight aberrations which are calculable based on the special theory of relativity. Starlight aberration components must be determined to 0.001 arc-second, and removed from the data in order to determine the relativity drifts to the desired accuracy. The aberration of starlight is not a purely detrimental effect because the aberration components can be used to calibrate the gyroscope drift readouts. For the chosen polar orbit, and for the tentatively chosen guide star, Rigel, the Earth's motion about the sun produces the polar and orbit-normal guide-star aberration components given in Table 7-2. In addition, the starlight of a roll-axis reference star (possibly Polaris) is aberrated. Because the perpendicular gyroscopes are used for the roll-axis control reference, the satellite does not follow the roll-star aberration. This aberration must be calculated and removed when the gyroscope roll orientation is determined two or three times during the mission.

For a perfect polar orbit, the orbital aberration of the guide-star image is along the orbit normal. This aberration is sinusoidal with an amplitude of about  $\pm 5$  arc seconds and a frequency of once per orbit. The positive or negative peaks of this aberration component are not present because the guide star is occulted for roughly 40 percent of each orbital revolution. The negative peaks are missing if the ascending node is  $78.3^\circ$  while the positive peaks are missing if the ascending node is  $258.3^\circ$ .

Other important features of the chosen polar orbit are that it is continuously illuminated by the sun for two seasons of the year. For the other two seasons, the satellite passes through the Earth's shadow for as much as about 35 percent of each orbit. Sunlight falls on the front and rear of the satellite, but never closer than about 30 degrees to the roll axis. In a polar orbit the geomagnetic field vector rotates twice per orbital revolution.



The magnitude of the magnetic field vector is roughly twice as large when the satellite passes over the poles as it is when the satellite crosses the Equator. The magnetic field vector does not rotate precisely in the orbit plane because the Earth's magnetic axis is tipped about  $11^\circ$  off its spin axis.

The line of action of the geogravitational acceleration rotates once per orbit in the orbit plane. For a polar orbit with no nodal drift, orbit-normal geogravity-gradient accelerations are inertially fixed. For a non-rolling satellite, the components can be treated independently of the in-plane gravity gradient accelerations. The worst case sum of disturbance forces and torques is about one-tenth the helium control capability.

The STADAN station at Fairbanks, Alaska, plays an extremely important role for polar orbiting satellites. Fairbanks can be used for 10 to 11 passes per day with Santiago, Chile, and Ororal, Australia, filling in on the remaining four or five passes.

#### 7.1.4 Orbit Trade-off Consideration

Trade-off considerations which led to choosing the orbit described in the Table 7-2 are summarized in Table 7-3. As discussed in Section 7.1.1, a substantial reduction in orbit altitude below 925 km is undesirable because the peak atmospheric drag disturbances might periodically exceed the control capability of the helium mass-expulsion jets. As can be seen from Fig. 7-1, reduction of 100 to 200 km is feasible because the peak atmospheric drag disturbances are only increased by a factor of 2 to 5. However, the advantages of increased relativity drift and increased booster payload capability are only a few percent as can be seen in Figs. 7-2 and 7-3.



Table 7-3  
ORBIT TRADE-OFF CONSIDERATIONS

<u>CHANGE</u>	<u>ADVANTAGE</u>	<u>DISADVANTAGE</u>
Orbit altitude reduction of 100 to 200 km	<p>Relativity drifts and booster payload capability increased by 3 to 8 percent.</p> <p>Radiation dosage decreased by a factor of 3 to 10.</p>	<p>Atmospheric drag disturbances increased by a factor of 2 to 5, and slight degradation in communication geometry.</p>
Orbit altitude increase of 100 to 200 km	<p>Slight improvement in communication geometry</p> <p>Slight reduction in gravity gradient and geomagnetic torques</p>	<p>Relativity drifts and booster payload reduced by 3 to 8 percent.</p> <p>Trapped particle radiation dosage increased by a factor of 3 to 10.</p>
Allow eccentricity $\gg 10^{-2}$		<p>Increased data reduction burden, higher peak atmospheric drag disturbances and lower relativity drift rates.</p>
Equatorial orbit	<p>Uniform solar, geomagnetic, and geogravitational geometry.</p>	<p>Motional drift not separable from geodetic drift unless prograde and retrograde satellites are flown.</p> <p>Factor of <math>\approx 2</math> reduction in booster capability.</p>
Mid-inclination orbit (for example, $30^\circ$ )	<p>Booster payload increase of about 40 percent, and solar geometry improvement.</p>	<p>Increased data reduction burden and possibility that the motional drift cannot be distinguished from the geodetic drift, to desired accuracy, and higher than desired gravity-gradient bias acceleration on gyros.</p>

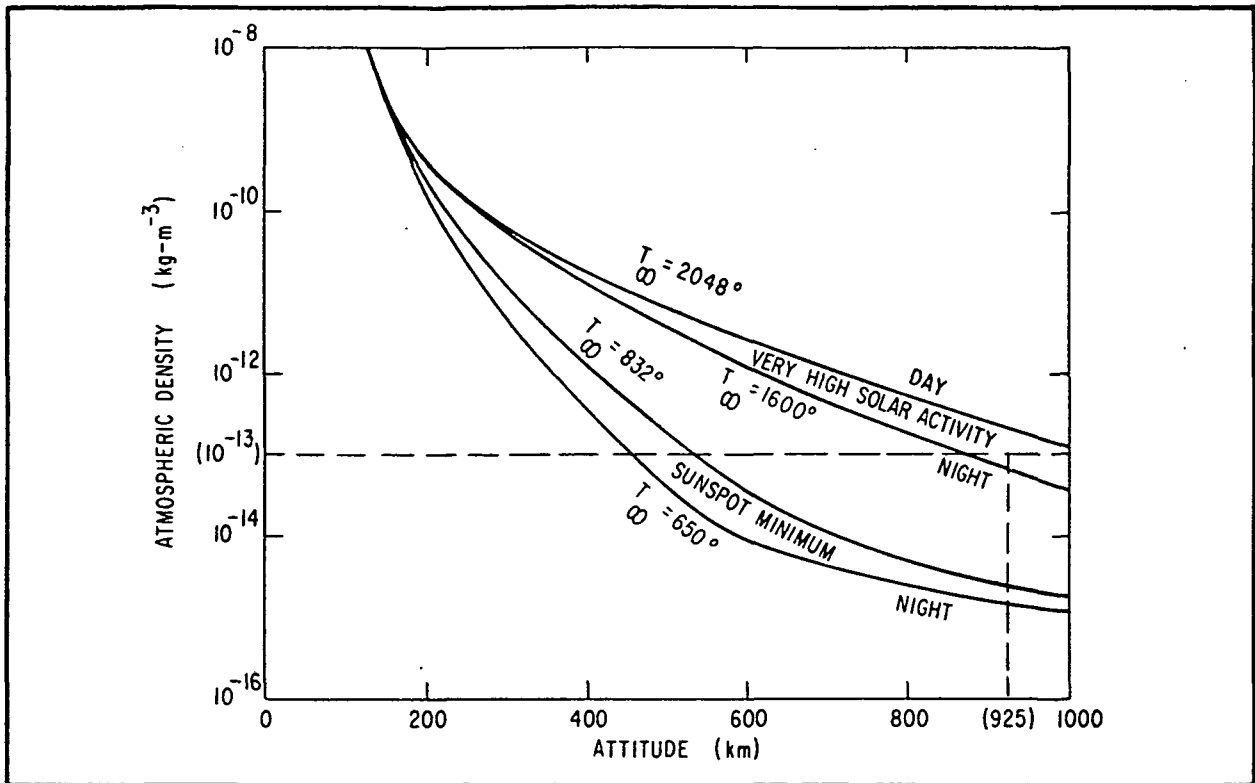


Fig. 7-1 Day and Night Density Profiles in the Upper Atmosphere

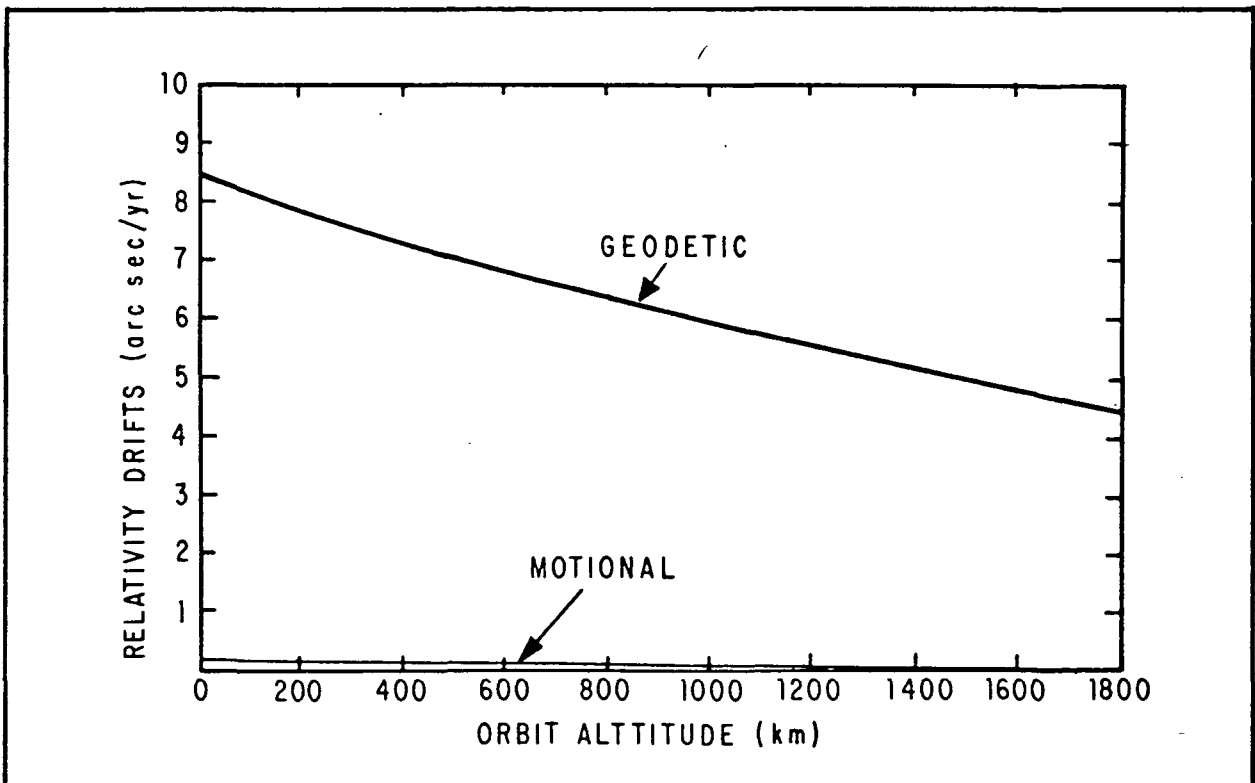


Fig. 7-2 Relativity Drift vs Circular Orbit Altitude

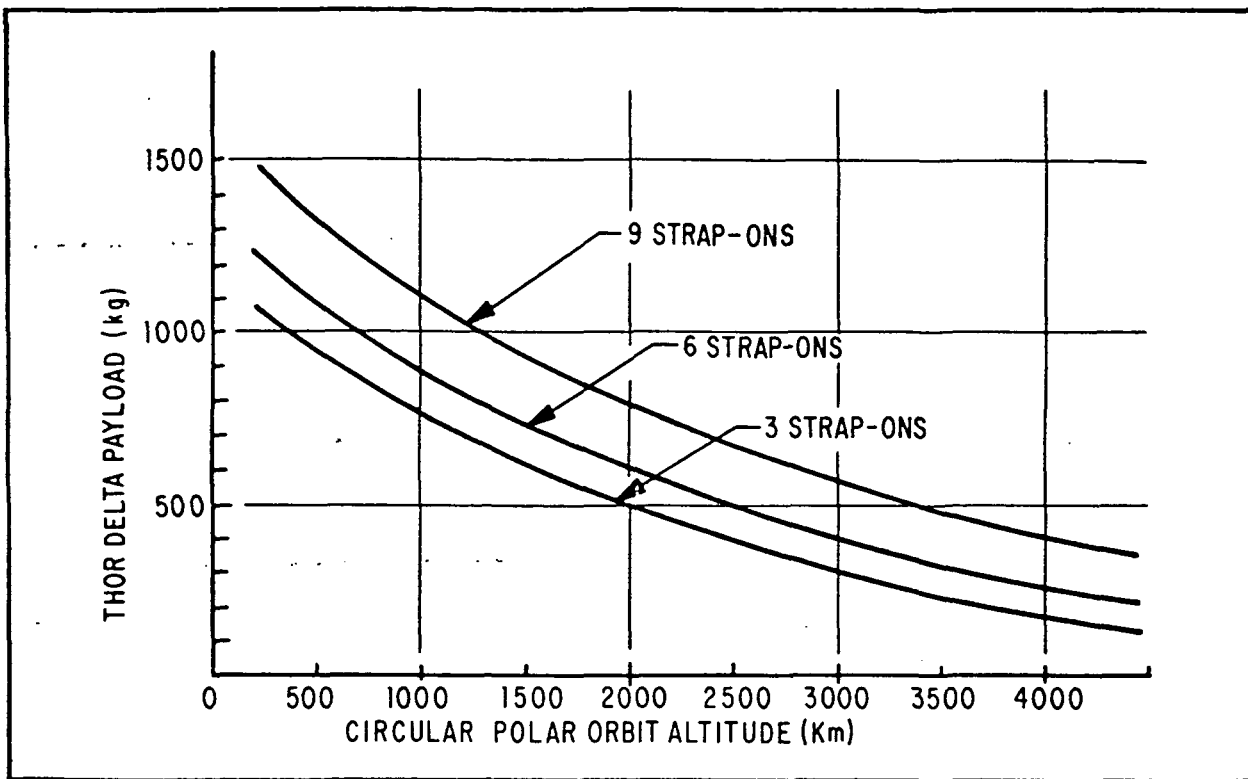


Fig. 7-3 Thor-Delta Payload Capability

A substantial increase in orbit altitude is undesirable because it could lead to a factor of 100 increase in the trapped particle radiation dosage. Figure 7-4 shows the steep rise in 0.5 MeV electrons below 200 km. An increase in altitude of only 100 to 200 km is undesirable because the relativity drifts are reduced by 3 to 8 percent (Fig. 7-2), the booster payload capability is decreased by about the same percentage (Fig. 7-3), and the trapped radiation dosage is increased by a factor of 3 to 10. The improvements associated with a 100 to 200 km increase in orbit altitude are very slight.

If the requirement on orbit eccentricity were dropped, the data reduction burden would be increased and the peak atmospheric drag disturbances would be increased or the relativity drift rate would be decreased (depending on whether apogee is higher or perigee is lower than for the chosen orbit).



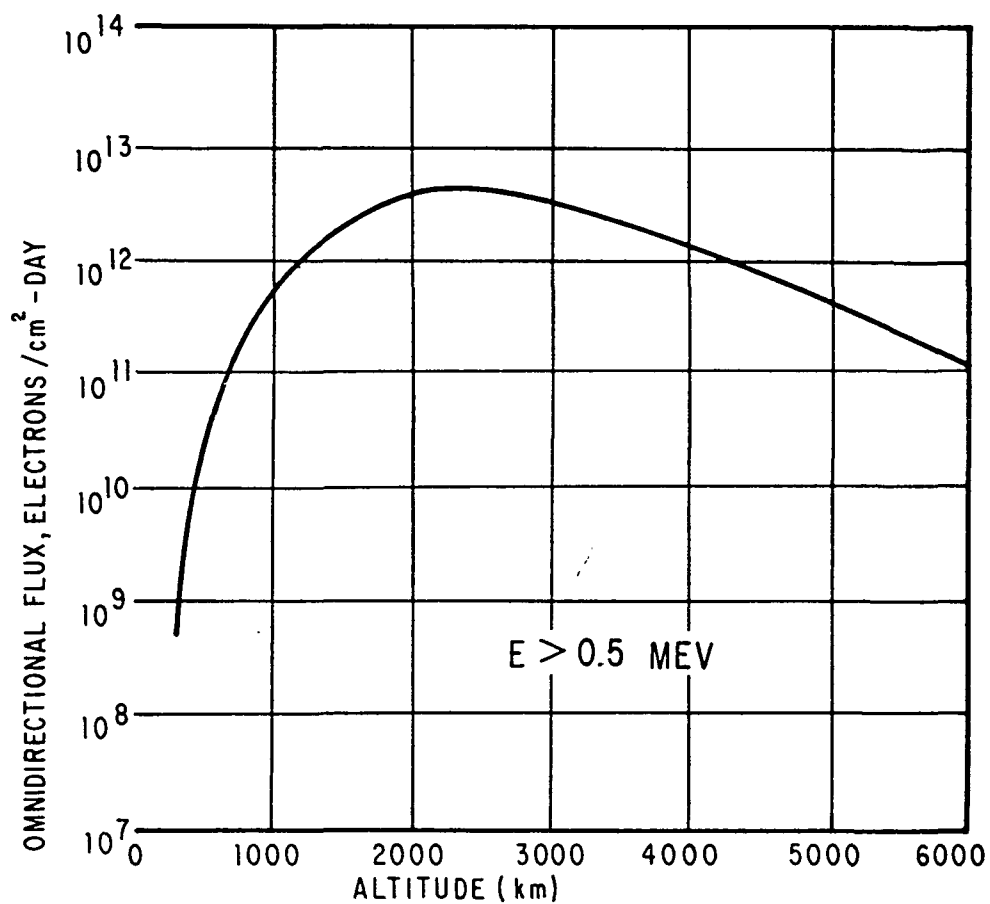


Fig. 7-4 Particle Radiation for Circular Polar Orbits



The most dramatic orbit options which were considered involve a change in orbit inclination. In a pure equatorial orbit the relativity motional drift is 2 to 3 times as large (but of opposite sense) as for a polar orbit. However, this drift is aligned with the geodetic drift and the two effects cannot be separated using data from a single flight. The booster payload capability, launching from Cape Kennedy, would be dramatically reduced in comparison to that required for a minimum energy ( $30^\circ$  inclination) orbit from Cape Kennedy or for a polar orbit launched south from either Cape Kennedy or the Western Test Range. Advantages associated with using an equatorial orbit are primarily the secondary advantages associated with solar, geomagnetic and gravitational geometry.

The disadvantage associated with using a mid-inclination orbit is that data reduction burden would be increased to the point that it is questionable whether a motional relativity drift measurement could be made. The problem for mid-inclination orbit is that the geodetic drift has a steady component along the Earth's polar axis (which is also the motional drift axis). The motional drift could only be separated from the polar component of the geodetic drift if the geodetic drift could be determined very accurately from its sinusoidal components. The advantage of using the mid-inclination orbit is that the booster payload capability is increased by a moderate amount and the solar illumination geometry is more uniform in that there are no seasons of continuous solar illumination of the satellite.

#### 7.1.5 Booster Requirements

Booster requirements are summarized in Table 7-4. The payload weight and dimension requirements leave a comfortable margin of growth from estimates for the preliminary satellite design. The requirements on characteristic velocity, inclination, and



Table 7-4  
BOOSTER REQUIREMENTS

<u>PARAMETER</u>	<u>REQUIREMENT</u>
Payload Weight	>700 kg
Payload Diameter	>2 m
Payload Height	>4 m
Characteristic Velocity	>9000 m/sec
Orbit Inclination	90°
Orbit Altitude	925 km
Orbit Injection Accuracy:	
Ascending Node	< ±0.5°
Inclination	< ±0.04°
Semi-major Axis	< ±30 km
Eccentricity	<0.009
Time from orbit injection to satellite separation	>1 hour (2 hours desired)
Satellite attitude error at separation	<0.6°
Satellite attitude rates at separation	<1 deg/sec (0.1 deg/sec desired)
Launch Window	±30 sec
Reliability	>0.9

orbit injection accuracy are for the chosen polar orbit.

The requirement that the orbit be polar makes it highly desirable to launch from the Western Test Range. Range safety considerations at the Eastern Test Range require that a dog-leg trajectory be employed for polar orbits. Such a trajectory substantially increases the required characteristic velocity.

A required orbit altitude of 925 km virtually eliminates the possibility of a "direct burn orbit injection". This remains



true even if the orbit altitude was reduced by 100 to 200 km as is discussed in Section 7.1.4 above. The alternative to a direct burn injection is a 5 to 50 minute coast in an elliptical transfer orbit followed by an "apogee kick" into the final circular orbit.

The orbit injection accuracy requirements are relatively tight, but are well within the capabilities of a number of today's inertially and radio-guided boosters. The requirement on semi-major axis accuracy could be relaxed by a factor of about 3, if necessary.

Inertial stabilization of the satellite to  $0.6^\circ$  by the launch vehicle is required for one hour following orbit injection. This requirement relaxes design requirements on the satellite's own coarse attitude acquisition system. This relatively severe requirement on the launch vehicle can be eliminated at the expense of a moderate increase in hardware for the satellite's attitude acquisition system. The requirement on satellite attitude rates at separation is another requirement which can be eliminated at the expense of added complexity of initial attitude acquisition by the satellite.

A relatively "soft and quiet ride" with respect to launch vibration accelerations and acoustic noise is desired because this might eliminate the need for the dewar's titanium launch-supports.

#### 7.1.6 Performance of the Thor-Delta Launch Vehicle

As can be seen from Table 7-5 the performance of the projected 1973 version of the Thor-Delta launch vehicle nicely fits the satellite booster requirement given in Table 7-4. Figure 7-3 shows that a 900 kg payload can be placed in a 925 km circular polar orbit using six solid strap-on rockets. A 730 kg payload



Table 7-5  
PERFORMANCE OF THE THOR DELTA LAUNCH VEHICLE

<u>Parameter</u>	<u>Performance</u>
Payload capability for a 925 km circular polar orbit	730 kg (using 3 solid strap-on rockets)
Shroud Diameter	2.2 m
Shroud Height	4.1 (5.7 m at reduced diameter)
Launch Pads:	2 at Cape Kennedy 2 at Western Test Range
Guidance System	Inertial with restartable, programmable second stage.
Orbit Injection Accuracy ( $3\sigma$ )	
Ascending Node	$<0.5^\circ$
Inclination	$< \pm 0.04^\circ$
Semi-major Axis	$< \pm 10$ km
Eccentricity	$<0.003$
Attitude error at orbit injection	$<0.2^\circ$ plus the misalignment between the Delta guidance package and the satellite
Attitude drift after orbit injection	$<0.25$ deg/hour
Attitude maintenance time after orbit injection	$>35$ minutes
Tip-off rate imparted to the satellite	$<1$ deg/sec
Probability of launch with a $\pm 10$ sec window	$>70\%$ on a given day, $>99\%$ for 1 out of 4 attempts
Projected booster hardware cost to NASA	3.5 million
Reliability	74 successes out of 82 launches. ( $R = 0.903$ )



could be placed into the desired orbit using only three strap-on rockets. With nine strap-on rockets, a payload weight of nearly 1200 kg could be accommodated. Fewer strap-on rockets are preferred because there is a slight decrease in cost, and because a softer, quieter ride results.

By folding the four solar array paddles, the preliminary satellite configuration was easily designed to the diameter and height constraints of the Delta shroud.

NASA currently maintains two launch complexes each for the Thor-Delta at both Cape Kennedy and the Western Test Range. The projected schedule for Delta missions from WTR through 1975 contains an average of four to five launches per year.

The guidance system for the projected 1973 version of the Thor-Delta is a relatively high quality inertial guidance system which will use the back-up inertial measurement unit used by the Apollo lunar excursion module and the guidance computer developed for NASA's Centaur stage. The three-sigma orbit injection accuracy of the system is well suited for this mission. The orbit orientation performance is precisely as required. The three sigma deviations in orbit altitude and eccentricity are substantially better than required.

The guidance system attitude error, one hour after orbit injection, barely meets the stated requirement, and the Delta second stage is not currently designed to maintain attitude control for more than about 35 minutes after orbit injection. It appears that the Delta can support the satellite during initial acquisition as desired; however, its capability in this area deserves further study. It is important to align the satellite with respect to the Delta guidance package to about  $0.2^\circ$ . It must also be assured that the Delta can maintain attitude control for the



required time interval. The expendables which might limit this time interval are: nitrogen attitude control gas, battery capacity, and a subliming coolant used with the attitude control computer. It appears that added quantities of any of the above expendables can be used, if required. Drift of the Delta's gyros would ultimately limit the useful attitude maintenance time interval. These drift rates must be reviewed when data on the improved Delta is available.

The quoted  $1^\circ$  per second tip-off rate that the Delta gives the satellite at separation is larger than desired. A rate of say  $0.1^\circ$  per second would simplify the satellite's initial acquisition. This lower rate could probably be achieved if the Delta backs away from the satellite instead of using separation springs. The ability of the Delta to perform this maneuver needs to be reviewed at a later stage in the program.

#### 7.1.7 Booster Trade-off Consideration

The payload capability and cost of a number of alternative booster and upper stage combinations are compared in Table 7-6. Only three booster stages are appropriately sized for this mission, the Thor, Atlas, and the Titan III. The Thor-Delta is NASA's standard vehicle for 900 kg payloads requiring 9000 meters per second characteristic velocity.

Combinations using the Agena upper stage are undesirable because the stage is expensive and the shroud is smaller than desired. The Titan/Burner and the Atlas/Centaur combinations are also undesirable because of cost. The Atlas F is attractive from the standpoint of cost, but is a refurbished ICBM with questionable reliability. Furthermore, only a limited number are currently available for use.



Table 7-6

PAYLOAD CAPABILITY AND COST COMPARISON FOR  
ALTERNATE LAUNCH VEHICLE CONFIGURATIONS

- Payload weight comparison for a 740 to 925 km circular polar orbit.

<u>Launch Vehicle Configuration</u>	<u>Payload (kg)</u>
Thor/Delta	730-1200
Thor/Agena	770
Atlas F (+ kickmotor)	730
Atlas F/Agena	2100
Atlas F/Burner II	1140
Atlas SLV-3A (+ kickmotor)	1140
Atlas (3A)/Agena, Burner	1700
Titan IIIBS/Burner II	1820
Atlas/Centaur (ETR only)	640 (dogleg)
	2270 (due South)

- Cost Comparison

<u>Launch Vehicle Configuration</u>	<u>Costs (\$ x 10<sup>6</sup>)</u>
Thor/Delta	5.6 (3.5*)
Thor/Agena	8.0
Atlas F (+ kickmotor)	2+
Atlas F/Agena	9+
Atlas F/Burner II	2.5+
Atlas SLV-3A (+ kickmotor)	5.1
Atlas (3A)/Burner II	5.1+
Titan IIIBS/Burner II	9.0
Atlas/Centaur	12.0 (10.5*)

\* Hardware cost applicable to a NASA launch.





The closest competitor to the Thor-Delta is an Atlas SLV-3A with some kind of velocity package. The only standard velocity package which currently exists for use with the Atlas is the Burner II. Burner II was developed by the Air Force and significant interface problems might be involved in using an Atlas/Burner combination for a NASA mission. The estimated cost for this combination in Table 7-6 may be optimistic. The orbit injection accuracy of the radio-guided Atlas is excellent, and the vehicle apparently gives a slightly softer and quieter ride than a Thor with strap-on solid rockets. If the Atlas, with a suitable upper stage, is used for future NASA launches from WTR, that combination would deserve serious consideration for this mission.

## 7.2 TRACKING AND DATA SUPPORT

The ground station coverage for minitrack, telemetry and command is very adequate for this mission. We will have ground station contact with the spacecraft at least every 108 minutes. The minitrack, telemetry and command link margins are also very adequate and require no special ground station equipment. Time correlation between spacecraft time and GMT will be relatively easy to accomplish.

### 7.2.1 Ground Station Coverage

Our analysis has shown that three STADAN stations (Fairbanks, Santiago and Ororal) will allow a 4-minute memory dump at least every 108 minutes. The analysis was run out for 10 consecutive days, which is adequate to cover all possibilities for one year in orbit. Figures 7-5 and 7-6 give the results of the first 24 hour period of this pass analysis. The orbit parameters used in the analysis are given on Fig. 7-6. The elevation angle above the horizon is limited to 5°.

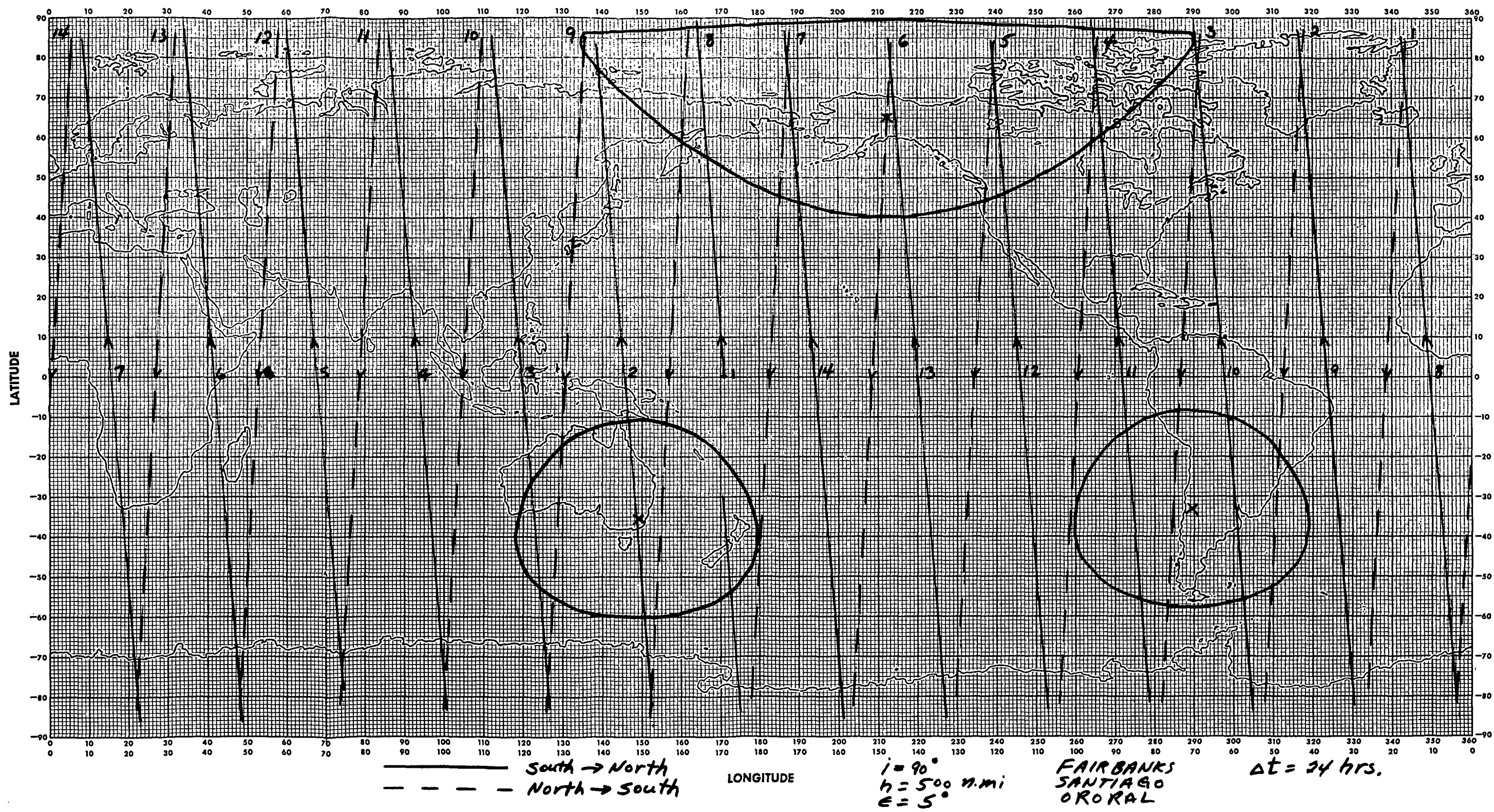


Fig. 7-5 Ground Station Visibility Plot  
7-21



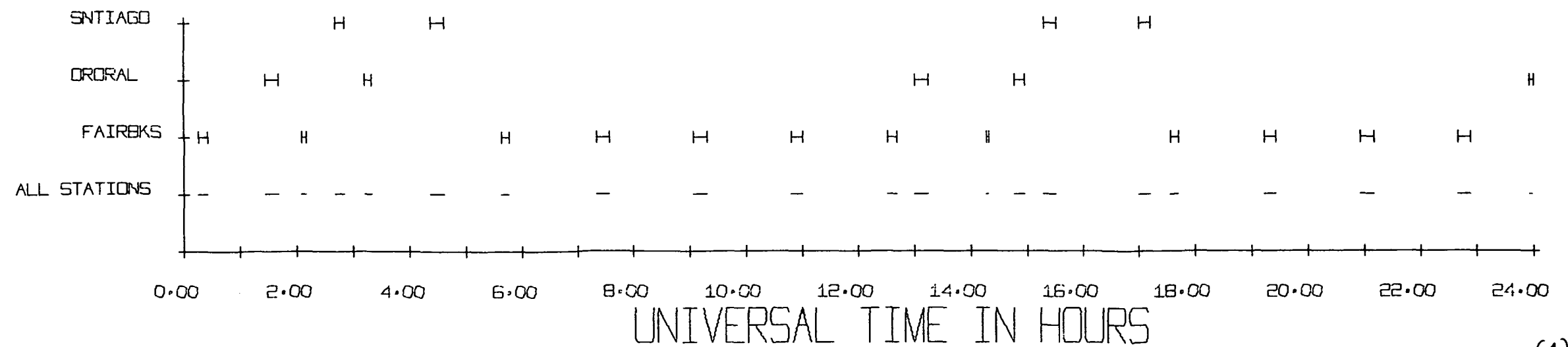
# COMMUNICATIONS TIME CHART

## ORBIT DATA

INCLINATION = 90.0000 DEGREES  
 R. A. OF NODE = 0.0000 DEGREES  
 ARG. OF PERIGEE = 0.0000 DEGREES  
 SEMI-MAJOR AXIS = 7304.1572 KILOMETERS  
 ECCENTRICITY = 0.0000  
 TRUE ANOMALY = 0.0000 DEGREES  
 ELEVATION ANGLE = 5.0000 DEGREES  
 APOGEE ALTITUDE = 500.0000 N.MI.  
 PERIGEE ALTITUDE = 500.0000 N.MI.

## COMMUNICATIONS DATA (IN HOURS)

PER CENT TIME	TOTAL TIME
3.444	0.826
3.541	0.850
8.588	2.061



(1)

Fig. 7-6 Communications Time Chart



Fairbanks will provide a memory dump for at least 10 passes per day. Santiago and Ororal will cover the remaining passes. The longest time between dumps will be 108 minutes. A dump time of 4 minutes will allow at least one minute of real-time data during each pass for spacecraft status checking and for time correlation. Occasionally, it will be necessary to dump the memory after only 20 to 30 minutes of data storage, but this will not cause any problem.

#### 7.2.2 Orbit Determination Requirements

Orbit determination requirements for the chosen polar orbit are summarized in Table 7-7. The orbit orientation (both its inclination and ascending node) must be known to 10 arc-seconds to limit the errors made in removing the effects of starlight aberration. It is possible that the starlight aberration can be deducted to the required accuracy from the form of the gyroscope output signals without the need for a priori aberration determination from tracking data. If this is true, the ascending node determination accuracy requirement might be relaxed. The determination accuracy requirement on inclination cannot be relaxed because this requirement also limits the corruption of the relative motional drift by the geodetic drift.

If errors in the a priori point-by-point determination of the starlight aberration contribute direct one-for-one errors in the relativity drift estimates, the orbital aberration of starlight must be determined to a fraction of an arc-second at each point around each orbit. This can be done only if the instantaneous satellite velocity is known to 0.5 meter per second at each point in the orbit. The 0.1 second requirement on the time correlation between telemetered and simulated data is equivalent to a 0.5 m/sec velocity when the satellite is near the poles.



Table 7-7  
ORBIT DETERMINATION REQUIREMENTS

<u>PARAMETER</u>	<u>DETERMINATION ACCURACY</u>	<u>JUSTIFICATION</u>
Inclination	10 arc-sec	Limit geodetic corruption of the motional drift to 0.0003 arc-second, limit annual aberration corruption of both relativity drifts, and allow determination of the orbital aberration to 0.0003 arc-second.
Ascending Node	10 arc-sec	Limit annual aberration corruption of the relativity drifts.
Instantaneous velocity at every point in the orbit	0.5 m/sec*	Allow determination of the orbital aberration to 0.0003 arc-second point-by-point in the orbit.
Radius and speed at some point in each orbit	300 m and 0.1 m/sec	Allow the relativity drifts for each orbit to be computed to 1 part in 20,000 from a first order perturbation analysis.
	300 m and 0.03 m/sec*	Allow the orbital aberration to be determined to 0.0003 arc-second point-by-point in the orbit from a first order perturbation analysis.
Time correlation between computed and telemetered data	0.1 sec*	Equivalent to the requirement on instantaneous velocity determination.

\* It may not be necessary to determine the orbital aberration point-by-point in each orbit. This will depend on the results of a data reduction error analysis.



Orbit injection errors and the Earth's equatorial bulge cause the satellite altitude and velocity to vary during each orbital revolution. These variations, and the variation in gravitational attraction caused by the Earth's bulge, must be taken into account if the relativity drifts are to be computed to an accuracy of a fraction of a millisecond of arc per year. If the first order perturbation analysis of D. C. Wilkins of Stanford is used to calculate the relativity drifts, then the radius and speed of the satellite must be known to 300 meters and 0.1 meter per second, respectively, at the integration starting point for each orbit. Because of error "propagation" from initial values, the velocity of the satellite must be known to 0.03 meter per second at the integration starting point in order that the point-by-point velocity error will remain within 0.5 meter per second throughout the orbit.

Several alternative procedures might be applied to reduce the telemetered gyroscope readout data to obtain relativity drift estimates. The most important alternatives involve the method used for removing the starlight aberration from the data, including use of the aberrations to calibrate the gyroscope readout signals. A data reduction error analysis should be conducted in the near future, to provide a basis for selecting among the alternative data reduction approaches.

### 7.2.3 Orbit Determination Performance

Two orbit determination systems are used by the NASA STADAN network to track unmanned satellites. The standard minitrack system is used where orbit determination requirements are moderate. A system called GRARR (Goddard Range and Range Rate) has been developed for applications where beacon tracking is not adequate. (GRARR will be used for the forthcoming NASA ERTS and Atmospheric Explorer missions.)



Minitrack performance, as applied to the meteorological satellites (improved Tyros), is adequate for this mission. This performance includes location of the satellite at each point in its orbit to 300 meters. A 300-meter cross-track satellite position error near the pole corresponds to an ascending node error of about 10 arc-seconds. A 300-meter cross-track position error near the Equator corresponds to an inclination error of 10 arc-seconds. The allowable satellite radius error is given in Table 7-7 as 300 meters (at some point in the orbit). Minitrack should be capable of determining the satellite radius at every point in the orbit to 300 meters. The average satellite speed can be determined very accurately from consecutive measurements of the orbital period. This velocity will change less than 3 meters per second during the entire year, because the satellite is controlled to follow a nearly drag-free orbit. This makes it easier to determine satellite velocity accurately enough to remove the starlight aberration based on a priori estimates.

#### 7.2.4 Link Margins

All communication links have margins which will give good performance. The telemetry link margin is +12.1 dB. The command link margin is +23.7 dB. This large margin is desirable to provide reliable command performance even when one satellite receiver channel has failed. The minitrack link margin is +5.9 dB. The calculations for these three links follow.



## TELEMETRY LINK

		<u>Remarks</u>
Transmit Power	+27 dBm	1/2 watt minimum
S/C Antenna Gain	-8 dB	Polarization diversity
Circuit Losses	-1.5 dB	
Space Loss	-144.1 dB	3041 km, 136 MHz
Polarization Loss	-1 dB	
Ground Antenna Gain	+22.2 dB	SATAN Antenna
Received Power	-105.4 dBm	
Receiver Noise Density	-164.1 dBm/Hz	10 log KT +3 dB
SNDR	+58.7 dB/Hz	
Dump Bit Rate	+33.6 dB	10 log (2.3 x 10 <sup>3</sup> )
Data Modulation Loss	-1 dB	67 ± 8° deviation
Data E/No.	+24.1 dB	Energy per bit to noise-density ratio
Required E/No.	+12 dB	10 <sup>-6</sup> BER, PSK
Margin	+12.1 dB	

## COMMAND LINK

		<u>Remarks</u>
Transmit Power	+60 dBm	1 kW
Ground Antenna Gain	+23.7 dB	SATAN Antenna
Space Loss	-146 dB	3041 km, 149 MHz
S/C Antenna	-10 dB	
Circuit Losses	-2 dB	
Received Power	-74.3 dBm	
Receiver Sensitivity	-98 dBm	for $\frac{S+N}{N} = 10$ dB
Margin	+23.7 dB	





## MINITRACK LINK

		<u>Remarks</u>
Transmit Power	+27 dBm	1/2 watt minimum
S/C Antenna Gain	-11 dB	Linear component
Circuit Losses	-1.5 dB	
Space Loss	137 dB	45° elevation, 1234 km
Ground Antenna Gain	+16 dB	Data Sys. Std. Spec. Value
Modulation Loss	-7.6 dB	67 ± 8° deviation
Received Power	-141.1 dBm	
Required Power	-120 dBm	Data Sys. Std. Spec. Value
Margin	+5.9 dB	

7.2.5 Time Correlation

There are two time correlation requirements; correlation between telemetry data words within 15 milliseconds and between space-craft time and GMT within 0.1 second. The accuracy of the space-craft timing oscillator is 0.001 percent so time correlation between the first and last word in a major frame of data will be within 1 millisecond. This is well within the requirement.

Time correlation with GMT is done as follows:

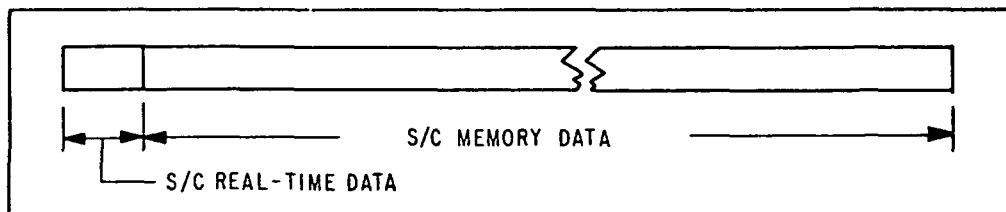


Fig. 7-9 Ground Station Tape (One Pass)

1. At the beginning of a ground station pass, allow 1/2 to 1 minute of real-time data to be recorded on the ground before commanding the satellite memory to dump.



2. GMT should be recorded on a track of the ground station recorder. The uncertainty between GMT and satellite time at this point is about  $\pm 0.015$  second. This uncertainty is made up of propagation time and equipment delays.
3. The end of the satellite memory dump and the real-time data are the same data, so this time correlation can be made without any uncertainty.
4. The uncertainty from the end to the beginning of the memory data is due only to the satellite clock. The clock is accurate to 1 part in  $10^5$ . The maximum memory dump is 110 minutes, giving an uncertainty of 0.067 second.
5. Thus, the total uncertainty is 0.067 plus 0.015 second or 0.082 second.

The spacecraft clock discussed above is a 13-bit major frame counter and a 5-bit submultiplexer channel identification word. The frame count number will change every 96 seconds. Between frame counts, the 5-bit word will provide time marks every 3 seconds.

### 7.3 OPERATIONS

The following paragraphs describe the equipment, facilities and processes required to build, launch and operate the satellite.

The operations related to the spacecraft as an orbiting platform are relatively straightforward; those related to the experiment involve more sophisticated techniques.

Special facilities and equipment are required to activate the



experiment, verify its performance, and support it during test, are as follows:

- A large cryogenic dewar for demagnetizing the experiment
- A servo-aligned artificial star source for experiment testing
- A static polar axis fixture for the complete satellite
- A vacuum station for the main dewar for use during test and prelaunch operations

It may not be economically feasible to completely evaluate experiment performance after integration into the satellite. Therefore, compromises must be made by performing less sophisticated functional tests late in the program. These tests can be arranged so that they will assure with reasonable confidence that the satellite has not degraded during environmental testing.

#### 7.3.1 Satellite Fabrication, Assembly and Test

The complete satellite consists of three main parts: the experiment, the main dewar and the girth ring to which are attached the spacecraft components. Construction of each of the main parts of the satellite proceeds simultaneously. Experience has shown that the satellite is more likely to perform properly as a system, with a minimum amount of retest or modification, if sufficient functional and environmental testing is conducted on the sub-assemblies, so that proper performance is confirmed and the likelihood of their survival under test and orbital conditions is high;



if, periodic system level tests, interspersed between environmental tests, are conducted under conditions as nearly as possible to those of operational environment, without breaking interfaces between the subsystem elements; and if fabrication, assembly and test are conducted under rigidly controlled conditions by a skilled and tightly knit team having a strong identification with the hardware.

The facilities, equipment and methods described generally here are those employed by Ball Brothers Research Corporation in building space hardware. Successful construction of the Stanford Relativity Experiment, by any contractor, will require a comparable degree of sophistication.

#### 7.3.1.1 Component Fabrication Assembly and Test

Figure 7-7 shows a typical fabrication, assembly and test sequence. This sequence involves highly specialized assembly and test operations performed under rigid control with periodic inspection, but also has flexibility for performing custom tasks such as the selection of parts and intermediate testing to achieve optimum performance.

Piece-Part Inspection. As indicated on the chart, piece part components are divided into three main categories and the level of piece part testing is adjusted accordingly: Active electronic parts are 100 percent inspected, including x-ray. They are powered if previous experience indicates infant mortality or changes in performance parameters with age. Passive components are generally sample inspected except in those cases where reject rates have been high. Non-critical parts, such as fasteners, which can be made precisely in large quantities are sample inspected. State-of-the-art piece parts or unusual components may require special testing under laboratory conditions.

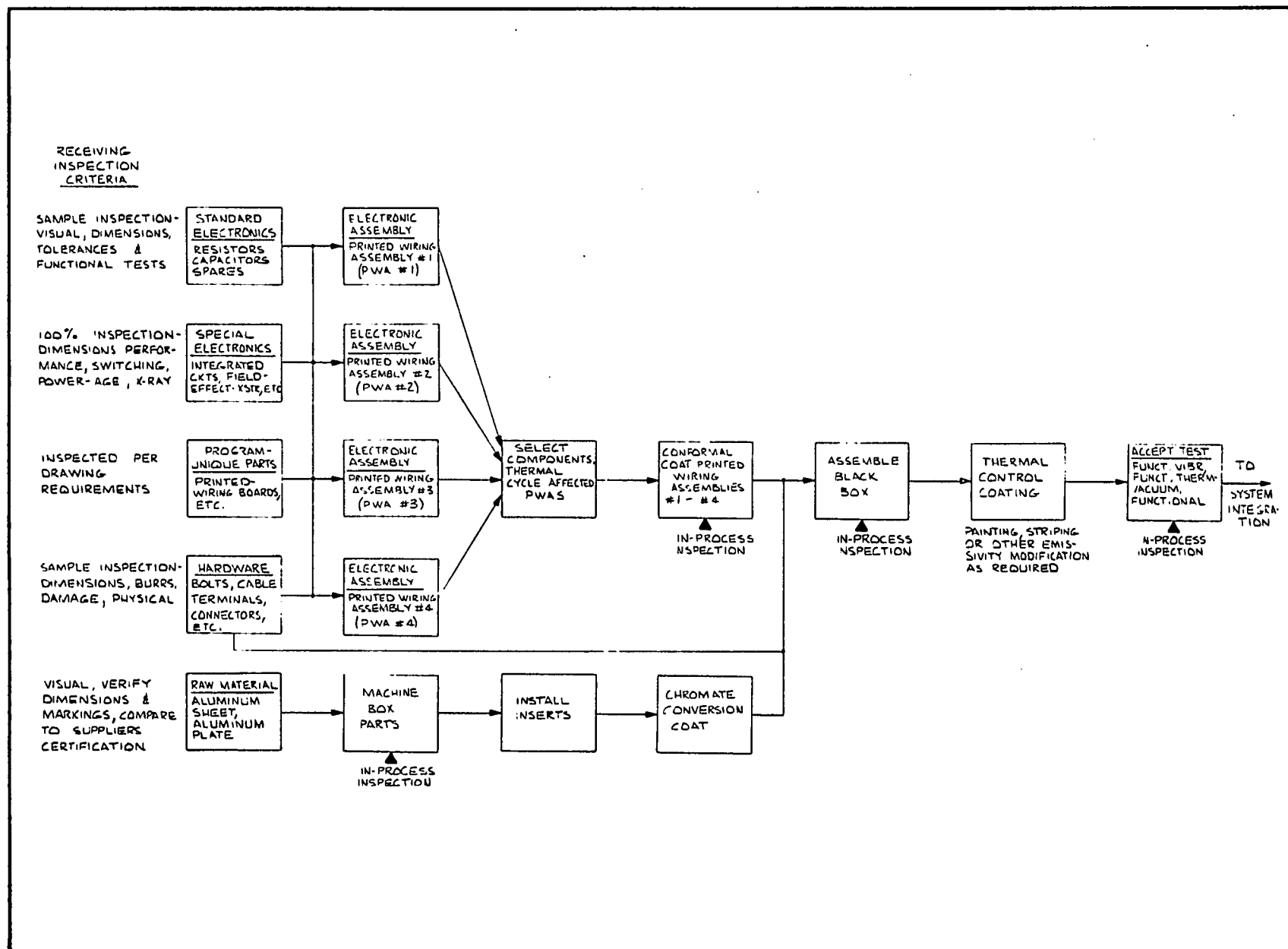


Fig. 7-7 Typical Black Box Fabrication, Assembly and Test Sequence





Electrical Assembly. These processes have been highly standardized and the inspection criteria are firmly established. Later assembly steps are performed in a clean-room environment. In-process inspection is conducted at regular intervals in the assembly processes, and if a portion of the work is to be obscured by a subsequent operation, the work is inspected prior to proceeding with the next step.

In those cases where it is necessary to select a piece part to achieve optimum performance, a test setup is provided and a selection made as early as possible in the assembly process.

Subassembly Testing. Individual electrical test fixtures are provided for the main subassemblies. These test fixtures are portable so that they can also be used during environmental testing of the subassembly. They provide power and simulate the electrical interface with the appropriate spacecraft subsystems.

After completion of the component assembly or black box, the unit is subjected to functional and performance tests to obtain baseline data and verify the performance. These tests are repeated between major phases of the subassembly testing as indicated on the flow diagram.

Mechanical Fabrication. Mechanical fabrication and assembly processes are also performed to rigidly controlled drawing requirements. The quantities involved in this size program do not justify elaborate production flow planning. Machine shop and assembly personnel are broadly skilled and qualified to perform most of the operations on a single part or assembly. In-process and final inspections are performed by independent Quality Assurance personnel. After detail parts are fabricated, they are cleaned and transferred to a clean room or assembly area.



Small subassemblies such as the pneumatics, star and solar sensors, and small cryogenic components are assembled on laminar flow Class 100 clean benches. Larger assemblies are completely assembled in a Class 10,000 integration and test clean room.

#### 7.3.1.2 Experiment Assembly and Test

As shown in the Fig. 7-8 the assembly and test of the experiment and main dewar involves five areas of activity: the fabrication and assembly of the experiment electronics, the experiment assembly containing the gyroscope and telescope, the inner dewar, the main dewar and a test support dewar.

After assembly and room temperature testing, the experiment is installed in the inner dewar. This assembly is a self-contained unit including all the optics and the end closure for the main dewar.

The inner dewar is equipped with a liquid helium reservoir which will keep the dewar cold for several hours.

The inner dewar and experiment assembly may be inserted in the test dewar during periods of inactivity. The test dewar is similar to but somewhat smaller than the flight dewar. It is equipped with external electrical harness and electronic equipment associated with the experiment.

As the experiment is assembled, the gyro alignment, gimbal suspension and telescope performance is evaluated. The equipment is then installed in the inner dewar, the entire assembly is placed in the low magnetic field environment, and cryogenically filled. From this time on, the experiment cavity must remain at liquid helium temperatures. Additional description of the low magnetic field facility is given in para. 7.3.1.5.

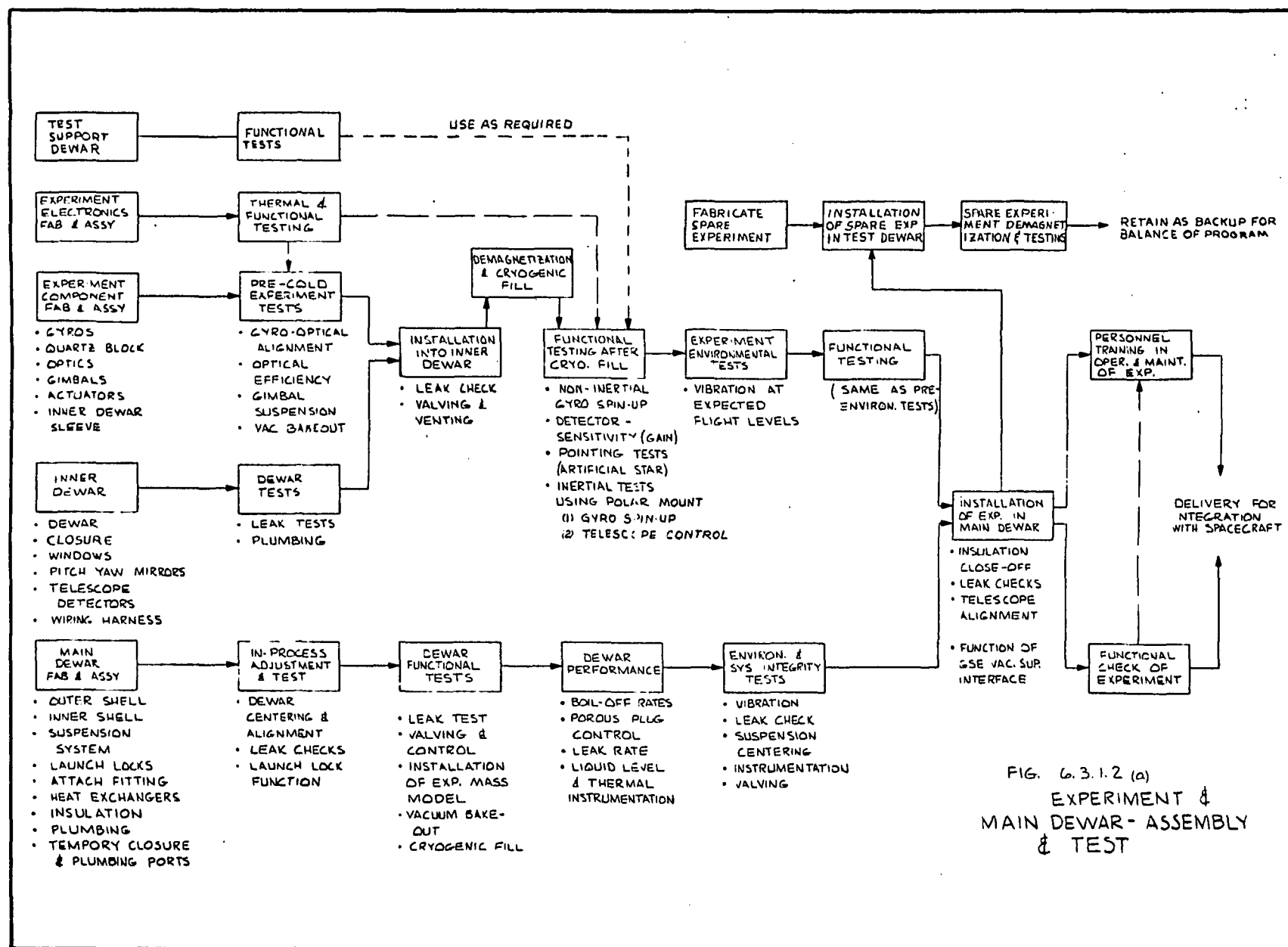


FIG. 6.3.1.2 (a)  
EXPERIMENT &  
MAIN DEWAR - ASSEMBLY  
& TEST

Fig. 7-8 Experiment and Main Dewar Assembly and Test





Several different levels of testing will be used: The telescope performance is verified during assembly prior to integration in the satellite by using a servo-aligned artificial star source. Gyroscope spin-up, stability and readout performance will be verified by orienting the experiment so that the earth serves as a rate table. Open loop performance of the experiment and satellite control system is tested using a servo-controlled artificial star source with the satellite installed on a static polar fixture. A lens cap source is used for qualitative testing of the telescope. Transfer function or block testing of electronics is performed by observing response to injected signals.

Experiment Alignment. It is desirable to have a simple method of periodically verifying basic experiment alignment during the environmental test problem. Figure 7-10 shows how the alignment between a reference surface on the quartz block and the telescope optical system is verified by using an autocollimating alignment telescope.

Alignment is indicated when the reflected image of the autocollimator target (cross-hairs) is coincident with the image of the experiment roof prisms. Using this method and performing several readings, it should be possible to verify perpendicularity of the telescope axis with the quartz block to within an arc-second.

Telescope Performance Testing. The linear range of the telescope is about 0.05 arc-seconds. To test the experiment telescope performance, it is desirable to have a target with stability approaching the noise level of the system, or 30 milliarc-seconds. Fairly good results would be obtained with a source stability of 50 milliarc-seconds. The source should have this stability over a one-hour period so that instrument drift or instability could be detected. These requirements cannot be met using actual stars as

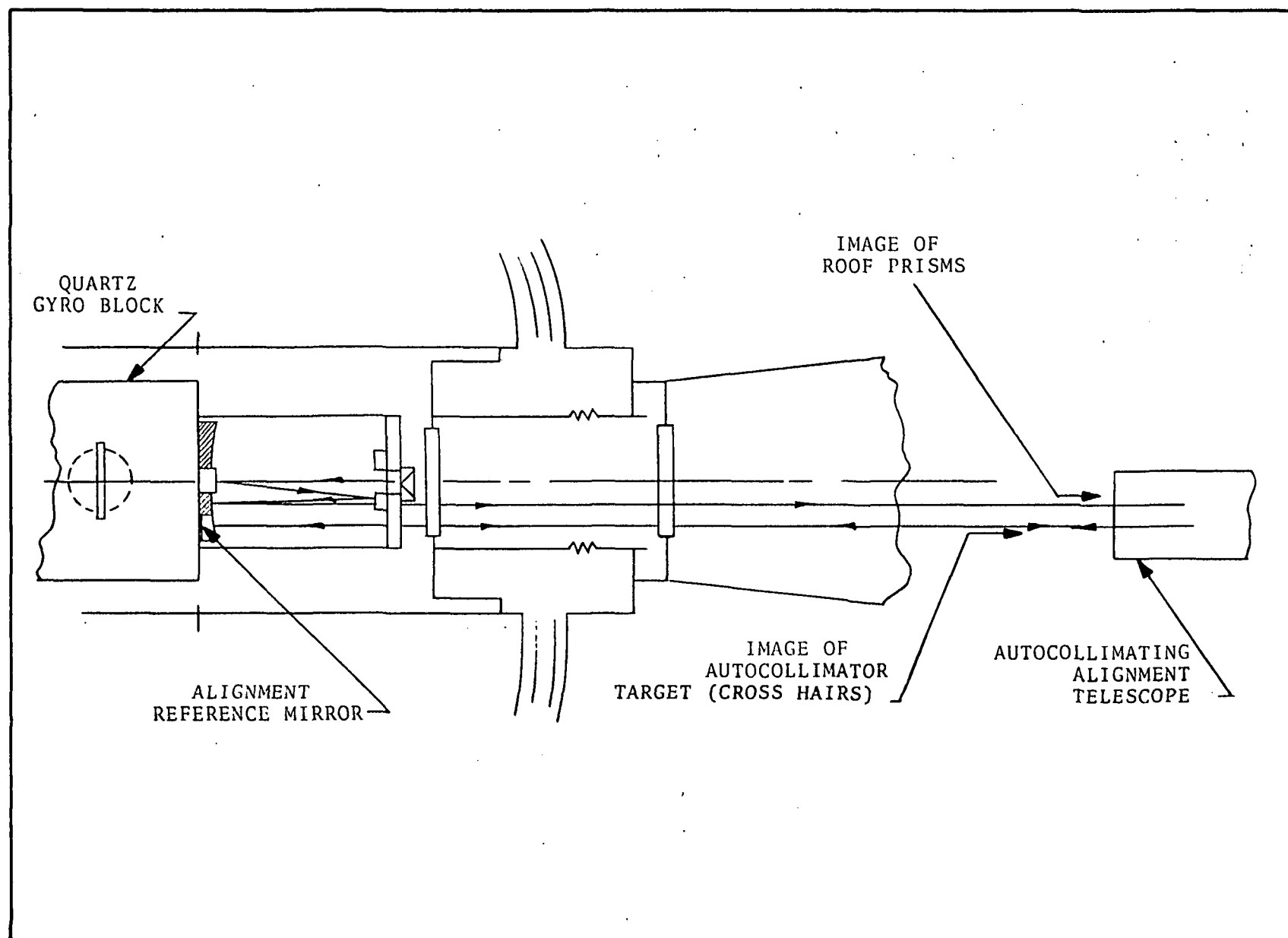


Fig. 7-10 Verification of Optical Alignment Using Autocollimating Telescope



targets. Atmospheric shimmer, even under the best conditions, would be greater than 1 arc-second and frequently 3 to 5 arc-seconds. Therefore, even with a perfect inertial fixture, completely isolated from seismic effects, the target noise would exceed the telescope system noise level by a large factor.

The artificial star source described in para. 7.3.1.4 eliminates atmospheric shimmer and minimizes other instabilities. It uses servo-control similar to the experiment telescope system to provide automatic alignment with respect to the inner dewar.

This source is used for initial telescope testing on either a horizontal slab or with the experiment and source inertially positioned on a static polar fixture, described later.

PAMITS Testing. It is also desirable that some kind of closed-loop testing be done on the complete experiment/satellite control system. One concept thought earlier to be useful was to perform a simulation by installing the experiment and control hardware in the Polar Attitude Mounted Inertial Test Stand (PAMITS) described in para. 7.3.1.5. This fixture directs the experiment toward fixed stars in response to signals generated by the experiment telescope, and conditioned by external compensation, to produce a response similar to that of the satellite when in orbit.

Because of the presence of atmospheric shimmer and the severe requirements on stability there is some question as to the usefulness of the PAMITS fixture with a real star. However, tests using an artificial star may be of value.

Environmental Tests. The experiment assembly is subjected to vibration testing at the levels expected during subsequent testing and launch. This vibration test assures that the workmanship and basic stability of the experiment are adequate, so that it



can be installed in the main dewar with a good likelihood of proper operation subsequently. Following the vibration tests, the functional testing of the experiment is repeated.

Main Dewar. The main dewar is equipped with a temporary closure, pumping ports and experiment mock-ups, so that the performance of the dewar valving and cryogenic control may be completely evaluated before installation of the experiment. Leak checks and verification of the instrumentation, are performed during and after the dewar assembly.

When proper operation of both the dewar and the experiment have been confirmed, the experiment will be transferred from the test dewar to the main dewar, and the final insulation close-off completed. This will be followed by a second set of leak checks, alignment measurements and verification of the interface with the vacuum support equipment.

During the post environmental functional testing, the personnel who will be handling and operating the experiment and dewar during spacecraft operations will be given instruction and training. A description of the dewar vacuum support station is given in para. 7.3.1.4.

#### 7.3.1.3 Spacecraft Fabrication and Test

The fabrication, assembly and test of the spacecraft girth ring and associated components can be accomplished using straightforward methods. The girth ring will be installed on a dummy dewar, and spacecraft subsystem testing will be performed as shown in Fig. 7-11 prior to integration with the actual dewar. The operation will be substantially simplified when it is not necessary to use the dewar support equipment. Some of these tests will be performed using a fixture to simulate the interface with the

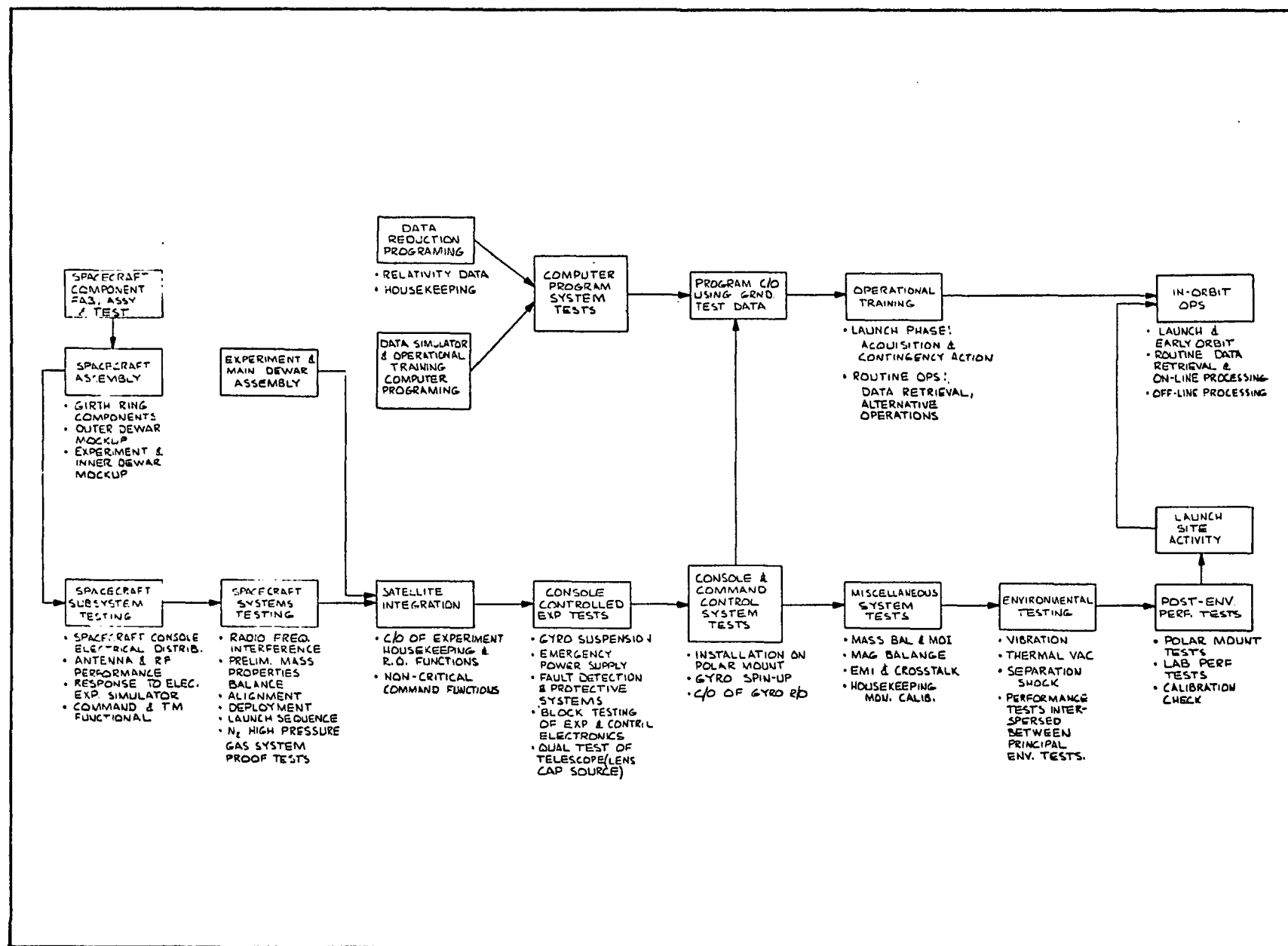


Fig. 7-11 Satellite Integration and Test Sequence



experiment. The transfer functions of various subsystems can be evaluated, however, and many functions not directly related with the experiment such as deployment, launch sequence, communication system and high pressure gas system checkout can be performed.

After mating with the flight dewar and experiment, the satellite system will undergo functional checks to assure that the command and instrumentation readouts and the fault detection and protective functions operate properly. The subsystems will be given "block" or transfer-function tests to assure that the interfaces are correct.

Experiment-Control System Testing. Following functional tests, the entire spacecraft will be mounted on a nonrotating polar fixture, described in para. 7.3.1.4, for all-up systems testing. The purpose of these tests is to prove that the experiment pointing control in the flight-ready condition works properly as an open-loop system. Detailed quantitative performance evaluation will have been done during earlier stages of testing. The polar fixture positions the satellite so that the earth rotation is around the roll axis and essentially removed from the other axes.

The satellite roll position can be changed during gyro spin-up so that misalignment errors are minimized. The target for the experiment telescope is an artificial star source described in para. 7.3.1.4. The star source is self-aligned by its own servo system which makes it possible to inject offset signals to evaluate the response of the experiment and control system.

The behavior of the control loops can be monitored electrically and the data generated can be processed through the telemetry link and ground data reduction system.



This is still an open-loop test in that the position of the spacecraft is not changed in response to telescope or gyroscope error signals. The function of the proportional thruster control valves is verified by monitoring poppet position. The position-to-thrust transfer function for the valves, derived during engineering testing, can then be used to infer the dynamic response of the satellite.

A possible refinement which should be considered would be to use valve position data and the valve-thruster transfer function to derive attitude errors with which to drive the star source.

Magnetic Balance. The spacecraft will be balanced magnetically so that the residual dipole is less than 200 dyne cm per gauss. This is sufficiently low to prevent unwanted drift, due to reaction with the earth's field in-orbit. This level of dipole moment is easily obtainable, using presently available equipment. If necessary, magnetic balance can be performed on the dewar-experiment and spacecraft before satellite integration.

Mass Balance. The spacecraft will undergo mass balance and center of gravity measurements using presently available equipment. Because of the wind resistance of the solar panels, it will be necessary to replace them with simulated masses during balancing.

Some attention will be required in the fabrication and assembly of the dewar and experiment to assure that the experiment proof mass and helium cavity centroid are reasonably close to the figure axis of the spacecraft. Preliminary calculations show that it will be necessary to align the vehicle attach fitting and the main dewar cavities during fabrication to prevent excessive shift in the center of mass with helium usage. Figure 7-12 shows the various contributions to a change in the center of mass location.

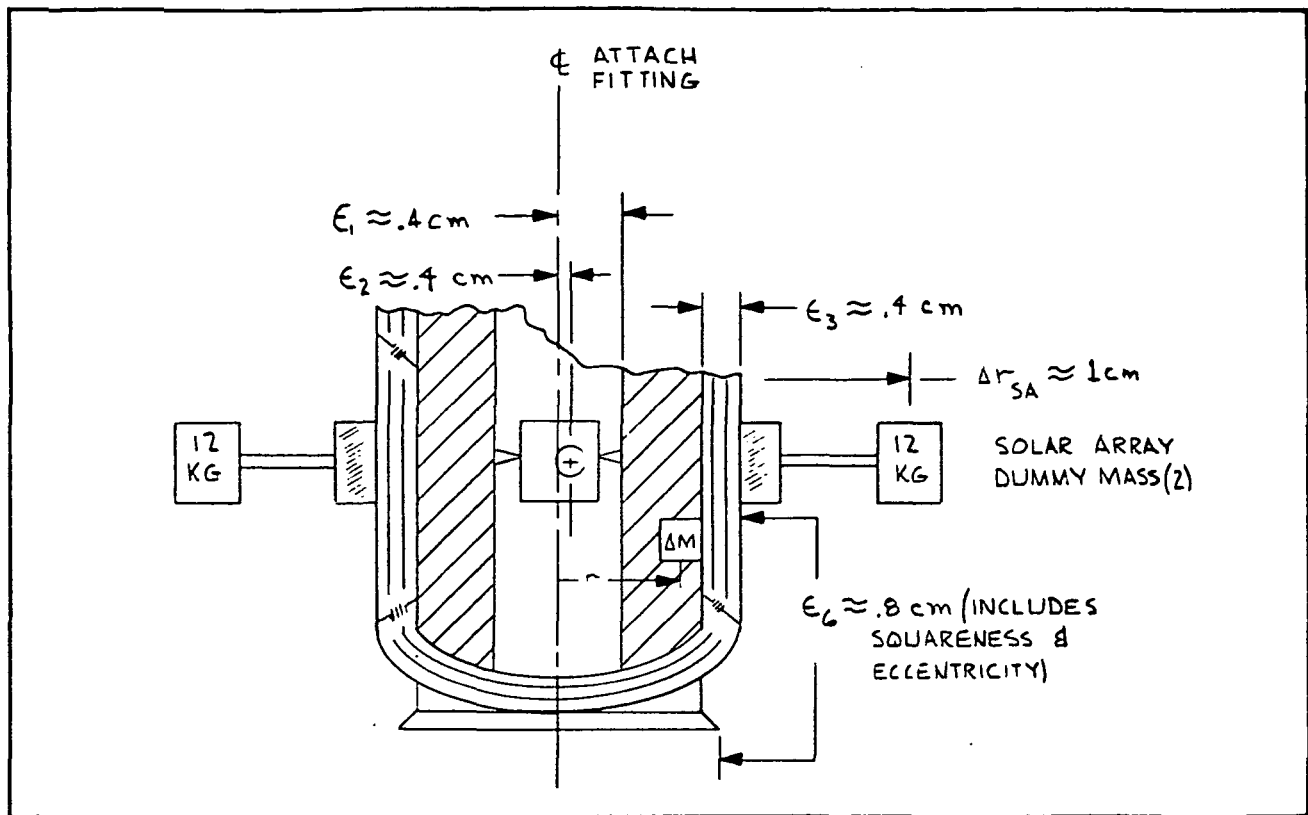


Fig. 7-12 Centering Errors Affecting Center of Mass Location

Table 7-8 shows the offset resulting when routine balancing techniques are used after the dewar has been assembled with the inner shell and experiment cavity centered reasonably well with respect to the attach fitting. This offset falls within the 1 cm static balance requirement.

Similar restraints are needed on squareness and parallelism of the dewar shells to achieve adequate dynamic balance. Table 7-9 shows the contributions to dynamic imbalance and the RSS dynamic balance errors immediately after launch and at the end-of-life when the helium is depleted.

The most difficult contribution to control is the uncertainty in the position of the solar array panels.





Table 7-8  
STATIC BALANCE-CENTER OF MASS LOCATION ERRORS

	Radial Distance from Attach Fitting Centerline	Mass	Moment Change
Helium	$\epsilon_3 + \epsilon_6 = 1.2 \text{ cm}$	136 kg	(1.2) kg-mtr
Exp. Cavity Filled with "Not Helium"	$\epsilon_1 = .4$ $m = 60$	20 $\Delta m = 0.5$	(.08) 0.3
Solar Array Dummy Mass (2 Panels)	$\Delta r_{SA} = 1$	24	2.4
Ground Test Static Balance Accuracy			.1
Static Bal Un- certainty At Launch (Worst Case)			<u>2.8 kg-mtr</u>
Corresponding C.M. Offset (600 kg)			.48 cm
Uncertainty of Proof Mass Loca- tion - $\epsilon_2$			.4
Expected Offset of Proof Mass from C.M. at Launch (Worst Case)			<u>.88 cm</u>
Expected Offset at Helium Depletion (Worst Case)			1.09 cm



Table 7-9  
DYNAMIC BALANCE ERRORS

	<u>Location</u>		<u>Mass</u>	<u>Dynamic Imbalance</u>
	X	Z		
Non-Repeatability in Position of Solar Panel No. 1	2 m	±0.1 cm	10 kg	0.2 kg
Non-Repeatability in Position of Solar Panel No. 3	2	±1	10	0.2
Helium (Empty Dewar -vs- Full)	2° runout of outer dewar shell W.R.T. Fig. Axis (.4)			
Helium-Flow from Distribution Control Cells	0.5	0.7 m	±0.5	0.17
Dynamic Balance Accuracy				0.1
• RSS Error - Start of Life				<u>0.35 kg-m<sup>2</sup></u>
Requirement (During 0.2 rpm Gyro Spin-Up)				0.4
MARGIN				<u>0.05</u>
• End-of-Life (Dewar Empty)				0.75
Requirement (Rolling at 0.2 Rev/Hr)				1 to 10 kg-m <sup>2</sup>



The accuracy with which balance adjustments can be made is considerably better than that given in the Tables. The uncertainty has been increased to allow for possible error introduced by not having the dewar completely filled during balancing.

Data Reduction Programming and Operational Training. During the assembly of the flight spacecraft, the required programming for off-line and on-line data processing will have started. The data generated during system testing will afford an excellent opportunity to check out the data programming and operational procedures. A description of the data processing sequence and facility requirements is given in para. 7.3.3.

Environmental Testing. The entire satellite will undergo environmental testing at the levels expected during launch and in orbit. Vibration testing consists of both sinusoidal and random excitation on all three axes of the spacecraft. Thermal vacuum testing verifies the transfer or block function of the various experiment and spacecraft systems, using externally-generated signals injected at key points in the instrumentation and control loops. The temperature range will be that expected at the outer surface of the dewar. The prototype spacecraft will have undergone thermal testing using local heaters to achieve most of the expected gradients on the satellite, and therefore, a complete thermal test will not be necessary on the flight satellite.

Before shipment to the launch site the spacecraft will again be installed on the polar mount for all-up system testing.

#### 7.3.1.4 Support Equipment

The requirements for ground support equipment are listed in Table 7-10. Most of the items are straightforward and in many cases the



Table 7-10  
SYSTEMS TEST EQUIPMENT

Special Test Equipment

Lab Dolly, Dewar/Satellite	Mount for Satellite in Vacuum Chamber
Lifting Harness, Dewar	Command Encoder and Transmitter
Shipping Container, Dewar/Satellite	TM Synchronizer and Decommulator
Mechanical Mockup, Dewar	Mass Balance Machine
Electronic Simulator, Experiment	MOI Measurement Fixture
Lab Dolly/Solar Fixture, Spacecraft	Vehicle Attach Fitting and Clamp
Checkout Console, Satellite	Artificial Star Source
Adapter-Attach Fitting	Lens-Cap (Qualitative Response) Source
Adapter-Attach Fitting to 18"	
Vacuum Maintenance Station, Portable	Polar Mount
Hi Pressure N <sub>2</sub> Service Cart	Spacecraft Simulator
Vacuum Chamber Feedthrough, Auxiliary Pumping	Closure Hat, Dewar
	Temporary Outer Dewar

Commercial Equipment

Ultec CFR Sorption Roughing Pump  
 Leak Detection Equipment  
 Theodolite with Autocollimator  
 Precision Levels  
 Other Electronic Test Equipment  
 Contamination Monitoring Equipment  
 Thermal Surface Measuring Equipment



fixtures and test equipment used for satellites of similar size can also be used on the satellite when equipped with the proper interface adaptors. Ground support equipment items peculiar to this satellite are described in the following paragraphs.

Satellite Checkout Console. This portable unit includes the power supply, battery charger, and controls necessary to turn on and operate the satellite subsystems. Readouts are provided for the basic modes and primary housekeeping points, so they can be read out without using telemetry, if desired. The same console is used for initial spacecraft checkout, monitoring during environmental testing, and during prelaunch preparations.

The console will be equipped with a storage battery bank for use during gyroscope spin-up when the spacecraft batteries are not usable. Using a battery supply protects against damage to the gyroscopes which could occur if power to the suspension system is interrupted.

Vacuum Support Unit, Pumping Hat and Vacuum Feedthrough. Figure 7-13 shows the schematic for the portable vacuum support equipment for the dewar. These vacuum systems exhaust the dewar jacket, the experiment cavity, the gyro spin-up exhaust port, and the porous plug or boil-off vent.

An individual ion pump is used to hold vacuum in the dewar jacket. An external connection is provided for connection of a sorption roughing pump during bake-out and initial evacuation.

Vacuum is held in the experiment cavity and gyro exhaust system by a second ion pump. During gyro spin-up the high volume system consisting of a mechanical pump and Roots booster is used to evacuate the experiment cavity.

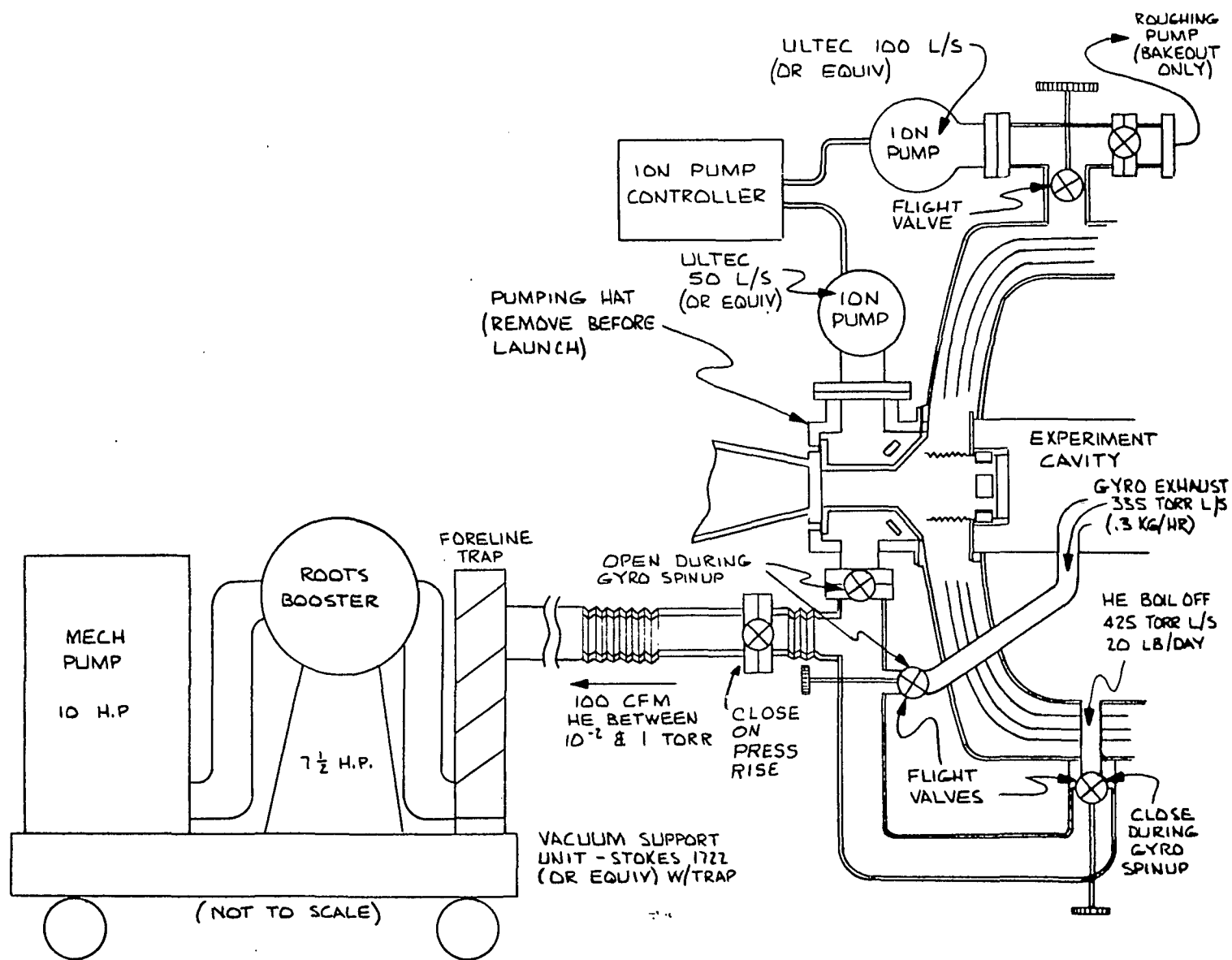


Fig. 7-13 Vacuum Support Unit



Connections to the experiment cavity are made via a temporary pumping hat installed behind the light shield. This pumping hat and the two ion pumps will be attached to the spacecraft until just before launch.

The Roots blower is also used to exhaust the heat exchanger and porous plug system.

Ion and sorption pumps were selected instead of diffusion pumps to minimize the possibility of back-contamination which can occur due to operator errors or pumping system failures. Also, the ion pumps make short, large ports feasible and fewer high-vacuum valves and manifolds are required.

The entire pumping system will be mounted on a portable cart usable in the lab, environmental test areas and on launch stand.

During thermal vacuum testing, the exhaust ports will be fed through a bulkhead fitting to the pump unit located outside the chamber.

Polar Mount. Figure 7-14 shows a fixture for testing of the complete satellite while pointing at an artificial star source. The spacecraft is positioned with the telescope axis parallel to the polar axis of the earth. Therefore, the earth rate is removed from one axis of the gyros and is introduced almost wholly into the other axes.

The attach fitting mount is equipped with a spindle so that the roll position of the satellite can be changed, as necessary, during gyro spin-up to minimize spin-up alignment errors.

Some instability will exist in the dewar suspension and in the satellite structure itself. The effects of these instabilities

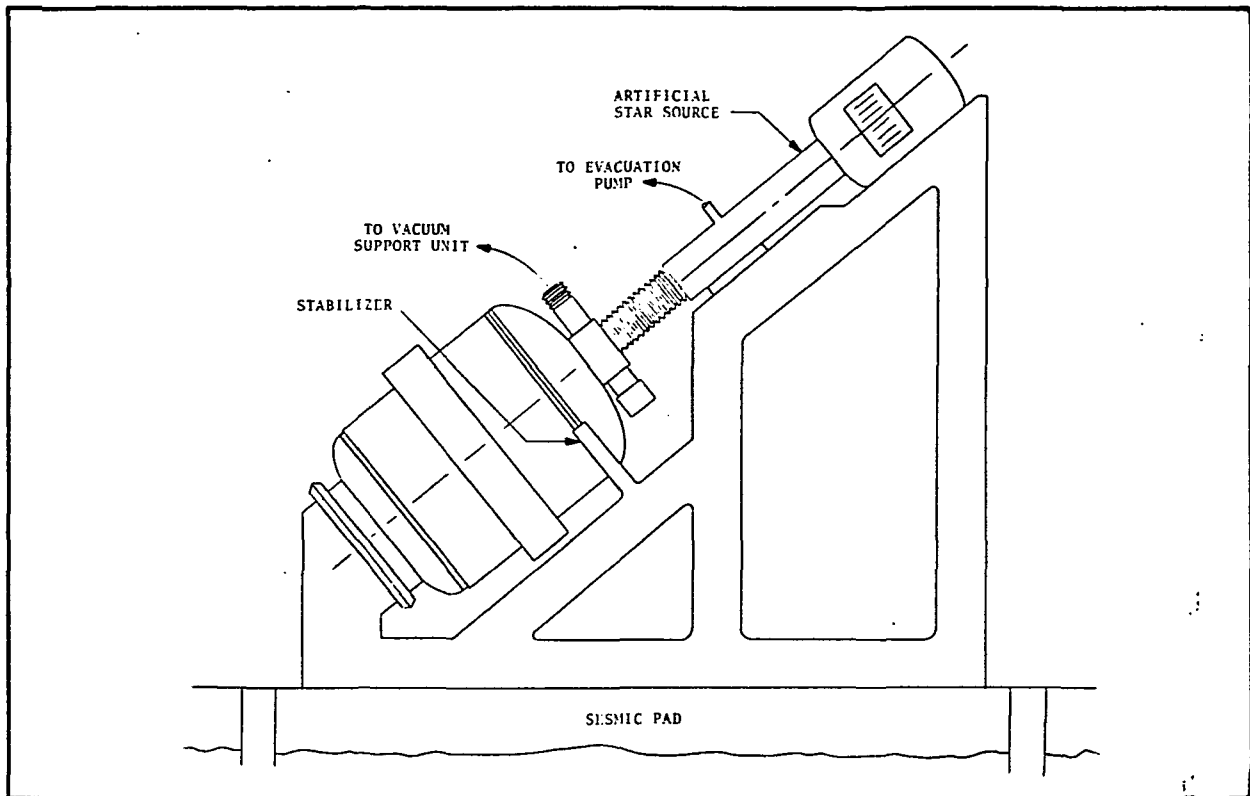


Fig. 7-14 Polar Mount for Experiment and Control System Tests

are minimized, however, since the spacecraft remains fixed relative to the force of gravity. An auxiliary stabilizer is provided for attachment to the forward part of the satellite.

The artificial star source is mounted directly on the test stand eliminating external mirrors.

Lens Cap Telescope Source. This fixture provides a qualitative check of the telescope optics and detector system by using a low-intensity source such as a photodiode positioned on a disk which closes off the optical entry to the telescope. The lens cap would be equipped with a cursor so that the position or intensity gradient of the source could be varied to make go-no-go checks on the four quadrants of the detector system.





Temporary (test) Dewar. This dewar is used to store the inner dewar and experiment prior to integration with the main flight dewar. It has proper interfaces with the inner dewar and accommodates the electronics and cryogenic control equipment required to functionally test the experiment. The dewar also has a suspension system simulating that of the flight dewar to permit environmental testing of the experiment when installed in the dewar.

Artificial Star Source. The stability requirements on the stellar source used as a telescope target are much more difficult to meet than those for either resolution or intensity. The stability must be better than 50 milliarc-seconds over a period of one half hour.

The contributions to instabilities will arise (1) within the source itself, (2) at the air currents between the source and experiment, (3) in the structural support connecting the experiment and source, (4) in the satellite structure and the dewar supports (especially if the satellite is rotated so that the force of gravity changes direction relative to the structure). Any one of these sources is likely to be several times the allowable instability.

One solution to these difficulties is to use a servo-controlled, self-aligning star source.

Figure 7-15 shows the concept for a servo-controlled source which maintains the incident beam perpendicular to a mirror attached to the cold window of the experiment. Only the "elevation" axis is shown, for clarity.

The stellar source uses optical detection and servo components similar to those in the satellite experiment.

The light from the source passes through an iris and is reflected from a half-silvered servo-controlled mirror into the experiment

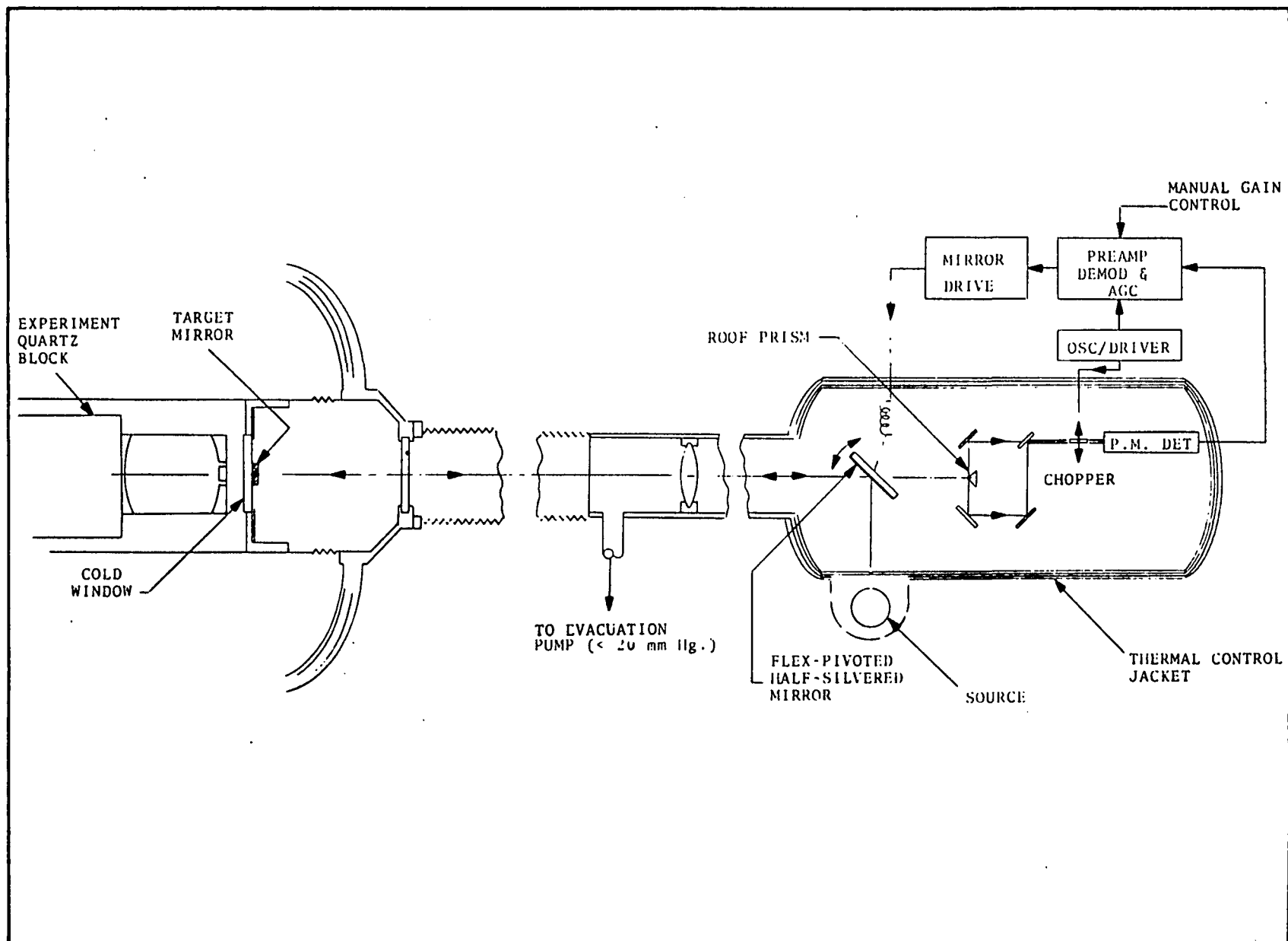


Fig. 7-15 Self-Aligning Artificial Star Source



telescope. The beam reflected from the target mirror passes through the half-silvered mirror and is split by a roof prism.

The chopper, PM detector and the demod electronics, also like the corresponding experiment components, are followed by a mirror drive amplifier.

The optical system is enclosed in a thermal control jacket. An evacuated tube connects the source to the satellite or experiment. The pointing performance of this source should approach that of the satellite telescope control.

Targets smaller than 1 arc-second will not be resolved by the experiment telescope (15 cm aperture, 6000 Å light). If the focal length of the stellar source is 3 meters, the spot size corresponding to a 1 arc-second angle is about  $2.3 \times 10^{-3}$  mm (.0006") diameter.

#### 7.3.1.5 Facilities

Test facility requirements are listed in Table 7-11. Most of the required facilities are straightforward and their use is routine for spacecraft of this size and type. Special facilities peculiar to this satellite are described below:

Polar Axis Mounted Inertial Test Stand (PAMITS). This fixture (Fig. 7-16) stabilizes an experiment or test specimen in precise attitude with respect to a fixed star. The fixture is equipped with a synchronously driven polar axis which counter-rotates the experiment at the earth rate. A cross-axis gimbal allows pointing off the polar axis. A vernier drive system provides fine attitude control about all three axes. Auxiliary function generators are used to generate control signals for the PAMITS fixture in response to signals from the experiment control system, so that closed loop simulation is possible. The spacecraft can be



Table 7-11

## STANDARD FACILITIES REQUIREMENTS, INTEGRATION AND TEST

CLEAN ROOMS - Horizontal Laminar Flow System

Floor area - 600 sq. ft.

Temperature - Controlled at  $70 \pm 5^{\circ}\text{F}$

Relative Humidity - 40% maximum

Federal Standard 209 Class 100; Class 10,000 under working conditions

ELECTRODYNAMIC EXCITER - Ling Model L-200 or Equivalent

Frequency Response - 5-200 Hz

Maximum Displacement 1 in. peak-to-peak

Force Capability 9000 force lbs. random  
14,000 force lbs. sine

DYNAMIC/STATIC BALANCER

Sensitivity - At 60 rpm: 4.0 oz-in. static unbalance,  
200 oz-in.<sup>2</sup> dynamic unbalance

THERMAL VACUUM CHAMBER

Dimensions - 10 ft diameter, 15 ft long

Pressure -  $8 \times 10^{-9}$  torr (clean, dry and empty)

Temperature -  $+150^{\circ}\text{C}$  to  $-200^{\circ}\text{C}$

MAGNETIC TEST FACILITY

Dipole Moment Measurements to  $60 \text{ gauss-cm}^3$  on objects up to 6 feet diameter and weighing 600 lbs.

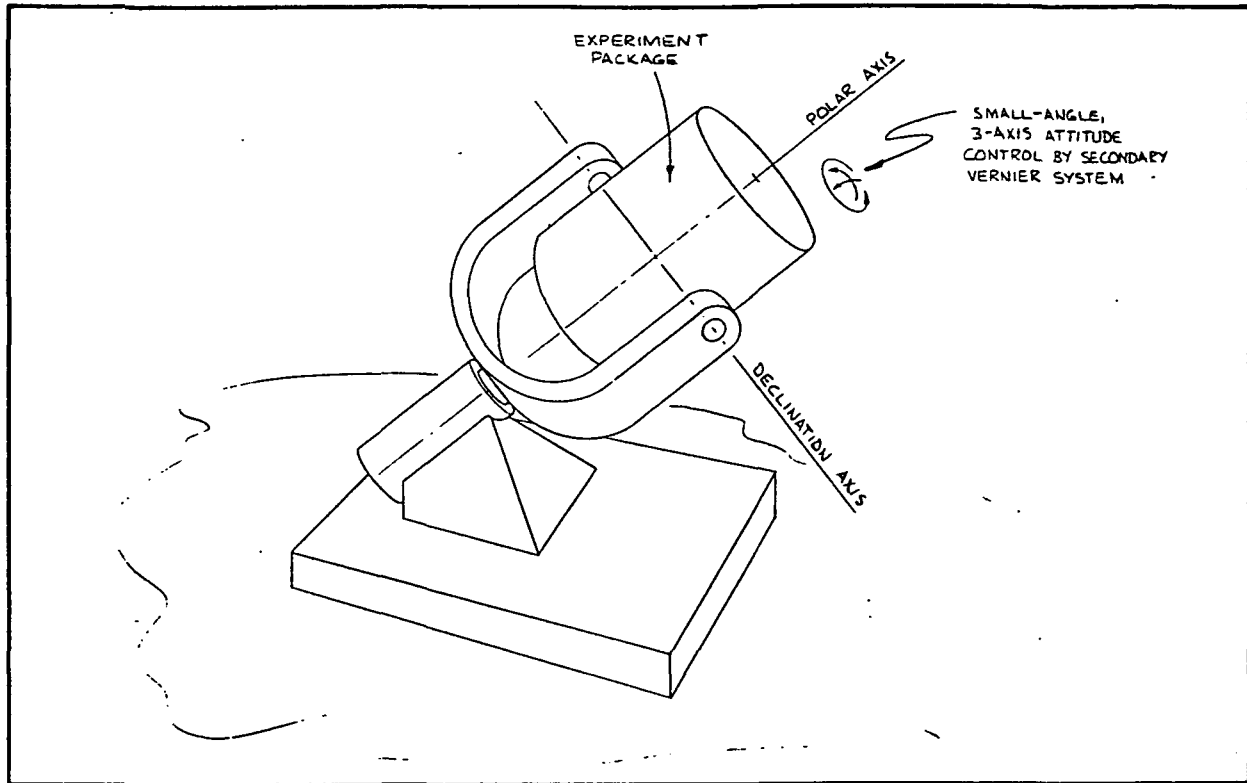


Fig. 7-16 Polar Axis Mounted Inertial Test Stand

rotated continuously during gyro spin-up to accurately align the spin axis of the gyroscopes with the polar axis. It also permits off-axis testing of the gyroscope instrumentation system since the spacecraft may be positioned at various declination angles.

The PAMITS fixture is mounted on a large seismic pad.

Low Magnetic Field Facility. To achieve a very low magnetic field in the experiment, the experiment is placed in a low magnetic environment prior to reducing the experiment to liquid helium temperatures. Figure 7-17 shows a cross section view of the low magnetic field facility. This chamber consists of superconducting lead shield submerged in liquid helium. Insulation for the helium cavity is provided by additional cavities pumped to hard vacuum and surrounded by walls containing liquid nitrogen. The experiment or test specimen is lowered into the cavity in its own dewar, and

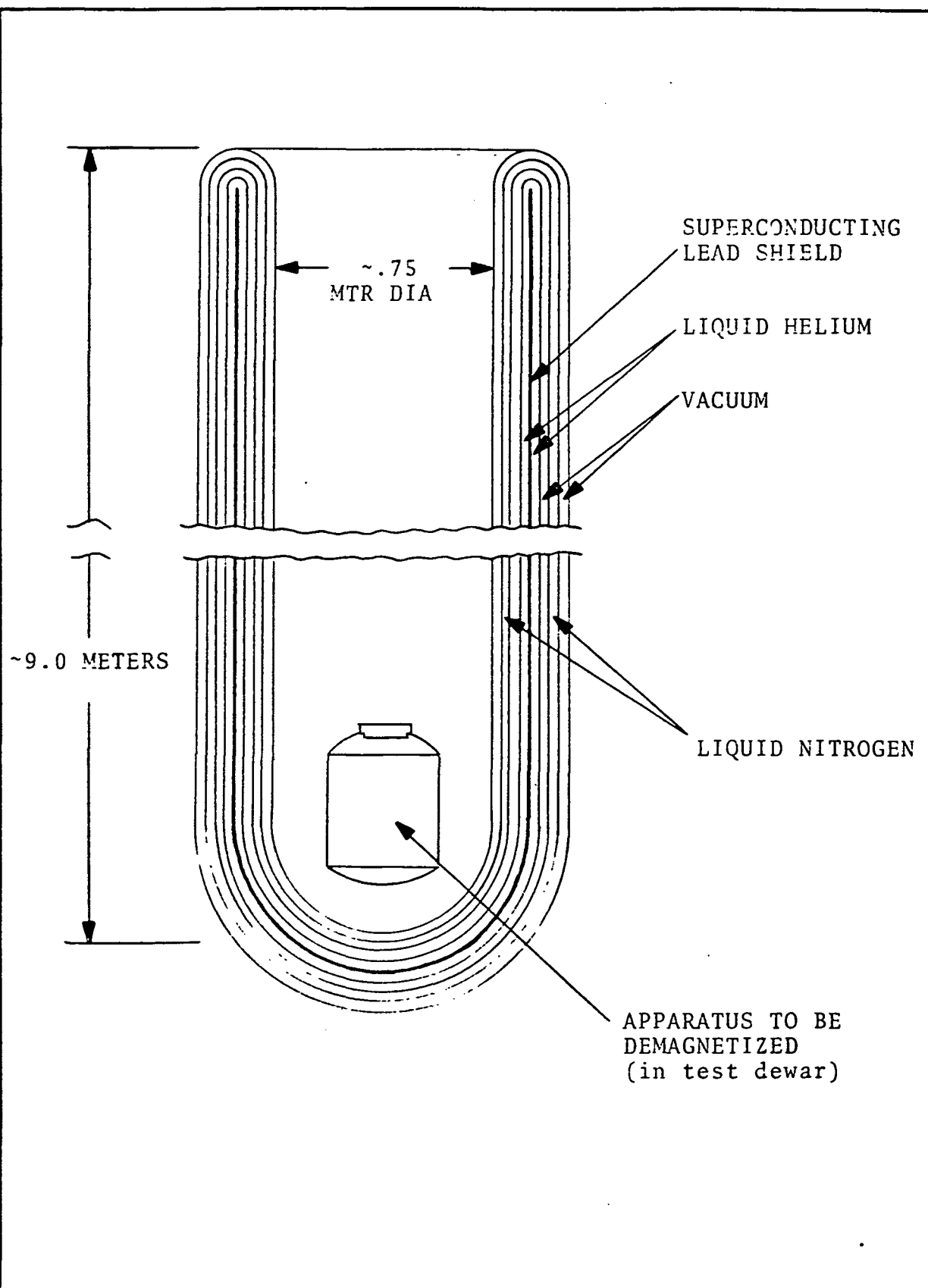


Fig. 7-17 Cross-Section Schematic, Ultra-Low  
Magnetic Field Facility



brought to cryogenic temperatures before removal.

A facility similar to the one described is under construction at Stanford University, and the magnetic field achieved by the facility will be less than  $10^{-6}$  gauss.

Liquid Helium Storage and Service. Substantial quantities of liquid helium will be required to replenish the test and flight dewars. As much as 5 kg of helium per day may be used. This may be reduced if the launch locks are retracted during periods of inactivity. On the other hand, the usage may be as high as 10 kg per day if the launch locks are left engaged continuously.

Three possible methods of supplying and storing helium were investigated: (1) buy the helium outright from a cryogenic supply company, (2) install a facility for recovering and liquefaction of the boil-off helium, (3) recompress the helium and return it to the supplier for liquefaction.

Helium is a semi-precious commodity; however, at the present time the Government has no program for regular recovery of the gas. The cost of helium produced by a supplier is presently less than the other alternatives.

A portable dewar can be supplied by the helium producer. The dewar and transfer equipment are available on a lease basis for up to a year for less than would be expended for a fixed storage facility.

Data Reduction Computers. Flow diagrams for real-time and off-line data processing are given in Figs. 7-18 and 7-19 respectively. Computer requirements are summarized in Table 7-12.

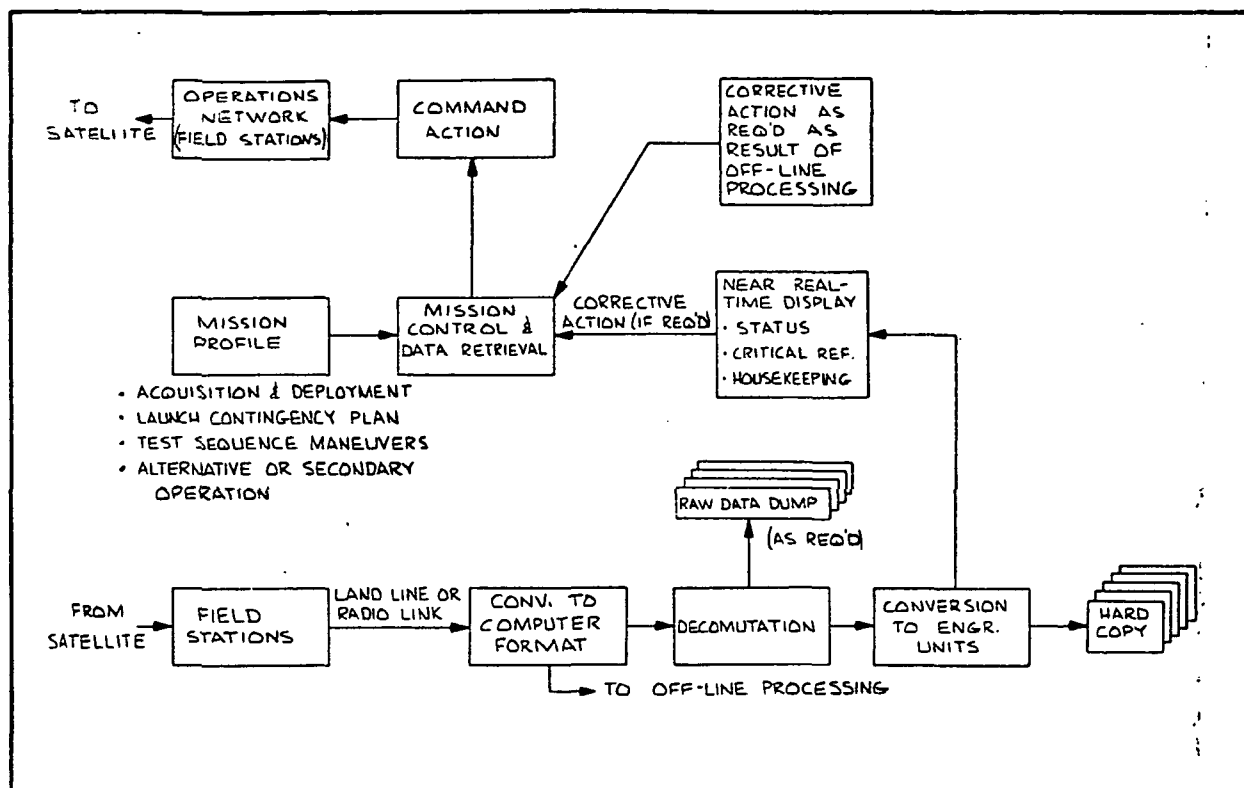


Fig. 7-18 On-Line (Near Real-Time) Data Processing and Operation

### 7.3.2 Launch and Early Orbit Operations

The sequence of pre-launch activities is outlined in Fig. 7-20. the Launch site operations are with one or two exceptions compatible with an established practice. The satellite will undergo a series of functional checks after arrival at the launch site to confirm the basic integrity of the satellite before transfer to the launcher tower. The same test equipment used for qualitative testing during the test program will be employed.

The functional test will consist mainly of the block (transfer function) tests on portions of the satellite circuitry, and verification of the response to simulated signals injected at test points. The vacuum support equipment and liquid helium supply dewar will be used both in the hangar and on the launch stand. No umbilical connection to the spacecraft will be required since



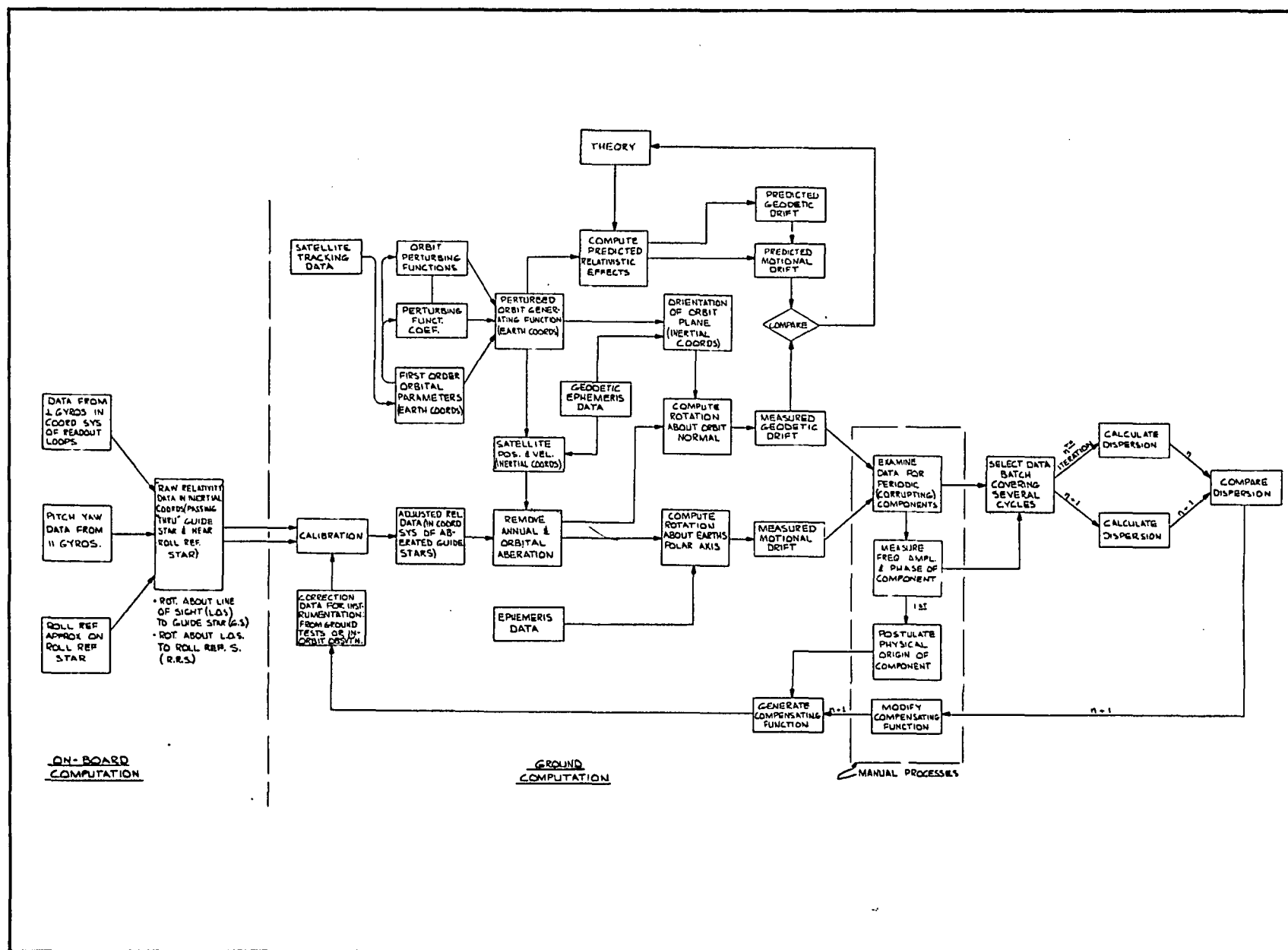




Table 7-12  
COMPUTER REQUIREMENTS

	<u>Real-Time Processing</u>	<u>Off-Line Data Reduction</u>
Word Length	16 Bit Floating Point	24 Bit Floating Point
Core Storage	16 K	24 K with overlay capability
Special Input/Output Equipment	Telemetry Buffer, Display Board	
Special Features	Real-Time Priority Interrupt Direct Digital Interface Adapter	Mag Tape
Typical Manufactur- ers Types	SDS-SIGMA-3  PDP-10 Honeywell- 301 Data General NOVA General Auto- mation SPC-16 Vacian 622I	SIGMA-3 IBM 370-135 CDC-3000 Series  PDP-16

the dewar is capable of standing for several hours in a sealed condition without pumping.

After mating with the launch vehicle, an all-system test will be run to assure compatibility between the spacecraft and the launch vehicle electrical systems. Before launching, the spacecraft will be given another series of functional checks to verify proper operation of the command and telemetry system, and to set up the spacecraft in the launch state. The satellite dewar will be topped off during final prelaunch preparations.

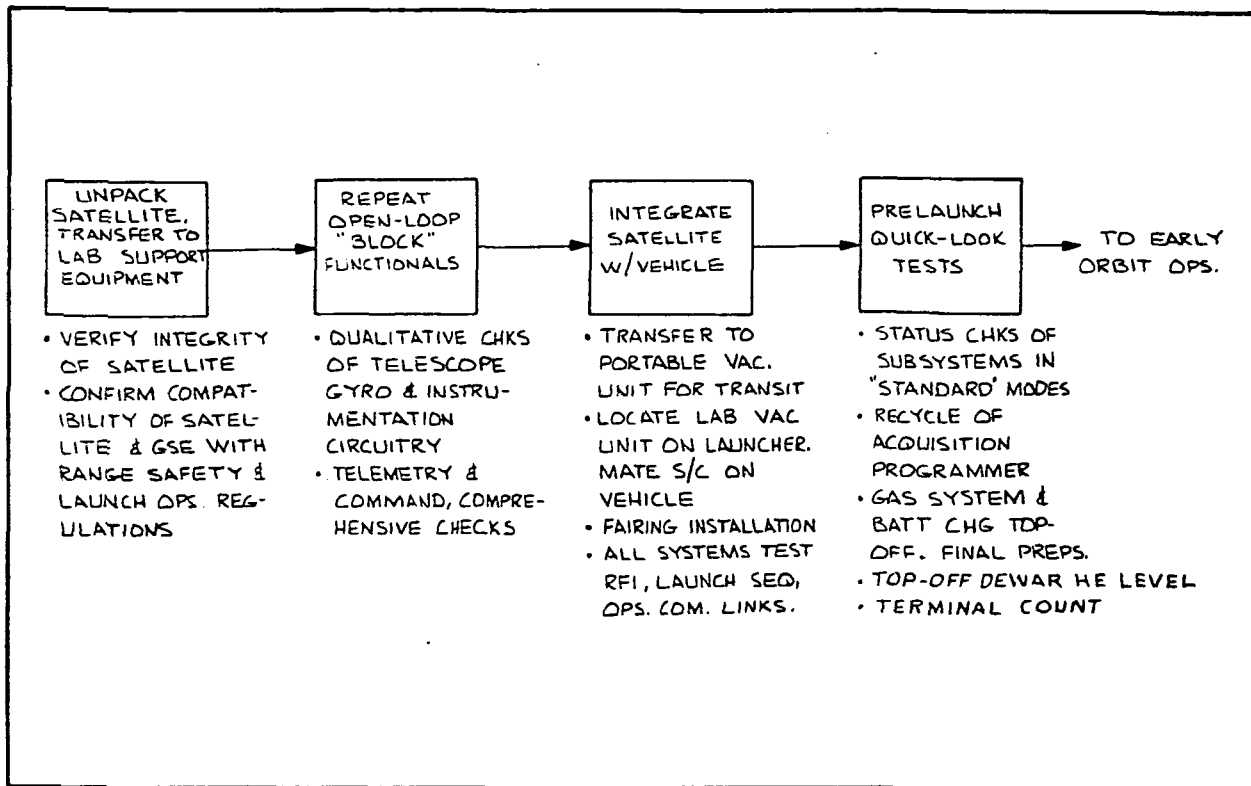


Fig. 7-20 Launch Site Operations

### 7.3.2.1 Launch, Acquisition and Early Orbit Operation

Figure 7-21 shows the schedule for the acquisition sequence. A detailed description of this sequence is given in Section 3.1.4. The acquisition sequence can be accomplished in about 16 hours with ample time between sequential operations to retrieve and analyze the satellite data.

### 7.3.2.2 Contingency Action

In preparation for possible contingency action a comprehensive plan is developed for diagnosing and correcting the principal failure modes of the satellite. The actions prescribed by this plan are rehearsed beforehand, using an operational simulator computer routine, so that the basic strategy and methods for contingency action have been rehearsed prior to the actual launch.

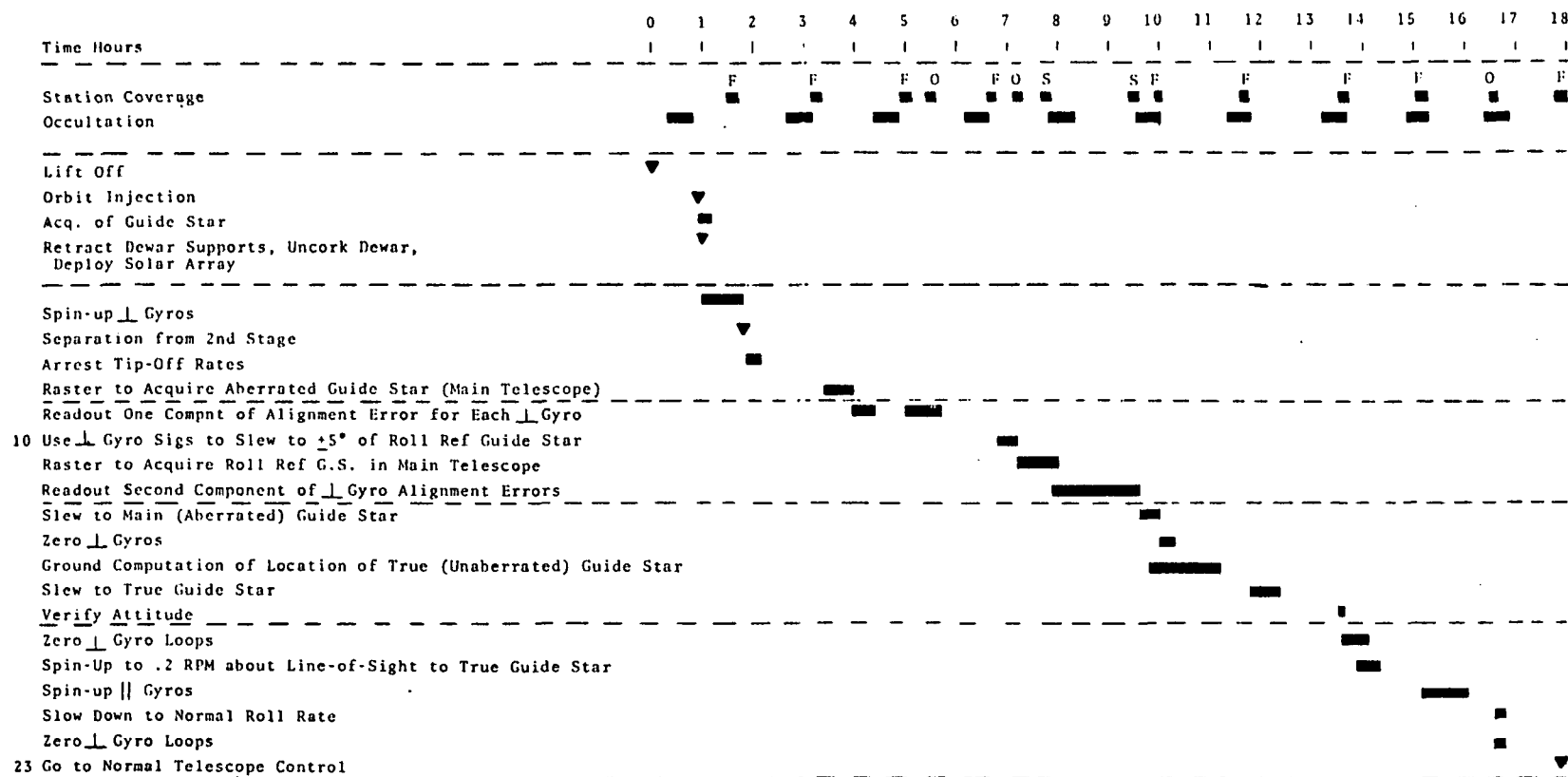


Fig. 7-21 Launch and Initial Acquisition Sequence



If there should be a malfunction in the initial acquisition sequence, the acquisition would be made using ground commands as indicated in Fig. 7-22. This contingent action would require about 29 hours.

### 7.3.3 In-Orbit Operations

The command action and real-time data processing takes place in a satellite control center which is the central focal point for all instructions and data retrieval from the spacecraft. Off line processing occurs as the data is accumulated and will be done by a larger computation facility shared by other programs.

#### 7.3.3.1 Real-Time Data Processing and Operational Control

Figure 7-18 shows the flow of information to and from the satellite, and indicates the various processing steps related to operating the spacecraft in orbit. The basic operation is prescribed by a mission profile which outlines the procedures for in orbit operation, contingency action, routine orbit operation, and alternative or secondary operations. This specification also indicates the types of changes which can be made on a routine basis, if the housekeeping data indicates a need.

The satellite data is decommutated and displayed in a raw data form, and also converted to engineering units so that the spacecraft status and housekeeping monitors can be readily examined. A copy of the computer formatted data tapes is also transmitted to the off-line data processing facility.

A satellite control center is usually capable of retrieving the data and exercising operational control over several satellites, and therefore, the satellite might share a control center with other satellites.

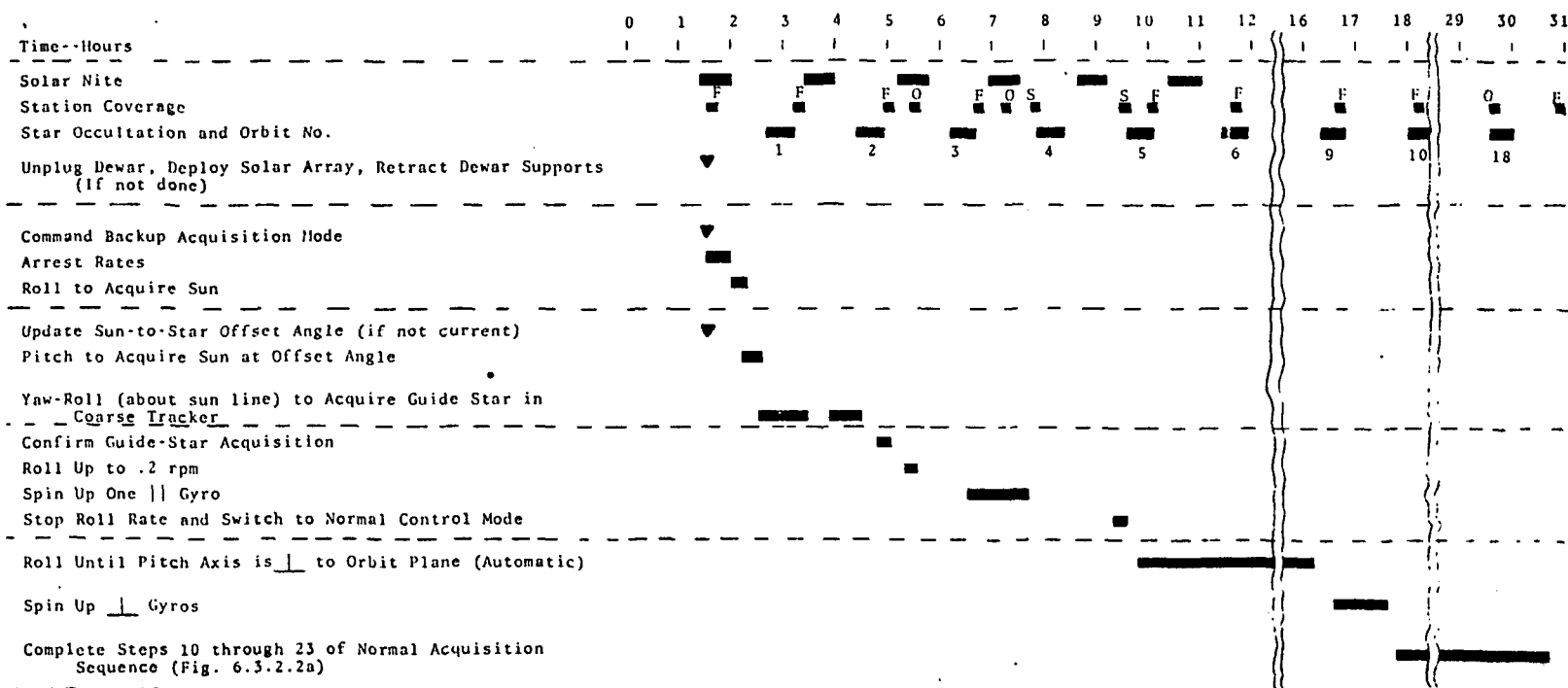


Fig. 7-22 Backup Acquisition Sequence



### 7.3.3.2 Off-line Data Processing

Figure 7-23 shows the angles to the aberrated guide star, relative to the drift-free reference axes of the gyros, for a spring launch, with the descending node of the satellite orbit on the dark side of the earth.

The orbital aberration is shown as clipped sine waves superimposed on the declination component of the annual aberration.

Figure 7-24 shows the look angle components after they are resolved into a coordinate system containing the orbit normal and the polar axis of the earth.

This figure also indicates the presence of statistical noise and possible corrupting modulation which might occur at the satellite roll frequency.

The data reduction process must remove the known and postulated components so that all that remains is the secular drift. As data is accumulated it will be compared with a machine calculated profile such as that shown in Fig. 7-24.

Figure 7-19 shows the off-line data reduction sequence. The raw relativity data which is generated by the spacecraft is first resolved into components in a coordinate system containing the guide star and the roll reference star. At this time, compensation is made for nonlinearities or corrupting functions if they have been pre-established by ground testing or the orbit observations.

To accurately remove the annual orbital aberration, a fairly sophisticated generating function is needed to calculate satellite position and velocity. This will be done by deriving the first

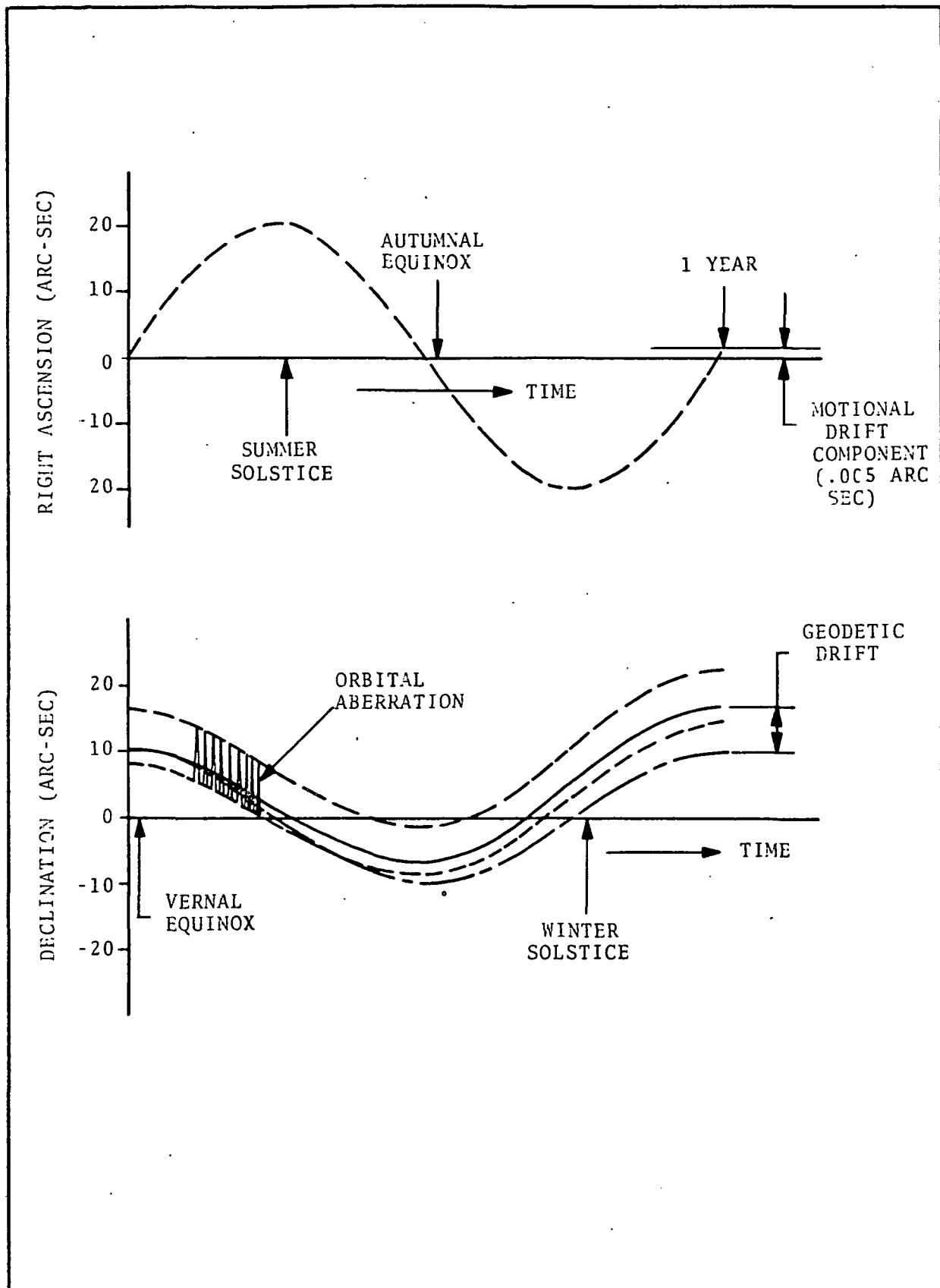
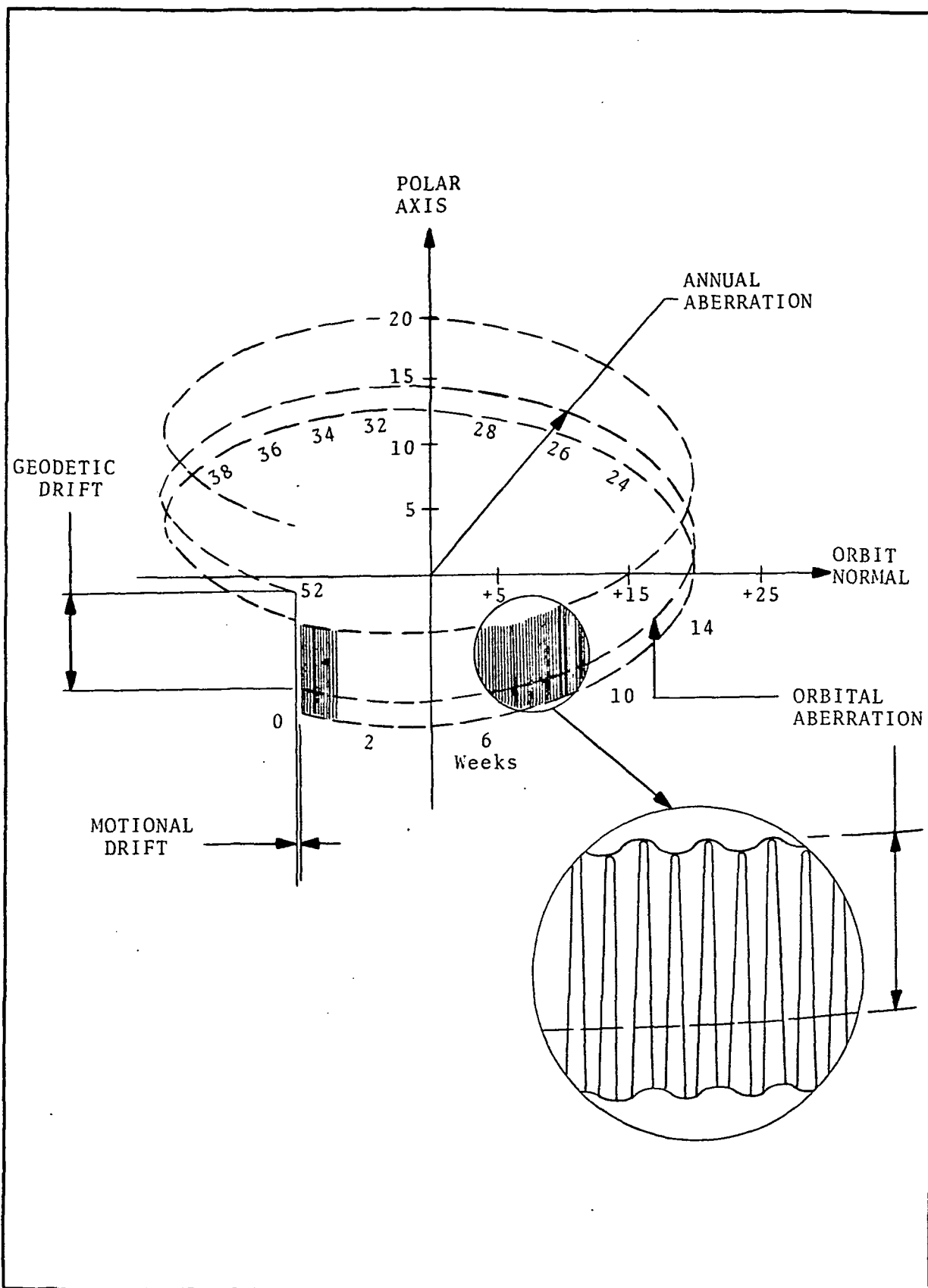


Fig. 7-23 Aberrated Guide Star Motion







order orbital parameters from tracking data and then adding perturbing functions and coefficients to the tracking data to reflect the effects of gravitational anomalies, orbital accelerations, atmospheric drag etc.

The instantaneous satellite position and velocity developed by these techniques will be used to remove annual and orbital aberration from the adjusted relativity data. Coordinate transformations will then be performed to resolve the relativity data into rotational components about the orbit normal and about the Earth's polar axis.

The resulting data will represent the first approximation to geodetic and motional data; however, it may still contain corrupting functions having periods equal to the satellite roll period or from other variations in the satellite environment. The removal of these corrupting functions will be a combination of manual and machine processing, and will rely heavily on the ability to present the data in a manner which makes the corrupting components evident.

When a periodic corrupting component has been identified, the frequency, amplitude, and the phase of the component is measured and the physical origin of the component postulated. Using a batch of the data covering several cycles of the corrupting component, the data is recycled and a compensating function inserted to lessen the effects of the corrupting element. The dispersion caused by the corrupting element is measured and compared with the dispersion measured after the injection of a compensating function to indicate whether or not the effects of the corrupting element have been reduced. This iterative process is repeated until the dispersion is minimized.

The development of this data reduction process should be carried on simultaneously with the development of the spacecraft, and



tested on both simulated data and on data generated at the systems level during experiment and satellite testing.

It is possible that the noise level on the data may be so severe that the presence of periodic components is not easily discernible by manual inspection. On the other hand, some corrupting components may be so evident that the iterative correlation process is not justified. Additional information on the noise level and types of corrupting functions will become evident as the experiment and control system development proceeds.

#### 7.3.3.3 Alternative and Back-up Operation

Even though part of this satellite should become inoperative, it is frequently possible to retrieve data and maintain effective operation of the satellite by using indirect methods. The spacecraft is equipped with redundant equipment in many cases. Section 3.3 discusses the main failure modes and the alternative action which could be used, if they should occur. More of these will become evident during the detailed design of the satellite and experiment.